IMPINGEMENT OF OFFSET JETS ON RIGID AND MOVABLE BEDS

Thesis submitted in accordance with the requirements of The University of Liverpool for the degree of Doctor in Philosophy

by

ALI AKBAR SALEHI NEYSHABOURY, Msc.

October, 1988.

ABSTRACT

The present thesis describes an experimental and theoretical investigation of the flow field and scour action of an offset jet.

The hydraulic characteristics of the offset jet and the resulting scour developed in the bed were investigated in the laboratory.

Tests were carried out using a fixed bed and a single offset ratio (height of jet above bed / jet thickness). Three flow rates were used. Velocity measurements in two directions, especially in the recirculating zone, were of help in understanding the flow field and in providing the necessary data for comparison with the theoretical results.

The development of scour, on a uniform sand, was monitored at set time intervals, in most cases until the asymptotic state was reached. A new effective and simple method for measuring the scour profile, while the experiment was running, was devised. The experiments were conducted using four different offset ratios and several flow-rates. Results showed dependency of the scour characteristics on Froude number, time and especially the offset ratio. The findings of each experiment were combined dimensionlessly to produce relationships which describe the development of scour characteristics for the tested range of parameters. Scour profiles were found to be similar for a given offset ratio, but differed from one offset ratio to another.

The second part of the work was concerned with developing a general integral method capable of the prediction of velocity fields of different flow situations, including those of offset jet impinging on rigid

and eroded beds. The combination of strip integral method in a curvilinear system with the k-ε and algebraic stress turbulence models provided such a method. Application of this method to a variety of selected test cases revealed the ability of the model to capture the main features of the flow within the considered range of interest. The algebraic stress model was found to give better results in curved and wall effected flows.

ACKNOWLEDGEMENTS

The author wishes to express his deep gratitude and sincere thanks to his supervisor Dr. K.H.M. Ali, Senior Lecturer, Department of Civil Engineering, for his patient guidance and his invaluable assistance throughout this study.

The author wishes to express his appreciation to the Islamic Republic of Iran for their financial help during the course of his postgraduate studies.

I am particularly grateful to the Technical Staff in the Department of Civil Engineering for their assistance and excellent workmanship in the construction of the experimental models.

Finally the assistance of all the other who have in one way or another contributed in the completion of this thesis is also acknowledged.

TABLE OF CONTENTS

Chapter 1. INTRODUCTION 1

1.1 General Introduction 1

1.2 Scope of Thesis 1

1.3 Layout of the Remaining Chapters 3

Chapter 2. BACKGROUND AND LITERATURE REVIEW 5

2.1 Introduction 5

2.2 The Concept of Local Scour 5

2.3 Types of Localised Scour 7

2.4 Literature Review 10

2.4.1 Local Scour due to a Horizontal Turbulent Jet 11

2.4.1.1 EXPERIMENTAL INVESTIGATIONS 12

2.4.1.2 Summary of theoretical work 21

2.4.2 Local Scour due to Impinging Jets 25

2.4.3 Local Scour Caused by an Offset Jet 29

2.5 Concluding Comment 31

Chapter 3. OFFSET-JET LITERATURE REVIEW 32

3.1 Introduction 32

3.2 Definition of the Problem 34

3.2.1 The Free-Turbulent Submerged Plane Jet 34

3.2.2 Shallow Plane Jets 36

3.2.3 Basic Features of the Two-Dimensional Offset-Jet . . . 39

3.3 Literature Review 41

3.3.1 Review of Experimental Investigations 41

3.3.1.1 Attachment Point 41

3.3.1.2 Pressure Distribution 43

3.3.1.3 Velocity Distributions 44

3.3.1.4 Shear Stress 47

3.3.2 Review of Theoretical Investigations 47

3.4 Concluding Remarks Regarding The Literature Review 50

Chapter 4. EXPERIMENTAL FACILITIES AND PROCEDURES 52

4.1 Objectives 52

4.2 Experimental Equipments and Arrangements 52

4.2.1 Characteristics of the Bed Material 54

4.3 Experimental Investigations 54

4.3.1 Measurements of the Scour Characteristics 54

4.3.1.1 The Photographic Method 55

4.3.2 Instrumentation and Velocity Measurements 57

4.3.3 Summary of the Test Programme 59

Chapter 5. EXPERIMENTAL RESULTS OF THE OFFSET JET 61

5.1 Introduction 61

5.2 Analysis of Results 61

5.2.1 Velocity Distribution 61

5.2.1.1 Attachment Length 63

5.2.1.2 Locus of Maximum Velocity 64

5.2.1.3 Velocity Decay; 66

5.2.1.4 Jet Spread 67

Chapter 6. PRESENTATION AND DISCUSSION OF SCOUR EXPERIMENTS . . 68

6.1 Introduction 68

6.2 General Description of the Mechanism of Scour by Jets . . . 69

6.2.1.1 Scouring Process by Offset Jets 71

6.2.1.2 Development of the Scour Hole 72

6.2.1.3 Concept of a Limiting Scour Condition 73

6.3 Dimensional Consideration 74

6.3.1 Introduction 74

6.3.2 Variables Affecting the Scouring Process 75

6.3.3 Dimensional Analysis 75

6.4 Analysis of the Experimental Results 78

6.4.1 Presentation of Data 78

6.4.1.1 Effect of Dimensionless Time Ratio 79

6.4.1.2 Dependency On The Densimetric Froude Number 79

6.4.1.3 Dependency on Height of Jet above the Bed 80

6.4.1.4 General Formulation 80

6.4.2 Characteristics and Similarity of the Scour Profiles . 81

6.4.3 Analysis of Scour at the Asymptotic State 82

6.4.4 Analysis of the Flow Characteristics in a Local Scour Hole 84

Chapter 7. THE GOVERNING EQUATIONS AND THE PROBLEM OF CLOSURE . 86

7.1 Introduction 86

7.2 General Flow Equations 87

7.2.1 Time-dependent equations 87

7.2.2 The Time-Averaged Continuity and Momentum Equations . . 89

7.3 Approaches to Closing the Equations 90

7.3.1 The Problem of Closure 90

7.3.2 The Turbulent Model Approach 91

7.3.3 Literature Review 91

7.3.3.1 Zero-Equation Models 92

7.3.3.2 One-Equation Models 94

7.3.3.3 Two-Equation Models 96

7.3.3.4 Reynolds-Stress Models 98

7.3.3.5 Algebraic-Stress Models 100

7.4 Equations of Flows in A Curved System 102

7.4.1 Mean Flow Equations 102

7.4.2 Reynolds-Stress Transport Equations 106

7.4.3 Turbulence Modelling for Curved Flows 108

7.4.3.1 Curvature Effects on Turbulence 108

7.4.4 Review of Turbulence Modelling 110

7.4.4.1 The Standard k-E Model 112

7.4.4.2 The Algebraic-Stress Model 114

Chapter 8. METHOD OF SOLUTION 121

8.1 Introduction 121

8.2 Methods of Solution 121

8.2.1 Differential Methods 122

8.2.2 Integral Methods 123

8.2.2.1 Energy Method 124

8.2.2.2 Entrainment Method 125

8.2.2.3 Moment of Momentum Method 125

8.2.2.4 Strip Integral Methods 125

8.2.3 Literature Review 125

8.2.4 Concluding Remarks 128

8.3 Method of Solution (SIM) 131

8.3.1 Integration of Mean-Flow Equations 132

8.3.1.1 The Closure Problem 135

8.3.1.2 Numerical Solution of the Equations 138

Chapter 9. THEORETICAL RESULTS 139

9.1.1 Studies on the modelling of turbulent free jets . . . 139

9.1.1.1 Free-jet results 141

9.1.2 Two-dimensional Wall Jets 143

9.1.2.1 Wall Jet on a Flat Surface 145

9.1.2.2 Wall Jets on Curved Surfaces 147

9.1.2.3 Two-Dimensional Offset Jets 151

9.1.2.4 Offset jet in scour hole 156

9.1.3 Conclusions 158

Chapter 10. CONCLUSIONS AND RECOMENDATIONS 160

10.1 introduction 160

10.2 Conclusions on the Experimental Part 160

10.2.1 Offset-Jet Impinging on a Rigid Bed 160

10.2.2 Scour Experiments 161

10.2.3 Conclusions on the Theoretical Work 163

10.3 Suggestions for Future Work 165

Appendix A. 184

GLOSSARY

A_v = coefficient

A, A_1, A_2 = constants

a, a_1, a_2 = constants

B_1, B_2, B_3 = constants

b = half-width of the velocity profile

b_A = half-width of jet at the end of rigid apron

b, b_1, b_2 = constants

B = constant ; width of scour hole ; width of 2-D channel

b_0 = jet nozzle thickness, sluice gate opening

b_u = upper half-depth

c = constant

C_n = coefficient

$C_\mu, C_{\varepsilon 1}, C_{\varepsilon 2}$ = coefficients in turbulence model

C_1, C_2 = ASM constants

C'_1, C'_2 = ASM constants

C_k, C_ε = ASM constants

D_{ij} = diffusion transport tensor

d = submergence of jet

$d_{15.9}$ = sieve diameter which passes 15.9%

d_{50} = median size of sediment

d_{90} = mean size of sediment of with 90% by weight is finer

d_s = depth of scour at any distance x from the jet exit

d_m = maximum depth of scour for a particular run time

d_{p1}, d_{p2} = height of the upstream and downstream dune, respectively

E = coefficient

F = empirical curvature correlation

f, f_1, f_2 = indicates "function of"

f_w = wall function in ASM

F_r = Froude number of flow = $U_0/\sqrt{gb_0}$

F_0 = densimetric Froude number = $U_0/\sqrt{(S - 1)gd_{50}}$

F_D = drag force on a typical particle lying on the bed surface

F_L = lift force on a typical particle lying on the bed surface

F_d = disturbing forces

F_s = stabilising forces

g = acceleration due to gravity

g, g_1, g_2 = functions of

g_i, g_s, g_n = body forces in i, s and n directions

$g(B)$ = rate of sediment transport out of the scour hole

$g(S)$ = rate of supply to the area under scour

H = downstream tailwater depth

h = impingement height of vertical jet

= distance between the sluice opening and the original bed level

h = 1+n/R = ratio of local to reference radius of curvature

J = momentum of an offset jet

k = turbulent kinetic energy (= $\frac{1}{2}\ u_i\ u_i$)

K = s/R, curvature parameter of logarithmic spiral

L, ℓ = dissipation length scale ($L = k^{1.5}/\varepsilon$)

= Width of shear layer

L_i = characteristic length of scour hole

l_m = mixing length

l_v = length scale of turbulence

n = exponent

= unit normal vector to the s

$\tilde{P}$ = instantaneous pressure

P = mean pressure

p' = fluctuating part of pressure

P_{ij} = generation tensor for turbulent kinetic energy

P_h = hydrostatic pressure

P_c = $P_N + \rho u^2 = P_N + \rho v^2$

= pressure on the centreline of an offset jet

P_N = excess pressure

P_a = atmospheric pressure

P_k = production of turbulent kinetic energy

q_B = bed load transport in vol. per unit time per unit width

Q = flow rate

Q_i = volume rate of sediment being transported into the scour hole

Q_s = volume rate of sediment transport out of the scour hole

R_e = Reynolds number of flow

R = radius of curvature of the curved surface

= hydraulic radius

r = radial dimensional space coordinate (= R + n)

S = specific gravity of sediment = ρ_s/ρ

= curvature parameter

s = coordinate along longitudinal direction

t = time, time of scouring action

T = turbulent time scale

T_k, T_ε = Diffusion term in k and ε transport equations

$\tilde{U}$ = instantaneous velocity at a point in the x or s direction

U = mean velocity in x or s direction

u = fluctuation component of U

U_i = instantaneous velocity component in x_i direction

U_i = mean velocity in x_i direction

U_m = maximum velocity at a section

U_{MA} = maximum velocity at the end of rigid apron

U_{mx} = maximum horizontal velocity at the section of maximum

scour depth

U_j = mean velocity of incoming jet

U_τ = friction velocity [$= (\tau_w/\rho)^{0.5}$]

$u_i u_j$ = Reynolds stress

U_0 = external flow velocity

$\tilde{V}$ = instantaneous velocity at a point in the y or n direction

V = mean velocity in y or n direction

v = fluctuation component of V

V_{max} = maximum total velocity of offset jet

V_h = volume of scour hole

V_s = volume of scour per unit width

w = mean fall velocity of sediment

= fluctuating part of the velocity in z direction

x = longitudinal distance measured from the jet exit

= coordinates, usually in the flow direction

x_i = direction

x_A = attachment length

X_m = distance of the section of maximum erosion from jet exit

X_D = extent of scour measured from the jet inlet to

the crest of the dune

X_{p1}, X_{p2} = distance of the upstream and downstream dune

from the sluice

X_L = X_D at the asymptotic state

x_s = downstream distance from attachment point

y = normal distance from the boundary

= coordinate, usually normal to water surface (vertical)

y_m = vertical distance between the point of maximum

velocity and the bed

Z = coefficient

z = coordinate, usually transverse to the horizontal

flow direction

α = coefficient

β = constant, coefficient

δ = boundary layer thickness

δ_{ij} = Kronecker delta (= 1 for i=j and = 0 for i≠j)

ε = dissipation rate of turbulence energy

η = non-dimensional crosswise space coordinates = n/b

κ = Von Karman constant

μ = dynamic viscosity of fluid

μ_t = turbulent eddy viscosity

μ_{eff} = $\mu+\mu_t$

ν = kinematic viscosity of fluid

ρ = mass density of fluid

ρ_s = mass density of sediment grain

$\sigma_k, \sigma_\varepsilon$ = turbulent Prandtle number for diffusion of k and ε

σ = spread parameter for free jet

σ_g = geometric standard deviation of particle sizes

τ = shear stress

τ_b = shear stress along the bed

τ_c = critical shear stress

τ_{ij} = shear stress

ϕ = angle of repose of sediment

ϕ_1, ϕ_2 = indicates "function of"

ϕ_{ij} = pressure-strain redistribution tensor

∞ = infinity ; suffix denoting scour at the asymptotic state.

i,j,k,m = orthogonal space planes

CHAPTER 1. INTRODUCTION

1.1 GENERAL INTRODUCTION

In hydraulic engineering, the prediction and control of erosional problems is an important subject. Amongst different flow cases, the action of an offset jet can result in the erosion of bed material. This scour can cause severe damage to the bed and nearby structures. For example near cooling pools of power plants or under sluice gates.

It is therefore essential that the erosive power of an offset jet is understood, enabling adequate safety factors to be included in the design of any structure where scour is to be expected.

To date, little work has been carried out on the effect of this type of flow on any nearby bed sediments.

1.2 SCOPE OF THESIS

The main purpose of the present work is to contribute to an understanding of the flow field resulting from an offset jet and the characteristics of the scour hole caused by it. The detailed computations of flows presented herein and the reported experimental velocity data may also be of use to investigators who seek to predict the scour profiles caused by different jets.

Prediction of the flow field of an offset jet is of considerable interest to the engineer. Offset jets are found in a wide variety of practical situations, for example at the pool of a power plant.

Calculation of flow fields is perhaps in its third phase of development. In the first phase there was an almost exclusive reliance on experimental correlations of overall flow behaviour with relevant non-dimensional groupings of variables. The next phase saw an increasing effort to develop mathematical models of the flow phenomena and then to deduce the behaviour of flows through mathematical reasoning. The advent of high-speed and large-capacity computers, and new and better finite difference and finite element techniques have led to the present phase. It is now possible and practicable to use advanced turbulence models for computing complex flows. In an effort to reduce the empiricism in models, attention is usually focused on basic transport mechanisms in the flow.

The present study, in the theoretical part, evaluates the performance of an integral method of solution in conjunction with the use of advanced turbulence models in predicting different flows. Comparisons with published experimental data enable an assessment of the model and help to identify corrections and further improvements that can be made in future work. The second aim is to use these analytical methods to predict the behaviour of the flow in a scour scour hole caused by an offset jet and to provide a basis for further work on the prediction of the scour-hole development. The computations are compared with velocities obtained by the writer in the experimental part of his research.

1.3 LAYOUT OF THE REMAINING CHAPTERS

A comprehensive survey of experimental and analytical work of scouring action of jets, with particular emphasis on that caused by an offset jet, is given in CHAPTER TWO.

In terms of the scouring action of the offset jet, the survey revealed that little work had been carried out, and as yet nothing was known about the temporal development of the scour. It was also found that most of the analytical work was based on the scouring action of a wall jet.

A similar survey was conducted into the nature of the offset jet itself, and this is given in CHAPTER THREE. It was found that limited theoretical work, in this field had been carried out.

As a result of the overall lack of data in this field, a study was carried out to provide adequate measurements of velocity on which verification of the present theory could by made. These velocities would also provide a better understanding of the flow field.

The details of the experimental arrangements and procedures for both the rigid bed and scour hole experiments are described in CHAPTER FOUR. A new method for measurement of the scour profile is introduced in this chapter.

Results of the present experimental work on the offset-jet impinging on a rigid bed is then described in CHAPTER 5.

CHAPTER 6 deals with the experimental results of the scouring action of the offset jet. The effects of the jet's height and jet discharge on the scouring action of the offset jet are studied. Some basic relationships between the duration of the scouring action, and different characteristics of the scoured profile are given.

CHAPTER 7 deals with the theoretical aspects of the problem. The basic equations and turbulence modelling involved in computing the various flows are presented, especially in the curved coordinate system appropriate for the present investigation. Also, a selection of the relevant literature on turbulence modelling is reviewed. CHAPTER 8 is concerned with solution methods and includes a review of the different methods of solving the governing equations. An integral modelling technique is developed for prediction of the flow-field.

In CHAPTER 9, computation of the velocity fields of a wide range of flows using different turbulence models are compared with various experimental results. Theoretical computation of the velocity distributions in a scour hole is also presented.

Finally CHAPTER 10 draws conclusions from this study and makes recommendations for further related work.

CHAPTER 2. BACKGROUND AND LITERATURE REVIEW

2.1 INTRODUCTION

The localised scour phenomenon has been the subject of extensive investigations by many researchers and numerous literature exists for scour caused by 2- and 3-dimensional turbulent jets. Most of the studies conducted on scour have been empirical because of the complexity of the physical processes. In this chapter much of the work carried out by others into scour, with particular reference to that produced by jets, has been summarised. A survey of literature revealed a limited amount of published material concerning offset-jet scour.

2.2 THE CONCEPT OF LOCAL SCOUR

Scour or erosion may be defined as the enlargement of a flow section by the removal of material comprising the boundary through the action of the moving fluid. This phenomenon generally takes place when water flows on a movable bed. Within the context of this work, it refers to the removal of soil particles by water. Implicit in this definition is the fact that the moving fluid exerts shearing and normal forces on the boundary particles, thereby causing their movement. The amount of material which the fluid can move or transport, in unit time, is termed the capacity of the flow.

Erosion may be divided into land or soil erosion, and local scour. Land erosion as an engineering problem applies primarily to the accel-

erated erosion of agricultural land as distinguished from normal or geological erosion.

Localised scour is regarded as the erosive action in a stream bed caused by an increase in the shear stress on the bed. A scour hole develops when the capacity of the water to carry sediment is greater than the incoming supply. Hence, the stream bed material is forced into motion by the local increase in transport capacity, which further disrupts the normal flow pattern. Therefore, localised scour occurs where the flow is being accelerated as it moves past the obstruction in the stream, or where large vortices are generated as the flow separates from the obstruction.

The problem of sediment transport caused by an offset jet, and any study of its development, must involve the concept of local scour.

Generally, local scour is classified into two types;

1. clear water scour
2. scour with continuous sediment transport

Clear water scour occurs when the bed shear stress of the undisturbed upstream region is less than the critical tractive value. If the former becomes larger than the later then scour with continuous sediment motion occurs.

Clear water scour is often split into two periods (Fig. 2.1a). As the scour hole develops, the local flow is concentrated in the proximity of the hole. Thus a rapid increase in the eroded depth with time occurs. As the scour time increases, the size of the hole becomes too big

to concentrate the flow. This results in the flow becoming scattered and weakened. As a result, there is a gradual decrease in the rate of erosion. The eroded profile therefore begins to stabilise and an equilibrium state is reached.

In the case of scour with continuous sediment motion, the equilibrium depth is obtained as a result of the balance between the amount of sediment eroded by scouring action, and that supplied from the upstream region. Under these circumstances the depth of scour fluctuates with time about the equilibrium value (Fig. 2.1b).

2.3 TYPES OF LOCALISED SCOUR

Local scour in alluvial channels and rivers, occurs under a variety of conditions and the following cases have been observed.

a) Scour in Meandering Rivers: Meandering channels usually occur on lower, gentler slopes towards a river mouth. Secondary currents occur at each meander loop and cause scouring of the outer bank and deposition on the inner bank. A consequence of this phenomenon is that the meandering loops extend outwards and gradually migrate downstream (Fig. 2.2a).

b) Scour Around the Foot of Hydraulic Structures:

1. Scour around bridge piers :

When designing a bridge to span a stream where the supporting material for the foundation is erodible, the engineer is confronted with

the problem of designing foundations that must be safe from washout due to scour. A downward flow in front of the pier should exist as a result of the horizontal curvature of the streamlines in front of the pier and the fact that the velocity near the bed is reduced by friction (Fig. 2.2b). This downward velocity component gives rise to the so-called "horseshoe vortex" that is wrapped around the pier near the junction with the bed. The vortex as well as the downward velocity component itself is effective in initiating and extending the scour around and close to the pier. During floods, scouring of the supporting material from the vicinity of the foundations may permit them to tilt or settle and cause partial or complete failure of the bridge.

2. Scour Around Spur-Dikes:

A spur-dike is an armoured projection in an alluvial channel. Once the stream is obstructed by a spur-dike, a scour hole is developed in the vicinity of the dike (Fig. 2.2c). The flow accelerates through the contracted section, thus increasing the bed shear stress. In addition, a vertical and a horseshoe type of vortex may develop and increase the tendency for granular material to be entrained in the main flow. This effect is enhanced by the street vortices that shed from the nose of the dike and travel along the flow separation line.

c) Scour by jets:[1]

---

[1] A jet is defined as a stream of high velocity fluid of discrete cross sectional area issuing into a mass of fluid; the properties

Scour caused by water jets may be classified under three conditions:

1. Two dimensional horizontal jet:

Examples of this are the cases of a water jet issuing underneath a sluice gate opening (wall jet), a jet entering stilling basin and the case of the flow downstream of a spillway or a weir (Fig. 2.3a-c). The water jet will attack the erodible bed at the end of the solid floor. Local scour occurs downstream of the solid floor and a scour hole is developed. Deep scour holes might result in the undermining and failure of the solid floor.

2. Two dimensional vertical jet:

As in the case of a water jet issuing from solid (full) or hollow circular (annular) jet impinging vertically on a flat erodible boundary. Other typical examples are associated with free overfalls, flip buckets and ski-jump spillways (Fig. 2.4a-c).

3. The offset jet:

This is the case of a horizontal submerged jet with its entrance above the original bed (Fig. 2.5), as in the case of a cooling pool for a power plant. The combined action on the erodibel bed caused by attachment of jet, pressure inside the vortex under the curved jet and wall jets flowing upstream and downstream of the attachment point cause

---

of the jet and the fluid into which it emerges need not, necessarily, be the same.

a complicated process of sediment movement and hence localised scour (the offset-jet will be discussed in detail in Chapter 3).

It should be mentioned that scour around bridge piers, spure-dikes and scour due to long constriction are typical examples of scour with continuous sediment. However the clear water scour is usually connected with jets

2.4 LITERATURE REVIEW

Since only group "c" of the above mentioned categories of localised scour are related to the present investigation, the following review is restricted to this group.

The work on localised scour can be grouped as analytical and experimental. In most of the experimental work, model studies were utilised to investigate some aspects of the problem and to find functional relationships between the parameters of localised scour. Due to the complexity of this problem, the number of analytical studies on this subject is very limited.

Understanding of the scour problem has been aided considerably by investigations on scour caused by water jets. Such investigations permit the initial flow patterns to be more simply described and, thus, the other basic variables to be systematically studied.

This section reviews local scour of a non-cohesive bed[2] in the following flow situations:

1. scour due to horizontal turbulent jets,
2. scour caused by impinging jets, and
3. scour caused by offset jets.

Although sections (1), and (2) are not directly relevant to our investigations, they however belong to the same class of problems. These studies also show the similarity of scour profiles and the logarithmic progression of the scour depth with time. The detailed process of scour itself is different from one problem to another because of the variation in the flow structures.

2.4.1 Local Scour due to a Horizontal Turbulent Jet

Since there were both experimental and analytical investigations on this type of scour, our review is split into two sections. First, experimental results and then analytical methods are reviewed.

---

[2] Bed materials, from the point of view of erosivity, may be classified as: i) non- cohesive sediments ii) cohesive sediments

Non-Cohesive sediments: are those of discrete particles, the movement of which, for given erosive forces, depends only on particle properties such as shape, size and density, and on the relative position of the particle with respect to surrounding particles.

Cohesive Sediments: are those for which the resistance to initial movement or erosion depends also on the strength of the cohesive bond between particles.

2.4.1.1 EXPERIMENTAL INVESTIGATIONS

Laursen (1952)

The pioneering study in this field was probably that by Laursen (1952). As this work is important in understanding the scour process, we review it in more detail.

His experiments were conducted with a horizontal 2-D submerged wall jet directed over a sandy bed. Laursen carried out a wide range of tests with varying incoming flows and three types of bed material. The jet thickness in all runs was kept constant.

Laursen showed that the scour pattern was similar in shape and, hence, similarity of scour profiles was established by plotting dimensionless coordinates of the profiles using the horizontal distance from the inlet to the crest of the dune, X_D, as the length scale. Fig. 2.6a shows the similarity of the scour profiles, obtained by Laursen, using the length scale, X_D. It can be seen that except for the profiles representative of an initial transitory stage of scour, all the profiles of a run superpose, if plotted in this manner. Moreover, Laursen found that the profile forms for all runs of one sand were almost identical and the forms for the various sands differed only slightly. Having established the profile similarity, the results of the experiments were analysed, by Laursen, using X_D as the key variable and were plotted as a function of time as shown in Fig. 2.6b. A separate curve is obtained for each value of U_j/w and the curves show that the extent of the scour increases linearly with the logarithm of $U_j t/b_0$, and can be expressed as:

$$X_D/b_0 = A \log_{10}(U_j t/b_0) + B \qquad (2.1)$$

where b_0 is jet thickness, w is the fall velocity of the sediment, t represents time, U_j is the velocity of the incoming jet, and A and B are constants (for a given U_j/w and medium size of the sediment, d_{50}).

Laursen stated that a limit exist for the extent of the scour profile, as time reaches a certain value. To prove this idea, he used the following indirect method. By reducing the velocity of flow after a scour hole had developed, he imposed conditions such that the sand particles rarely moved at the point of impingement, and movement of any particle over the ridge was hardly conceivable. A slight increase in velocity would increase the amount of movement. The limiting velocity for any given size of scour hole was defined by Laursen as the velocity which appeared to carry particles to, but not over, the ridge, during a period of observation of several minutes. This limiting velocity was measured and the asymptotic extent of scour, X_L, was found to be given by the following equation:

$$X_L/b_0 = c\ (U_j/w)^{0.5} F_0^{0.75} \qquad (2.2)$$

where $F_0 = U_j/\sqrt{((S-1)gd_{50})}$ is the densimetric Froude Number, S is the specific gravity of sediment, and c is a constant.

Laursen deduced that the scouring process has the following general characteristics which are typical of any local-scour phenomenon:

1. The rate of scour will be equal to the difference between the capacity for transport out of the scoured area, g(B), and the rate of supply of sediment, g(S), to the area.

2. The rate of scour will decrease as the flow section is enlarged by erosion.

3. There will be a limiting extent of scour for given initial condition, and

4. The limit will be approached asymptotically with respect to time.

The first principle can be viewed as a form of a sediment continuity equation, expressed symbolically as:

$$df(B)/dt = g(B) - g(S) \qquad (2.3)$$

where f(B) = a mathematical description of the boundary, and df(B)/dt is local rate of scour or deposition.

In general, Eq. 2.3 should describe the rate of erosion. If for any reason a local change in the transport rate occurs, then there will be a corresponding local change in the bed configuration. If g(B) > g(S), localised scour occurs. Conversely, if g(B) < g(S), localised fill or deposition occurs.

The application of Eq. 2.3, in general, depends on the establishment of mathematical functions to describe the bed geometry, the capacity, and supply, as functions of the flow conditions and time. Laursen made an attempt to determine the scour depth, using Eq. 2.3, which will be given later in this chapter.

Altinbilek and Basmaci (1980)

Altinbilek and Basmaci (1980) conducted an experimental and theoretical study of localised scour caused by a two-dimensional submerged wall-jet issuing from a sluice gate. Three different bed materials were used.

Fig. 2.7 shows the results obtained by Altinbilek and Basmaci with the maximum depth, d_m, plotted against the logarithm of time. Although there is considerable scatter, the data points followed reasonably the semi-logarithmic law . As shown in Fig. 2.7, the equilibrium scour condition was attained in some of the runs. On the basis of these runs, an empirical equation was obtained for the asymptotic scour depth, viz

$$d_{m\infty}/b_0 = (\tan\phi)^{0.5}(d_{50}/b_0)^{0.75}F_0^{1.5} \qquad (2.4)$$

where ϕ is the angle of repose of the sediment.

It was found by Altinblik et al. that $d_{m\infty}$ computed from Eq. 2.4 agreed favourably with the results obtained by Laursen (1952) and by Tarpore (1956).

Rajaratnam et al (1981, 1983)

Recently, Rajaratnam and his co-workers contributed several interesting papers on erosion caused by 2-D turbulent wall jets on a bed of erodible sand. Their work were mainly experimental and two extremes in the submergence of the jet outlet were studied:

a. The deeply submerged jet where the tailwater depth, H, is many times the height of the jet opening, d_0 ($H >> d_0$).

b. The minimum submerged jet, where $H \simeq b_0$.

The conclusions reached by Rajaratnam et al, regarding the similarity of the scour profiles and the exponential nature of the scour depth versus time relationship were in general conformity with the findings of the other workers (Altinblik et al (1980), Laursen (1952)). However, some interesting experiments were performed, particularly for scour at the asymptotic state.

In the case of scour by 2-D jets, (Rajaratnam (1981)), the tests were conducted for the high submergence, and both air and water jets were used. The time evolution of scour was examined in these experiments. At the asymptotic state, Rajaratnam (1981), deduced from dimensional analysis that:

$$d_{m\infty}/b_0 = f_1(F_0,\ U_j b_0/\nu,\ b_0/d_{50}) \qquad (2.5)$$

Neglecting the jet Reynolds number, $U_j b_0/\nu$, as the effect of the fluid viscosity would be small if the Reynolds number is large, Eq. 2.5 becomes:

$$d_{m\infty}/b_0 = f_2(F_0,\ b_0/d_{50}) \qquad 2.6)$$

It was also shown that at the asymptotic state, the normalised scour profiles (using $d_{m\infty}$ and $X_{m\infty}$ as length scales) for experiments with different F_0 were similar and can be approximated by a sine curve (Fig. 2.8a).

In addition, Rajaratnam (1981) also studied the characteristics of the ridge: the distance of the ridge, X_D and the height of the ridge were both found to be functions of the densimetric Froude number, F_0.

Rajaratnam and MacDougall (1983) did experiments on the scour by two-dimensional water jet with minimum tailwater depth. They studied the asymptotic state of erosion in details.

It was shown that, in the case of minimum tailwater depth, the normalised scour profiles at the asymptotic state (using length scales $d_{m\infty}$ and $X_{m\infty}$), scatter considerably (Fig. 2.8b).

As expected, because of the small jet submergence ($H \simeq b_0$), no ridge was observed for the case of scour with minimum tailwater depth.

Figs. 2.9a and 2.9b show asymptotic data of the above mentioned experiments of Rajaratnam (1981), and Rajaratnam et al (1983) for the 2-D wall jets with $H >> b_0$ and $H \simeq b_0$.

Lim (1985)

Recently, S.Y. Lim (1985) conducted extensive investigations on localised scour by two- and three-dimensional turbulent wall jets with shallow tailwater depths.

Much of his research effort and time was spent on the measurement and analysis of the flow patterns and boundary shear stress distributions in the scour holes.

He also observed time development of the scour holes to develop a method of predicting the scour characteristics, i.e. the maximum depth and volume of the scour holes.

It was shown by Lim that the hydraulic radius of the jet outlet, R(=Area of jet/perimeter of jet) was a useful characteristic length for describing the shape of the jet outlet and in the collation of the experimental results.

Variations in the dimensionless volume V_h/R^3 and maximum depth of scour, d_m/R, with the parameter $U_j t/R$ were found to be well represented by the following relationships:

$$V_h/R^3 = A1\ (U_j t/R)^{B1} \tag{2.7a}$$

$$d_m/R = A2\ (U_j t/R)^{B2} \tag{2.7b}$$

where A1, B1, A2 and B2 are coefficients.

To check for similarity of the scour profiles, Lim used two different length-sclaes d_m and x_{mh} for the vertical and horizontal dimensions, respectively. The dimensionless scour profiles, for various jets, and at different times, were well represented by an exponential relation, viz:

$$d_s/d_m = -\exp[-a_1(x/x_{hm}-b_1)^2] \tag{2.8}$$

where a_1 and b_1 are constants and x_{hm} is the distance from the jet exit to the point where $d_s=0.5d_m$ (Fig. 2.10).

Lim found that the scour development was greatly affected by the tailwater depth, H. A larger and deeper hole was obtained for tests with non-submerged jet outlets, i.e. $H < b_0$, than those with intermediate values of H.

Lim also found that the tailwater depth profoundly affected the asymptotic scour depth, $d_{m\infty}$. He showed that there existed a critical tailwater depth at which either an increase or a decrease in tailwater causes an increase in $d_{m\infty}$.

He made extensive measurements of the velocity distribution in 2-D and 3-D scour holes. Because of the transient nature of the problem, Lim used a method of 'fixing' the scour hole for any desired scouring time.

Based on these measurements, he showed that the velocity profiles for those sections from the jet exit to the location of maximum depth were similar, irrespective of the period of scouring (Fig. 2.10), and were well expressed by the following reltionship:

$$U/U_m = \exp[-0.693((y-\delta_1)/(y_m-\delta_1))^2] \qquad (2.9)$$

The different parameters are defined in Fig. 2.10.

Lim used Rossinskii's (1961) analysis to determine the theoretical velocity distribution for a two-dimensional scour hole.

To calculate the boundary shear stress, τ_b, along a scour hole, Lim developed a method which estimated the boundary shear stress from the mean floor velocity data.

The distribution of the boundary shear stress showed that in the scoured region of the hole, the shear stress was less than τ_c, (τ_c = critical shear stress for the initiation of particle motion). Lim stated that the entrainment and transport of sediment particles were not unique

functions of the boundary shear stress but they also depended on the intensity of turbulence over it.

Nik Hassan (1985)

At the same time as Lim (1985), Nik Hassan (1985) investigated scouring due to a 2-D submerged turbulent jet of water issuing out from a sluice gate, with and without a solid apron. He studied the effects of sand size, sluice opening, efflux velocities and length of apron on the scour. However, no attempt was undertaken by him to establish the equilibrium scour depth.

Nik Hassan measured velocity distributions, associated with the development of a scour hole. For decay of maximum horizontal velocity in the scour hole, he found the following empirical relationships:

A) With rigid apron

$$U_m/U_{mA} = e^{-0.138}(x/b_A)^{1.055} \qquad \text{for } 0<x/b_A<4.28 \qquad (2.10a)$$

$$U_m/U_{mA} = 0.61\ (x/b_A)^{-0.1} \qquad \text{for } x/b_A > 4.28 \qquad (2.10b)$$

where U_m is the maximum horizontal velocity at a distance x from the beginning of the scour hole, U_{mA} and b_A are respectively, maximum velocity and half-depth of the mean velocity distribution at the end of the rigid apron.

B) Without rigid apron

$$U_m/U_j = 1 \qquad \text{for } x/b_0 < 5.2 \qquad (2.11a)$$

$$U_m/U_j = 2.28\ (x/b_0)^{-0.5} \qquad \text{for } 5.2 < x/b_0 < 18.0 \qquad (2.11b)$$

$$U_m/U_j = 10.77\ (x/b_0)^{-1.04} \qquad \text{for } x/b_0 > 18.0 \qquad (2.11c)$$

He found that the line joining the positions of the maximum velocity mostly curved inward into the scour hole as a result of entrainment which is typical of reattaching flows.

2.4.1.2 Summary of theoretical work

In general, most of the analytical methods attempt, in one way or another, to find a solution for the sediment continuity equation (Eq. 2.3). Assuming that the control volume is the scour hole volume, Eq. 2.3 can be re-written as:

$$d\ V_s/dt = Q_s - Q_i \qquad (2.12)$$

where, $d\ V_s/dt$ is the rate of change of the volume of sand removed from the scour hole with time, Q_s and Q_i are volume rates of sediment transported out of scour hole and into the scour hole, respectively.

In the case of localised scour caused by turbulent jets, the analysis assumed that no sediment was transported into the scour hole other than the sediment that would slide from the side into the scour hole. Hence, the rate of supply, Q_i, in Eq. 2.12 is zero. The solution of Eq. 2.12 was based upon a separate determination of dV_s and Q_s in terms of the

scour hole geometry. The final function relating the scour depth to time was then obtained by the integration of Eq. 2.12.

In the following sections, the analytical methods used by Laursen (1952), Carstens (1966) and Altinblik and Basmaci (1980), based upon the above criteria, are summarised first,and then a semi-empirical approach developed by Nik Hassan is given. It should be mentioned that in all cases, the scour depth versus time relationships were derived for a 2-D turbulent wall jet with the jet outlet deeply submerged.

Usually, due to the difficulty in obtaining analytical expressions for the parameters in Eq. 2.12, researchers resorted to experiments to determine these functions.

Laursen (1952) obtained the values of Q_s experimentally by supplying a known rate of sediment into the scour zone. In Carstens' (1966) and Altinblik et al's (1980) case, Q_s was derived empirically, from a consideration of the forces acting on a particle which is scoured from the bed. In the Altinblik et al's work, the rate at which sediment is scoured from the scour hole was assumed to be given by the sediment pick-up function obtained by Le Feuvre (1970).

All three methods derived the differential volume function, dV_s, by assuming that the volume of the scour hole is given by an isosceles triangle having side slopes equal to the tangent of the angle of repose, ϕ, of the sediment (Fig. 2.11). Thus

$$V_s = (2B/\tan\phi)\ d_m^{\,2} \tag{2.13a}$$

and differentiating

$$d V_s = (4Bd_m/\tan\phi) \; d(d_m) \qquad (2.13b)$$

where B is the channel width.

Although Laursen's differential volume function is different from Eq. 2.13, it has been shown that both functions are similar and utilise the same assumption, as mentioned above.

Finally, the scour depth versus time function should be such that it approximates to a semi-logarithmic relationship, i.e. a linear variation of scour depth with the logarithmic of time over a considerable time period.

A different approach was proposed by Nik Hassan (1985), to predict the temporal rate of maximum scour depth by relating the mean velocity in the scour hole to the scour potential, thereby predicting the scour depth as a function of time.

He used similarity of scour profiles in ascertaining the character of flow. This enabled him to identify a characteristic mean velocity in the scour hole. A brief review of his method is given below.

Nik Hassan assumed that the disturbing forces F_d which are trying to dislodge the particles out of the scour hole were proportional to the following parameters:

$$F_d \sim \rho \; d_{50}^{\,2} \; U_{mx}^{\,2}. \qquad (2.14a)$$

where ρ is fluid density, and U_{mx} is the maximum horizontal velocity at the vertical section passing through the position of the maximum scour depth d_m.

On the other hand, the stabilising force F_s resisting the fluid forces is proportional to the submerged weight of the sediment i.e.,

$$F_s \sim (\rho_s - \rho) g d_{50}^{\ 3} \qquad (2.14b)$$

The scour potential is expected to be proportional to the ratio F_d/F_s of these forces which is $[U_{mx}^{\ 2}/gd_{50}(S-1)]$. In addition, taking account of the dimensional homogeneity, the rate of scour with respect to time may be written as,

$$d(d_m)/dt = \beta\, U_{mx} [U_{mx}^{\ 2}/(gd_{50}(S-1))] \qquad (2.15)$$

where β is a coefficient of proportionality.

The above equation assumes that all the sediment particles that are dislodged from the bed are removed from the hole to be dumped downstream. Evidently this is not the case because some particles do not make the full journey out of the scour hole. The fraction of sediment that will leave the scour hole was considered to be proportional to some power of the relative magnitude of the kinetic energy to the potential energy of the sediments, i.e $[U_{mx}^{\ 2}/g(S-1)d_m]^n$.

So, the equation for the rate of the scour depth becomes,

$$d(d_m)/dt = \beta[U_{mx}^{\ 2}/(g(S-1)d_m)]^n\, U_{mx}[U_{mx}^{\ 2}/(g(S-1)d_{50})] \qquad (2.16a)$$

or

$$1/(n+1)\ d[d_m^{(n+1)}]/dt=\beta\ [U_{mx}^2/(g(S-1))]^n U_{mx}[U_{mx}^2/(gd_{50}(S-1))] \quad (2.16b)$$

Finally, by integrating Eq. 2.16b, the temporal variation of d_m can be found. At any step of integration, it is necessary to know U_{mx}. Nik Hassan used similarity of scour profile for that purpose. Knowing the initial value of d_m at that step, the value of x_m can be obtained. By using Eqs. 2.11 and 2.12 with $x=x_m$, the value of U_{mx} can be found.

2.4.2 Local Scour due to Impinging Jets

Here, scour is caused by a jet impinging at an angle of 90° to the initially horizontal sand bed. Many investigators in the past have published results on this problem (Rouse (1939), Rao et al (1967), Rajaratnam et al (1977, 1981)). This section intends to give a brief description only of some of the more important findings.

Generally speaking, most of the investigators found that:

a. The development of scour varied linearly with the logarithm of time for an appreciable part of the time, and

b. The eroded bed profiles were similar.

These two criteria will be assumed in the following review unless otherwise stated.

Rouse (1939)

The pioneering work in this field was done by Rouse (1939) who investigated experimentally the scour resulting from a vertical, deeply submerged two-dimensional jet with the upstream face against the wall (Fig. 2.12). This nature of study could result in two possible types of flows; a) the jet may be deflected either 180° or b) it may follow the boundary of the scour hole as far as the crest. The transition from (a) to (b) depended upon certain conditions such as the jet velocity, sediment fall velocity and boundary geometry.

Rouse observed that the particle transport out of the scour hole was mainly a phenomenon of suspension. The particles falling upon the upstream side of the dune would gradually slide back towards the zone of erosion. These would then be carried again into suspension as they met the deflected jet. As the flow stopped, the suspended particles settled down and the dune's slope adjusted itself to the natural angle of repose of the material. Rouse suggested a functional relationship for the maximum scour depth, d_m, viz.

$$d_m/b_0 = f_2(wt/b_0,\ U_j/w,\ \sigma_g) \qquad (2.17)$$

where σ_g is the geometric standard deviation of the sediment.

Rouse argued that scour is an ever increasing phenomenon and neither in model nor in prototype situations can a limiting depth of scour be expected. Rouse, however, stated implicitly that in the case of graded bed material, where selective sorting of the bed material occurred, the scour hole would eventually be paved with material of non-scourable sizes and that scour would not progress any further.

Rao and Sarma (1967)

A comprehensive study of the erosion characteristics of a 2-D submerged vertical jet was conducted by Rao and Sarma (1967). In this study, the jet outlet was located just above the original flat bed level. Three sizes of jet thickness, together with two types of sand were used.

From dimensional analysis, Rao and Sarma obtained:

$$d_m/b_0 = f_3(U_j/w,\ wt/H,\ H/b_0) \tag{2.18}$$

Comparing Eqs. 2.17 and 2.18, it can be seen that the effect of the tailwater depth, H/b_0 has been ignored by Rouse. Rao and Sarma's paper, however, reported that the tailwater depth used in their experiment was constant for all the runs. Hence, neglecting the term H/b_0 in Eq. 2.18, Rao and Sarma proposed an empirical scour depth versus time relationship of the form:

$$d_m/b_0 = A_2(U_j/w)\ \tan^{-1}[B_2(wt/H)^D] \tag{2.19}$$

where A_2, B_2, and D are constants, to be determined experimentally. At the asymptotic state, Eq. 2.19 becomes:

$$d_{m\infty}/b_0 = A_2(U_j/w)(\pi/2) \tag{2.20}$$

The asymptotic scour depth was obtained indirectly using the artificially imposed condition employed by Laursen (1952). From a plot of $d_{m\infty}/b_0$ against U_j/w, the constant A_2 was found to be equal to 0.883. Eq. 2.20 was then reduced to a straight line when plotted on a log-log axis. The constants B_2 and D were found to have the same value of 0.4. Hence, Eq.2.19 becomes:

$$d_m/b_0 = 0.883(U_j/w)\ \tan^{-1}[0.4(wt/H)^{0.4}] \qquad (2.21)$$

Fig. 2.13 shows the experimental data of Rao and Sarma together with Eq. 2.21.

Rajaratnam et al (1977, 1981)

In Rao and Sarma's experiments, the vertical distance between the jet exit and the original flat bed level, referred to here as the height of impingement, h,is zero. For h > 0, Rajaratnam (1981) and Rajaratnam and Betlaos (1977) conducted extensive tests with 2-D and 3-D submerged impinging air and water jets. Significant in these studies is the fact that the results were found to be well correlated using the following length scales:

1. For large impingement height, i.e h > $8.3b_0$, the length scale used was h, and

2. For small impinement height, i.e. h < $5.5b_0$, the length scale was b_0.

As in the case of the horizontal jets, Rajaratnam et al were more interested in the asymptotic scour depth and most of the experiments were conducted with large impingement height.

For the 2-D jets, $d_{m\infty}/h$ was found to be a function of $F_0/\sqrt{(h/b_0)}$ only. Similarly, for the 3-D circular jets, $d_{m\infty}/h$ when plotted against $F_0/\sqrt{(h/b_0)}$ was found to be uniquely described by a straight line for both air and water jets, viz:

$$d_{m\infty}/h = 0.5[F_0/\sqrt{(h/b_0)} - 0.18] \qquad (2.22)$$

In the 3-D case, with small impingement heights, Rajaratnam et al found that $d_{m\infty}/b_0$ was a function of F_0 only.

2.4.3 Local Scour Caused by an Offset Jet

Balfour (1973) conducted experiments to study the scouring action of a two-dimensional offset jet discharging parallel to a movable bed into a tailwater of finite depth. In his experiments only one type of sediment was used and all the parameters except the jet discharge were kept constant (with b_0=2.5 cm, h=1.5 cm and H=10.5 cm). His experiments can be divided into two parts:

1. The object of the first part was to obtain a series of instantaneous bed shapes during the development of a scour hole through the action of a two-dimensional submerged jet with shallow tailwater depth, issuing from a sluice positioned a short distance, above an initially horizontal sand bed.

2. From the data produced in (1), fixed-bed models of the scour hole at various stages of its development were produced. Having, with these shapes, 'frozen' the instantaneous scour hole shape, a detailed analysis of the fluid flow that would be acting at that instant of time, could be undertaken by measuring velocities and shear stresses.

As his experiments were undertaken for a shallow tailwater depth, Balfour observed different flow situations which are summarised below:

Initially, the jet started at a position 1.5 cm above and parallel to a horizontal flat bed (Fig. 2.14a). Immediately the jet attached itself to the bed and began scouring away-at the sand. After about 5 minutes a considerable scour hole was produced with the jet apparently still attached to the bed (evidenced by the tranquil free surface) (Figs. 2.14b-d). At this stage, the scouring has nearly finished and the large hump excavated material is being held up by the action of the jet. Shortly afterwards the free-surface began to boil signifying that the jet had deflected to the surface (Fig. 2.14e). At this point the mound of sand just downstream of the scour hole slumped back into the hole. While the deflected jet remained at the surface, the backflow under the jet aided the filling in of the scour hole. This continued until a point was reached at which the jet could no longer stay at the surface and reattached once again to the bed. Scouring started immediately and the whole cycle was repeated. This process can also be noticed in Fig. 2.15 which shows the development of volume of scour hole with time.

The above observations indicates that the character of the scour hole development could be explained in terms of whether or not the jet attaches to the bed after leaving the sluice.

In the second part of his experiment, Balfour measured horizontal velocity distributions in fixed-bed scour holes. A typical velocity distribution related to the scouring period of the cycle is shown in Fig. 2.16. Using the velocity distributions for the different stages of the scouring and filling periods, Balfour was able to describe the above mentioned scouring cycle.

In a similar investigation, King (1985) studied scour by an offset water jet. His experiments were conducted under shallow tailwater conditions and small jet height situations. However, because of time limitations, King was not able to investigate this problem thoroughly.

An interesting investigation on the use of turbulent jets to induce scouring near the bed in a dock was undertaken by Ali and Halliwell [1980]. The main object was to obtain a good distribution of high velocities (generated by properly-directed water jets) near the bed at a certain area. The experiments were conducted to study the influence on the floor velocities of the following parameters; 1) Elevation of the water jet above the bed, 2) Operating head, 3) Downstream water level, 4) Size, shape and direction of the jet nozzles and 5) Form of the bed , whether rigid or composed of erodible sand bed. It should be stressed that their experiments were conducted using three-dimensional jets which usually behave very differently from two-dimensional offset jets, as will be shown later in this thesis.

2.5 CONCLUDING COMMENT

To the best knowledge of the present writer there has been no work reported on scour by a two-dimensional offset-jet under a deep tailwater condition. Also, in all of the work to date no conclusion could be drawn concerning the rate of development of scour induced by an offset jet under shallow tailwater conditions. Further work was therefore required. In order that such work would have a sound basis, it was decided that the flow-field produced by a two-dimensional offset-jet under deep tailwater conditions impinging on a rigid bed had to be investigated first.

CHAPTER 3. OFFSET-JET LITERATURE REVIEW

3.1 INTRODUCTION

The free jet has long been of interest in the study of turbulent shear flows. Besides having many engineering applications, the free turbulent jet provided early investigators with a simple geometry upon which to base various speculative models. In the recent years, considerable attention has been directed towards better understanding and also the need for obtaining an improved theoretical model for turbulent submerged flows discharged into quiescent and moving ambient.

These efforts have been motivated largely by needs arising from problems of pollution control, such as the dispersion of affluent from industrial chimneys and cooling towers, and the discharge of condenser water and sewage into rivers, lakes, and oceans. These problems introduce such complicating factors as ambient fluid motion, buoyancy, discharge geometry and jet-boundary interaction.

Although much attention has been focused on the development of theoretical models to predict the jet characteristics in unbounded flows, the effect of the possible jet-boundary interaction has not been fully explored. Three types of jet-boundary interactions are commonly encountered in many engineering applications (see Fig. 3.1):

1. the wall jet, where the fluid is discharged at the boundary,
2. impinging jets, where the the discharge is aimed towards the boundary, and

3. the offset jet, where the fluid is discharged at some distance from the boundary and eventually attaches to it because of the bending of the jet by forces acting upon it. The wall jet may be considered as a limiting case of the offset jet.

The third of the above categories is mainly the subject of this study.

The phenomenon of jet attachment to an adjacent surface is one in which a jet of fluid after being deflected by the adjacent surface would flow along it. The importance of its study is twofold:

1. When the attachment is undesirable, one ought to know the method by which it can be prevented;
2. when it is desirable, the variables involved can be chosen so that a precise control on the flow can be established.

The case of a submerged jet in the vicinity of a solid boundary is of special interest because of its practical application, e.g. in thermal discharges from power plants which emerge near the bottom of rivers and lakes. The subsequent interaction with the solid surface may significantly alter the plume's behaviour. Furthermore, pressure and shearing forces by the floor-bound jet give rise to scouring and bed erosion resulting in discharge structural problems.

In this chapter, it is tried to define the offset-jet flow and also to review the previous work done on it.

3.2 DEFINITION OF THE PROBLEM

To have a better understanding of the general problem, we start by considering the free-turbulent submerged plane jet.

3.2.1 The Free-Turbulent Submerged Plane Jet

This flow situation refers to the case where a two-dimensional plane jet issues from a slot opening into a still medium which has no restricting solid or free-surface boundaries (Fig. 3.2).

The diffusion of submerged jets has been studied by many researchers and the paper by Albertson, Dai, Jensen and Rouse (1950) gives an analysis for both two-dimensional and three-dimensional free-turbulent submerged jets.

Consider the flow emerging from a two-dimensional slot as shown in Fig. 3.2. The flow emerges into the ambient fluid as a uniform jet (constant velocity core) of width b_0 and velocity U_j.

The jet enters an initial region known as the Zone of Flow Establishment. At the edges of the constant velocity core there is a velocity discontinuity, which produces high shearing forces and mixing of the jet and surrounding fluid. These regions of mixing are highly unstable and turbulent; they progressively eat away at the central velocity core while the surrounding fluid is accelerated or entrained. This results in the total quantity of flow and overall breadth of the jet increasing with distance from the efflux section, while the width of the central core decreases. The end of the zone is reached when the two mixing

layers meet at the centre-line of the jet. The whole jet is now turbulent and the flow may be considered as fully established. This region is called the Zone of Established Flow. The diffusion process continues thereafter without essential change in character. Further entrainment of the surrounding fluid is now balanced inertially by a continuous reduction in the velocity of the whole central region.

The velocity profiles in the zone of established flow become 'flatter' and 'wider' with increasing distance from the jet orifice.

When the velocity distributions are plotted in dimensionless form, it is found that the velocity profiles, at all sections of the fully developed zone, are geometrically similar. This implies that at any section,

$$U/U_m = f(y/x) \qquad (3.1)$$

where, U_m = maximum velocity (i.e. on the centre-line) and U = horizontal velocity at distance y from the centre-line. (see Fig. 3.2).

If the assumption of the geometric similitude holds for the two-dimensional free-turbulent submerged jet, then the increase in thickness of the jet (2B) is given by

$$B = \text{constant}.x \qquad (3.2)$$

in which B, is defined as the value of y, where U≅0 (Fig. 3.2).

Gortler (1942) established a non-dimensional relationship for the decay of the centre-line velocity, in the zone of established flow, as

$$U_m/U_j = \text{Const}.x^{-0.5} \qquad (3.3)$$

Gortler also established that the velocity profiles could be represented by

$$U/U_m = \text{Sech}^2(\sigma y/x) \qquad (3.4)$$

where σ is a constant called spread parameter.

Albertson et al (1950), on the other hand, found that their experimental data for the velocity distributions were well defined by a Gaussian normal probability function. They were then able to represent their results for the decay of the centre-line velocity as

$$U_m/U_j = 2.28\sqrt{(b_0/x)} \qquad (3.5)$$

3.2.2 Shallow Plane Jets

The term 'free' submerged jet implies that there are no external boundaries to impede the diffusion of the jet. However, the characteristics of the jet will change when a bed and /or a surface boundary are in close proximity to the jet.

As has been outlined in the discussion of the free jet, the jet entering a reservoir immediately entrains the fluid that was originally at rest. Due to the high shearing forces at the edges of the jet, mixing and entrainment increase as the jet progresses further from the efflux section. This outward spreading and deceleration of the jet in the downstream direction is symmetrical about the centre-line for a free jet. However, if a free surface is relatively close to the efflux section, then only the bottom half of the jet has an infinite supply of water available for entrainment, whereas the supply of water available for entrainment in the upper half is restricted by the free surface

(Fig. 3.3). Hence, the ambient fluid entrained into the jet from the upper half must be replenished by a backflow of water near the free surface. The limit to the backflow region will be signified by a region of 'boiling' on the free surface. A vortex will be established in this region enclosed by the upper surface of the jet, the wall containing the slot and the free-surface (Fig. 3.3). The pressure in this region will be lower than the pressure below the jet and results in a pressure difference that produces a net lift effect that deflects the jet towards the free-surface.

Mahajan and John (1971) and Stoy, Stenhouse and Hsie (1973) investigated the conditions shown in Fig. 3.3, where the tailwater depth was slightly above the level of the jet's outlet. Stoy, Stenhouse and Hsie (1973) concluded from their studies that the Froude number was not a significant parameter for the shallow submerged jet and that the submergence ratio, (d/b_0), was of primary importance in determining the flow pattern and the resulting dividing streamline.

If, the solid bed is the boundary that limits the entrainment of fluid, then jet deflection is somewhat like that of the free-surface mentioned above. This time, however, the jet deflects towards the bed. This case is explained in more details in the next section.

In the situation where both the free-surface and the bed boundary are close enough to affect the jet, attachment of the jet to either boundary is possible. Whether or not it is the nearest boundary which will influence the jet is not certain; external forces such as ambient turbulence, surface turbulence, jet buoyancy and bed shape may affect the jet to a greater or lesser extent.

One of the observations by Balfour (1973) during his general experimental study once again demonstrated the instantaneous flow pattern changes possible when two boundaries reacted on the flow instantaneously (see Fig. 2.14 in Chapter 2). In this case the boundaries had the effect, under suitable conditions, of changing the path of the jet from the surface to the bed. (The problem was mentioned in more details in Chapter 2).

This phenomenon is of particular practical significance to the engineer concerned with hydraulic structures where shallow jet conditions prevail.

Coates (1976) investigated the possible flow conditions present in shallow water jets and showed that the predominant boundary affecting the jet's diffusion could be established if several parameters were known. These included, the Froude Number ($U_j^2/(gb_0)$), the dimensionless submergence ratio of the jet (d/b_0) and the offset ratio, (h/b_0) (Fig. 3.4). From these studies he was able to classify three possible separate zones of jet diffusion under various conditions. In one zone the jet would become attached to the bed and in another it would be dominated by the free surface boundary and would become attached to the surface. In the intermediate zone the jet could become attached to either of the boundaries and could be physically flicked between boundaries by mechanical means.

In a similar work, Johnson (1978) conducted experimental investigations on two-dimensional shallow jets. In addition to the mean-flow features, he measured some components of the fluctuating velocity and bed shear stress. He also distinguished between four separate zones of

jet diffusion compared with the three zone classified by Coates. (Fig. 3.5).

3.2.3 Basic Features of the Two-Dimensional Offset-Jet

The studied flow geometry is shown in Fig. 3.6. A plane, incompressible, turbulent water jet is discharged into quiescent ambient surroundings in the vicinity of a plate offset from and parallel to the axis of the jet. When the jet enters the tailwater, its action is similar to that of a turbulent free jet, in that it entrains fluid from the surrounding tailwater. However, when the jet efflux is close to a solid boundary there is only a finite volume of fluid which is available to be entrained between the jet and the bed boundary. Therefore, the surrounding fluid being entrained must be replenished by a back flow near the plate. This will set up vortices in the surrounding fluid. Because of the back flow and the vortices set up in the region, the pressure below the jet will be considerably lower than that above the jet, and consequently the jet deflects toward the boundary and eventually attaches to it.

By attaching to the boundary, the jet encloses a region of eddying motion known as the recirculation region (Fig. 3.6).[3] The jet region

---

[3] It is clear that the attached flow to the bed will not be established in practice unless the flow is nearly two-dimensional. If spanwise flow from the edge of the jet is permitted, the vortex will not be very strong as entrainment will bring fluid from the sides.

extending from the nozzle's exit to the point of attachment is commonly referred to as the pre-attachment region. A dividing streamline is defined as that which extends from the lower nozzle's exit to a location on the wall which separates the forward and reversed jet flow. Across this streamline there is no mass flow. The portion above the dividing streamline is accelerated along the boundary because of the jet's positive pressure and the fluid below this streamline is assumed to be the part of a recirculating region, on average, contains a fixed amount of fluid. Thus, any fluid entrained on the lower side of the jet is returned to the recirculation region in the impingment zone.

In the pre-attachment region, pressures are generally lower than hydrostatic. As the jet approaches the boundary, the pressure inside the jet increases, reaching a maximum as the jet attaches to the boundary.

In the second, or impingment region the pressure decreases, eventually reaching a hydrostatic value, and the acceleration ceases. The jet then undergoes turbulent diffusion analogous to that of a plane turbulent wall jet in what is known as the wall jet region. A typical velocity profile before and after reattachment is shown in the Fig 3.6.

The important parameters associated with this flow geometry are as follows: The length of the offset plate, the ratio of the jet offset to the nozzle thickness (h/b_0), the jet Reynolds number, $U_j b_0/\nu$, the initial turbulence intensity of the jet, and the uniformity of the in-

---

Hence, a pressure difference large enough to cause the jet to deflect will not occur.

itial jet velocity profile. A relatively wide range of these flow parameters has been considered by previous investigators.

3.3 LITERATURE REVIEW

The problem of an offset jet interacting with an adjacent parallel boundary has been previously described along with the important flow parameters which must be considered. This particular problem is relatively new with the first reported study being that of Bourque and Newmam (1960]. Since that time several investigators have attempted to study various aspects of the problem. The following review is an attempt to cover the significant results obtained by these investigators. A review of some relevant experimental findings will be given first. Later, a description of some of the important analytical solution will be presented.

3.3.1 Review of Experimental Investigations

To have a better understanding of the different experimental investigations, every parameter is considered separately.

3.3.1.1 Attachment Point

The primary objective of most of the offset jet attachment studies was to determine the length of the pre-attachment region, X_A, that is, to find the point of flow attachment (Fig. 3.6). Experimentally, many different techniques have been used to find the location of the at-

tachment point: Bourque and Newman (1960) and Parameswaran and Alpay (1975) used tufts on the offset plate, Rajaratnam and Subramanya (1968) used coloured dye injection technique. Parameswaran and Alpay (1975) also used a suspension of Titanium oxide in penetrating oil on the side walls and the offset plate. Kumada et al. (1973) and Sawyer (1960) defined the attachment point as the point of maximum wall static pressure.

Using dimensional analysis, Bourque and Newman (1960) showed that the attachment length became independent of Reynolds number, offset ratio, and plate length as each became sufficiently large. They also found that the attachment flow characteristics were not influenced by the length of the offset plate as long as it was approximately 3.7 times the attachment length. They also found that the flow characteristics became independent of Reynolds number when it was sufficiently large, approximately 6000 at an offset ratio of twelve and approximately 2500 at an offset ratio of fifty. All the subsequent studies were performed at Reynolds number well above these values and well within the turbulent range. Attached flow at high Reynolds number and long offset plate values thus became dependent only upon the offset ratio.

Nearly all the studies on offset jets involved offset ratios between zero and 24. Bourque and Newman (1960), Parameswaran and Alpay (1975), Sawyer (1963), and Rajaratnam et al. (1968) found that the attachment length became almost a constant for large values of the offset ratio. Bourque and Newman (1960) found the limiting value of the offset ratio to be 35. Nozaki et al. (1981) studied the effects of turbulence intensity on attachment and found that the flow was independent of turbulence intensity for initial turbulence level larger than 0.06.

3.3.1.2 Pressure Distribution

The variation of the static pressure along the offset wall was measured by virtually all of the previous investigators who observed the same general trends (Figs. 3.7 and 3.8 where P_a shows pressure of ambient and j is jet momentum per unit span). The wall static pressure, at the beginning of the pre-attachment region was negative and reached a minimum value at a point which corresponded closely to the centre position of the vortex. The centre position of the vortex was measured by Parameswaran and Alpay (1975) who found it to be located approximately two-third of the distance to the attachment point. From the minimum pressure point, the wall static pressure then increased rapidly becoming positive and reaching a maximum value very near to the attachment point. In fact, Kumada et al. (1973) and Sawyer (1960) defined the attachment point as the point of maximum wall static pressure.

After attachment, the wall static pressure decreased monotonically in the downstream direction and tended toward zero. As the offset ratio was increased, the magnitudes of the maximum and minimum wall static pressure decreased. The distance from the nozzle's exit at which these extremes occurred, however, increased with increasing offset ratio. At larger offset ratios, the pressure profiles tended to merge into one, corresponding to a limiting value of the attachment distance.

Kumada et al. (1973) suggested that a distinct change in the wall static pressure profile occurred at an offset ratio of approximately six, suggesting a change in the character of the recirculation region at that point. They stated that the values of the maximum and minimum wall static pressures remained essentially constant for offset ratios between two and six, although the locations of these points moved as

the ratio changes. The suggestion of a change in recirculation region's character at an offset ratio of six has not been brought forward by any of the above investigators.

3.3.1.3 Velocity Distributions

Sawyer (1960), Rajaratnam and Subramanya (1968), and Ayukawa and Shakouchi (1976) measured velocity profiles normal to the curved jet and found them to be similar to those of a free jet, as given by Gortler (1942). Sawyer (1960) found that the velocity profiles of the jet as it curved towards the boundary exhibited no obvious asymmetry (Fig. 3.9). This observation was in apparent disagreement with the argument put forward by Prandtl (1929). The later indicated that there should be enhanced entrainment in the outer portion of a curved jet, and reduced mixing in the inner portion, due to the influence of centrifugal forces on particles of fluid which transfer momentum from layer to layer.

In a later paper, Sawyer (1963) resolved this discrepancy by postulating that there must be a flow of fluid across the jet's centreline for the observed symmetry of the velocity profiles to be compatible with different entrainment rates on the two sides of the jet. A first-order mixing length theory was used to show that the effects of different entrainment rates on the two sides of the jet did not substantially alter the velocity profiles from their free jet shapes. He therefore, concluded that the total entrainment to the jet would remain unchanged.

Pelfrey (1984) in his experimental work on an air offset-jet made detailed mean velocity measurements using a directionally sensitive LDA

system (Fig. 3.11). By using the velocity profiles he determined the jet entrainment and found it to be significantly different from that of either a free jet or a wall jet. Pelfrey also showed that the entrainment parameter in the pre-attachment region was influenced by the recirculation region's pressure. Pelfrey also obtained turbulence characteristics, including: distribution of higher order moments, energy spectra, autocorrelation functions, and integral scales.

Except those of Pelfrey (1984) no other velocity measurements have been reported for the flow within the recirculation region.

In the impingment and wall jet regions, the flow is assumed to be essentially parallel to the wall and to behave like a wall jet. Parameswaran and Alpay (1975) divided the velocity profile downstream of attachment into an inner region, below the point of maximum velocity, and an outer region, above the point of maximum velocity. They found that the inner region was fairly well represented by a power law profile, the exponent of which depended upon the offset ratio, the attachment length, and the Reynolds number. For offset ratios from one to seven a one eleventh power law profile seemed to best fit their data. The flow in the outer region was found to be similar to one-half of the Gortler profile.

Hoch and Jiji (1981) also divided the flow downstream of attachment into an inner region and an outer region. They said that in the inner region, except for the excess pressure, the jet behaviour was similar to a one-seventh power law profile. The outer region was well represented by one-half of a Gaussian distribution.

Rajaratnam and Subramanya (1968) stated that the decay of the maximum velocity of the attached wall jet could be separated into two regions (Fig. 3.10):

1. a characteristic decay region, where the rate of maximum velocity decay was dependent upon the value of the offset ratio; and
2. the classical wall jet decay region, where the decay rate was the same as that of the classical wall jet.

As the jet left the nozzle and flowed toward the plate, the maximum velocity decayed quickly up to the attachment point. After attachment, the rate of decay recovered somewhat and approached that of the classical wall jet at further distance downstream of the nozzle (Fig. 3.10). Kumada et al. (1973) stated that in the attached wall jet region the gradient of the velocity decay equalled that of the wall jet regardless of the offset ratio. Parameswaren and Alpay (1975) stated that the decay of maximum velocity for various offset ratios behaved in the same manner as that of a plane wall jet in stagnant surroundings. Hoch and Jiji (1981) gave measurements of maximum velocity decay which seemed to agree with those of Rajaratnam and Subramanya (1968).

Parameswaran and Alpay (1975) found that the rate of growth of the outer layer of the attached wall jet, beyond the attachment point, was similar to that of a plane wall jet. The angle of inclination of the line joining points at which the velocity was equal to one-half the maximum velocity and passing through the virtual origin of the attached wall jet for offset ratios greater than three was found to be 3.8 degree and appeared to be independent of the jet's exit velocity. The growth of the inner layer beyond attachment, however, did not exhibit any kind of similarity.

a

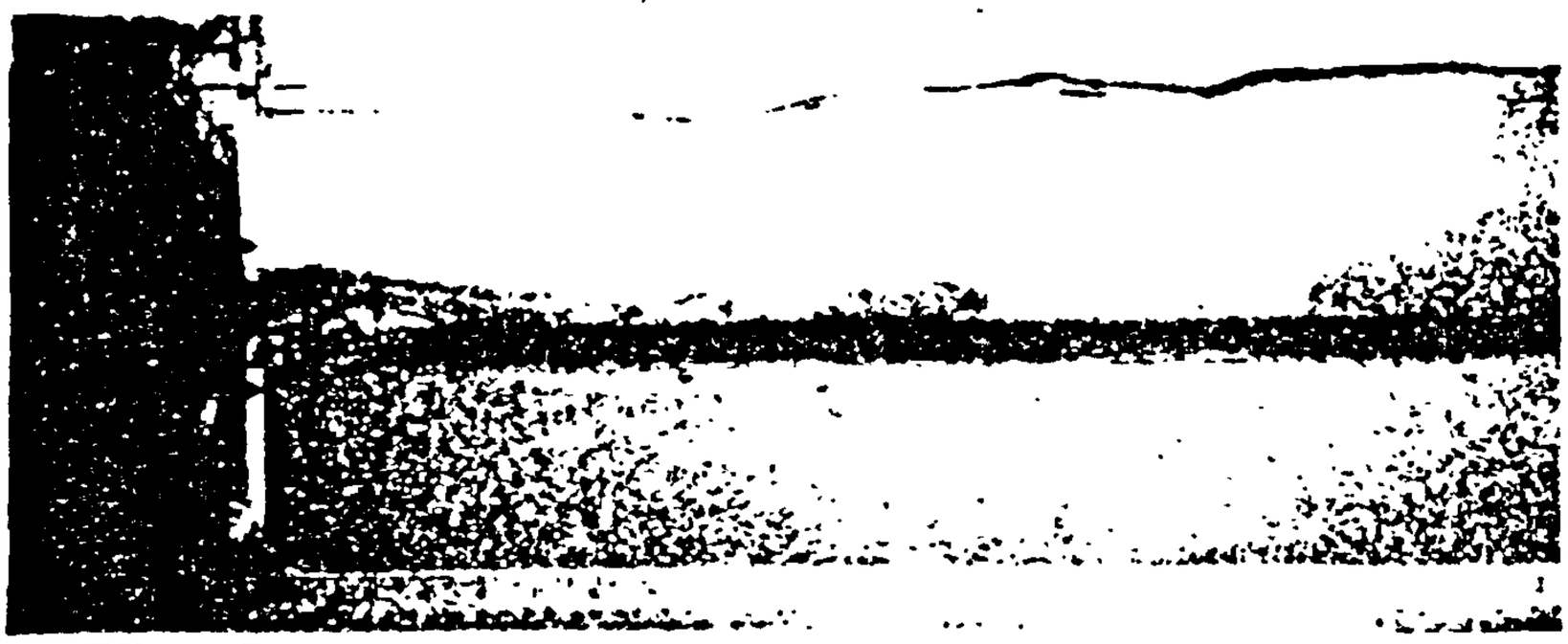

b

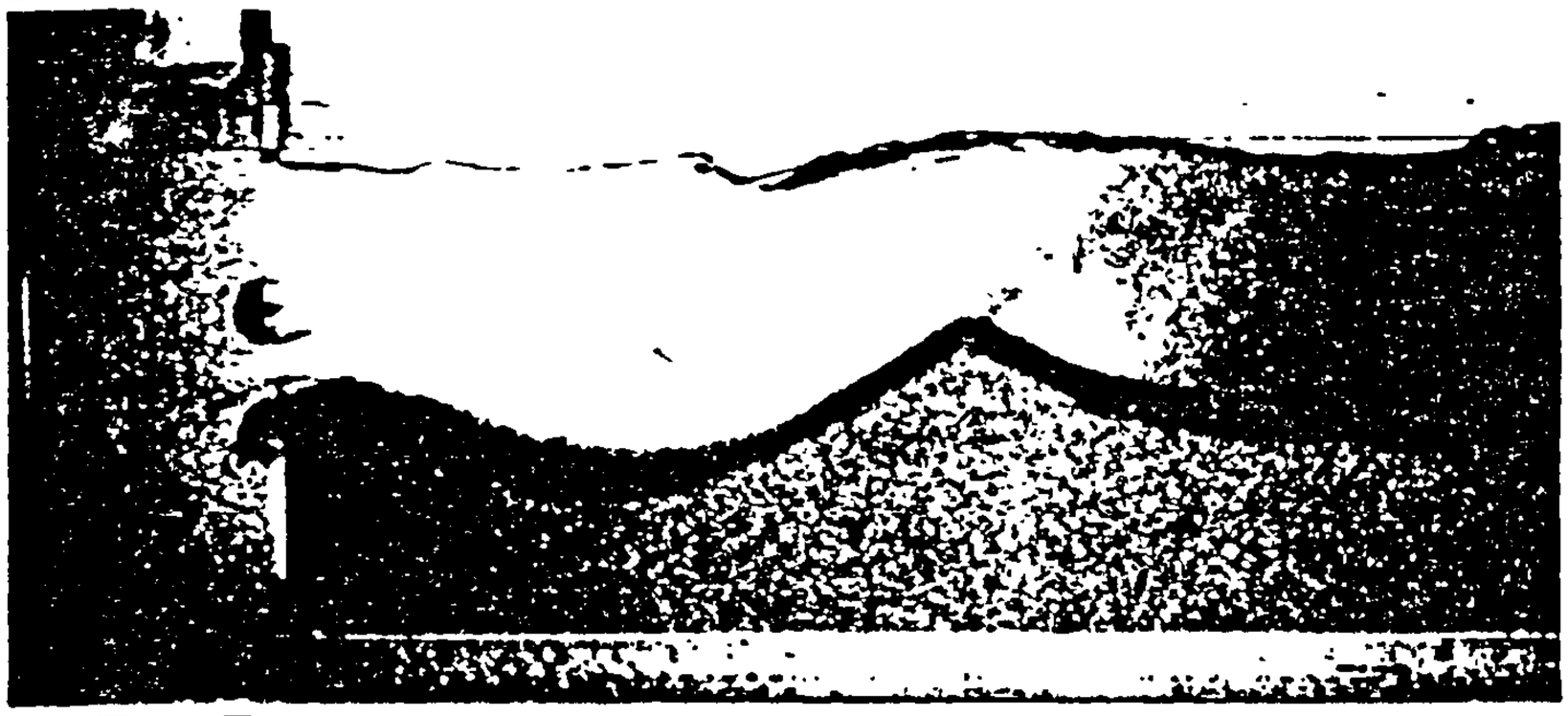

c

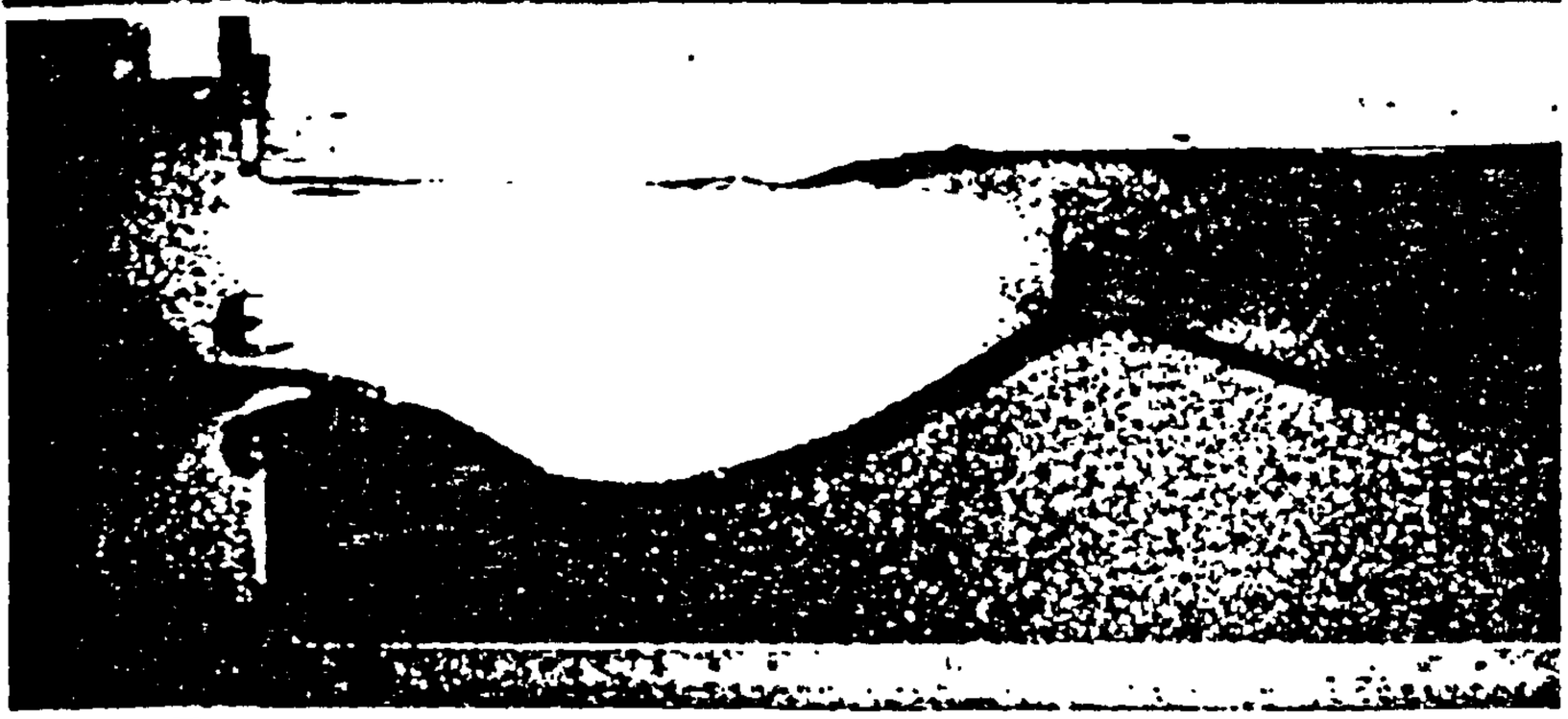

d

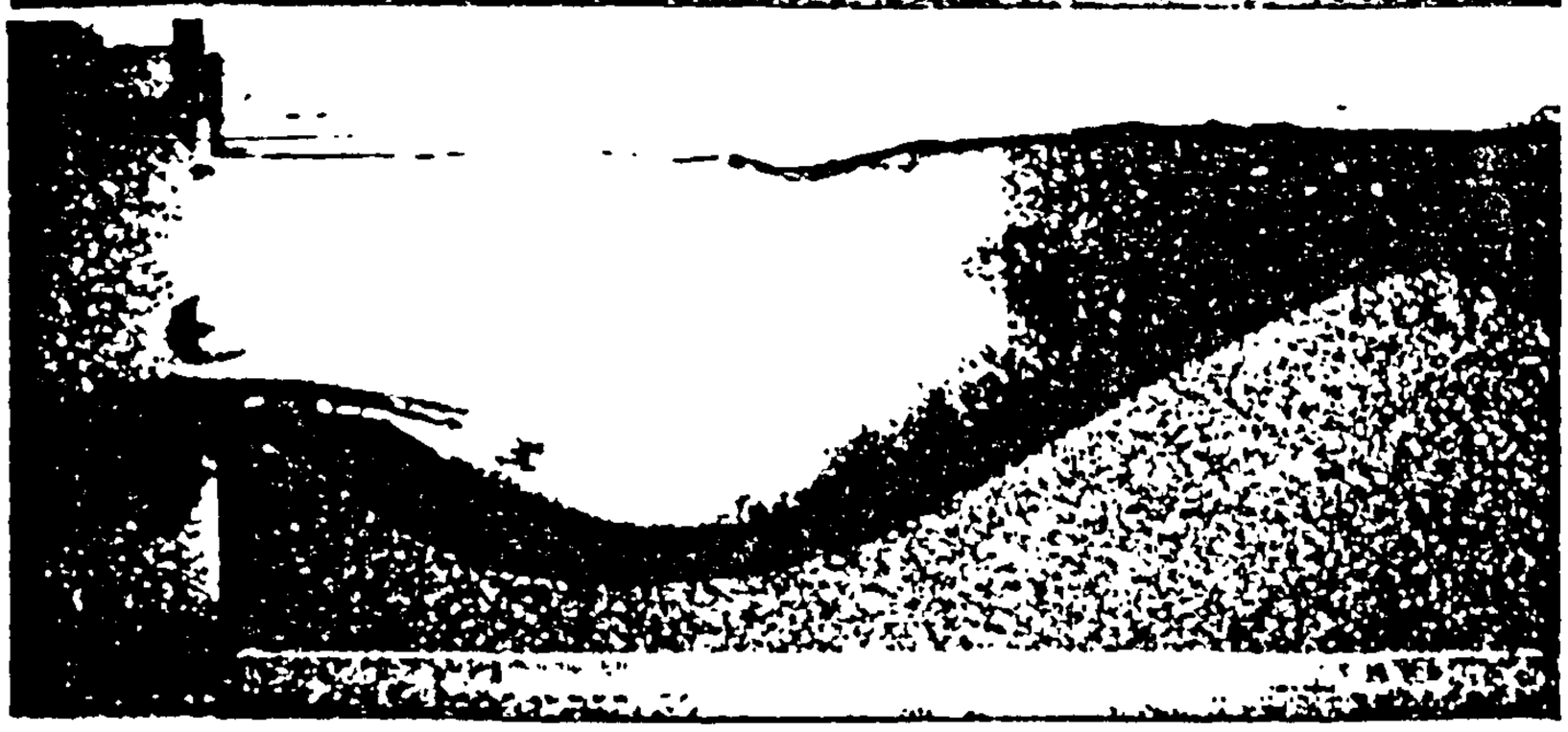

e

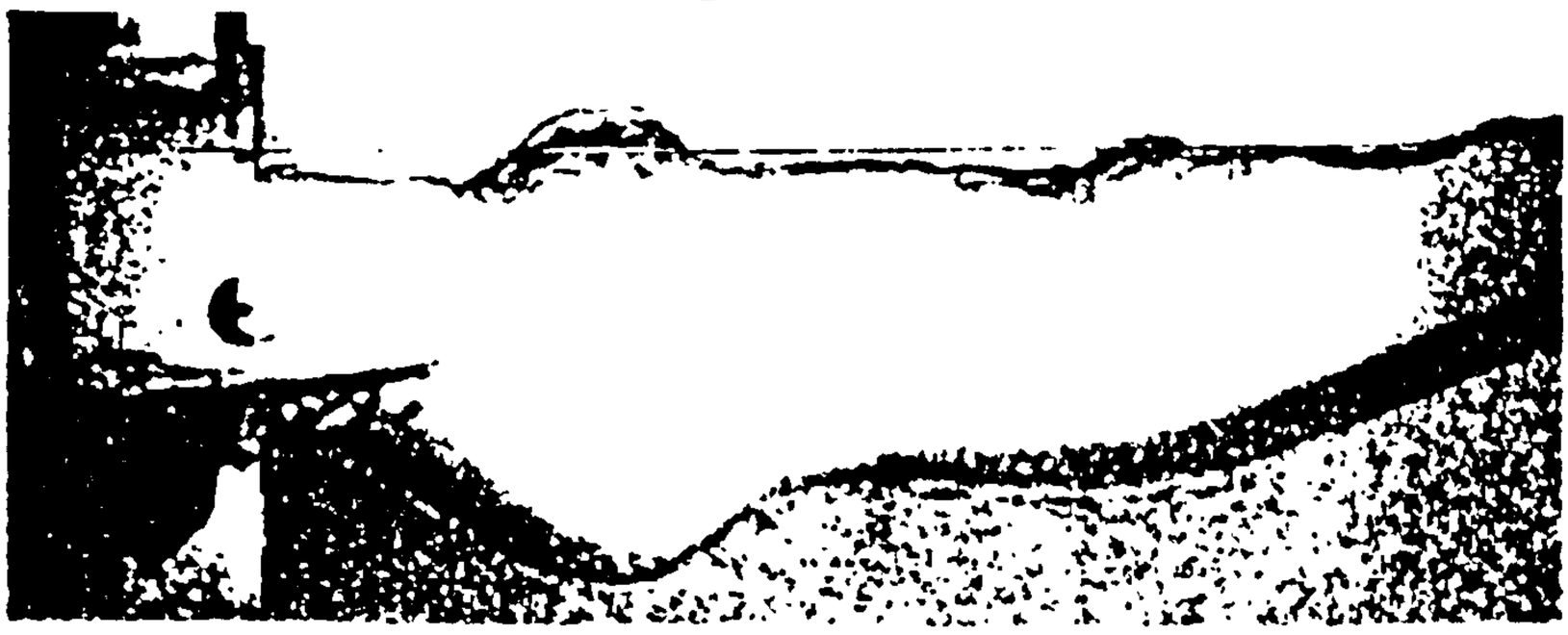

2.14 Progress of scour hole by a shallow submerged jet

(after Balfour, 1973)

3.3.1.4 Shear Stress

The shear stress along the wall, downstream of the attachment point, was measured by Parameswaran and Alpay (1975) and Rajaratnam and Subramanya (1968). Rajaratnam and Subramanya (1968) found that the time-averaged wall shear stress was zero at the attachment point, then increased rapidly to a maximum, and finally decreased monotonically in the downstream direction (Fig. 3.12). The shear stress distribution did exhibit some similarity in shape beyond the attachment point. Rajaratnam and Subramanya (1968) suggested dimensionless parameters which reduced the shear stress profiles to a single curve which was independent of the offset ratio (Fig. 3.13). No measurements of shear stresses in the pre-attachment region were reported.

3.3.2 Review of Theoretical Investigations

Most of the theoretical studies pertaining to offset jets were confined only to predicting the reattachment point. The pioneering work was undertaken by Bourque and Newman (1960). Much of the investigation that followed their work was essentially similar with minor modifications and improvements.

Bourque and Newman (1960) were among the first to investigate the velocity and pressure distributions of a two-dimensional jet in the vicinity of a solid boundary. The problem was greatly simplified by assuming that the presence of the boundary had little effect on the velocity distribution of the jet. Thus, the velocity field was taken from the solution of the two-dimensional free turbulent jet. This assumption implied a zero pressure gradient along the jet trajectory. This

was accomplished by assuming that the radius of curvature of the jet centreline and the pressure inside the recirculation region were constant.

With the velocity known, the introduction of an additional equation, or closure assumption, was necessary to determine the only remaining unknown: the radius of curvature. This was achieved by applying the horizontal component of momentum locally at the point of re-attachment while neglecting local pressure variation.

Bourque and Newman (1960) applied this solution using the Gortler (1942) velocity distribution for a two-dimensional free turbulent jet (Eq. 3.4). This velocity distribution was in terms of a constant jet spread parameter, σ. Some adjustment of this parameter was necessary to obtain satisfactory agreement with the experimental results. The value of the jet spread parameter differed from its free jet value because of reduced entrainment on the lower side of the jet.

Though reasonable results for the position of the reattachment point were obtained, the assumption of constant radius of curvature and base pressure were not borne out by the experimental results. For example, measurements by Bourque and Newman (1960) and Rajaratnam and Subramanya (1968) have shown that the pressure distribution within the recirculation region is not uniform (Fig. 3.8). The wide variation of the wall static pressure in the pre-attachment region would indicate that a uniform recirculation pressure is not possible. This model also failed to account for the rise in pressure and deceleration of the jet as it approached the point of reattachment.

A similar analysis was developed, independently, by Sawyer (1960) at Cambridge. Sawyer in his later paper (1963) modified his earlier analysis to account for the different entrainment rates along the inner and outer edges of the jet and to account for the initial mixing region of the jet. He also included pressure forces for the momentum balance near the reattachment point. In a later paper, Bourque (1967) also made some improvement to his predictions, by assuming the path of the dividing streamline to be a sine curve. Bourque (1967) pointed out that this assumption compensated for the unrealistic model of constant pressure in the recirculation region. He still, however, failed to obtain a detailed pressure distribution and relate it to the velocity field.

Boucher (1968), instead of the Gortler profile, used a power law distribution for the jet velocity as proposed by Brown and Simpson (1964). Boucher obtained good agreement with experiments for jets attaching to an inclined as well as a parallel offset surface. He also concluded that the entrainment rate was not much affected by curvature.

Perry (1967) by modifying the model of Bourque and Newman (1960), and using a spread parameter, (σ), of 10, obtained a good prediction for low offset ratio attaching jets and inclined plates.

To solve the flow field of a jet curving towards a surface, Stoy et al. (1973), applied an integral method for the solution of governing equations and used the entrainment assumption as the closure. Also, they assumed an empirical relationship for the pressure on the centreline of the jet which will be followed in the present work.

Hoch and Jiji (1981) used a fifth degree polynomial to approximate the jet trajectory and left the recirculation region pressure as a parameter to be obtained in the solution. They assumed a Gaussian-shaped velocity profile for the curved jet. They also took into account the zone of flow establishment.

Recently, Raghunath and Liburdy (1986), applied a modified k-ε closure model to solve the offset-jet problem. The impingment distance was determined to within 2% of the experimental results. However, the velocity profiles both upstream and downstream of impingment, were not well predicted.

3.4 CONCLUDING REMARKS REGARDING THE LITERATURE REVIEW

Most of the prior investigations of two-dimensional jet-boundary interaction were primarily concerned with the pre-attachment region, focusing on the determination of the point of reattachment. To achieve this, simplifications such as the assumptions of constant pressure in the recirculation region and constant jet-axis radius of curvature were introduced. These assumptions facilitated the use of the free jet velocity distribution, thus bypassing the need to solve for the velocity.

Although these models gave reasonable results for the position of the point of jet-attachment as a function of the offset height, the assumptions regarding velocity, pressure and radius of curvature were unrealistic.

It is apparent that there is a need for a more substantive model, based on sounder physical reasoning which could be extended to give the

velocity, and pressure distributions in all regions of the jet. Also, detailed velocity measurements, especially in the recirculating zone are necessary for a better understanding of this type of flow.

CHAPTER 4. EXPERIMENTAL FACILITIES AND PROCEDURES

4.1 OBJECTIVES

In the experimental part of the present study,the behaviour of a two-dimensional offset jet impinging on a rigid bed and the clear-water scour produced by this type of jet were investigated. The offset jet experiments consisted of velocity measurements in both of the horizontal and vertical directions. These velocities were measured at various sections along the centreline of the channel.

The scour experiments were conducted to study the following :

a) Change of scour hole geometry with time

b) Change of scour depth and length with time

c) Change in flow conditions.

4.2 EXPERIMENTAL EQUIPMENTS AND ARRANGEMENTS

The experimental set up is shown in plate 4.1, and diagrammatically in Fig. 4.1. The glass open channel was 3.4m long, 0.6 m wide and 1.0 m deep. A vertical sluice gate was constructed from a 1 inch thick perspex cut to the width of the channel. The gate was supported by a metal frame and could be lifted using a gear box. The sluice gate opening was measured by using two dial gauges located on top of the gate and having an accuracy of 0.01 mm. A bottom vertical weir was fixed to the channel wall and had a height of 30.3 cm. To ensure uniform and 2-dimensional flow, two pieces of half-rounded perspex pipes were used to form a well designed sluice entrance (Fig 4.1).

For the scour experiments, the working section of the channel was 1.7 m from the downstream end of the channel. This section was filled with sand to the desired height. At the end of the channel, a vertical sharp-crested weir of adjustable height was used to regulate the water level in the channel.

A centrifugal pump was connected between the storage tank and the header tank and was used to produce the required discharge. The flow rate was adjusted using a valve. The incoming flow was efficiently streamlined by the header tank and its gradually convergent sections (Fig 4.1).

Downstream of the end weir, water was guided and collected in the storage tanks, thus completing the flow circulation.

The flow-rate was calculated by measuring the average incoming velocity at the sluice entrance using a propeller meter. Depth gauges were used to measure the water levels upstream and downstream of the sluice gate. These depths were used to calculate the theoretical discharge.

The profile of the scour hole was measured, sometimes, using a depth gauge mounted on a gauge carriage positioned over the flume. This carriage could be moved across or along the channel.

To level the sand bed, a piece of wooden sheet cut to the internal width of the downstream tank was used. This piece of wood was bolted onto a handle, so that the whole assembly could slide along the top edge of the channel.

4.2.1 Characteristics of the Bed Material

Only one type of bed material was used in this study. The bed material was non-cohesive sand and its cumulative size distribution is shown in Fig 4.2. From the curve, the median size, d_{50}, corresponding to the sieve diameter which retains 50% by weight of a representative sample of the bed material is 0.82 mm. The geometric standard deviation, σ_g, is 1.126 and is the ratio of the sieve diameter which passes or retains 50% of the sample to that which passes 15.9%, or the ratio of the sieve diameter which passes 84.1% to that which passes or retains 50% or the average of the two ratios. i.e.

$$\sigma_g = d_{50}/d_{15.9} = d_{84.1}/d_{50} \qquad (4.1)$$

or

$$\sigma_g = 0.5(d_{50}/d_{15.9} + d_{84.1}/d_{50}) \qquad (4.2)$$

The specific gravity, S, angle of repose, ϕ, and the porosity of the bed material were, 2.66, 33^0 and 0.403 respectively. The fall velocity, w, of the bed material corresponding d_{50} is 11.0 cm/s.

4.3 EXPERIMENTAL INVESTIGATIONS

4.3.1 Measurements of the Scour Characteristics

The general experimental procedure was as follows. For a particular run, the bed was levelled and covered with a piece of suitably sized aluminium sheet (plate 4.2). This piece of metal prevented the levelled

bed from being disrupted once the flow began. Trial runs showed that this method was satisfactory and the levelled sand bed was found to be well protected from the jet. The inflow was started, the flow rate and tailwater depth were set to the desired values and the whole system was left until a steady condition was reached.

The scour experiment was begun by carefully removing the covering metal sheet. This was done gently so as not to cause too much disturbance to the flow. With some practice, the removal could be achieved with minimum disruption.

This is the starting time, after which the development of scour hole with time was measured photographically and will be described later.

At the end of the run, the flow was stopped by switching off the pump. The water in the downstream tank was allowed to drain off slowly by means of a siphon at the downstream end of the flume and by a small drainage valve upstream of it, so that the scour profile was not disturbed. After the water was drained, measurements of the scour hole geometry were made using the depth gauge arrangement.

4.3.1.1 The Photographic Method

Generally, obtaining scour dimensions from a scale fixed to the side wall of the channel is not reliable due to the three dimensional nature of the flow and the scoured hole. Asymmetry of the flow is caused by the retarding effects of the channel walls. As the fluid near to the channel wall is, in general, travelling more slowly than the fluid in the centre of the channel, experiments show that there will be a "hol-

lowing" of the bed in areas where the sediment is being scoured.In areas of deposition there will be a "humping" of the channel bed. Both these features can be clearly seen by inspection of plates 4.3.a and 4.3.b. Therefore, the bed shape at the wall usually differs from the bed shape at the channel centrline. Hence, a method is required to measure the scour profile directly at the centreline. One method involved taking photographs of a series of gauges, located along the centrline of the channel.

Two types of gauges were tried, one was made of aluminium strips of different widths and thicknesses. The second type was made of brass rods of different diameters. To find the most appropriate gauge, three requirements were tested. The first requirement was the rigidity of the gauge, so that it does not bend when it is inserted in the sand bed. This condition was mainly affected by the thickness of the strips or by the diameter of the rods. The second requirement was the visibility of the gauges, so that the graduations on them can be seen in the photographs in order to enable measurement of the scoured depth. This condition was mainly controlled by the width of the strips. Finally, the third and most important requirement was that these gauges should not disturb the flow field or the scour hole profile. This condition controls the thickness of the strips, diameter of rods, type of gauge (rod or strip), and the distance between the gauges and whether to use gauges in one or two rows.

All of the requirements mentioned above, were checked using different gauges and different spacing (sample photographs are shown in plates 4.4-a and 4.4-b). Finally, it was found that aluminium strips, 1 cm wide, 2 mm thick and 110 cm long gave the best results. The second choice was a 3 mm brass rod with 100 cm length. Few experiments were

conducted using the rod gauges, but the majority were conducted using the strip gauges. The strips and rods were marked along their lengths using coloured tapes at 1.2 cm intervals.

Measurement of the scour profile, at various times during the erosion process was made by using photographic records of the gauges. Two cameras were positioned on fixed frames on either side of the scour hole. Essential lightings on both sides of the channel and a black background were also provided.

4.3.2 Instrumentation and Velocity Measurements

All velocities were measured using a streamflow miniature current meter manufactured by Nixon Instrumentation Ltd. (see Plate 4.5) The measuring head of the current meter was 16 mm in diameter and consisted of five bladed P.V.C. rotor mounted on a hard stainless steel spindle. The spindle terminated in fine burnished conical pivots which run in jewelled bearing mounted in an open frame. Minimum frictional resistance was thus ensured. The head was attached to the end of a stainless steel tube containing an insulated gold wire terminating 0.1 mm away from the rotor. As water passed the immersed sensing head, the passage of the rotor blades past the gold wire tip varied the measurable impedance between the tip and the tube. This variation was used to modulate a 15 K Hz carrier signal which was passed via a coaxial cable to a Type 401 Analogue Frequency Indicator (see Plate 4.5).

The frequency indicator was connected to a Speedomax XL Pen Recorder (Plate 4.5) so that the frequency variations could be recorded on chart paper. These variations were usually recorded for a time period of

40-120 seconds. However, if the turbulent fluctuation was large, (judged by the relative movements of the pen), then a longer frequency variation was recorded. To get a velocity reading, first an average value of the frequency trace was established. This value was then correlated using a calibration curve which converted the frequency readings to linear velocities.

For each streamflo probe, the calibration curve mentioned above was usually provided by the manufacturer. The quoted accuracy of the probe was:

5% from 2.5-7.5 cm/s

2% from 7.5-15. cm/s

1% from 15.-150 cm/s

Velocity measurement

Velocity measurements for an offset jet impinging on a rigid bed and for a scour hole were taken over a grid of location in both the horizontal and vertical planes. To do so, two types of probes were used, one straight probe to measure the horizontal velocities, and a bend probe to measure the vertical velocities The streamflo probes were held in a perspex block which was attached to a depth gauge. This assembly was fixed to a carriage which could be positioned at any desired point in the experimental area.

At various horizontal distances, x, two components of velocity at various vertical distances, y, above the bed were measured. In this study, the "floor velocity" was measured at y=0.8 cm (equal to half the diameter of the streamflo rotor) above the bed. Since the probe only

recorded positive velocities, negative velocities were noted when the rotor reversed its direction of turn.

4.3.3 Summary of the Test Programme

In the study on the two-dimensional offset jet impinging on a rigid bed, a single jet height and nozzle thickness was used. However experiments were done using four different flow rates (Experiments No.1 to No.4). The characteristics of these four experiments are given in Table 4.1.

In the scour part of the study, different sets of experiments were conducted to investigate the effect of the following parameters on the scour development.

a) Flow rate (Q)

b) Jet height (h)

c) Running time (t)

The experiments are classified according to a series number. A series number is given to each complete set of experiments pertaining to one value of Q, h, and running time.

A total of 18 runs were performed. A summary of the experimental investigations is given in Table 4.2.

Velocity measurements were made for one test only, (test no. S205), during the "asymptotic" stage. It is only at this stage that, as the scour hole becomes large, the rate of scour is so small that a velocity

profile taken over a period of 5 to 6 hours may be regarded as instantaneous.

CHAPTER 5. EXPERIMENTAL RESULTS OF THE OFFSET JET

5.1 INTRODUCTION

An experimental study is presented which details the mean flow characteristics of a two-dimensional offset jet.

One single offset ratio was used with three different discharges. The ratio of the height of the nozzle above the solid wall to the nozzle height was 26.2.

Velocities were measured, in the horizontal and vertical directions, in the pre-attachment jet region using a velocity meter.

To establish confidence in our experimental setup, and measuring techniques, our experimental results were compared with previously published data.

5.2 ANALYSIS OF RESULTS

5.2.1 Velocity Distribution

In order to obtain information about the flow field, detailed mean velocity profiles were obtained at several downstream locations. The horizontal components of velocity, U, are shown in Fig. 5.1a with the magnitude of the velocity represented by displacement of the profile

in the x-direction. Note that the traverse location indicator also marks the zero velocity position for that profile.

As the flow depth above the nozzle is not infinite, the entrainment of the upper portion of the jet causes a replacement backflow near the surface, which can be seen in Fig. 5.1a.

In Fig. 5.1b, the maximum velocity of the flow near the bed is shown. Examination of Fig. 5.1b shows that after impingement of the jet, (x/b_0=40.0), the flow behaves like a wall jet in pressure gradient (Fig. 3.8, chapter 3). As the wall-pressure gradient in the area between the point of attachment and point of minimum pressure is negative, the maximum velocity of the backflow increases. However, from the point of minimum wall-pressure towards the vertical wall, the pressure gradient is positive, therefore the maximum velocity of the backflow decreases in this direction.

The vertical components of velocity, V, are shown in Fig. 5.2, with the magnitude of the velocity represented by displacement of the profile in the x-direction (a downward V velocity is represented by a negative x displacement). Again, the traverse location indicator in each figure represents the zero velocity position for a particular profile.

The resultant velocity vectors for this flow are shown in Fig. 5.3 with the length of each vector corresponding to the velocity magnitude in the indicated direction. The point represented is located at the "tail" of the velocity vector. It can be observed in Fig. 5.3, that between the lower portion of the jet, the bed and the wall containing the sluice, a clockwise vortex or eddy has been formed by the entraining effect of the jet.

Details of the recirculation region of offset jet flows have been previously reported only by Pelfrey (1984) for air-flow with an offset ratio of 7. As can be seen from Fig. 5.3, the primary jet flow curves slowly towards the bed, through the first half of the recirculation region and then turns sharply downward as the jet impinges on the offset channel floor. This trend has been observed in previous studies of this geometry and also in backward-facing step flows. The division between the forward and reversed jet flow along the offset channel is observed to occur in the vicinity of x/b_0 =40. Downstream of this point the flow approaches that of a wall jet.

5.2.1.1 Attachment Length

The exact location of the intersection of the dividing streamline with the offset channel, i.e. the attachment length, x_A, was obtained by considering detailed mean velocity measurements in the x direction, in the jet impingement region. Based upon these results, the average attachment length was determined within $0.1b_0$ to be x_A =40.3 b_0.

The attachment length, x_A, for deeply submerged homogeneous flow can be expressed as:

$$x_A = f(U_j, b_0, h, \rho, \nu) \qquad (5.1)$$

where U_j is the mean velocity at the nozzle, b_0 is height of the nozzle, h is the jet height, ρ and ν are density and kinematic viscosity of the fluid, respectively.

By dimensional analysis Eq. 5.1 can be rewritten;

$$x_A/h = f_1(U_j b_0/\nu,\ h/b_0) \tag{5.2}$$

For large values of Reynolds number, $R_e = U_j b_0/\nu$, viscosity is known to have negligible effects on turbulent mixing. Hence Eq. 5.2 becomes

$$x_A/h = f_1(h/b_0) \tag{5.3}$$

In Fig. 5.4, the present attachment length data are plotted along with other investigators' results. The present results for the offset ratio agree well with the experimental results presented in previous studies, where different measurement techniques were used to obtain the attachment length.

It is interesting to note that in Fig. 5.4, all of the attachment lengths of the present experiments are the same, although different discharges were used. This confirms the assumption that the effects of viscosity are negligible when the Reynolds number is high.

5.2.1.2 Locus of Maximum Velocity

To define a trajectory for the offset jet is very useful in the theoretical work. The locus of the position of the maximum velocity was chosen as the reference streamline, s, and the cross-stream coordinate, n, is normal to s.

Fig. 5.4 gives the attachment length as a function of the offset ratio and works well for the present experiments and the results of the previous investigators. This quantity was, therefore, chosen as the nondimensionlizing parameter for the expressions representing the

characteristics of curved jets, such as the data points representing the trajectory of maximum velocity locations.

A least square curve fit was performed in order to smooth out the data for the locus of maximum velocity, and obtain an nth order polynomial of the form;

$$y_m/h = \Sigma\ C_n (x/x_A)^n \qquad (5.4)$$

where y_m is the vertical distance between the point of maximum velocity and the bed. C_n is a coefficient to be calculated by fitting a curve to the experimental results.

A fifth order polynomial with coefficients

$$C_0 = 1.00 \qquad C_1 = 0.581 \qquad C_2 = -4.452$$
$$C_3 = 10.708 \qquad C_4 = -12.31 \qquad C_5 = 4.850$$

was found to best fit the data of the present work and those of the previous investigators, based on minimum residuals, and is shown in Fig. 5.5 along with the measured points. The expression for y_m/h is, therefore, given by

$$y_m/h = C_0 + C_1(x/x_A) + C_2(x/x_A)^2 + C_3(x/x_A)^3 + C_4(x/x_A)^4 + C_5(x/x_A)^5 \qquad (5.5)$$

5.2.1.3 Velocity Decay;

The maximum total velocity, V_{max}, was determined as a function of distance along s. A plot for the decay of the non-dimensional maximum velocity, (V_{max}/U_j), in the downstream direction, s, was next produced for the results of the present experiments (Fig. 5.6). Due to turbulent diffusion, V_{max}, in general, decreases with s. The present results indicate that at $s/b_0 > 32$, decay of the maximum velocity, in the pre-attachment region, is different from that of the free jet flow shown in the same figure. In free jet flow, decay of the maximum velocity is inversely proportional to the square root of the distance from the jet's virtual origin, and is given by the following relationship (Rajaratnam 1976):

$$V_{max}/U_j = 1 \qquad \text{for } s/b_0 < 6 \qquad (5.6a)$$

$$V_{max}/U_j = 2.47/\sqrt{(s/b_0)} \qquad \text{for } s/b_0 > 6 \qquad (5.6b)$$

The present results show that for $s/b_0 > 12$, the velocity decay is linear with the downstream distance. V_{max}/U_j decreases rapidly to the reattachment point and the rate of decay appears to be greater than that of the free jet. One important reason for this behaviour is that in this region the emerging stream is a curved plane turbulent free jet. However, in the impingment zone (approximately $s/b_0 > 41$), where the jet 'scrubs' the bed, the rate of decay of maximum velocity decreases; this is possibly due to the small acceleration of the flow in this region caused by the favourable pressure gradient.

Fig. 5.6 also shows that the length of the potential core is smaller than that of a free jet. The cause of this might be the presence of

the negative velocities on the upper and lower boundaries of the offset jet.

5.2.1.4 Jet Spread

To determine the upper jet spread, linear interpolation of the velocity components was used along the line perpendicular to the s axis, to find the value of n where the jet velocity is equal to one-half the maximum velocity.

A plot of the upper jet spread, b_u, (value of n where U = 0.5 V_{max}), is given in Fig. 5.7. Also given is the line for the spread of a two-dimensional free jet whose equation is (Rajaratnam, 1976):

$$b_u = 0.11\ s \qquad (5.7)$$

Fig. 5.7 shows that the variation of b_u/b_0 with s/b_0 is almost linear for $s/b_0 < 27$, where the effect of curvature is negligible. However, for bigger values of s/b_0, the flow is curving towards the bed sharply and it results in a sharp increase in b_u/b_0.

Fig. 5.7 clearly shows the effect of curvature on the progress of a jet and also indicates that the values of b_u/b_0 are generally higher than those for a self-preserving free jet.

CHAPTER 6. PRESENTATION AND DISCUSSION OF SCOUR EXPERIMENTS

6.1 INTRODUCTION

This chapter presents the results obtained in this study for clear water scour caused by 2-dimensional offset turbulent jets.

The flow of an offset jet on an erodible bed, often results in the scouring of bed material. With the exception of Balfour (1973), and King (1985) no other work could be found which dealt with the scouring action of an offset jet. No relationship could be found which described the temporal development of offset-jet scour. The development of the scour profiles were therefore monitored at set time intervals, for each experiment, so that a relationship could be found describing the scour profile at any instant in time. At each of these set intervals a photograph was taken of the scour hole, and a scour profile was measured from it later. Plate 6.1 shows examples of the scour holes obtained.

Experiments were carried out using four different jet heights, each with several jet discharges. Only one type of bed material was used in these experiment/. Downstream water depth and slot thickness were kept nearly constant in all the runs, with average values of 1.175 cm and 90 cm, respectively.

The experimental results are presented and discussed under the following headings:

a. Time development of scour

b. Characteristics of the scour profiles

c. Analysis of scour at the asymptotic state

d. Analysis of the flow patterns

First, a description of the development of the scour hole is given. This will help in understanding the scour phenomenon.

6.2 GENERAL DESCRIPTION OF THE MECHANISM OF SCOUR BY JETS

The entrainment, transportation and deposition of sediment depends as much on the properties of the sediment as upon the hydraulic characteristics of the flow. Generally speaking, the scouring mechanism involves a combination of two relative motion: that of the flow field relative to the boundary, and that of the bed material relative to the overlying flowing fluid.

Consider a turbulent jet issuing from a two-dimensional nozzle. As the diffused jet starts to flow over the initially flat erodible bed, the scouring potential of the jet, created by the high incoming velocity, is usually so strong that the sand grains are immediately dislodged from the surface and transported in the direction of the flow, at a rapid rate. For a small time period, the bed material is transported mainly as bed load.

As the scour hole gradually enlarges with time, the depth of flow also increases. From the principle of continuity, the expanding cross sectional area would require a reduction in the mean flow velocity.

Accordingly, the local velocity near the scoured bed decreases as the depth of the hole increases. Hence, the rate of erosion decreases as time progresses. For larger time periods, the bed velocity eventually reduces to a certain "critical" value whence the flow (near the bed) becomes incapable of removing further bed material from the scoured area. At this point, we could say that the scour geometry has reached its "equilibrium" or "asymptotic" condition. Implicitly, this suggests that the local bed velocity is directly related to the concept of a threshold of particle movement. Conventionally, it has been widely accepted that the boundary shear stress is a logical choice of a key variable to characterise the incipient motion of particles. However, the bed shear stress is a function of the local bed velocity and measurements of the bed velocity distribution in a scour hole will enable the scouring process to be examined.

In accordance with the above description, Laursen (1952) has deduced that the scouring process has the following general characteristics:

a) The rate of scour will equal the difference between the capacity for transport out of the scoured region and the rate of supply of material, as demanded by the principle of continuity;

b) The rate of scour will decrease as the flow section is enlarged. This is due to the velocity and presumably the forces exerted on the sediment particles within the scour hole decreasing as the scour hole deepens;and

c) The extent of scour may be expected to reach a limiting value asmptotically.

6.2.1.1 Scouring Process by Offset Jets

In the present work, the following general process of scouring was observed.

Immediately the aluminium plate protecting the horizontal sand bed was removed, scour began to take place.

The jet in this case was impinging on the bed and was then divided in the upstream and downstream directions. Therefore, sand grains which were scoured mainly from the region of the attachment were moved in both of the downstream and upstream directions until the flow could no longer carry them. They were then deposited and began to form two dunes (Plate 6.2). During the early stages of scour, the scour hole was changing shape very rapidly and scour was taking place at a very high rate which is shown in Plate 6.3 and also in plates 6.8-a to 6.8-b. Plate 6.4 also shows sand grains lifted from the bottom of the scour hole and thrown over the dune. In this period, the dimensions of the upstream dune (the one near the sluice) increased faster than those of the downstream dune.

After a while the scour hole became deep and the dunes were so high that the sediment was thrown mainly on top of, rather than over, them (Plate 6.5). In this stage, in contrast to the initial stage, the progress of the downstream dune was faster than that of the upstream dune. The jet at this stage was virtually digging into the dune. At the point of maximum scour the angle of the scour hole was greater than the angle of repose of the sand (the angle of repose of the sand in water was approximately equal to the slope of the lee of the dune, Plate 6.6). This means that the jet was holding the sand up against the action of

gravity. The location of the most active scour was at the point of attachment of the jet to the bed. The sand was entrained by the flow largely at the point of attachment and was lifted in suspension by eddy motion. A large part of the sediment in suspension was settled on the upstream face of the dune. The remainder passed the crest of the dune and settled on its downstream face. That part of the sediment constituted the portion removed from the scour hole.

During the later periods of a run, very few particles were carried by the flow. Those particles were moving over the scour hole's bottom. There was no sediment in suspension. However, it was observed that there were occasional turbulent bursts near the bed which brought sand particles from the sloping face of the hole to the section of maximum erosion (Plate 6.7). At that period of time, the configuration of the scour hole and the dunes was stabilised, and it was assumed that the scour hole has reached a state of equilibrium.

6.2.1.2 Development of the Scour Hole

Plates 6.8-a to 6.8-c are photographic records of the development of a typical scour hole. From the photographical record of the scour hole development, graphs representing variations with time of the maximum scour depth, (d_m), the height of the dunes (d_{p1} and d_{p2}) and their distances from the sluice (X_{p1} and X_{p2}), were drawn. (Figs. 6.2-6.7). The volumes of scour holes were also calculated and are given in Fig. 6.8. The various parameters are defined in Fig. 6.1.

As mentioned above, scour development can generally be analysed in three stages, as is clearly shown in Figs. 6.2-6.8. In the first stage,

there is a rapid change in the scour hole configuration. Sediment was transported mainly as bed load. That stage of development of scour took a short period of time. In the second stage, the scour hole developed logarithmically with time. In that stage a practical terminal scour depth was reached due to the logarithmic character of the development of the scour. The mode of transport of the sediment was both as suspended load and as bed load. Type of jet, flow characteristics and sediment properties were the influencing factors. In the final stage, the development of scour reaches a limiting condition. The rate of transport of sediment approaches zero. The scour hole configuration was stabilised in this stage.

6.2.1.3 Concept of a Limiting Scour Condition

The argument about the existence of an asymptotic scour depth for localised scour problems has been debated fervently by many investigators (Anderson (1963), Laursen(1952), Sarma(1967), and Rajaratnam and Berry (1977)).

In general, localised scour can occur in two ways: (1) clear-water scour; and (2) live-bed scour. Clear-water scour refers to the situation when no sediment is supplied from the upstream into the scour zone. Live-bed scour, on the other hand, occurs when there is a general bed load transported by the stream. Sediment is continuously being supplied to the areas subjected to scour.

In the case of clear-water scour, where there is no bed movement from upstream of the jet, the scour hole will deepen and eventually reach an equilibrium condition as explained earlier in Section 6.2 . At this

equilibrium state the depth of scour will be such that the shear stress on the bed boundary is at the "threshold" value appropriate to the bed material. There is then no movement of sediment into or out of the hole. The scour depth should then be a function of the erosive force as determined by the mean velocity of flow. Hence an increase in the incoming water flow will increase the limiting scour depth if all the other variables are held constant.

6.3 DIMENSIONAL CONSIDERATION

Dimensional analysis was used to show the relative importance of the various parameters influencing the scouring action of an offset jet.

6.3.1 Introduction

For a complex flow such as that of scour caused by jets, dimensional analysis can be very useful in combining the variables involved into a dimensionless and useful form. Basically, the Buckingham π theorem states that if there is a functional relationship between n physical quantities, all of which can be expressed in terms of K fundamental quantities (e.g. mass, length and time), then (n-K) dimensionless numbers can be formed from the original n quantities, such that there is a functional relationship between them. Often, through a sound physical reasoning of the problem, the dimensionless parameters can be combined or neglected to make the problem more compact for theoretical analysis. Such a technique will be used in the following section.

6.3.2 Variables Affecting the Scouring Process

Referring to the definition sketch shown in Fig. 6.1, the variables affecting scour due to a two-dimensional offset jet can be classified into the following groups:

1. Variables characterising the fluid : density of fluid, ρ, kinematic viscosity of fluid, ν.

2. Variables characterising the flow: mean velocity of jet, U_j, downstream tailwater depth, H, scouring duration, t, and acceleration due to gravity, g.

3. Variables characterising the bed material: density of the sediment, ρ_s, and median size of sediment, d_{50}.

4. Variables characterising the geometry: height of jet above the original bed level, h, nozzle thickness, b_0, and channel with ,B.

6.3.3 Dimensional Analysis

To efficiently combine all of the variables listed above into characteristic, meaningful dimensionless parameters requires a suitable measuring system. Whittington (1963) has presented a simple dimensional method for hydraulic problems in which the measuring system ρ, L (length), V (velocity) was shown to be an ideal one for most hydraulic phenomena. In the present study, the following measuring system is chosen:

1. unit of length [L] = b_0,

2. unit of time [T] = b_0/U_j,

3. unit of mass [M] = ρb_0^3.

Using the method proposed by Whittington, the following dimensionless groups, or Whittington's "dynamic numbers" were obtained:

$$\phi_1 \left[V_s/b_0^2,\ d_m/b_0, U_j/\sqrt{(gb_0)},\ U_j b_0/\nu, U_j t/b_0,\ \rho_s/\rho,\right.$$
$$\left. d_{50}/b_0,\ H/b_0,\ h/b_0\right] = 0 \qquad (6.1)$$

There are many ways in which the above dimensionless parameters may be combined to give different dimensionless groups which reflect the phenomenon better. In the field of sediment transport, it is customary to use a densimetric Froude Number instead of the conventional one, and it is defined as:

$$F_0 = U_j/\sqrt{(gd_{50}\ (\rho_s-\rho)/\ \rho)} \qquad (6.2)$$

Another important dimensionless number is Reynolds number, R_e, defined as :

$$R_e = U_j b_0/\nu. \qquad (6.3)$$

However, for large values of Reynolds number, viscosity is known to have negligible effect on turbulent flow, so R_e can therefore be neglected.

With the above considerations, Eq. 6.1 may be reduced to

$$\phi_2 \left[V_s/b_0^2,\ F_0,\ U_j t/b_0,\ d_{50}/b_0,\ H/b_0,\ h/b_0\right] = 0 \qquad (6.4)$$

In the present investigations, different length characteristics of scour profiles like: maximum depth of scour, d_m, distance of maximum scour from sluice gate, X_m, height of the downstream dune, d_{p2}, and its distance from the gate, X_{p2} were measured extensively. Also, values of the scour volume, V_s, were calculated from measured scour profiles. Therefore, writing V_s and the above mentioned length parameters (e.g. d_m) as the dependent variables, we obtain:

$$V_s/b_0^2 \text{ or } d_m/b_0 = \phi_3 \left[F_0,\ U_j t/b_0,\ d_{50}/b_0,\ H/b_0,\ h/b_0\right] \qquad (6.5)$$

Eq. 6.5 forms the functional relationship for scour studies in which the grain properties are varied. However, in the present case only one type of grain is considered, and the above equation may be reduced to:

$$V_s/b_0^2 \text{ or } d_m/b_0 = \phi_4 \left[F_0,\ U_j t/b_0,\ H/b_0,\ h/b_0\right] \qquad (6.6)$$

showing that the eroded profile is dependent on

(i) the densimetric Froude number

(ii) the ratios h/b_0 and H/b_0, and

(iii) a dimensionless time ratio

6.4 ANALYSIS OF THE EXPERIMENTAL RESULTS

6.4.1 Presentation of Data

The means used for the graphical representation of the data is Eq. 6.6 which was obtained using dimensional analysis and a systematic simplification of the problem. We study the effect of every dimensionless parameter in Eq. 6.6 on the scour profiles, and then try to combine these effects in a general equation. However, before analysis of data, one point about the experimental results should be mentioned.

Generally, various researchers have shown that the limiting conditions of scour were reached after a very long time. It was 24 days in the experiment by Tarpore (1956), and it was above 370 hours in the data reported by Valentin (1967). In some of the experiments of the current investigation, the jet was allowed to scour the bed until the asymptotic state was reached, or the scour depth attained a value close to that of the final state. The time for which each experiment was run varied from test to test, with maximum runs of 4 days being needed in some cases. This was in contrast to Balfour (1973), or King (1985), who conducted limited research into the scouring action of offset jet (with maximum run time of 2 hours for Balfour's experiments, and 6 hours for King's experiments).

6.4.1.1 Effect of Dimensionless Time Ratio

Figs. 6.9 to 6.15 show different parameters of the scour profiles plotted against the time parameter $U_j t/b_0$, for constant values of F_0 and h/b_0.

Observations during the experiments indicated that for large scouring duration (as the scour approaches the equilibrium condition), the rate of erosion at the section where the maximum depth of scour was measured became imperceptibly small. The hole, however, was continually being enlarged in the downstream direction, thus giving a larger value of V_s without altering the value of x_m. In Figs. 6.16 to 6.22, the results were plotted in a semi-log from.

6.4.1.2 Dependency On The Densimetric Froude Number

Figs. 6.23 to 6.29 show different parameters of the scour profiles plotted against the time parameter $U_j t/b_0$ for different values of F_0 and for constant h/b_0. In Fig. 6.26, for instance, the family of curves shown is for the variation of d_m/b_0 with $U_j t/b_0$ for F_0 values of 5.4-6.4.

By analysing these figures the effect of the densimetric Froude number, F_0, on the development of different parameters of scour with time can be studied. Figures 6.23 to 6.28 show that generally the extent of scour increases with the increase in F_0. however the effect of F_0 is more pronounced on d_m, X_{p2} and d_{p2}.

6.4.1.3 Dependency on Height of Jet above the Bed

Figs. 6.30-6.36 show the effect of the height of the jet on the time development of scour. Three different jet heights were considered. Figs. 6.33 and 6.35 show that a deeper hole (bigger d_m and d_{p2}) is scoured with the lower height. The opposite effect is observed for X_{p1}, X_m and X_{p2}(Figs 6.30,6.32 and 6.34). Figures 6.31 and 6.34 also show that changing h/b_0 from 8.64 to 17.15 has little effect on d_{p1} and X_{p2}during the early periods of scouring.

6.4.1.4 General Formulation

After the inspection of the effect of separate parameters on the scour hole, we can now combine these effects. The following relationship was tried to see if it can explain a general relationship;

$$L_i/b_0 = A \quad \text{Log} \left[(U_j t/b_0)^B F_0{}^C \ (h/b_0) \right] + D \qquad (6.7)$$

where L_i stands for any of the length parameters in the scour hole profile, and A, B, C and D are constants which are different for each L_i. A least square curve fit was performed in order to find the constants. Figs 6.37 to 6.40 show the results of these calculations for the most important parameters in the scour profile. It can be seen that by this method most of the experimental points for different jet heights, initial discharges and different time scales can be expressed by a single relationship.

The equations for the best fit lines are given on Figures 6.37 to 6.40. Values of A_i,$B_i$and C_i for the different cases are given in Table 6.1.

6.4.2 Characteristics and Similarity of the Scour Profiles

Most of the bed profiles measured in this study refer to the centreline profiles of the scour holes.

Bed profiles were measured for different discharges and scouring durations. Typical development of scour profiles with time is shown in Fig 6.41. which shows that two characteristic dunes were formed at the upstream and downstream ends of the scour hole. Fig. 6.41 shows the rapid changes of the scour hole profile in the initial stages of scour and also the equilibrium stage, where it approaches at a very much longer time.

To correlate the bed profile data, different length scales were tried and results of this effort are shown in Figs. 6.42 to 6.44. Amongst these scales, d_m and X_{p2} seem to be the proper length scales (for depth and length, respectively) to bring the different scour profiles together.

Figs. 6.45 to 6.46 show plots of d_s/d_m versus X/X_{p2} for the data of different jet heights, discharges and scouring durations. It can be seen that the plotted data in each of these Figures could satisfactorily be represented by one curve, at least for the scour hole part of the eroded bed profile.

Fig. 6.47 shows a comparison between the dimensionless scour hole profiles for the various values of h and for t=300 mins. Upstream of the section of maximum scour, the increase in h results in a steeper upstream face and a higher ridge. Downstream of this section, the in-

crease in h results in a decrease in the height of the downstream ridge except for h=0.

6.4.3 Analysis of Scour at the Asymptotic State

It follows from the considerations in Section 6.3.5, that the asymptotic scour condition is a function of the flow velocity, U_j, sediment size, d_{50}, particle density, ρ_s, downstream tailwater depth, H and jet height, h. If the asymptotic scour depth, $d_{m\infty}$, is taken as the dependent variable, dimensional analysis shows that:

$$d_{m\infty}/b_0 = g_1 \left[F_0,\ d_{50}/b_0,\ H/b_0,\ h/b_0\right] \qquad (6.8)$$

However, as mentioned before, in the present study values of H and d_{50} were kept constant. Therefore, Eq. 6.8 reduces to:

$$d_{m\infty}/b_0 = g_2 \left[F_0,\ h/b_0\right] \qquad (6.9)$$

Eq. 6.9 will be used to analyse all the existing data on scour due to offset jets.

For each experiment the value of $d_{m\infty}/b_0$ and the corresponding values of F_0 and jet height were determined and are shown in Fig. 6.48. As can be seen from Fig. 6.48, for a constant h/b_0, increasing F_0 causes nearly a linear increase in the value of $d_{m\infty}$. However, for a constant F_0, it can be seen that increasing h/b_0 causes a decrease in the value of $d_{m\infty}$. It was therefore possible, that for a constant h/b_0 to derive a relationship of the form

$$d_{m\infty}/b_0 = E.F_0 + Z \qquad (6.10)$$

where E and Z are coefficients which are functions of h/b_0.

By a linear regression analysis the values of E and Z were obtained for different h/b_0 and are given in table 6.2. Also the E and Z values are plotted against h/b_0 in Fig. 6.49. By analysis of Fig. 6.49, the following relationship can be derived between the E and Z values in terms of h/b_0 :

$$E = 2.45 - 0.022(h/b_0) \qquad (6.11\text{-a})$$

$$Z = -4.85 - 0.114(h/b_0) \qquad (6.11\text{-b})$$

Finally, by substituting Eqs. 6.11-a and 6.11-b in Eq. 6.10 we get:

$$d_{m\infty}/b_0 = [2.45-0.022(h/b_0)]\ F_0 - 0.114(h/b_0) - 4.85 \qquad (6.12)$$

by which the maximum eroded depth may be calculated, for the range of parameters used.

It is interesting to note that the relationship given by for $d_{m\infty}$ for the case of a two dimensional vertical jet is given by:

$$d_{m\infty}/h = 0.5[F_0/\sqrt{(h/b_0)} - 0.18] \qquad (2.22)$$

For the case of a two dimensional wall jet, the variation of $d_{m\infty}$ is given by Eq. (2.4):

$$d_{m\infty}/b_0 = (\tan\phi)^{0.5}(d_{50}/b_0)^{0.75}\ F_0^{1.5} \qquad (2.4)$$

6.4.4 Analysis of the Flow Characteristics in a Local Scour Hole

While scour is taking place, the behaviour and movement of the sediment-water mixture along the bed of the scour hole represents a very complex, unsteady and non-uniform shear flow problem. A thorough analytical study of the flow patterns would be very difficult, even for the two-dimensional case because the scoured bed profiles and hence, the velocity distributions are continuously changing as the scour progresses with time.

Although some work (Rajaratnam and Berry (1977), Chatterjee and Ghosh (1980)) has been performed to observe the flow characteristic in local scour holes caused by wall jets, or at bridge piers, there appears to be little measured data on the flow patterns in a scour hole caused by turbulent offset jets. In this section, the results of a detailed experimental investigation into the hydrodynamic behaviour of turbulent offset jets in the asymptotic state of the scouring process are presented.

As the flow condition was considered to be in the asymptotic state, and therefore, it was hardly changing with time, there was no need to freeze the scour hole in the same way that most of the previous investigators did. Figs. 6.50 and 6.51, show the horizontal and vertical velocity distributions at a number of vertical sections in the scour hole. Note that each vertical line represents zero velocity for that section. Also, the velocity vectors are shown in Fig. 6.52. It is seen from this Figure that as with the case of the rigid horizontal bed condition the jet, on leaving the sluice, soon begins to dip towards the bed and finally attaches to the boundary. The jet then runs along

the bed until it reaches the dune of the scour hole where it separates from the bed.

Plates 6.9a and 6.9b were obtained by injecting dye through the jet. They confirm the above mentioned flow behaviour.

The absolute value of floor velocities at different point along the scour hole are shown in Fig. 6.53. It is seen from Fig. 6.53 that the minimum floor velocity occurs at the point of maximum scour and just downstream of the jet's exit, where the slope of the bed is nearly zero. Also, it is observed that the maximum floor velocity occurs on the downstream slope of the hole.

CHAPTER 7. THE GOVERNING EQUATIONS AND THE PROBLEM OF CLOSURE

7.1 INTRODUCTION

In hydraulics, the flows of practical relevance are almost always turbulent; this means that the fluid motion is highly random, unsteady and three-dimensional. Due to these complexities, the turbulent motion and the heat and mass-transfer phenomena associated with it are extremely difficult to describe and thus to predict theoretically. Yet, the basic task of hydraulic engineering is that of predicting water-flow phenomena, and, because "predictions" by way of experiments are usually very expensive, calculation methods are in great practical demand. Empirical methods simply correlate experimental results and can therefore be used with confidence only for direct interpolation of these results; the Chezy equation is a typical example.

With the aid of dimensional analysis, experimental data were condensed into many useful empirical formulae. However, these can describe only the simplest phenomena of interest and are not suitable for complex geometries. Whenever there are more than just a few parameters determining the problem in question, generally valid empirical correlations are difficult if not impossible to attain.

At an early stage in this research an analytical approach was followed and methods were developed which made use of our theoretical knowledge of fluid-flow phenomena. These methods were based on the conservation laws for mass, momentum and energy and were therefore, at least potentially, of greater general validity than strictly empirical relations.

The purpose of this chapter is to present the basic equations which govern turbulent flows, and to introduce the problems which their solution poses. After reviewing general equations of motion and problems associated with their solutions, in the rest of this chapter the special form of the equations and turbulence models suitable for the present work are discussed.

7.2 GENERAL FLOW EQUATIONS

7.2.1 Time-dependent equations

Laminar and turbulent flows alike are governed by the laws of mass and momentum conservation. For a Newtonian fluid with constant density and viscosity, these laws are expressed in tensor forms as follows;

Mass conservation: continuity equation

$$\partial \tilde{U}_i / \partial x_i = 0, \tag{7.1}$$

Momentum conservation: Navier-Stokes equation

$$\partial \tilde{U}_i / \partial t + \tilde{U}_j \, \partial \tilde{U}_i / \partial x_j = -1/\rho \, \partial \tilde{P} / \partial x_i + g_i + \partial / \partial x_j [\nu \, (\partial \tilde{U}_i / \partial x_j + \partial \tilde{U}_j / \partial x_i)] \tag{7.2}$$

where U and P denote velocity and pressure, respectively, x is direction, t denotes the time, ν and ρ represent kinematic viscosity and the fluid density respectively, g_i is the body force in the ith direction. The ~ over variables in the equations denote the instantaneous values of the quantities in question. Here, and in all the following

equations, the summation convention [4] applies where repeated indices appear.

Equations (7.1) and (7.2) constitute a closed set; so all we need to predict for the solution of a given flow problem, it seems, are boundary conditions and a method of solution. For many laminar flows the equations can indeed be solved by currently available methods, but this is not the case for turbulent flows of engineering interest. The reasons are that (i) turbulence is always three-dimensional, and (ii) many of the important processes take place on very small scales (about 0.1 mm). The equations can be solved only by means of numerical techniques which calculate the dependent variables at discrete points in the flow. So, with a mesh size of 0.1 mm in all three directions, we would need 10^6 grid points for a volume of one cubic centimetre. Therefore it seems to be very expensive and sometimes impossible to solve equations (7.1) and (7.2) for realistic turbulent flows.

Fortunately, however, the design engineer is not interested in every detail of the turbulent motion, but mainly in the time-averaged velocity and pressure. The next section will present equations governing these quantities.

---

[4] The summation convention implies that whenever the same index is repeated in a single expression, the sum over all three directions has to be taken, thus, for example:

$$\partial U_i/\partial x_i = \sum_{i=1}^{3} \partial U_i/\partial x_i = \partial U_1/\partial x_1 + \partial U_2/\partial x_2 + \partial U_3/\partial x_3 = 0$$

7.2.2 The Time-Averaged Continuity and Momentum Equations

Following Reynolds (1895), the instantaneous dependent variables are assumed to be equal to the sum of a time-averaged and a fluctuating component. Thus

$$\tilde{U}_j = U_j + u_j \qquad (7.3\text{-a})$$

$$\tilde{P} = P + p' \qquad (7.3\text{-b})$$

where, for steady mean flow, the time-averaged (or mean) values of U and P are defined by

$$U_i \equiv \text{Lim}\ ((1/T) \int^T U_i\ dt), \qquad (7.4\text{-a})$$

$$P \equiv \text{Lim}\ ((1/T) \int^T P\ dt), \qquad (7.4\text{-b})$$

where T is a time scale which is long compared with that of the turbulent motion.

Substituting equations (7.3-a and 7.3-b) into the governing equations (7.1 and 7.2), and time-averaging, the equations that result for steady state, are (Hinze 1959):

Momentum equation:

$$U_j\ \partial U_i/\partial x_j = -1/\rho\ \partial P/\partial x_i + g_i + \nu\ \partial^2 U_j/\partial x^2{}_j\ -\partial(u_i u_j)/\partial x_j \qquad (7.5)$$

Continuity equation:

$$\partial U_j/\partial x_j = 0 \qquad (7.6)$$

These are two very important equations; they govern the mean motion and will therefore, in one form or another, be part of any prediction method which does not solve the time-dependent equations (Eqs.7.1 and 7.2). The products of fluctuating quantities, $-\rho u_i u_j$, are usually called the turbulent shear stresses.

7.3 APPROACHES TO CLOSING THE EQUATIONS

The momentum equation (7.5) contains a product of the time-averaging process: the Reynolds stress $-\rho u_i u_j$. This stress represents the transfer of momentum by the turbulent motion. Because of its presence, equations (7.5) and (7.6) do not constitute a closed set. Our basic task is therefore to find a means for evaluating $u_i u_j$ (exactly or approximately by modelling) in order for the equations to be closed. This section contains a brief description of approaches taken to close the momentum equations.

7.3.1 The Problem of Closure

Exact transport equations can be derived from the Navier-Stokes equations for the correlations, $u_i u_j$, appearing in equation (7.5). However, correlations of the next higher order (e.g. $u^2_i u_j$) are thereby introduced; and equation (7.5) shows, for example, that the number of unknowns grow faster than the number of equations. Thus, we may conclude, that closure cannot be achieved by resorting to equations for correlations of higher and higher order.

7.3.2 The Turbulent Model Approach

In order to close the system, some of the correlations are usually approximated in terms of quantities that can be calculated. "Model" assumptions about turbulence are thereby introduced which may not always be entirely realistic. Instead of the real turbulent fluid we thus consider an idealised "model" fluid which is governed by the laws prescribed by a "turbulence model". Therefore, a turbulent model is defined as a set of equations (algebraic or differential) which determine the turbulent transport terms in the mean-flow equations and thus close the system of equations.

This turbulence-model approach is the only practicable one at present. It avoids the difficulty of the Navier-Stokes-equation approach, i.e. the requirement for an extremely large number of grid points, because the time-averaged quantities vary much more gradually than do the time-dependent ones.

Our first task is to select the type of model which is to be employed. Thus, in section 7.3.3, we review models of various levels of complexity.

7.3.3 Literature Review

The number of turbulence models suggested in the literature over the last 70 years is rather large, therefore not all the models can be included in this review. Some of the suggested models have not been tested properly (or not at all) and are therefore difficult to assess; others are used no longer because they have been found to perform poorly. The

present review concentrates on those models which are still in use and have been tested to a fair degree.

The specification of Reynolds stresses may be made in terms of algebraic equations or in terms of a combination of algebraic and differential equations, and this has given rise to terminology involving the number of differential equations. The division of this review is based on this terminology.

7.3.3.1 Zero-Equation Models

The models of this group do not employ differential equations for turbulence quantities. They relate the shear stress uniquely to the local mean flow conditions.

Boussinesq (1877) proposed what is commonly referred to as the "eddy viscosity" concept, to evaluate the turbulent shear stresses in the momentum equations. Models based on this concept are often called "Eddy Viscosity Models" (EVMs). Bousinesq suggested that the Reynolds stresses, τ_{ij} may be treated in the same manner as are molecular shearing stresses, so that (for two-dimensional thin shear flow)

$$\tau_{ij} = - \rho u_i u_j = \mu_t \, \partial U_i / \partial x_j \qquad (7.7)$$

where the eddy viscosity, μ_t depends upon the turbulent structure of the flow, and has the same dimensions as the molecular viscosity, μ.

About half a century later, Prandtl (1925) proposed that the eddy viscosity could be prescribed in terms of a mixing-length, l_m. He based his proposal on the assumption that the transport of turbulent eddies

in a fluid is similar to that of molecules in a gas. The mixing-length of the turbulent eddies in the fluid is then the quantity that corresponds to the mean free path of the molecules in the gas. The Reynolds stresses, τ_{ij} were prescribed as follows :

$$\tau_{ij} = \rho l_m^2 \left| \partial U_i/\partial x_j \right| \partial U_i/\partial x_j \qquad (7.8)$$

Prandtl was successful in obtaining reasonable estimates of the turbulent shear stress in near-wall flows by assuming that the mixing-length was proportional to the distance from the wall. With the constant of the proportionality, κ, (the von Karman constant), equation (7.8) may be rewritten :

$$\tau_{ij} = \rho \kappa^2 x_j^2 \left| \partial U_i/\partial x_j \right| \partial U_i/\partial x_j \qquad (7.9)$$

Using equation (7.9), the momentum equation (7.5) may be closed and this approach is usually referred to as the "mixing-length" hypothesis. This approach has been and still is applied with great success, at least for turbulent boundary layers, where the effects of turbulence transport are weak.

For thin shear layers, the mixing length, l_m is normally taken as proportional to the width of the shear layer.

The mixing-length hypothesis of Prandtl (1925) is doubtless the best known of the zero-equation models. The simpler model for free shear-layers proposed later by Prandtl (1942), and the models of Cebeci and Smith (1974), and Crawford and Kays (1975) are also zero-equation models. Cebeci and Smith used an eddy viscosity formulation which involves empirical corrections to account for the effect of low Reynolds number, transition region, compressibility, mass transfer, pressure gradient

and transverse curvature. Crawford and Kays tuned their zero-equation model specifically for boundary layers. Models such as these continue to be useful for many engineering applications.

Zero-equation models work well for boundary layers (e.g. far field of jets and wakes) where the turbulence structure changes but slowly in the main flow direction. However, the empirical constants involved vary from one flow situation to another and are thus valid for restricted flow regions only.

7.3.3.2 One-Equation Models

About two decades after the introduction of the eddy-viscosity concept, Prandtl (1945) proposed the use of a turbulence velocity scale in evaluating the eddy viscosity. The kinematic eddy viscosity, $\nu_t = \mu_t/\rho$ is assumed to be related to the turbulent kinetic energy, $k(=1/2[u_i^2 + u_j^2 + u_k^2])$ and a length scale of turbulence, l_v by (Kolmogrove Equation);

$$\nu_t = C_v\, k^{0.5}\, l_v \tag{7.10}$$

$k^{0.5}$ is turbulence velocity scale and can be found by the following transport equation for the turbulent kinetic energy, (which is obtained by halving the sum of the transport equations for three normal stresses, Hinze, 1959):

$$\begin{aligned} U_j\, \partial k/\partial x_j = &- \partial/\partial x_j \left[u_j(P/\rho + k) - u_i u_j\, \partial U_i/\partial x_j \right] \\ &+\nu_t\, \partial/\partial x_j \left[u_i(\partial u_i/\partial x_j + \partial u_j/\partial x_i) \right] \\ &-\nu_t\, \partial u_i/\partial x_j(\partial u_i/\partial x_j + \partial u_j/\partial x_i) \end{aligned} \tag{7.11}$$

The left hand side of eq. (7.11) is the convective transport of kinetic energy. The first and second terms on the right hand side of this equation are respectively, diffusion and production of k. The last term in the eq. (7.11) is referred to as the dissipation rate of turbulence energy since it serves as a sink for the turbulent kinetic energy.

Equation (7.5), applied to two-dimensional flows, can now be closed using equations (7.7) and (7.10). When equation (7.11) is the only partial differential equation (pde) used in addition to the mean-flow pde's to solve the flow, the turbulence model is termed a "one-equation model". In these models, the length scale, l_v is prescribed algebraically to mimic as closely as possible that observed in experiments.

In accounting for the behaviour of flows influenced by walls, Wolfshtein (1969) found that the use of expressions similar to those proposed by van-Driest (1956) in specifying the length scale gave results that were in agreement with the experimental data for Couette and fully developed turbulent duct flows. The length scale was specified as follows:

$$l_v = B_3\, y\, [\, 1 - \exp(-A_v y^*)\,] \qquad (7.12)$$

where the turbulent Reynolds number, $y^* = k^{0.5} y/\nu$ and y is the perpendicular distance to the wall, and A_v and B_3 are coefficients. Far from the wall, where y^* is large, the length scale is proportional to y whereas as the wall is approached, the length scale is dampened by a factor approaching $A_v y^*$. This behaviour is in accordance with that experimentally observed of fluids influenced by walls in unseparated flows. Norris and Reynolds (1975) prescribed length scales in the viscous sublayer as well as in the fully turbulent regions so that their models can be used right down to the walls.

A one-equation model which does not employ the eddy viscosity concept is that of Bradshaw and his co-workers (Bradshaw, Ferris and Atwell, 1967 and Ferris, 1973) who assume that $u_i u_j$ is proportional to k.

One equation models are superior to mixing-length and other zero-equation models when the convective and diffusive transport of the turbulent velocity scale is important (for example in boundary layers with free-stream turbulence). However, the requirement of a prescription for the length-scale distribution makes it very difficult to apply one-equation models to more complex flows; for it is only for well documented boundary layers that these distributions are known.

7.3.3.3 Two-Equation Models

In more complex flows, difficulties are often found in specifying empirically the distribution of the length-scale. For this reason a third approach was developed which used a transport equation to calculate the length scale, l_v. The dependent variable (a scalar quantity) of the second turbulence equation is not the length scale itself and varies in form but is usually a derivative of the general variable $z=k^a\ l_v^{\ b}$ where a and b are constants. These "two-equation" models (involving two pde's in addition to the mean flow pde's) are usually designated by the two turbulent scalar quantities being solved in the transport equations. The variables that have been used include $\varepsilon = k^{1.5}/l_v$ (e.g. Jones and Launder, 1972), kl_v (Rotta, 1951), $k^{0.5}/l_v$ (Kolmogorove, 1942) and $k/l_v^{\ 2}$ (e.g. Spalding, 1971).

Of the two-equation models, the energy-dissipation or k-ε model (where $\varepsilon=k^{1.5}/l_v$) proposed by Jones and Launder (1972) has been par-

ticularly popular and was applied successfully to a wide variety of two-dimensional flows. These include strongly accelerated boundary layer flows (Jones and Launder, 1972), duct flows (Stephenson, 1976), free shear flows (Launder, Morse, Rodi and Spalding, 1973), and recirculating flows (e.g. Gosman, Khalil and Whitelaw, 1979). The model has also been tested successfully for three-dimensional wall boundary layers (Rastogi and Rodi, 1978), and jets (McGuirk and Rodi, 1979). A detailed description of the k-ε model and applications of the model (by various authors) to nine different flows was presented by Launder and Spalding (1974). In particular, its capabilities are well established for shear-layer and confined recirculating flows. For this reason, the k-ε model is one of the two turbulence models applied to the main region of the flow fields studied in this work and will be given in more detail in this chapter.

The capabilities of two-equation models and in particular the k-ε model have been established for a wide range of flows, as the brief survey above has shown. However, in flows such as those of weak shear layers and axisymetric jets, some of the constants have had to be replaced by functions in order to obtain agreement with the experimental results. Furthermore, neglect of the transport of the individual turbulent stresses, implicit in the assumption of an eddy viscosity concept, has contributed to errors in the predictions. For example, in a wall jet, because there is the diffusive transport of shear stresses, the surfaces of maximum velocity and zero shear stress are not coincident in reality, as is implied by the eddy viscosity concept.

7.3.3.4 Reynolds-Stress Models

In highly anisotropic flows where all the Reynolds stresses need to be calculated (e.g. strongly swirling jets), the models reviewed so far will fail.

If we had a transport equation for $u_i u_j$ then the most direct way to determine $u_i u_j$ would be to solve this equation. Indeed, such an equation does exist. It can be derived in the following way. The momentum equation (7.5) is subtracted from the Navier-Stokes equations (7.2) for both of the i and j components. The resulting equation for component i is multiplied by the fluctuating velocity u_j, and the equation for the component j is multiplied by u_i .Summation of the two equations, and subsequent time-averaging yields the desired equation for $u_i u_j$ (detailed derivation can be found in Hinze 1959).

The Reynolds stress equation may be written:

$$\begin{aligned} U_k \, \partial(u_i u_j)/\partial x_k = & - (u_j u_k \, \partial U_i/\partial x_k + u_i u_k \, \partial U_j/ \partial x_k) \\ & + P/\rho \, (\partial u_i/\partial x_j + \partial u_j/\partial x_i) + \partial/\partial x_k \, [\, \nu \, \partial/\partial x_k \, (u_i u_j) \\ & - u_i u_j u_k - P/\rho \, (\delta_{jk} u_i + \delta_{ik} u_j) \,] \\ & - 2\nu \, \partial u_i/\partial x_k \partial u_j/\partial x_k \end{aligned} \qquad (7.13)$$

or

$$U_k \, \partial/\partial x_k \, (u_i u_j) = P_{ij} + \phi_{ij} + D_{ij} - \varepsilon_{ij} \qquad (7.14)$$

where P_{ij} is the "generation" tensor (and being explicit in $u_i u_j$ requires no modelling); ϕ_{ij}, the pressure-strain "redistributive tensor"; D_{ij}, the diffusive transport tensor; and ε_{ij}, the dissipative correlation.

The Reynolds-stress equation (7.13) contains terms corresponding to the ones just discussed. In addition, it contains the pressure-strain term which redistributes energy among its components (when i = j) and reduces shear stresses (when i ≠ j). This term therefore tends to make turbulence more isotropic.

The turbulence diffusion, pressure-strain, and dissipation terms in equation (7.14) introduce new unknowns in the form of higher order correlations. To find these unknowns, a number of workers (for example, Hanjalic and Launder, 1972, and Daly and Harlow, 1970) have proposed approximations for ϕ_{ij}, D_{ij} and ε_{ij} in terms of Reynolds stresses and mean velocity components. Some of these approximations (modelling) will be described later in this chapter.

There have been some computations of simple flows and mildly complex flow (mostly two-dimensional) using RSM's. Gibson and Rodi (1981) employed the RSM to compute the flowfield in a highly curved jet measured by Castro and Bradshaw (1976). RSM predicted the growth of the jet and maximum shear stress very well, but the recovery of k downstream of the curve was not predicted adequately by this model. Gibson et al. (1978, 1981a, 1981b) have employed the RSM to predict a variety of complex flows, including curved free flows, curved wall jet, etc. For wall jets, the RSM accurately predicted the location of the zero shear stress and the zero mean velocity gradient. The stabilising action of the convex surface is also predicted.

The resulting "Reynolds stress models" (RSMs) provide a more realistic physical simulation of turbulent flow and is potentially the superior model. However, it is very complex, expensive to use and the least tested model so far. Even this model does not constitute a com-

plete closure for turbulence, as the additional physics associated with the turbulence is not simulated properly.

In summary, for very complex flows, the RSM may be much superior. But for moderate-to-simple shear layers, the k-w and k-ε models may be adequate.

Based on the above discussion, the use of RSM is considered inappropriate for this work.

7.3.3.5 Algebraic-Stress Models

A number of workers recognised that the only terms containing gradients of Reynolds stresses in the stress equation (7.13) were convective and diffusive terms. By eliminating these gradients by suitable approximations, the stress equations represented by the tensor equation (7.14) could be reduced to a set of algebraic equations. Substantial saving in computing time could then be obtained since this set of algebraic equations replaced the six strongly coupled and highly non-linear differential equations for the stresses in the RSM that required solution. Launder (1971), Rodi (1972), Launder and Ying (1973) and Tatchell (1975) developed and applied this approach, known as the Algebraic Stress Model (ASM), for calculating turbulent flows.

ASM has been explored in a few recent work. One such form was used by Ljuboja and Rodi (1980) to calculate turbulent wall jets. The empirical constants C_v in the Kolmogorove-Prandtl eddy viscosity relation ,(Eq. 7.10), was replaced by a function which was derived by reducing a modelled form of the Reynolds stress transport equation to algebraic

expressions while retaining the wall damping correction to the pressure-strain relation used in these equations. The predicted streamwise profiles of jet half-width, maximum velocity and skin friction coefficient, and the lateral profiles of streamwise velocity, shear stress and kinetic energy were all in close agreement with the experimental results of Tailland (1970).

The success in predicting these flows opened the way for the ASM to be used as a suitable approach between that of ~~a~~ the isotropic eddy viscosity and full Reynolds stress models in calculating turbulent flows.

The ASM is suitable for use when the notion of isotropic turbulent viscosity is inadequate and when computing economy is an important consideration. The ASM is the second model used, herein, for predicting the main region of the flow fields. This model is described in more detail in Section 7.4.4.2.

As the main flows considered in the present work (offset jet and flow in a scour hole) are curved flows, it is suitable to express the equations of motion in a curvilinear system.

In the following section, we consider two-dimensional flow, and assume that it is mainly in the longitudinal direction , by which we can use the principal of boundary-layer approximation.[5]

---

[5] A boundary layer can be characterised as a region, in a moving fluid, in which there is a single predominant direction of flow; and in which transfers of momentum, heat and matter by molecular

7.4 EQUATIONS OF FLOWS IN A CURVED SYSTEM

The governing equations of two-dimensional flow with curved streamlines are most conveniently expressed in a curvilinear orthogonal (s,n)-coordinate system, Fig (7.1), where s follows a reference streamline and n is normal to s. The radius of curvature of the reference streamline R is in general a function of s, and the local radius of curvature r is related to R by r=R + n. R is defined to be positive for flow on a convex path and negative for flow on a concave path. The velocity components in the s and n directions are U and V, respectively. The corresponding fluctuating velocity components are u and v and the fluctuating part of velocity in the third direction (z) is w. The only non-zero components of the Reynolds stress tensor are u^2, v^2, w^2 and uv. The transport equations appropriate to this system are obtained by transforming the corresponding equations written in Cartesian tensor notation.

7.4.1 Mean Flow Equations

The basic governing equations, in curved coordinates, for two-dimensional, steady, incompressible, turbulent boundary-layer flows with horizontal free-surface, may be obtained from the tensoral form of the equations of motion (eqs 7.5-7.6) as follows (Bradshaw 1973):

---

and turbulent intermingling occur mainly at right angles to the predominant direction. Therefore, if x_i is the predominant direction, we have:

$$U_i >> U_j \text{ and } \partial/\partial x_i << \partial/\partial x_j$$

1- Continuity Equation

$$\partial U/\partial s + \partial(hV)/\partial n = 0 \qquad (7.15)$$

where $h = 1+n/R$ is the ratio of local to reference radius of curvature.

2- Momentum Equations

s-direction

$$U\,\partial U/\partial s + hV\,\partial U/\partial n + UV/R = -(1/\rho)\,\partial P_N/\partial s - h\,\partial(uv)/\partial n$$
$$-2\,uv/R - \partial u^2/\partial s + U_0 dU_0/ds \qquad (7.16)$$

n-direction

$$U\,\partial V/\partial s + hV\,\partial V/\partial n - U^2/R = (h/\rho)\,\partial P_N/\partial n - \partial(uv)/\partial s$$
$$-h\,\partial v^2/\partial n - (v^2 - u^2)/R \qquad (7.17)$$

where P_N is the excess pressure, ρ the fluid density, and U_0 is the external flow velocity in the s direction.

It should be mentioned here, that as we are concerned with the flows with horizontal free-surfaces, the body force terms (gravity terms) and gradient of hydrostatic pressure which should be on right of Eqs. (7.16) and (7.17) cancel out.[6]

---

[6] In general form, terms relating to pressure gradient and gravity force are presented on the right-hand side of the momentum equation as follows:

s-momentum Eq. $\quad -1/\rho\ \partial P_t/\partial s + g_s$

n-momentum Eq. $\quad -1/\rho\ \partial P_t/\partial n + g_n$

where $P_t = P_h + P_N$, is the total pressure, P_h denotes the hyrostatic pressure and P_N is the pressure due to other parameters, like curvature. g_s and g_n are components of gravity force in the s and n direction, respectively.

Referring to Fig. 7.1 we have:

The terms on the left-hand side of Eqs. 7.16 and 7.17 have arisen from the transformation of the Cartesian mean-flow transport (convection) term, $(U\partial/\partial x + V\ \partial/\partial y)$, into the (s-n) coordinate system. The transformed terms are of two distinct types. The first type may be represented, for compactness and ease of reference, by the operator D/Dt which is defined as :

$$D/Dt \equiv U\ \partial/\partial s + Vh\ \partial/\partial n \qquad (7.18)$$

The second type of terms which appear in equations (7.16)-(7.17) is a consequence of analysing the flow with respect to the curved axes. Since the directions of the curved axes change with position in the flow, it follows that the directions of U and V change accordingly. The terms UV/R and U^2/R appear in the mean-flow equations as a consequence of the change in momentum arising from the change in the direction of the velocity components. Thus, irrespective of whether or not the flow is curved with respect to the Cartesian system, the mere fact that the flow is analysed by reference to curved axes leads to the appearance of these terms which, for convenience, will henceforth be referred to as the 'curvature-of-axes' terms. The remaining terms in equations (7.15-7.17) are easily identified by analogy to their Cartesian counterparts.

$g_s = g \sin(\theta)$

$g_n = -g \cos(\theta)$

$P_h = \rho g\ h_s$

$\partial P_h/\partial s = \rho\ g \sin(\theta)$

$\partial P_h/\partial n = -\rho\ g \cos(\theta)$

where h_s is the depth below water surface, and θ is the angle between the n direction and the vertical direction. Finally substituting the above terms into the relevant terms of the momentum Eqs. we obtain:

$$-1/\rho\partial P_t/\partial s + g_s = -1/\rho\partial P_N/\partial s - g \sin(\theta) + g \sin(\theta) = -1/\rho\ \partial P_N/\partial s$$

$$-1/\rho\partial P_t/\partial n + g_n = -1/\rho\partial P_N/\partial n + g \cos(\theta) - g \cos(\theta) = -1/\rho\ \partial P_N/\partial n$$

The above mean flow equations are applicable to high Reynolds number flows where molecular diffusion is negligible and the small-scale turbulent motions are isotropic. These equations apply everywhere in the flow except in the viscous sublayer since all the viscous terms have been neglected.

There is no need to retain all the terms which appear in the transformed equations in the numerical solution method. The dominant terms can easily be identified by applying the well known boundary layer approximations to these equations; see for example Schlichting (1966). Terms which turn out to be of an order of magnitude smaller than the dominant terms may be discarded without significantly affecting the accuracy of the solution. In assigning orders of magnitude to the various terms, the normal distance, n, is taken to be of order L, the thickness of shear layer. The radial velocity, V, is then found from the continuity equation to be of order L.U/R. Note that the ratio (s/R) was taken to be of order unity which is appropriate to flows with sharp curvature. Indeed one of the present test cases concerns the development of a wall jet on a logarithmic spiral defined by R/s = 1.0.

Further, if we put $\tau/\rho = -uv$ and assume:

$$P_c = P_N + \rho u^2 = P_N + \rho v^2,$$

the axial- and the radial-momentum equations are written, with terms of order (L/R) retained, as

$$DU/Dt + UV/R = -(1/\rho)\ \partial P_c/\partial s - h\ \partial uv/\partial n - 2\ uv/R + U_0 dU_0/ds \qquad (7.19)$$

$$(h/\rho)\ \partial P_c/\partial n = U^2/R \qquad (7.20)$$

Since the radial velocity component is small, its transport equation is reduced to the simple form (7.20) which represents (in the s-n coordinate system) a balance between the radial pressure gradient and the oppositely-directed centrifugal force. Irwin and Smith (1975) neglected the radial momentum equation altogether in their calculations of curved flows. The errors introduced in a calculation method as a result of ignoring the radial variation of static pressure arising from curvature cannot be exactly quantified. What is certain, however, is that such a method can only be valid for flows with small curvature.

7.4.2 Reynolds-Stress Transport Equations

Transport equations for the Reynolds stresses are obtained from the Navier-Stokes equations as described by Bradshaw (1973). For boundary-layer flows at Reynolds numbers high enough for the small scale motion to be assumed isotropic, the Reynolds stress equations, in s-n system, are (Irwin and Smith, 1975):

$$Du^2/Dt = -\partial(vu^2)/\partial n + (2/h)(p/\rho)\partial u/\partial s - 2[u^2\ \partial U/\partial s + uv\ (\partial U/\partial n + U/r)] - 2/3\varepsilon \qquad (7.21)$$

$$Dv^2/Dt = -\partial(v^3 + 2vp/\rho)/\partial n + 2p/\rho\ \partial v/\partial n + 2(v^2\ \partial U/\partial s + 2uv\ U/r) - 2/3\varepsilon \qquad (7.22)$$

$$Dw^2/Dt = -\partial(vw^2)/\partial n + 2\ (p/\rho)\partial w/\partial z - 2/3\varepsilon \qquad (7.23)$$

$$D(uv)/Dt = -\partial(uv^2 + p/\rho u)/\partial n + p/\rho(1/h\ \partial v/\partial s + \partial u/\partial n) - [v^2\ \partial U/\partial n - (2u^2 - v^2)\ U/r] \qquad (7.24)$$

where p is the fluctuating part of the pressure.

Terms involving the longitudinal acceleration $\partial U/\partial s$ contribute to the production of u^2, v^2. These terms are often ignored in modelling plane flows but, since they are of the same order as the production terms involving U/r, they ought logically to be included when the effects of curvature are considered. However, it seems improbable that the two effects are significantly coupled, at any rate for a mild curvature. Also, the study of Irwin and Smith (1975) suggested that the turbulence structure is much less sensitive to the effects of acceleration than to those of curvature, these terms will be discarded in the present study.

The triple correlation terms in the Reynolds stress equations explicitly associated with curvature were omitted from eqs. (7.21-7.24), in view of the evidence (Castro and Bradshaw, 1976) that they are extremely small even in highly curved flows. Of the terms representing the rates of production of the Reynolds stresses, those involving the secondary strain rates (i.e. $\partial V/\partial s$, V/R and $\partial V/\partial n$) are of order (L/R) times the production terms involving the primary strain rates ($\partial U/\partial n$ and U/R) and were therefore neglected.

By taking half the sum of equations (7.21) -(7.23), the transport equation for turbulent kinetic energy is obtained as follows:

$$Dk/Dt=-\partial/\partial n\ (vk + pv/\rho)-[(u^2-v^2)\partial U/\partial s+uv(\partial U/\partial n-U/r)]-\varepsilon \qquad (7.25)$$

Note that the "curvature-of-axes" terms associated with the equations for u^2 and v^2, being equal in magnitude but opposite in sign, have vanished upon summation. That the k-equation does

not contain coordinate-dependent terms is hardly surprising in view of the fact that turbulence energy is a scalar quantity and thus would remain invariant under rotation of coordinates.

The dissipation rate transport equation for curved boundary layer flows takes the form

$$D\varepsilon/Dt = C_{\varepsilon}/\partial(h(k/\varepsilon)\, v^2\ \partial\varepsilon/\partial n)/\partial n$$
$$+ C_{\varepsilon 1}(\varepsilon/k) P_k - C_{\varepsilon 2}(\varepsilon^2/k) \qquad (7.26)$$

The dissipation rate ε is a scalar quantity and thus the above comments on the non-appearance of coordinate-dependent terms apply here as well.

7.4.3 Turbulence Modelling for Curved Flows

7.4.3.1 Curvature Effects on Turbulence

Turbulence in thin shear layers is known to be highly sensitive to streamline curvature in the plane of the mean shear.
It is not surprising that curved turbulent flows should behave differently from plane flows. It is well known that the effect of curvature on small disturbances in laminar flow is to create a stabilising effect depending on the sign of the angular momentum gradient,
$\partial(Ur)/\partial r$. It has been postulated that the same mechanism acts
on curved turbulent flows to influence the scale and intensity of the

turbulence. A fluid particle is considered to be displaced with a constant angular momentum from one fluid stratum to another of larger radius and the pressure gradient necessary for its equilibrium is noted. It is easily shown that the particle will be displaced further outwards in a negative, and hence unstable angular momentum gradient. In a similar way the positive gradient leads to stability.

Experiments have shown that in a region with an unstable angular momentum gradient, turbulence production is amplified and that the opposite occurs if the gradient is stable.

Sawyer (1962) studied the special case of curved wall jets flowing on surfaces whose radii were proportional to the width of the jet (R∝L): this particular geometry arose from a similarity study of the equations of motion. He found that the growth of the jets differed by as much as 50% from that of a plane wall jet when the ratio of wall-jet thickness to radius was about 0.1. Convex flow spread more rapidly, and concave flow less rapidly than the corresponding plane flow.

A wall jet flowing over a concave surface has a stable outer region and an unstable boundary layer region. The opposite is true for a wall jet flowing over a convex surface.

Therefore, turbulent transport of heat and momentum is reduced by curvature when the angular momentum of the flow increases in the direction of the radius of curvature and is increased when the angular momentum decreases with radius.

7.4.4 Review of Turbulence Modelling

Nearly all attempts to account for streamline curvature effects in calculation schemes have involved empirical modifications to eddy-viscosity formulae developed for flows with insignificant curvature.

In most cases, the eddy-viscosity or the mixing length is multiplied by an empirical curvature correction, F, defined as:

$$F = 1-\alpha S \tag{7.27}$$

where α is an empirical constant of order 10, whose exact value depends on the flow considered. According to Bradshaw(1973), the constant varies in the range $6<\alpha<14$ for wall flows. Here S is a dimensionless parameter characterising the ratio of the extra rate of strain produced by curvature to the inherent shear strain, i.e.;

$$S = (U/r)/(\partial U/\partial n) \tag{7.28}$$

Empirical modifications to the eddy viscosity and the mixing length theories have been reported by Rastogi and Whitelaw (1971), and Gillis et al. (1980) and have been applied with some success. However, as was stated above, a universal value for the empirical curvature coefficient α has not evolved .

The methods described so far are extensions of mixing length and other eddy-viscosity-type models that do not involve transport equations

for the turbulence quantities. These methods have been found to lack generality, in particular in situations when the turbulent shear layer is not in local equilibrium. Eddy-viscosity models that determine the velocity and length scale of the turbulent motion from modelled transport equations are superior in such situations. However, they also require additional curvature modifications. These may be classified in three categories. In the first, modifications are introduced to the model equation for the velocity scale, an example being the model of Wilcix and Chambers (1977), in which an extra production term is introduced into the mixing-energy equation. The second group comprises models which use a modified form of the length-scale-determining equation. The model of Launder et al. (1977) is of this type. In this model, the sink term in the model equation for the rate of dissipation ε of turbulent kinetic energy is made a function of the curvature parameter. While the modifications in the two schemes discussed so far are based on purely empirical arguments, the third group,

algebraic-stress models,

extract information from modelled Reynolds-stress equations. For example, the transport terms of the Reynolds stresses are related to the transport of the turbulent kinetic energy k (Rodi, 1976). For shear layers, an eddy-viscosity type formula results, but the eddy viscosity is now automatically a function of the curvature parameter S. The application of an algebraic-stress model to curved shear layers has been reported by Gibson (1979).

Bradshaw (1973) has argued that at least a turbulence closure involving the solution of modelled forms of the Reynolds-stress equations is necessary to account for the overproportional response of the turbulence structure to streamline curvature. Indeed, Irwin and Arnot Smith (1975), Gibson and Rodi (1981), Gibson et al. (1981),

and Gibson and
Younis (1981) have shown that models of this closure level produce the effects of prolonged influence of curvature with very good quantitative agreement.

Reynolds-stress equation models appear to be adequate for simulating the main features of curved shear layers. However, for reasons of computational economy, it is desirable to have available two-equation models that also respond realistically to curvature either by use of algebraic-stress relations, obtained from the Reynolds-stress equations, or by introducing proper empirical curvature modifications.

In the following sections two turbulence models,
(the k-ε and the ASM) used in this work,
are described.

7.4.4.1 The Standard k-E Model

In the standard k-ε model (Launder and Spalding, 1974), the shear stress -ρuv is related to the local strain rate (∂U/∂n - U/r) via the eddy-viscosity relation:

$$- uv = \nu_t \ (\partial U/\partial n - U/r) \tag{7.29}$$

The eddy viscosity ν_t is related to the turbulent kinetic energy, k, and the rate of its dissipation, ε, by:

$$\nu_t = C_\mu \ k^2/\varepsilon \tag{7.30}$$

The distributions of k and ε in the shear layer are obtained from modelled transport equations for these quantities (Eqs. 7.25 and 7.26), which can be rearranged as follows;

$$(U/h)\ \partial k/\partial s + V\ \partial k/\partial n = (1/h)\ \partial((\nu_t/\sigma_k)\, h(\partial k/\partial n))/\partial n + \nu_t(\partial U/\partial n)^2\ (1-S)^2 - \varepsilon \qquad (7.31)$$

$$(U/h)\ \partial \varepsilon/\partial s + V\ \partial \varepsilon/\partial n = (1/h)\ \partial((\nu_t/\sigma_\varepsilon)\, h\ \partial \varepsilon/\partial n)/\partial n - C_{\varepsilon 2}\ \varepsilon^2/k + C_{\varepsilon 1}(\varepsilon/k)\nu_t(\partial U/\partial n)^2(1-S)^2 \qquad (7.32)$$

where C_μ, $C_{\varepsilon 1}$, $C_{\varepsilon 2}$, σ_k, and σ_ε are empirical coefficients.

As can be seen from these equations, the main effect of curvature is the multiplication of the k production $\nu_t\ (\partial U/\partial n)^2$ in a plane-flow situation by the factor $(1-S)^2$. Positive S therefore leads to a reduction of k and hence also to a reduction of the shear stress $-\rho\ uv$, whereas negative S augments the turbulence. For the empirical constants in Eqs. (7.31)-(7.32), the "standard" values given by Rodi (1980) are adopted:

$$C_\mu = 0.09,\quad C_{\varepsilon 1} = 1.44,\quad C_{\varepsilon 2} = 1.92,\ \sigma_k = 1.0,\ \sigma_\varepsilon = 1.3.$$

The value of C_μ=0.09 was chosen on the basis of experiments in flows in which the production P_k and dissipation ε of the turbulence energy were in approximate balance. However, in weak shear flows, for example far-field jets and wakes, where the velocity difference across the flow is only a small fraction of the convection velocity (≃ free stream velocity), P_k is significantly different from ε and C_μ was found to take different values (Rodi, 1975). Rodi (1972) correlated the experimental data and proposed a function $C_\mu = f(P_k/\varepsilon)$ which is given in Fig. 7.2. This function is valid only for thin shear layers; the argument value

P_k/ε is the average value across the layer. Use of the function significantly improves the k-ε model's ability to predict weak shear flows (Launder et al. 1973).

7.4.4.2 The Algebraic-Stress Model

The algebraic-stress model is derived by modelling and simplifying the Reynolds-stress equations which are written in the curvilinear coordinate system (eqs. 7.21-7.24). These equations may be expressed in general form as

$$D\,u_i u_j\,/Dt = DIFF(u_i u_j) + P_{ij} + \phi_{ij} + \varepsilon_{ij}, \qquad (7.33)$$

where $D\,(u_i u_j)/Dt$ stands for the convective transport of $u_i u_j$ by the motion, $DIFF(u_i u_j)$ represents the diffusive transport by the turbulent motion; and P_{ij}, ϕ_{ij}, and ε_{ij} are, respectively, production, pressure-strain, and viscous-destruction terms.

Modelling of stress equations

The diffusion and pressure-strain terms of eq. (7.33) contain correlations for which model approximations must be introduced if the system is to be closed at the level of the stress-equations.

Pressure-Strain

It can be shown (e.g. Launder, Reece and Rodi, 1975) that two kinds of interactions give rise to these correlations: one involving only turbulence quantities and another arising from the presence of the mean rate of strain. If these terms are denoted by ϕ_{ij} and tensor notation is used for brevity then we get:

$$\phi_{ij} = \phi_{ij,1} + \phi_{ij,2} \tag{7.34}$$

where

$$\phi_{11} \equiv 2/h(p/\rho)\partial u/\partial s; \tag{7.35 a}$$

$$\phi_{22} \equiv 2(p/\rho)\ \partial v/\partial n \tag{7.35 b}$$

$$\phi_{33} \equiv 2(p/\rho)\ \partial w/\partial z; \tag{7.35c}$$

The two components of ϕ_{ij} are modelled as in model 2 of Launder, Reece, and Rodi (1975):

$$\phi_{ij,1} = -C_1\ \varepsilon/k\ (u_i u_j - 2/3\ \delta_{ij} k) \tag{7.36}$$

$$\phi_{ij,2} = -C_2(P_{ij} - 2/3\ \delta_{ij}\ P_k) \tag{7.37}$$

where δ_{ij} is the Kronecker delta defined as:

$$\delta_{ij} = 1 \text{ for } i=j$$

$$\text{and } \delta_{ij} = 0 \text{ for } i \neq j$$

C_1 and C_2 are coefficients which are constants for high-Reynolds-number turbulence and are determined by reference to plane-flow data.

Wall Effects

In a simple shear flow the proximity of a rigid wall modifies the fluctuating pressure field so as to impede the transfer of energy from the streamwise direction to that normal to the wall. The relative mag-

nitude of the shear stress is also reduced. The pressure-strain model introduced thus far does not produce these differences because it does not account for any wall effects. By introducing the unit vector n normal to the surface, Shir (1973) advanced the following near-wall addition to $\phi_{ij,1}$:

$$\phi'_{ij,1} = C'_1 (\varepsilon/k) (u_n^2 \delta_{ij} - 3/2\, u_n u_i \delta_{nj} - 3/2\, u_n u_j \delta_{ni}) f_w(L_w/x_n) \quad (7.38)$$

Later, Gibson and Launder (1978) extended this proposal by introducing an analogous correction for $\phi_{ij,2}$:

$$\phi'_{ij,2} = C'_2(\phi_{nn,2} \delta_{ij} - 3/2\, \phi_{ni,2} \delta_{nj} - 3/2\, \phi_{nj,2} \delta_{ni}) f_w(L_w/x_n) \quad (7.39)$$

where C'_1 and C'_2 are constants chosen to give the right stress levels in the uniform-stress layer close to a plane wall, x_n is the distance from the wall (which in the s-n system is the same as n). L_w is a characteristic turbulence length scale characterising the energy containing eddies and increases linearly with x_n. The function $f_w(L_w/x_n)$ is to reduce the effect of the wall correction with increasing x_n and a linear relationship for f_w was found to be adequate (Launder et al., 1975) which, with $L_w \propto k^{1.5}/\varepsilon$, can be written as

$$f_w = k^{1.5}/(C_w x_n \varepsilon) \quad (7.40)$$

The coefficient C_w in (7.40) was chosen such that the function f_w has a value of unity close to the wall where turbulence is in local equilibrium. This choice yielded $C_w = \kappa / C_\mu^{0.75}$. The mean value of 3.72 was

shown (Ljuboja et al. 1980) to be a proper substitute for C_w, and this value is used in the present investigation.

Finally the pressure-strain terms in the stress equations can be expressed as follows:

$$\phi_{11} = - C_1 (\varepsilon/k)(u^2 - 2/3\ k) + C_2(P_{11} - 2/3\ P_k) + C'_1(\varepsilon/k)\ f_w\ v^2 - C_2C'_2\ f_w(P_{22} - 2/3\ P_k) \quad (7.41)$$

$$\phi_{22} = - C_1 (\varepsilon/k)(v^2 - 2/3\ k) - C_2(P_{22} - 2/3\ P_k) - 2C'_1(\varepsilon/k)\ f_w\ v^2 + 2C_2C'_2\ f_w\ (P_{22} - 2/3\ P_k) \quad (7.42)$$

$$\phi_{12} = - C_1 (\varepsilon/k)\ uv - C_2\ P_{12} - 1.5C'_1\ (\varepsilon/k)\ f_w\ uv + 1.5\ C_2C'_2\ f_w P_{12} \quad (7.43)$$

P_{11}, P_{22} ,P_{12} and P_k are the production rate of u^2, v^2, uv and turbulent kinetic energy, respectively, which are given as follows:

$$P_{11} = -uv(\partial U/\partial n + U/r) \quad (7.44\ a)$$

$$P_{22} = 2\ uv\ U/r \quad (7.44\ b)$$

$$P_{12} = -v^2(\partial U/\partial n + U/r) + 2u^2\ U/r \quad (7.44\ c)$$

$$P_k = -uv(\partial U/\partial n - U/r) = -uv(\partial U/\partial n)\ (1-S) \quad (7.44\ d)$$

The modelled equations contain four empirical constants which are assigned the values determined by Gibson and Launder (1978), from plane-flow data:

C_1=1.8, C_2=0.6, C'_1=0.5, C'_2=0.3

Algebraic expression

Algebraic expressions for $u_i u_j$ can be obtained by approximating the convection and diffusion terms in the Reynolds stress equations. Here, the following proposal of Rodi (1976) is adopted:

$$D\,(u_i u_j)/Dt - DIFF(u_i u_j) = (u_i u_j)/k\,(Dk/Dt - DIFF(k)) \approx (u_i u_j)/k\,(P_k - \varepsilon), \qquad (7.45)$$

When the convection and diffusion terms in equations (7.33) are eliminated with the aid of (7.45), and the modelled form of pressure-strain terms given by eqs (7.41-7.43) are substituted, the following relations result for the individual stresses:

$$v^2/k = (2/3)(1-(P_k/\varepsilon)\phi_2)/(1+2\phi_5) - 4(S/(1-S))\,(\phi_2/(1+2\phi_5))P_k/\varepsilon \qquad (7.46)$$

$$u^2/k = (2/3)(1+P_k/\varepsilon\ \phi_4) + \phi_5 v^2/k + 4(S/(1-S))\ \phi_3\ P_k/\varepsilon, \qquad (7.47)$$

$$uv = -\phi_1[1-(2u^2/v^2 -1)S](v^2/k)\ (k^2/\varepsilon)\ \partial U/\partial n \qquad (7.48)$$

in which

$$\phi_1 = (1-c_2 + 1.5c_2c'_2f_w)/(\beta + 1.5\ c'_1\ f_w), \qquad (7.49\ a)$$

$$\phi_2 = (1-c_2 +2c'_2c_2f_w)/\beta, \qquad (7.49\ b)$$

$$\phi_3 = (1-c_2 +c'_2c_2f_w)/\beta, \qquad (7.49\ c)$$

$$\phi_4 = (2-2c_2 + c'_2 c_2 f_w)/\beta, \qquad (7.49\ d)$$

$$\phi_5 = c'_1 f_w/\beta, \qquad (7.49\ e)$$

$$\beta = c_1 + (P_k/\varepsilon) - 1 \qquad (7.49\ f)$$

These are the algebraic-stress relations derived already by Gibson (1981) and were used by Rodi and Scheuerer (1983). Equations (7.46-7.48) contain two scalar properties of turbulence as unknowns : k and ε. These parameters can be obtained by solving the differential transport equations (7.31 and 7.32). Equations (7.46) and (7.47) show that stabilising curvature (positive S) extracts energy from the normal-stress component v^2 and increases the streamwise fluctuations. In the shear-stress relation Eq. (7.48), an expression similar to that in Eq. (7.27) appears, with the coefficient α as

$$\alpha = (2u^2/v^2) - 1 \qquad (7.50)$$

For wall flows, α according to (7.50) is of the order of eight, which is in fairly good agreement with Bradshaw's (1973) estimate.

A comparison of Eq. (7.48) with relations (7.29) and (7.30), used in the k-ε model, reveals that the algebraic-stress model yields the same shear-stress relation as in that model. However, C_μ is now a function of the curvature parameter S and of the wall-damping function f_w, i,e:

$$C_\mu(S,f_w) = (\phi_1/(1-S))[1 - (2u^2/v^2 - 1)S]v^2/k \qquad (7.51)$$

For a plane layer remote from the wall, we have $S = 0$, $P_k = \varepsilon$ and $f_w = 0$. Eq. (7.51) gives $C_\mu = 0.1152$, which is slightly higher than the value of $C_\mu = 0.09$ used in the standard k-ε model.

CHAPTER 8. METHOD OF SOLUTION

8.1 INTRODUCTION

In this chapter, we first review the different methods for the solution of the governing equations of motion described in chapter 7. We, next, solve the present flow field using an integral method called the Strip Integral Method (SIM).

8.2 METHODS OF SOLUTION

Over the years, many attempts have been made to develop a general method for predicting turbulent flows. These methods can be divided into two main categories.: "integral" methods and "differential" methods. The integral methods involve ordinary differential equations while the differential methods involve governing equations in their original partial differential form. All the methods have a common basis: the equations of motion and continuity for turbulent flow.

The integral methods first integrate the equations of motion reducing them to ordinary differential equations and then incorporating empirical information. The differential methods first incorporate empirical information and then integrate [7] the partial differential equations numerically. The principal advantage of the integral methods

---

[7] "Integration", here means establishment of the solutions of the differential equations which describe the physical processes; so

lies in the use of ordinary differential equations, which are much easier to solve than partial differential equations. Integral methods also result in greater flexibility in utilising empirical data.

8.2.1 Differential Methods

Differential methods are based on the solution of the equations of motions in their partial-differential form. The differential methods require, in common with the integral methods, boundary conditions on both sides of the solution domain. The physical information required to describe the Reynolds shear stresses, may be provided in various forms and these may, in turn, require boundary conditions for turbulence properties.

Like other partial differential equations, there are different methods for their solution, such as finite difference or finite element methods.

With the use of finite-difference methods for the solution of the two -dimensional Navier-Stokes equations, the compromise between cost and numerical accuracy becomes very important. In common with all numerical methods, a grid of numerical nodes must be generated and the accuracy of the resulting calculations can depend heavily on the correct choice.

---

integration entails finding out what values of velocity, temperature, etc., prevail at each point in the domain of integration

Many calculation methods in current use are based on the schemes expounded by Bradshaw, Ferriss and Atwell [1967], Patankar and Spalding [1967], and Keller and Cebeci [1971, 1972]. In Bradshaw et al.'s solution, the turbulence assumptions led to hyperbolic equations which were solved by the method of characteristics. In the other two solutions the equations were parabolic and were solved using finite-difference approximations and an algorithm which allowed the calculation to march in the direction of the flow.

These methods have been applied to a wide range of flow configurations and detailed descriptions and appraisals are readily available in the literature. In general, more than thirty finite-difference nodes are used across the layer to describe the profiles and provide flexibility which is impossible with the small number of parameters allowed for in the profile assumptions of integral methods.

8.2.2 Integral Methods

General

As was mentioned before, integral methods for solving turbulent flows refer to methods based on integrated forms of the equation of motion (momentum equation) and/or the equation of continuity, using various weighting factors.

Integral methods are generally forward marching schemes.[8] Therefore, integral methods are applicable only to the parabolic flows, which are mainly flowing in one predominant direction and usually, the assumptions for boundary-layer approximation is used to simplify them.

Integral methods can be divided into the following groups: the Energy method, the Entrainment method, the Moment-of-Momentum method, and the Strip Integral method. A brief description of these methods is presented below.

8.2.2.1 Energy Method

In this method, the energy equation is solved. This equation is obtained by multiplying the longitudinal (s-direction) momentum equation by U and integrating it over the whole layer. In this method the weighting factor is the longitudinal velocity, U.

---

[8] "Marching" integration is that kind of integration which starts by determining the values at one end of the domain, then determining the values over a front displaced just a little from that end, and so gradually moves the "integration front" towards the other end of the domain until the required values have been determined everywhere. The direction of the "march" is always that of the predominant direction of the flow.

8.2.2.2 Entrainment Method

In this method, the continuity equation is integrated across the layer. The entrainment assumption is that the lateral velocity of the entrained mass is proportional to a velocity scale (e.g. centreline velocity of the jet). This assumption is used to provide closure of the governing equations. The constant of proportionality, or the entrainment coefficient, is determined experimentally.

8.2.2.3 Moment of Momentum Method

In this method the longitudinal momentum equation is multiplied by the transverse distance (n) and then integrated across the whole layer. It is seen that the transverse direction is used as weighting factor in this method.

8.2.2.4 Strip Integral Methods

Another group of integrated equations may be obtained by integrating the longitudinal momentum equation to some intermediate value of n, say n_s. n_s may equal to m.L where m is a constant and L is the shear layer thickness (Moses (1968)).

8.2.3 Literature Review

The following section contains a brief review of the application of the different integral methods.

Albertson [1950] was one of the first to use the integral method to solve for the centerline velocity distribution of both axisymmetric and two-dimensional free momentum jets. Employing a Gaussian-shaped velocity profile, Albertson proposed a linear rate of jet spread as his closure assumption. Theoretical results compared very well with experimental data.

The entrainment equation was first proposed for boundary layer calculation by Head [1958] on the basis of physical reasoning regarding the growth of entrainment of a developing boundary layer. The entrainment method was applied by Fan and Brooks [1969] and Anwar [1965] to buoyant discharges in a stagnant infinite ambient fluid. Fan and Brooks presented working charts for both round and two-dimensional outlets. Hirst [1971], using the moment-of-momentum method, solved the non-vertical round buoyant jet problem. However, Hirst did not use the moment-of- momentum method in the zone of flow establishment. He assumed a form for the entrainment function which was similar to that of the established flow and involved the use of the integrated kinetic energy equation.

Jiji and Hoch [1975,1976] applied the moment-of-momentum method in a slightly different manner to solve a variety of free jet problems for both the zone of flow establishment and the zone of established flow.

Squire and Trouncer [1944] investigated the flow in a round jet with an external flow parallel to it, using the integral method. The jet was assumed to have a uniform velocity over its cross section at the nozzle exit. Mixing with the outside stream caused a decrease of the core depth downstream and the core eventually disappeared. Downstream of the apex

of the core, the maximum mean velocity began to fall and finally reached a state for which the velocity profiles at all sections were similar.

Moses [1968] developed a procedure for calculating the development of the boundary layer by dividing the layer into two or more strips and applying an integral momentum equation for each strip. The velocity profiles were written in a parametric form using the logarithmic law and a polynomial. The turbulent shear stress was related to the local mean velocity using the eddy viscosity.

The streamwise development of a two-dimensional turbulent wall jet in an arbitrary pressure gradient was formulated by Gartshore and Newman [1969]. This method assumed a simple profile for the mean velocity by dividing the depth of the wall jet into an inner layer and an outer layer. For each of the layers, they developed two differential equations.

Integral methods have also been applied to the incompressible turbulent wall jet by Myers et al [1961]. Their analysis gave relationships for obtaining the shear stress, the decay of the maximum velocity, and the boundary layer thickness. They divided the distance downstream from the nozzle into two regions, one near the efflux section and the other farther downstream from the nozzle. In each region the cross section was divided into two layers; an inner layer and an outer layer. For each layer, the boundary layer equation in conjunction with the continuity equation were used. The shear stress was computed from the Blasius equation for the wall layer and from Prandtl's relationship for the outer layer.

In order to study the kinematics of the mean motion in the flow past a leaf gate, Narayanan [1972] developed the so-called strip integral method, in which the cross section of the flow was divided into various strips. Integral momentum equations as well as continuity equations were used to study the mean flow characteristics.

The internal flow in a hydraulic jump was studied by McCorqudale and Khalifa [1983] using the strip integral method. They applied an exponential form of the velocity distribution at the outer layer instead of the cosine form of Narayanan [1972] and extended this method to include the prediction of turbulent pressures.

The non-stratified steady flow hydrodynamics of rectangular sedimentation tanks was simulated by Abdel-Gawad and McCorquadel [1984], using a combination of the strip-integral and finite-element methods. They used a modified mixing-length approach to introduce the effect of recirculation into the solution. Also, the velocity distributions were chosen to allow for the recirculation above the mixing zone. Their numerical results were in good agreement with experimental velocity distributions obtained by laser anemometry.

8.2.4 Concluding Remarks

A few remarks may be made regarding the different methods described above. Digital computing machines are now readily available and are easy to programme. It is therefore becoming customary to obtain a complete numerical solution of the equations of motion. Great accuracy is obtained when the flow is laminar. This is not necessarily the case, however, when the flow is turbulent. Here, the apparent turbulent

stresses, and in particular the shearing stresses, are not known with any certainty and these stresses must be modelled at every node in the domain. So the main disadvantage of higher order methods (like finite difference and finite element) is that they require excessive computer time even for 2-D solutions. There is merit in the integral methods of the sort described here, because they only require an explicit knowledge of the shearing stresses at certain specified points across the flow rather than at all points.

Another feature of the integral approach is that the solution may be limited to the determination of a property of immediate interest, for example the variation of boundary layer thickness. Local flow properties can be determined subsequently from the assumed velocity profile.

Differential methods are applicable to both parabolic and elliptic flows, while integral methods are only restricted to parabolic flows. As in the present work, we are mainly concerned with parabolic flows, therefore, a simple yet an accurate method was sought, particularly for design purposes. In the research reported herein, the Strip Integral Method (SIM) was investigated as a possible calculation tool. The most important feature of the model is the computational efficiency both in time and storage. SIM will run one to two orders of magnitude faster than finite element or finite difference models.

The remaining uncertainty in this method is resolved by assuming a shape for the mean velocity profile, a sensible procedure since we have considerable knowledge, from a wealth of experimental data, of the mean velocity changes across various turbulent shear flows.

The motivation for the SIM, is in the retention of information contained in the original momentum equation, information which would have been lost by the spatial averaging of this equation in other integral methods.

8.3 METHOD OF SOLUTION (SIM)

As is usual with integral methods, the shape of the velocity profile is assumed, and the integral form of the governing equations are used to compute the shear-layer growth rate, and other dependent variables of the problem. In such a method it is necessary to compute the shear stresses at the limits of integration of the momentum equation. To find these stresses, most of the previous investigators have made use of simple turbulence model like mixing length, or eddy viscosity. However, as was mentioned in chapter 7, such simple models are not suitable for complex flows like the curved flows which are mainly dealt with in the present work. Therefore, it was tried to use more general turbulence models like the k-ε and ASM models. In the present study, the earlier integral approach was extended to include integrated forms of the transport equations for k and ε. One of the advantages of this integration is that, because the k and ε equations are integrated across the entire layer,the net lateral diffusion is zero, and no model for the lateral diffusion of k and ε needs to be specified. In this section we present the integral form of the conservation equations of motion and the integral form of the transport equations of k and ε

Fundamental assumptions

The following principal assumptions have been used in developing the analysis:

(1) The flow is two dimensional

(2) The usual boundary-layer approximations are used.

(3) The flow is completely turbulent.

(4) The normalised profiles of velocity.

are similar in shape at all axial stations.[9]

(5) The lateral dimension of the flow field is much bigger than the thickness of the shear layer, so that we can assume that the shear layer is flowing in infinite surrounding.

8.3.1 Integration of Mean-Flow Equations

Rearranging equations (7.19)-(7.20), yields:

s-momentum equation:

$$h\partial(U^2+P_c/\rho)/\partial s+\partial(h^2UV)/\partial n- U_0dU_0/ds =1/\rho\partial(\tau h^2)/\partial n \qquad (8.1)$$

n-momentum equation:

$$(h/\rho)\ \partial P_c/\partial n = U^2/R \qquad (8.2)$$

Integrating the s-momentum Eq. with respect to n, (between the arbitrary limits : $n=n_i$ and $n=n_j$), yields:

$$\int_{ni}^{nj} h\partial(U^2+P_c/\rho)/\partial s + h_j^{\,2}\ U_jV_j - h_i^{\,2}U_iV_i - U_0dU_0/ds(n_j-n_i) = 1/\rho(\tau_j h_j^{\,2} - \tau_i h_i^{\,2}) \qquad (8.3)$$

---

[9] The similarity hypothesis in turbulent flows is introduced by Townsend [1976] in these terms:

> The transverse distributions of mean velocity and other mean quantities change with distance downstream, but it is often assumed that the distributions retain the same functional forms by merely changing their transverse length scale and the scale of the mean-value quantities ....

and ε are similar in shape at all axial stations.[9]

(5) The lateral dimension of the flow field is much bigger than the thickness of the shear layer, so that we can assume that the shear layer is flowing in infinite surrounding.

8.3.1 Integration of Mean-Flow Equations

Rearranging equations (7.19)-(7.20), yields:

s-momentum equation:

$$h\partial(U^2+P_c/\rho)/\partial s+\partial(h^2UV)/\partial n- U_0dU_0/ds =1/\rho\partial(\tau h^2)/\partial n \qquad (8.1)$$

n-momentum equation:

$$(h/\rho)\ \partial P_c/\partial n = U^2/R \qquad (8.2)$$

Integrating the s-momentum Eq. with respect to n, (between the arbitrary limits : $n=n_i$ and $n=n_j$), yields:

$$\int_{ni}^{nj} h\partial(U^2+P_c/\rho)/\partial s + h_j^2\ U_jV_j - h_i^2U_iV_i - U_0dU_0/ds(n_j-n_i) = 1/\rho(\tau_jh_j^2- \tau_ih_i^2) \qquad (8.3)$$

---

[9] The similarity hypothesis in turbulent flows is introduced by Townsend [1976] in these terms:

> The transverse distributions of mean velocity and other mean quantities change with distance downstream, but it is often assumed that the distributions retain the same functional forms by merely changing their transverse length scale and the scale of the mean-value quantities ....

Now, to find the value of hV in the above equation, we integrate the continuity equation (Eq. 7.16), with respect to n (between n=0 and n), this yields;

$$hV - h_0V_0 = -\int_0^n (\partial U/\partial s)\, dn \qquad (8.4a)$$

or

$$hV = h_0V_0 - \int_0^n (\partial U/\partial s)\, dn \qquad (8.4b)$$

where h_0 and V_0 are values of h and V at n = 0

To evaluate the pressure gradient term in Eq. 8.3, the lateral momentum equation (Eq. 8.2) is integrated across the flow (between n and outer limit of the flow) to yield the pressure distribution:

$$P_\infty/\rho - P_c/\rho = \int_n^\infty U^2/(Rh)\, dn \qquad (8.5a)$$

$$\text{or} \quad P_c/\rho = P_\infty/\rho + (1/R) \int_\infty^n (U^2/h)\, dn \qquad (8.5b)$$

where P_∞ is value of P_c at $n = \infty$, which (with $u^2 \simeq 0$) is equal to atmospheric pressure and as we are concerned with relative pressure, it is neglected. This equation is then differentiated with respect to s, to yield the following expression for the longitudinal pressure gradient appearing in (8.3):

$$(1/\rho)\partial P_c/\partial s = +(1/\rho)d\left(\int_\infty^n (U^2/h)\, dn\right)/ds \qquad (8.6)$$

Non-Dimensional Velocity Profiles

Based on the similarity assumption for the velocity distribution, the following form for the velocity profiles is assumed;

$$U = U_0 + U_m\ f(\eta)$$

where f is a shape function for the velocity profile, whose form is dependent on the flow type, U_m is a velocity scale which is a function

of s only, $\eta = n/b$ and b is a length scale which is also a function of s only. In the present work the scales U_m and b are defined according to Fig. 8.1, as maximum (or deficit) velocity and half depth, respectively.

After substituting this expression for U in the integral form of the equation of continuity (Eq. 8.4.b) we get:

$$hV = h_0V_0 + U_m\ FP_0 11\ db/ds\ - b\ FE_0 01\ dU_m/ds$$
$$-b\ FE_0 00\ \ dU_0/ds \qquad (8.7)$$

where $FP_0 ij = {}_0\int^{\eta}\ \eta^i (f^j)'\ d\xi$ (8.8 a)

$$FE_0 ij = {}_0\int^{\eta}\ \eta^i\ f^j d\xi \qquad (8.8b)$$

and primes signify differentiation with respect to η.

Using the expression for U in the integral form of the n-momentum equation, (Eq. 8.5b), and after simplifying the expressions, we finally obtain;

$$P_c/\rho = (b/R)\ F_e \qquad (8.9)$$

where $F_e = \gamma U_0^{\,2} + \phi U_m^{\,2} + 2U_0U_m\ \psi$

and $\gamma = {}_{\infty}\int^{\eta}\ 1/h\ d\xi$

$\psi = {}_{\infty}\int^{\eta}\ f/h\ d\xi$

$\phi = {}_{\infty}\int^{\eta}\ f^2/h\ d\xi$

The pressure gradient becomes:

$$(1/\rho)\partial P_c/\partial s = .(b/R)\partial F_e/\partial s$$
$$+ F_e((1/R)db/ds - (b/R^2)dR/ds) \qquad (8.10)$$

Substituting for the different terms from Eqs. 8.7 and 8.10 into the typical integral-momentum equation, (Eq. 8.3), a set of first-order ordinary differential equations are obtained in the form:

$$A_{ij}\ db/dS + E_{ij}\ dU_m/dS + H_{ij}\ dU_0/dS = J_{ij}\ dR/dS + K_{ij} \qquad (8.11)$$

where the coefficients A_{ij}, E_{ij}, G_{ij}, H_{ij}, J_{ij} and K_{ij} are functions of b, U_m, U_0, and τ_{ij} and are given in Appendix A.

It should be mentioned that if we consider cases where the value of the external velocity, U_0, is constant or is proportional to U_m, we will be left with two unknowns in velocity profile (i.e. b and U_m). Therefore, Eq. (8.11) should be applied to two strips across the layer.

.

8.3.1.1 The Closure Problem

Because of the appearance of the Reynolds stress , τ_{ij}, Eq. (8.11) does not form a closed system and a turbulence model must be used to procure closure.

To evaluate the shear stress in Eq. 8.11, we use the k-ε or the ASM turbulence models. In both models we have to solve the transport equations for k and ε (Eqs. 7.31 and 7.32). In this case, we again reduce the partial differential equations for k and ε to ordinary ones, by integrating them in the n direction, across the entire shear layer, which yields;

$$_0\int^L (Dk/Dt)\ dn = {}_0\int^L T_k dn + {}_0\int^L hP_k\ dn - {}_0\int^L h\varepsilon\ dn \qquad (8.12\ a)$$

$$_0\int^L (D\varepsilon/Dt) dn = {}_0\int^L T_\varepsilon\ dn + C_{\varepsilon 1}\ {}_0\int^L \varepsilon/k\ hP_k dn - C_{\varepsilon 2}\ {}_0\int^L h\varepsilon^2/k\ dn \qquad (8.12\ b)$$

where L is the layer thickness and T_k and T_ε represent lateral diffusion of k and ε respectively.

The following procedure was used to calculate the different terms in these integrations:

(i) Diffusion Terms

By integrating the k and ε equation across the entire shear layer, the lateral diffusion terms disappears, i.e.;

$$\int_0^L T_k \, dn = 0 \qquad (8.13\ a)$$

$$\int_0^L T_\varepsilon \, dn = 0 \qquad (8.13\ b)$$

(ii) Turbulence Production

With reference to Eq. (7.44 d), we see that both terms on the right hand side of this equation are related to τ which is unknown and should be found by solving the k-ε or ASM models. To get rid of this interconnection, we use the following procedure:

We can express P_k in terms of the mean velocity parameters, by noting that

$$hP_k = (\nu_t/h)\ [h\partial U/\partial n - U/R]^2 = (\tau/\rho)(h\partial U/\partial n - U/R) = (1/\rho)\ \partial(Uh\tau)/\partial n - (U/\rho)(h\ \partial\tau/\partial n + 2\tau/R) \qquad (8.14)$$

The second term on the RHS of Eq. 8.14 could be found by using the s-momentum Eq., as:

$$(U/\rho)(h\ \partial\tau/\partial n + 2\tau/R) = (1/2)\ \partial U^3/\partial s + (1/2)\ \partial(hU^2V)/\partial n + U^2V/R + (U/\rho)\ \partial P_c/\partial s + U\ U_0 dU_0/ds \qquad (8.15)$$

and finally the production term, P_k, can be expressed as

$$hP_k = (1/\rho)\ \partial(hU\tau)/\partial n - (1/2)\ \partial U^3/\partial s - (1/2)\ \partial(hU^2V)/\partial n$$
$$- U^2V/R - (U/\rho)\partial P_c/\partial s + UU_0 dU_0/ds \qquad (8.16)$$

By using the production term in this form, the shape of the shear-stress profile need not be specified. The turbulence production is related only to the dissipation of mechanical energy of the mean flow, which in turn, is related to the mean flow profiles and the rate of the growth of the shear layer.

Now, similar to what we did regarding the velocity profiles, we use the following assumptions for the k and ε profiles

$$k = k_m g(\eta) \qquad (8.17a)$$

$$\varepsilon = \varepsilon_m q(\eta) \qquad (8.17b)$$

where k_m and ε_m are the turbulent kinetic energy and dissipation scales respectively, g and q are shape functions for k and ε. After substituting Eqs. 8.13 and 8.16 and using Eqs. 8.17 in the integral form of the k and ε equations (Eqs. 8.12-a and 8.12-b), they finally yield the following ordinary differential equations;

$$-ZK0\ dk_m/ds + ZK1\ db/ds + ZK2\ dU_m/ds + ZK4\ dU_0/ds + ZK5\ dR/ds$$
$$+ ZK6 = 0 \qquad (8.18)$$

$$-ZE0\ d\varepsilon_m/dS + ZE1\ db/dS + ZE2\ dU_m/dS + ZE4\ dU_0/dS + ZE5\ dR/dS$$
$$+ ZE6 = 0 \qquad (8.19)$$

where the coefficients ZK1, Zk2, ... and ZE1, ZE2, ... are given in Appendix A.

8.3.1.2 Numerical Solution of the Equations

By integrating the governing differential equations, four basic integral equations are obtained: (1) a momentum equation for the entire flow, (2) a momentum equation for the flow in the strip shown in the Fig. 8.2, (3) a turbulent kinetic energy equation for the shear layer and (4) a dissipation equation for the shear layer. The relevant equations are in the form of linear differential equations.

The shapes of velocity profile together with the k and ε profiles must be specified for any flow condition. After the system of linear equations is solved for the derivatives, the resulting differential equations are then numerically integrated using the Runge-Kutta technique. Details of this technique are well known, and the solution of the equations is straightforward.

In order to integrate the system of differential equations, initial values must be specified for each of the dependent variables.

CHAPTER 9. THEORETICAL RESULTS

All the components of the present prediction method have now been introduced. In what follows, we examine how well the method works. The principal turbulence models of this investigation are the ASM and k-ε models. However, due to the better performance of the ASM, this model was applied to a wider range of flows.

To complete the integral solution, appropriate profiles for velocity, k and ε, boundary conditions and closure assumptions are made, and outlined for the various flow regimes under consideration. Comparisons are made wherever possible with experimental data, in order to verify the accuracy of our solutions.

The author's method was applied to the following shear layers: (i) the free turbulent jet (ii) wall jets on flat and curved surfaces and (iii) offset jets on rigid and scoured beds.

9.1.1 Studies on the modelling of turbulent free jets

Before the calculation method is applied to complex flows, the present section presents applications of the method using both of the turbulence models , to free jet flows. The purpose of including these calculations in this work is twofold. Firstly, most of the flows investigated here are fairly simple and have been well documented experimentally. The study of the comparisons between the calculated results and measured values in these simple flows can thus provide direct indication of the deficiencies in the different models. If a complex flow

is regarded as being made up of several simpler types of flow, these case-by-case studies can arguably give hints as to the causes of failures in more complicated situations. Secondly, the need for this study arises through the relationship between the simple jet flow and the flow of primary interest here - that of an offset jet. An offset jet can be said to undergo three stages of development: the free jet region, the jet-impingement and the wall jet regions. Hence, in practice, the results obtained from the initial free jet calculation can be used as entry condition for the impingment region; similarly, the results obtained from the exit of the impingement region can be used as initial condition for the wall jet region.

The basic equations and turbulence models employed in this section are those described in chapter 8. However, for the free jet, the curvature parameter, S, and the wall damping function, f_w, are set to zero.

To evaluate the integrals in Eq. (8.11) (App. A1), a velocity profile must be introduced. Based on the various experimental results, the following Gaussian-shaped profile is used for the free jet:

$$U/U_m = \exp(-0.693\ \eta^2) \tag{9.1}$$

Turbulent Kinetic Energy Profiles

In order to calculate the shear stress in the governing equations, the shape of the k and ε profiles must also be specified. To find these profiles, we, first, assume a general form for them as follows:

$$g=k/k_m = \exp(p1\ (\eta - \eta_1)^2) \tag{9.2}$$

$$q=\varepsilon/\varepsilon_m = \exp(p2\ (\eta - \eta_2)^2) \qquad (9.3)$$

where p1, p2, η1 and η2 are coefficients which depend on the flow situation. To find these coefficients, we use another four strip integral of the momentum equation which will be solved simultaneously with the other two strip-integral momentum equations and two integral equations for the transport of k and ε. The solution of these 8 equations is the basis of the prediction in all the flow situation studied herein.

9.1.1.1 Free-jet results

For the plane jet issuing into stagnant surroundings ($U_0 = 0$), predictions are presented of both of the ASM and the standard k-ε models.[10]

Table 9.1 lists the predicted rates of spread obtained from various models and calculations. Progress of jet's half-width is shown in Fig. 9.1 along with the experimental data of Reichardt (1942) and Hussein et al. (1977). It can be seen from Fig. 9.1 and Table 9.1 that the predicted rate of spread given by the k-ε model, which assumes that C_u = 0.09, is in good agreement with the experimental value. This is so, for the k-ε, because, here, the overall ratio of production of turbulent kinetic energy to its dissipation is about 1 in the plane jet, which

---

[10] It should be mentioned that due to the time limitations regarding the completion of this work, calculation were started, in most cases, from the end of the developing zone. No attempt was made to solve for the initial mixing layer which follows the jet nozzle.

is consistent with the assumption from which C_u has been found. The value of db/ds predicted by the ASM is approximately 6% higher. It was mentioned before, that the ASM in such a case gives $C_u = 0.115$ which is higher than the appropriate value of 0.09. A comparison of the predicted values obtained by Rodi et al. (1970) shows generally consistent results.

Table 9.1 Prediction of rate of spread of the free jet

Turb. Model	k-ε Present	ASM Present	Rodi et. al (1970), k-ε	Exp. Rodi (1973)
db/ds	0.111	0.118	0.108	0.11

The predicted decay of the centre-line velocity and the development of k_m/U_m^2 are shown in Figs. 9.2 and 9.3, respectively. The comparisons reveal that the values predicted by the k-ε model are again better than those given by the ASM model. As can be seen from Fig. 9.3, k_m/U_m^2 increases sharply for small values of s/b_0. Both theoretical curves reach horizontal asymptotes at high values of s/b_0. This indicates that the flow becomes self-similar at these values of s/b_0. This developing phenomenon is seen to be predicted by the present method and it shows the ability of the method to predict flows in non self-preserving cases. Progress of the k and ε profiles in downstream direction, predicted by both models, is shown in Figs. 9.4 and 9.5. Although there are no experimental results available to compare with, the general behaviour of

these profiles is, however, physically correct. These profiles progress from quite a flat distribution at x/b_0=14.2 and then they gradually develop till x/b_0=40.0 after which they remain unchanged. Downstream of an initial development region, the profiles of the turbulence quantities attain similarity, and the jet spreads linearly so that db/ds becomes constant. In Figs. 9.6-9.8, distributions of k and ε and shear stress are shown along with the experimental results for the self-similar zone. It can be seen from Fig. 9.6 that the maximum value of k/U_m^2 predicted by the k-ε model is very close to the average experimental results. For dissipation rate it is seen in Fig. 9.7 that both methods overpredict this parameter. Howsoever, it is shown that except the shift in position of maximum ε the predicted and experimental curves are identical. Taking into account the uncertainty in measuring the turbulent quantities and especially ε which is estimated from the measurement of other turbulent parameters, the general agreement of the present prediction with k-ε model is satisfactory.

In Fig. 9.8, it is observed that the maximum shear stress is well predicted by the k-ε model, and is overpredicted by 24% by the ASM model. Here, again the reason is the high value of C_μ for the ASM compared with the proper value of this parameter given by the k-ε.

9.1.2 Two-dimensional Wall Jets

This section describes applications of the author's analysis to wall jets along plane, concave and convex surfaces of constant radius and of a logarithmic spiral form.

Turbulent wall jets are important test cases, because they contain a near-wall as well as a free layer, both interacting with each other. The two layers are identified in Fig. 9.9a , where the flow configuration is sketched.

In a two-dimensional discharge from a slot situated along a wall two flow regions exist. The first zone, which immediately follows the outlet, is characterised by a core region of uniform velocity. In this zone the outer layer of the jet mixes with the ambient fluid setting up a free jet boundary while a boundary layer is formed in the region between the core and the wall. The second zone begins at the point where these two mixing regions meet. In this zone, which is analogous to the zone of established flow for a free jet, the outer region has a structural similarity to a two-dimensional free jet, whereas the inner region behaves somewhat like a boundary layer flow over a flat plate. Wall jets were found to spread significantly less than free jets; this reduction in spreading rate appears to be due not so much to the action of the wall shear stress on the flow but mainly to the damping of lateral velocity fluctuations by the wall. This damping effect penetrates into the outer layer and, since the lateral momentum transfer is closely linked to the lateral fluctuations, the shear stress and thus the spreading of the jet is reduced. Inversely, the relatively high turbulence in the outer layer has a sort of free-stream-turbulence effect on the near-wall layer.

Commonly used eddy viscosity models do not account for the damping of lateral fluctuations by the presence of a wall (unless this is put in empirically) and thus tend to overpredict the spreading of the wall jet when empirical constants are used that give the correct spreading for the free jet.

The flow in wall jets is well documented and in recent years a number of detailed turbulence measurements have been published. The literature has recently been critically reviewed by Launder and Rodi (1983).

9.1.2.1 Wall Jet on a Flat Surface

Velocity Profile

Here, as in the case of the free jet, we have to assume the shape of the velocity profile. In this case however, the velocity profile is more complicated than that of the free jet and consists of two parts, an inner layer and an outer layer.

For the inner layer, which resembles boundary layer flow over a flat plate, a 1/7th power law is assumed, therefore:

$$U/U_m = (n/\delta)^{1/7}. \qquad (9.4a)$$

where δ is the boundary layer thickness.

In the outer region where the flow is similar in nature to that of a free jet, we will assume a Gaussian-shaped velocity profile:

$$U/U_m = \exp(-0.693((n-\delta)/(b-\delta))^2) \qquad (9\text{-}4b)$$

where b is half-width of the jet, and based on experimental evidence, we can assume: $\delta = 0.15b$.

Figs. 9.10 and 9.11 show the predicted values of the jet half width b, and the maximum velocity. These results were obtained using both the k-ε and the ASM models. Fig. 9-10 shows that the ASM model predicts

sufficiently well the rate of spread of the wall jet while the standard k-ε model produces a considerably high value. This capability of the ASM model to account for the wall effect on the development of the wall jet lies in its formulation which takes into account the damping effect of v^2 by including the wall function in modelled pressure-strain distribution (Sec. 7.4.4.2). On average, the calculated value for C_u by the ASM was significantly below 0.09 which explains the reduced rate of spread as compared with the spread obtained with the standard k-ε model using $c_u = 0.09$. The same conclusion is reached about the predicted decay of U_m in comparison with the experimental data of different investigators mentioned in Figs 9.10-9.11.

Figs. 9-12 and 9-13 show the distributions of the k and ε profiles in the developed region of the wall jet. It is seen from these figures that there is slight differences in the maximum value of k/U_m^2 predicted by the ASM model and those of the experiments. However, in both figures it is shown that the k-ε model overpredicts the maximum level for both k/U_m^2 and $\varepsilon b/U_m^3$. The shape of the k distribution for values of η below the point of maximum k/U_m^2 is reasonably well predicted by both models. In the case of $\varepsilon b/U_m^3$, the ASM predicted curve is similar to the experimental one, except for the shift of the peak. Another point to note is that near the wall, the turbulence structure is under an interaction between that of a boundary layer and that of a free shear flow. This causes the distribution of both k and ε not to be expressed by simple functions like those of Eqs. 9.2 and 9.3. It is due to this interaction that in the wall jet, the shear stress does not vanish at the point of maximum velocity and there is a small region where the shear stress $-\rho uv$ and the velocity gradient $\partial U/\partial n$ have opposite signs. Obviously, this region cannot be simulated correctly with an eddy-viscosity model which requires the shear stress to vanish at the point of maximum ve-

locity. Therefore, a Reynolds stress-equation model is necessary to reproduce correctly the observed behaviour. The problematic region is however so small that its poor-prediction should not be critical in an integral solution.

9.1.2.2 Wall Jets on Curved Surfaces

Constant Radius Surface

We next consider the case of a wall jet on a curved surface of a constant radius. To see the curvature effect on the prediction method and especially to check the performance of both turbulence models we examined one of the concave cases studied by Kobayashi et al. (1983). Kobayashi et al. (1983) in their experimental work on curvature effects on two-dimensional wall jets found that the velocity profiles were in agreement with those for the plane wall jet, so that they became similar in the s direction. They also found that the half width b and the value of $(U_j/U_m)^2$ were increased for the convex wall jets and decreased for the concave wall jets. The ratio δ/b of the position of the maximum velocity to the half width (b) remained unchanged and agreed with the value 0.15 for the plane wall jet. Also, the experimental results of Fujisawa et al. (1983), showed that the velocity profiles $U/U_m = f(n/b)$ were not affected by curvature, b/R, and they were approximately in agreement with the plane wall jet results.

Hence, in the present calculation we can assume the same velocity profile for the curved wall jet as that for the plane wall jet. Developments of flow characteristics of the curved wall jet were calculated starting from $s/b_0 = 100$, at which a fully developed plane

turbulent wall jet comes into a curved surface of constant radius (R/b_0=-100). Therefore, experimental results of Kobayashi et al. (1983) at s/b_0 = 100 from the nozzle's exit were used as the starting conditions for calculations. Figs. 9-14 and 9-15 show experimental results of Kobayashi et al. for the variation of the values of the half-width and maximum velocity with downstream distance. Also given are the predicted values using the ASM and k-ε turbulence models. As is expected, due to the stabilising effect of a concave curvature on the outer part of the wall jet, turbulent quantities should be reduced and hence the spread of the wall jet should become slower than that of a plane wall jet. This phenomenon is seen in Fig. 9-14 which also shows that the agreement of the ASM predictions are very good, but the predictions by k-ε model is even worse than the plane jet case. The reason is that in this case, in addition to the non-responding nature of the k-ε to wall damping effect, it is also not sensitive to curvature effects.

To show this sensitivity of the two models to curvature effects, in Figs. 9-16 and 9-17, variation of dimensionless turbulent kinetic energy and its dissipation with the downstream distance are shown. The ASM responds correctly to the fact that with increasing the concave parameter (b/R), the level of the turbulent quantities should be more damped, while k-ε predictions are in the wrong direction.

Wall jets on logarithmic spiral surfaces

The second curved wall jet examined in this study is the self preserving (or self-similar) wall jet on a convex logarithmic spiral.

The logarithmic spiral is a surface for which the radius of curvature at any point is proportional to the arc length measured from the origin

to the point in question (Fig. 9-9b). The parameter K, which is simply s/R, is a measure of the importance of curvature. For a curved wall jet a self-preserving form is achieved when the wall jet develops on a logarithmic spiral.

A wall jet developing around a logarithmic spiral surfaces provides an excellent test case for the computational procedures for complex turbulent flows. The effect of curvature on the mixing rate is truly dramatic (more severe than in the case of a circular cylinder) and the self-preserving character of the flow means that researchers cannot blame uncertainties in the initial conditions for discrepancies in their predictions.

Kamemoto (1974) in his work on turbulent wall jets over logarithmic spiral surfaces found the following results;

1) for any logarithmic spiral surface, non-dimensional velocity profiles of the jet region are strictly similar to those of a two-dimensional plane wall jet; and

2) the growth of the jet's width, and the decay of the maximum velocity vary with the characteristic value of K=(s/R) of the logarithmic spiral;

All experimental results on this flow exhibit an acceptably linear rate of growth, corresponding to that for a self-preserving flow, except perhaps that of Kamemoto (1974) for the steepest curvature, K = 1.25. There is evidently a much stronger dependence of the growth rate on b/R than in the case of the circular cylinder. Of the three sets of data reviewed in Launder et al. (1983), the most closely two-dimensional is that of Guitton and Newman (1977) which is also particularly suitable for stress model validation in that hot-wire data were provided for all four non-zero Reynolds stresses.

Guitton and Newamn (1977) measured the characteristics of wall jets on two logarithmic spirals with values of s/R of 2/3 and of 1. Launder and Rodi (1983) correlated their results for the increase in the rate of spread with those of other workers and obtained the following relationship:

$$b/s = 0.073 + 0.8b/R - 0.3(b/R)^2, \qquad (9.5)$$

where b is the jet half-width. For s/R=1 Eq. (9.5) results in a rate of spread of 0.26 which is more than three times the value observed in plane-wall jets. As the wall curvature changes gradually in this case, the assumption that the streamlines are concentric to the local shape of the wall is sufficiently accurate.

For a wall jet on a logarithmic spiral surface, the mean velocity profile undergoes a small but consistently reproduced change of shape as K increases, becoming less pointed - more rounded - in the vicinity of the maximum velocity. The ratio of δ/b increases monotonically with K and appears well correlated by the equation

$$\delta/b = 0.159 + 0.205\ b/R \qquad (9.6)$$

proposed in Kamemoto (1974). However, Giles et al. (1966) found that the non-dimensional velocity profiles for each logarithmic spiral are of identical shape within the errors in measurements.

As the above mentioned changes of velocity distribution were not found to affect significantly the predicted results, we, in our analysis, used the velocity profile of the classical wall jet for the present case.

Amongst two cases studied by Guitton and Newman, the more severe case (R/s=1) was chosen ,herein, for prediction purposes.

Comparison of the theoretical results with the data of Guitton and Newman (1977), for s/R = 1 is presented in Figs. 9-18 and 9-19. It is seen in both figures that the algebraic-stress prediction is close to the experimental values. This is due to the inclusion of the curvature and wall-damping effects in this model which also cause the well observed difference in the spreading between a free jet and a wall jet. In Fig. 9-20, the predicted distribution of kinetic energy is shown along with the data of Guitton and Newman (1977). The prediction by the k-ε of both the level and general distribution are worse than those of the ASM model. However, the results of Gibson and Younis (1983) with a Reynolds-stress equation model for the case of s/R = 1 gives no better agreement. The standard k-ε hardly produces any sensitivity to curvature.

9.1.2.3 Two-Dimensional Offset Jets

After evaluating the capability of the present analysis, we can now turn our attention to the case of the offset jet. In this section two general cases are considered, that of an offset jet impinging on a rigid bed and the case of on offset jet discharging into a scour hole.

Rigid Bed

The discharge of a two-dimensional jet in the vicinity of a boundary is characterised by three distinct flow regions. In the first or the pre-attachment region, the jet closely resembles a two-dimensional

curved free jet. In the second zone, or the impingement region, the wall pressure is higher than the hydrostatic pressure causing the fluid to accelerate. After a short distance, the pressure distribution in the jet becomes hydrostatic. Here, in the third region, the flow behaves as if it was a wall jet.

The unique characteristics of each of the flow regions necessitates different sets of profiles and initial conditions.

1. Pre-attachment Region

For a stationary ambient we will follow previous studies in assuming that the bending of the jet does not influence the shape of the velocity profile. Therefore, the velocity profile for a free jet, given by Eq. (9-1) is used in this region:

Closure of the Governing Equations

Even after using an appropriate turbulence model to evaluate the shear stresses, we are still left with a system of 8 equations, and 9 unknowns: where the local radius of curvature is the extra unknown. In order to obtain closure of the governing equations we use the same method as that used by Stoy et. al (1973). They derived an approximate expression for the pressure, by first using the equation of motion for a vortex, $dP/dn = \rho U^2/n$. Then they assumed that the pressure gradient at the jet centreline can be approximated by $dP/dn = Pc/b$. It means that the entire pressure change takes place over a distance proportional to the jet half-width, b. Furthermore, Stoy et. al. used U_m and h/2 for U and n respectively to get the following final relationship:

$$Pc = \alpha\ b\ U_m^2/h \qquad (9.7)$$

in which α is a coefficient which was found by them to be a constant (0.75) for the range of offset they studied. This relationship will in effect give us the value of the radius of curvature.

2.The Impingement Region

This region begins at the point of re-attachment (Fig. 3.6). We assume that the jet is inflected and is now parallel to the horizontal boundary. This region is characterised by its excess pressure. Except for this, the impingement region resembles a wall jet. Therefore, the velocity profile is given by equations 9-4a and 9-4b. However, the wall jet momentum equation must be modified to account for the excess pressure in this region.

As was pointed out by Hoch (1979), the variation of surface pressure downstream of the attachment point has a similar form to that of a free impinging jet, and can be expressed by the following relationship:

$$P_w/P_{wa}=\exp[-\beta(x_s/h)^2] \qquad (9.8)$$

where x_s is the distance along the surface measured from the stagnation point, (Fig 3.8), P_w is surface pressure at x_s, P_{wa} is the wall presure at the point of impingment, and β is an empirical constant. This constant is, in effect, a pressure spread parameter, which is independent of h. and was found to be 3.4.

Following Hoch, the variation of pressure across the jet is assumed to be linear with the zero pressure at n = 1.4 b.

The boundary conditions for the impingement region are obtained by matching with the pre-attachment region at the point of re-attachment. The values of U_m and b are taken directly from the velocity profile just prior to the point of impingement.

The Wall Jet Region

As X_s becomes sufficiently large, the pressure term vanishes and the flow situation resembles that of a simple plane wall jet which was predicted earlier in this chapter.

Theoretical results for velocity distributions of the two-dimensional offset jet are presented and compared with appropriate experimental results. In addition, experimental results are given which describe the general flow field. For the purpose of comparison, in addition to my experimental results, the work done by Pelfrey (1984) was also used. Calculations were started at the end of the developing zone, with the same initial condition as that of the free jet.

Velocity Distribution

Comparisons between the theoretical and experimental results, for the pre-attachment region, are given in Figs 9.21-9.22 and Figs 9-23(a-b). The variations of the jet's half-width and the maximum velocity with distance are shown in these figures. The experimental results of Pelfrey and those of the present author are used for comparison.

It is seen in both cases that in the early stages of offset-jet development, since the curvature effect is not very strong, the flow be-

haves more-or less like in the free jet case. So in this zone, as it was shown in the prediction of the free jet, the agreement of the k-ε made with the experimental data is better. However, as the curvature effects increase in the downstream direction, the sensitivity of the ASM cause it to predict better than the k-ε model. But, as the jet approaches the impinging zone, the flow is no longer of the parabolic type and so the assumptions made for the present work are not valid. This is why the prediction in this zone is not as good as in the other part.

To see the performance of the method for the flow after impingement, the experimental velocity measurement by Hoch (1979) for h/b_0=8.7 was chosen for prediction purpose. The result of prediction is shown in Fig. 9.24. It is seen that like the other two previous cases, the performance in the pre-attachment up to the impingemnet zone is good but near impingement, the velocity is slightly overprerdicted. After impingement, due to the negative pressure gradient, the velocity is increasing which is seen to be well predicted by the present method.

Jet Trajectory

By allowing the pressure to vary in the pre-attachment region, we were not forced to assume a constant radius of curvature for the jet's trajectory. Figures 9-25 and 6-26 show the predicted jet trajectories using the ASM model for two different jet heights using my and Pelfrey's experiments. Agreement is generally good for all three trajectories, i.e. locus of the maximum velocity, dividing streamline and the locus of the upper-jet's half-width, especially in Pelfrey's case.

It is seen in Figs. 9-25 and 9-26 that although the predicted attachment length for Pelfrey's experiment is near to the experimental

one, but in both cases and especially for the present experiment it is overpredicted. The reason for this is the overprediction of maximum velocity near the impingment zone, which leads to a shorter distance between the dividing streamline and the jet's trajectory.

Finally, a general view of the flow predicted by the ASM model for the upper part of the offset jet for Pelfrey's and the present author's experiments are shown in Figs. 9-27 and 9-28. These figures can be compared with the experimental results shown in Figs 2.11 and 5.3.

9.1.2.4 Offset jet in scour hole

The final prediction was made for an offset jet in a scour hole. Comparison was made with the test case (S205) of the author's experiments on scour holes. In this case it was assumed that the flow in the pre-attachment region behaved like an offset jet with its jet height equal to the difference between the level of the jet nozzle and that of half the maximum scour depth. The flow after impingement is a wall jet on a concave surface with excess pressure due to impingement.

Figs. 9-29 and 9-30 show the predictions for the maximum velocity and for the half width of the jet. Here, like the rigid-bed case, fair prediction is produced, especially using the ASM model. In Fig. 9.31 prediction of the jet's centerline and dividing streamline by the ASM model are shown along with the present experimental results for the position of maximum velocity. Generally, good agreement between the predicted and experimental results of the jet centerline is observed. However, similar to the case of the offset-jet impinging on a rigid bed, the position of the attachment point, which in this case is nearly the

same as the position of maximum scour section, is overpredicted. But the error in this case is less than in the case of the rigid bed. One of the reason for the better theoretical results in this case is that the impingment of the jet on the scour hole is not as sharp as in the rigid-bed case, so the deviation from the parabolic behaviour is less.

This method of predicting the velocity distributions can be used to find the progress of the maximum depth of the scour hole caused by an offset jet. The author's suggestion for the method of solution is similar to that of Nik-Hassan (1985) whose semi-empirical calculation required the local velocity to be known (see Sec. 2.4.1).

The suggestion for the method of calculation is as follows:

(1) Starting at t=0 and d_m=0, calculate the maximum velocity above the point of attachment using the author's theory.

(2) Solve Eq. 2.16 (Sec. 2.4.1, page 26) for the first time step and obtain d_m.

(3) Proceed to the next time step and repeat the calculation in (1) and (2) using now the calculated value of d_m from the previous step as the initial condition.

It must be pointed out that the present author's method doesn't rely on an assumption of similarity for the scour hole profiles or on using an empirical equation to find the local velocity as required in Nik-Hassan's (1985) method.

9.1.3 Conclusions

Predictions for the development of mean flow fields, for curved wall jets, were verified using various experimental results.

It was shown that using a simple method for the solution of the complicated governing equations of the flow together with sophisticated turbulence modelling techniques resulted in a generally efficient method for the prediction of complex flows.

From the point of view of the performance of different turbulence models, it was shown that except for the free-jet case, the best overall agreement for all of the other test cases was obtained using the algebraic-stress model. This model was derived by simplifying a Reynolds-stress-equation model and does not involve any curvature-specific empirical modification to the k-ε equations. In all test cases, this model was found to work well in regions where curvature was pronounced.

In conclusion, the algebraic-stress model is the most promising tool for obtaining economic solutions of flow problems involving streamwise curvature. The model produces results that, from a practical point of view, are only slightly inferior to those obtained with the parent Reynolds-stress-equation model. Certain details of the flow, like the differences in the locations of zero shear stress and zero velocity gradients in wall jets, can only be predicted with the latter more complex model. These details are of little practical importance.

The present method also proved adequate for the calculation of relatively more complex wall-jet flows.

It should be mentioned that one of the restriction of the present method, like other parabolic methods is that the main streamline of the flow should be defined in some way, as it was the case for the offset jet predictions.

CHAPTER 10. CONCLUSIONS AND RECOMENDATIONS

10.1 INTRODUCTION

Major conclusions of the experimental and theoretical studies are grouped and discussed separately in the following subsections. However, some aspects of the problem were not studied and some new questions also arise from this study and much scope remains for further work on both the computational and experimental part of the problem. Recommendations are therefore made at the end of the chapter concerning the clarifications needed and directions in which future research may be undertaken.

10.2 CONCLUSIONS ON THE EXPERIMENTAL PART

In the experimental part of this work, the two-dimensional offset jet and scour produced by it were investigated.

10.2.1 Offset-Jet Impinging on a Rigid Bed

The characteristics of the turbulent plane offset jet flow, with a single offset ratio but with different discharges were examined.

Comparison of the attachment length with the experimental results of previous investigations showed good agreement.

Detailed mean horizontal and vertical velocity components were measured in the pre-attachment region. Using these components, a plot of velocity vectors was made which provided a clear visualisation of the offset jets flow and in particular the recirculation region and the jets curvature. The jet is observed to curve slowly through the first half of the recirculation region and then turn sharply downward to the attachment point.

10.2.2 Scour Experiments

Clear water scour tests were conducted with deeply submerged offset jets of varying heights and with different discharges. In all these tests,the tailwater depth, the slot's thickness, and the sediment size were kept constant.

A new method for the measurement of scour profile, during its formation, was developed. The accuracy of the measurement by this method was confirmed by measurements of the scour profile using a depth gauge, especially at the asymptotic stage.

The maximum depth of scour was found to be not solely a function of the densimetric Froude number and time. But also, the jets height had a pronounced effect on the development of the scour profile. A larger and deeper hole was obtained for tests with a smaller jet height. Also, at the asymptotic state, it was found that an offset jet with a smaller height scoured a deeper hole than that caused by a jet with a bigger height.

Using dimensional analysis, a regression analysis was performed to provide a relationship by which the maximum scour depth, after any time, could be estimated. This relationship applies up to the asymptotic state.

The centreline bed profiles for any jet height, and for different scouring times and different discharges were found to be similar, provided d_m and X_{p2} were used for the depth and length scales, respectively where X_{p2} is the distance from the jet exit to the position of the second peak and d_m is the maximum depth of scour (Fig. 6.1). However, as the jet height increases, the non-dimensional profile changes and becomes steeper on the upstream face with the height of the upstream ridge increasing while that of the downstream ridge decreasing.

Measurement of the velocity distributions in one of the tests, at the asymptotic stage was undertaken. The velocity distributions along the centreline bed profile revealed that, as in the case of the offset jet impinging on a rigid bed, decay of the maximum velocity was enhanced as the curvature effect increased in the pre-attachment region. However, downstream of impingement, due to both negative pressure gradient and the decrease in the depth between the bed and the water surface, the maximum velocity increased for some distance and then continued to decrease.

It was also observed that the location of the position of maximum scour corresponded to the location of the jet's attachment.

10.2.3 Conclusions on the Theoretical Work

The present theoretical work was concerned with the development and verification of a numerical solution procedure capable of simulating steady, incompressible, two-dimensional turbulent jet flow under the influence of various geometries. The procedure allows flexibility with respect to flow curvature and wall effect. Two particular features of the solution algorithm, namely integration of the governing equations and the marching-forward solution allow substantial computer-storage and solution-time economy.

More often, in the integral methods, the absence of a hypothesis concerning the local structure of the turbulence appears to be a draw-back of the method. However, in the present study, by using advanced turbulence models (k-ε and ASM), it was tried to develop an integral method applicable to a wide range of flows without the need for prob-lem-dependent treatment.

Indeed, one major accomplishment of this work is in opening up some potential avenues for future refinement of the integral method accom-panied by the sophisticated turbulence modelling which have not previ-ously been reported.

A significant part of the present research effort was devoted to validation tests of the computational model, in which a total of six different geometries were considered. Four of the cases were not di-rectly related to the offset configuration, but share with the offset flow some fundamentally important physical features, or expedite an assessment of major aspects of the numerical algorithm.

The extensive validation programme showed that the computational model is capable of capturing the main features of each flow.

Comparing the results obtained by the two turbulence models, the algebraic stress model gave a clearly superior performance in most of the flows tested, especially in curved flows. The k-ε model failed to respond to the introduction of wall and curvature effects and therefore the results predicted using this model were inferior. However in the case of a free turbulent jet it was k-ε which gave a better agreement with the experimental data because of a proper choice for its C_u coefficient.

In the case of an offset jet impinging on rigid and moveable beds, agreement between the predicted flow field and the experimental results is satisfactory. Some discrepancies persist when the impingement zone is approached. The reason for this disagreement around this zone is that in the derivation of the integral method, the flow was assumed to be parabolic, while the flow field near the impingement zone is clearly of an elliptic type.

The predicted trajectories of the offset jet were in sufficiently good agreement with the experimental results. However, due to the overprediction of the velocity near the impingement region, the attachment length was overpredicted.

Good agreement between the theoretical and experimental velocities in the scour hole, provided a basis for further work on the prediction of the development of the scour hole.

10.3 SUGGESTIONS FOR FUTURE WORK

The work presented, herein, on the scouring action of an offset jet is only an initial step, in a very complex field. The relationships already established require further verification before they could be generally accepted for use in any situation. The need to study the effect of wider ranges of parameters is of great importance. For example, the effect of the sediment size and downstream water depth on scour development were not investigated. Effects of the jet's height and jet discharge were investigated for a limited range and all these parameters need further investigation.

Effect of the eroded profile on the diffusing jet was studied only for the asymptotic stage by measuring the velocity distributions. Measurements of the velocities within the scour hole, during its development, using fixed-bed models is needed for an overall understanding of the scour process.

Further work is required to verify the proposed theoretical method for the calculation of velocities in the offset jet. This could be achieved by the measurement of mean and turbulent velocity and also by the measurement of the pressure distribution for a number of different offset ratios.

To combine the experimental and theoretical work to find scour hole development, it is highly recommended to apply the present flow prediction method in conjunction with some scour-hole prediction model requiring only the information about mean velocity field.

The observed disagreement between the predicted and measured velocity field near the impingement region necessitates further consider-

ation. One way to solve this problem might be to use a combination of parabolic and elliptic schemes for simulation of the offset jet.

REFRENCES

1. Abdel-Gawad, S.M. and McCorquodale, J.A., "Strip integral method applied to settling tanks", J. of Hyd. Div., ASCE, 1984, 110, No. HY1, pp. 1-17.

2. Albertson, M.L., DAI,Y.B.,Jensen, R.A.and Rouse, A., "Diffusion of submerged jets ",Trans. A.S.C.E., VOL. 115, Paper No. 2409, 1950, PP. 639-664.

3. Ali, K.H.M. and Halliwell, A.R. "The use of water-jets for scouring and dredging", 3rd. Int. Symp. on Dredging Technology, BHRA, Bordeaux, France, March 1980, PP. 239-266.

4. Altinbilek, H.D. and Basmaci, Y. "Localised scour below submerged vertical gates", Proc. of the Speciality Conf. on "Computer and Physical Modelling in Hydraulic Engineering", Chicago, Illinois, Aug. 6-8, 1980, PP. 39-50.

5. Anderson, A.G., closure of "Sedimentation Transportation Mechanics: Erosion of sediment", by the Task Committee on Sedimentation, J. of Hyd. Div., ASCE, Vol. 89, no. HY6, Nov. 1963, PP.237-247.

6. Ayukawa, K., and Shakouchi, T., "Analysis of a Jet Attaching to an Offset Parallel Plate," Bull. of JSME, V19, 1976, PP. 395-401.

7. Anwar, H.O., "Behavior of Buoyant Jet in Calm Fluid", ASCE J. of Hydraulics Div., 91, HY 4, 1965.

8. Beltaos, S. and N. Rajaratnam, "Plane Turbulent Impinging Jets", J. of Hydraulic Research, 11, 1973.

9. Beltaos, S. "Oblique Impingement of plane Turbulent Jets", ASCE J. of the Hydraulic Division, 102, HY9, 1976.

10. Boussinesq, J., "Theorie de l'ecoulement tourbillant", Memories Presentes par Divers Savants Sciences Mathematique at Physiques, Academies des Sciences, Paris, Vol. 23, 1877, pp. 46.

11. Bourque, C., "Reattachment of a Two-Dimensional Jet to an Adjacent Flat Plate," Advances of Fluidics, ed. by F. T. Brown, ASME, New York, 1967, PP. 192-204.

12. Bourque, C., and Newman, B. G., "Reattachment of a two-Dimensional Incompressible Jet to an Adjacent Flat Plate", Aeron. Quar., V11, Aug. 1960, PP. 201-232.

13. Bradbury, L.J.S., "The structure of a self-preserving turbulent plane jet", Journal of Fluid Mechanics Vol. 23, Part 1, 1965, pp. 31-46.

14. Bradshaw, P., "The effects of streamline curvature on turbulent flow", AGARDograph, No. 169, 1973.

15. Bradshaw, P., Ferriss, D.H. and Atwell, N.P., "Calculation of boundary layer development using the turbulent energy equation", J. Fluid Mech., Vol. 28,PP. 593-616, 1967.

16. Bradshow, P, and Ferriss, D.H., "Applications of a general method of calculating turbulent shear layers", J. Basic Eng., Trans. ASME, Series D, 94, P. 345, 1973.

17. Bradshaw, P. and Gee, M. T., "Turbulent wall jets with and without external stream", Aero. Res. Council, RM 3252, 1960.

18. Boucher, R.F., "Incompressible jet reattachment analysis using a good free jet model", Third Cranfield Fluidics conference, 8-10 May, 1968, F1-I.

19. Brown, F.T., and Simpson, A.K., M.I.T. Department of Mechanical Engineering Report, 1964.

20. Balfour, J.A.D, "Flow patterns during the development of a scour hole", Project Thesis, Heriot-watt University, Edinburgh, 1973.

21. Castro, I.P. and Bradshaw, P., "The turbulence structure of highly curved mixing layer", J. of Fluid. Mech., Vol. 73, 1976, pp. 265-304.

22. Coates, A.D, "The numerical and experimental studies on the Dynamics of Fluid", Ph.D. Thesis, Heriot-watt University, Edinburgh, 1976.

23. Carstens, M.R., "Similarity Laws for Localised Scour ", J. of Hyd. Div., Proc. ASCE, Vol. 92, No. HY3, May 1966, PP. 13-36.

24. Cebeci, T. and Smith, A.M.O., "Analysis of Turbulent Boundary Layers", Applied Mathematics and Mechanics, Vol. 15, Academic Press, New York, 1974.

25. Chatterjee, S.S and Ghosh, S.N., "Submerged horizontal jet over erodible bed", J. of Hyd.,Proc. ASCE, Vol. 106, No. HY 11,Nov., 1980.

26. Crawford, M.E. and Kays, W.M., "STAN-5 A program for numerical computation of two-dimensional internal / external boundary layer flows", Stanford University, Dept. Mech. Eng., Report HMT-23, 1975.

27. Daly, B.J. and Harlow, F.H., "Transport equations of turbulence", Phys. Fluids, 13, P.2634, 1970.

28. Fan, L.N., and Brooks N.H., "Numerical Solutions of Turbulent Buoyant Jet Problems", W. M. Keck Laboratory for Hydraulics and water Resources, California Institute of Technology, Pasadena, California, Report No. KH-R-18, 1969.

29. Forthmann, E., "Uber turbulente srahlausbreitung", Ing. Arch., 5, 42,, 1934.

30. Gartshore, I.S. and Newman B.G., "The turbulent wall jet in an arbitrary pressure gradient", Journal of Aeronautical Quarterly, 1969, pp. 25-57.

31. Gibson, M.M., Jones, W.P. and Younis, B.A., "Calculation of turbulent boundary layer on curved surfaces", phys. Fluids, 24, p.386, 1981.

32. Gibson, M.M. and Launder, B.E., "Ground effects on pressure fluctuations in the atmospheric boundary layer", J. Fluid Mech., 86, P. 491, 1978.

33. Gibson, M.M. and Younis, P.A., "Calculation of a turbulent wall jet on a curved wall with a Reynolds stress model of turbulence", Proc. 3rd. Symposium on turbulent shear flows, Davis, calif,1981.

34. Gibson, M. M. and Rodi, W., "A Reynolds-stress closure model of turbulence applied to the calculation of a highly curved mixing layer", J. of Fluid Mech., Vol. 103, 1981, pp. 161-182.

35. Gillis, J.C. and Johnston, J.P., "Turbulent boundary layer on a convex curved surface", Mech. Eng. Dept., Stanford Univ., Stanford, CA, Rept. HMT-31, 1980.

36. Giles, J.A., Hays, A.P. and Sawyer, R.A., "Turbulent wall jets on logarithmic spiral surfaces", Aeronautical Quarterly, Vol. 17, p.201, 1966.

37. Guitton, D.E. and Newman, B.G., "Self-preserving wall jets over convex surfaces", Journal of Fluid Mechanics, Vol. 81, p.155, 1977.

38. Guitton, D. E., "Some contributions to the study of eqilibrium and non-equilibrium wall jets over curved surfaces", PhD thesis, McGill University, 1970.

39. Gortler, H., "Berechunug von Aufgaben der freien Turbulenz auf Grund eines neuen naherungsansatzes", Z. Angew. Math. Mech., V22, 1942, P. 244.

40. Gosman, A.D., Khalil, E.E., Whitelaw, J.H., "The calculation of two-dimensional turbulent recirculating flows", Turbulent Shear Flows I, Springer Verlag, Heidelberg, 1979.

41. Gutmark, E. and Wygananski, I. J. Fluid Mech. Vol. 73, 1976, p. 465.

42. Hanjalic, K. and Launder, B.E., "A Reynolds-stress model of turbulence and its application to thin shear flows", J. Fluid Mech., 52, P. 609, 1972.

43. Head, M. R., "Entrainment in the Turbulent Boundary layer", ARC RM 3152, Sept. 1985.

44. Hinze, O., "Turbulence", McGraw Hill, New York, 1959.

45. Hirst, E., "Analysis of Round, Turbulent, Buoyant jets Discharged to Flowing. Stratified Ambients," ORNL Report 4685, Oak Ridge National Lab., Oak Ridge, Tenn., 1971.

46. Hoch, J., "Two-dimensional jet-boundary interaction for submerged thermal discharges", Doctoral Dissertation, The City Univ. of New York, 1979.

47. Hoch, J., and Jiji, L. M., "Two-Dimensional Turbulent Offset Jet-Boundary Interaction", ASME J, of Fluids Enger., V103, Mar. 1981, PP. 154-161.

48. Hussain, A.K.M.F. and Clark, A.R., Phys. of Fluids, Vol. 20, 1977, pp 1416.

49. Irwin, H.P.A.H. and Arnot Smith, P., "Predictions of the effect of streamline curvature on turbulence", Phys. Fluids, Vol. 18, No. 6, PP. 624-630, 1975.

50. Jiji, L. M. and J. Hoch, "Submerged Thermal Discharges", Department of Mechanical Engineering, The city University of New York, Report No. 101, 1975.

51. Jiji, L. M. and J. Hoch, "Analysis of the zone of flow Establishment for Buoyant Turbulent Jets in Cross Flow", International Center for Heat and Mass Transfer, Dubrovnik, Yugoslavia, September 1976.

52. Johnston, A.J., "An experimental study of shallow submerged turbulent jets". PHD Thesis. Department of civil Engineering, Heriot-watt University, 1978.

53. Jones, W.P. and Launder, B.E., "The prediction of Laminarization with a two-equation model of turbulence", Int. J. Heat and Mass Transfer, 15, 301, 1972.

54. Keller H. B. and Cebeci, T., "Accurate numerical methods for boundary-layer flows - I. Two-dimensional laminar flows", Lecture Notes in Physics, 8, Proceedings of the Second International Conf. on Numerical Methods in Fluid Dynamics, p. 92, Springer-Verlag, Berlin and New York, 1971.

55. Keller, H. B. and Cebeci, T., "Accurate numerical methods for boundary-layer flows - II. Two-dimensional turbulent flows", AIAA J., 10, p. 1193, 1972.

56. King, R., "The effects of scouring by a two-dimensional water jet", BSc Project. Liverpool Univ., Dept. of Civil Eng., 1985.

57. Kolmogorov, A.N., "Equations of turbulent motion of an incompressible Fluid", Izv. Akad. Nouk. SSR, Seria fizicheska Vi., No. 1-2, PP. 56-58, 1942 (English translation : Imperiol College, Mech. Eng. Dept. Rept. ON/6, 1968.

58. Kumads, M., Mabuchi, I., and Oyakawa, K., " Studies in Heat Transfer to Turbulent Jets with Adjacent Boundaries (3rd Report, Mass Transfer to Plane Turbulent Jet Reattached on an Offset Parallel Plate)", Bull. of JSME, V16, 1973, PP. 1712-1722.

59. Kememoto, K., "Investigation of turbulent wall jets over logarithmic spiral surfaces. Part 1: Development of jets and similarity of velocity profile. Part 2: Properties of flow near wall", Bulletion of the Japan Society of Mechanical Engineers, Vol. 17, No. 105, p.335, 1974.

60. Kobayashi, R. and Fujisawa, N., "Curvature effects on two-dimensional turbulent wall jets", Ingenieur Archiv. Vol. 53, p. 409, 1983.

61. Launder, B.E., Priddin, C.H., and Sharma, B.I., "The calculation of turbulent boundary layers on spinning and curvaed surfaces", J. Fluids Engng., 99, pp. 231-239, 1977.

62. Launder, B.E. and Rodi, W., "The turbulent wall jet", Progress in Aerospace Science, Vol. 19, p. 81, 1981.

63. Launder, B.E and Rodi, W., "The turbulent wall jet - measurements and modelling", Annual Review of Fluid Mechanics, Vol. 15, p. 429, 1983.

64. Kobayashi, R and Fujisawa, N., "Turbulence measurements in wall jets along strongly concave surfaces", Acta Mech. 47, 1983 pp. 39-52.

65. Launder, B.E., Morse, A.P., Rodi, W. and Spalding, D.B., "The prediction of free-shear flows -a comparison of the performance of six turbulence models", Proc. NASA Langley free Turbulent shear flows Conf., Vol. 1, NASA SP 320, 1973.

66. Launder, B.E. and Ying, W.M., "The prediction of flow and heat transfer in ducts of square cross section", Proc. Inst. of Mech. Engrs., Vol. 187, 1973, pp.37-73.

67. Launder, B.E. and Spalding, D.B., "The numerical computation of turbulent flow", Comp. Meth. in Appl. Mech., and Eng., 3, P. 269, 1974.

68. Laursen, E.M., "Observations on the nature of scour" Proc. of 5th Hyd. Conf., Bull. 34, Univ. of Iowa. Iowa, 1952, PP. 179-197.

69. Le Feuvre, A.R., Altinbilek, H.D., and Cartens, M.R., "Sediment pickup function", J. of Hyd. Div., Proc. ASCE, Vol. 96, No. HY 10, Oct. 1970, PP. 2051-2063.

70. LIM S. Y. Scour and particle diffusion caused by water jets. PHD thesis, University of Liverpool, 1985.

71. McGuirk, J.J. and Rodi, W., "The calculation of three-dimensional turbulent free jets", Turbulent Shear Flows I, Springer Verlog, Heidelberg, 1979.

72. Mahajan, B. M., and John, J. E. A., "Mixing of a Shallow Submerged Heated Water Jet with an Ambient Reservoir", AIAA Journal, American Institute of Aeronautics and Astronautics, Vol. 9, No. 11, Nov., 1971,pp. 2135-2140.

73. Mc Corquodale J.A. and Khalifa A.M., "Internal flow in hydraulic jumps", J. of Hyd. Engng., ASCE, Vol. 109, No. 5, 1983, pp. 684-701

74. Moses, H.L., "A strip-integral method for predicting the behaviour of the turbulent boundary layers", Stanford Conference, Stanford, Calif., 1968.

75. Myers, G.E., Schauer, J.J., and Eustis, R.H., "Plane turbulent wall jet flow development and friction factor", Tech. Rep. No. 1, Mech. Engng. Dept., Stanford Univ., Stanford, 1961.

76. Narayanan, R., "Theoretical analysis of flow past leaf gate", J. of Hyd. Div., ASCE, Vol. 98, No. HY6, 1972, pp. 993-1011.

77. Nik-Hassan, "Erosion of alluvial bed downstream of a sluice gate", PhD thesis, UMIST, England, 1985.

78. Norris, L.H. and Reynolds, W.C., "Turbulent channel flow with a moving wavy boundary", Stanford Univ., Dept. Mech. Eng., Rept. FM-10, 1975.

79. Nozaki, T., Hatta, K., Sato, N., and Matsumura, H., "Reattachment Flow Issuing from a Finite Width Nozzle (Report 2. Effects of lnitial Turbulence lntensity)", Bull. of JSME, V24, n188, Feb. 1981, PP. 363-369.

80. Paizis, S. T., and Schwarz, w. h., "Entrainment rates in turbulent shear flows", J. of Fluid Mech., V68, 1975, PP. 297-308.

81. Parameswaran, V., and Alpay, S.A., "Studies on Re-attaching Wall Jets", Trans. of Canadian Socity of Mech. Engr., V3, 1975, PP. 83-89.

82. Patanker, S.V. and Spalding, D.B., "Heat and mass transfer in boundary layers", Morgan-Grampian, London, 1967.

83. Perry, C. C., "Two-dimensional Jet Attachment", Advances in Fluidics, ed. by F. T. Brown, ASME, New York, 1967, PP. 205-217.

84. Pelfrey, J.R.R., "Characteristics of a turbulent plane offset jet", PhD Diss., Clemson Univ., 1984.

85. Prandtl, L., "Influence of stabilising forces on turbulence", Vortrage vas dem Gebeite der Aerodynamik und verwandte Gebite, Achen, 1929.

86. Prandtl, L., Uber die ausgebildete Turbutenz, ZAMM, 5, P.136, 1925.

87. Prandtl, L., Bemerkungen zur Theorie der freien Turbulenz, ZAMM, 22, PP. 241-243, 1942.

88. Prandtl, L., Uber ein neues Fromelsystem fur die ausgebildete turbulenz, Nachr Akad. Wiss., Gottingen, Math.-Phys. Klasse, p. 6, 1945.

89. Rao, R., and Sarma, K.V.N., "The scour function", journal of institution of Engineers, India, vol. 47, C13, part 5, 1967, pp. 260-286.

90. Rajaratnam, N., "Turbulent Jets", Elsevier Scientific Publishing Co., Amsterdam, The Netherlands, 1976.

91. Rajaratnam, N., "Erosion by plane turbulent Jets", J. of Hydr. Res., IAHR, Vol. 19, No. 4, 1981, Delft, PP. 339-357.

92. Rajaratnam, N. and Beltaos, S. "Erosion by Impinging Circular Turbulent Jets", J. of Hyd. Div., Proc. ASCE, Vol, 103, No. HY10, Oct. 1977, PP. 1191-1205.

93. Rajaratnam, N. and Berry, B., "Erosion by Circular turbulent wall jets", J. of Hydr. Res., IAHR, Vol. 15, No. 3, 1977, Delft, PP. 277-289.

94. Rajaratnam, N. and Humphries J.A., "Diffusion of bluff Wall Jets in Finite Depth Tailwater", J. of Hyd. Engineering, Vol. 109, No. 11, Nov. 1983, PP. 1471-1486.

95. Rajaratnam, N., and Macdougall,R.K. "Erosion by plane wall jets with minimum tailwater", Technical Notes, J. of Hyd. Engineering, ASCE Vol. 109, No. 7, July, 1983, PP.1061-1064.

96. Rajaratnam, N., and Subramanya, N., "Plane Turbulent Reattached wall Jets", ASCE J. of Hydraulics Div., V94, HY1,1968, PP. 95-112.

97. Raghunat, G., Liburdy, J.A., "Predictions of a turbulent offset jet", AIAA/ASME 4th Joint Fluid Mech., Plasma Dynamics and Laser Conference, May 12-14 1986, Atlanta, GA, USA.

98. Reynolds, O., 1895 On the Dynamical theory of incompressible viscous fluids and the Determination of the Criterion. Trans. Royal soc., A, 186, p. 123.

99. Rodi, W., "The prediction of free turbulent boundary layers by use of a two-equation model of turbulence", Ph.D. Thesis, University of london, 1972.

100. Rodi, W., "A note on the empirical constant in the Kolmogorov-Prandtl eddy-viscosity expression", J. of Fluids Engg., Trans. ASME, PP. 386-389, sept. 1975.

101. Rodi, W.," A new algebraic relation for calculating the Reynolds stresses", ZAMM 56, T219-T221, 1976.

102. Rodi. W, "Turbulence models and their applications in hydraulics-A state of the art review", IAHR. Delft, 1980.

103. Rodi, W. and Scheuerer, G., "Calculations of curved shear layers with two equations turbulence models", The Physics of Fluids, Vol. 26, 1983, pp. 1422-1436.

104. Rossiniski, K.I., "Hydraulic of Scouring Pits", Chapter 2 from "Problems of River Runoff Control", Acad. Sci. Ussr., Section for Scientific Study of Water Engineering Problems, 1961.

105. Rastogi, A.K. and Rodi, W., "Calculation of general three-dimensional turbulent boundary layers", AIAA Journal, 16, PP. 151-159, 1978.

106. Rastogi, A.K. and Whitelaw, J.H.,"Procedure for predicting the influence of longitudinal curvature on boundary-layer flows", ASME Paper 71-WA/FE-37, 1971.

107. Reichardt, H. "Gesetzmassigkeiten der freien turbulenz", VDI-Forschungsheft, 414, 1942.

108. Robins, E., "The structure and development of a plane free jet", ph.D. thesis, University of London, 1971.

109. Rotta, J.C., "Statistische Theorie nichthomogener Turbulenz", Zeitschrift f. Physik, Bd. 192, PP. 547-572, and Bd. 131, PP. 51-77, 1951 (English translation : Imperial College, Dept. of Mech. Eng., Reports TWF/TN/38, 39, 1968.

110. Rotta, J.C., "Turbulente Stromungen", B.G. Teubner, Stuttgart, 1972.

111. Rouse, H., "Criteria for Similarity in the Transportation of Sediment", Proc. Hyd. Conf. Studies Engineering Bull., Univ. of Iowa, 1939 PP. 33-49.

112. Saffman, P.G., "A model for inhomogeneous turbulent flow", Proc. Roy. Soc., Ser. A, 317, P. 417, 1970.

113. Sarma, K.V.N., "Existence of limiting scour depth", Journal of the Instn. of Engineers (India), Vol. 48, No. 1, Cl, Sept. 1967, PP. 84-92

114. Sawyer, R.A., "Two-dimensional turbulent jets with adjacent boundaries", PhD. thesis, Cambridge University, 1962.

115. Sawyer, R. A., "The flow due to a two-dimensional jet issuing parallel to a flat plate", J. of Fluid Mech., V9, 1960, PP. 543-560.

116. Sawyer, R. A., "Two-dimensional reattaching jet flows including the effects of curvature on entrainment", J. of Fluid Mech., V17, 1963, PP. 481-498.

117. Schichting, H., "Boundary Layer Theory", McGraw Hill, New York, 1966.

118. Spalding, D.B., "The k-W model of turbulence", Imperial College, Dept. Mech. Eng., Report (TM/TN/A/16), 1971.

119. Squire, H.B. and Trouncer, J., "Round jets in a general stream", Aeronautical Research Committee, Rep. and Mem. No. 1974, 1944.

120. Stoy, R. L., Stenhouse, M. H., and Hsia, A., "Vortex Containment of Submerged Jet Discharge", Journal of the Hydraulics Division, ASCE, Vol. 99, No. HY9, Proc. Paper 9999, Sept., 1973, pp. 1585-1597.

121. Stephenson, P.L., "Theoretical study of heat transfer in two- dimensional turbulent flow in a circular pipe and between parallel and diverging plates", Int. J. Heat Mass Transfer, Vol. 19, pp. 413-423, 1976.

122. Shir, C.C., "A preliminary numerical study of atmospheric turbulent flow in the idealized planetary boundary layer", J. Atmos. Sci. 30, p. 1327, 1973.

123. Tatchel, D.G., "Convection processes in confined three-dimensional boundary layers", PhD. Thesis, University of London, 1975.

124. Tailland, A., "Contribution ltude dun jet plan dirig tangentiellement une paroi plane", Th se de Docteur es Sciences, Univ. Claude Bernard, Lyon, 1970.

125. Tarapore, Z.S., "Scour below a submerged sluice gate", MSC Thesis presented to the Univ. of Minnesota, Minneapolis, Minn., 1956.

126. Townsend, A.A., "The structure of turbulent shear flows", Cambridge Univ. Press, Cambridge, 1976.

127. VALENTIN, F., "Considerations concerning scour in the case of flow under gates", 12th. Congr. IAHR, Vol. 3, Fort Collins, 1967, PP. 92-96.

128. Van Driest, E.R., "On turbulent flow near a wall", J. Aero. Sci., 23, P. 1007, 1956.

129. Van der Hegge, B.G., "Measurements of the velocity distribution in a plane turbulent jet of air", Appl. Sci. Res., Sec. A, 7, 256-272 1958.

130. Verhoff, A., "Steady and pulsating two=dimensional turbulent wall jets in a uniform stream", Princeton University Rept. No. 723, 1970.

131. Whittington, R.B.,"A simple dimensional method for hydraulic problems", J. of Hyd. Div., Proc. ASCE, Vol. 89, No. HY5, Sept. 1963, PP. 1-27.

132. Wilcox, D.C. and Chambers, T.L., "Streamline curvature effects on turbulent boundary layers", AIAA journal, Vol. 15, 1977, pp. 574-580.

APPENDIX A.

The final form of Eq. (8.3) after using Eqs 8.7 and 8.10 and simplifying the expression, is:

$$A_{ij}\ db/dS + E_{ij}\ dU_m/dS + H_{ij}\ dU_0/dS = J_{ij}\ dR/dS + K_{ij}$$

where

$$A_{ij} = U_m\ (-2U_0\ HFP111 - U_m HFP112 + h_j U_j\ FP11_{0j} - h_i U_i FP11_{0i}) + b/R$$
$$[U_m^2(HP011 - FE12) + 2U_0 U_m(HS011-FE11) + U_0^2(HM011-FE10)]$$

$$E_{ij} = b(2U_0\ HF011 + 2U_m\ HF012 - h_j U_j\ FE01_{0j} + h_i U_i\ FE01_{0i})$$
$$+(2b^2/R)(U_m\ HP011 + U_0\ HS011)$$

$$H_{ij} = b(2U_0\ HH01 + 2U_m\ HF011 - h_j U_j\ FE00_{0j} + h_i U_i\ Fe00_{0i})$$
$$+(2b^2/R)(U_m\ HS011 + U_0\ HM011)$$

$$J_{ij} = (b/R)^2(U_m^2\ HP011 + 2U_m U_0\ HS011 + U_0^2\ HM011)$$
$$K_{ij} = -h_0 V_0\ (h_j U_j - h_i U_i) + h_j^2\ \tau_j/\rho - h_i^2\ \tau_i/\rho$$

and different integral values (between η_i and η_j) are defined as follows:

$$FEab = \int \eta^a\ f^b\ d\eta$$
$$GGab = \int \eta^a\ g^b\ d\eta$$
$$QQab = \int \eta^a\ q^b\ d\eta$$
$$FPab = \int \eta^a\ (f^b)'\ d\eta$$
$$FGab = \int \eta^a\ (fg)^b\ d\eta$$
$$FGPab = \int \eta^a\ (fg^b)'\ d\eta$$
$$GPab = \int \eta^a\ (g^b)'\ d\eta$$

$$-ZK0\ dk_m/ds + ZK1\ db/ds + ZK2\ dU_m/ds + ZK4\ dU_0/ds + ZK5\ dR/ds + ZK6 = 0 \qquad (8.18)$$

$$-ZE0\ d\varepsilon_m/ds + ZE1\ db/ds + ZE2\ dU_m/ds + ZE4\ dU_0/ds + ZE5\ dR/ds + ZE6 = 0 \qquad (8.19)$$

where

$$ZK0 = b(U_0\ GG01 + U_m\ FG01)$$

$$ZK1 = WK1 - k_m[U_m(g_j FP11_{0j} - g_i\ FP11_{0i} - FGP11) - U_0\ GP11]$$

$$ZK2 = WK2 - bk_m[FG01 - g_j\ FE01_{0j} + g_i FE01_{0i}]$$

$$ZK3 = WK3 - k_m[U_m(g_j\ FP01_{0j} - g_i FP01_{0i} - FGP01) - U_0\ GP01]$$

$$ZK4 = WK4 - bk_m[GG01 - g_j\ FE00_{0j} + g_i FE00_{0i}]$$

$$ZK5 = WK5$$

$$ZK6 = WK6 - k_m h_0 V_0(g_j - g_i) - b\varepsilon_m\ HQ01 + (h\nu_t/\sigma_k\, \partial k/\partial n)\big|_{ni}^{nj}$$

$$ZE0 = b(U_0\ QQ01 + U_m\ FQ01)$$

$$ZE1 = CC1\ WK1 - \varepsilon_m[U_m(q_j FP11_{0j} - q_i\ FP11_{0i} - FQP11) - U_0\ QP11]$$

$$ZE2 = CC1\ WK2 - b\varepsilon_m[FQ01 - q_j\ FE01_{0j} + q_i\ FE01_{0i}]$$

$$ZE3 = CC1\ WK3 - \varepsilon_m[U_m(q_j\ FP01_{0j} - q_i\ FP01_{0i} - FQP01) - U_0\ QP01]$$

$$ZE4 = CC1\ WK4 - b\varepsilon_m[QQ01 - q_j\ FE00_{0j} + q_i\ FE00_{0i}]$$

$$ZE5 = CC1\ WK5$$

$$ZE6 = CC1\ WK6 - \varepsilon_m h_0 V_0(q_j - q_i) - CC2\ b\varepsilon_m\ HQ01 + (h\nu_t/\sigma_e\, \partial\varepsilon/\partial n)\big|_i^j$$

$$CC1 = C_{e1}\ \varepsilon_m/k_m$$

$$CC2 = C_{e2}\ \varepsilon_m/k_m$$

and different integral values (between $\eta_i = 0$ and $\eta_j = \infty$) are defined as follows:

$$WK1 = U_m[3/2(U_0^2\ FP11 + U_0U_m FP12 + U_m^2/3\ FP13) + (UP_i\ FP11_{0i} - UP_j FP11_{0j}) + (b/R\ FTP111)] - b/R[U_0(FET001 - uh0121) + U_m(FET011 - uh1121)]$$

$$WK2 = -b[3/2(U_0^2\ FE01 + 2U_0U_m\ FE02 + U_m^2\ FE03) + (UP_i\ FE01_{0i} - UP_jFE01_{0j}) + (b/R\ FET011) + 2b/R(U_0(U_0\ SS01 + U_m\ PP01) + U_m(U_0SF011 + U_m\ PF011))]$$

$$WK3 = U_m[3/2(U_0^2\ FP01 + U_0U_mFP02 + U_m^2/3\ FP03) + (UP_i\ FP01_{0i} - UP_jFP01_{0j}) + (b/R\ FTP011)] + b/R[U_0uh0021 + U_m\ uh1021]$$

$$WK4 = -b[3/2(U_0^2\ FE00 + 2U_0U_m\ FE01 + U_m^2\ FE02) + (UP_i\ FE00_{0i} - UP_jFE00_{0j}) + (b/R\ FET001) + 2b/R(U_0(U_0\ MM01 + U_m\ SS01) + U_m(U_0MF011 + U_m\ SF011))] + bU_0(U_0\ FE00 + U_m\ FE01)$$

$$WK5 = (b/R)^2\ (U_0\ FET001 + U_m\ FET011)$$

$$WK6 = (h\ U\ \tau/\rho - UP\ h_0\ V_0)\Big|_{ni}^{nj}$$

Table 4.1 : Summary of the offset-Jet experiments

Experiment No.	Jet height h(cm)	Jet velocity U_j(cm/s)
1	30.3	62.0
2	30.3	78.0
3	30.0	90.0
4	30.0	150.0

Table 4.2 : Summary of scour experiments

Series No.	Jet height h, (cm)	Jet velocity U_j(cm/s)	Duration t (min)	Time develop.
S001	0.0	64.0	3000	YES
S002	0.0	71.8	2625	NO
S051	5.15	61.0	3210	YES
S052	5.15	73.0	3174	YES
S101	10.15	37.0	650	NO
S102	10.15	46.2	460	NO
S103	10.15	57.5	645	NO
S104	10.15	64.2	300	YES
S105	10.15	78.2	385	NO
S106	10.15	98.0	480	NO
S201	20.15	47.5	1343	NO
S202	20.15	56.5	660	NO
S203	20.15	63.0	1500	YES
S204	20.15	66.0	800	NO
S205	20.15	69.0	4770	YES
S206	20.15	75.0	360	YES
S207	20.15	80.5	1845	YES
S208	20.15	81.0	695	NO

Table 6.1 : Coefficients of best fit lines in Eq. 6.7

Parameters	A	B	C	D
X_m/b_o	23.05	0.14	1.45	-39.52
d_m/b_o	- 3.34	- 0.55	-5.88	+17.81
X_{p2}/b_o	23.61	0.35	4.45	-99.51
d_{p2}/b_o	- 5.12	-0.44	- 4.99	+22.37

Table 6.2 Values of E and Z vs. h/b_o

h/b_o	0	4.4	8.6	17.1
E	2.45	2.3	2.24	2.07
Z	-4.85	-5.3	-6.3	-6.8

LIST OF FIGURES

2.1a Clear-water scour

2.1b Scour with continous sediment transport

2.2 Scour around hydraulic structures

2.3 Local scour caused by horizontal jets

2.4 Scour by vertical jets

2.5 Local scour by offset jet

2.6a Similarity of scour profiles (after Laursen, 1952)

2.6b Scour due to horizontal submerged jet (after Laursen, 1952)

2.7 Scour depth versus time (after Altinbilek et al, 1980)

2.8a Similarity of scour profiles at the asymptotic state with $H>>b_0$ (after Rajaratnam, 1981)

2.8a Similarity of scour profiles at the asymptotic state with $H\approx b_0$ (after Rajaratnam and Mcdougall, 1983)

2.9 Variation of scour depth at the asymptotic state for 2-D turbulent wall jets with (a) $H>>b_0$, (b) $H\approx b_0$ (after Rajaratnam et al, 1981, 1983).

2.10 Definition of typical scour hole (after Lim, 1985)

2.11 Schematic scour hole (after Carstens 1966)

2.12 Scour due to a vertical jet with the upstream face againts the wall

2.13 Variation of wt/H against $A(w/U_j)(d_m/b_0)$ (after Rao and Sarma, 1967)

2.14 Progress of scour hole by a shallow submerged jet (after Balfour, 1973)

2.15 Plot of volume of sediment scoured vs. time (after Balfour, 1973)

2.16 Distribution of horizontal velocity on various vertical sections (after Balfour, 1973)

3.1 Jet-boundary interaction

3.2 Schematic representation of jet diffusion.

3.3 Schematic representation of a shallow jet near to the surface

3.4 The shallow jet with the bed offset and parallel to the slot

3.5 Location of non-buoyant jets observed by Coates (1976) and measured by Johnston (1978).

3.6 Definition sketch for an offset jet

3.7 Static pressure distribution along plate (after Sawyer, 1960)

3.8 Static pressure contoures for case $h/b_0 = 5.62$ (after Sawyer, 1960)

3.9 Velocity profiles for case $h/b_0 = 5.62$ (after Sawyer, 1960)

3.10 Decay of the maximum velocity for offset jets (after Rajaratnam et al, 1968)

3.11 Velocity vectors of an offset jet (after Pelfrey, 1984)

3.12 Bed shear stress plots (after Rajaratnam et al, 1968)

3.13 Distribution of the bed shear stress (after Rajaratnam et al, 1968)

4.1 Sketch of laboratory layout

4.2 Cumulative size distribution curve

5.1a Horizontal velocity distribution of offset Jet (no. 4)

5.1b Distribution of maximum velocity of near-bed flow for offset jet.

5.2 Vertical velocity distribution of offset Jet (no. 4)

5.3 Velocity vector for offset jet (no. 3)

5.4 Attachment length vs. offset ratio

5.5 Locus of maximum velocity

5.6 Streamwise decay of maximum velocity of offset jet

5.7 Streamwise development of half-width of upper jet

6.1 Definition sketch for a scour hole

6.2 Variation of d_m with time

6.3 Variation of d_{p1} with time

6.4 Variation of d_{p2} with time

6.5 Variation of X_m with time

6.6 Variation of d_{p1} with time

6.7 Variation of d_{p2} with time

6.8 Variation of Scour Volume with time

6.9 Variation of d_m/b_0 with time

6.10 Variation of d_{p1}/b_0 with time

6.11 Variation of d_{p2}/b_0 with time

6.12 Variation of X_m/b_0 with time

6.13 Variation of X_{p1}/b_0 with time

6.14 Variation of X_{p2}/b_0 with time

6.15 Variation of Scour Volume with time

6.16 Variation of d_m/b_0 with log of time

6.17 Variation of d_{p1}/b_0 with log of time

6.18 Variation of d_{p2}/b_0 with log of time

6.19 Variation of X_m/b_0 with log of time

6.20 Variation of X_{p1}/b_0 with log of time

6.21 Variation of X_{p2}/b_0 with log of time

6.23 Effect of F_0 on the variation of X_{p1} with log of time

6.24 Effect of F_0 on the variation of d_{p1} with log of time

6.25 Effect of F_0 on the variation of X_m with of time

6.26 Effect of F_0 on the variation of d_m with log of time

6.27 Effect of F_0 on the variation of X_{p2} with log of time

6.28 Effect of F_0 on the variation of d_{p2} with log of time

6.30 Effect of h on the variation of X_{p1} with log. of time

6.31 Effect of h on the variation of d_{p1} with log. of time

6.32 Effect of h on the variation of X_m with log. of time

6.33 Effect of h on the variation of d_m with log of time)

6.34 Effect of h on the variation of X_{p2} with log of time)

6.35 Effect of h on the variation of d_{p2} with log of time)

6.37 Best fit curve for X_m

6.38 Best fit curve for d_m

6.39 Best fit curve for X_{p2}

6.40 Best fit curve for d_{p2}

6.41-a Progress of Scour Hole Profile with time (test no.S205)

6.41-b Progress of Scour Hole Profile with time (test no. S205)

6.42 Effect of Choice of Length Scale on the Dimensionless Scour Profile (test no S051)

6.43 Effect of Choice of Length Scale on the Dimensionless scour profile (test no S051)

6.44 Effect of Choice of Length Scale on the Dimensionless scour profile (test no S051)

6.45-a Dimenionless scour profile (d_s/d_m vs. x/X_{p2}) (test no s001)

6.45-b Dimenionless scour profile (d_s/d_m vs. x/X_{p2}) (test no s052)

6.46-a Dimenionless scour profile ($d_s d_m$ vs. x/X_{p2}) (test no s104)

6.46-b Dimenionless scour profile ($d_s d_m$ vs. x/X_{p2}) (test no s205)

7.1 The (s,n) coordinate systems

7.2 Variation of C_μ with P/ε (after Rodi, 1972)

8.1 Definition sketch for velocity profiles

8.2 Strips for mementum equation

9.1 Streamwise development of half-width for plane free jet

9.2 Streamwise decay of max velocity for plane free jet

9.3 Streamwise development of $k_m U_{m2}$ for plane free jet

9.4 Development of k-profile of free jet (pred. by k-ε)

9.5 Development of ε-profile in free jet (Pred by k-ε)

9.6 Distribution of turb. kinetic energy in free jet

9.7 Lateral distribution of ε in free jet

9.8 Shear-stress distribution in free turbulent jet

9.9a Sketch of a wall jet

9.9b Sketch of a wall jet on a logarithmic spiral

9.10 Streamwise development of half-width for plane wall jet

9.11 Streamwise develop. of max. vel. for plane wall jet

9.12 ε-profile of plane wall jet

9.13 Lateral distribution of k in plane wall jet

9.14 Variation of half-width with s/b_0 for concav wall jet (R/b_0=-100)

9.15 Streamwise variation of $(U_j U_m)^2$ for concave wall jet (R/b_0=-100)

9.16 Streamwise variation of $k\ U_m^2$ for concave wall jet (R/b_0=-100)

9.17 Streamwise variation of $e_m b/U_m^3$ for concave wall jet (R/b_0=-100)

9.19 Development of Half-Width of Wall Jet on Logar. Spiral

9.20 Decay of Max. Vel. of Wall Jet on Logar. Spiral (R/s=1)

9.21 k-profile of wall jet on logarithmic spiral (R/s=1)

9.22a Development of Half-Width of Offset Jet (h/b_0= 7 Exp. of Pelfrey (1984)

9.22b Decay of Max. Vel. of Offset Jet (h/b_0=7, Exp. (h/b_0=7, Exp. of Pelfrey ,1984)

9.24 Decay of Max. Vel. of Offset Jet (h/b_0=8.7, Exp. of Hoch 1979)

9.25 Pred. of Different Trajectories of Offset Jet with ASM (h/b_0=7, Exp. of Pelfrey 1984)

9.27 Predicted Velocity Vectors with ASM Model for Offset jet, (h/b_0=7, Exp. of Pelfrey 1984)

9.28 Predicted Velocity Vectors with ASM Model for Offset jet (h/b_0=26.2)

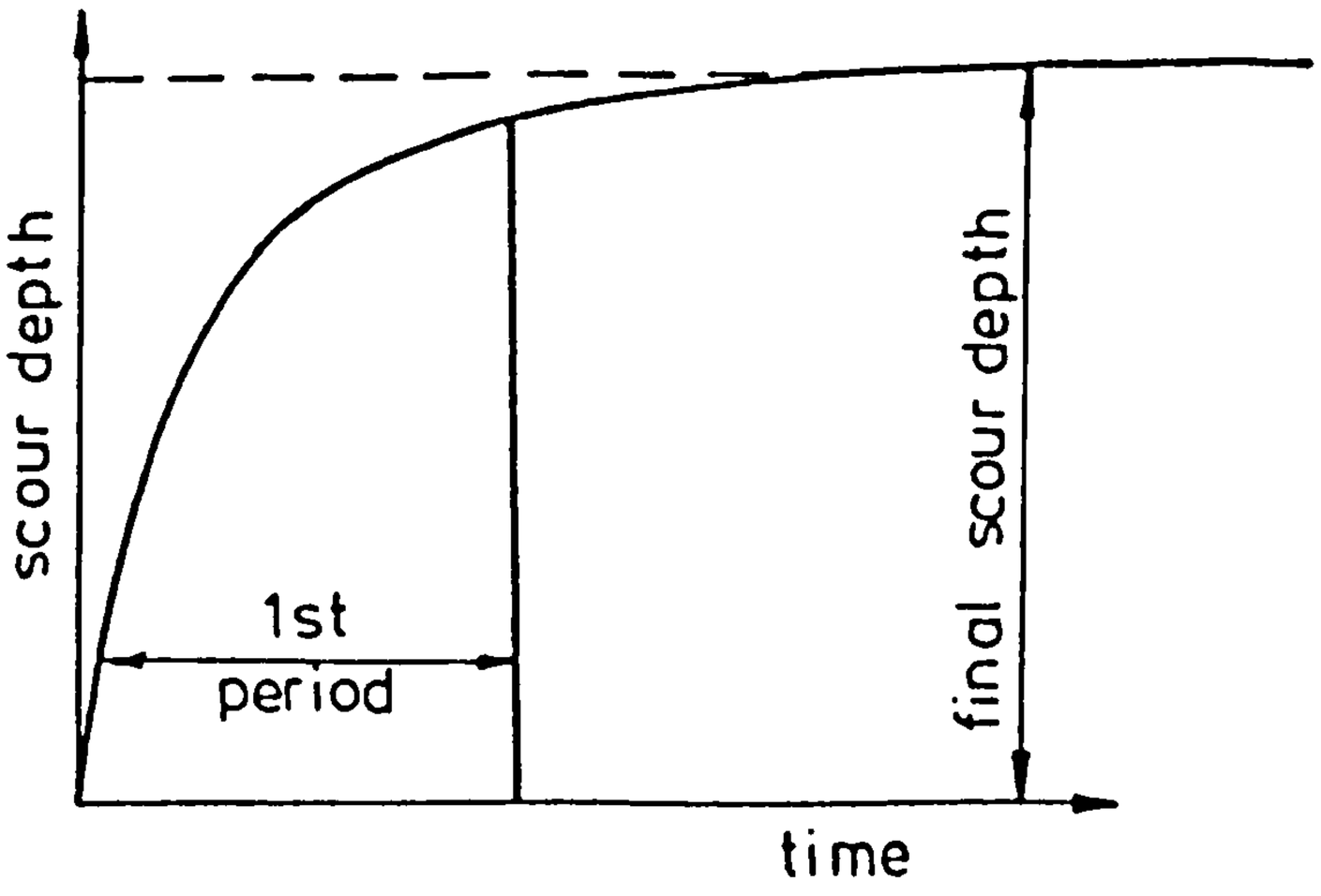

Fig. 2.1-a Clear water scour

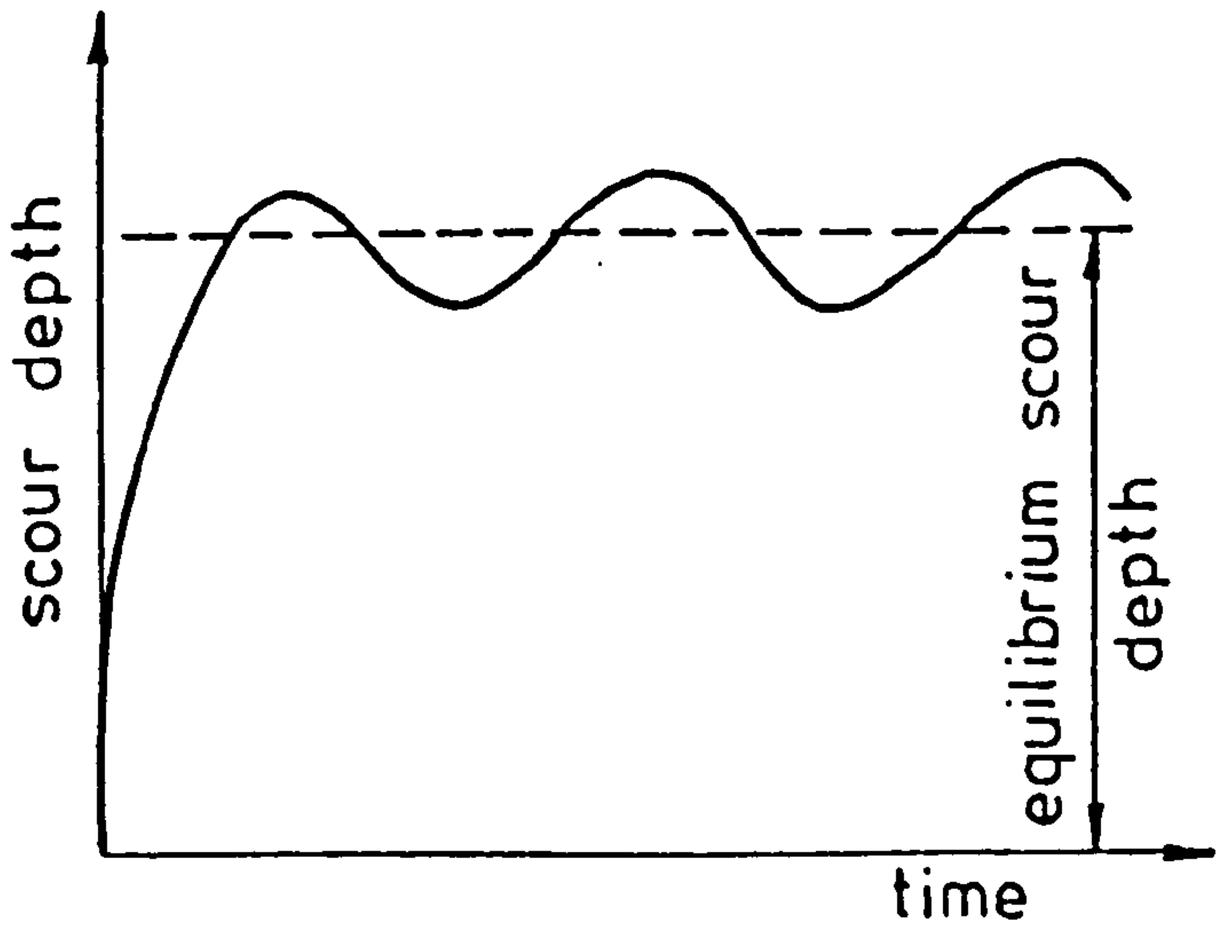

Fig. 2.1-b Scour With Continous Sediment Transport

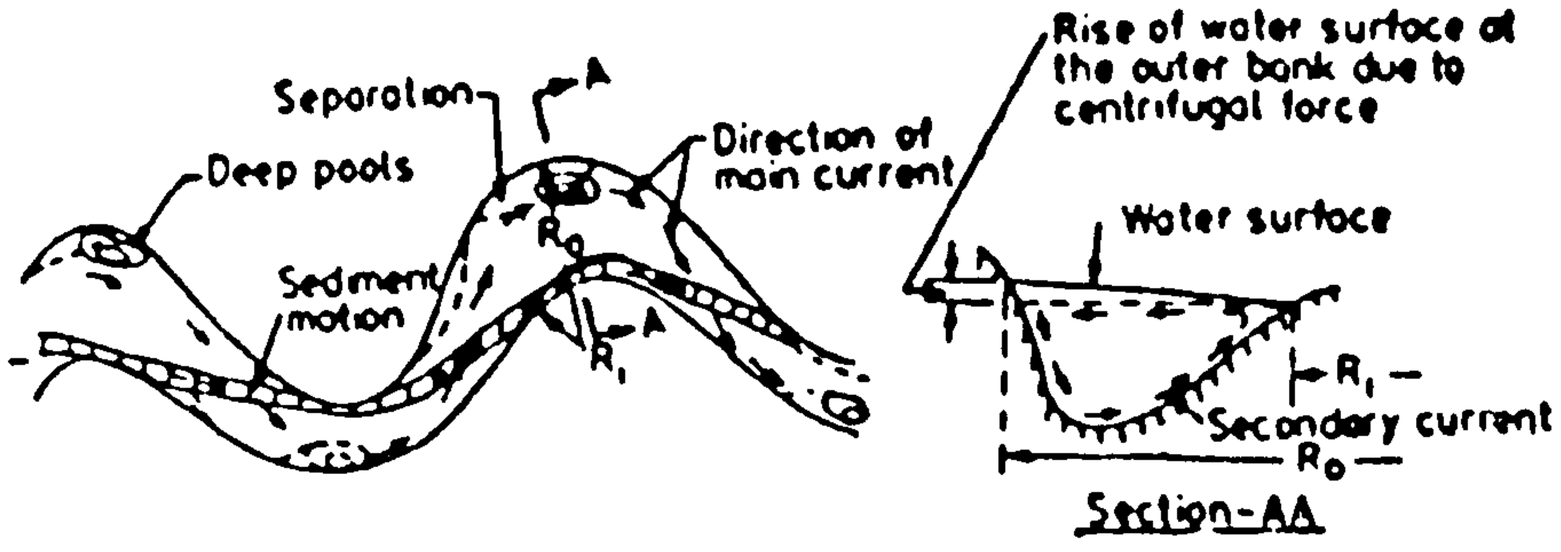

a) Scour in Meandring Channel

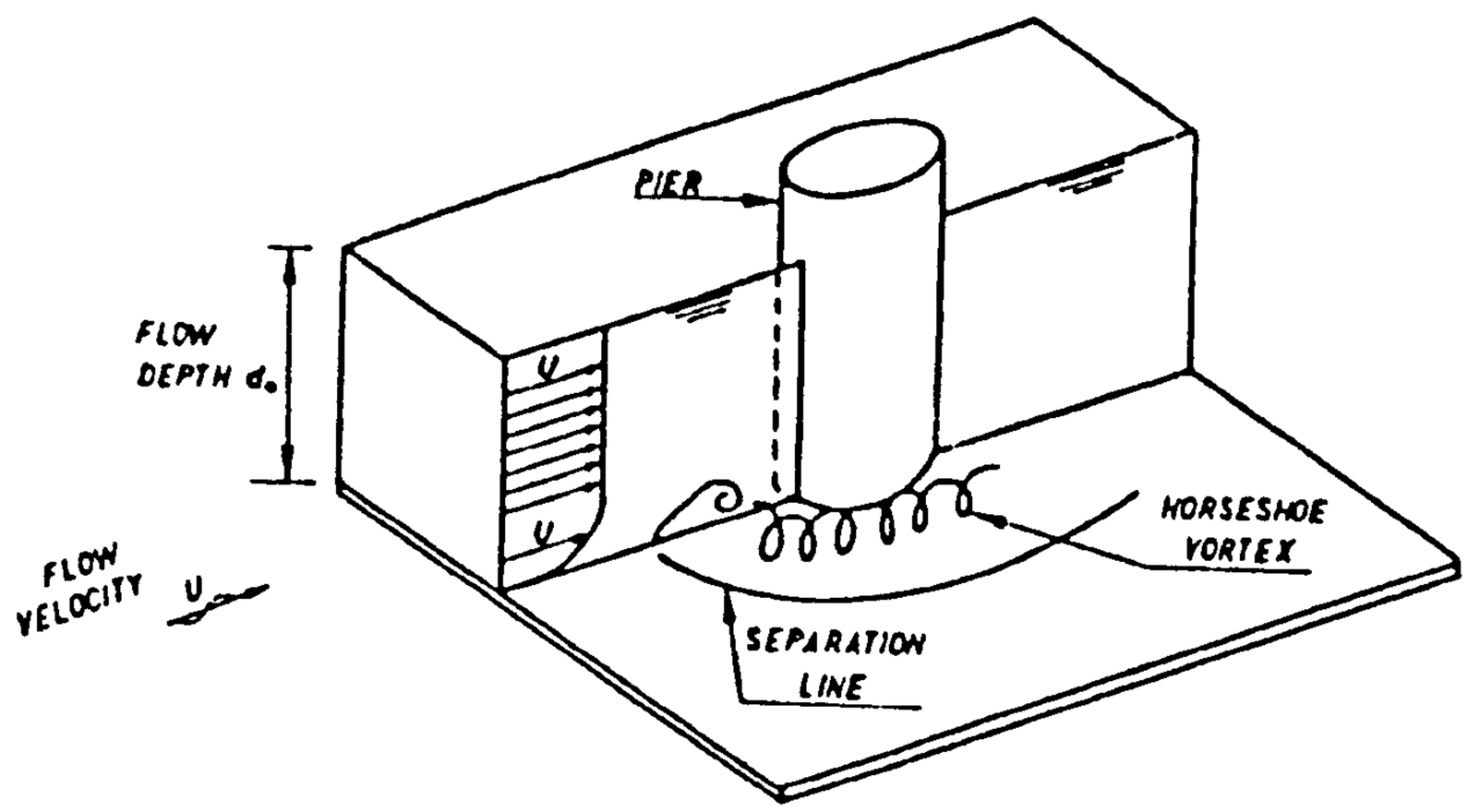

b) Bridge Piers

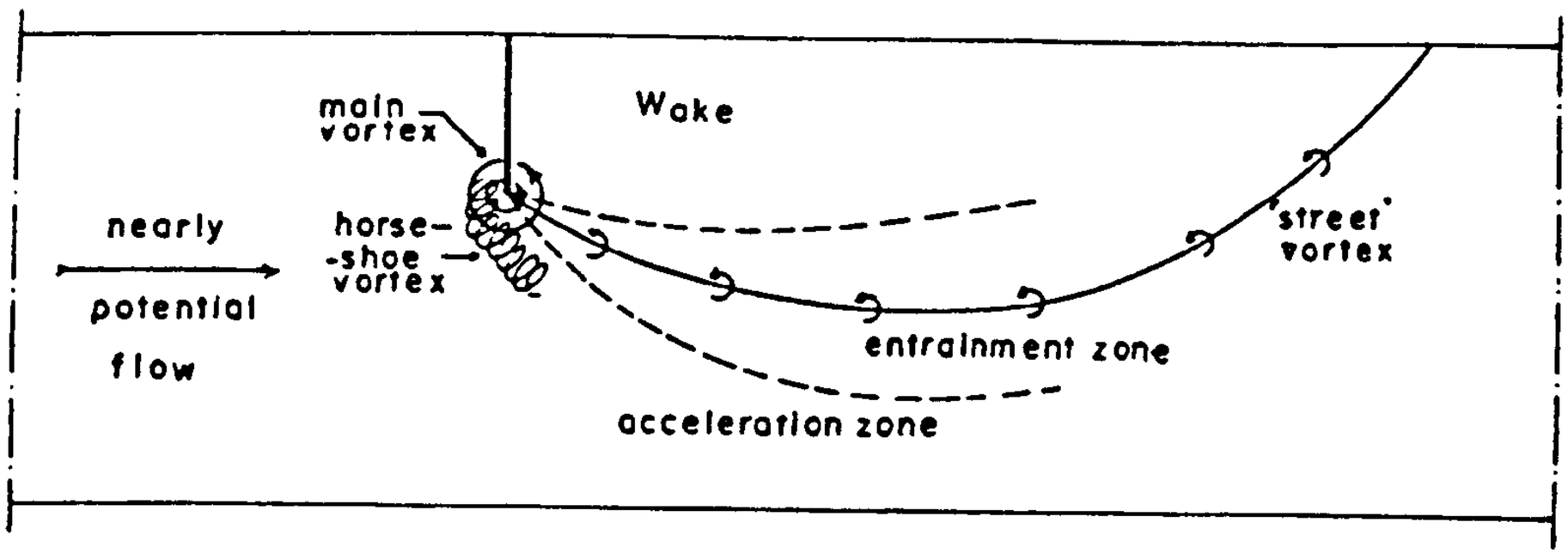

c) Spur-dike

Fig. 2.2 Scour Around Hydrulic Structers

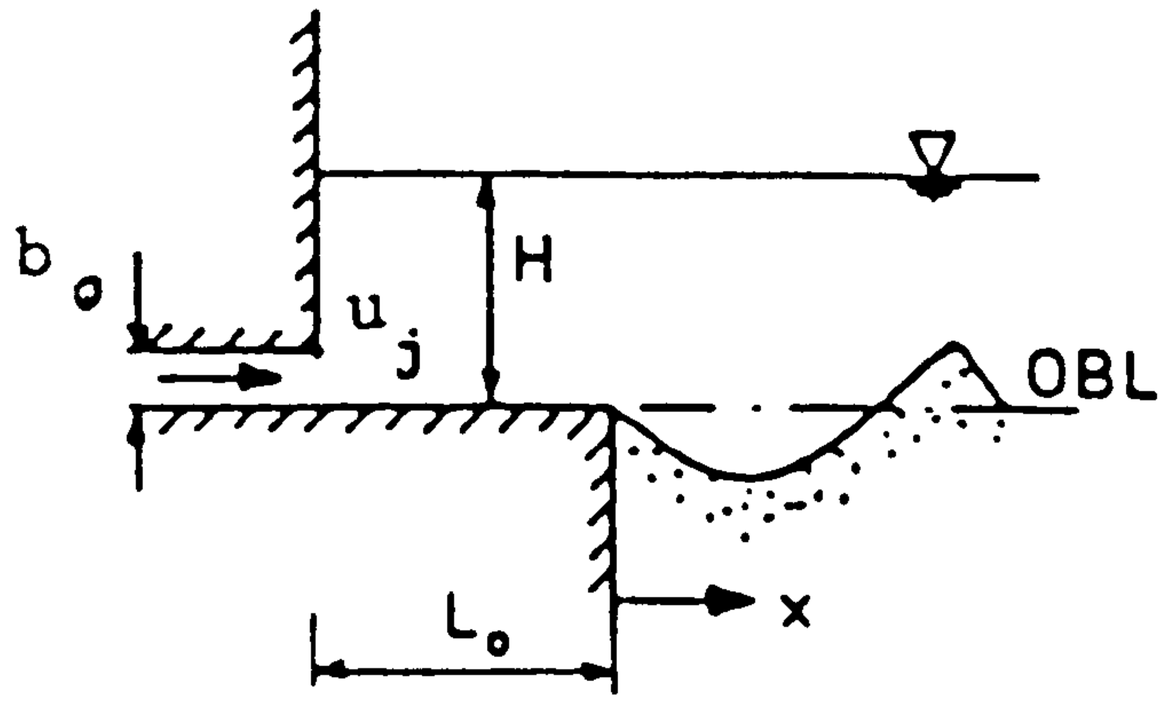

a) wall jet

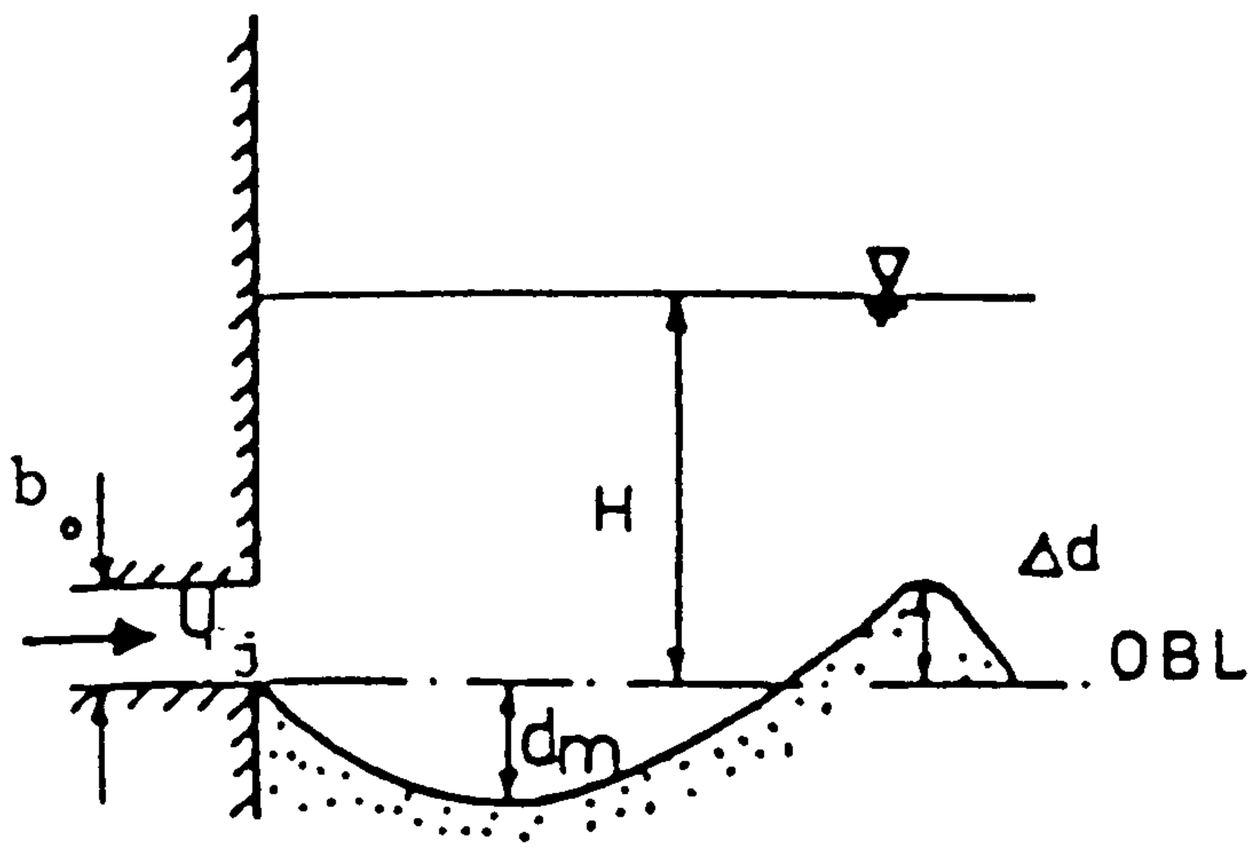

b) sluice gate

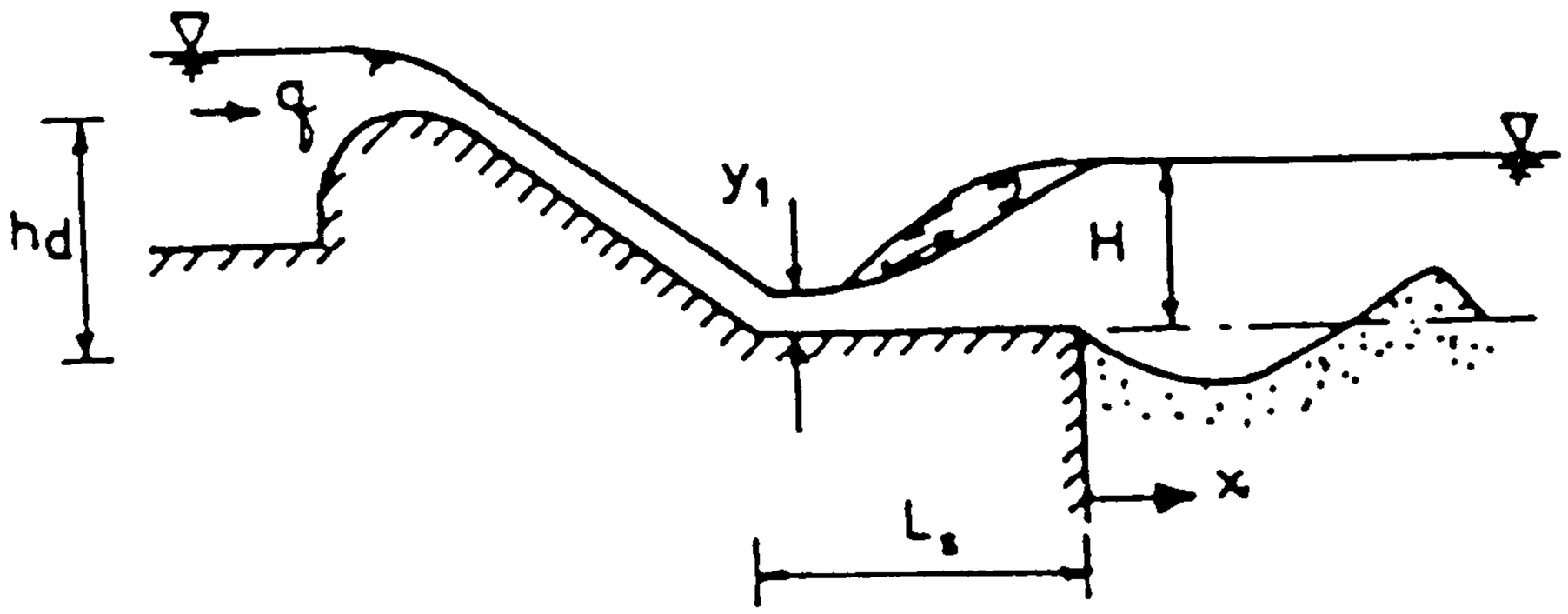

c) spillway

Fig.2.3 Local Scour Caused by horizontal Jets

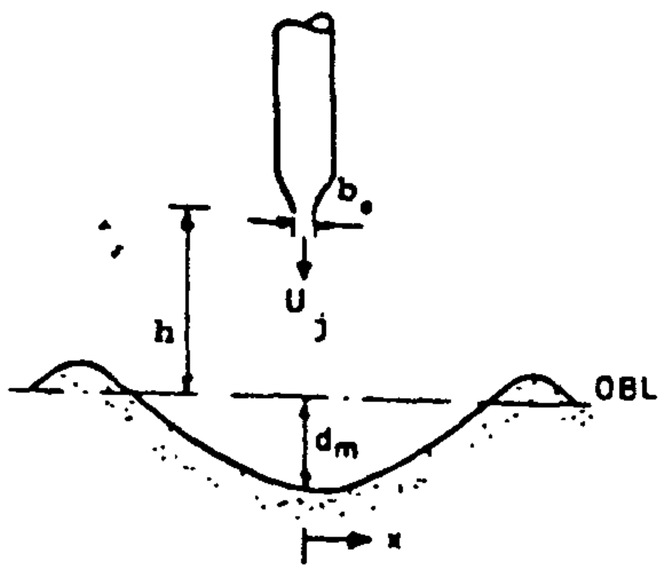

a) VERTICAL JET

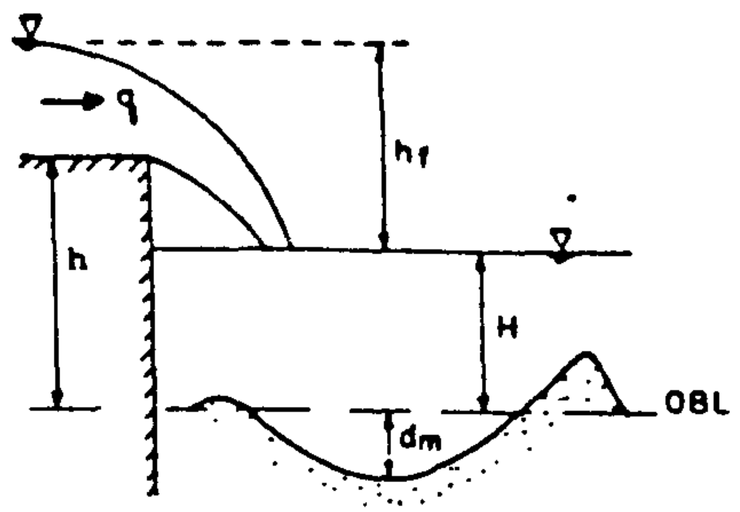

b) FREE OVERFALL

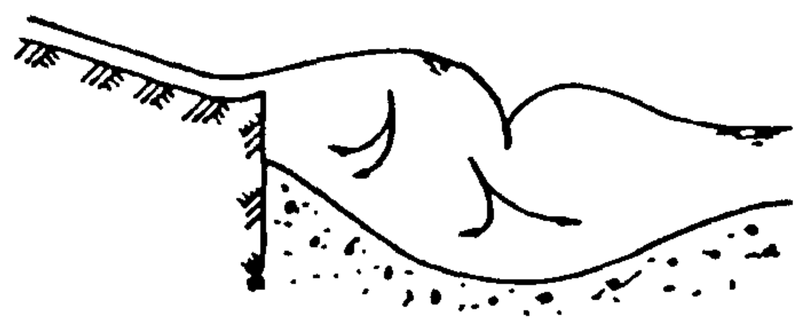

c) Ski- Jump

Fig. 2.4 Scour by vertical jets

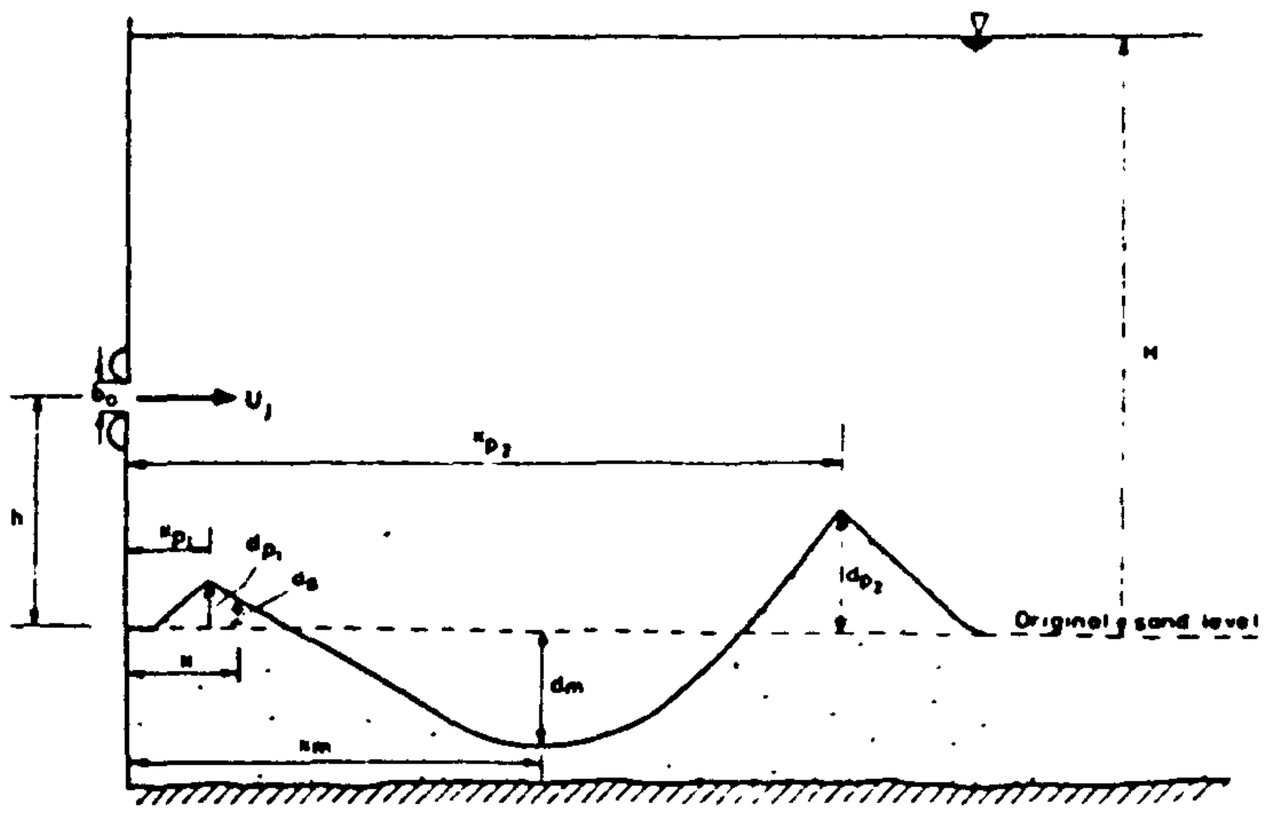

d) offset jet

Fig. 2.5 Local scour by offset jet

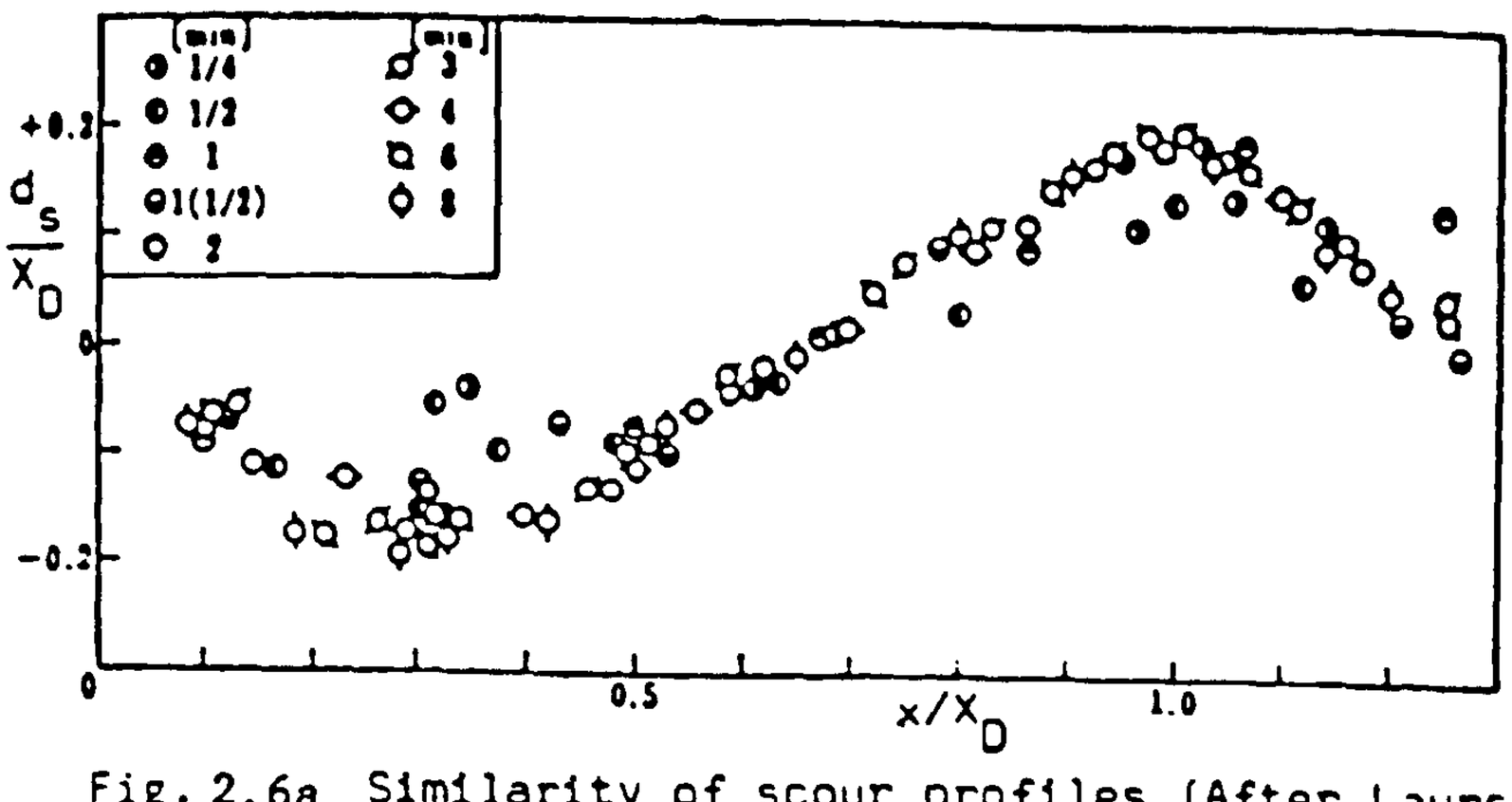

Fig. 2.6a Similarity of scour profiles (After Laursen, 1952)

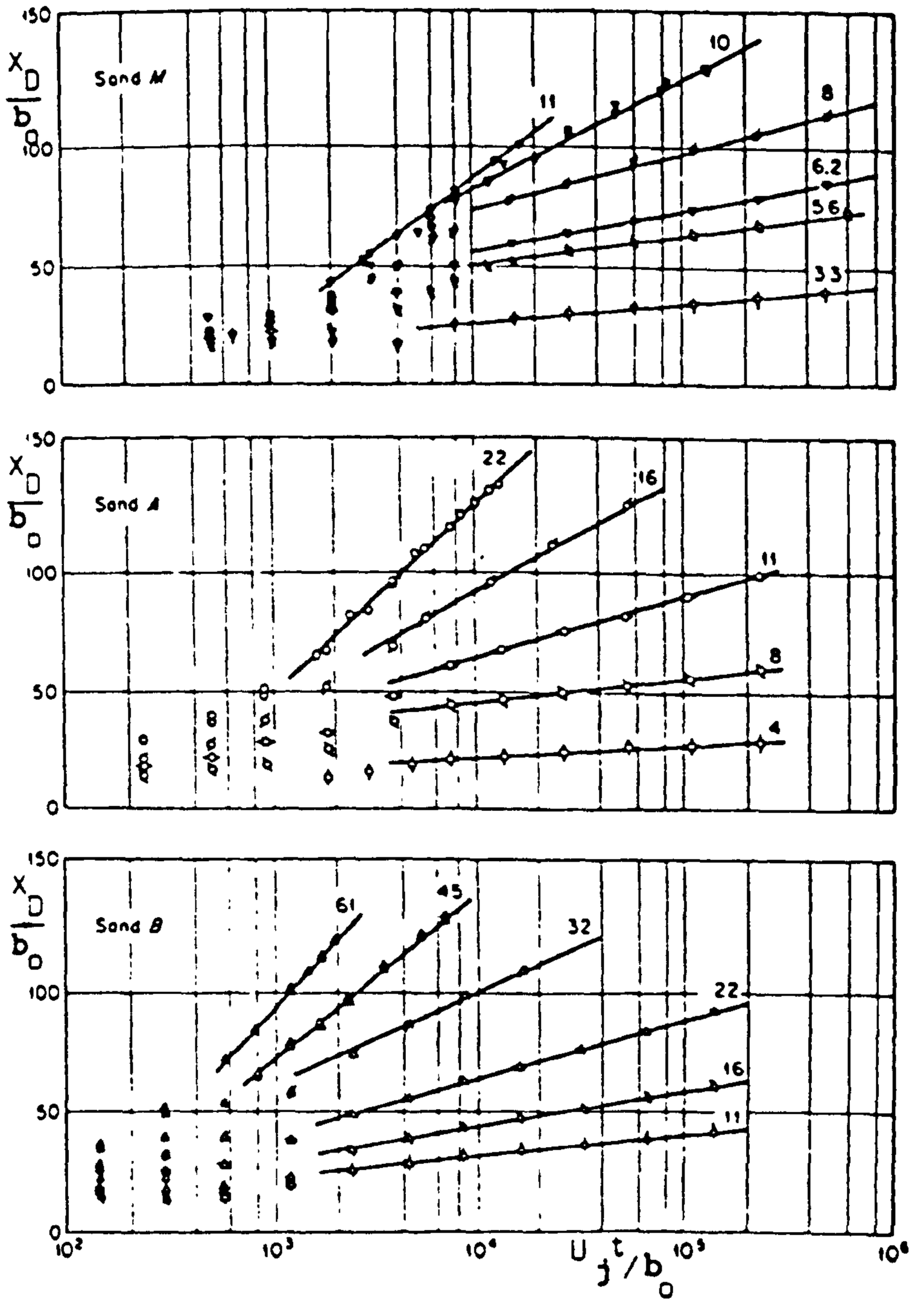

Fig. 2.6b Scour due to horizontal submerged jet (After Laursen, 1952)

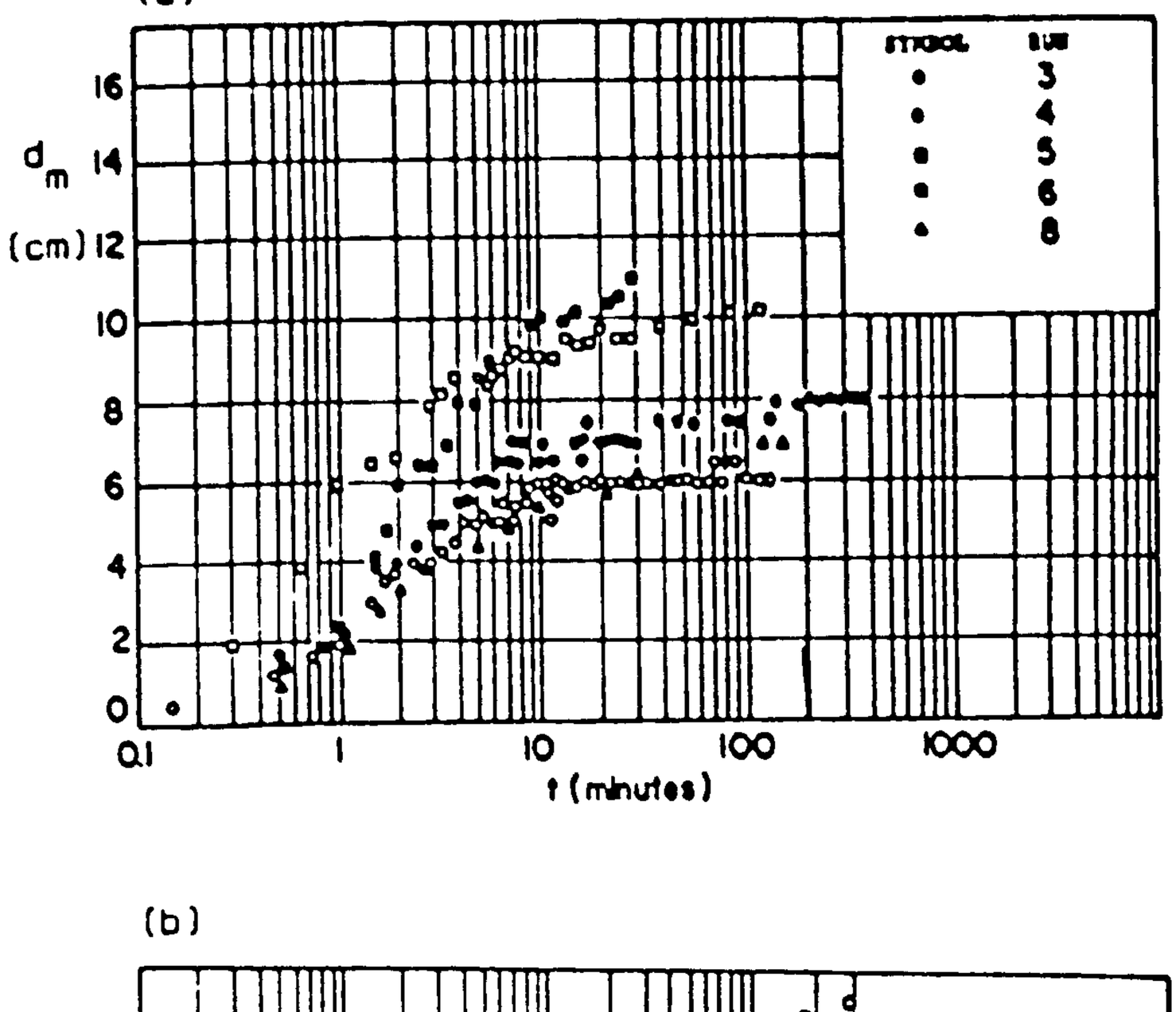

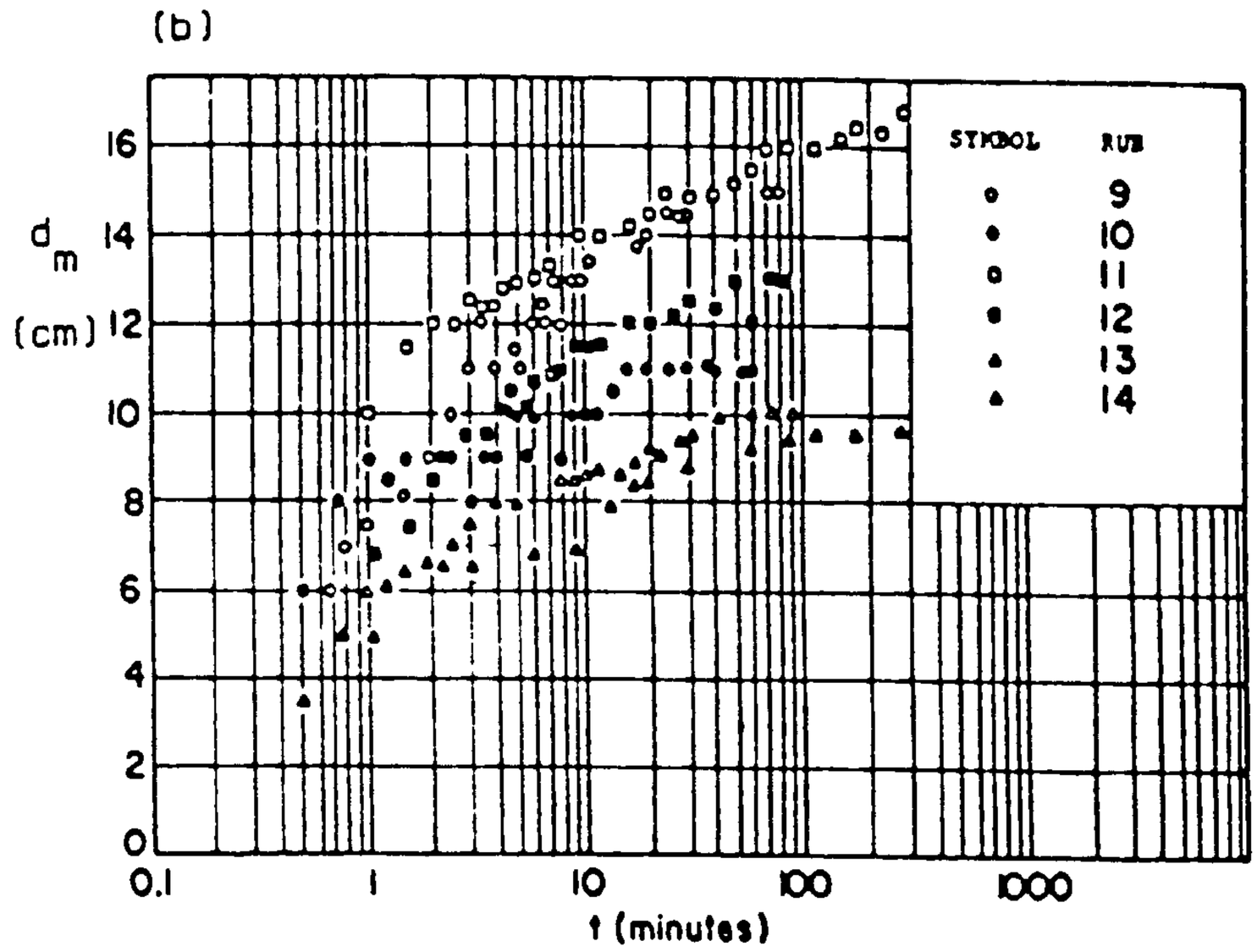

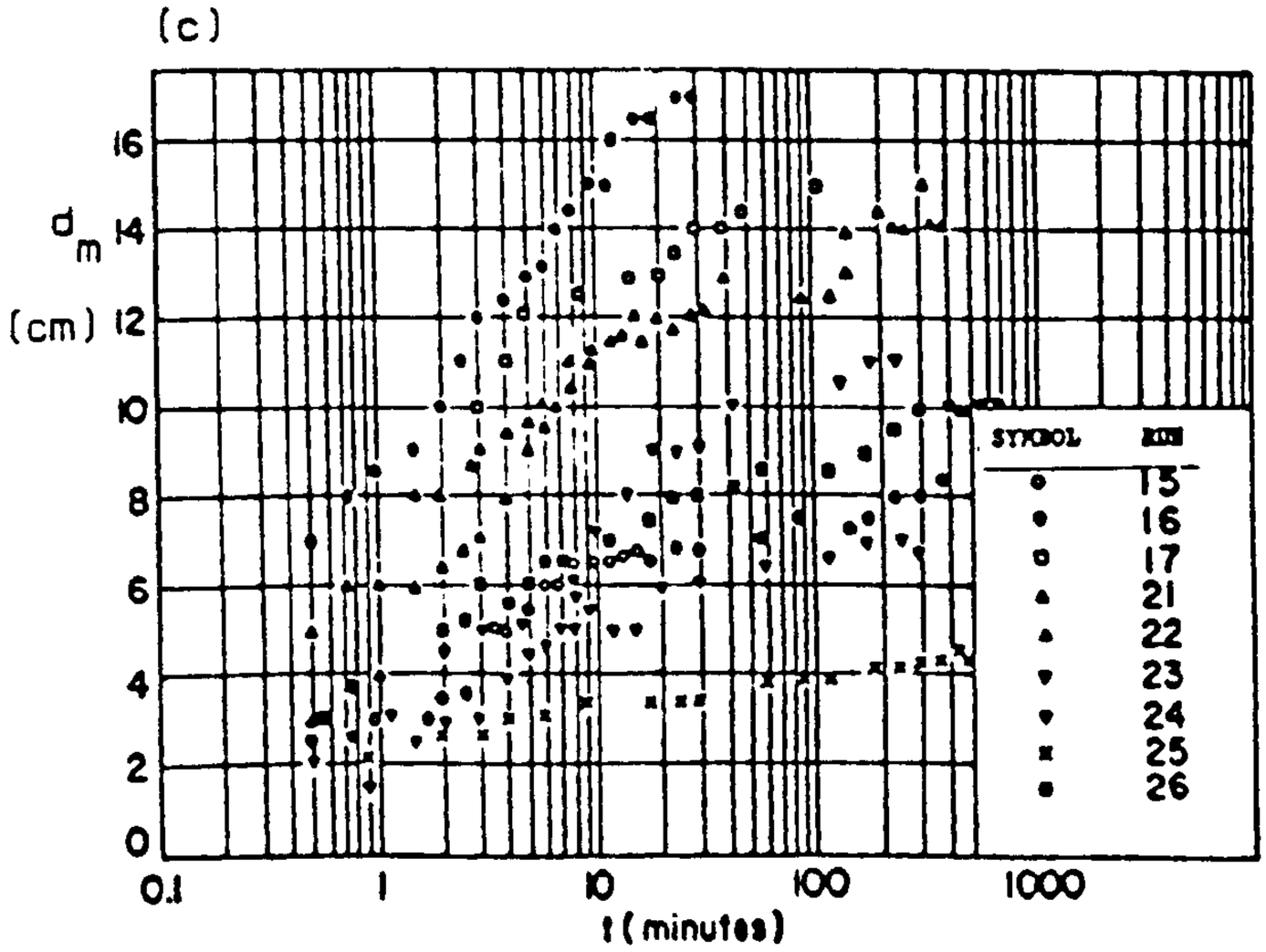

Fig. 2.7 Scour depth versus time for (a) d_{50} = 6.5 mm, (b) d_{50} = 2.65 mm, (c) d_{50} = 1.3 mm (After Altinbilek et al, 1980

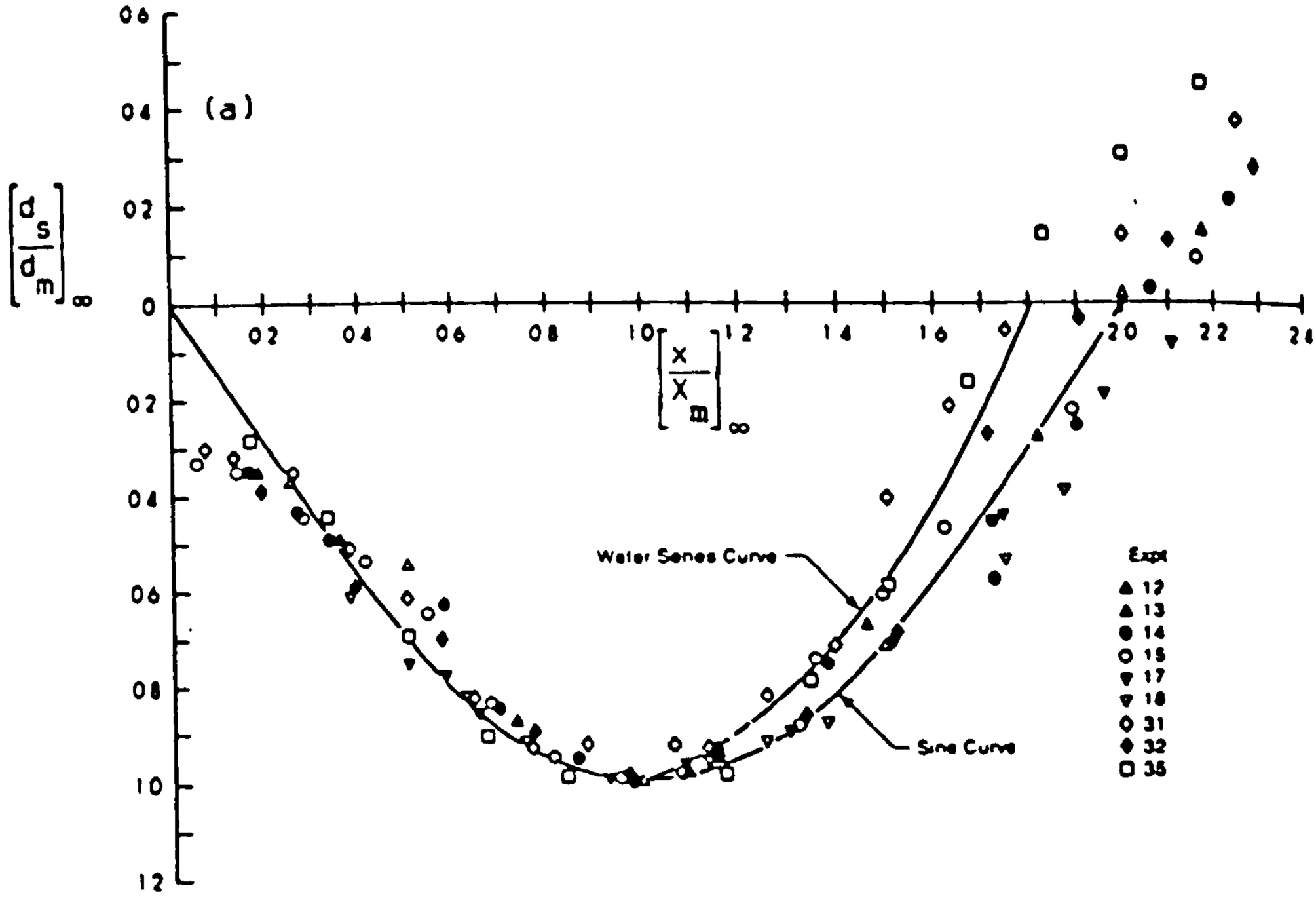

Fig. 2.8(a) Similarity of scour profiles at the asymptotic state with $H >> b_o$ (After Rajaratnam, 1981)

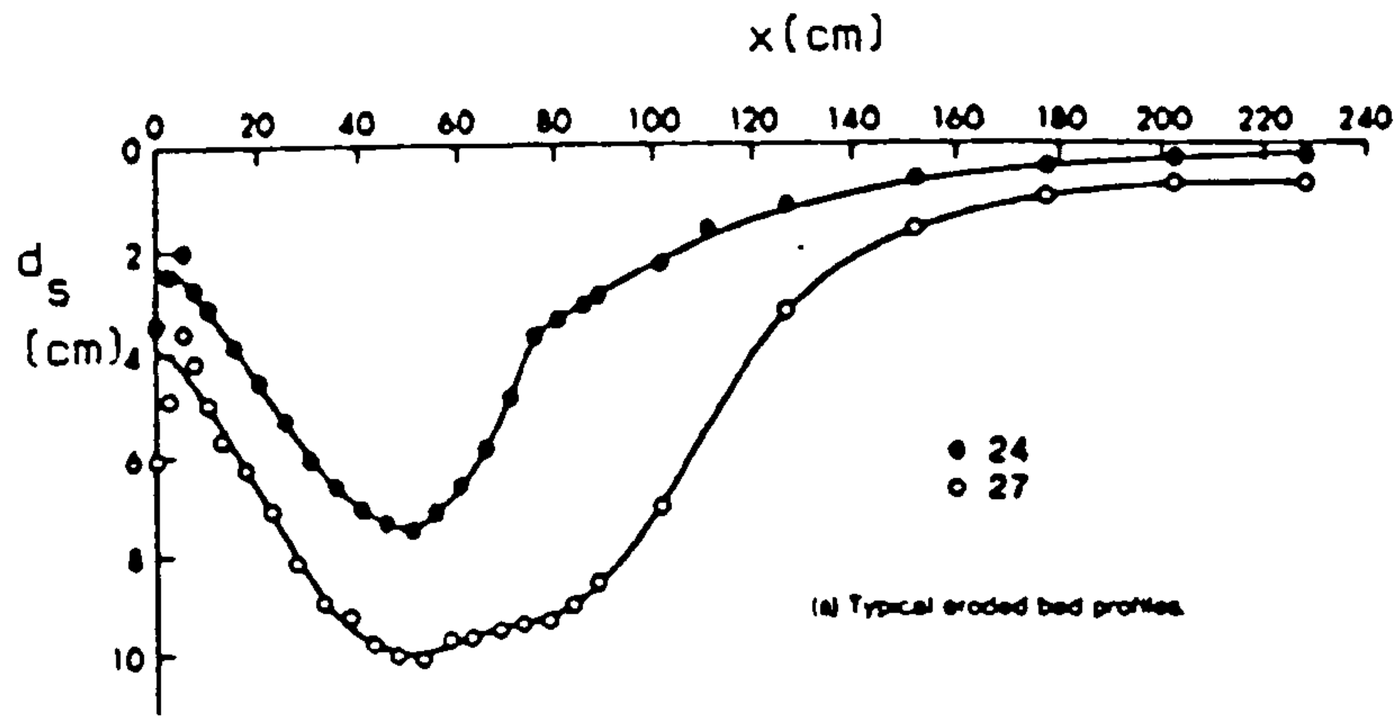

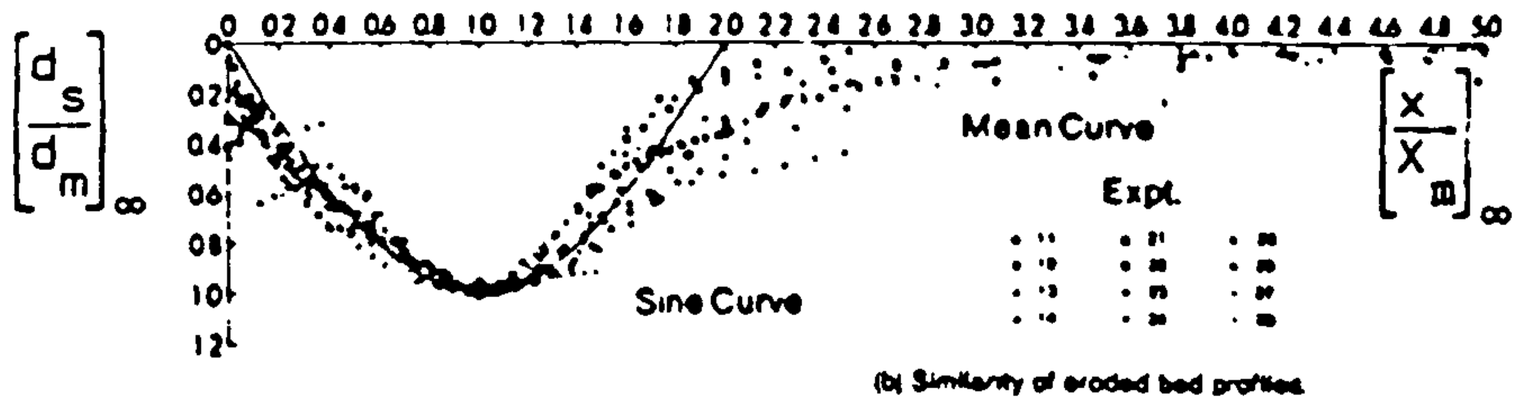

Fig.2.8(b) Similarity of scour profiles at the asymptotic state with $H \simeq b_o$ (After Rajaratnam & Macdougall, 1983)

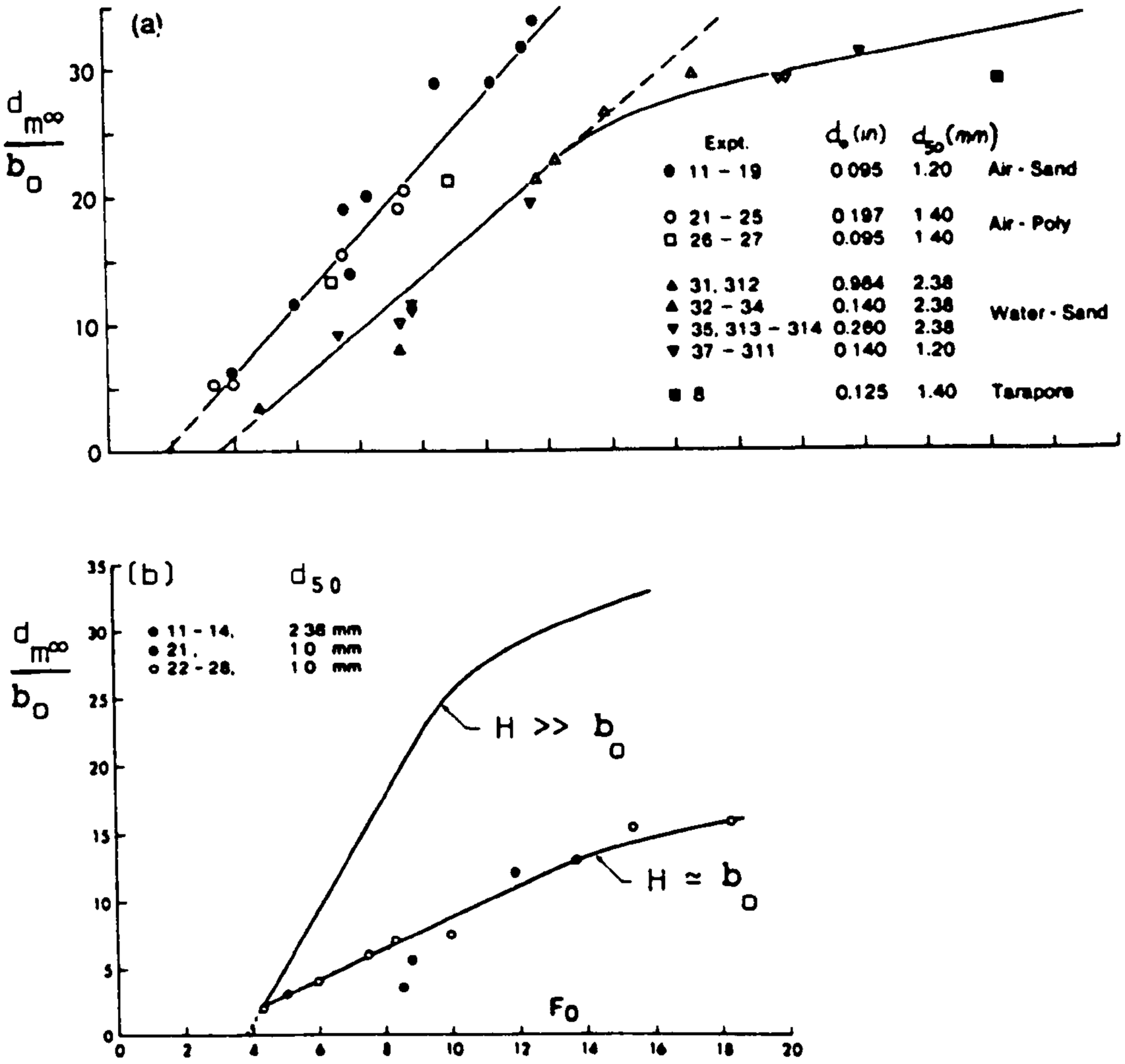

Fig. 2.9 Variation of scour depth at the asymptotic state for 2-D turbulent wall jets with (a) $H \gg d_o$, (b) $H \simeq d_o$ (After Rajaratnam et al, 1981, 1983)

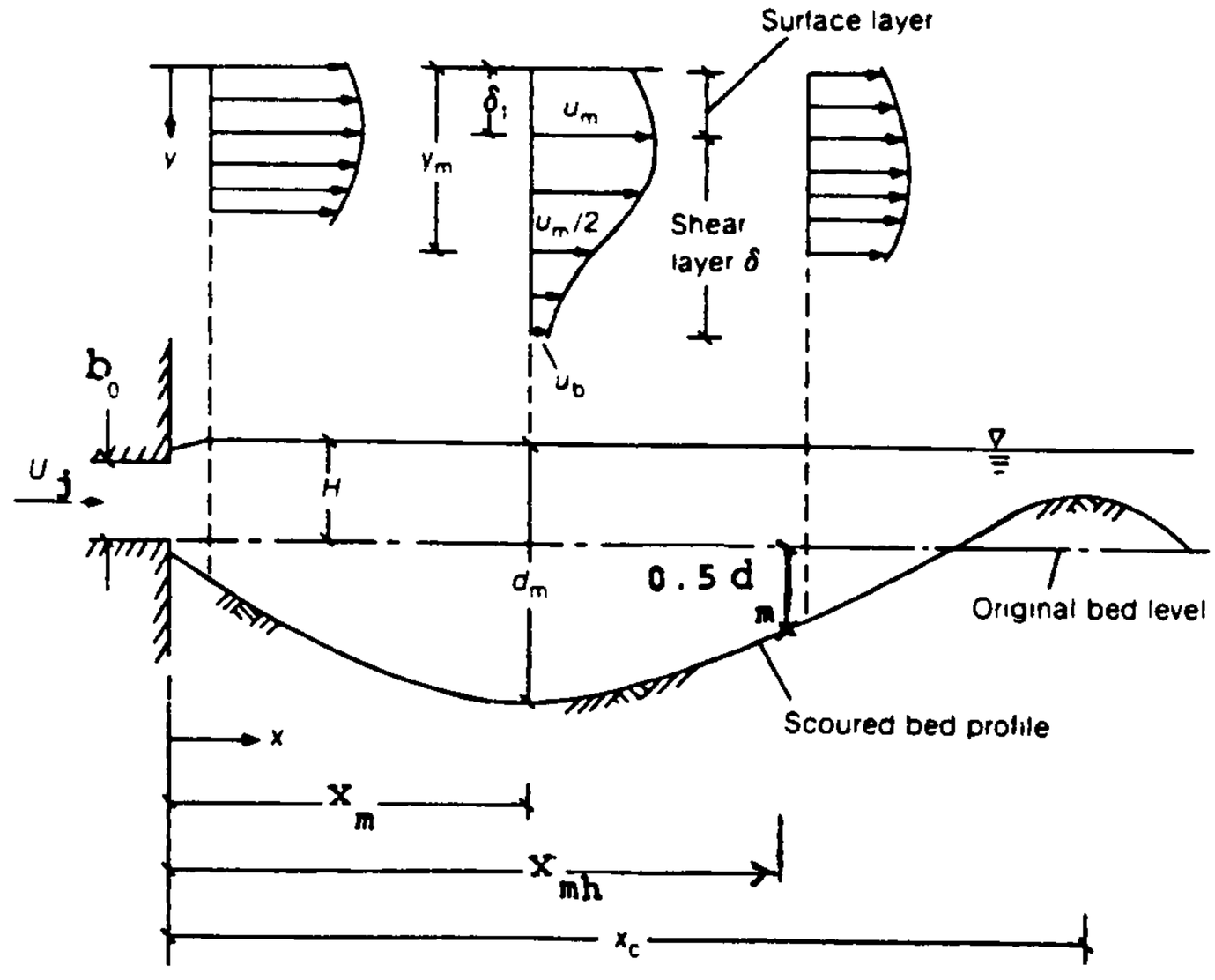

Fig. 2.10 Definition of Typical Scour Hole

(After Lim (1985))

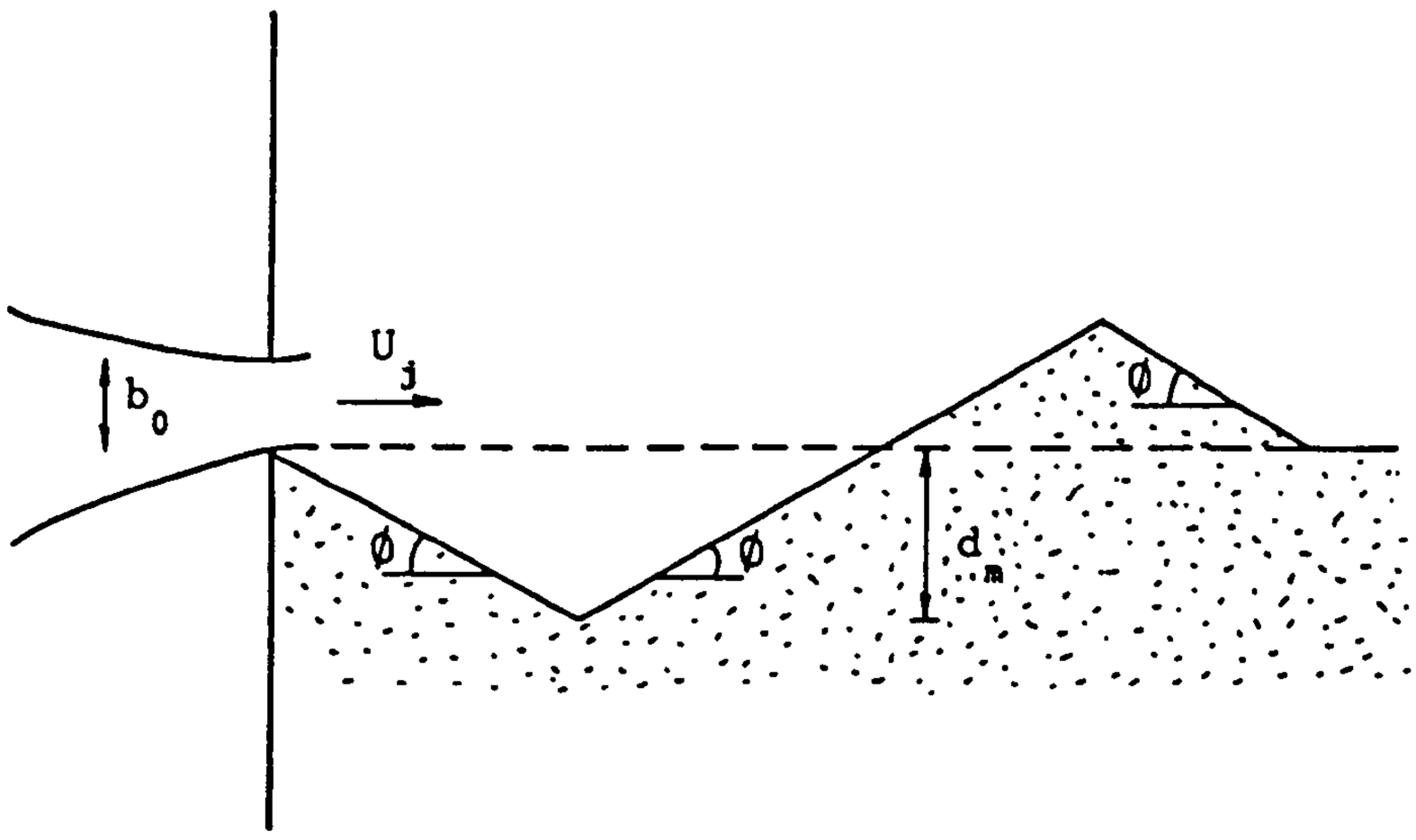

Fig. 2.11 Schematic Scour Hole (After Carstens 1966)

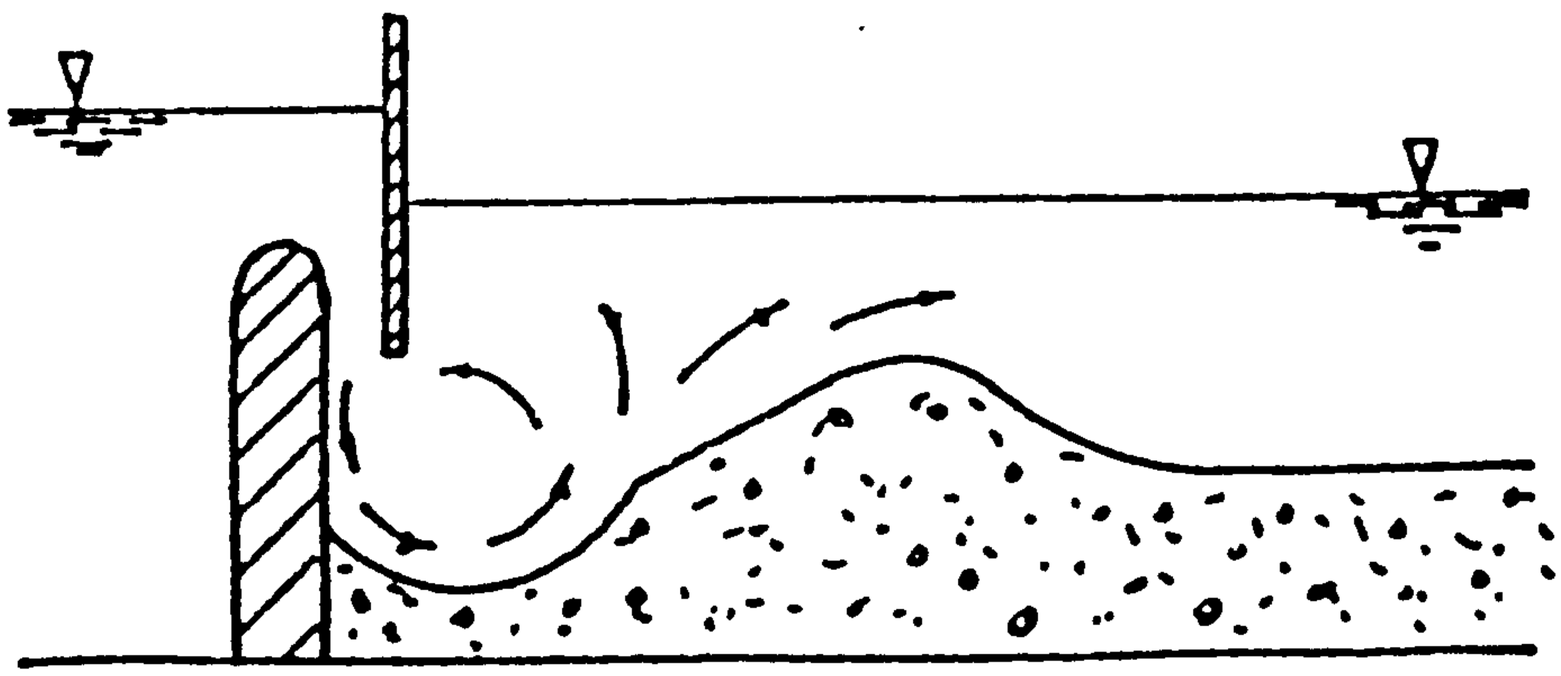

Fig. 2.12 Scour Due to a Vertical Jet With the Upstream Face Againts the Wall

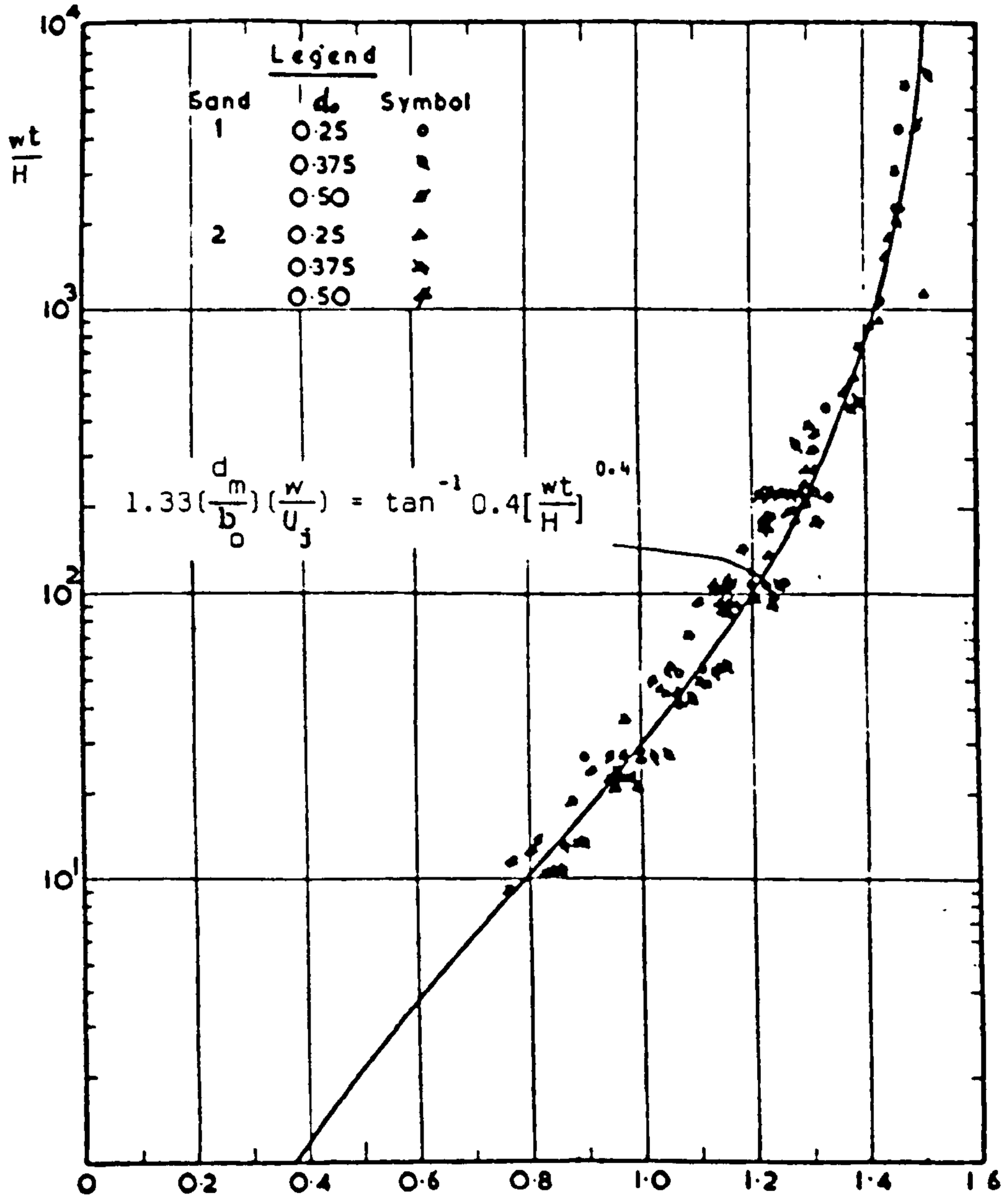

Fig. 2.13 Variation of $\frac{wt}{H}$ against $A(\frac{w}{U_j})(\frac{d_m}{b_o})$ (After Roa & Sarma, 1967)

a

b

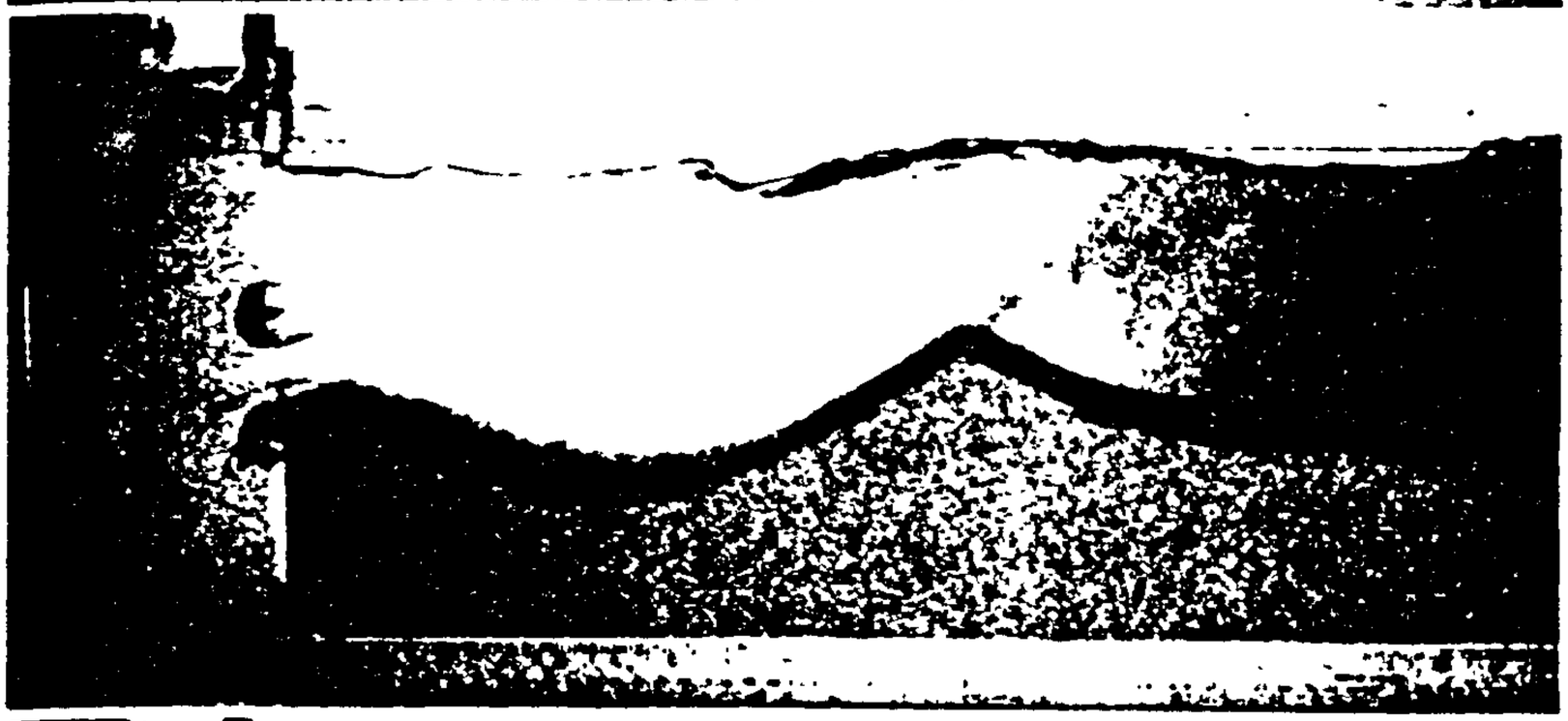

c

d

e

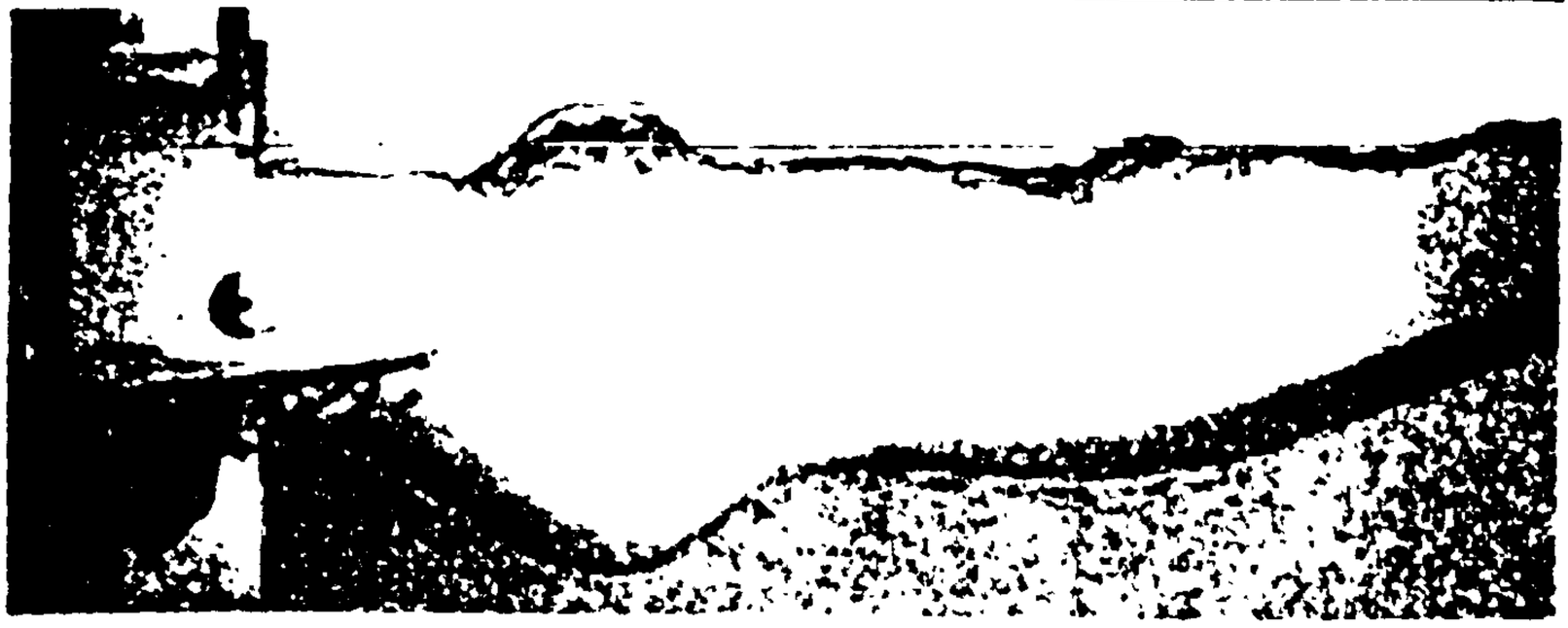

2.14 Progress of scour hole by a shallow submerged jet

(after Balfour, 1973)

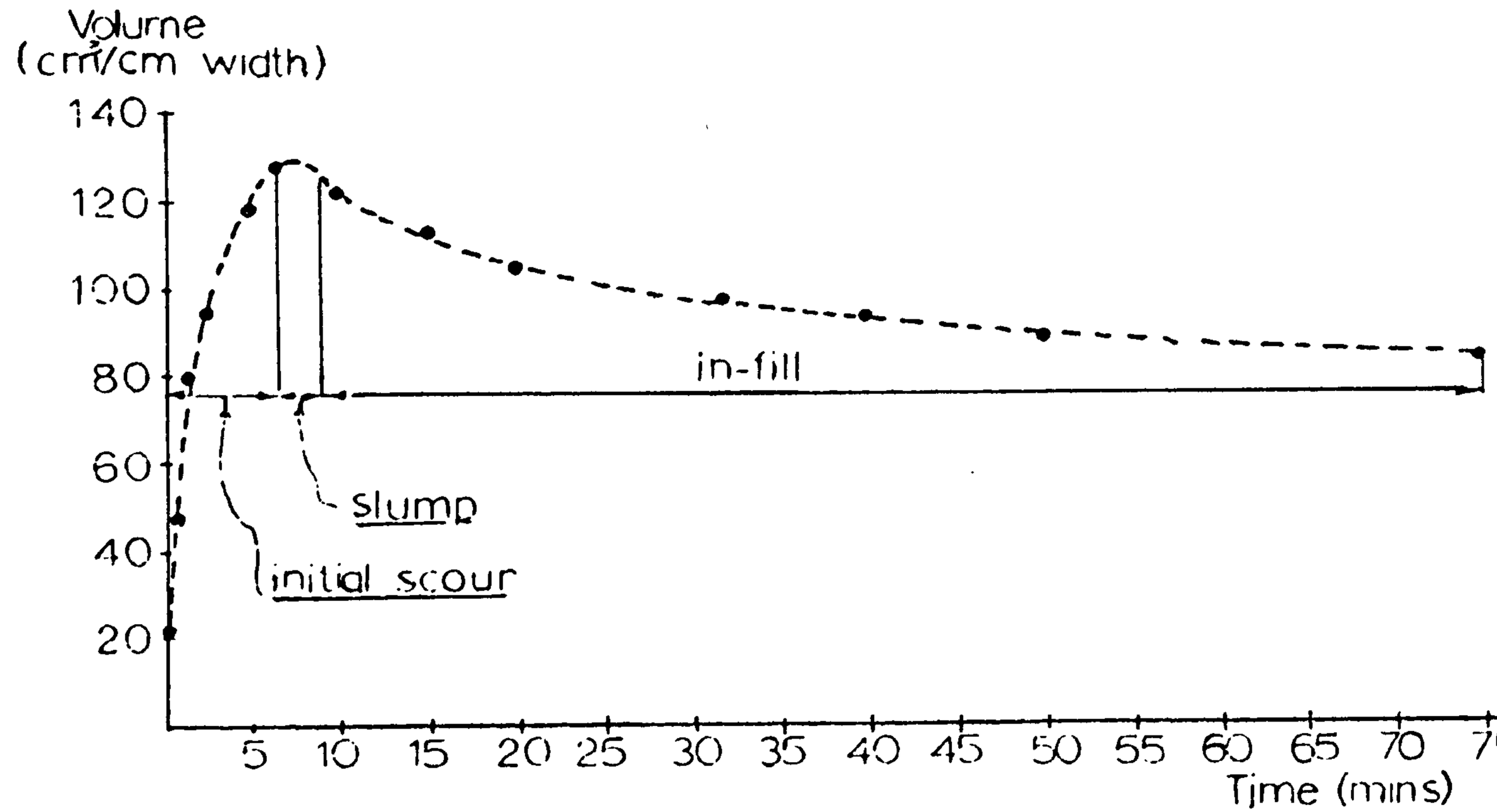

Fig. 2.15 Plot of Volume of Sediment Scoured Vs. Time (After Balfour (1973))

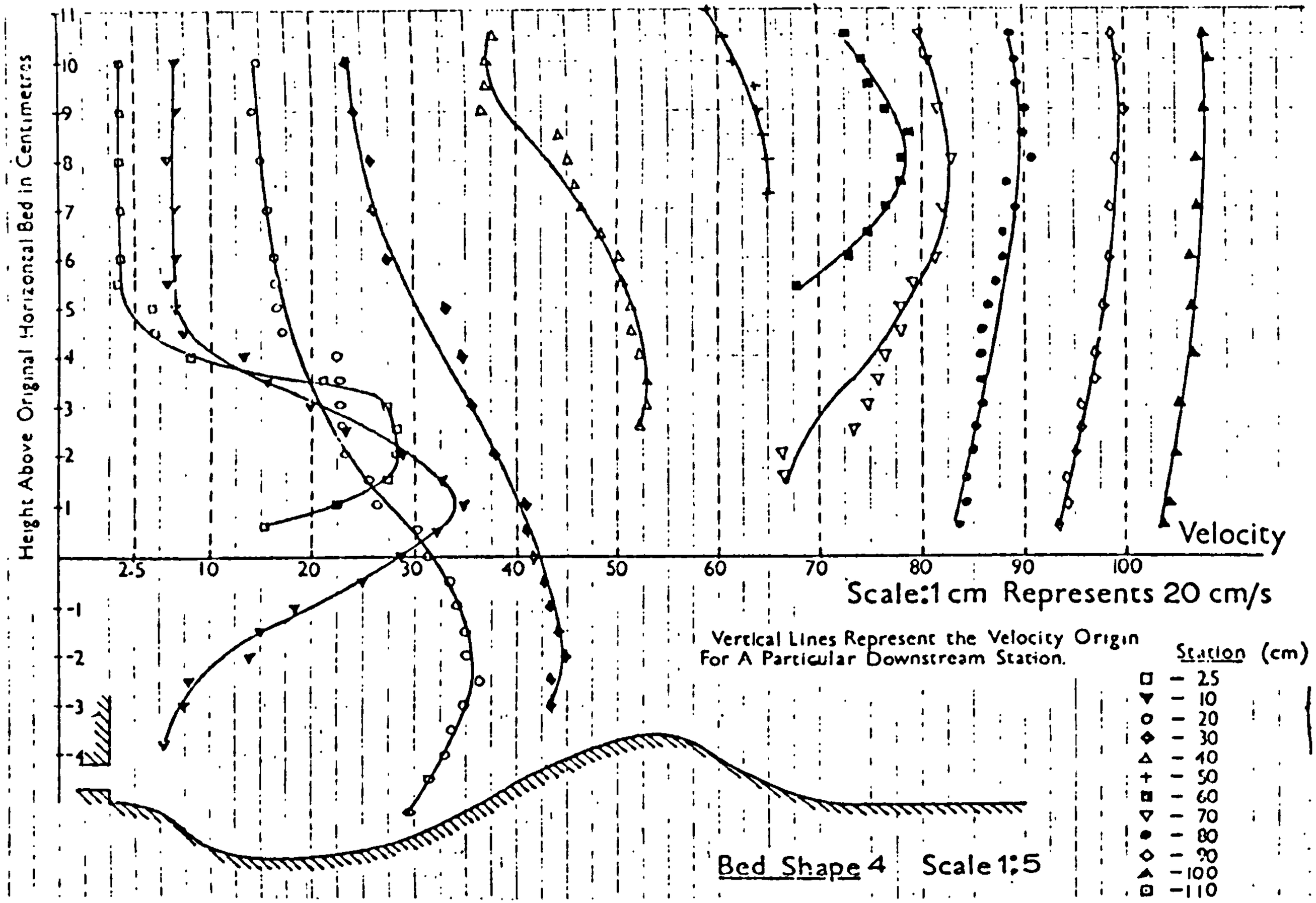

Fig. 2.16 Distribution of Horizontal Velocity on Various Vertical Sections (After Balfour (1973))

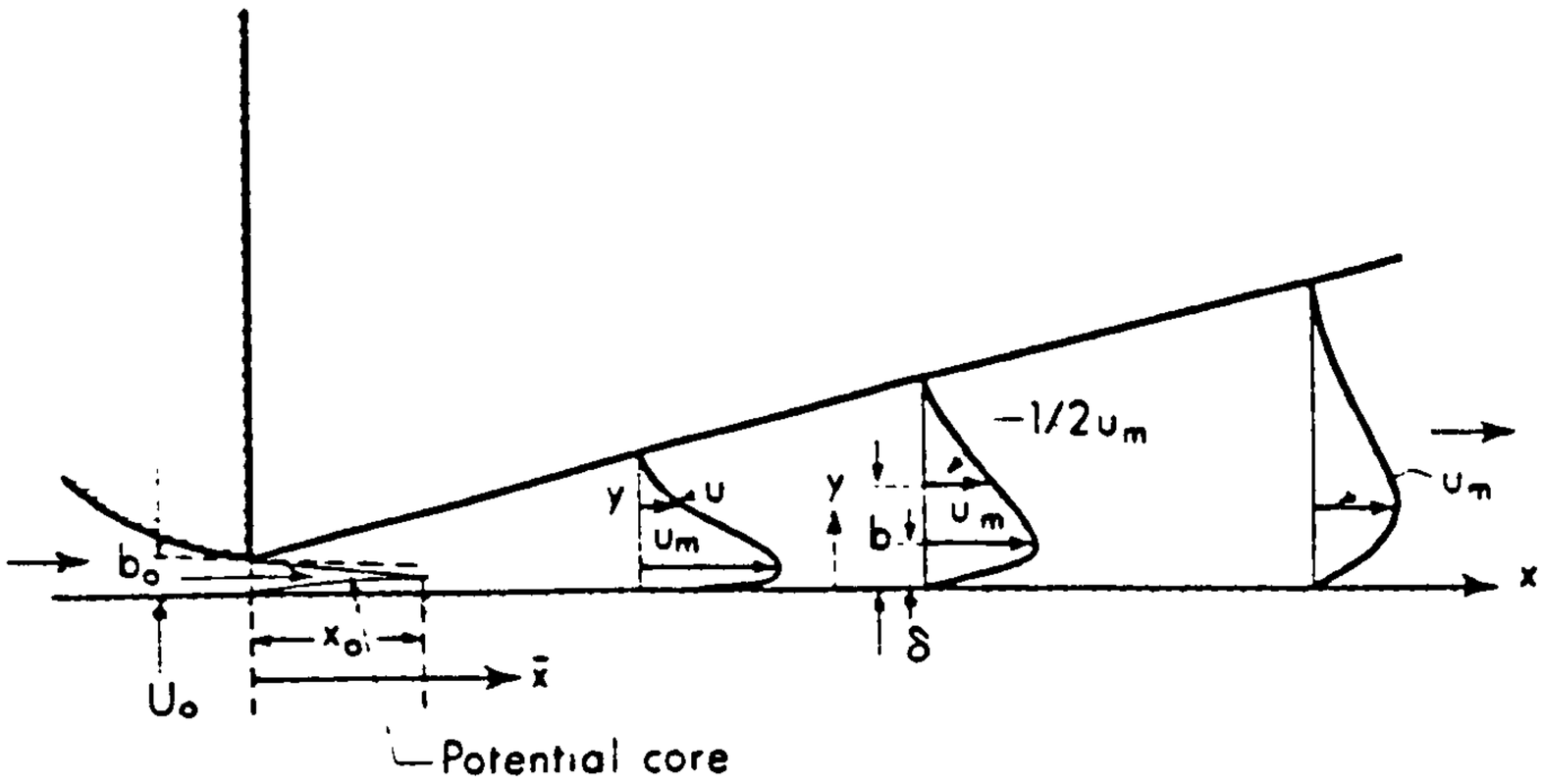

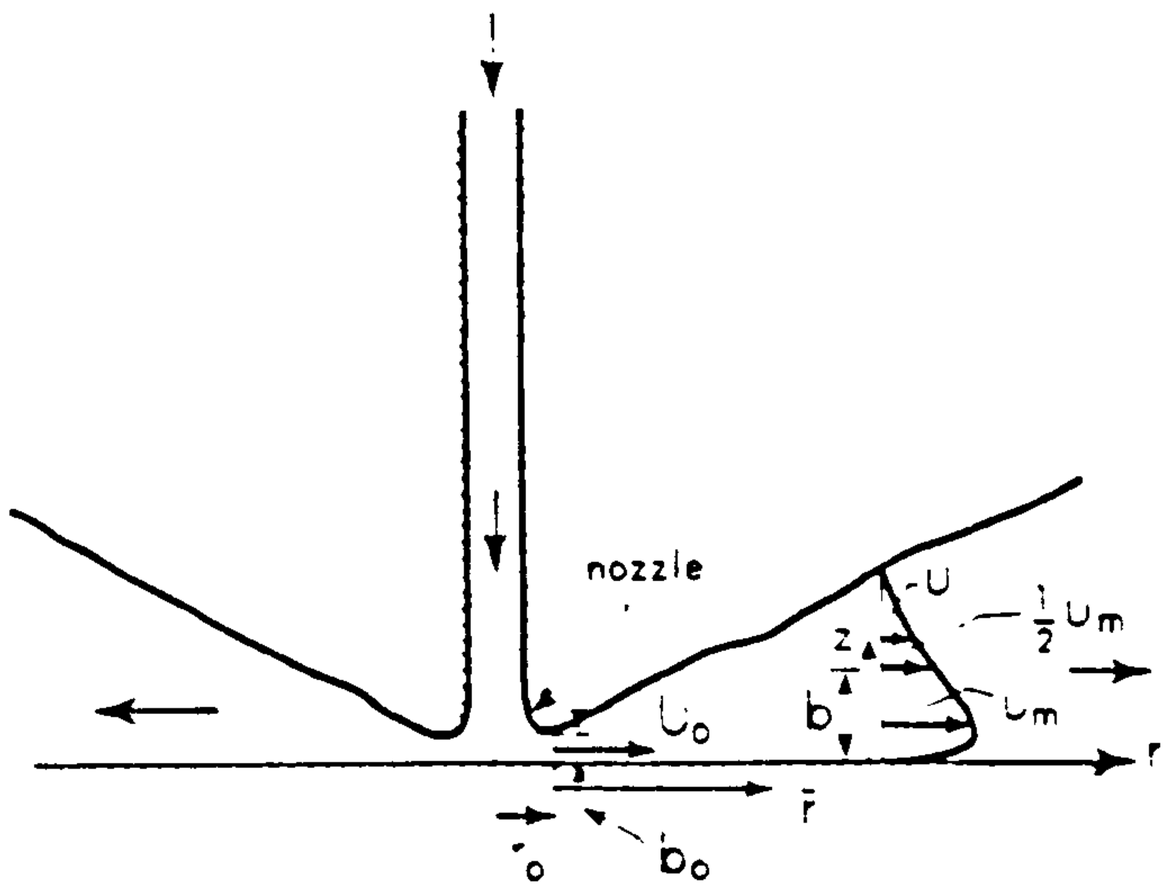

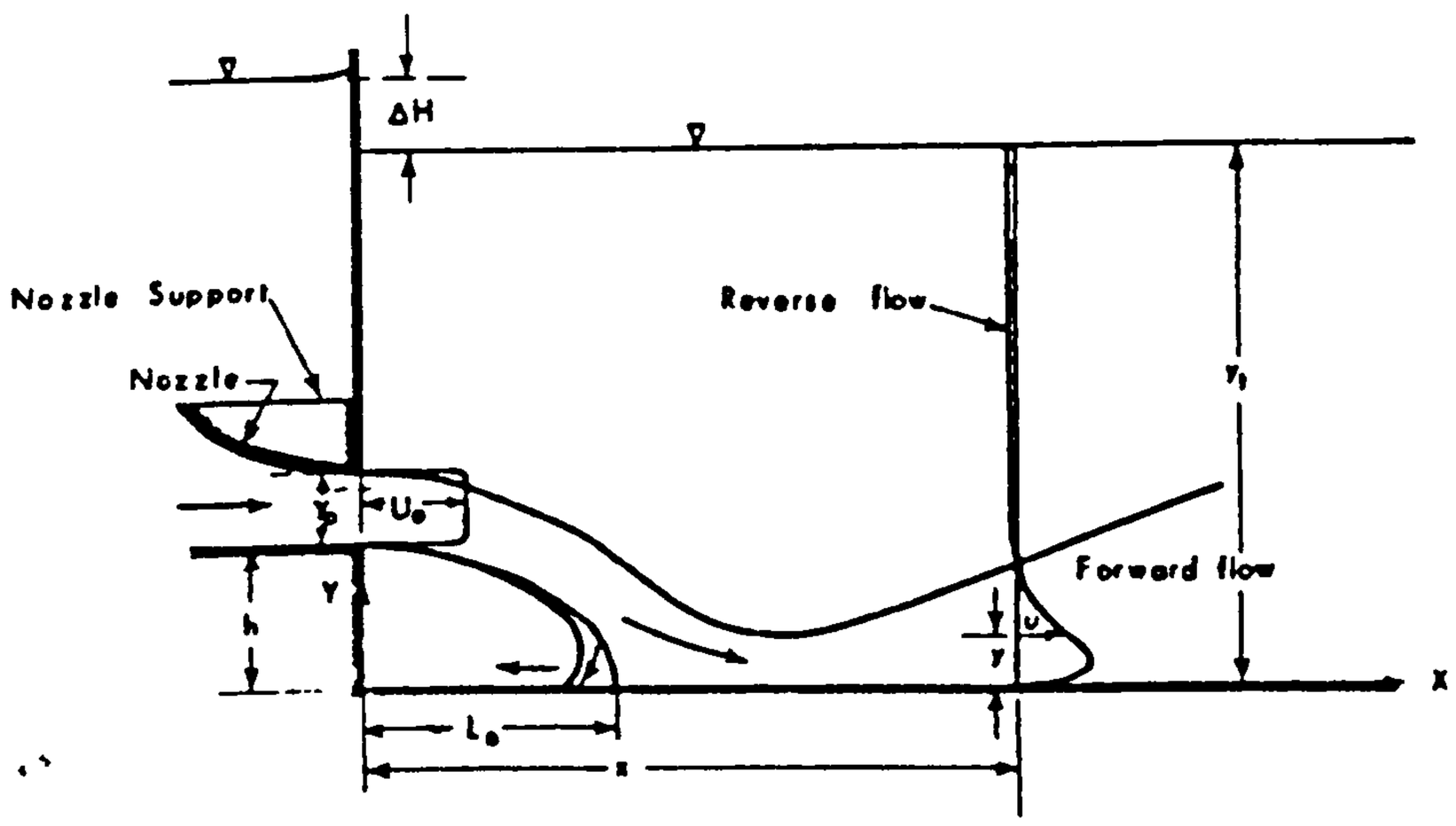

Fig. 3.1 Jet-boundary interaction

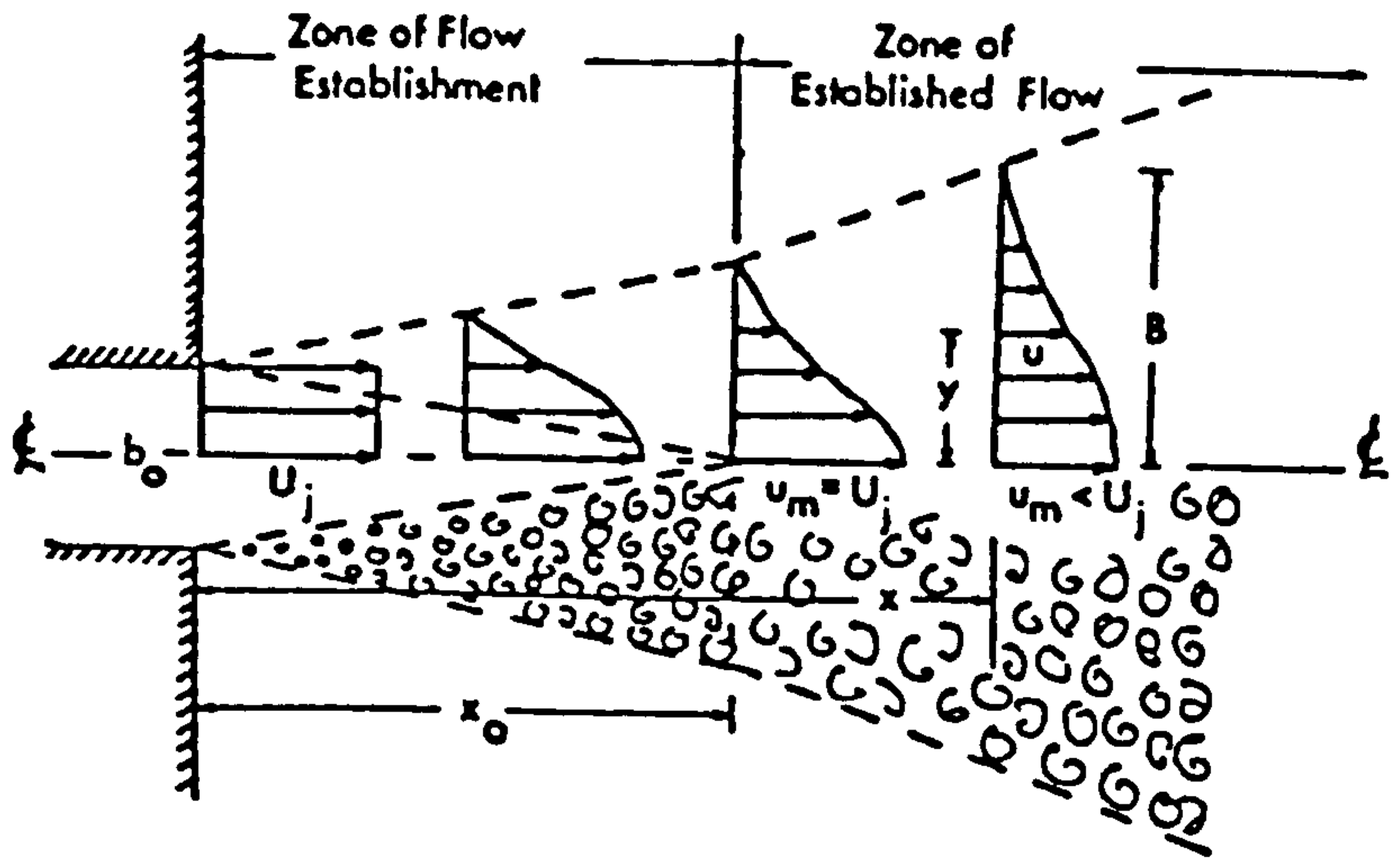

Fig. 3.2 Schematic Representation of Jet Diffusion

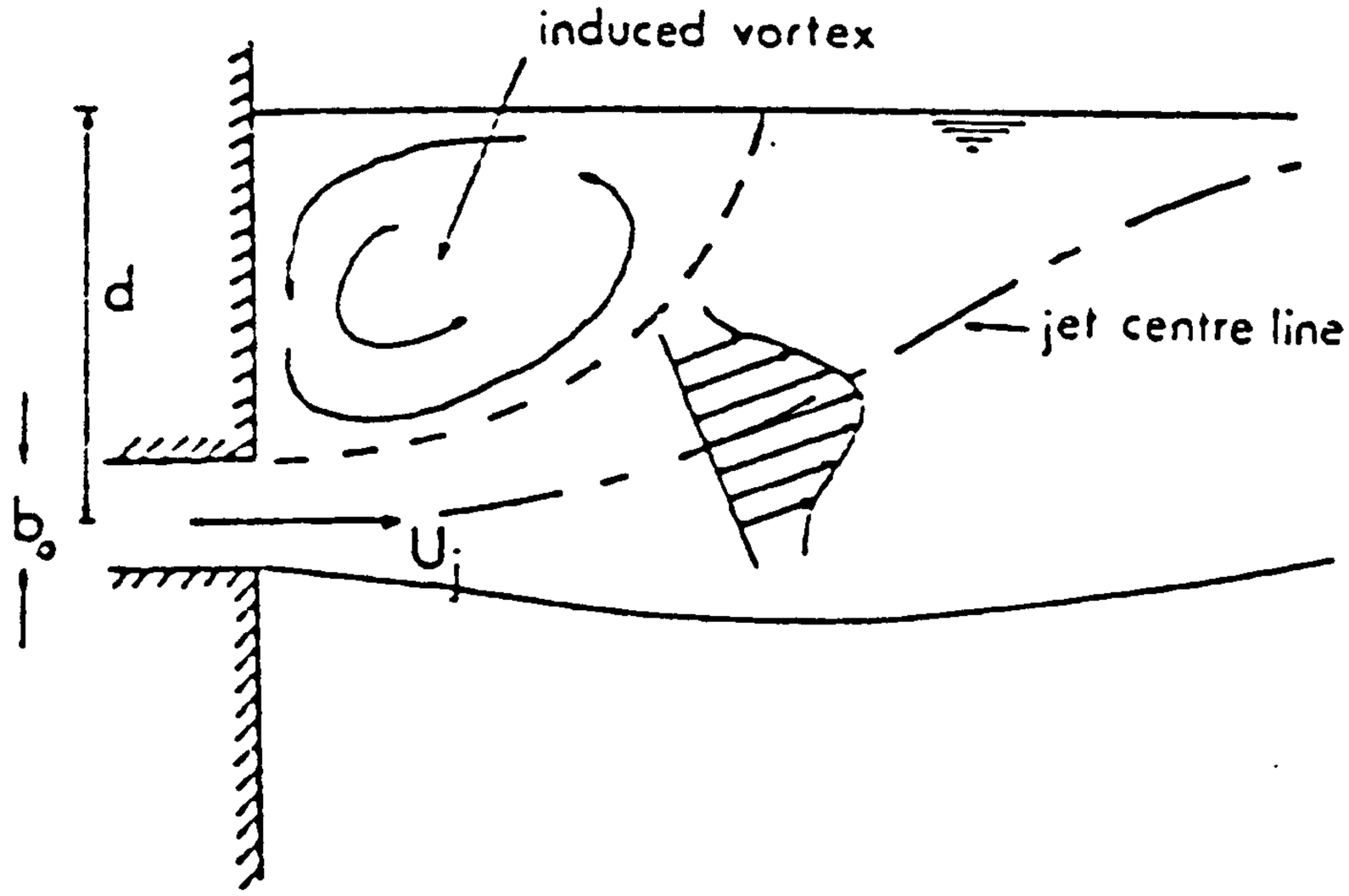

Fig. 3.3) Schematic Representation of a Shallow Jet Near to the Free-Surface

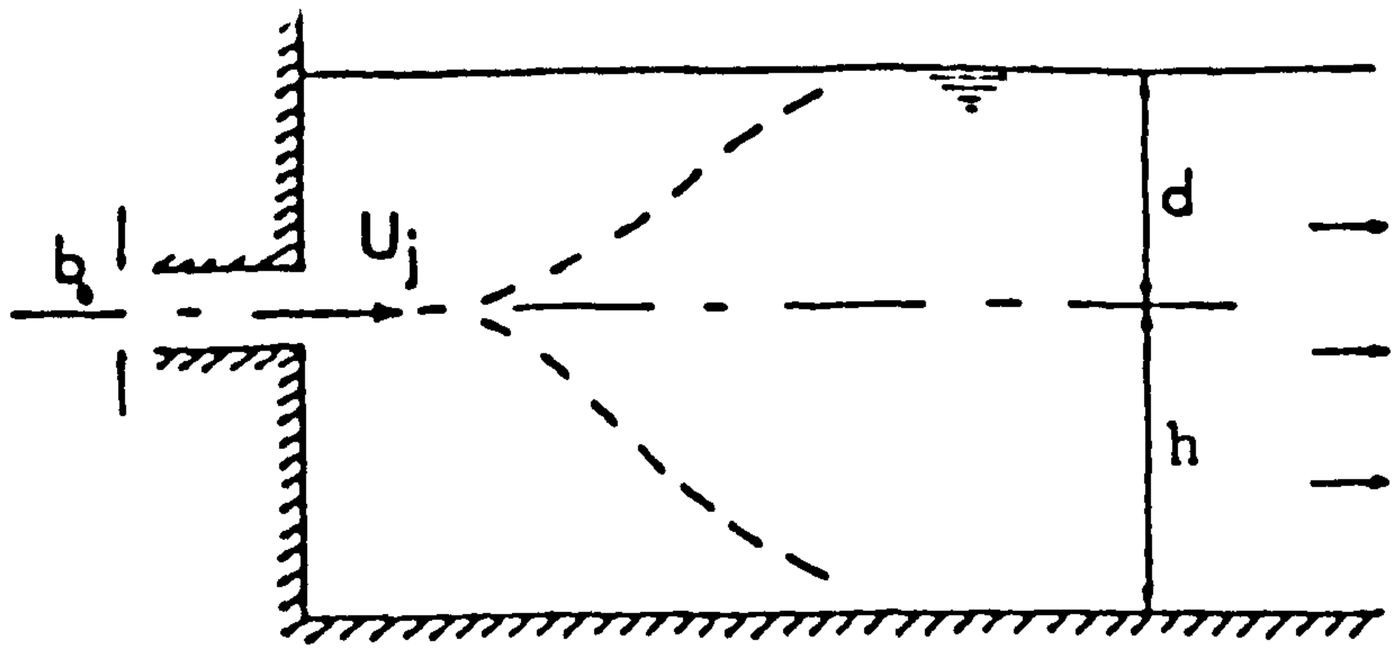

Fig. 3.4 The Shallow Jet With the Bed Offset and Parallet to the Slot

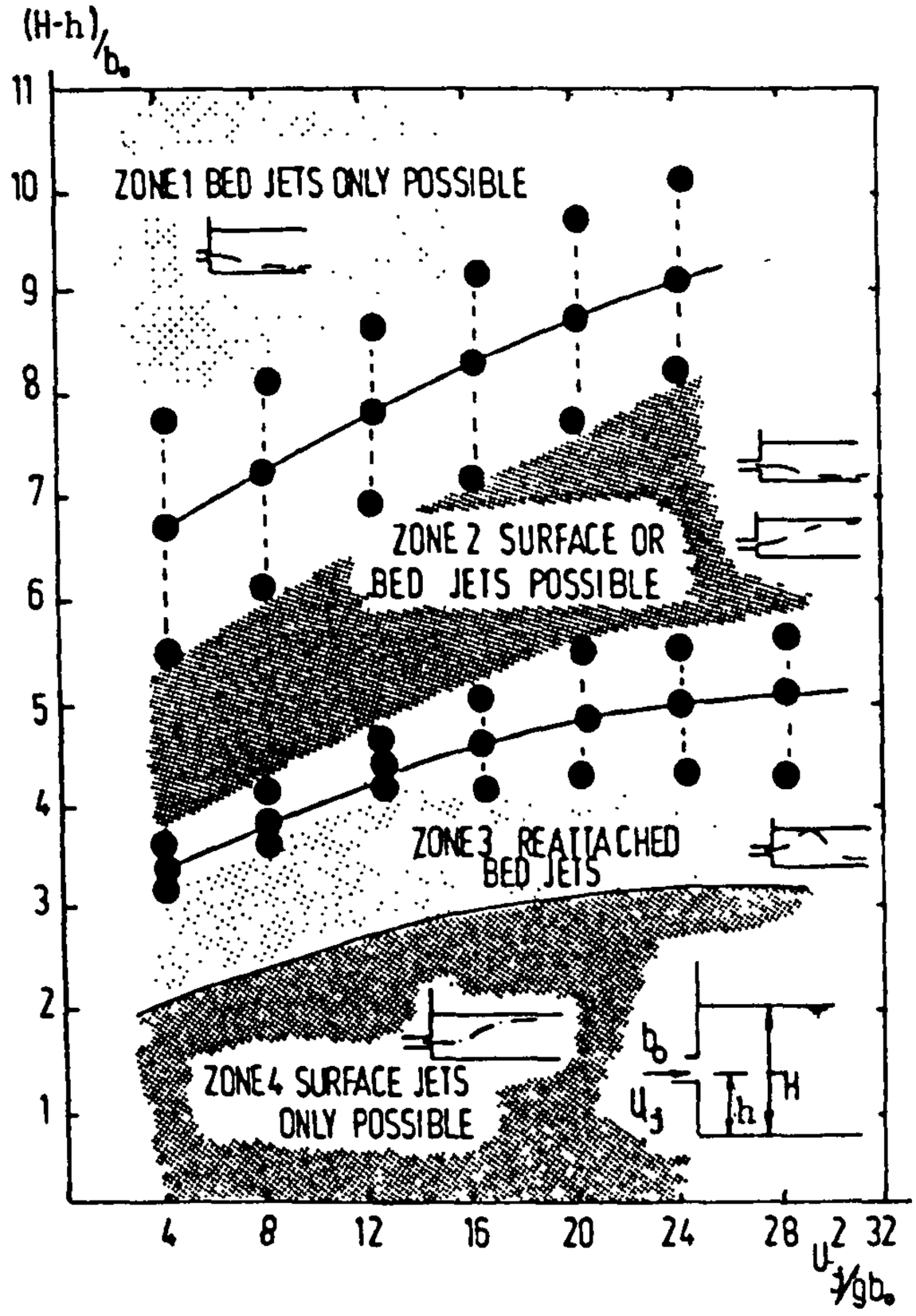

Fig. 3.5 Location of Non-buoyant Jets Observed by Coates (1976) and Measured by Johnston (1978)

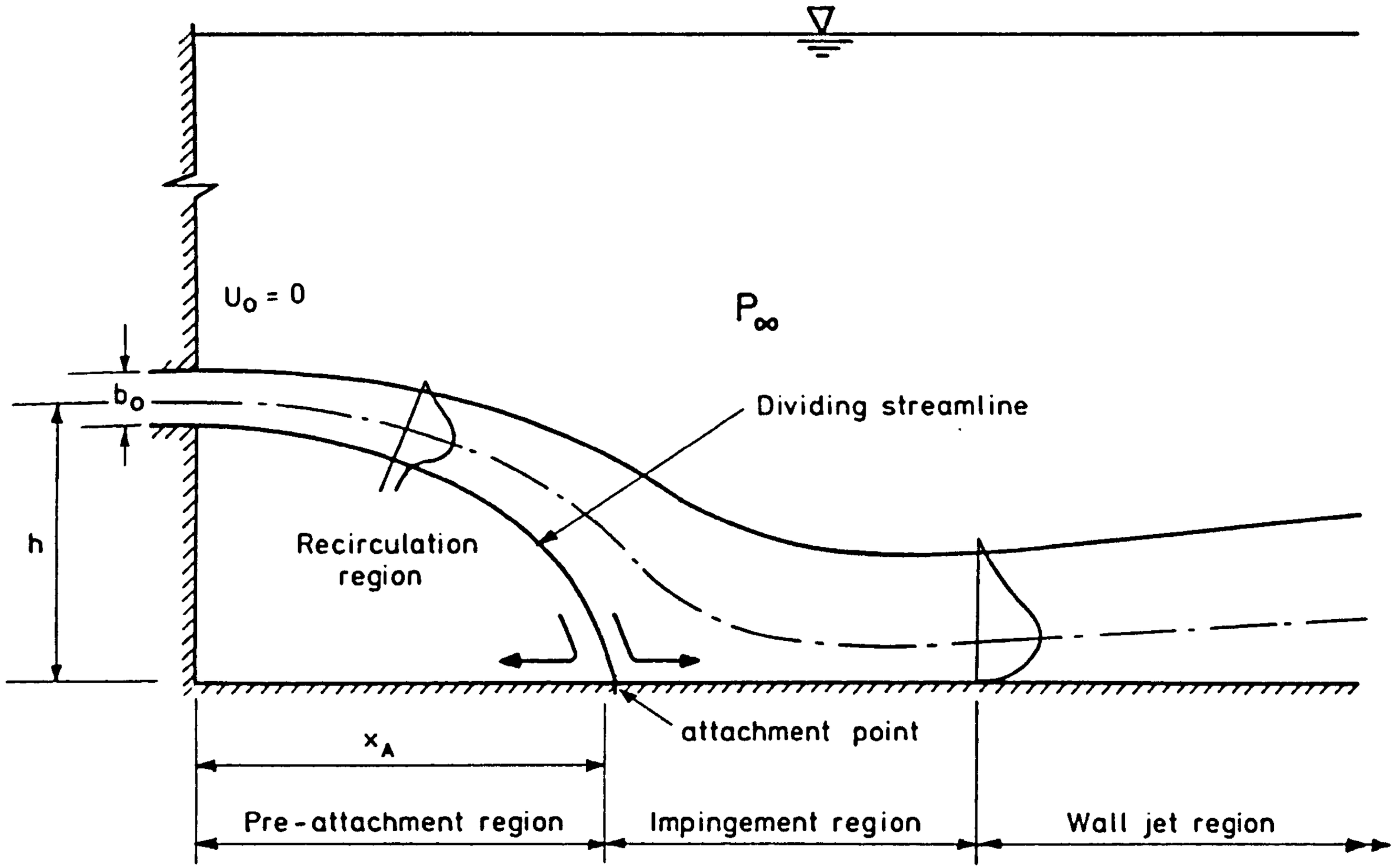

FIG. 3. 6 DEFINITION SKETCH FOR AN OFFSET JET

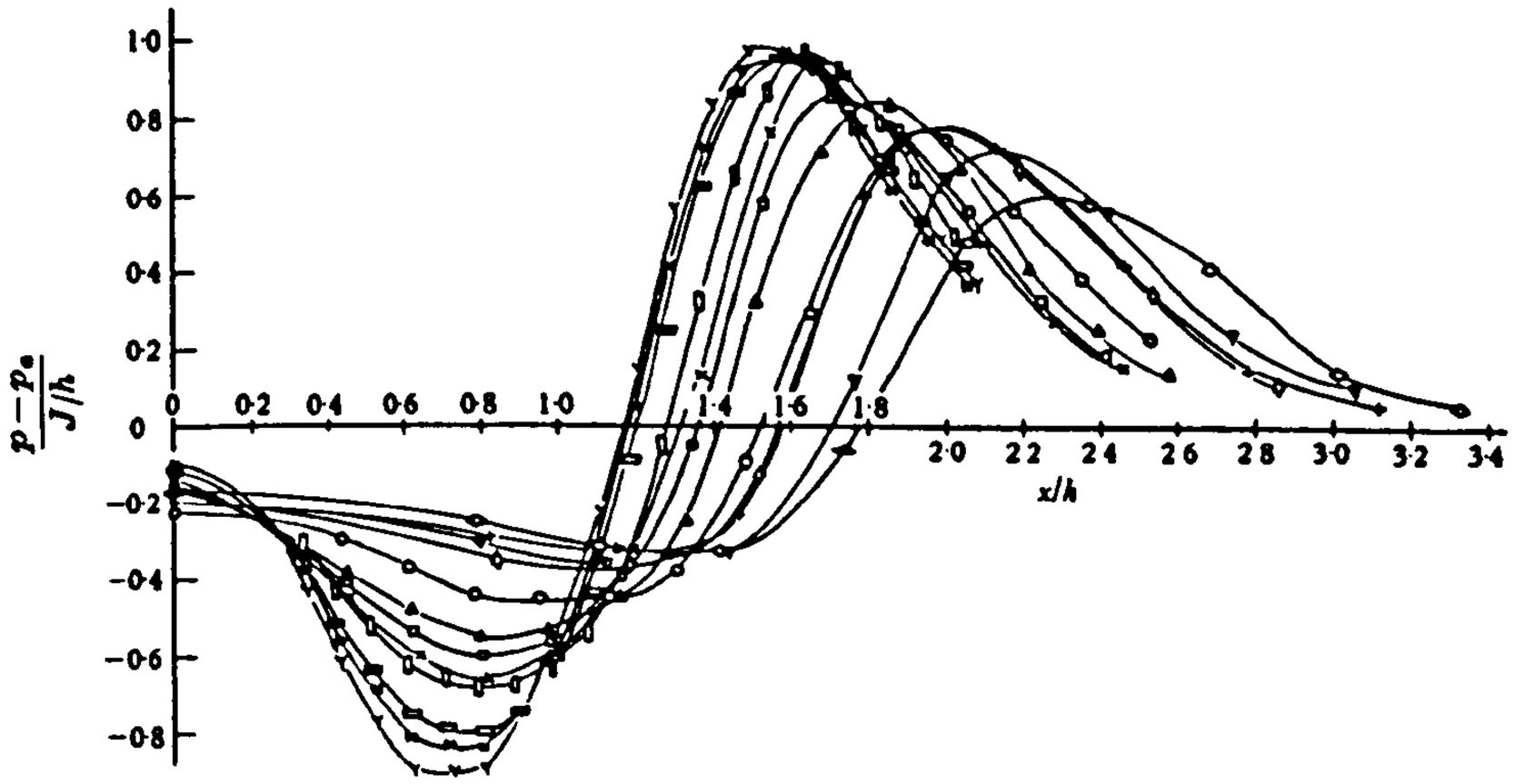

Symbol	h/b_o	Symbol	h/b_o
◇	4·15	□	9·13
▽	4·81	×	10·64
+	5·92	▯	10·65
◇	6·99	⬭	14·06
○	5·62	*	16·74
△	7·35	Y	24·40

Fig. 3.7 Static Pressure Distribution Along the Plate

(After Sawyer (1960))

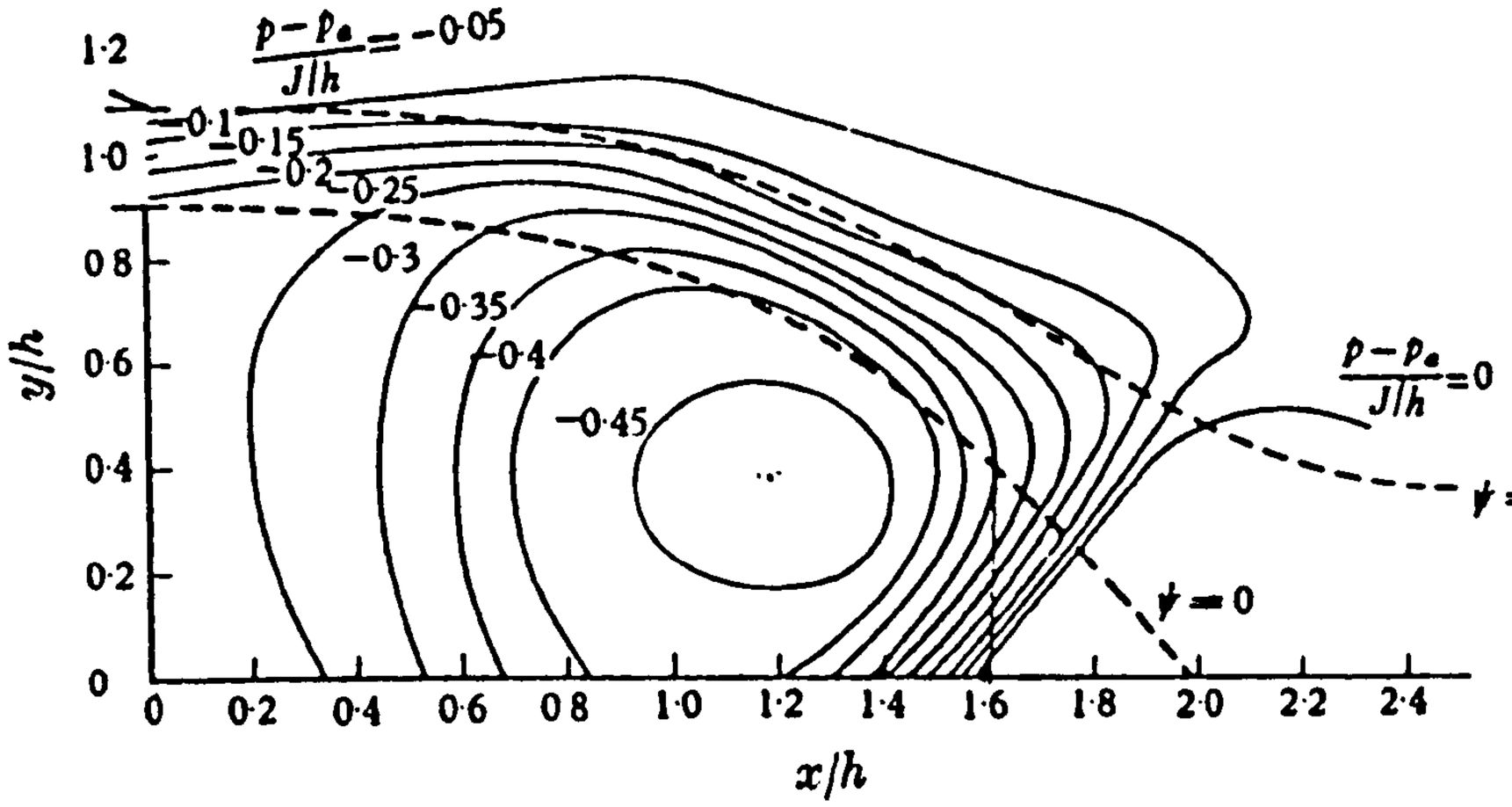

Fig. 3.8 Static Pressure Contoures for Case h/b_o = 5.62

(After Sawyer(1960))

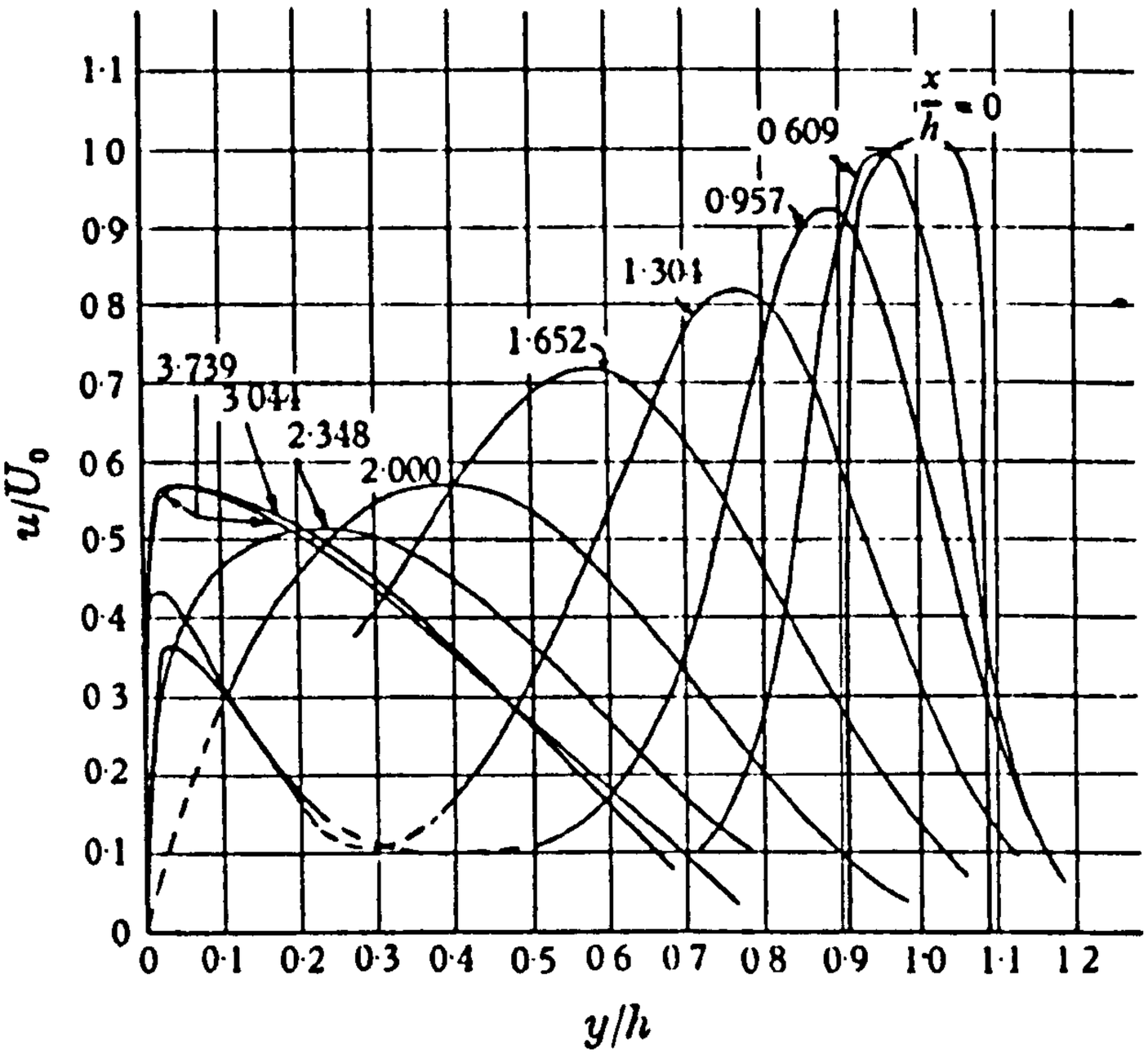

Fig. 3.9 Velocity Profiles for case h/b_o = 5.62

(After Sawyer (1960))

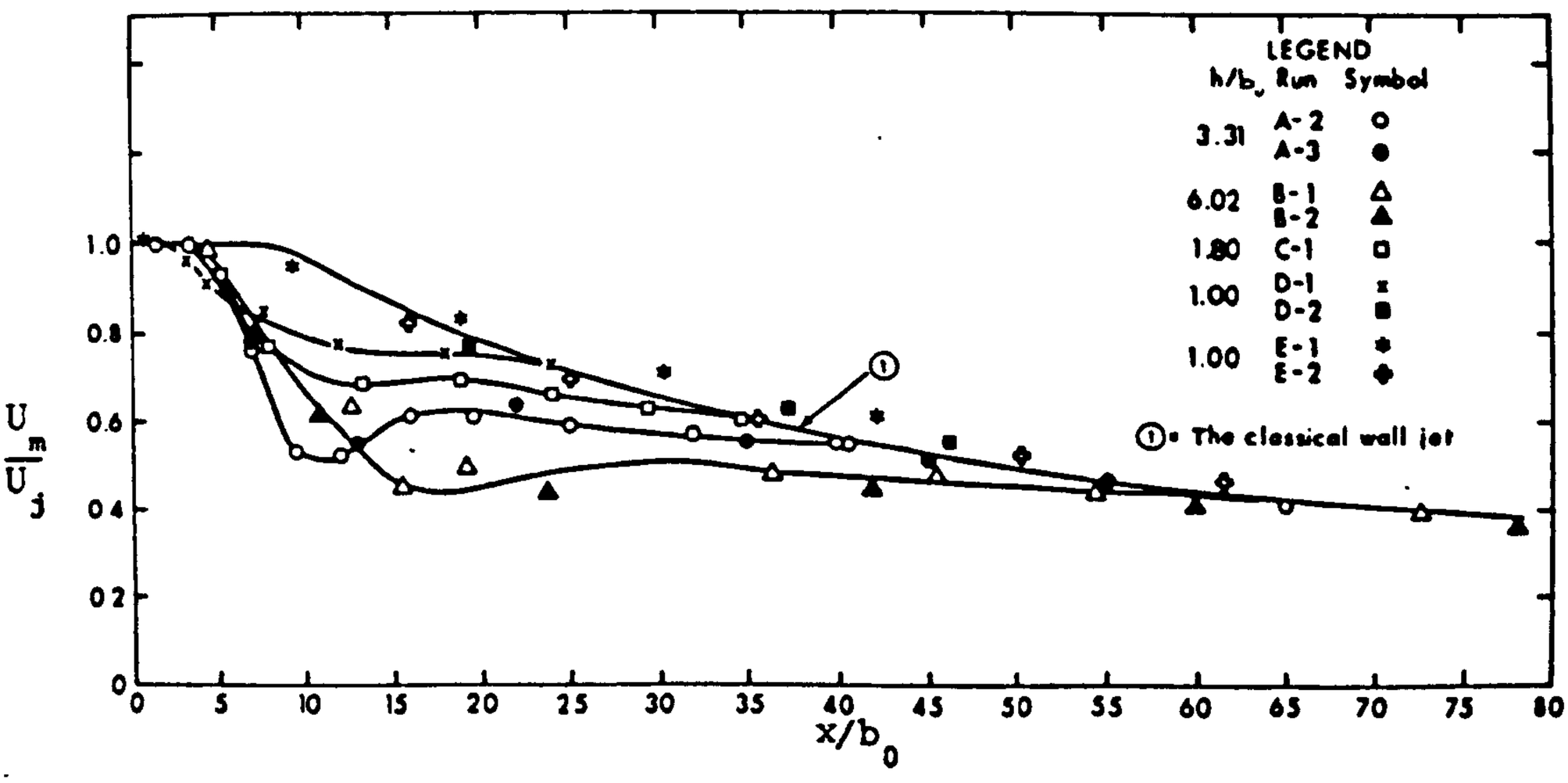

Fig. 3.10 Decay of the Max. Velocity for Offse Jets

(After Rajaratnam (1968))

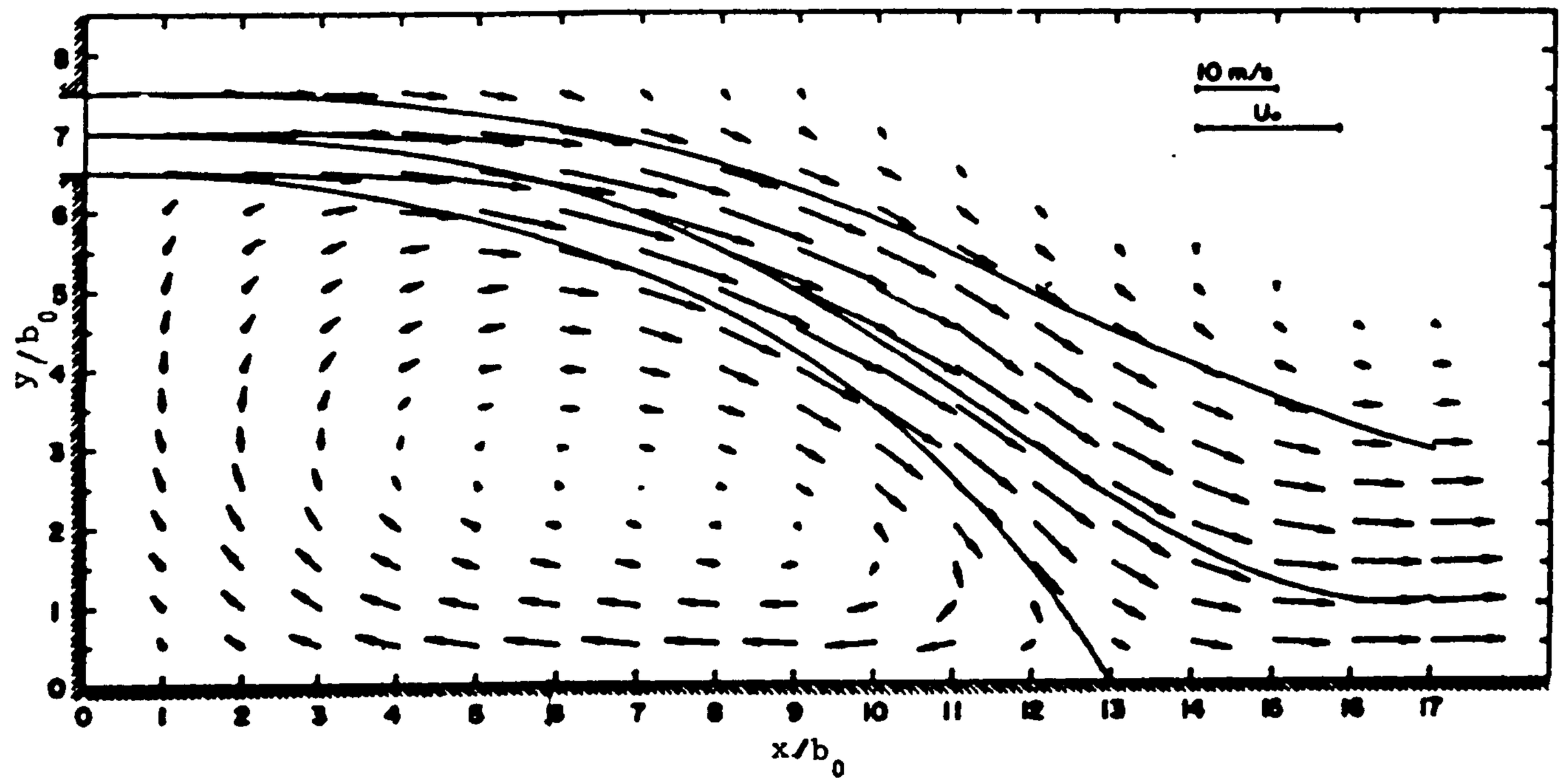

Fig. 3.11 Velocity Vectors of an Offset Jet (After Pelfrey (1984))

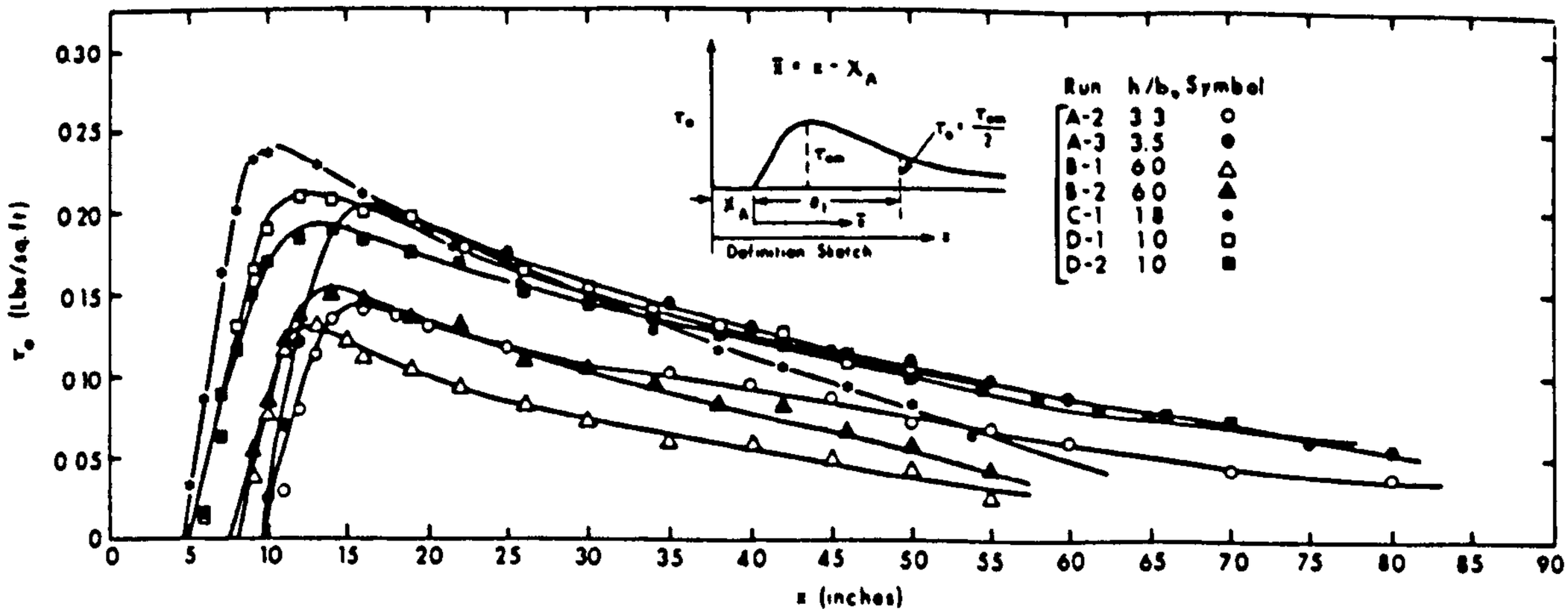

Fig. 3.12 Bed Shear Stress Plots (After Rajaratnam (1968))

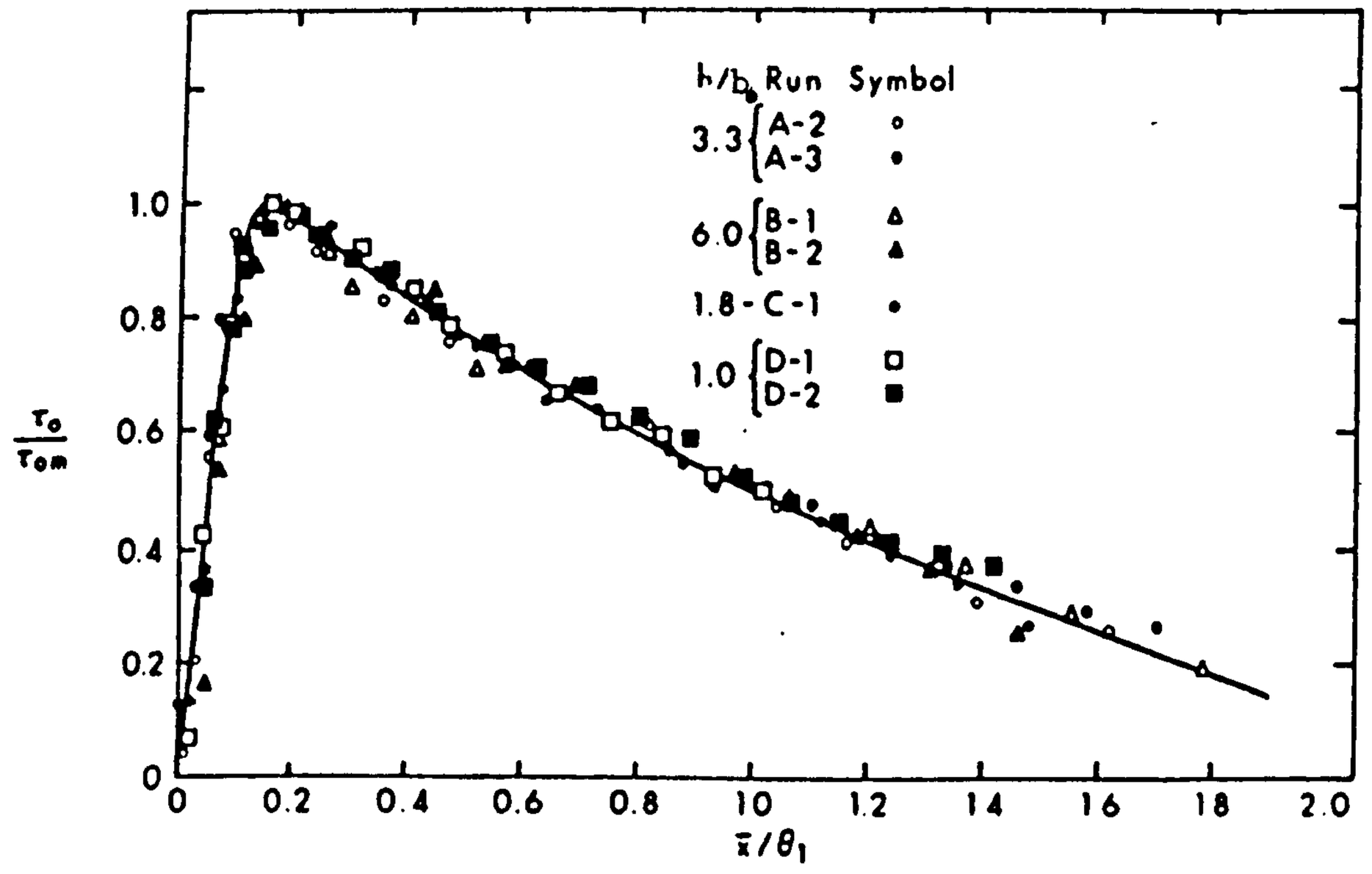

Fig. 3.13 Distribution of the Bed Shear Stress

(After Rajaratnam (1968))

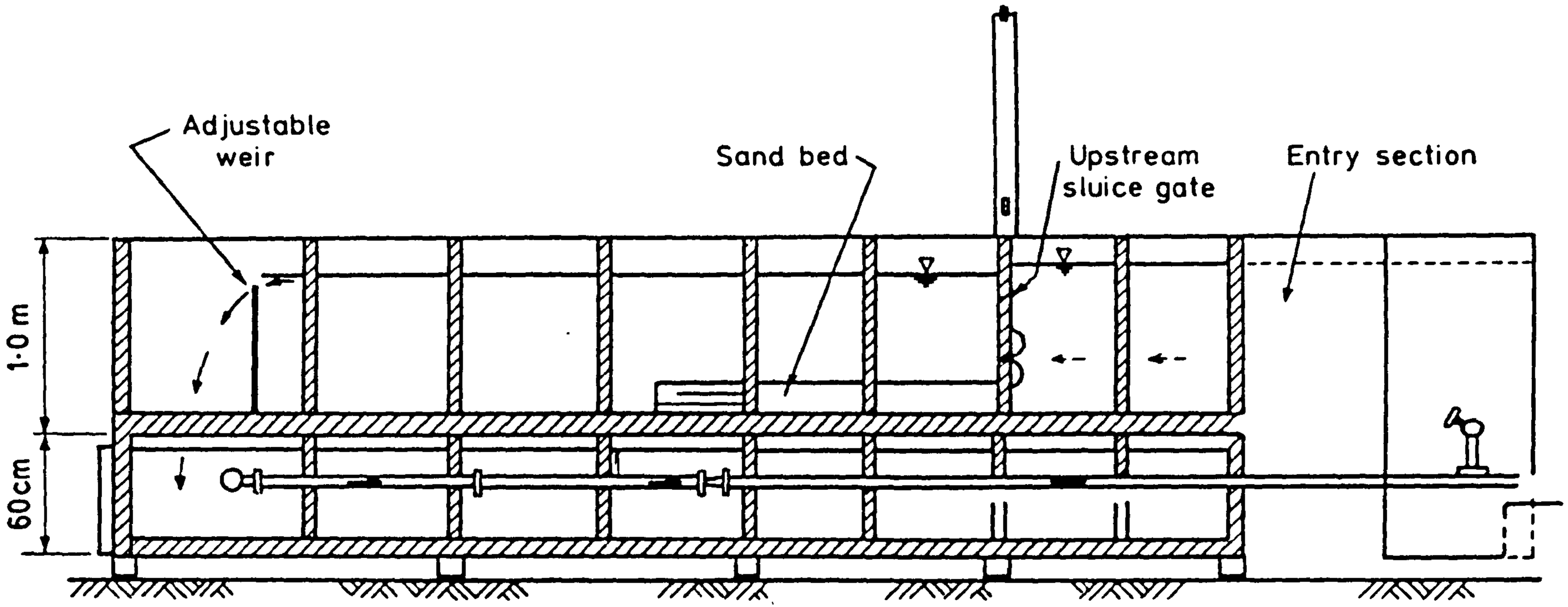

FIG 4.1 SKETCH OF LABORATORY LAYOUT

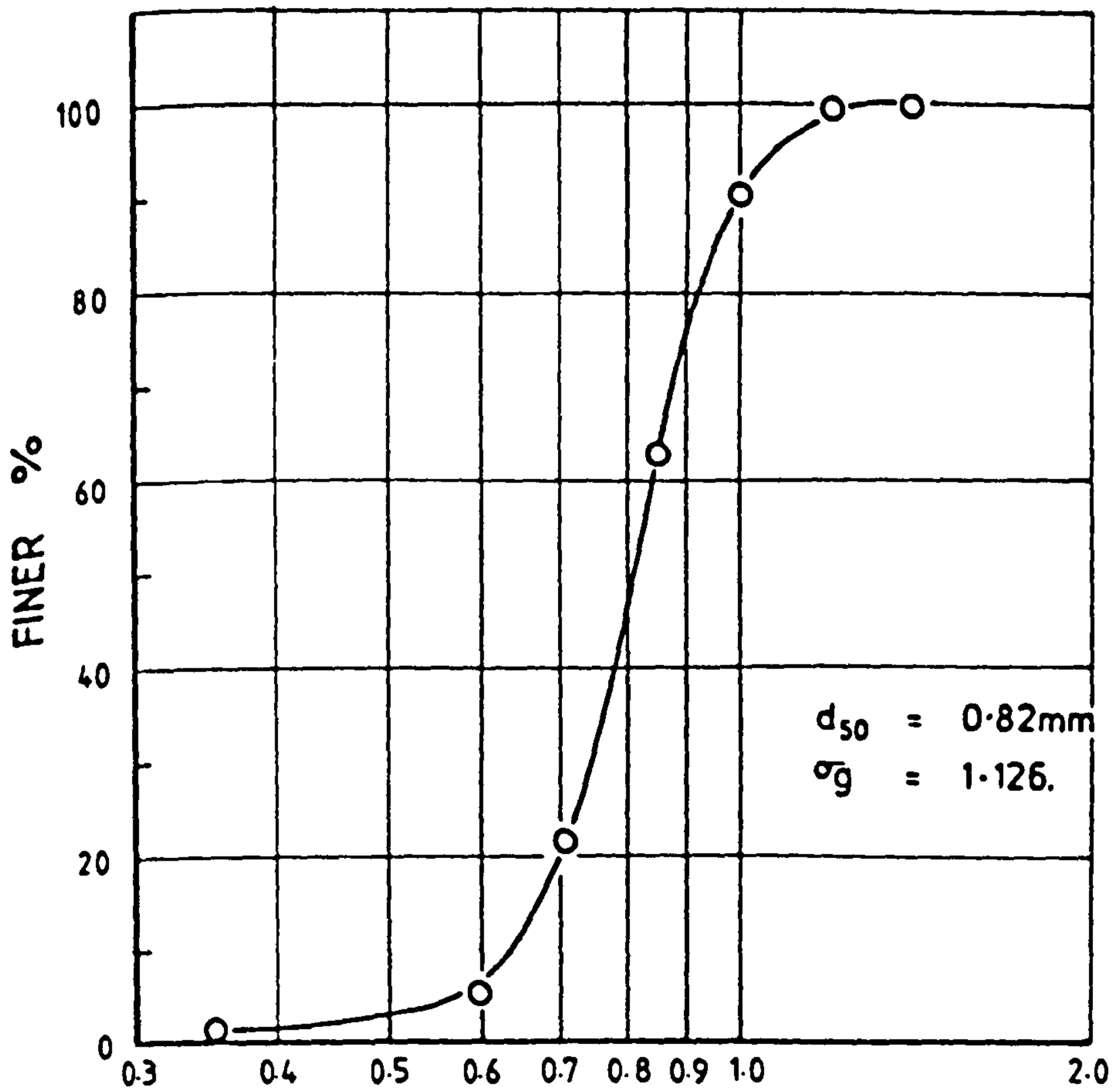

FIG. 4.2 CUMULATIVE SIZE DISTRIBUTION CURVE

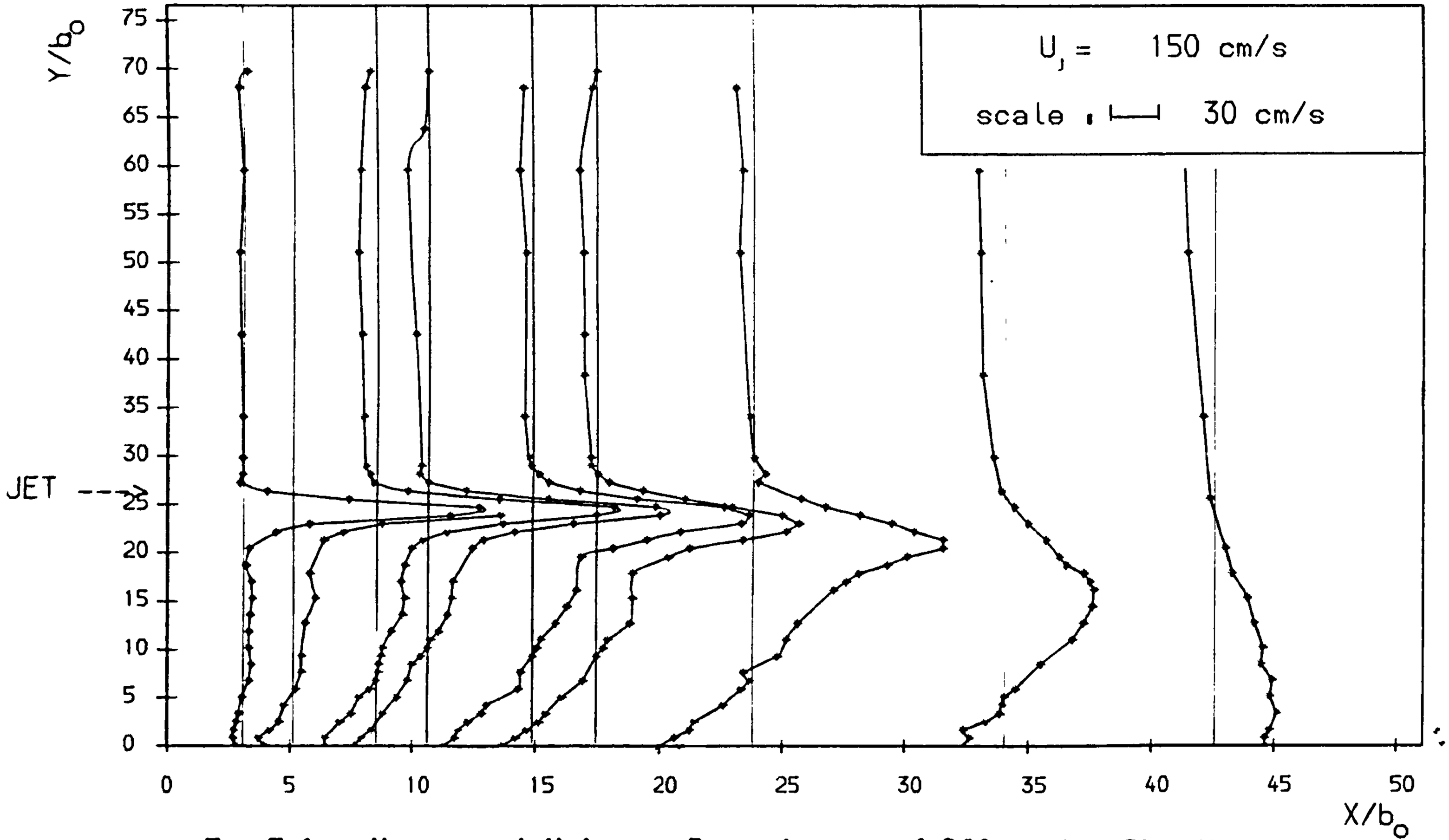

Fig 5.1-a Horizontal Velocity Distribution of Offset Jet (No. 4)

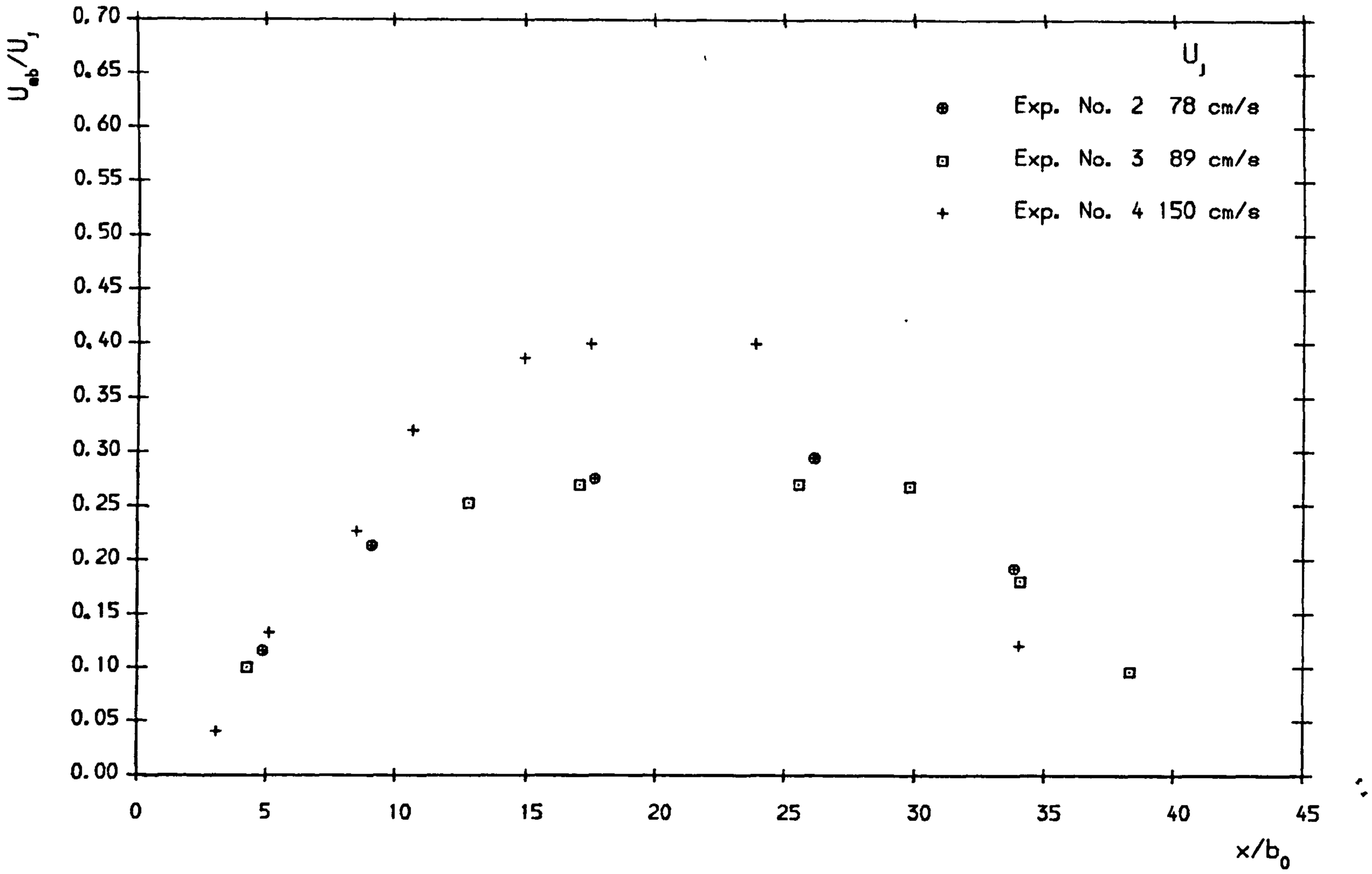

Fig. 5.1b Distr. of Max. Vel. of Near-bed Flow for Offset-Jet

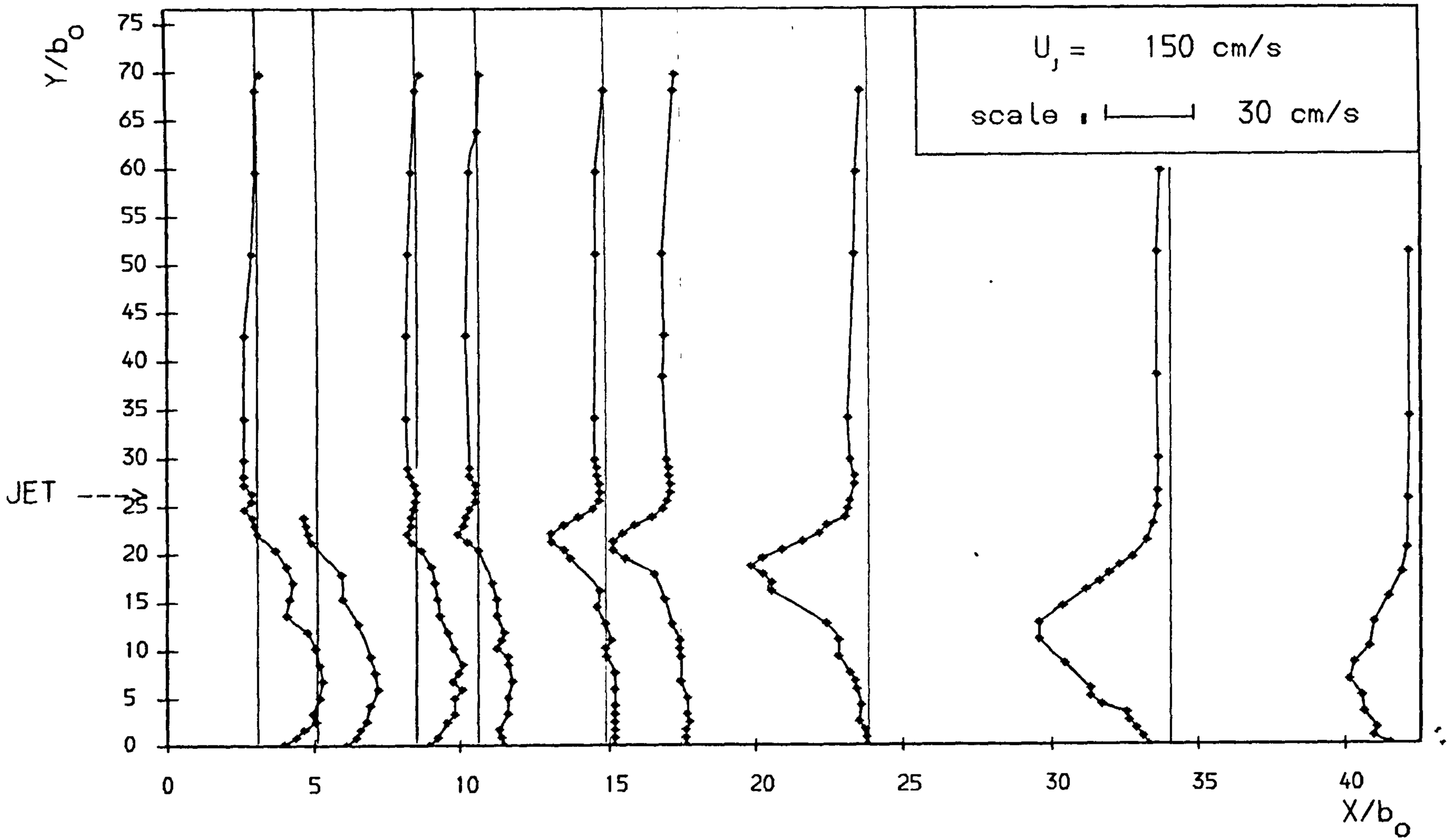

Fig 5.2 Vertical Velocity Distribution of Offset Jet (No. 4)

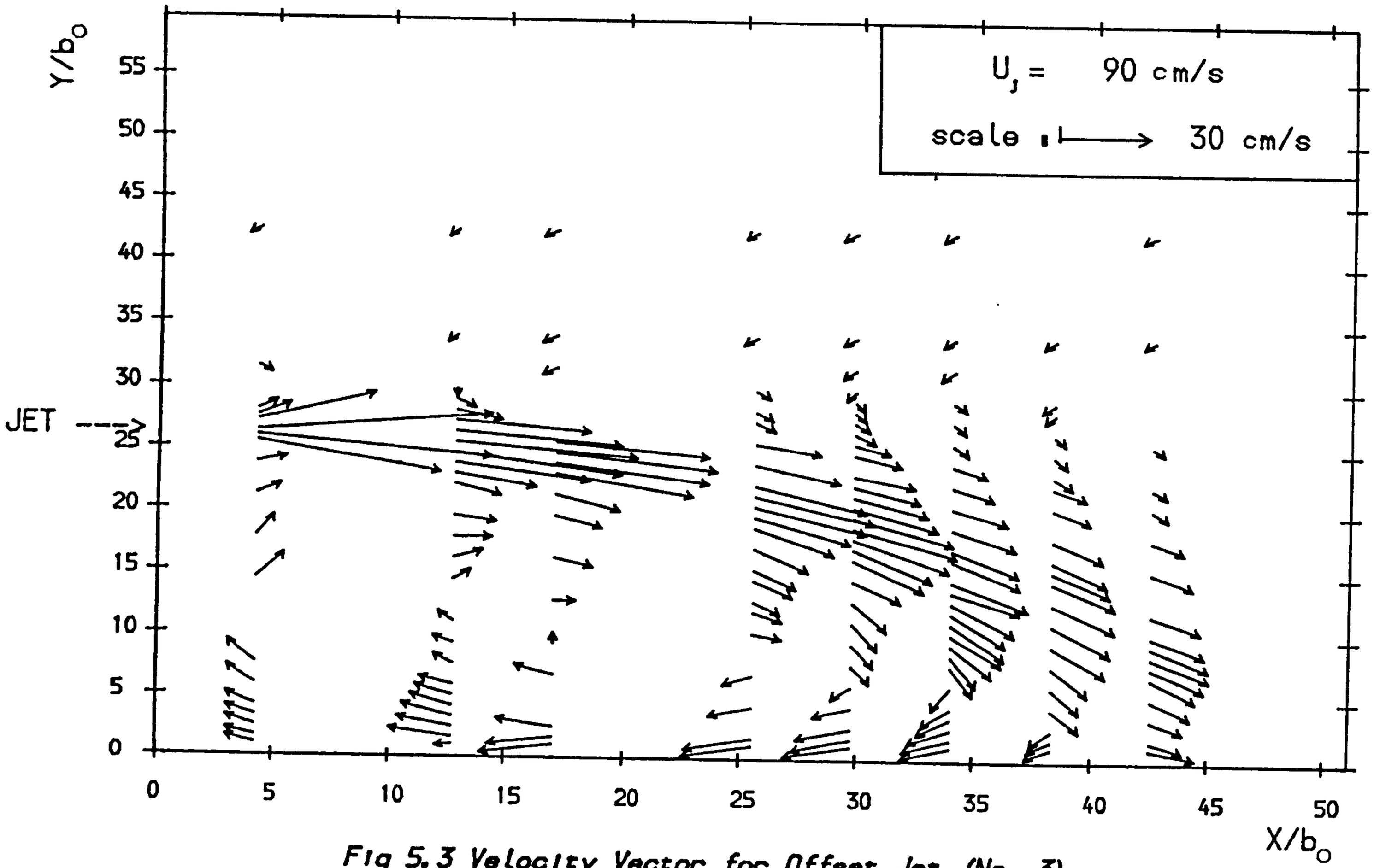

Fig 5.3 Velocity Vector for Offset Jet (No. 3)

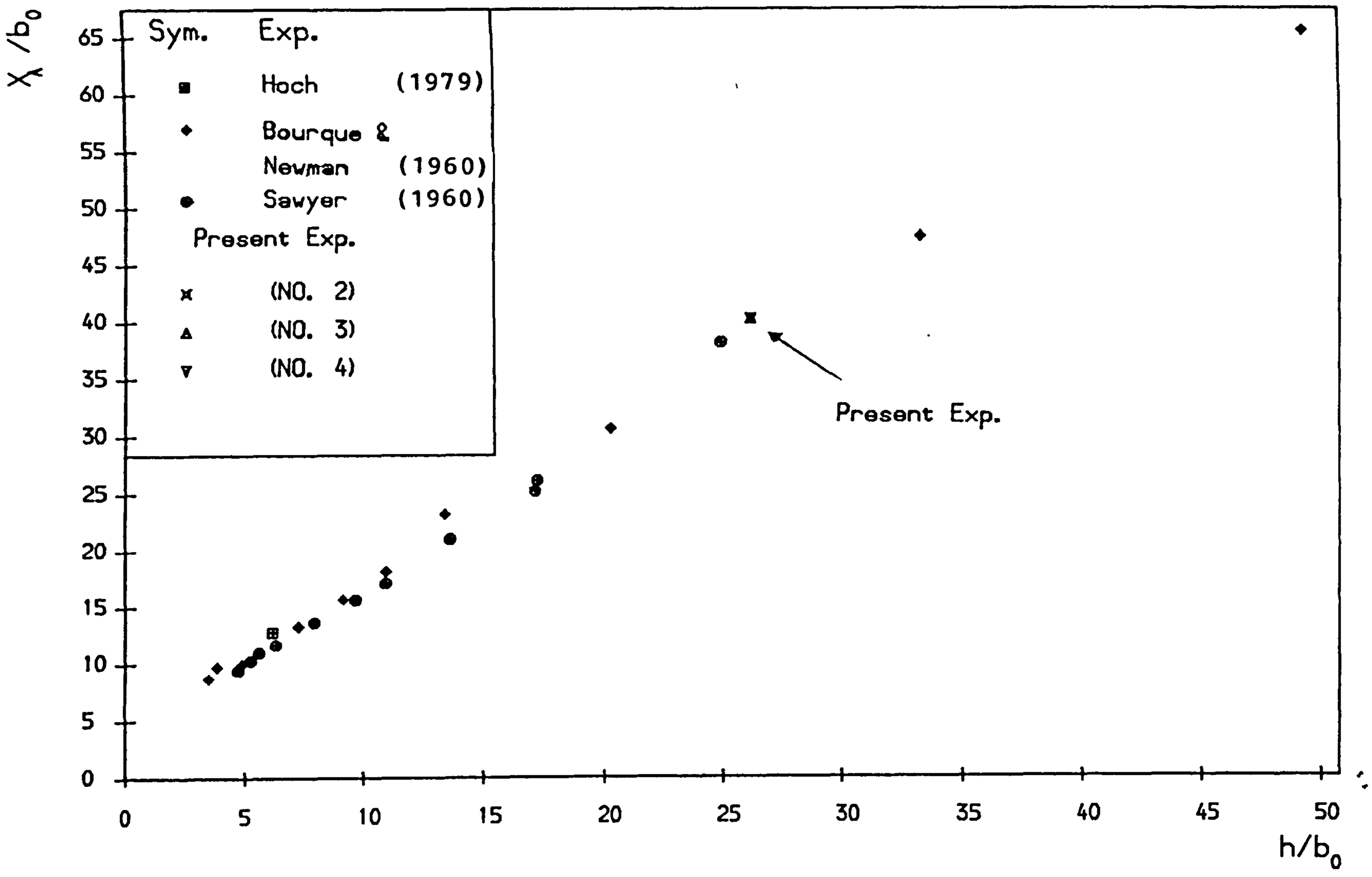

Fig 5.4 Attachment Length vs. Offset Ratio

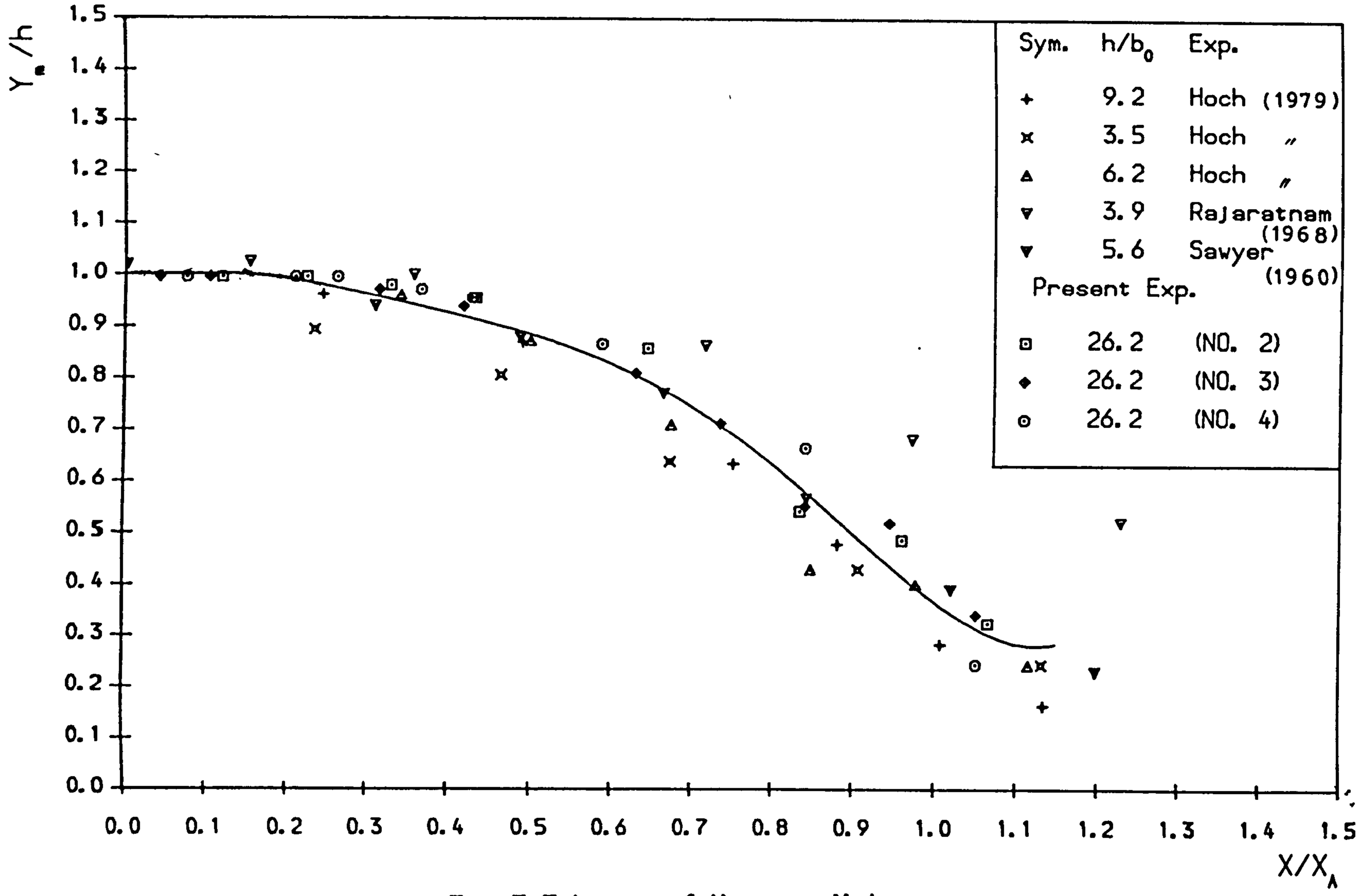

Fig 5.5 Locus of Maximum Velocity

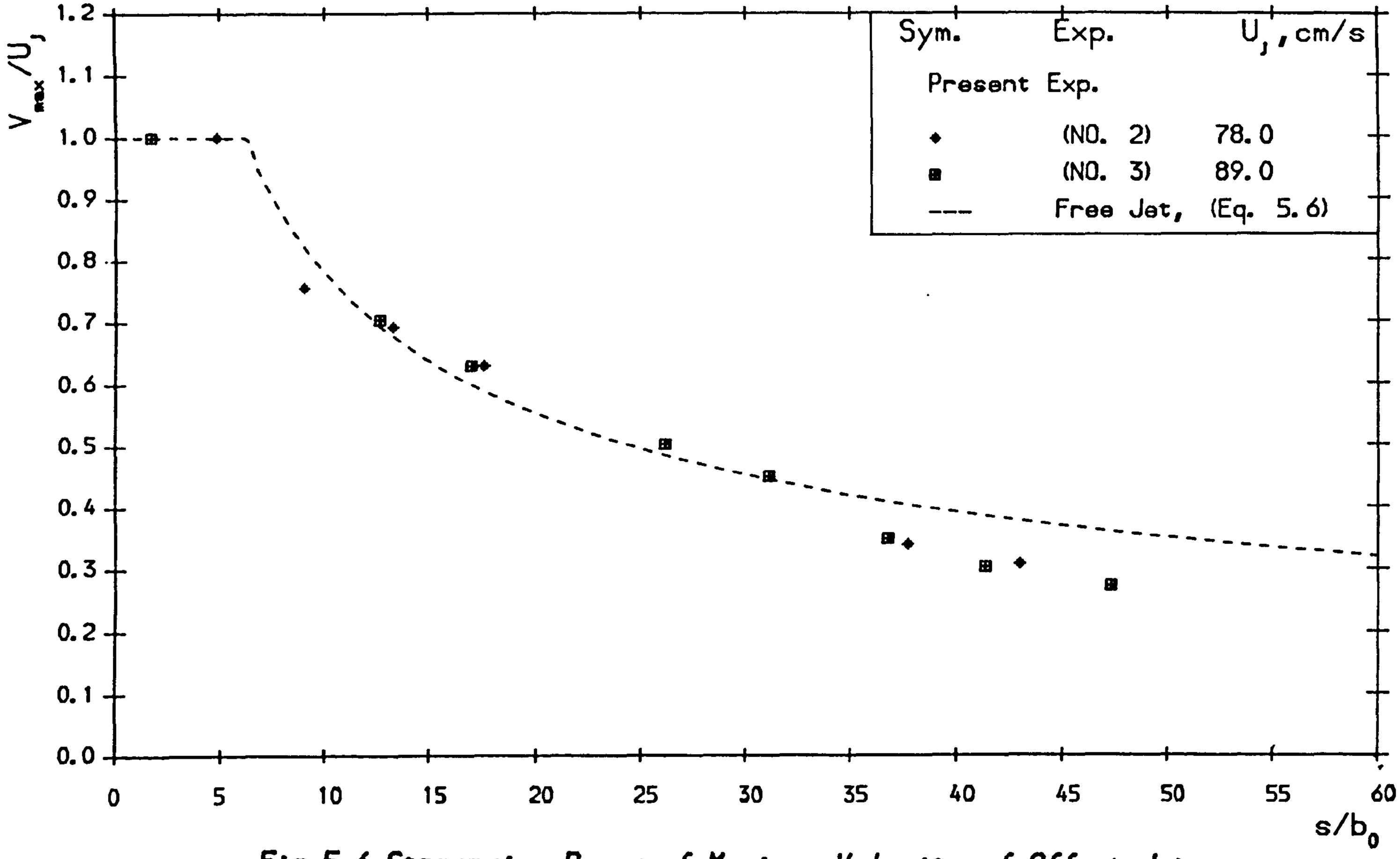

Fig 5.6 Streamwise Decay of Maximum Velocity of Offset Jet

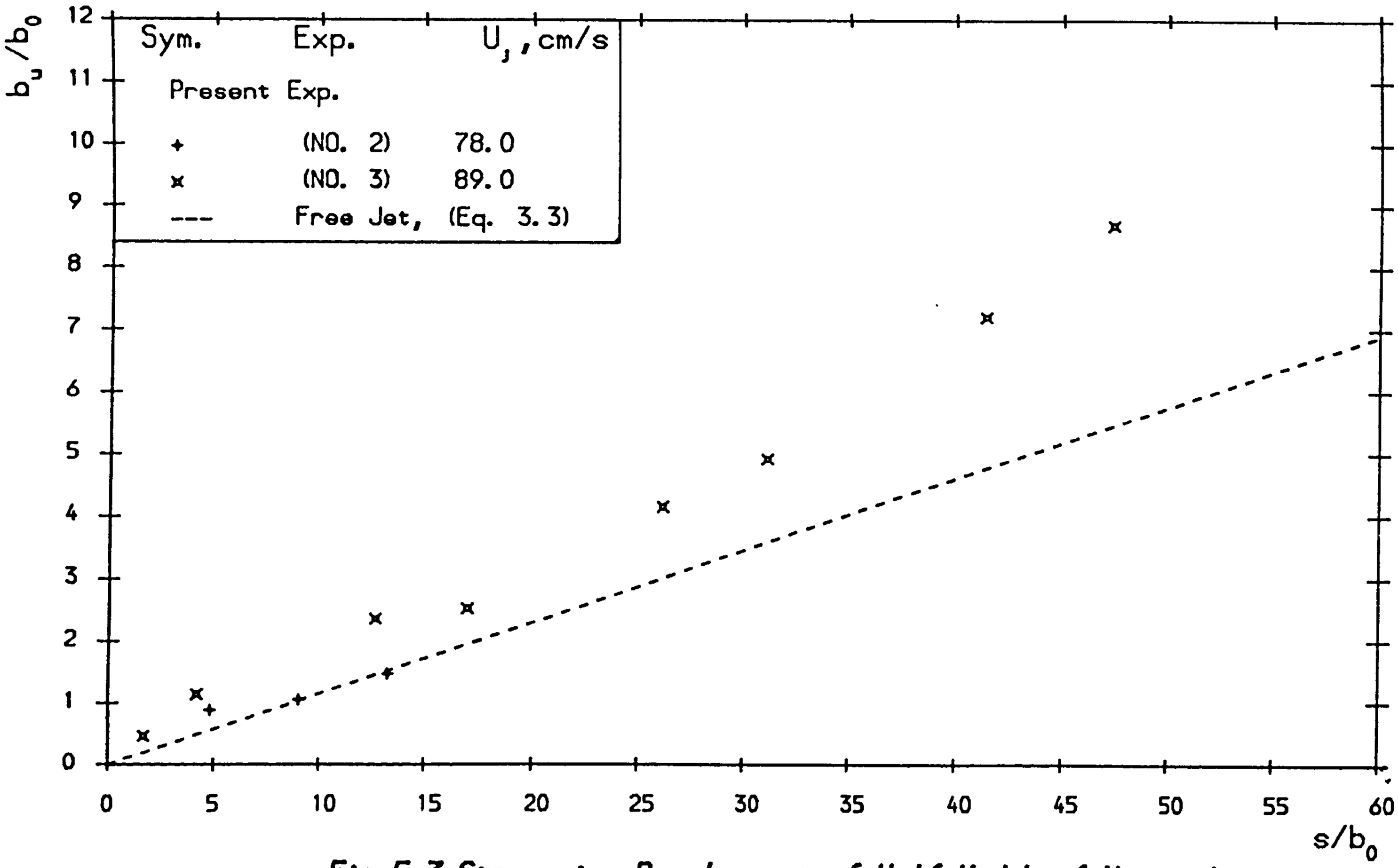

Fig 5.7 Streamwise Development of Half-Width of Upper Jet

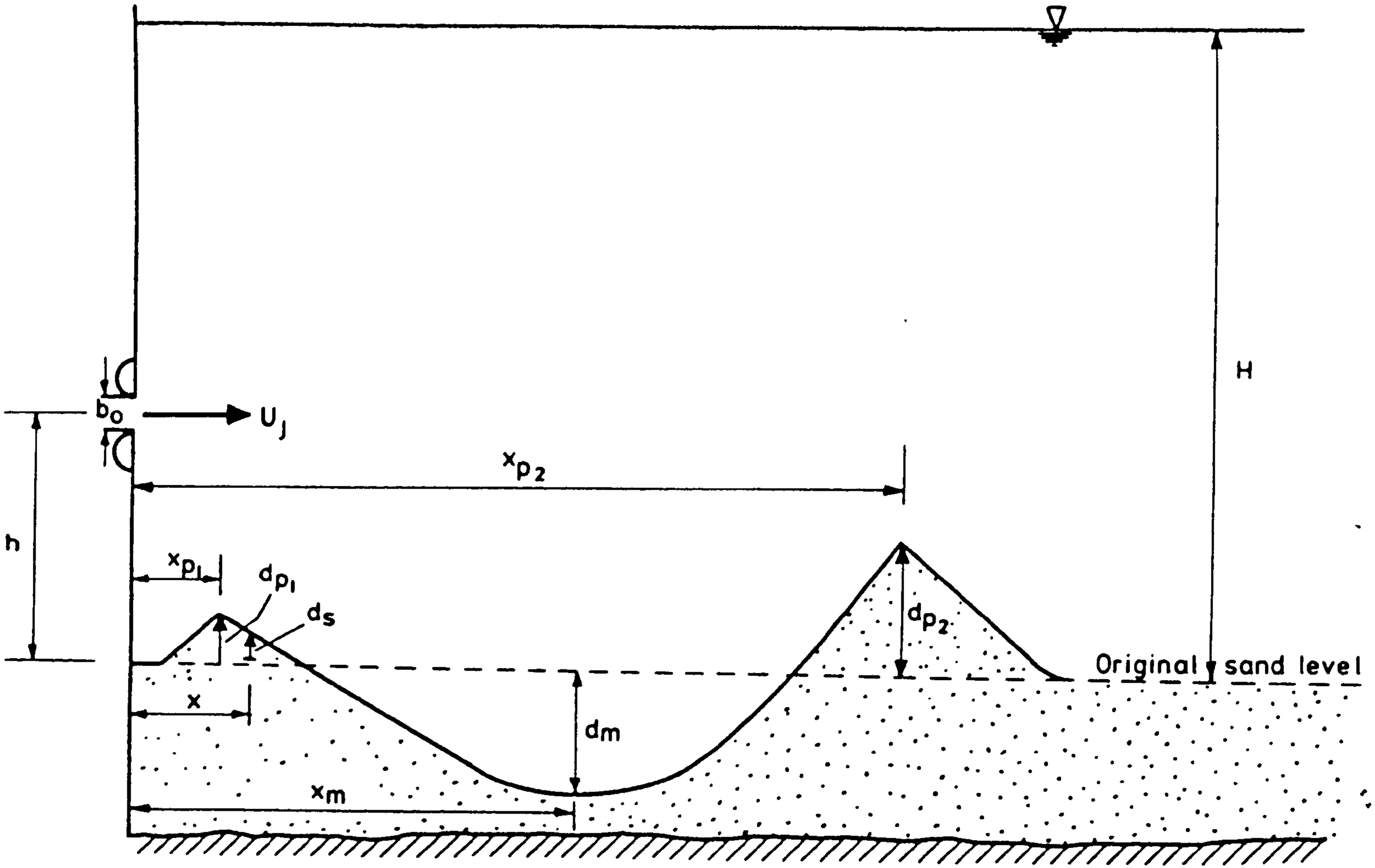

FIG. 6.1 DEFINITION SKETCH FOR A SCOUR HOLE

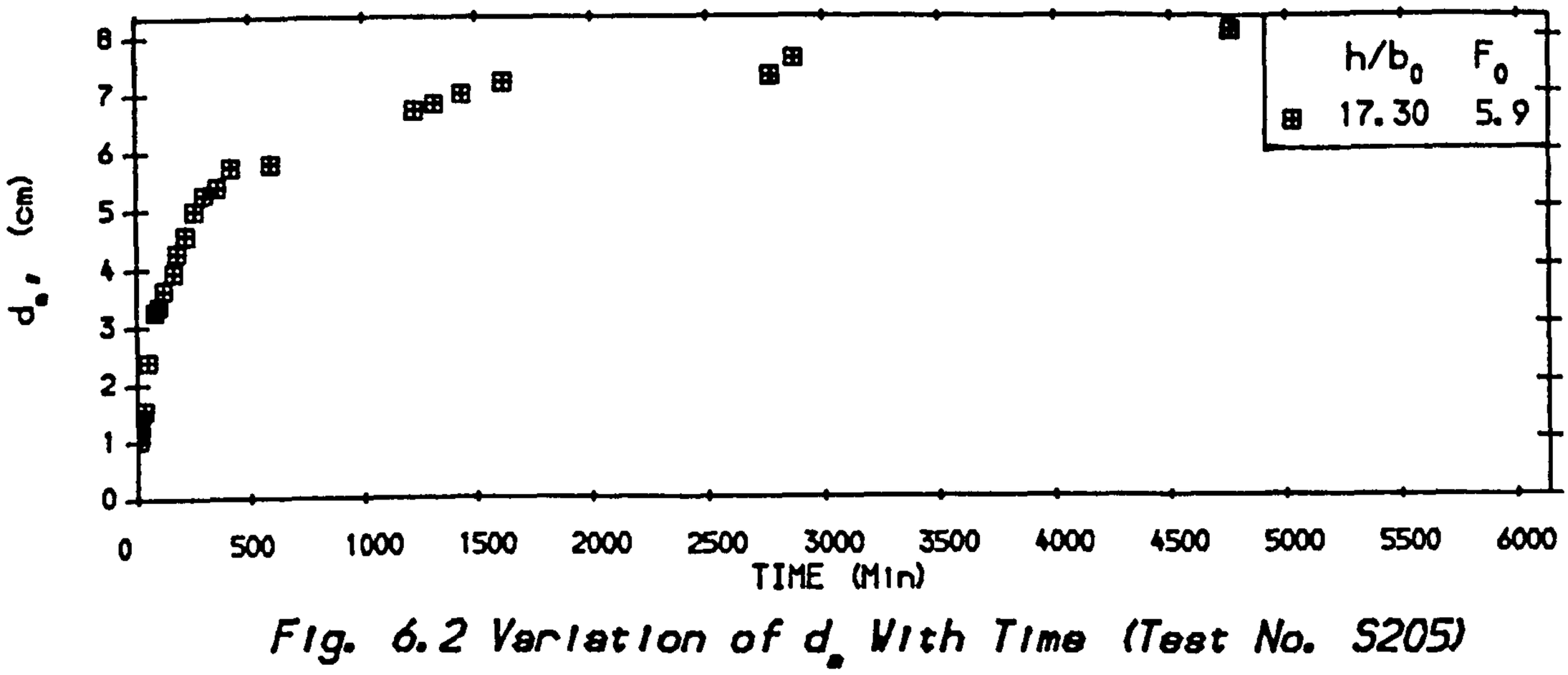

Fig. 6.2 Variation of d_* With Time (Test No. S205)

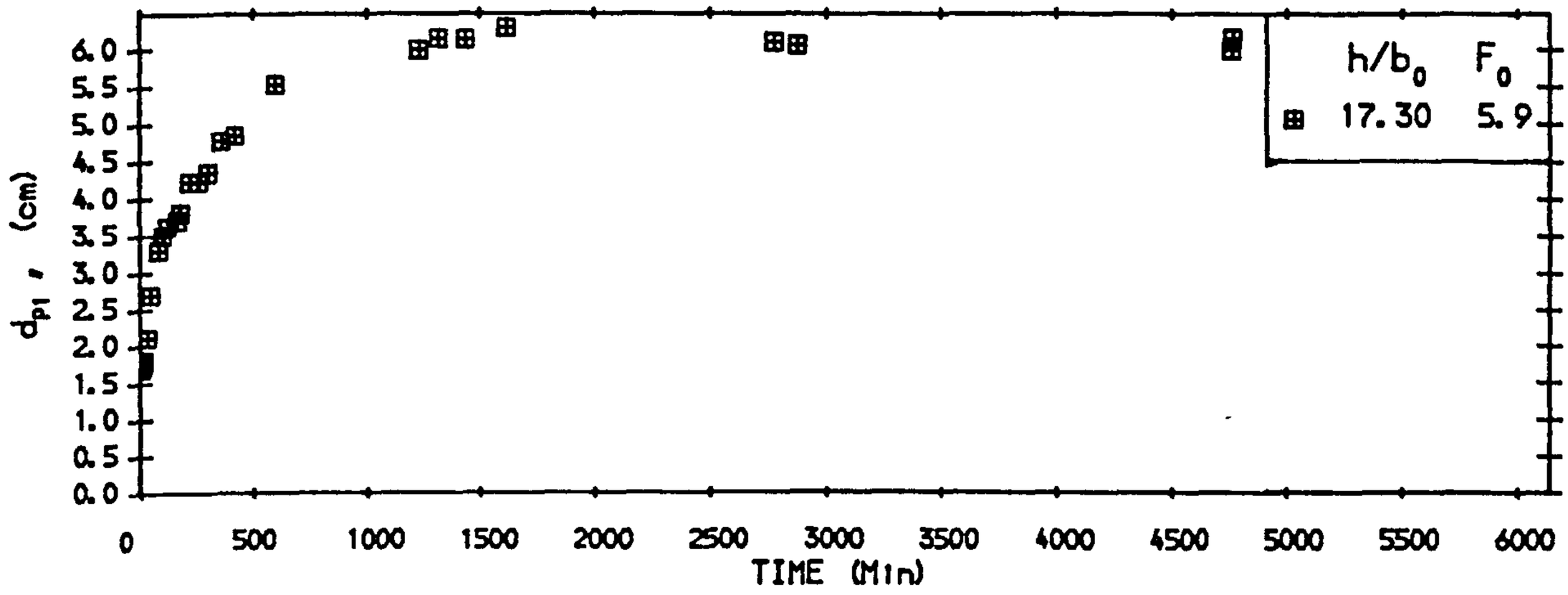

Fig. 6.3 Variation of d_{p1} With Time (Test No. S205)

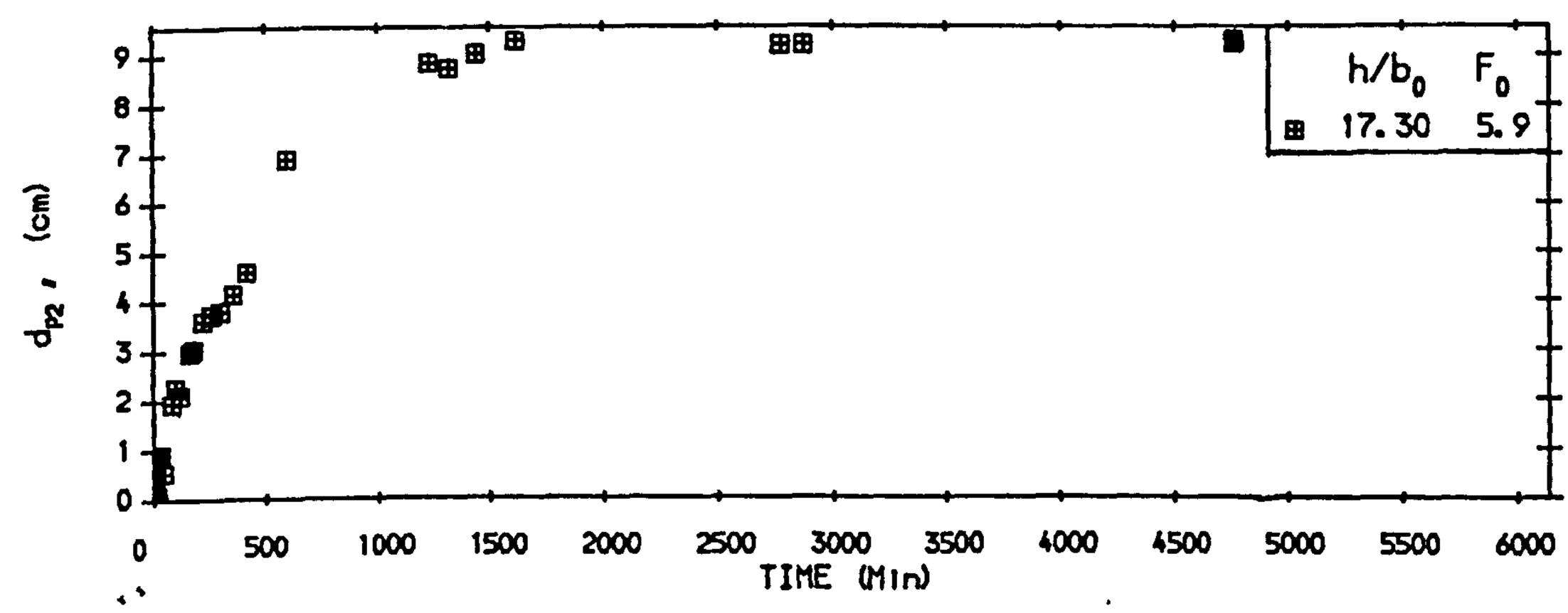

Fig. 6.4 Variation of d_{p2} With Time (Test No. S205)

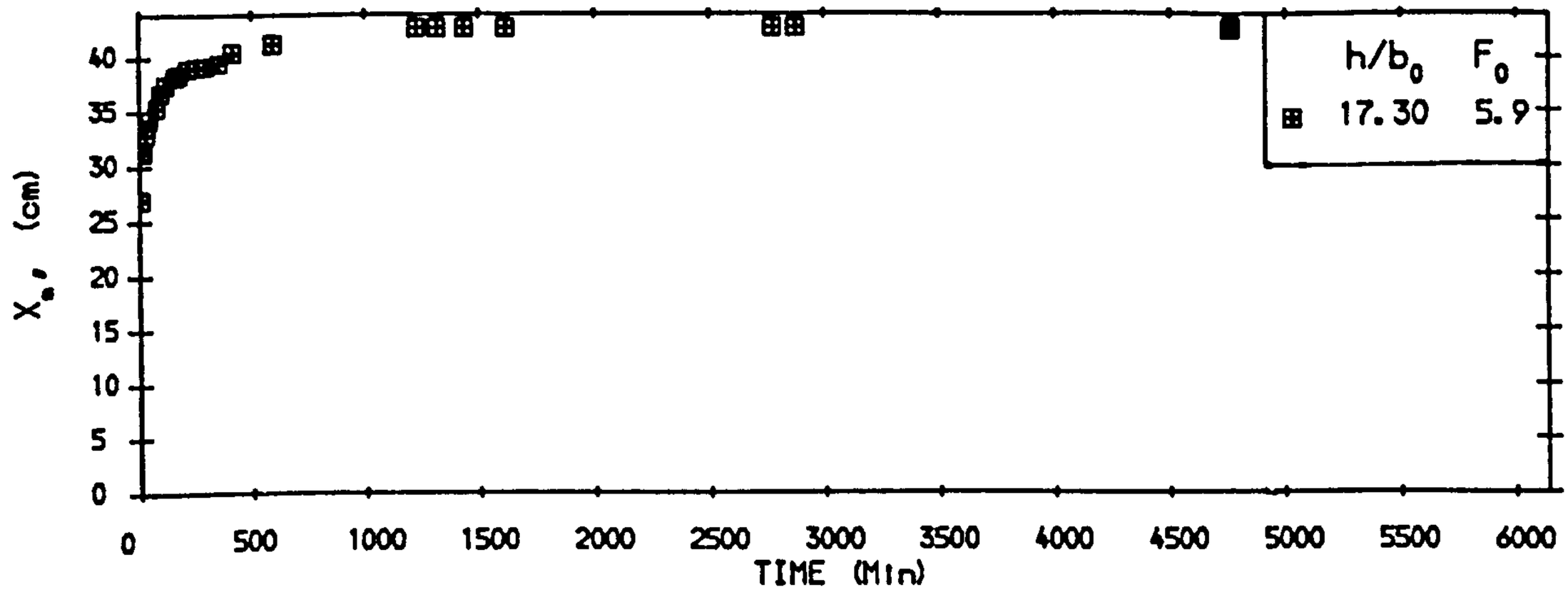

Fig. 6.5 Variation of X_a With Time (Test No. S205)

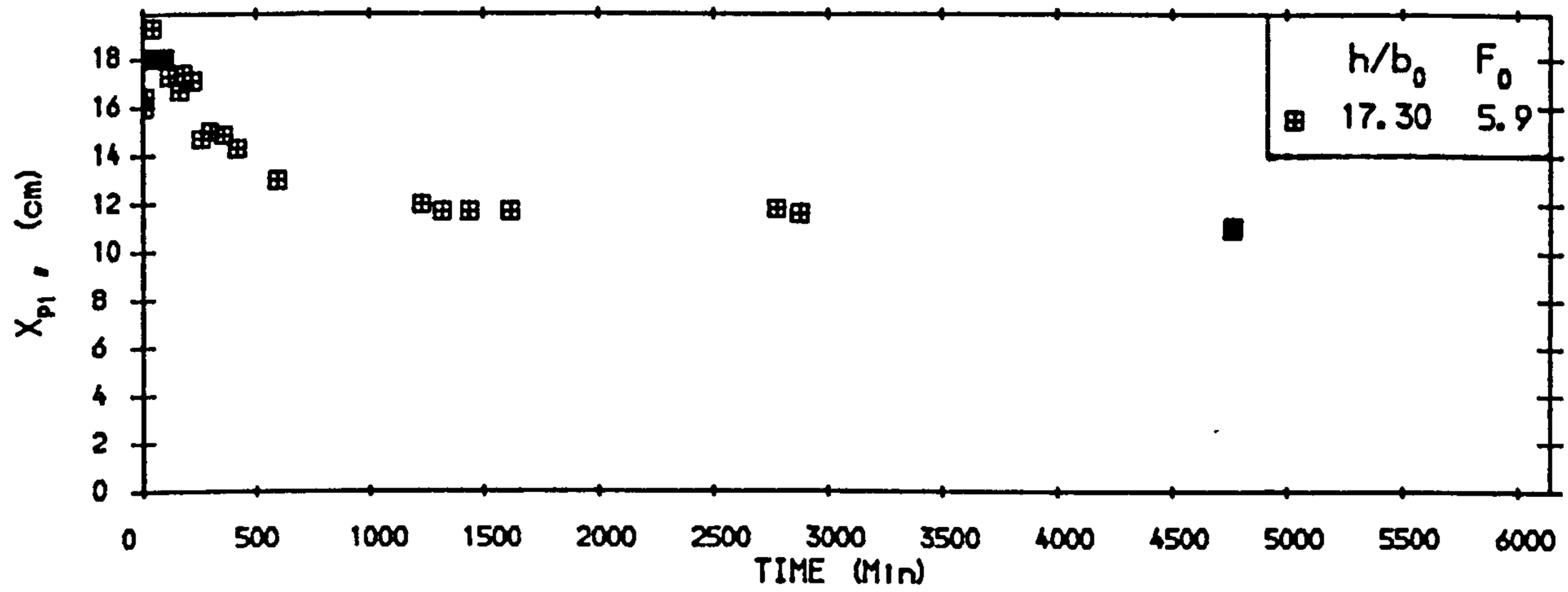

Fig. 6.6 Variation of X_{p1} With Time (Test No. S205)

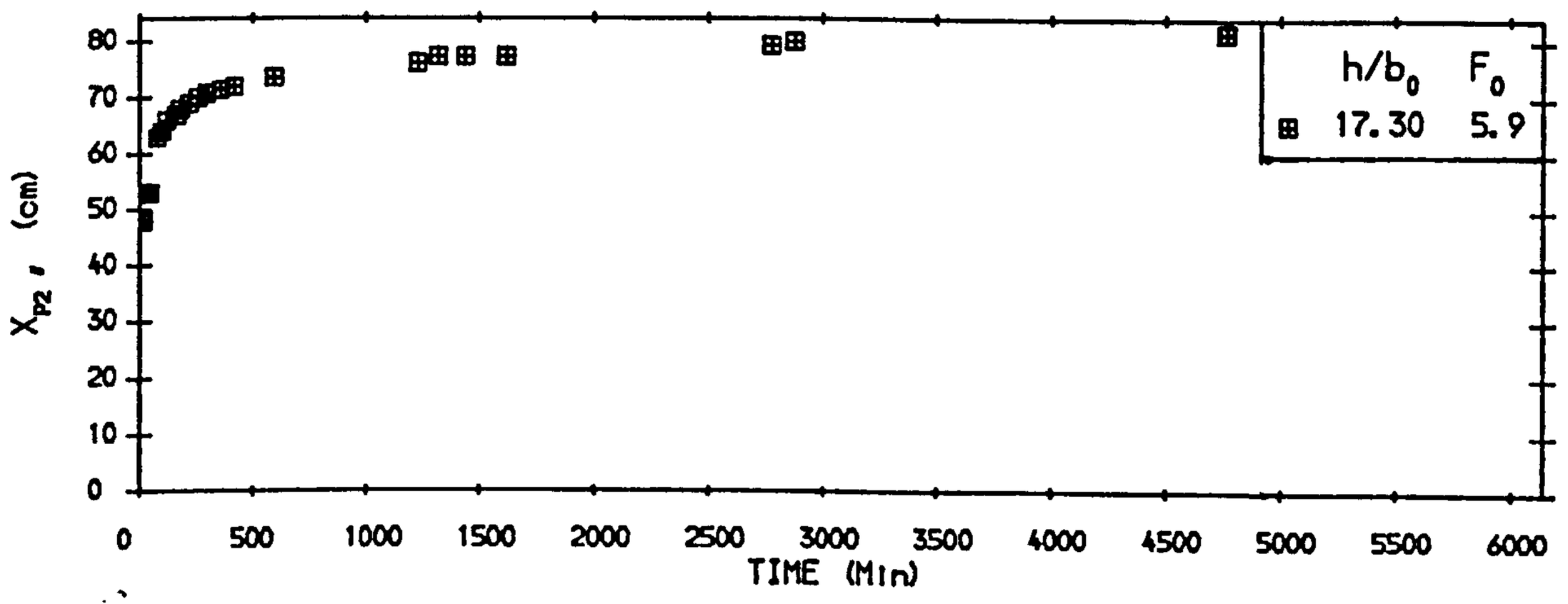

Fig. 6.7 Variation of X_{p2} With Time (Test No. S205)

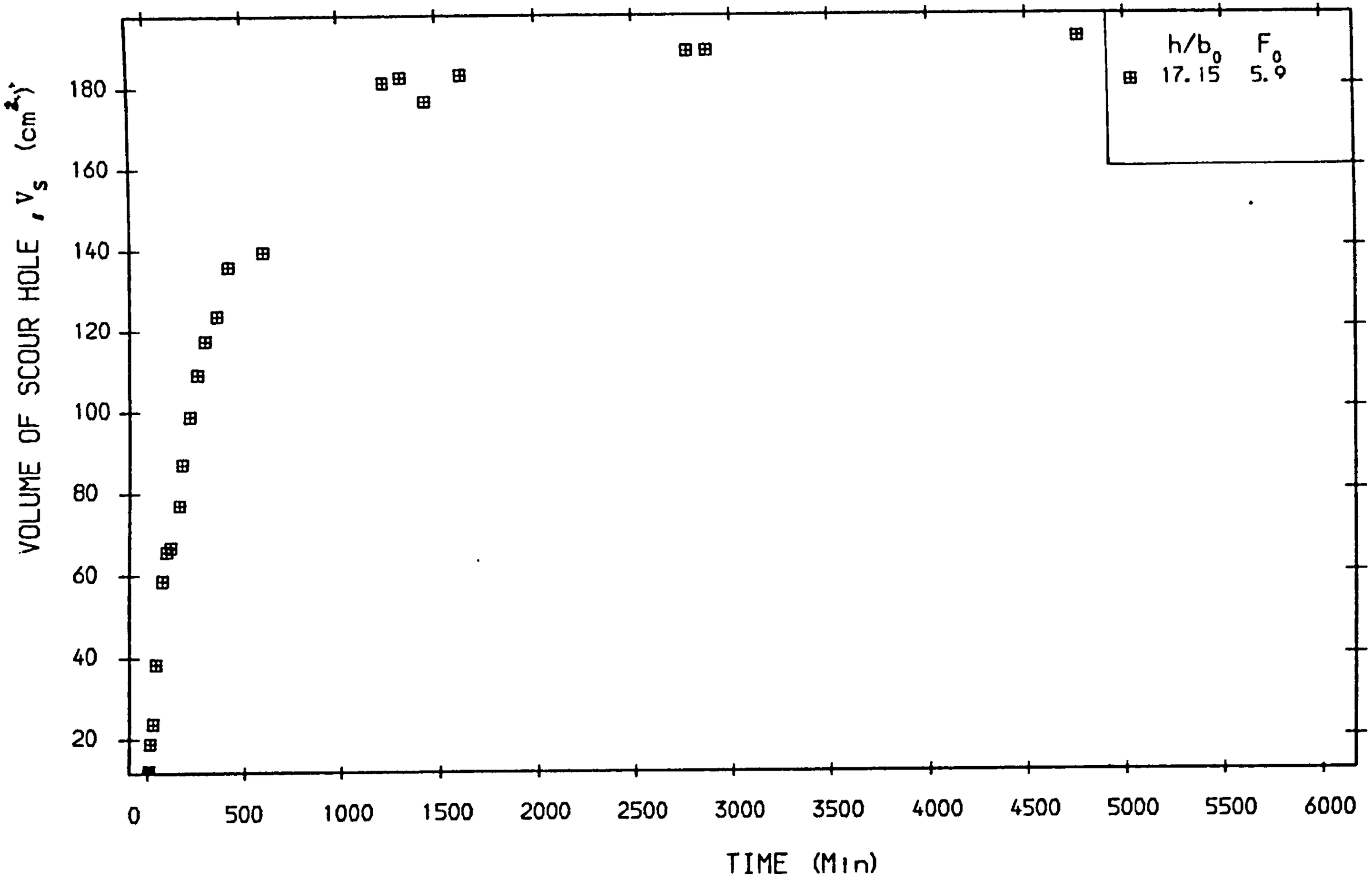

Fig 6.8 Variation of Scour Volume With Time (Test No. S205)

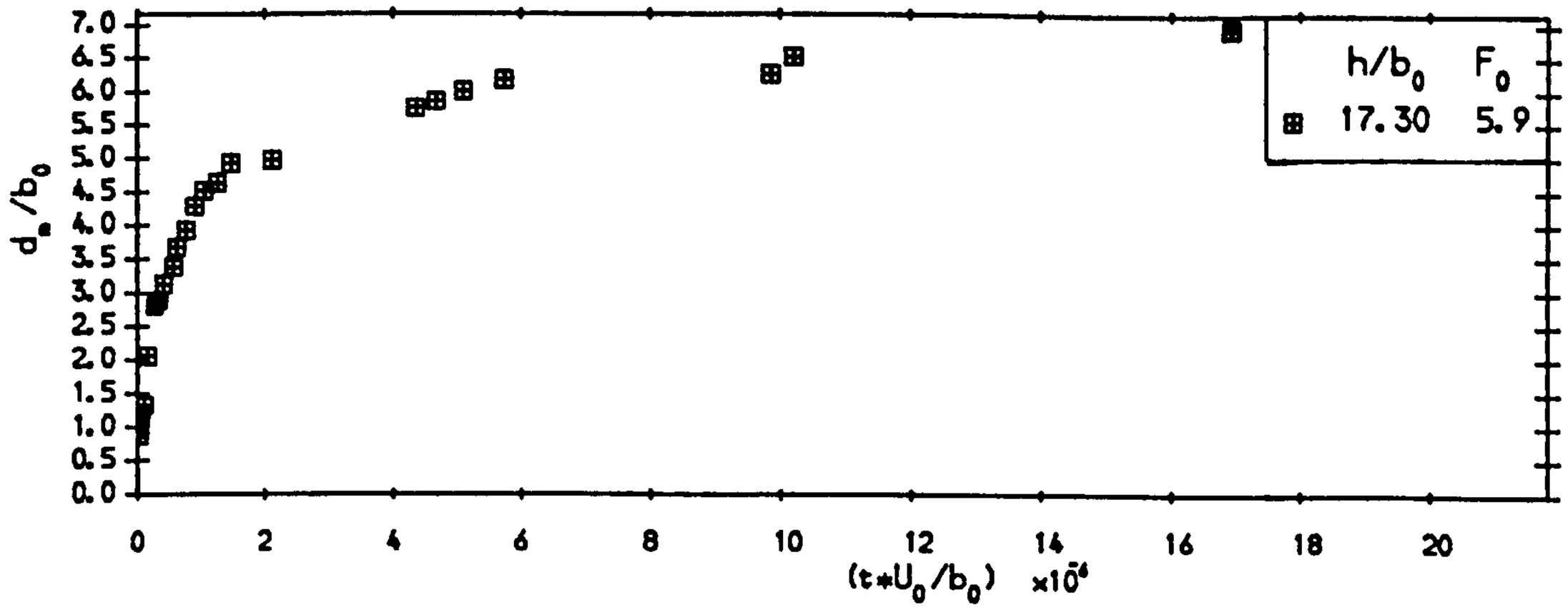

Fig. 6.9 Variation of d_*/b_0 With Time (Test No. S205)

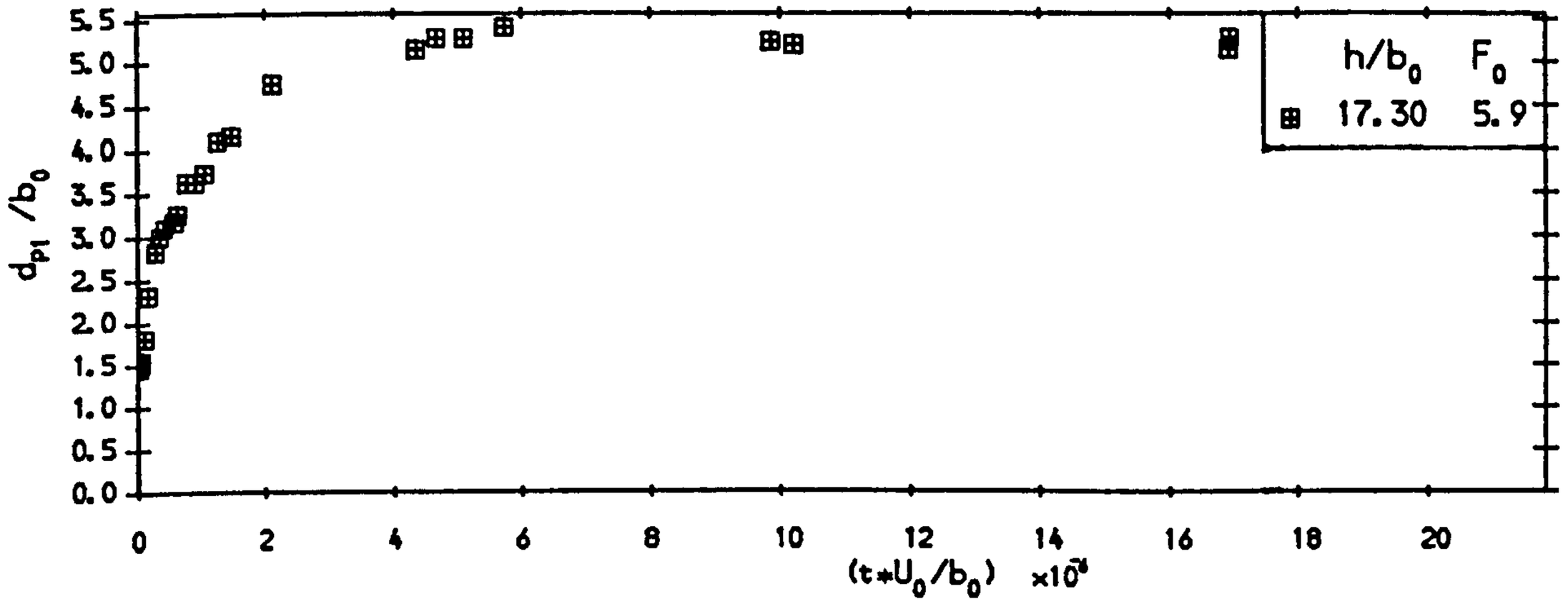

Fig. 6.10 Variation of d_{p1}/b_0 With Time (Test No. S205)

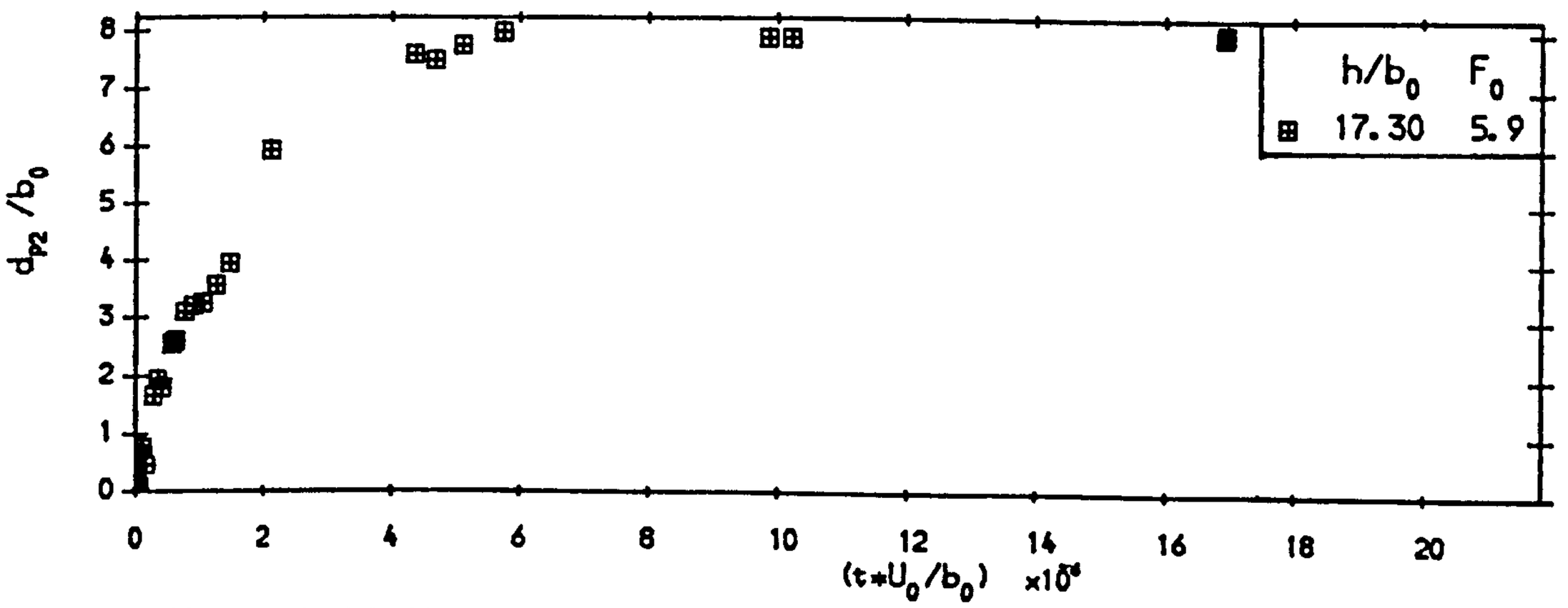

Fig. 6.11 Variation of d_{p2}/b_0 With Time (Test No. S205)

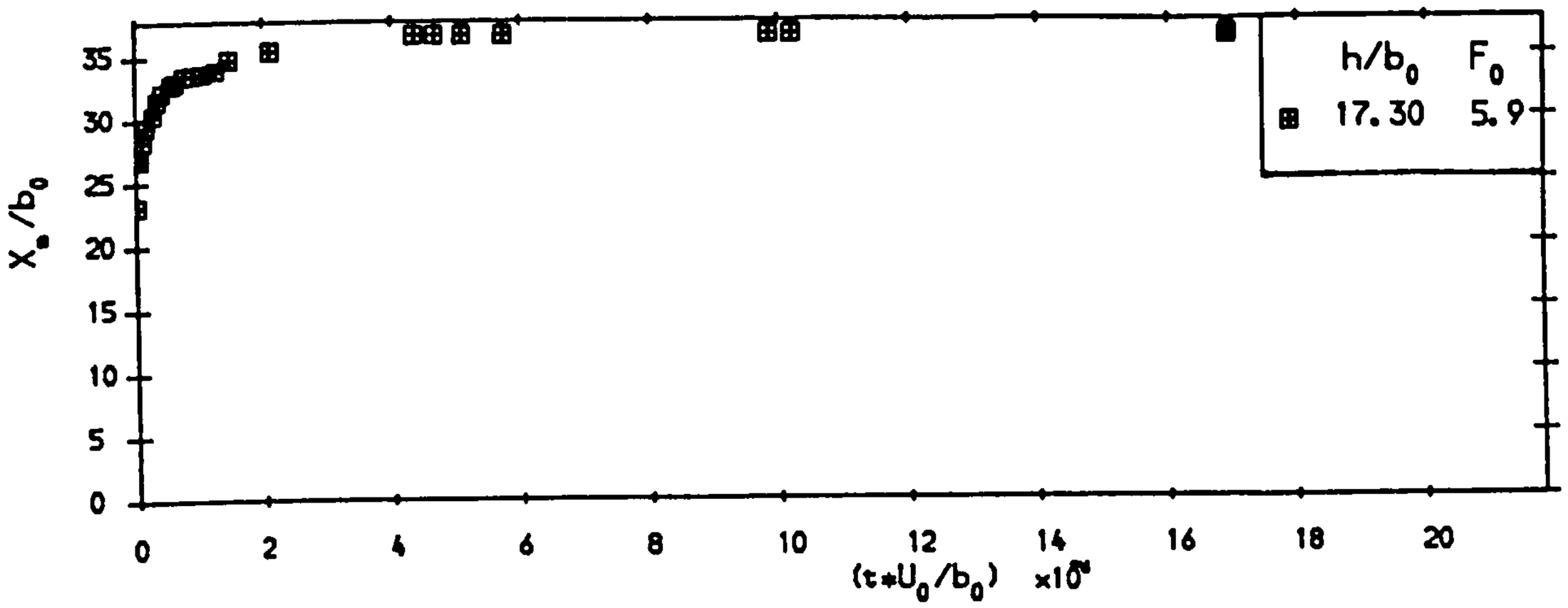

Fig. 6.12 Variation of X_*/b_0 With Time (Test No. S205)

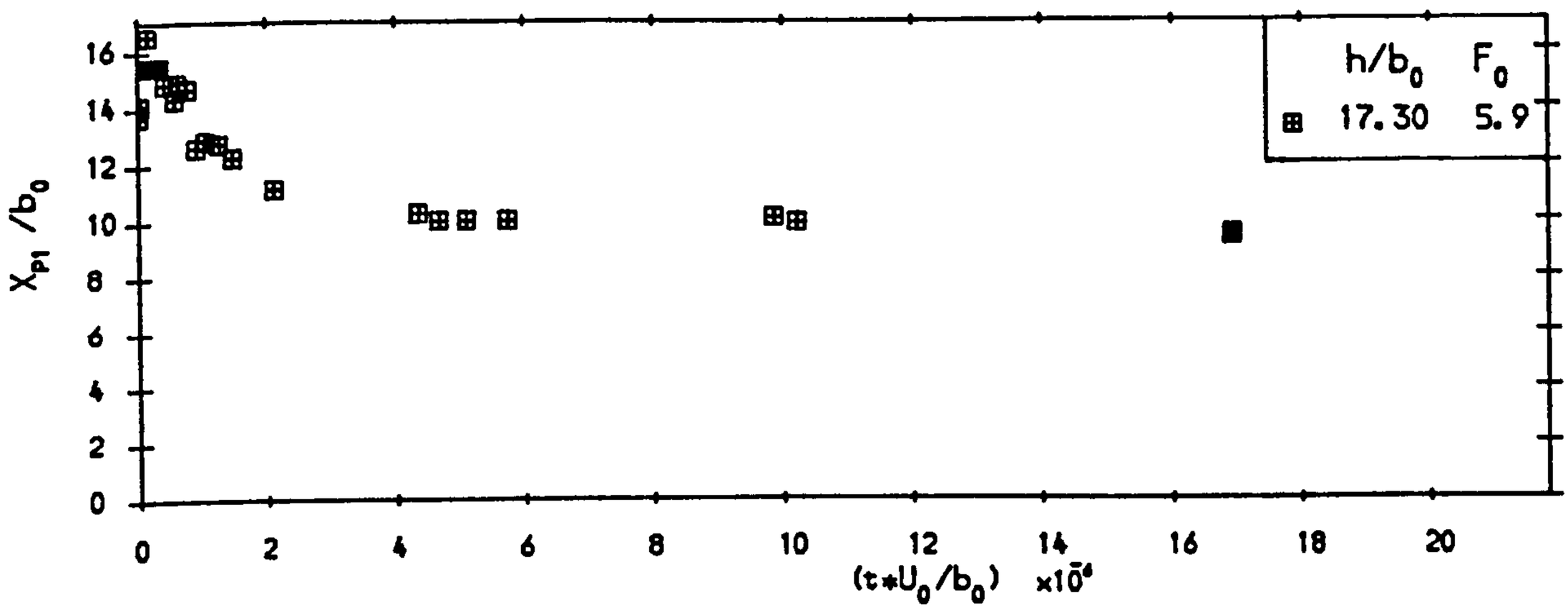

Fig. 6.13 Variation of X_{p1}/b_0 With Time (Test No. S205)

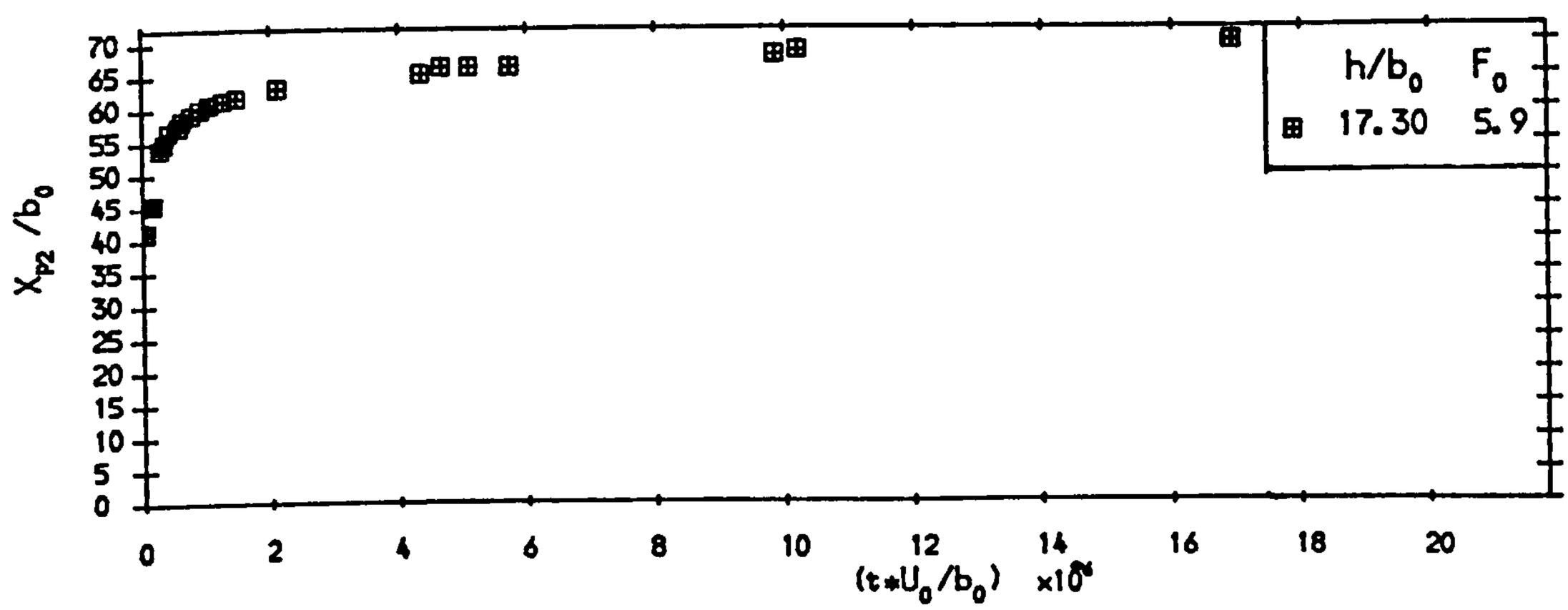

Fig. 6.14 Variation of X_{p2}/b_0 With Time (Test No. S205

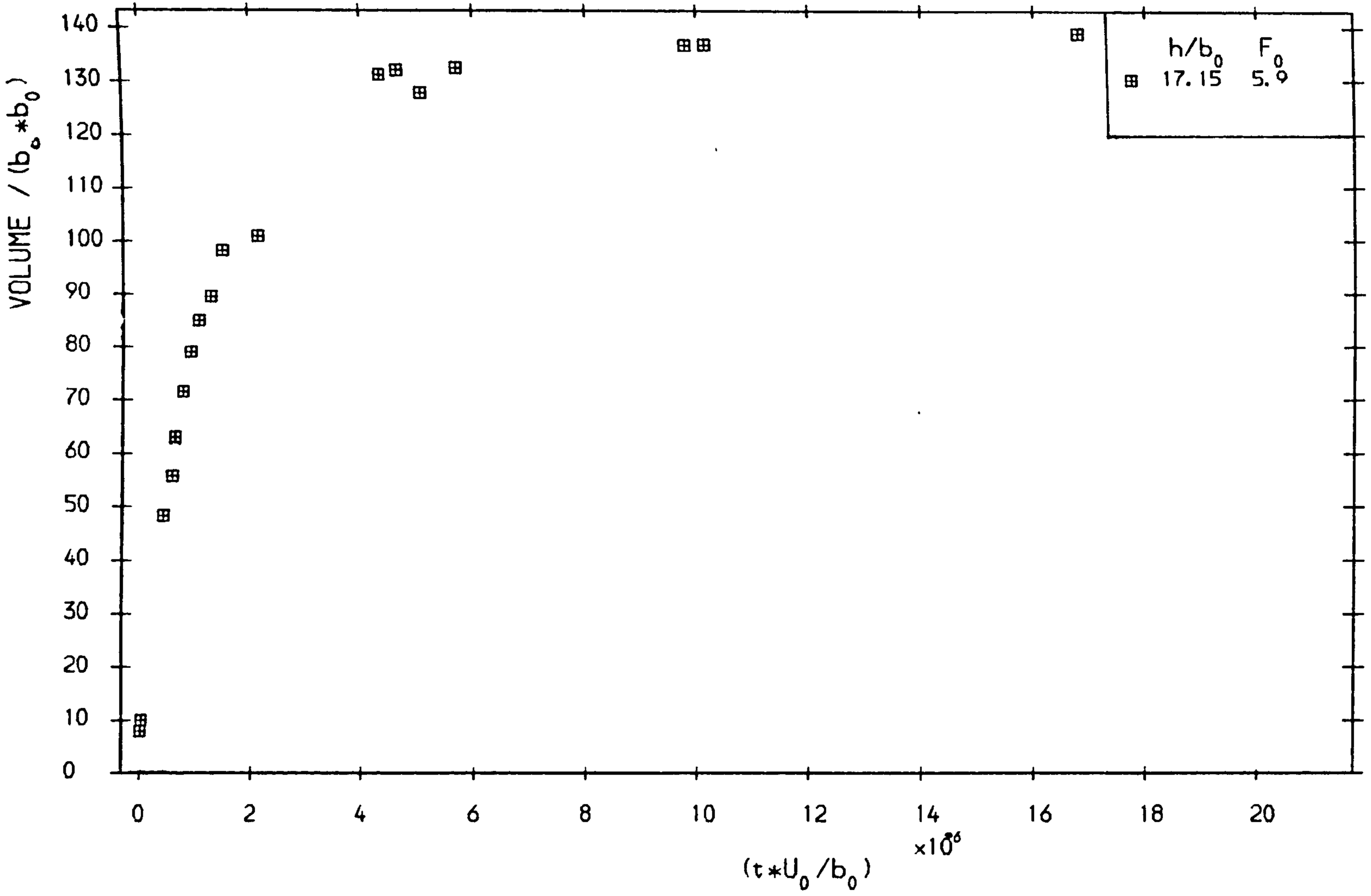

Fig 6.15 Variation of V_e/b_0^2 With Time (Test No. S205)

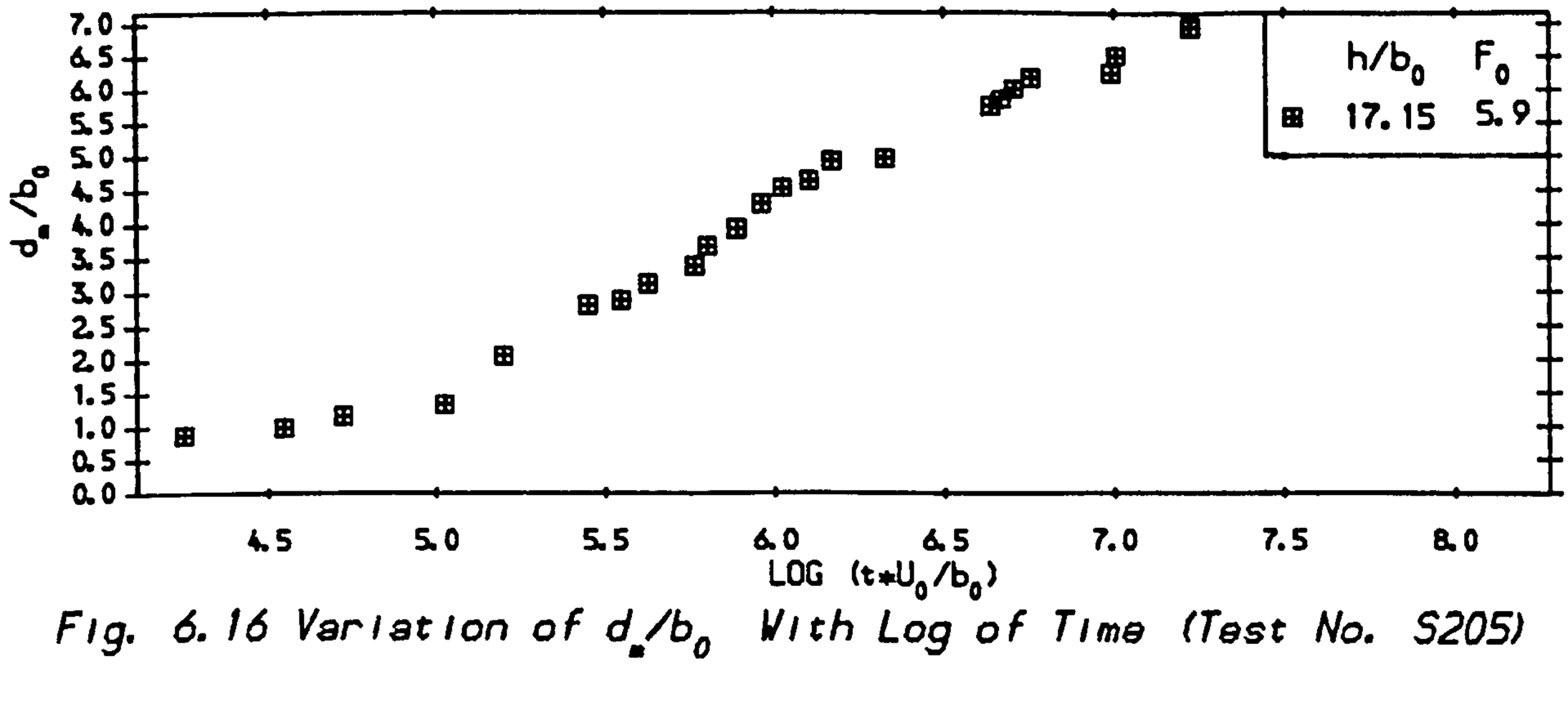

Fig. 6.16 Variation of d_s/b_0 With Log of Time (Test No. S205)

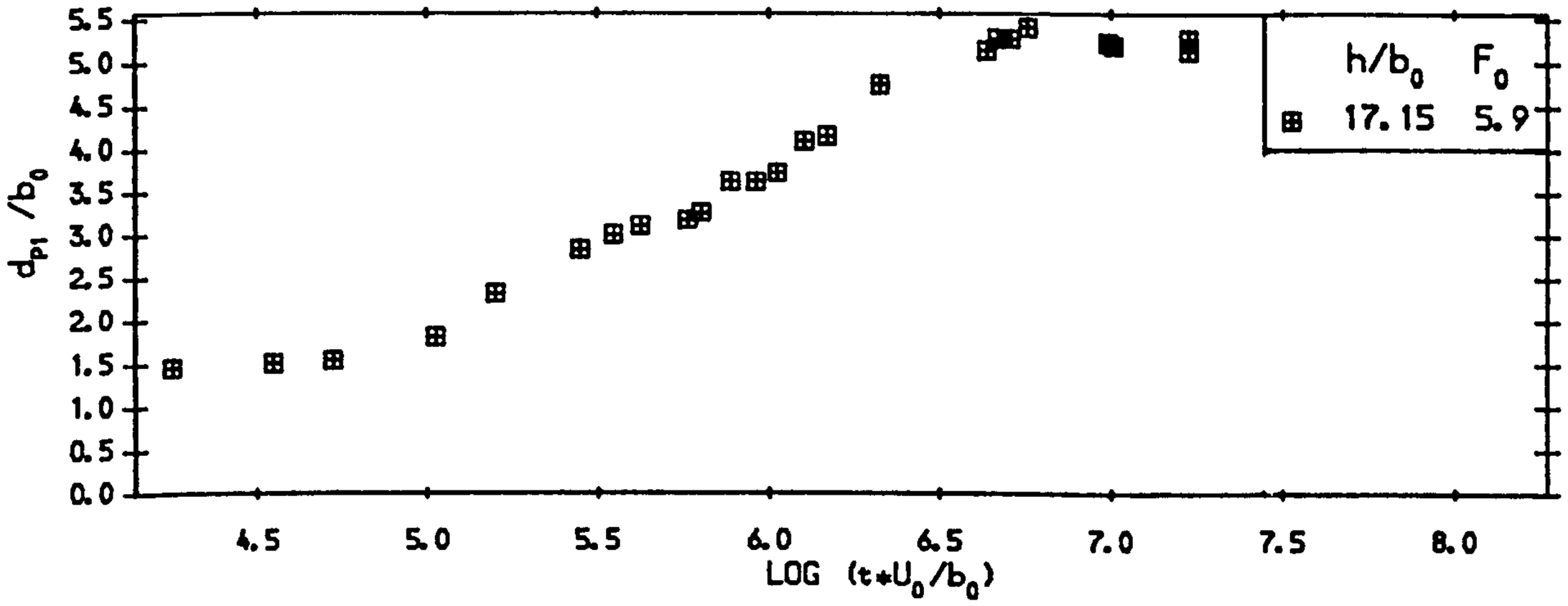

Fig. 6.17 Variation of d_{p1}/b_0 With Log of Time (Test No. S205)

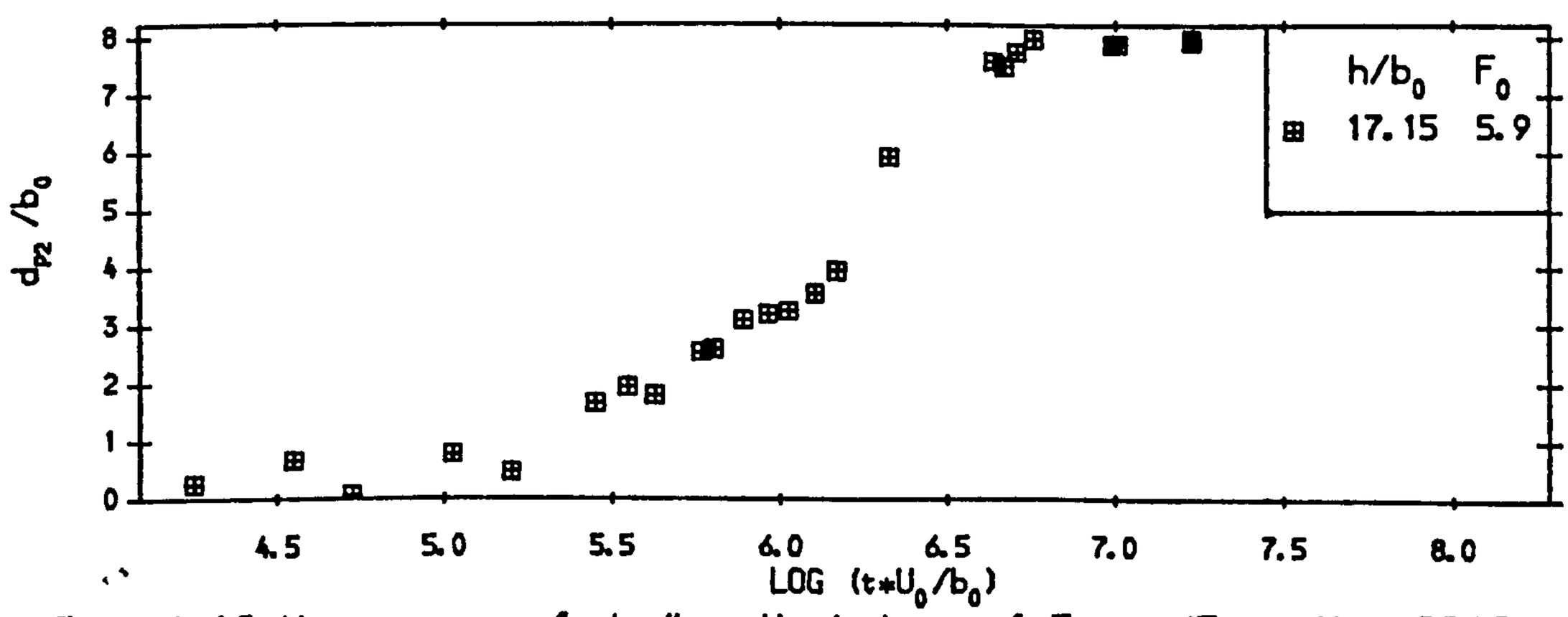

Fig. 6.18 Variation of d_{p2}/b_0 With Log of Time (Test No. S205)

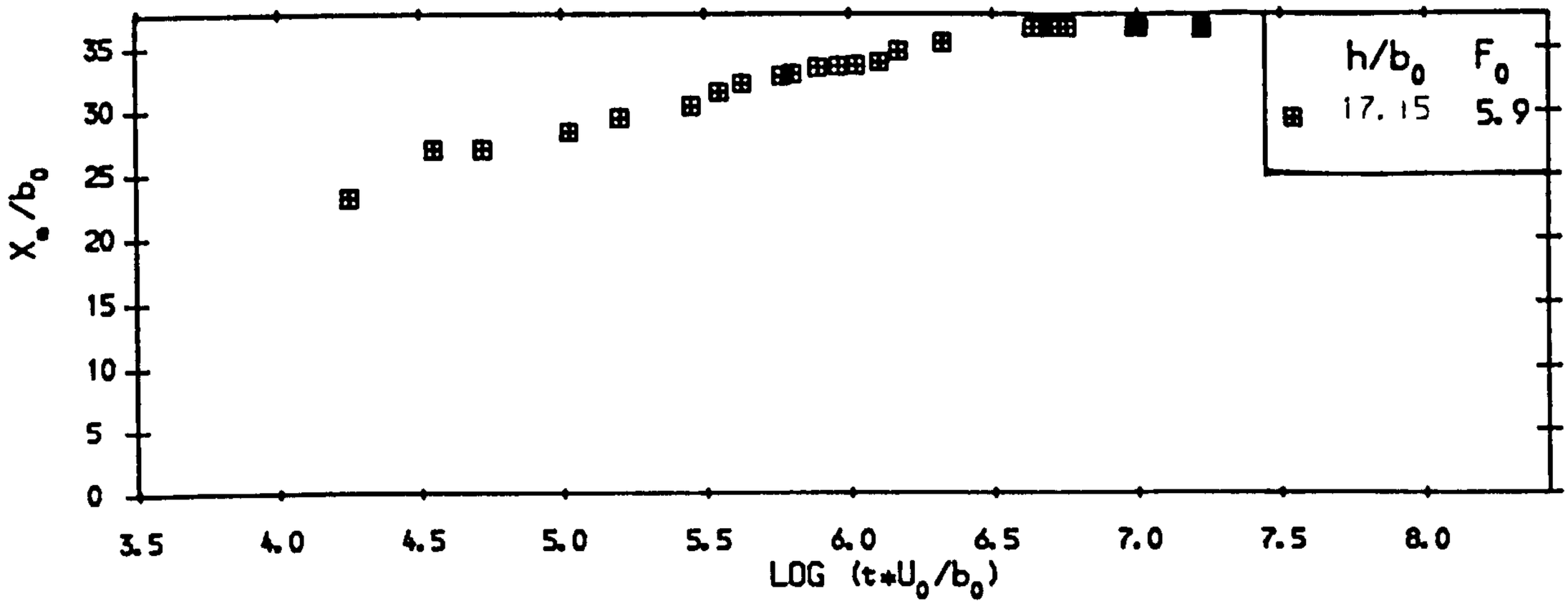

Fig. 6.19 Variation of X_*/b_0 With Log of Time (Test No. S205)

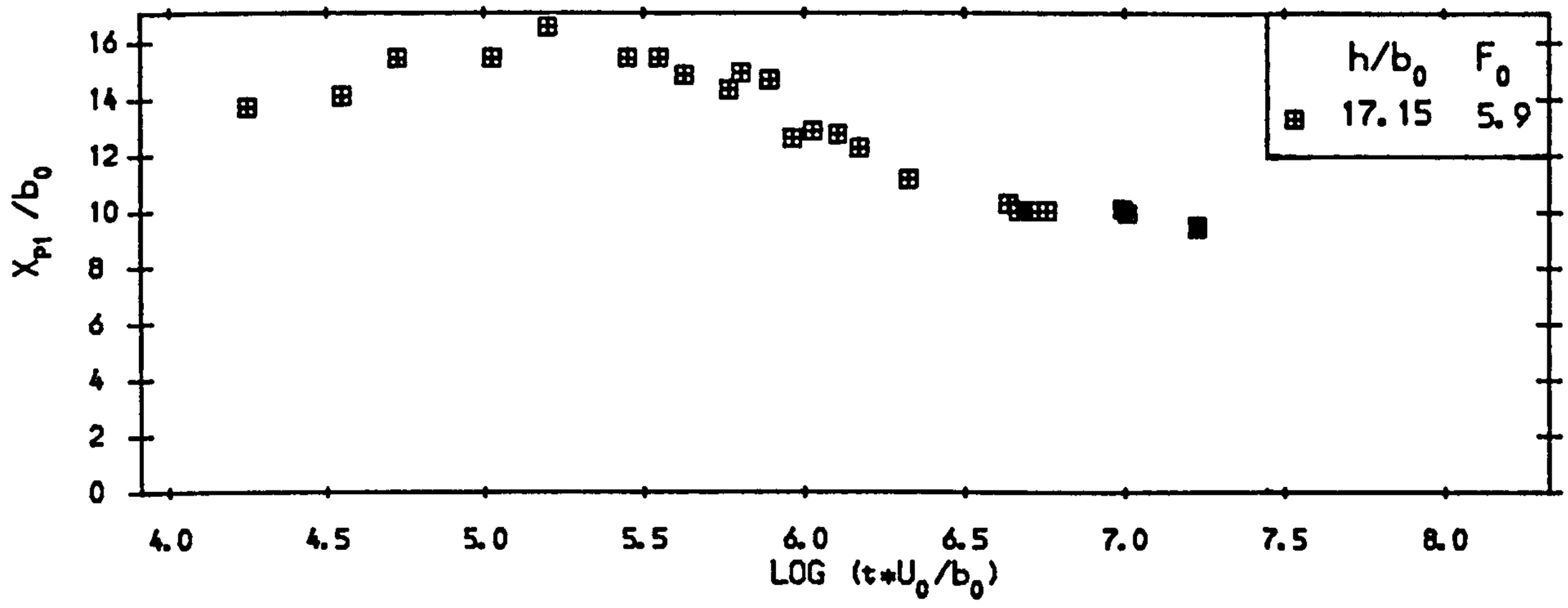

Fig. 6.20 Variation of X_{p1}/b_0 With Log of Time (Test No. S205)

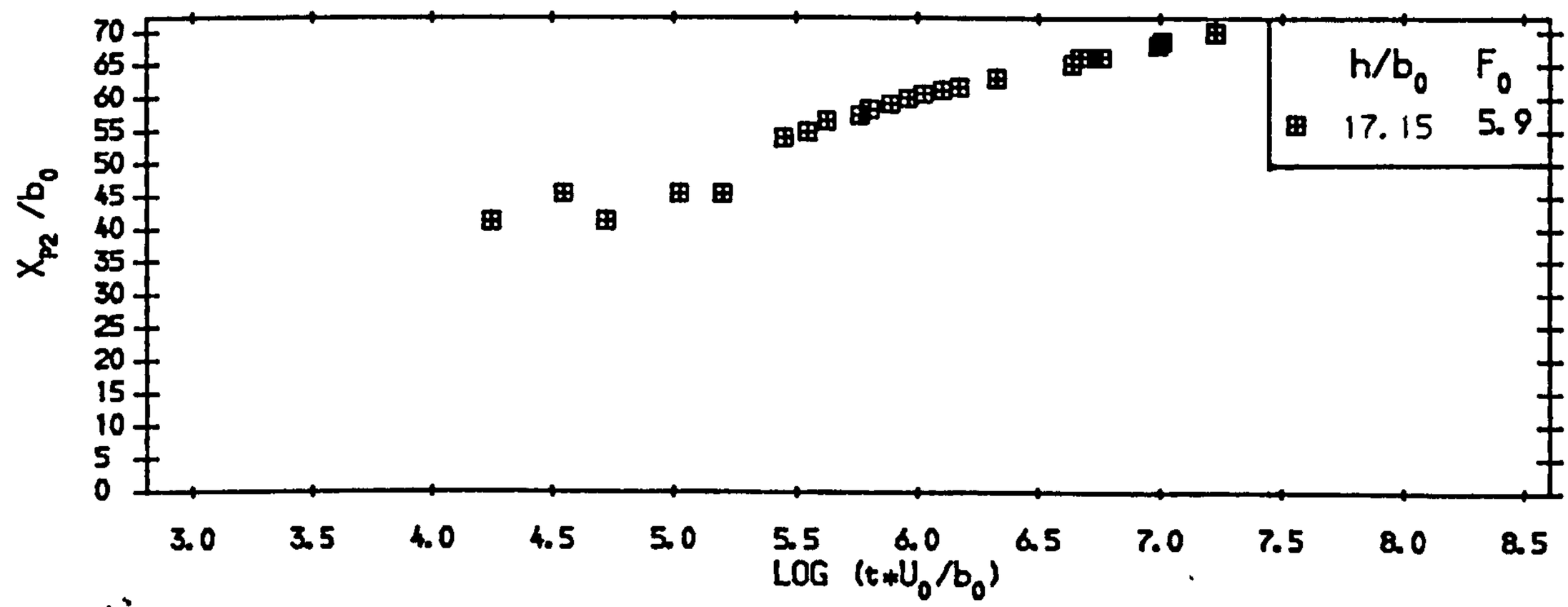

Fig. 6.21 Variation of X_{p2}/b_0 With Log of Time (Test No. S205)

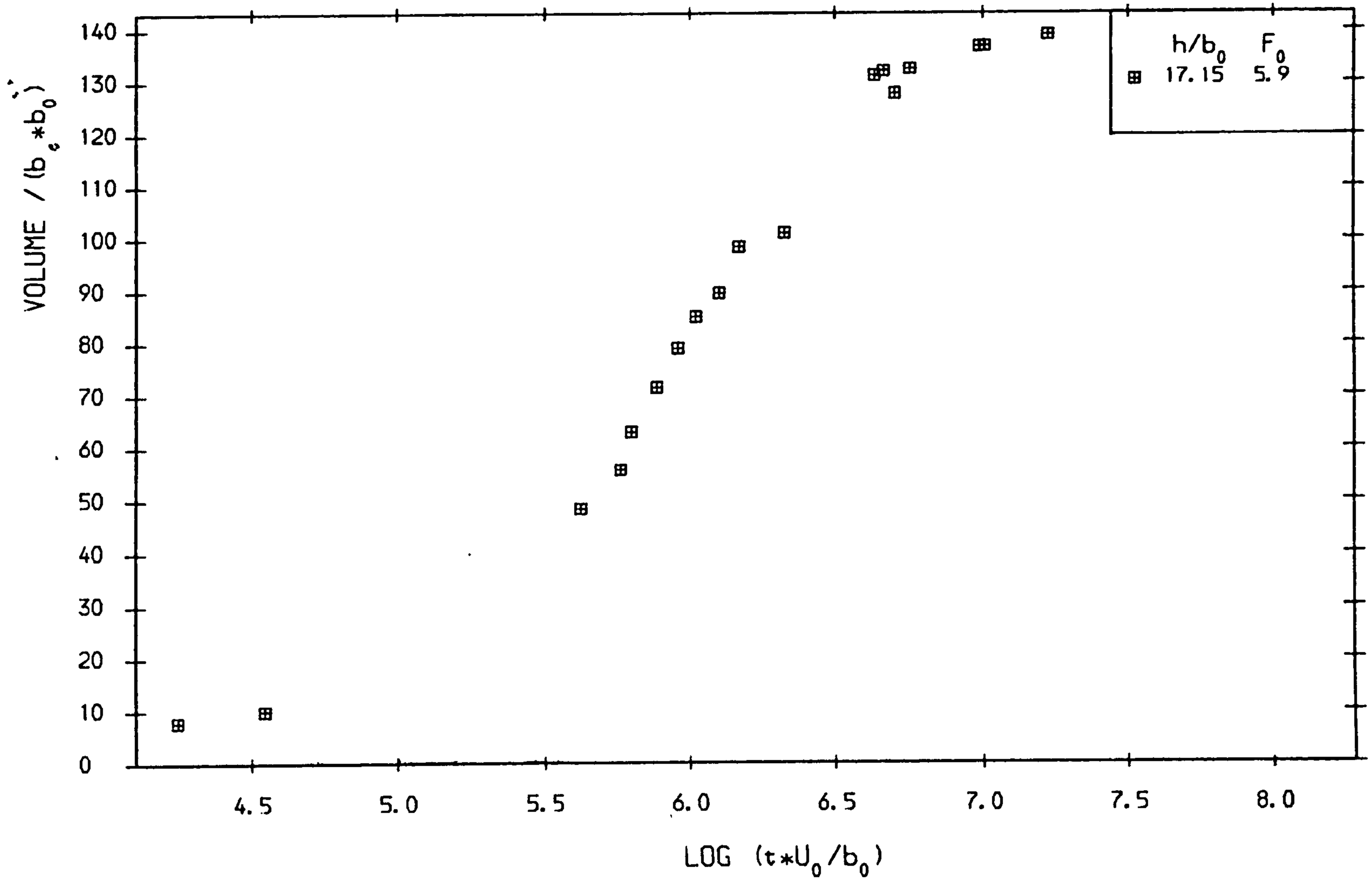

Fig 6.22 Variation of V_e/b_0^2 With Log. of Time (Test No. S205)

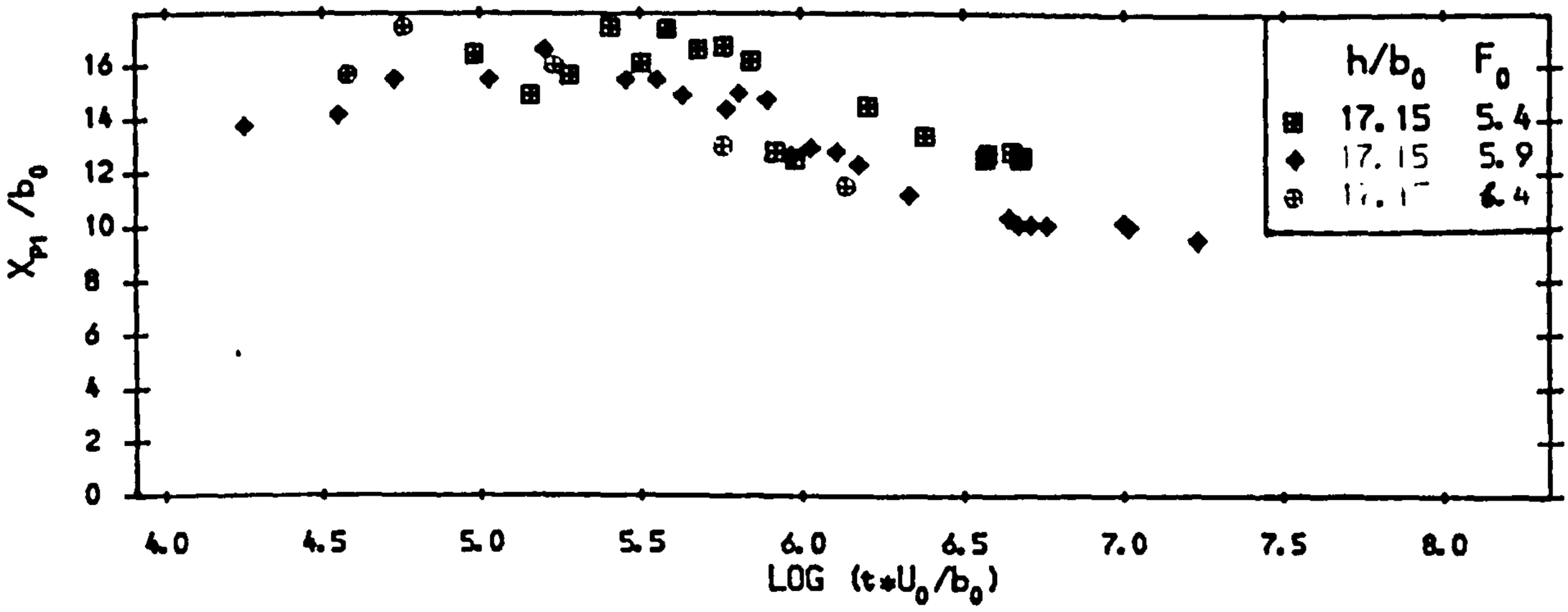

Fig. 6.23 Effect of F_0 on the Variation of X_{pl} With Log of Time

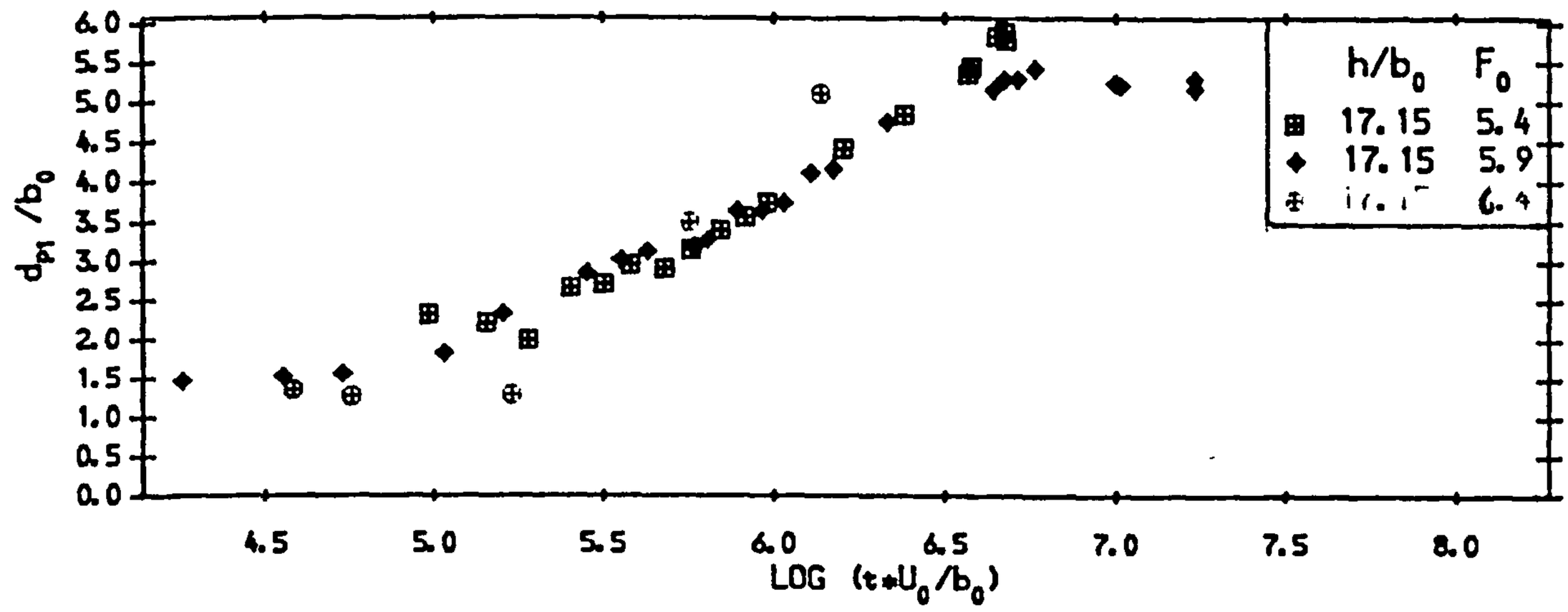

Fig. 6.24 Effect of F_0 on the Variation of d_{p1} W th Log. of Time

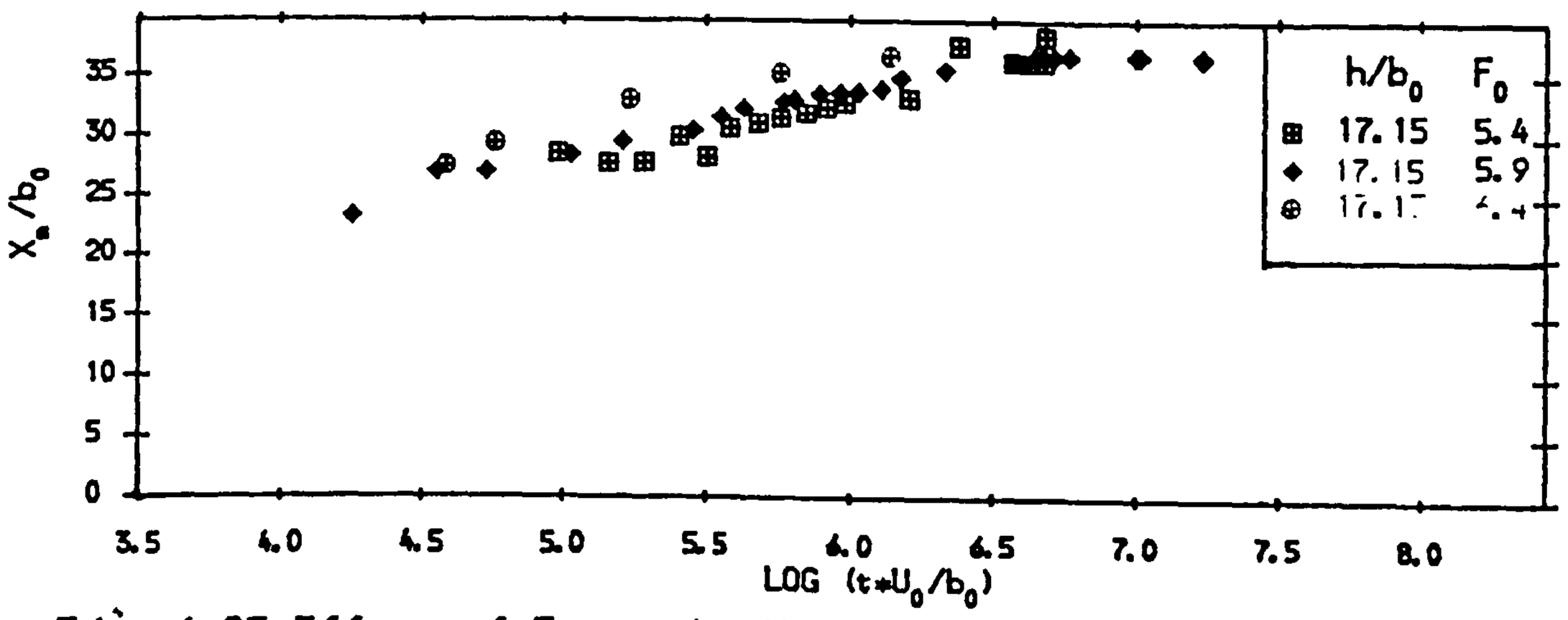

Fig. 6.25 Effect of F_0 on the Variation of X_a With Log. of Time

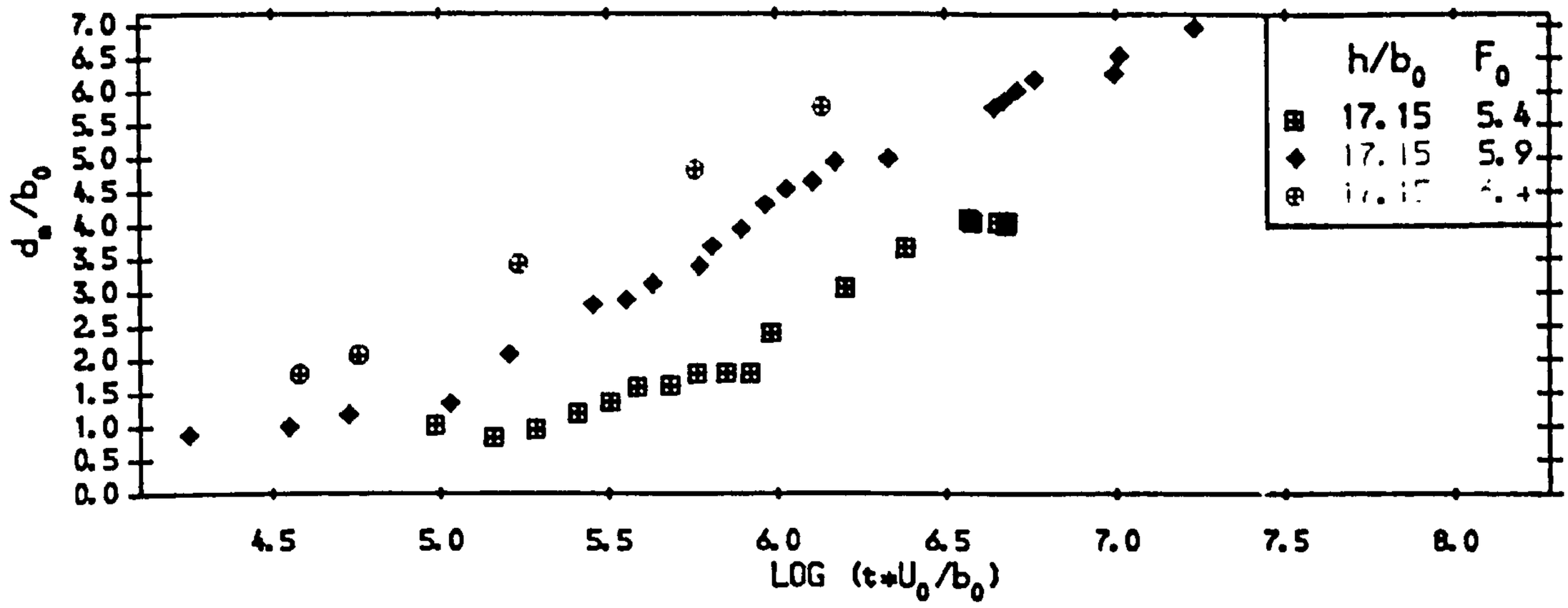

Fig. 6.26 Effect of F_0 on the Variation of d_* With Log. of Time

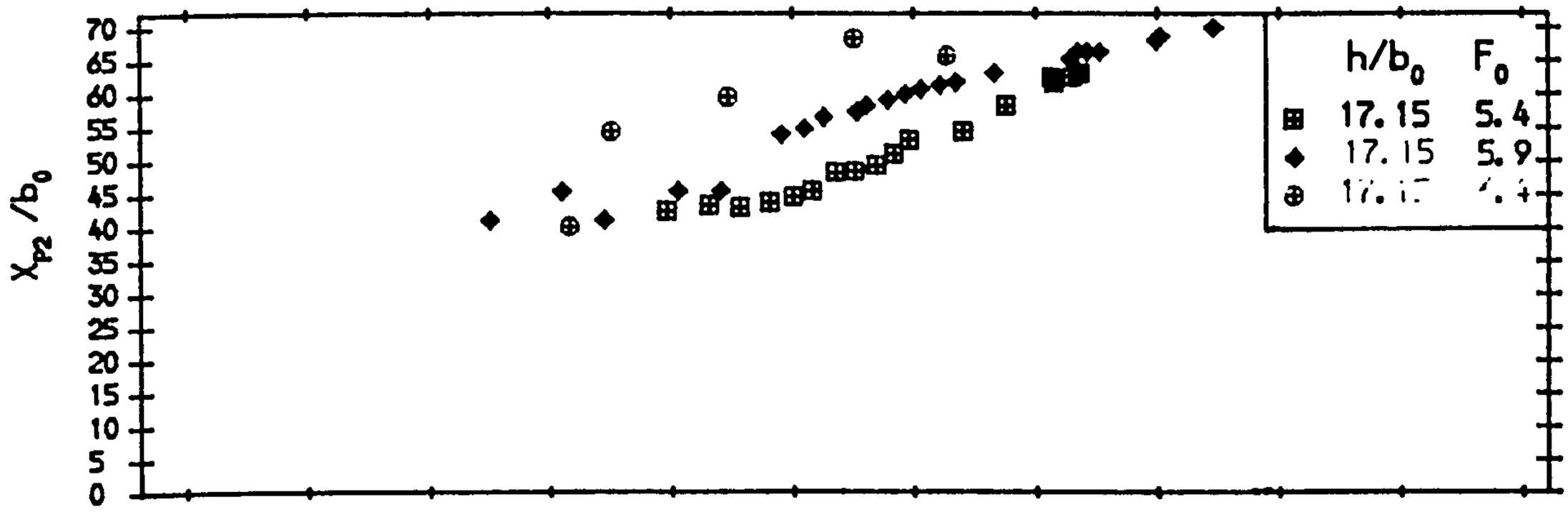

Fig. 6.27 Effect of F_0 on the Variation of X_{p2} With Log. of Time

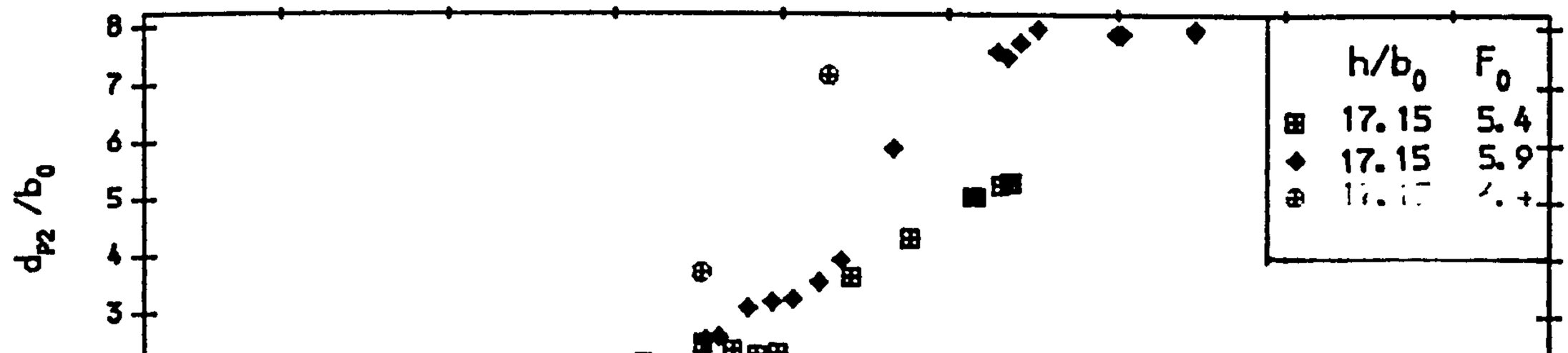

Fig. 6.28 Effect of F_0 on the Variation of d_{p2} With Log. of Tim

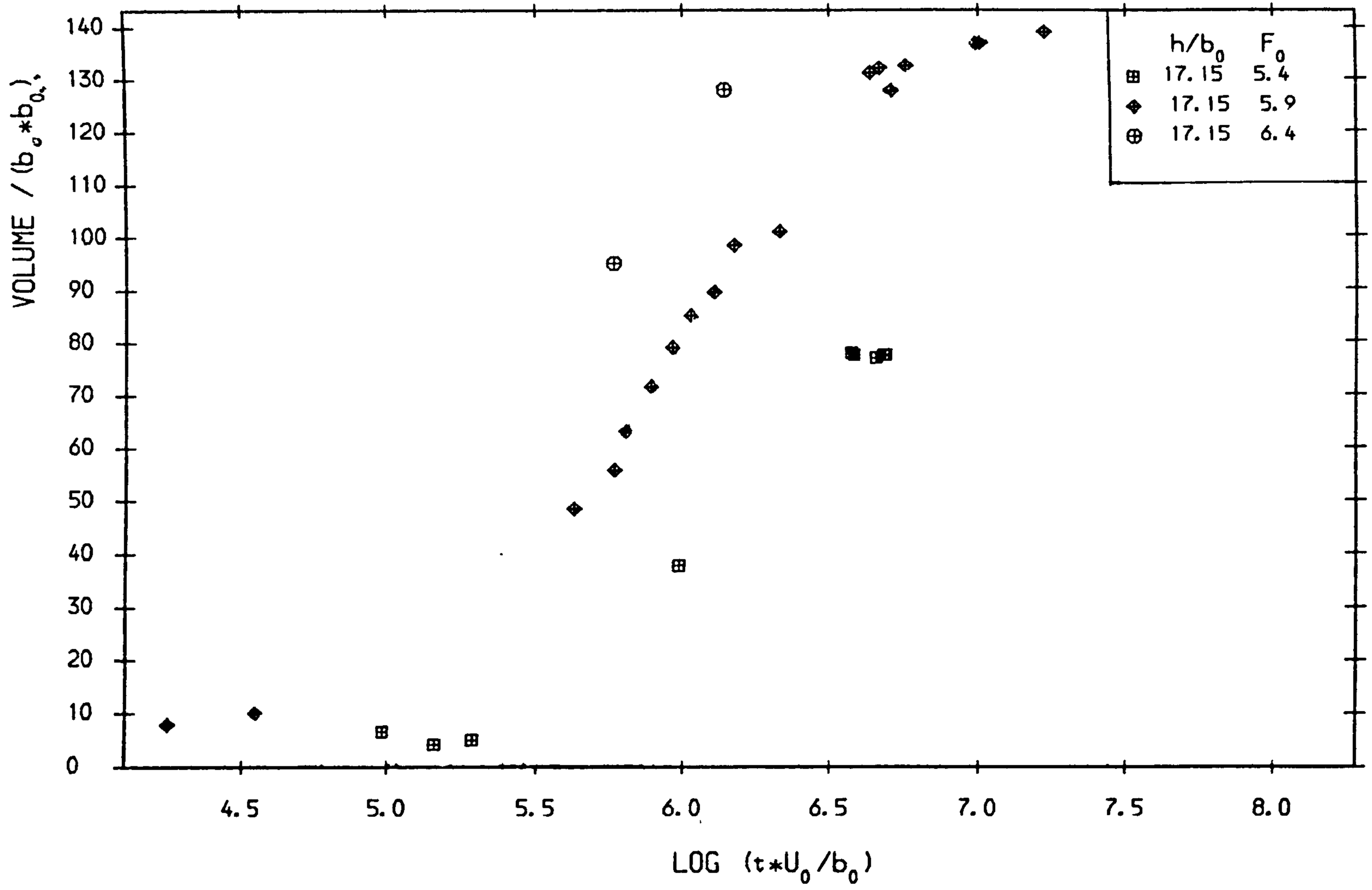

Fig. 6.29 Effect of F_0 on the Time Variation of Scour Volume

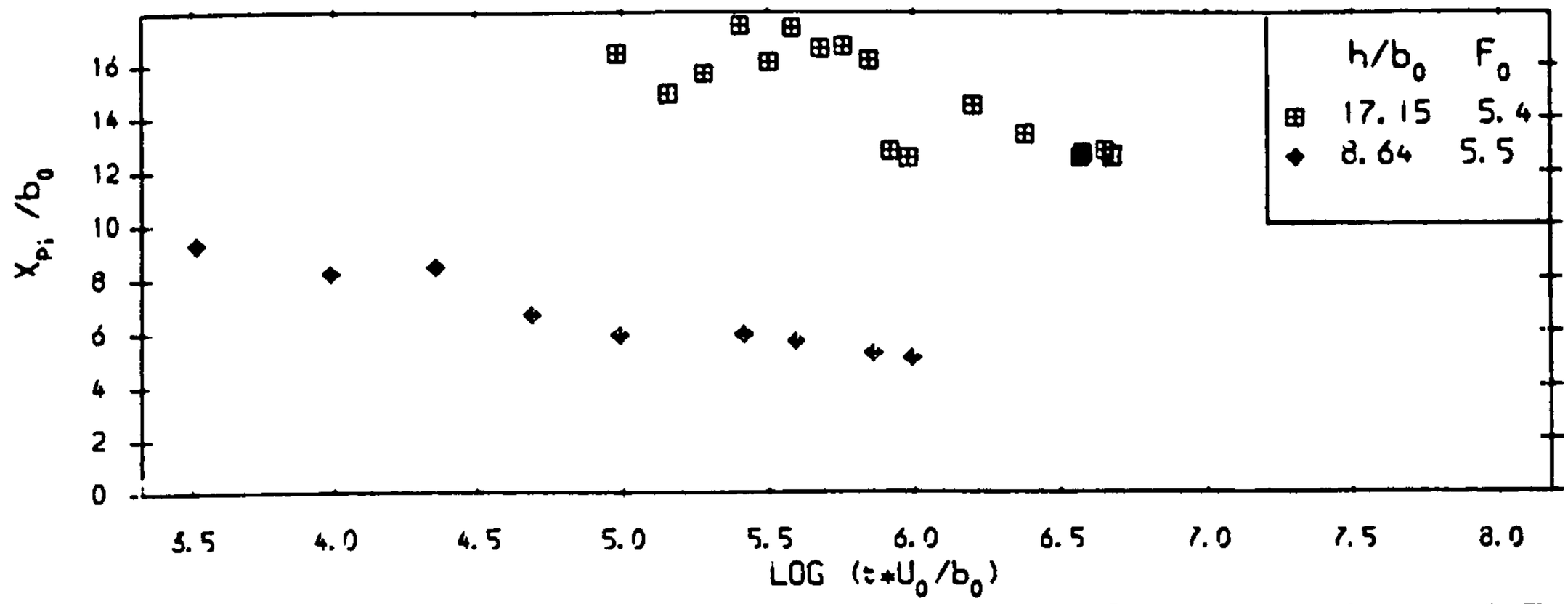

Fig. 6.30 Effect of h on the Variation of X_{pl} With Log of Time

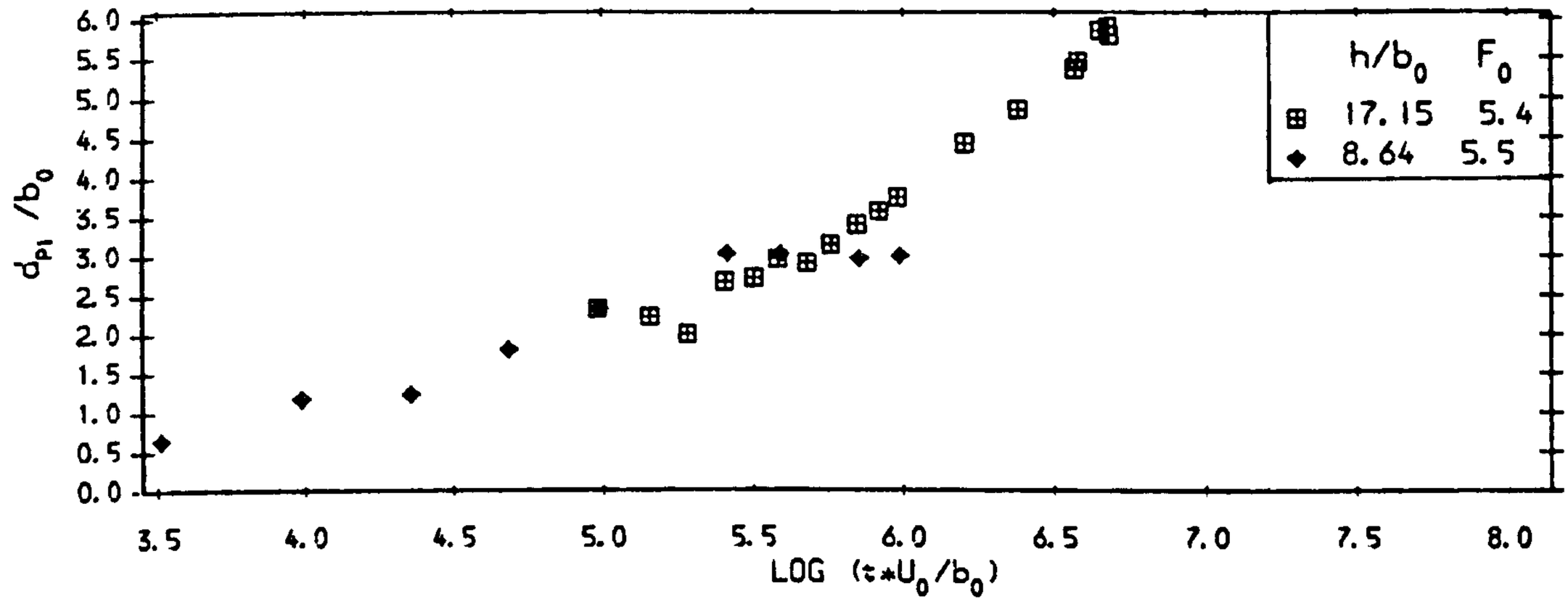

Fig. 6.31 Effect of h on the Variation of d_{pl} With Log of Tim

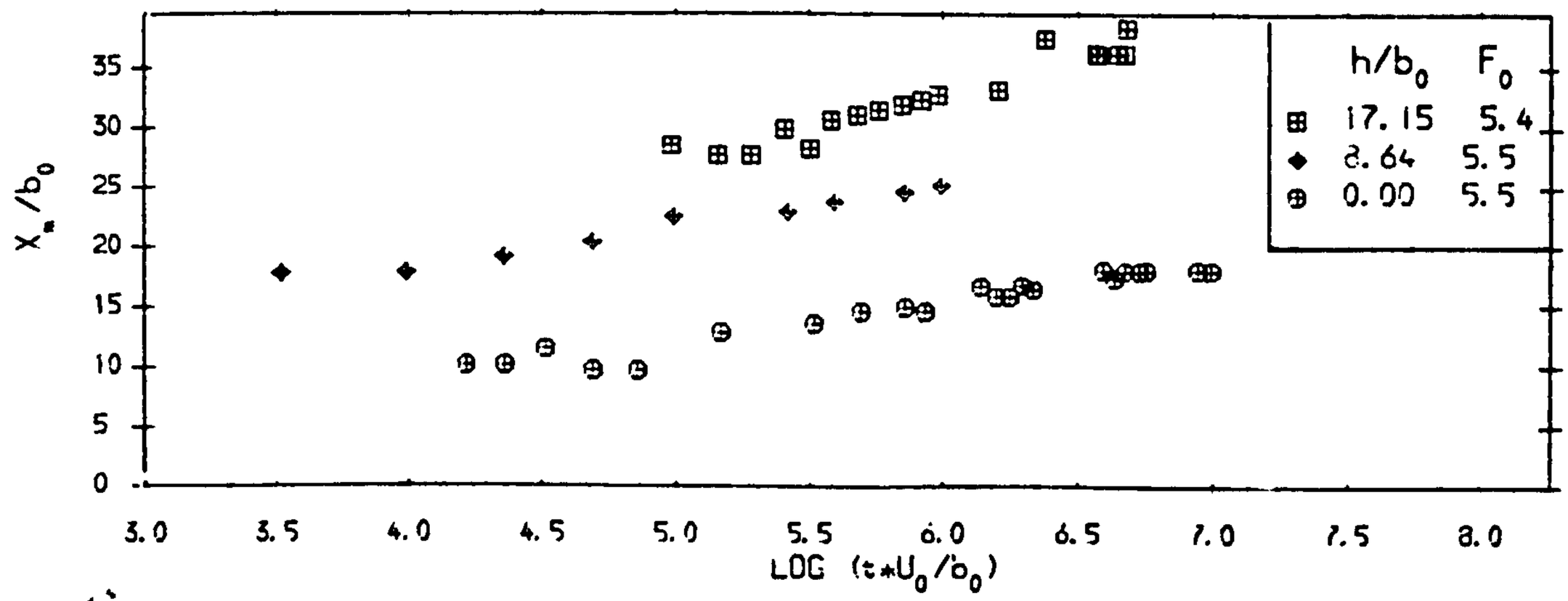

Fig. 6.32 Effect of h on the Variation of X_* With Log of Time

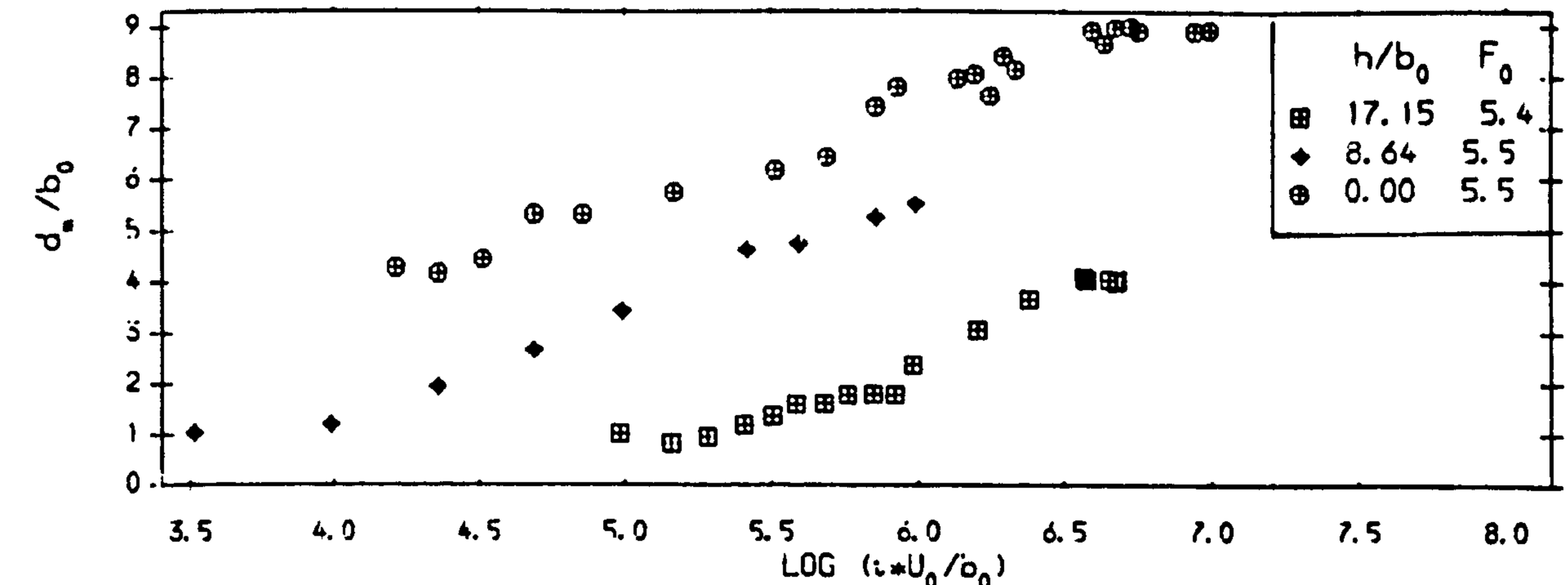

Fig. 6.33 Effect of h on the Variation of d_* With Log of Time

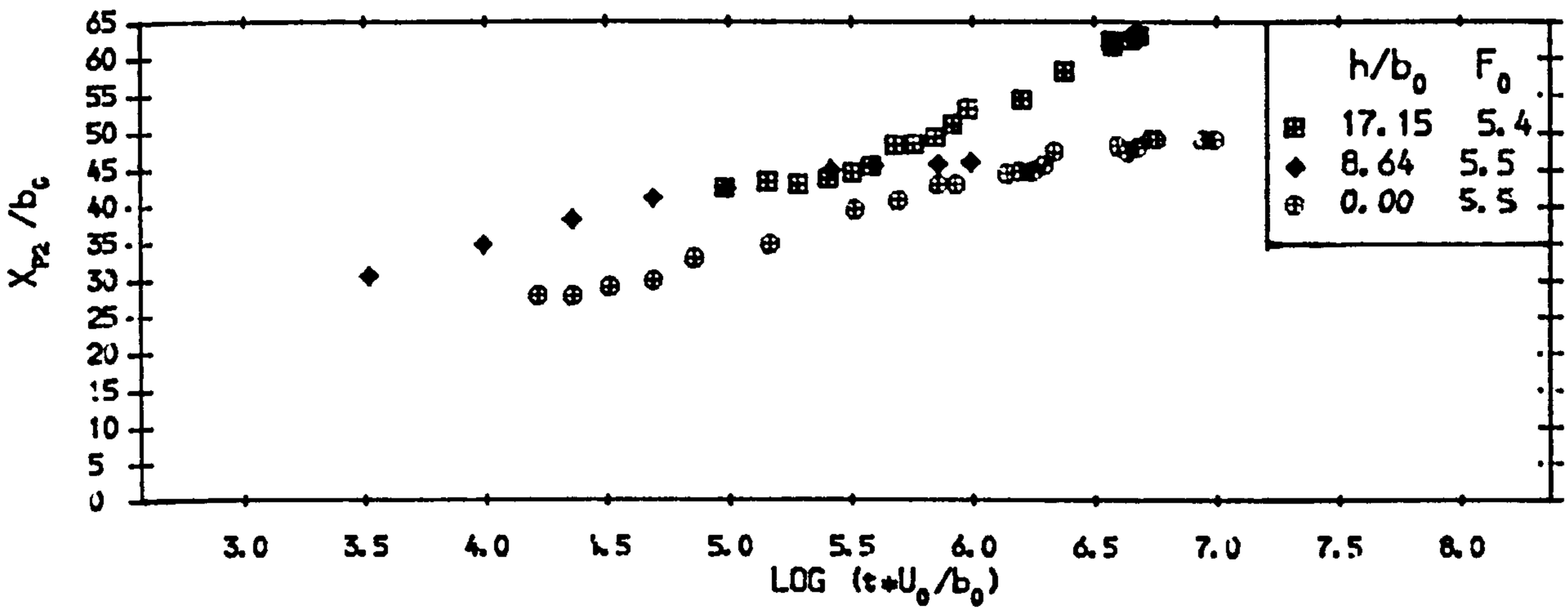

Fig. 6.34 Effect of h on the Variation of X_{p2} With Log of Time

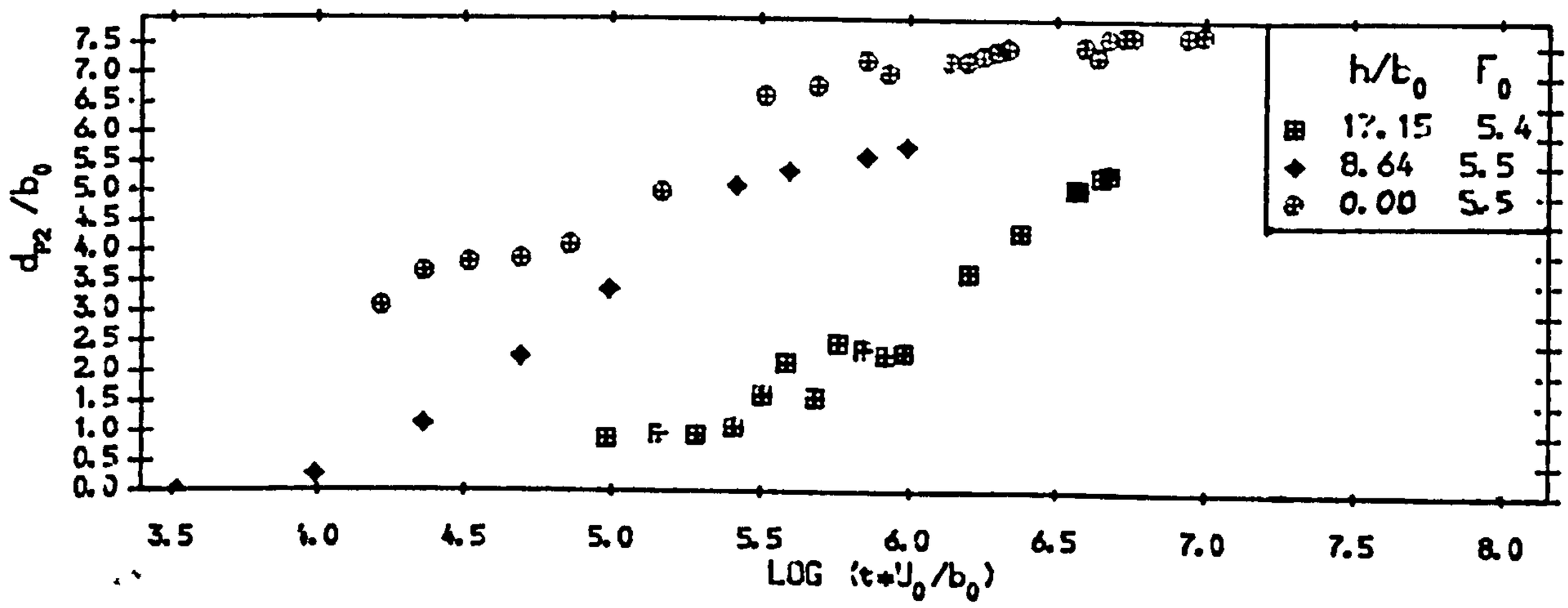

Fig. 6.35 Effect of h on the Variation of d_{p2} With Log of Time

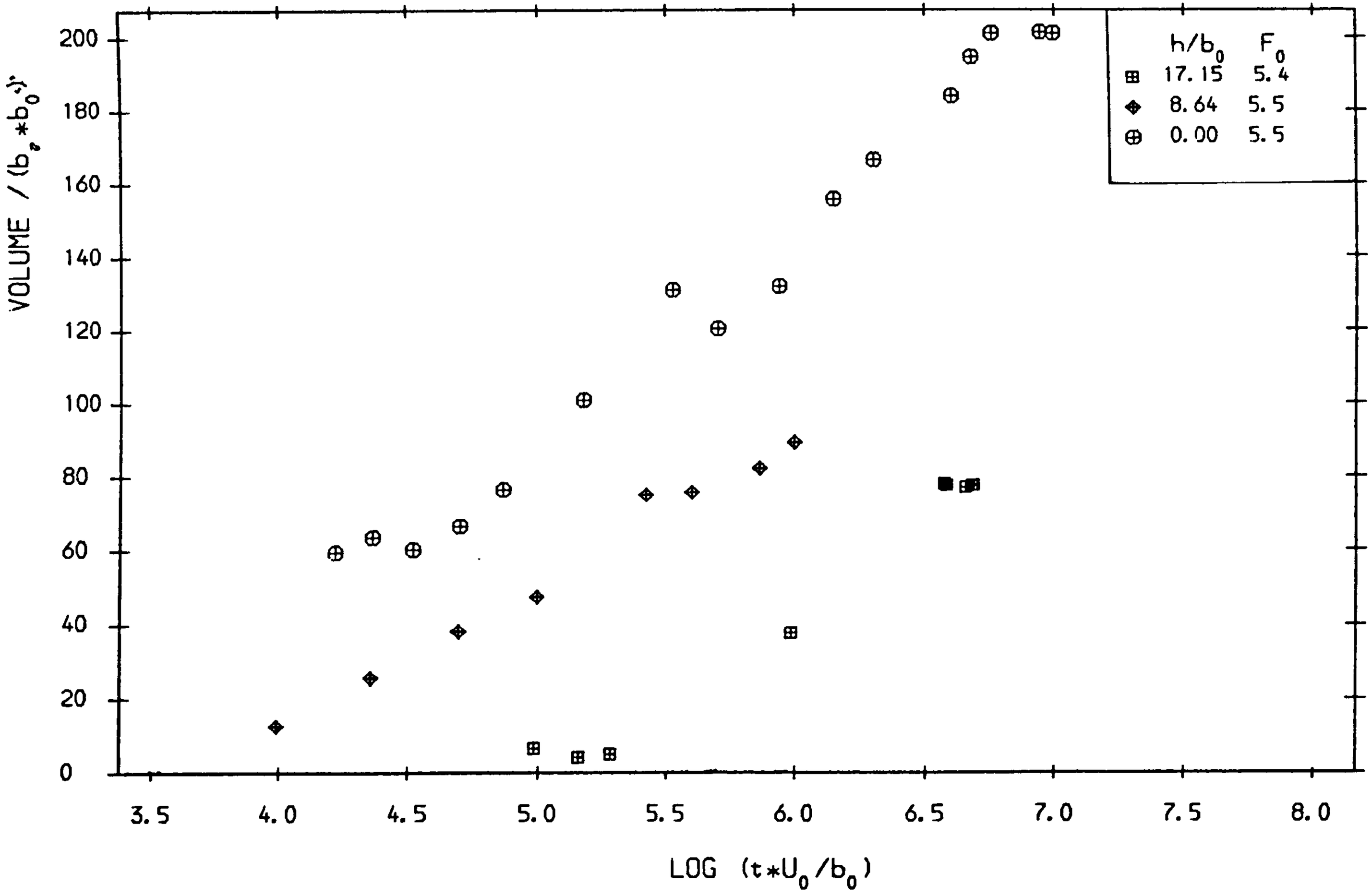

Fig. 6.36 Effect of h on the Time Variation of Scour Volume

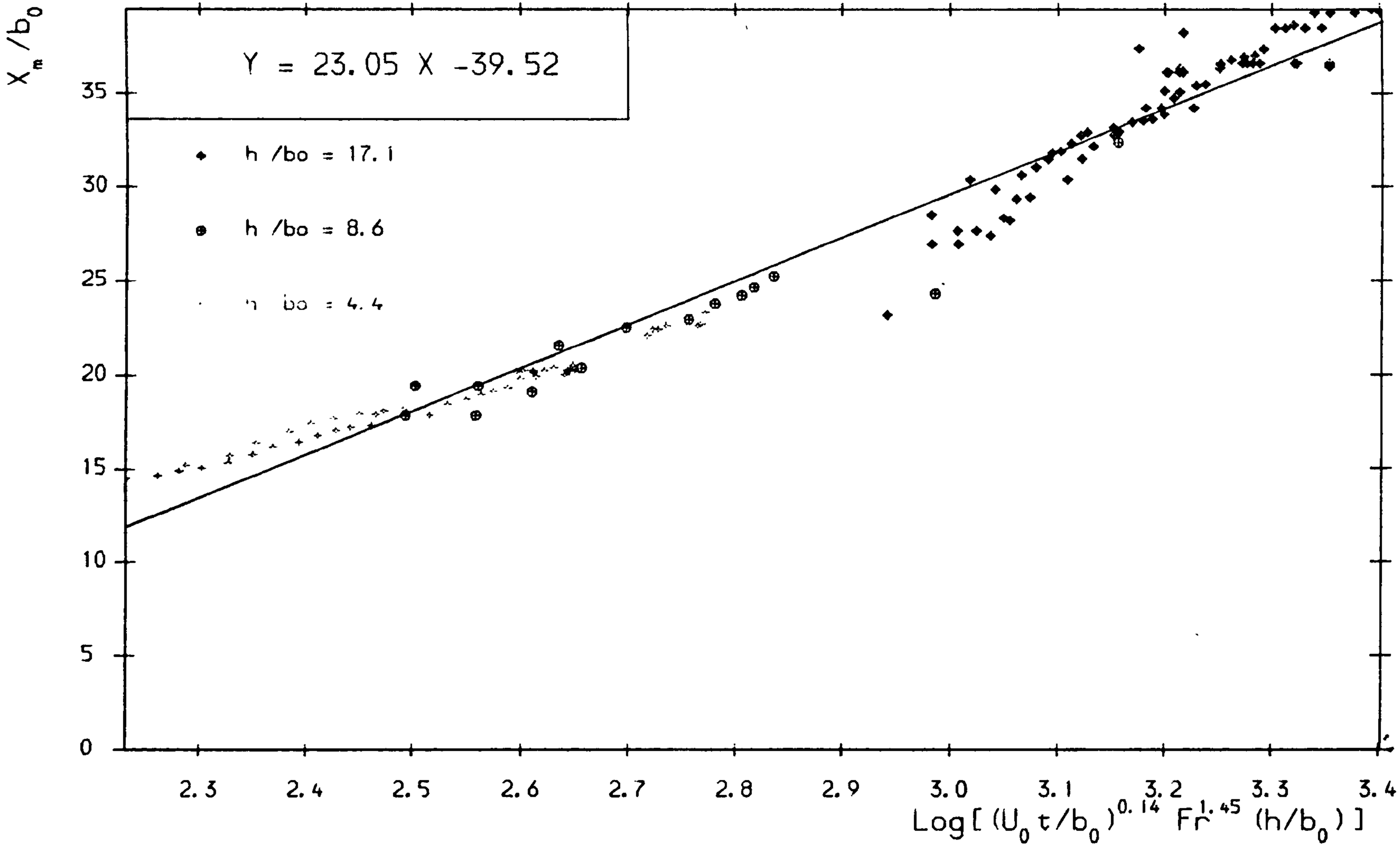

Fig. 6.37 Best-Fit Curve for X_m

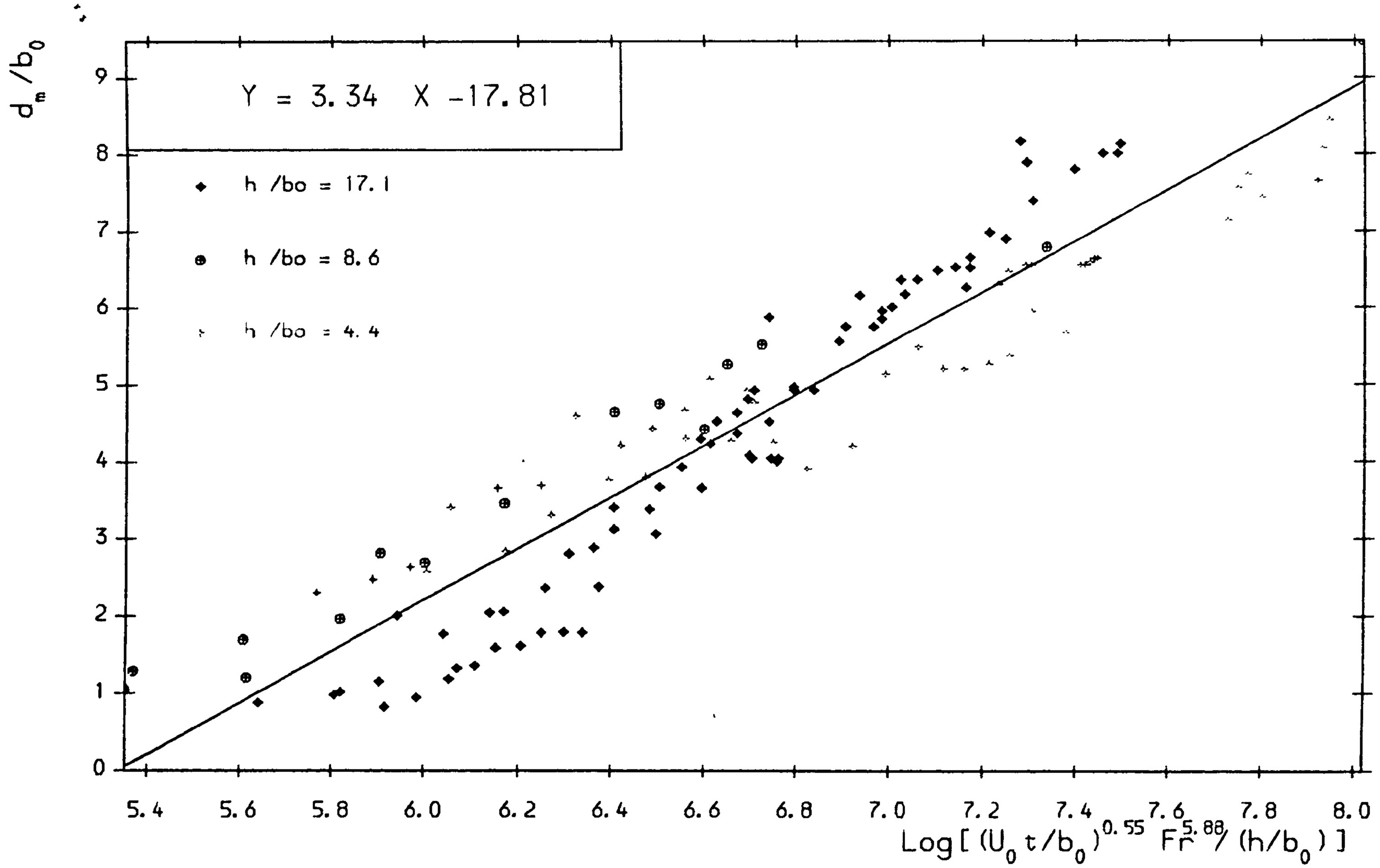

Fig. 6.38 Best-Fit Curve for d_m

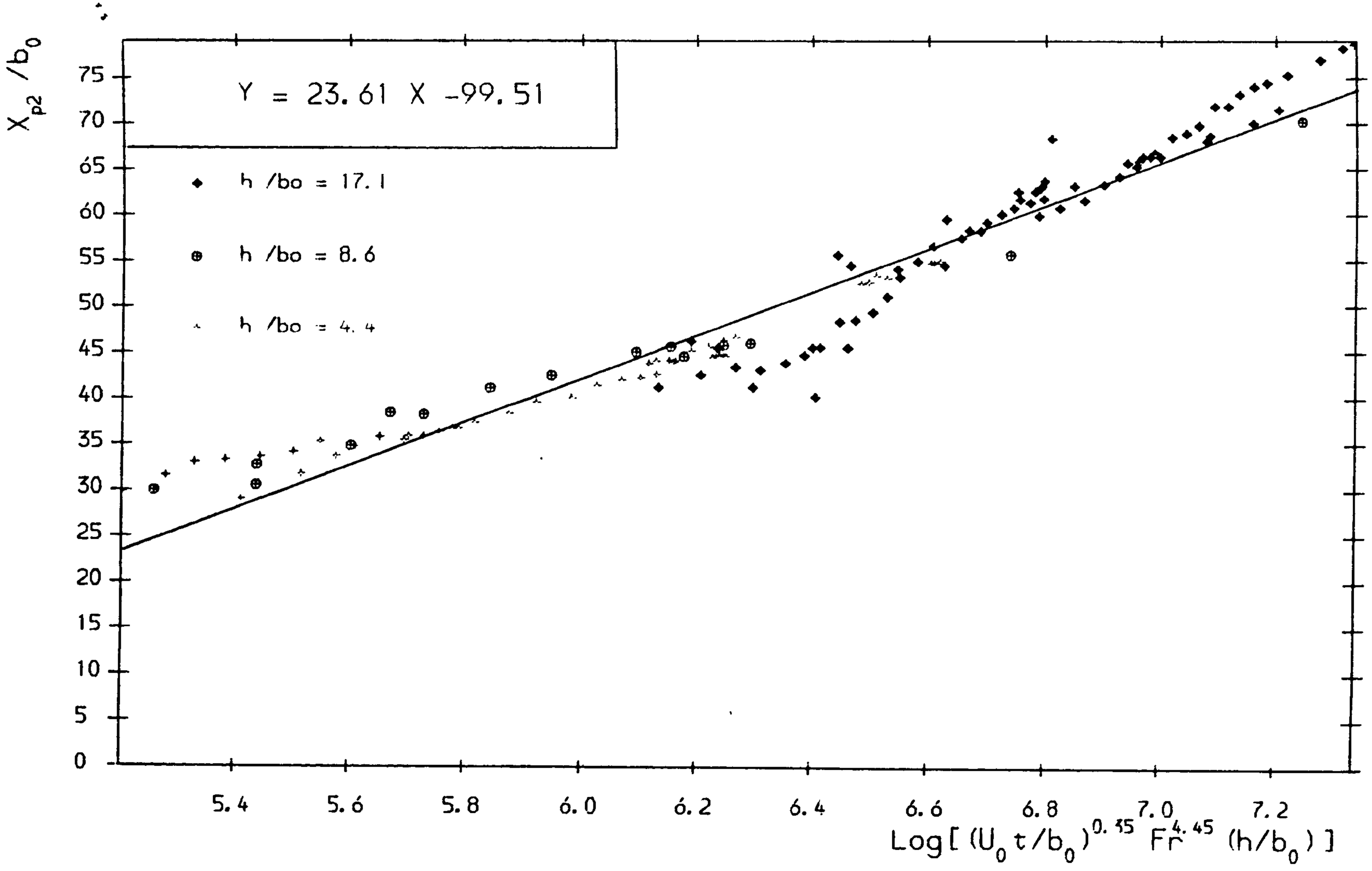

Fig. 6.39 Best-Fit Curve for X_{p2}

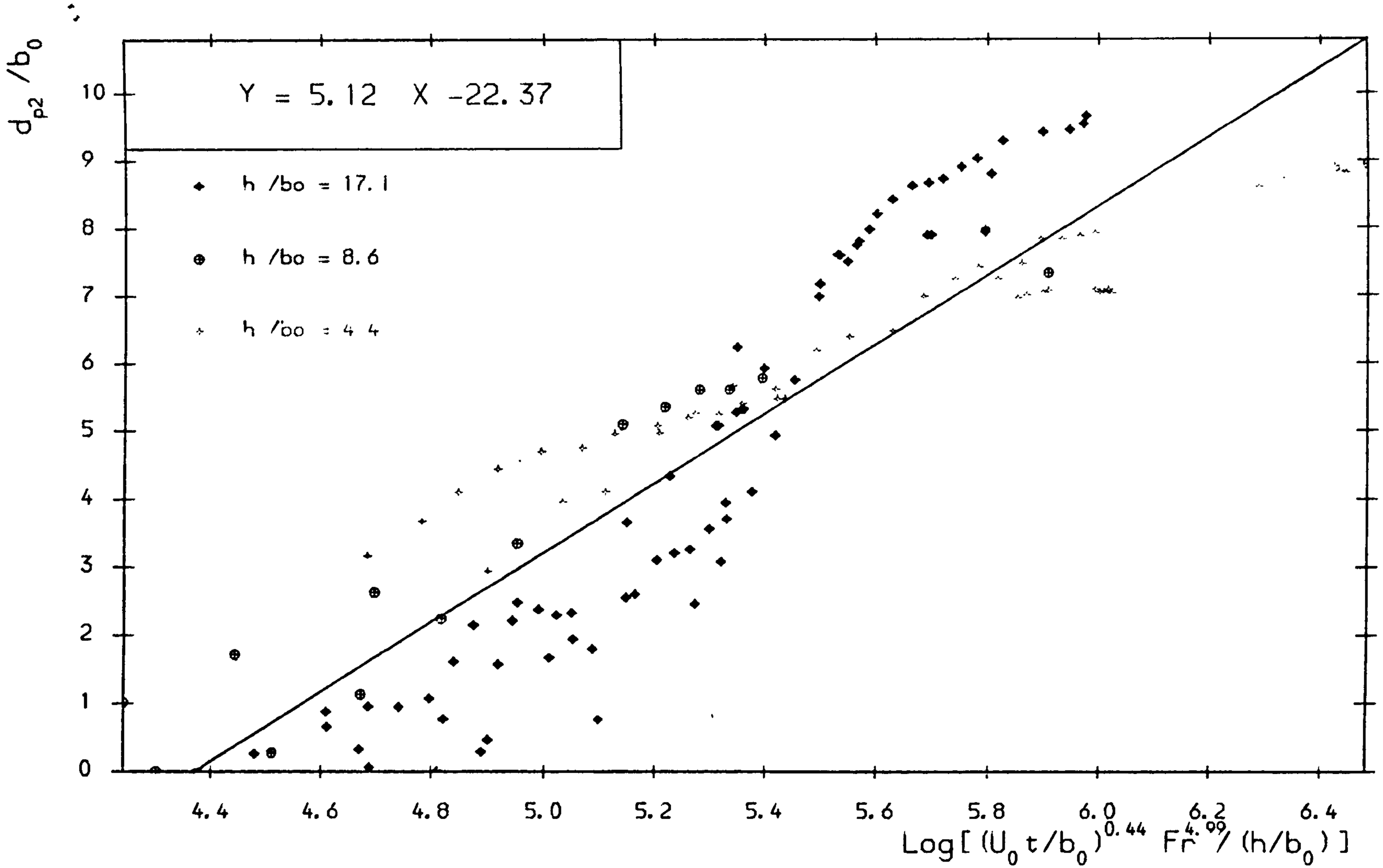

Fig. 6.40 Best-Fit Curve for d_{p2}

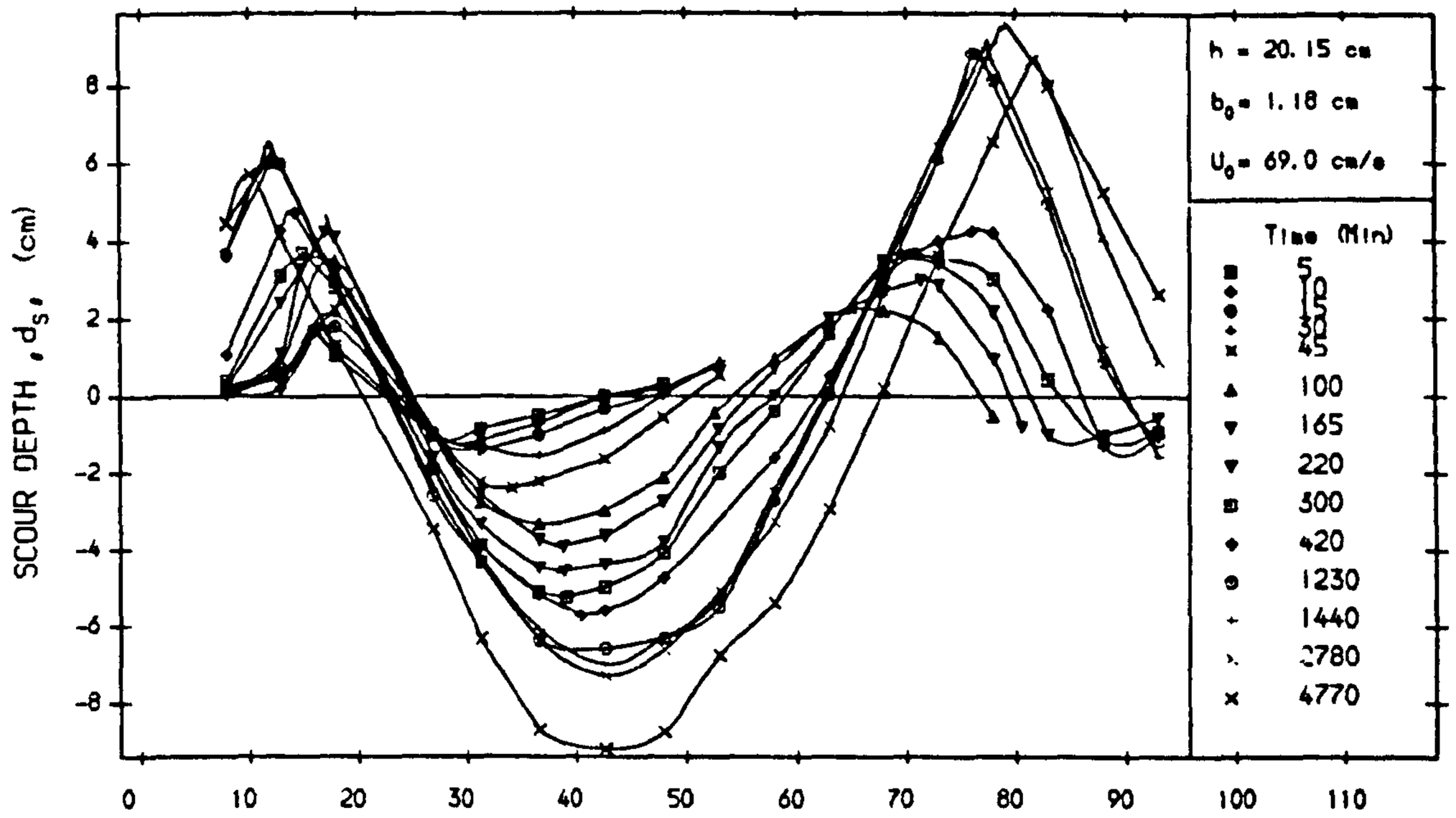

Fig. 6.41-a Progress of Scour Hole Profile With Time (Test No. S205)

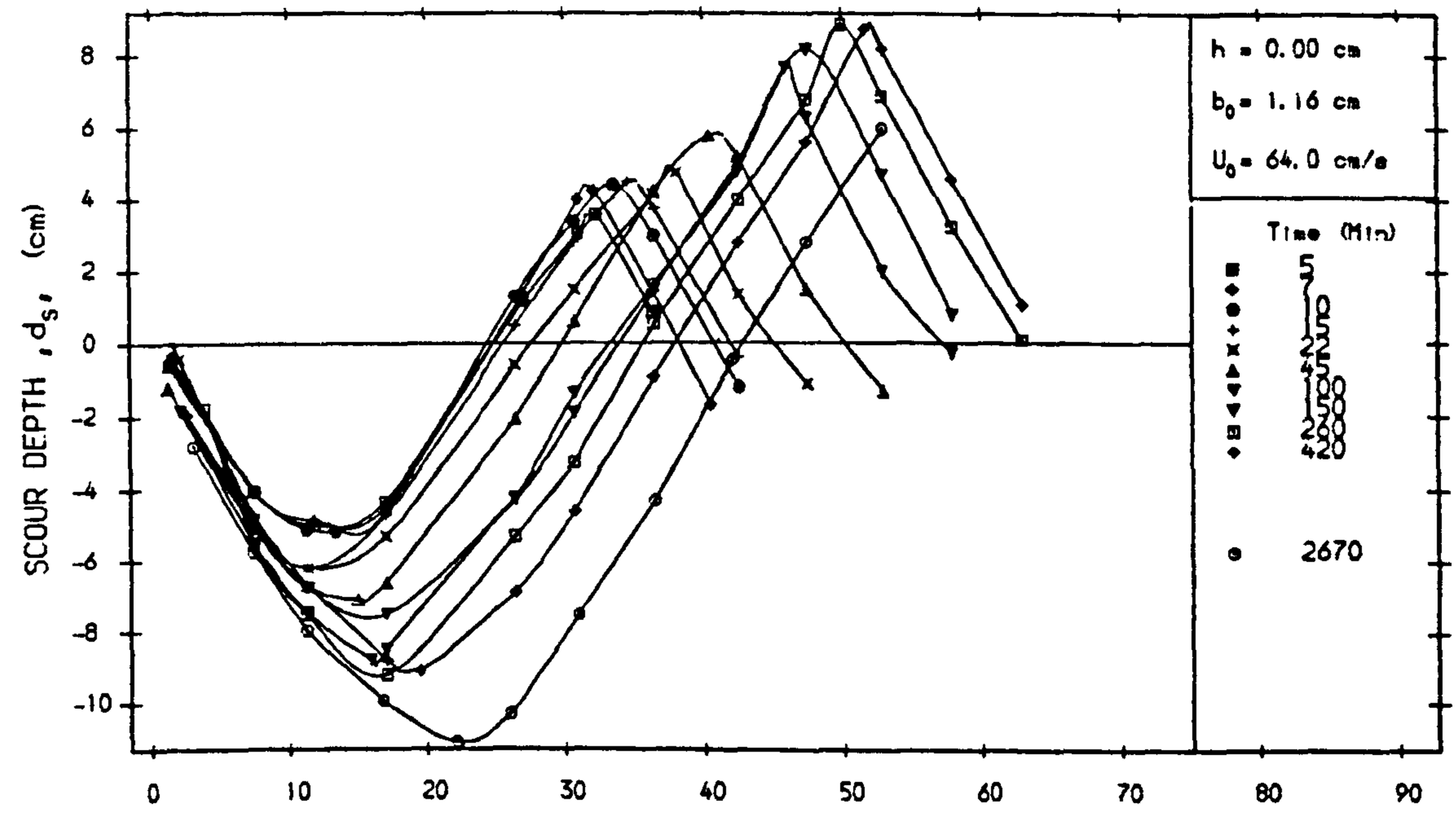

Fig. 6.41-b Progress of Scour Hole Profile With Time (Test No. S001)

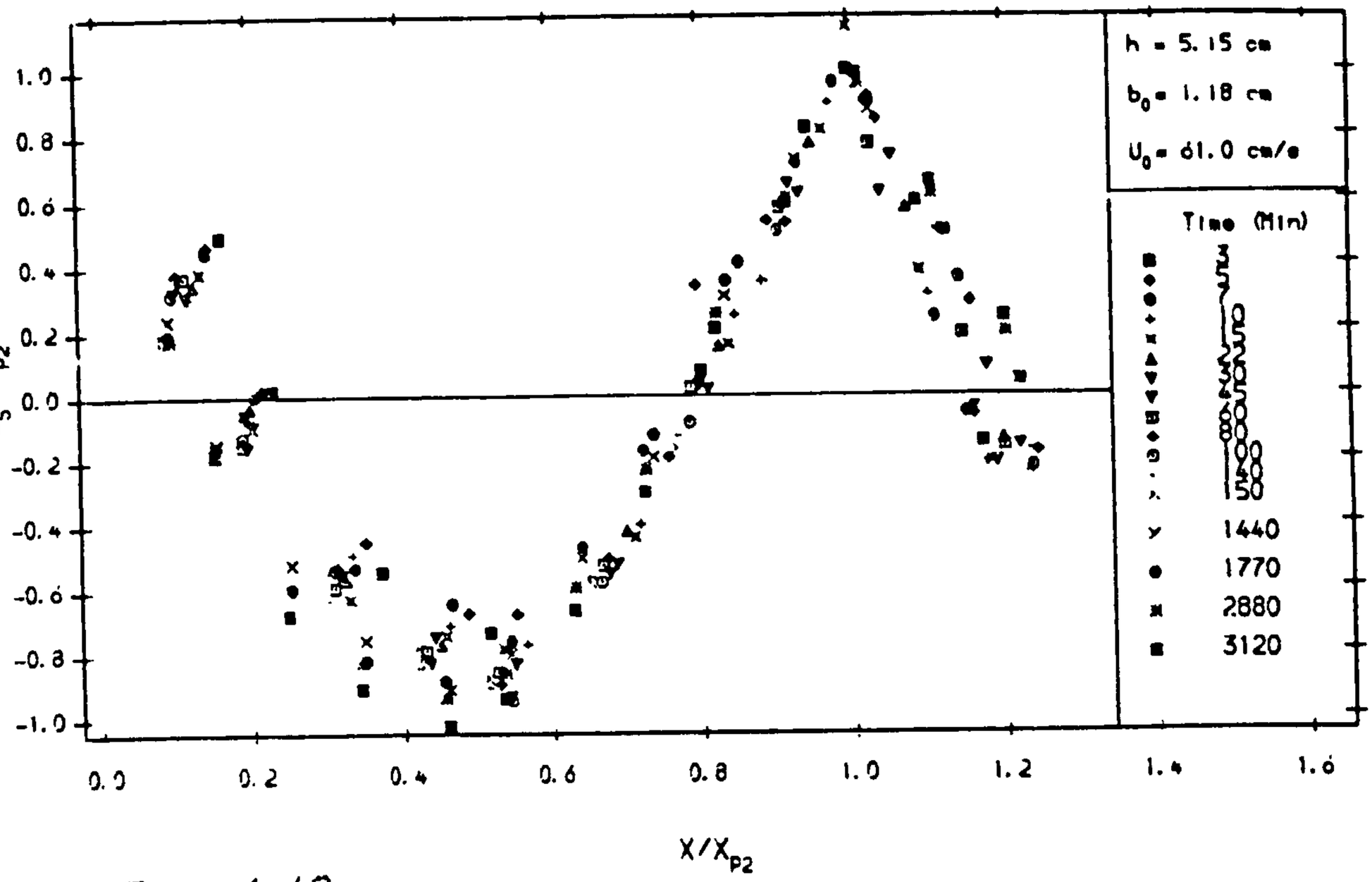

Fig. 6.42-a

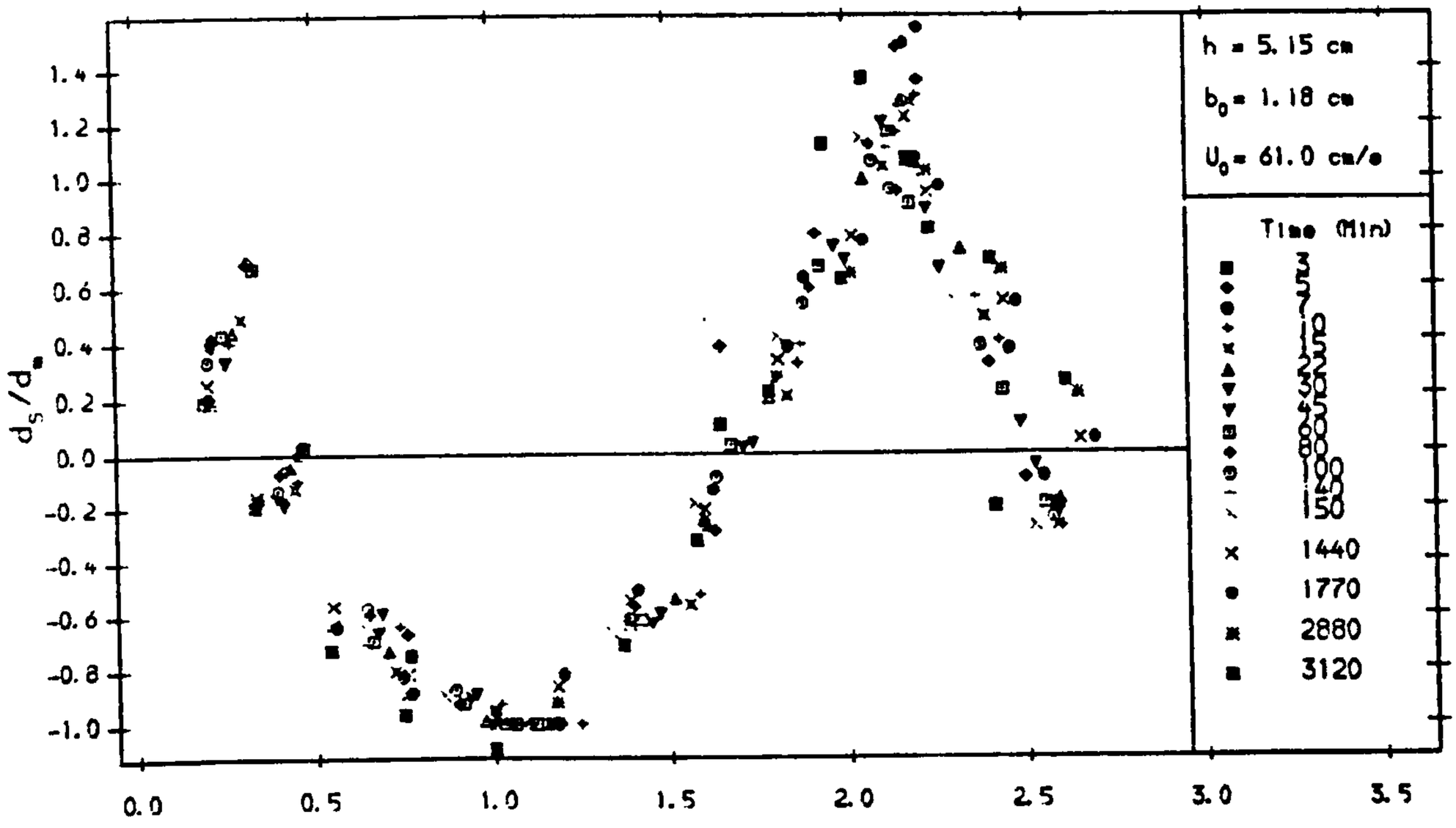

Fig. 6.42-b Effect of Choice of Length Scale on the Dimensionless Scour Profile (Test No. S051)

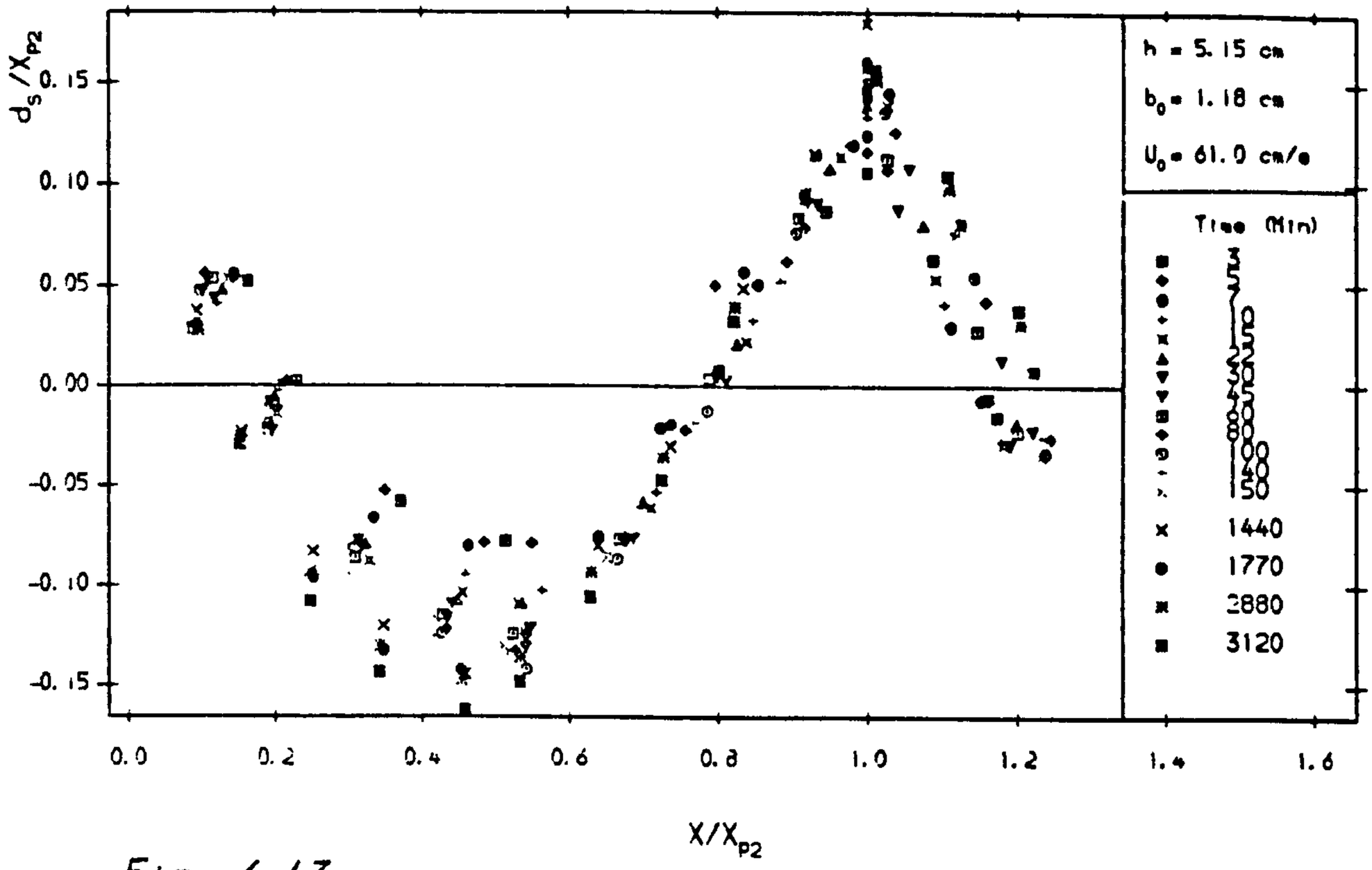

Fig. 6.43-a

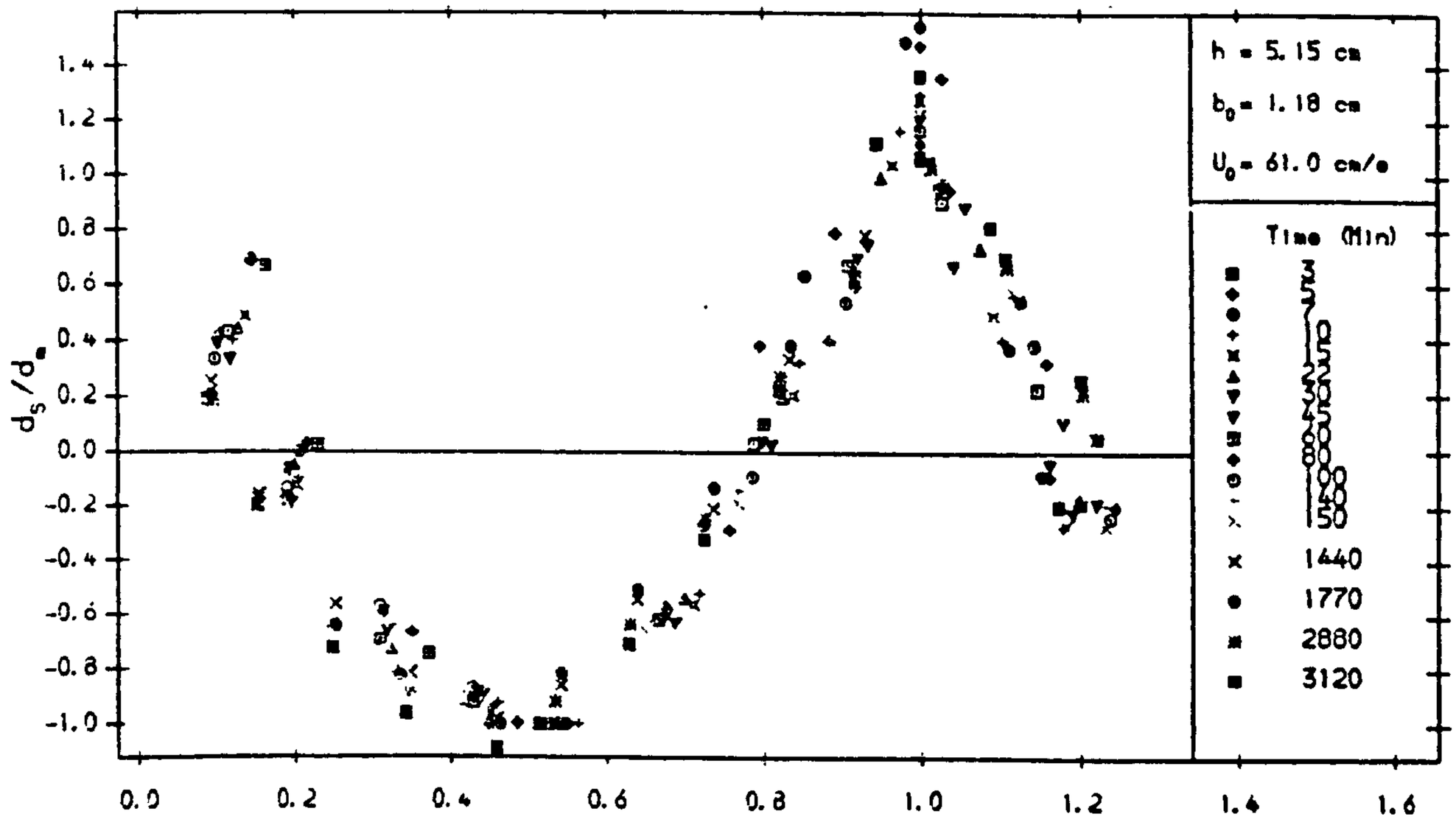

Fig. 6.43-b Effect of Choice of Length Scale on the Dimensionless Scour Profile (Test No. S051)

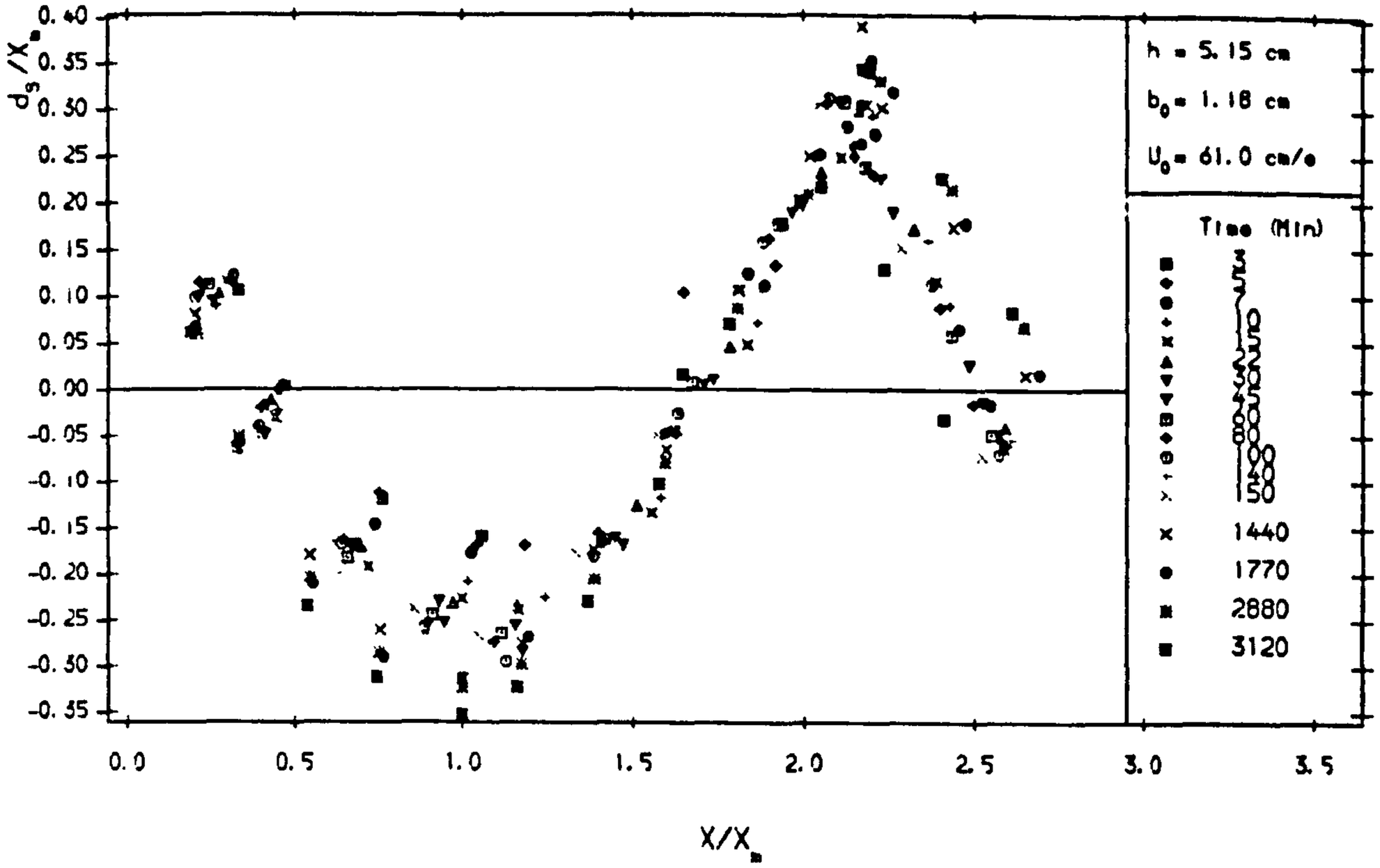

Fig. 6.44-a

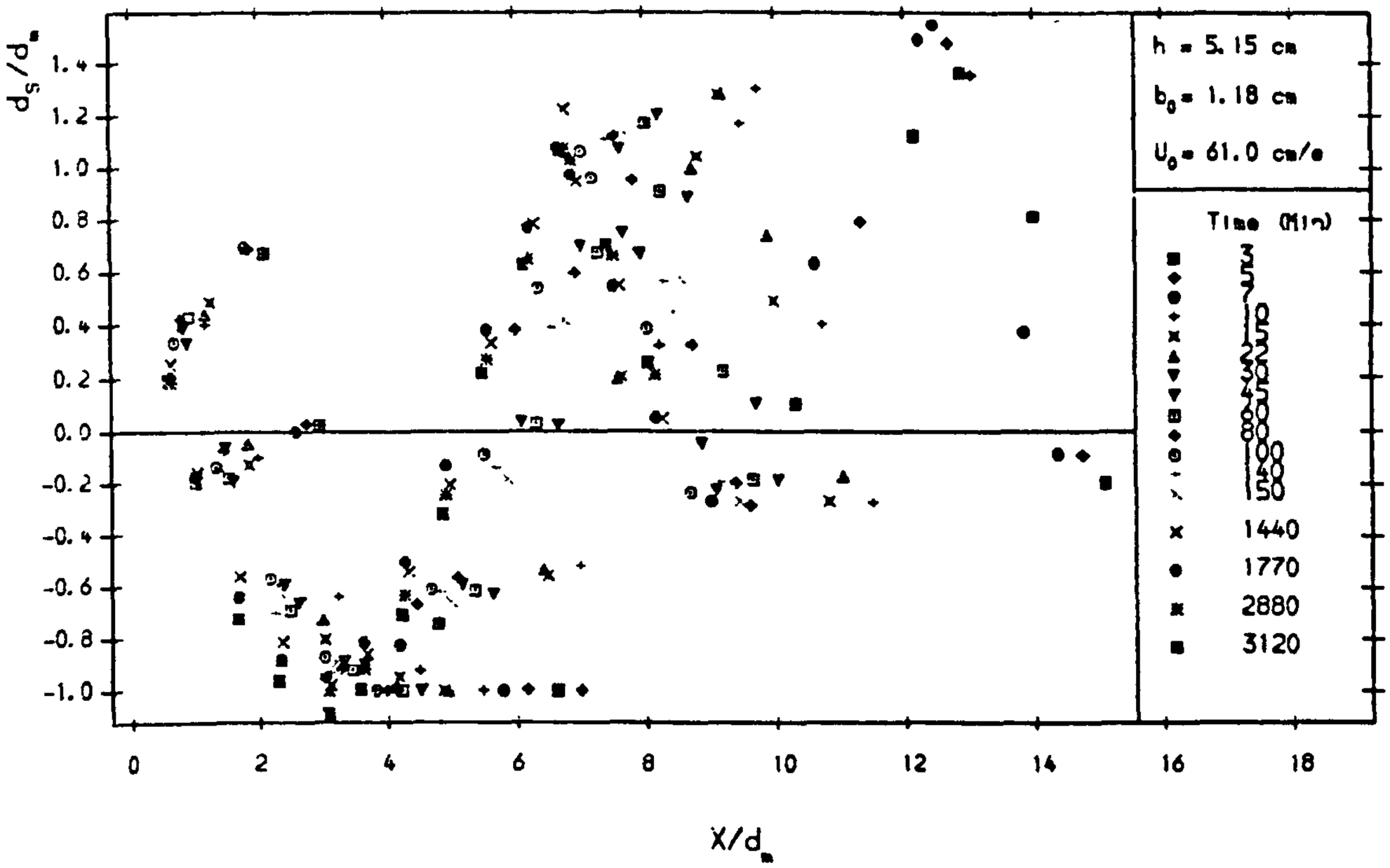

Fig. 6.44-b Effect of Choice of Length Scale on the Dimensionless Scour Profile (Test No. S051)

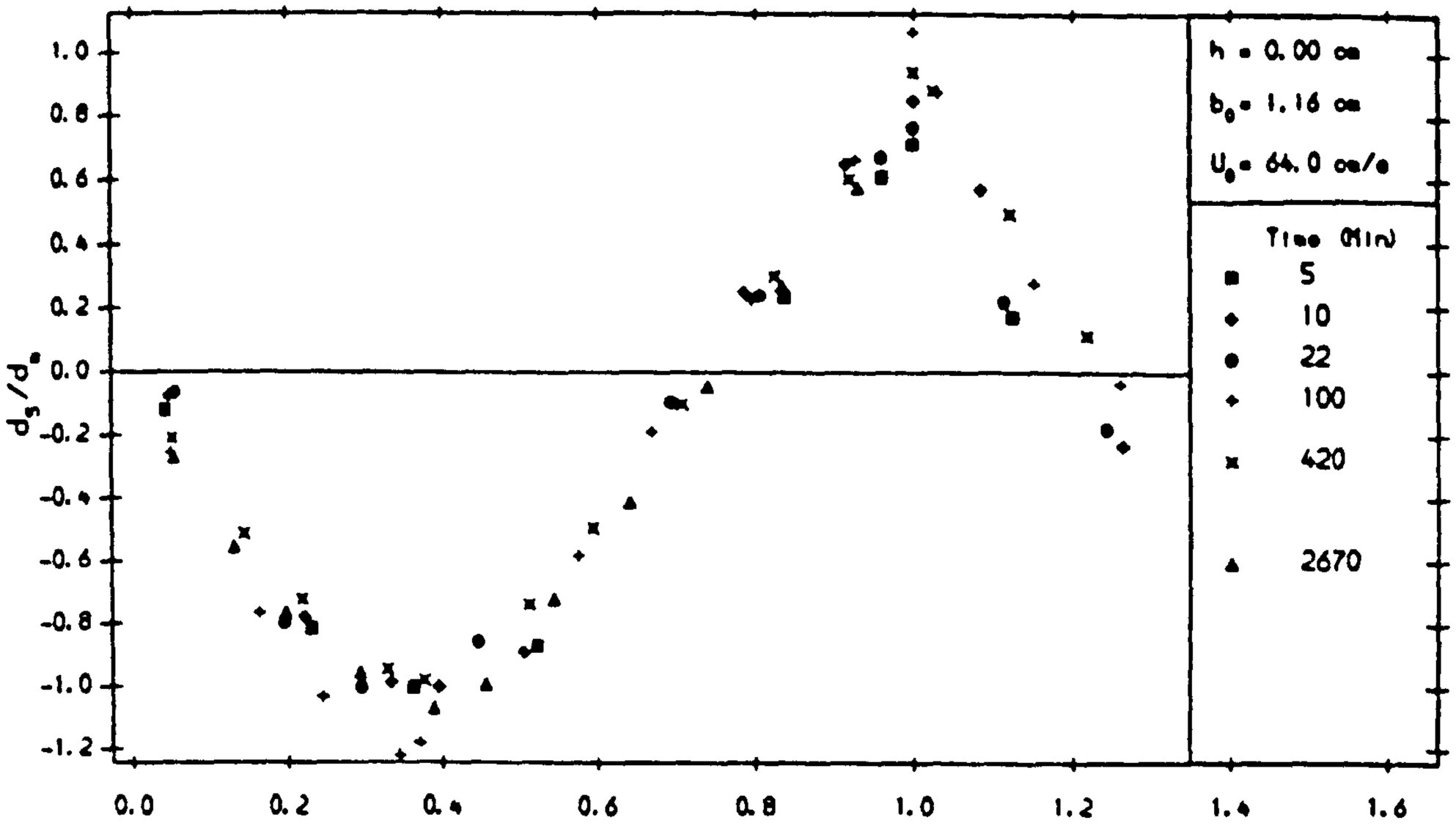

Fig. 6.45-a Dimenionless Scour Profile (d_s/d_s vs. X/X_{P2})
(Test No. S001)

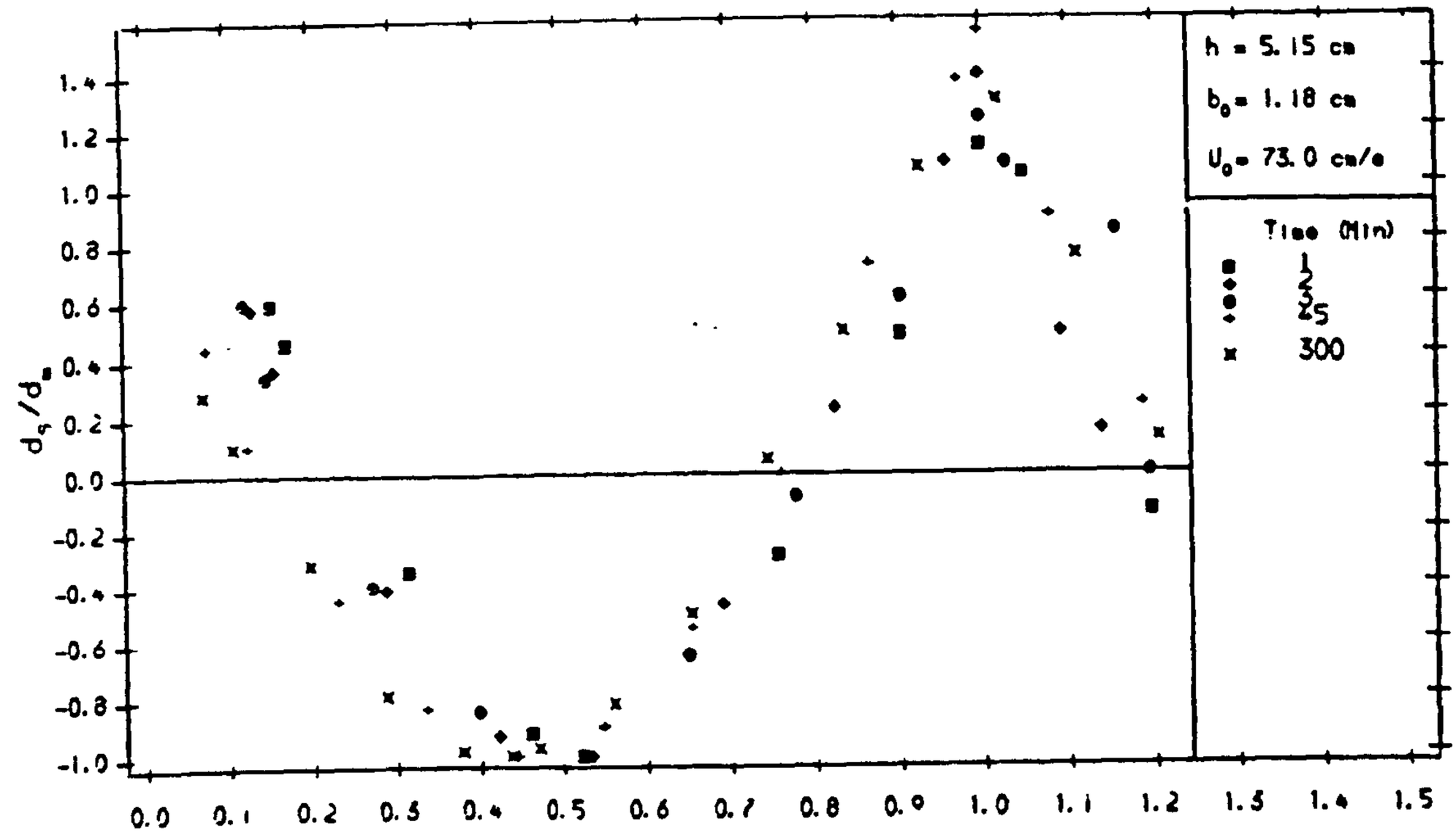

Fig. 6.45-b Dimenionless Scour Profile (d_s/d_s vs. X/X_{P2})
(Test No. S052)

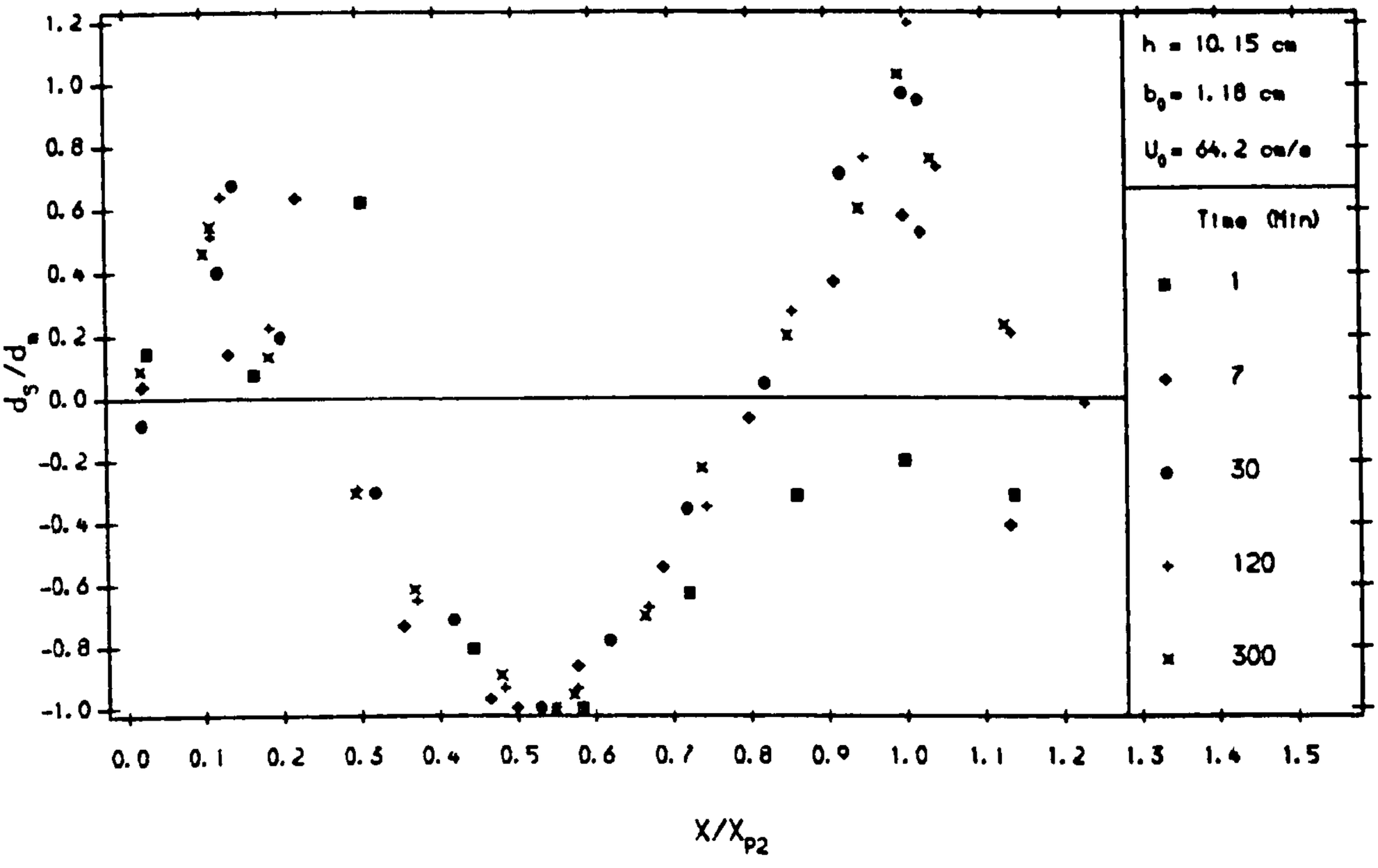

Fig. 6.46-a Dimenionless Scour Profile (d_s/d_s vs. X/X_{P2})
(Test No. S104)

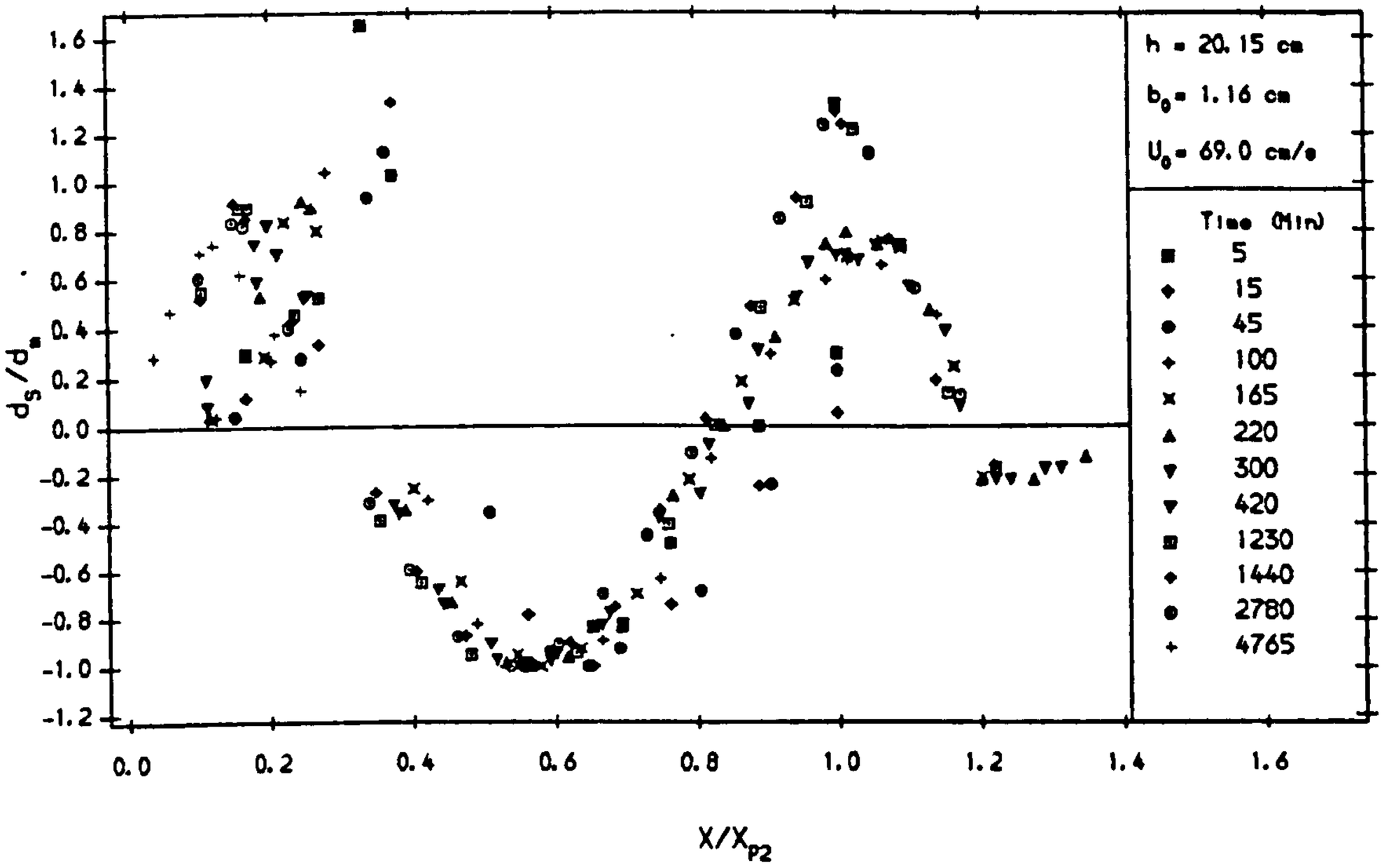

Fig. 6.46-b Dimenionless Scour Profile (d_s/d_s vs. X/X_{P2})
(Test No. S205)

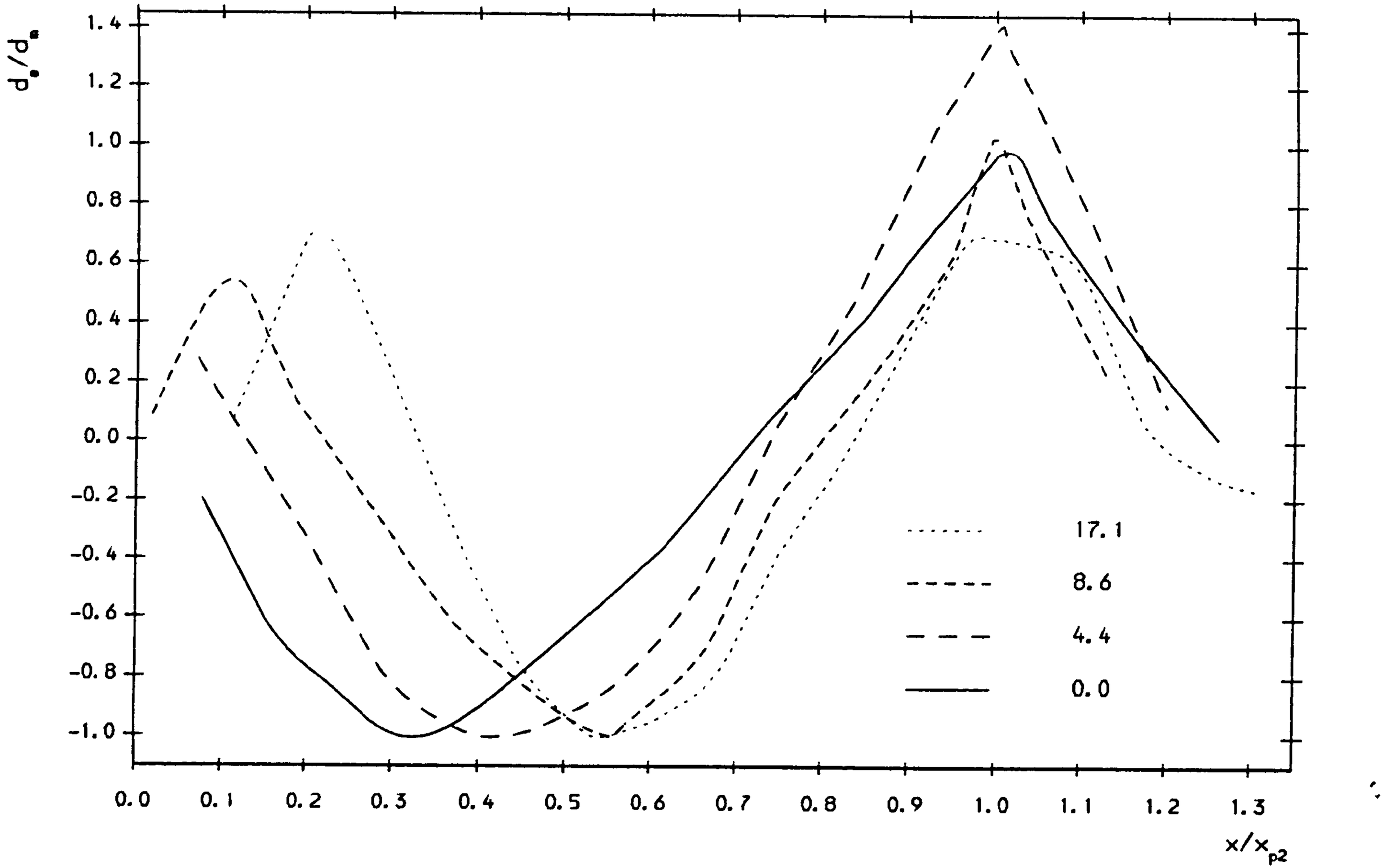

FIG. 6.47 Effect of h/b0 on the scour profile

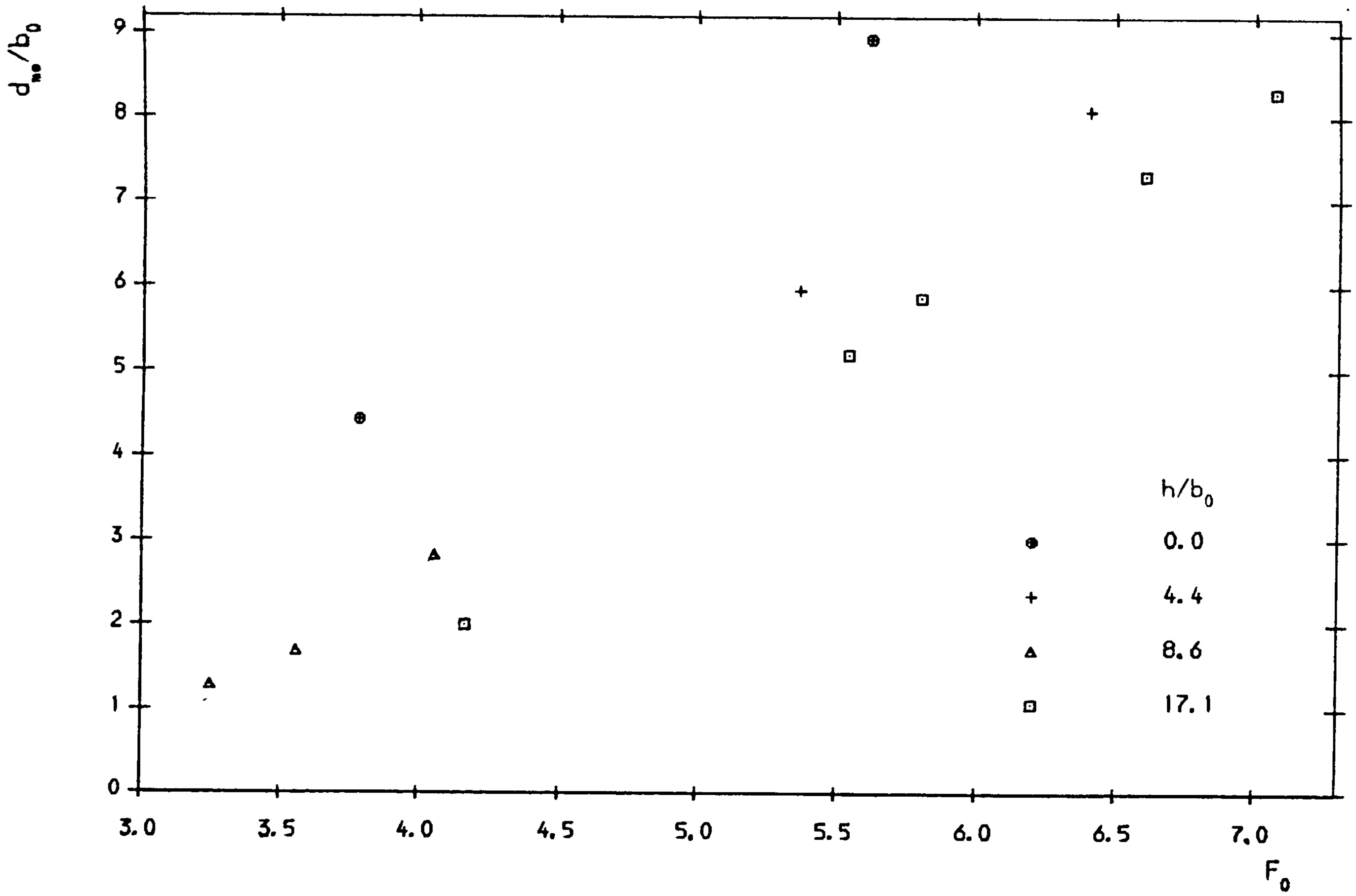

Fig. 6.48 Asymptotic Maximum Depth of Scour Hole vs. Froude No.

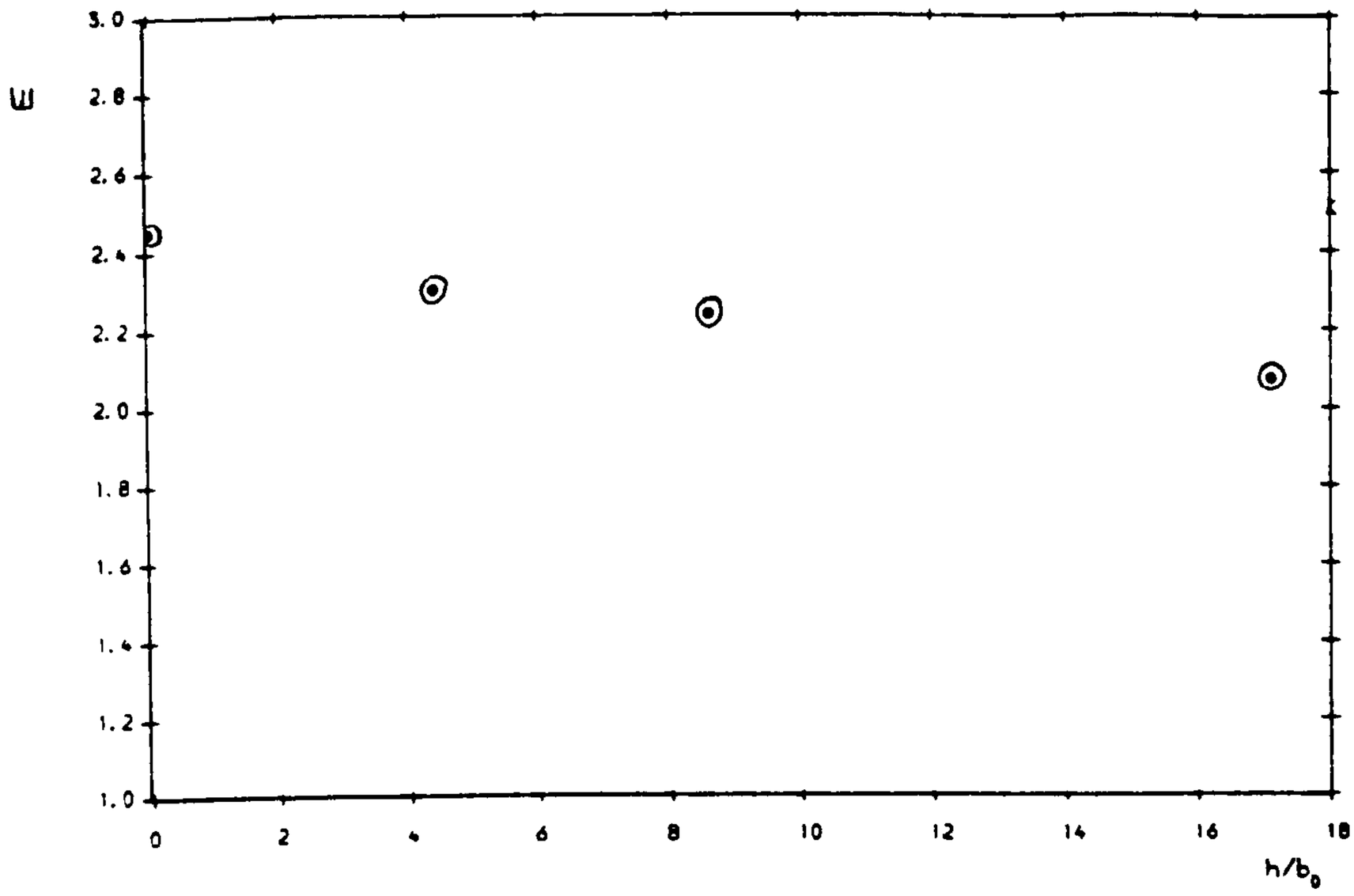

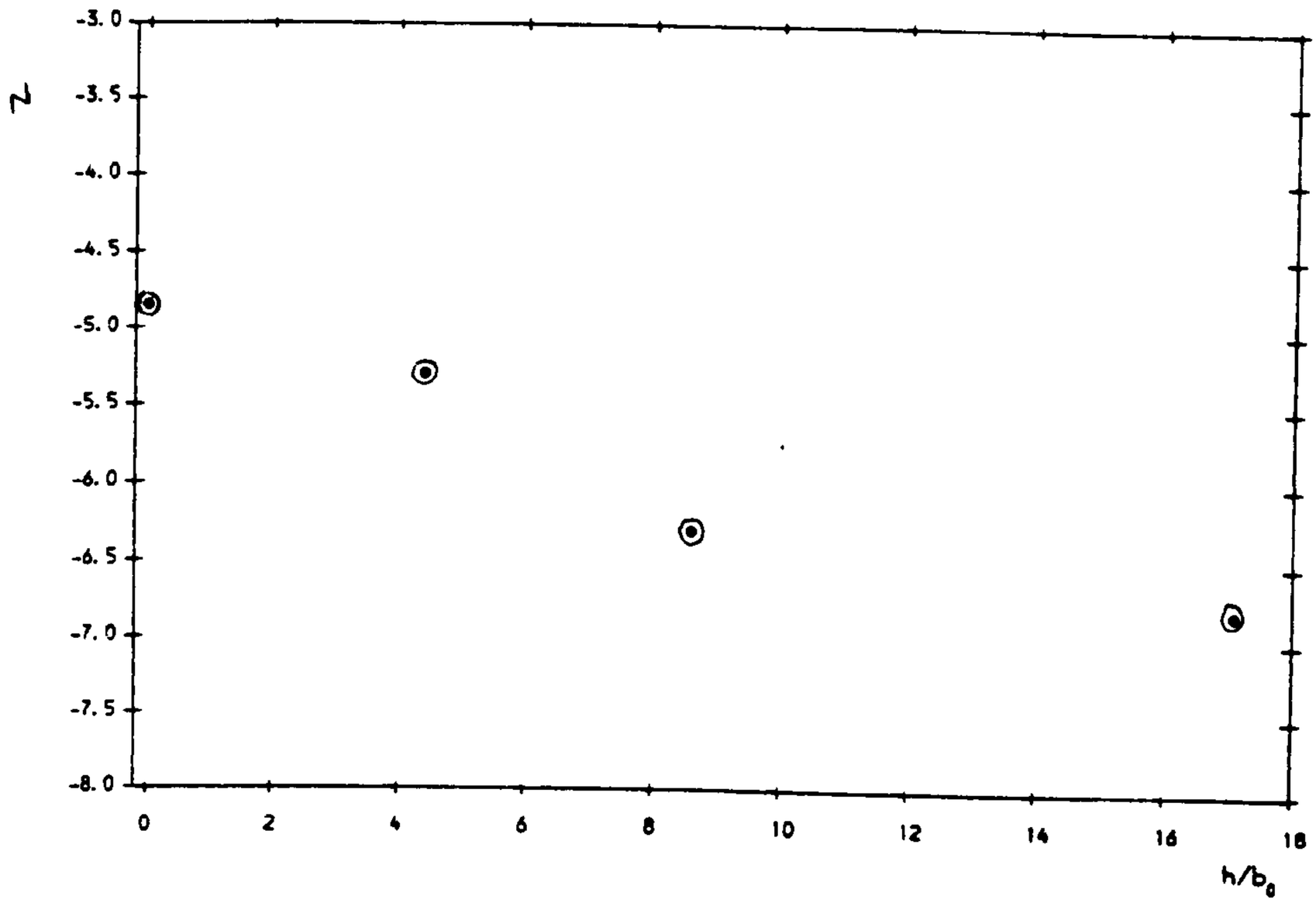

Fig. 6.49 Variation of E and Z with h/b0

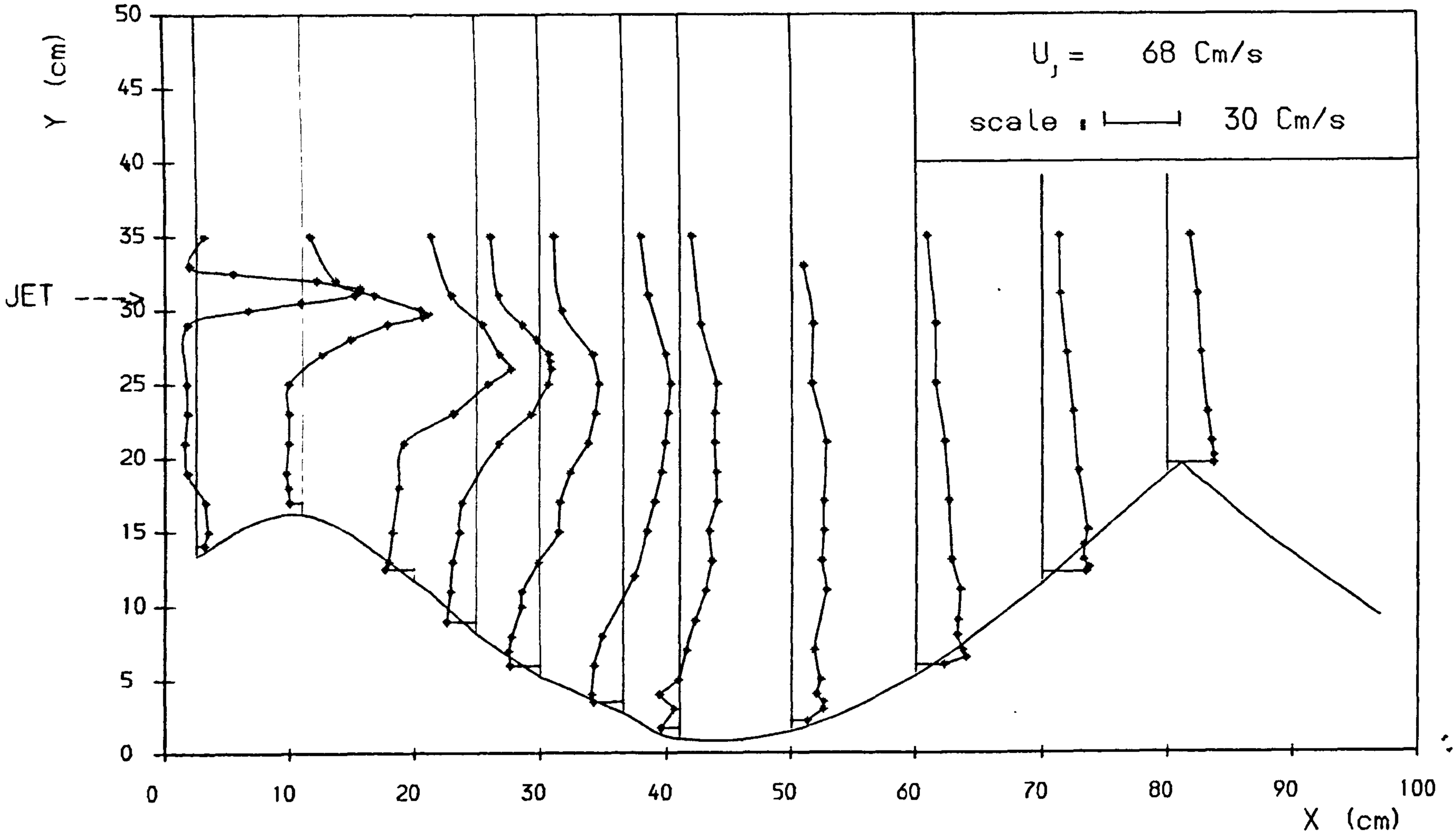

Fig 6.50 Horizontal Velocity Distributions in Scour Hole (Test No. S205)

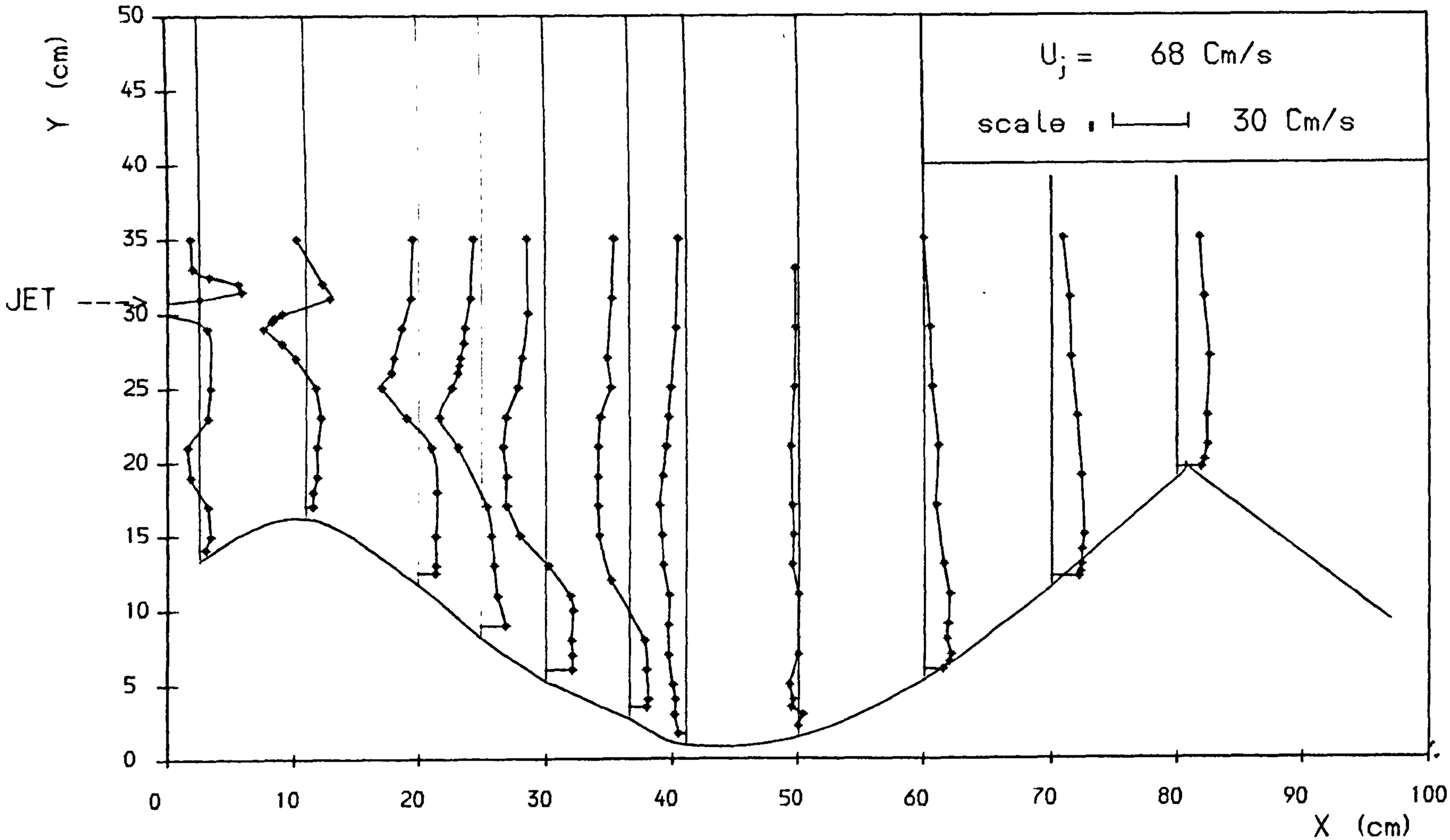

Fig 6.51 Vertical Velocity Distributions in Scour Hole (Test No. S205)

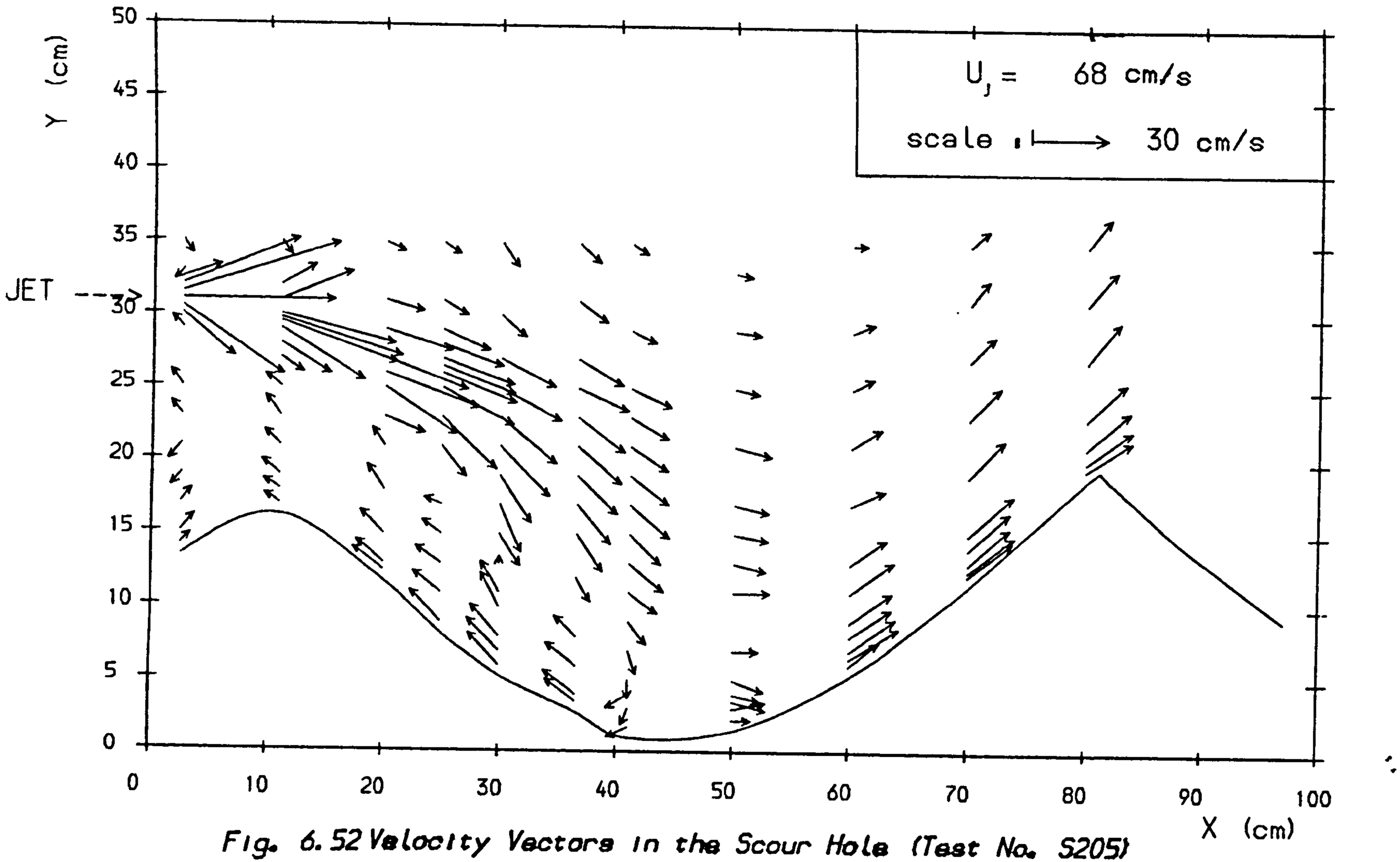

Fig. 6.52 Velocity Vectors in the Scour Hole (Test No. S205)

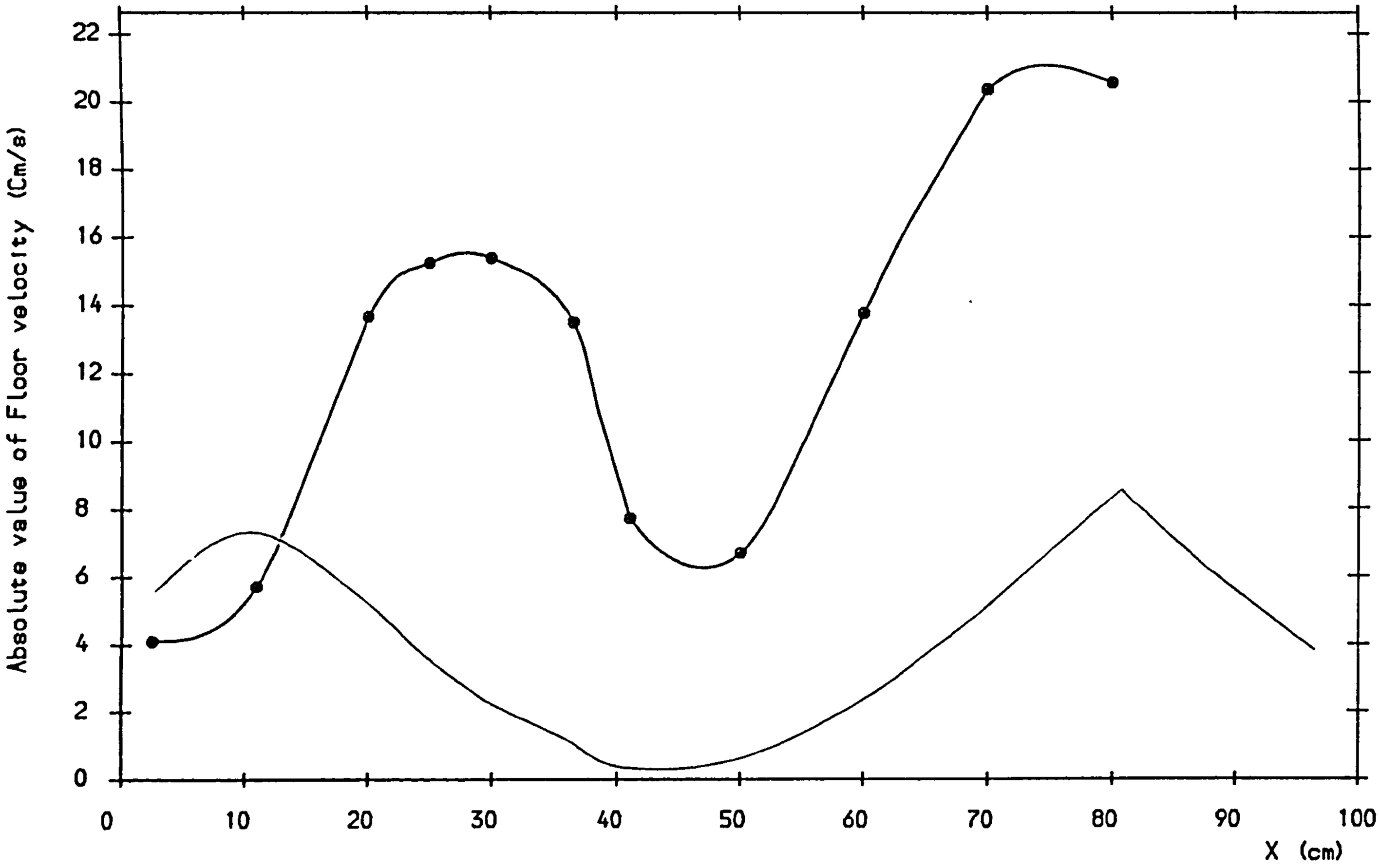

Fig. 6.53 Absolute Value of Floor Velocity in the Scour Hole (Test No. S205)

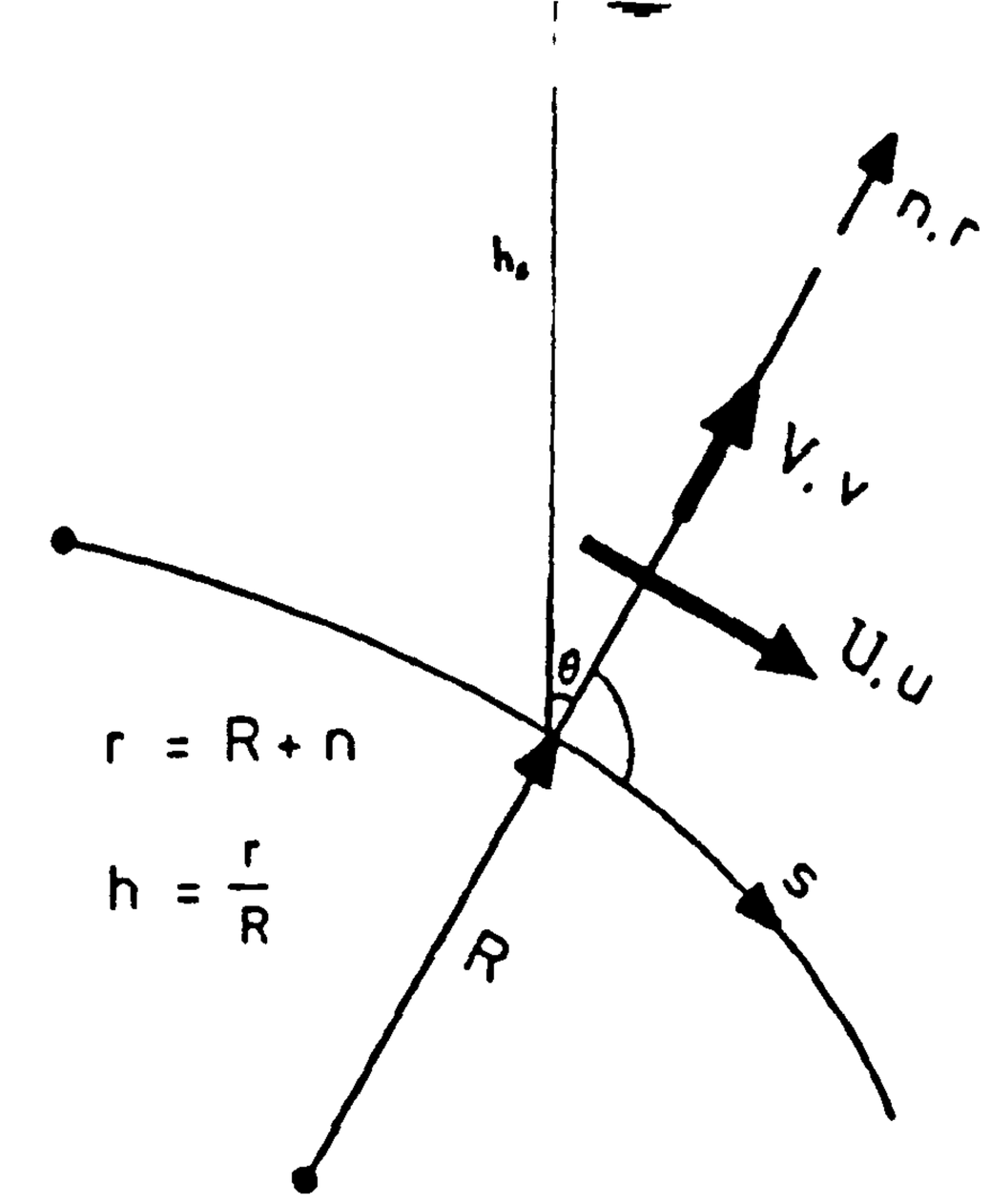

Fig. 7.1 The (s,n) Coordirate System

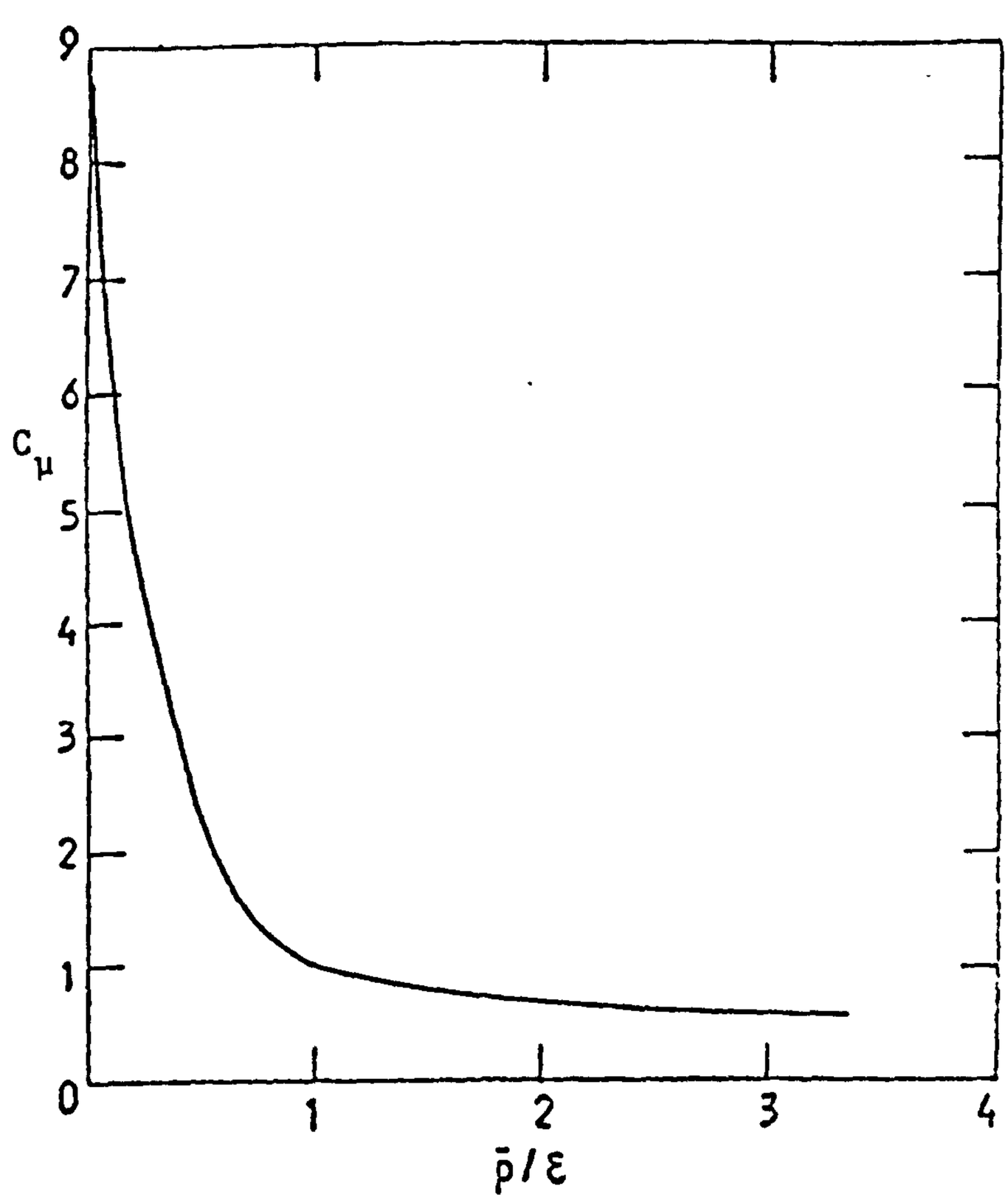

Fig. 7.2 Variation of C_μ With P/ϵ

(After Rodi (1972))

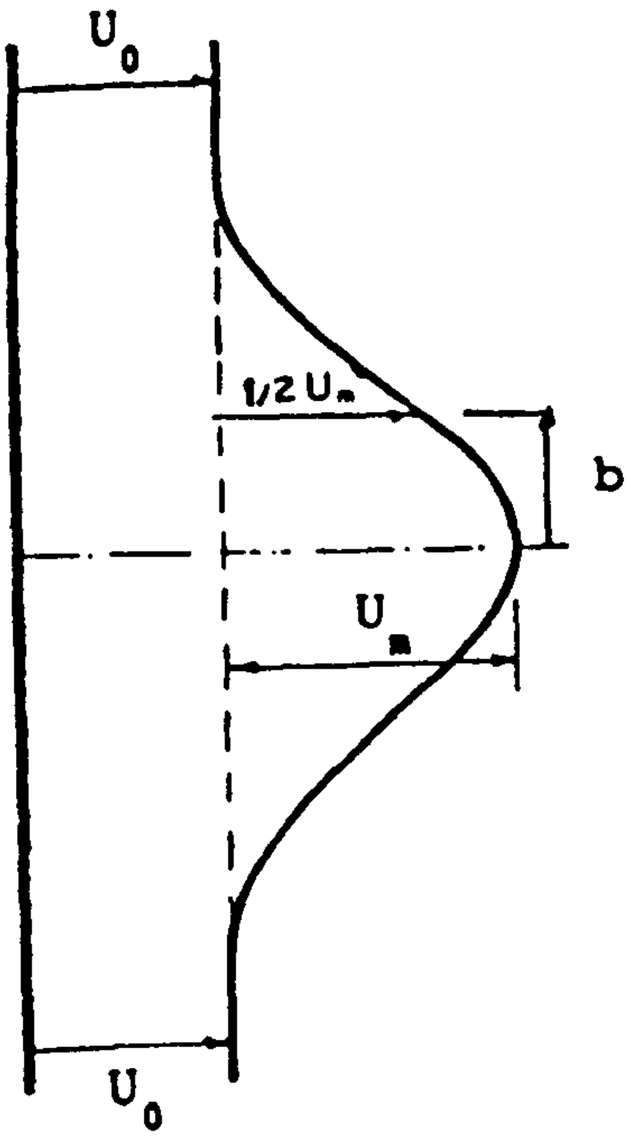

a) Free Jet

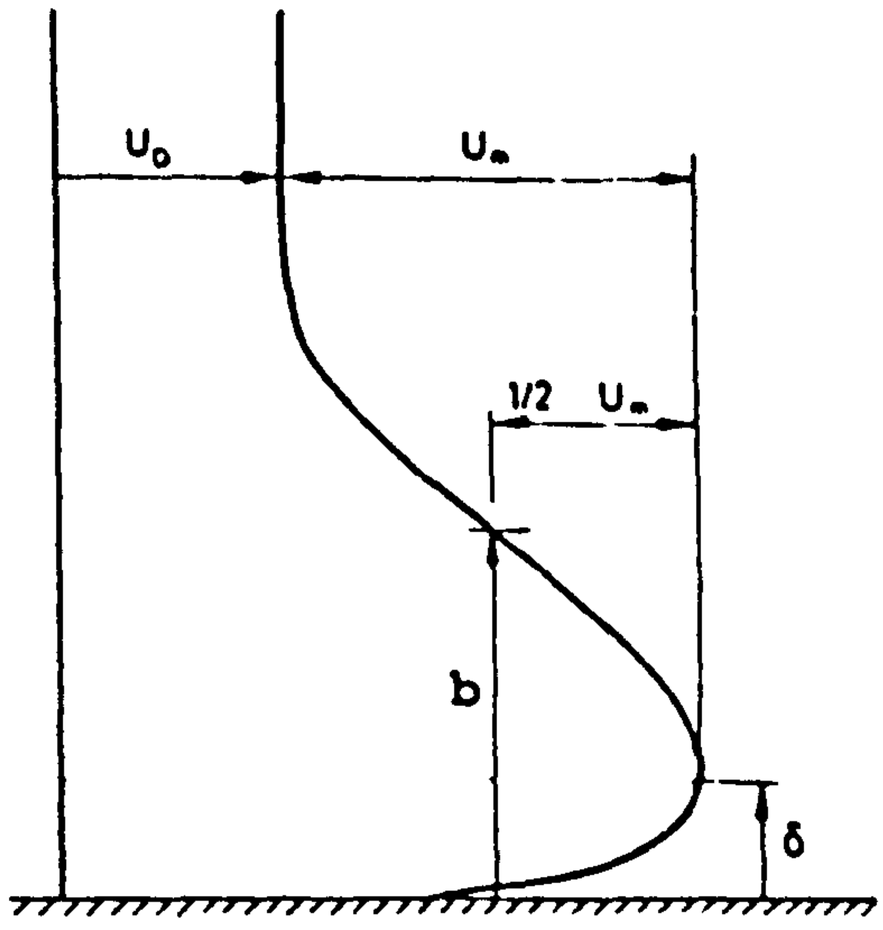

b) Wall Jet

Fig. 8.1 Definition Sketch for Velocity Profile

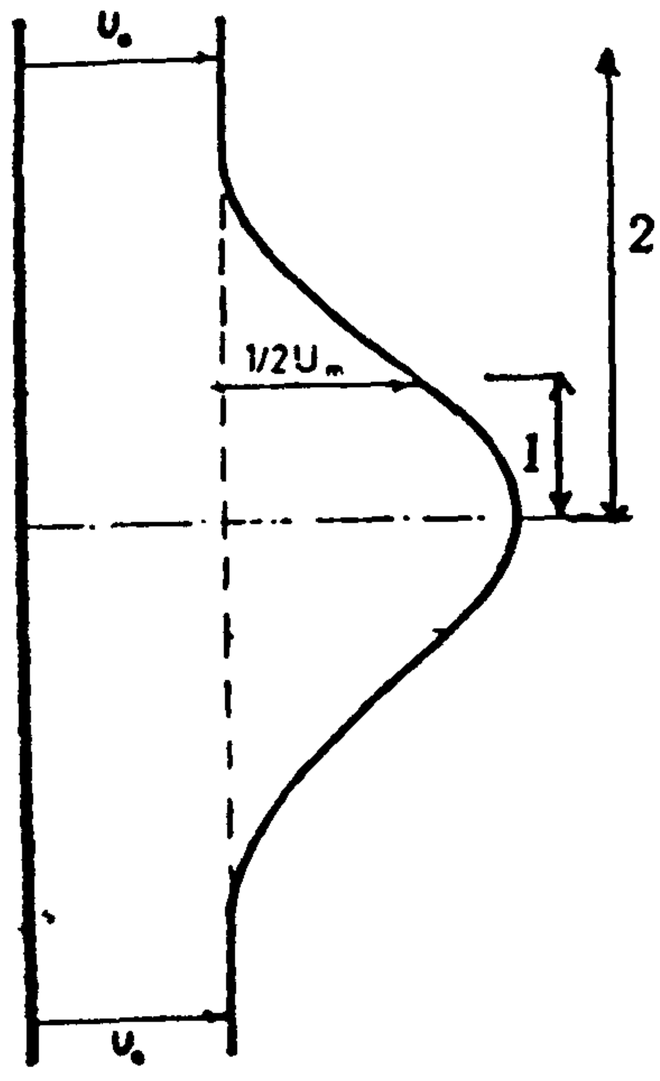

a) Free Jet

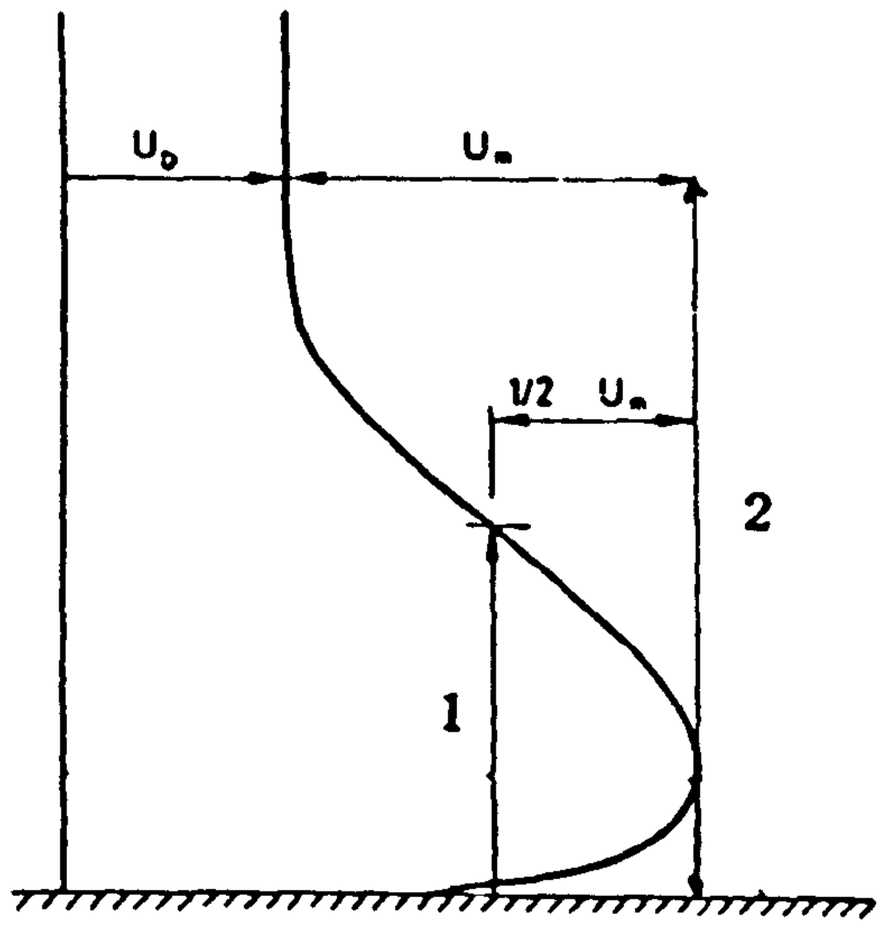

b) Wall Jet

Fig. 8.2 StripS for Momentum Equation

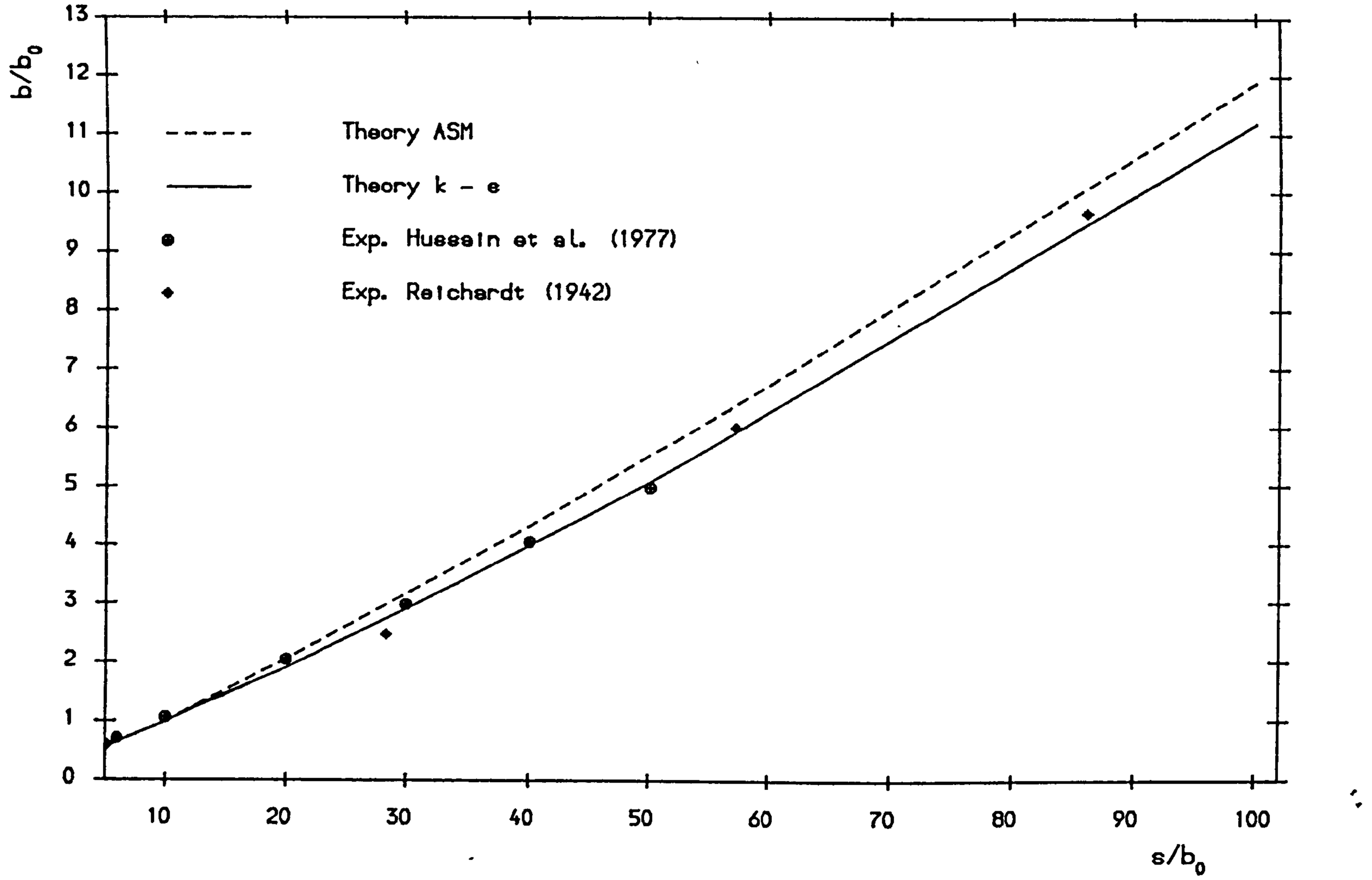

Fig 9.1 Streamwise development of half-width of free jet

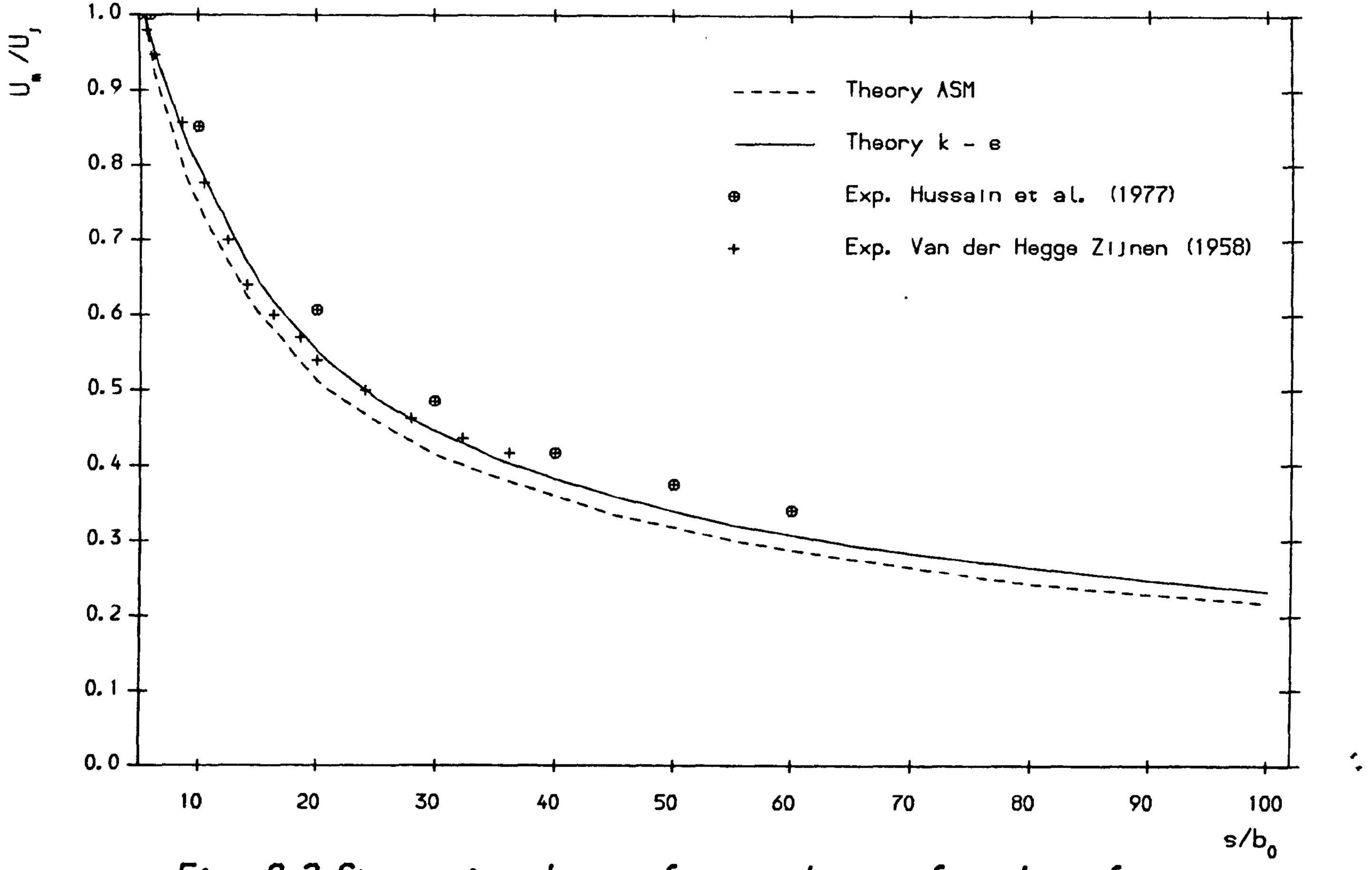

Fig. 9.2 Streamwise decay of max velocity for plane free jet

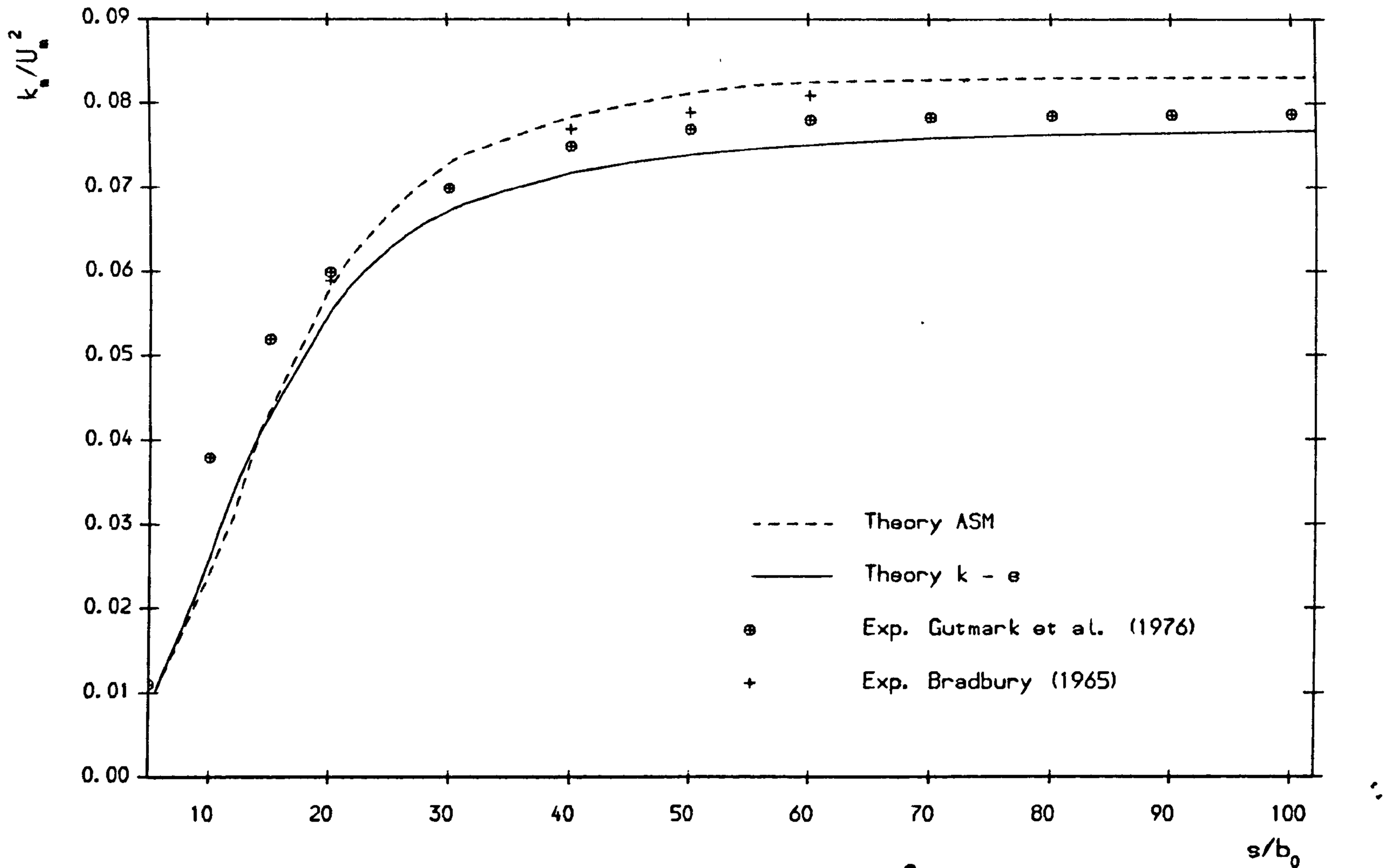

Fig. 9.3 Streamwise development of k_m/U_m^2 for plane free jet

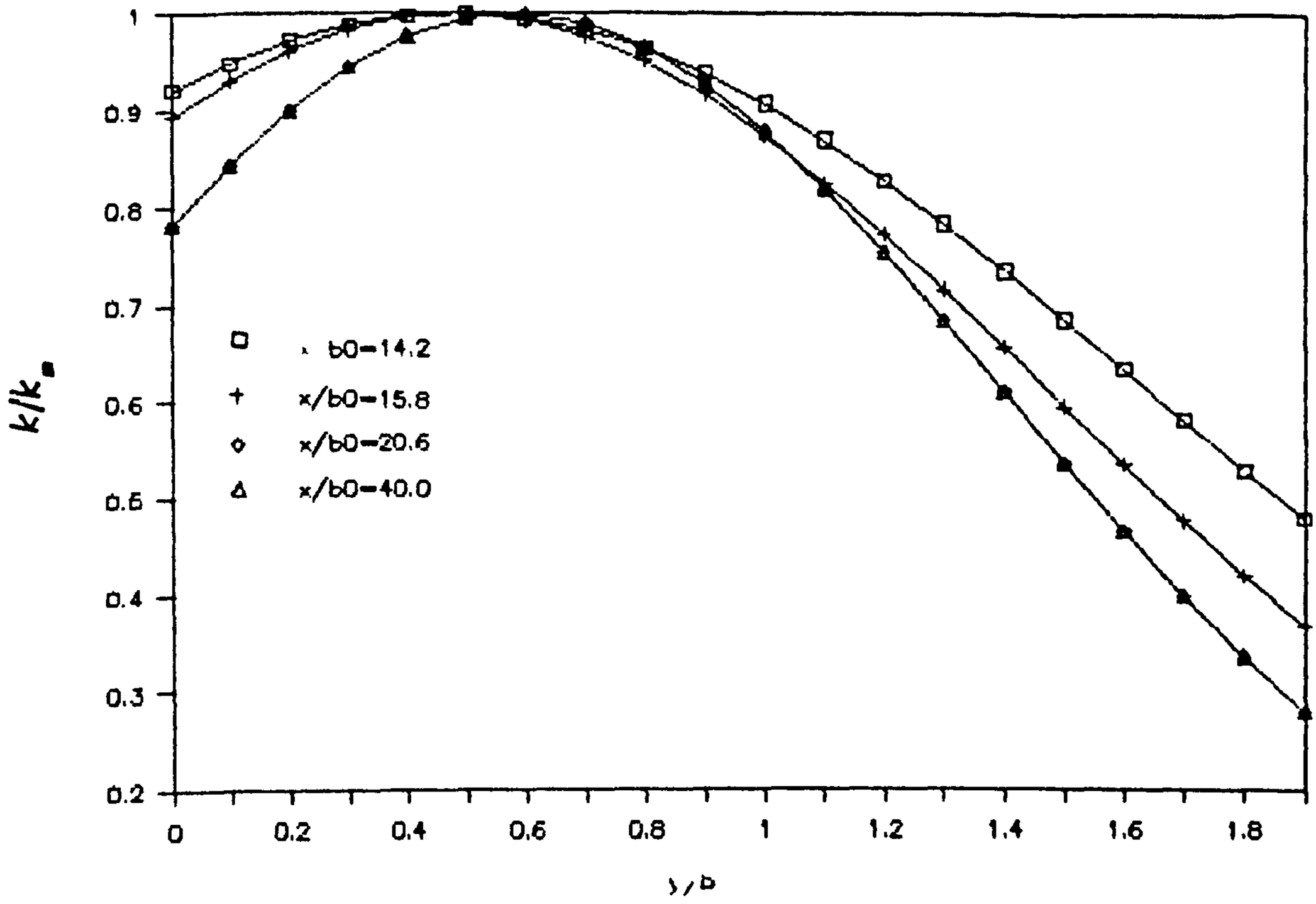

Fig. 9.4 Development of k-profile of free jet (pred. by k-e)

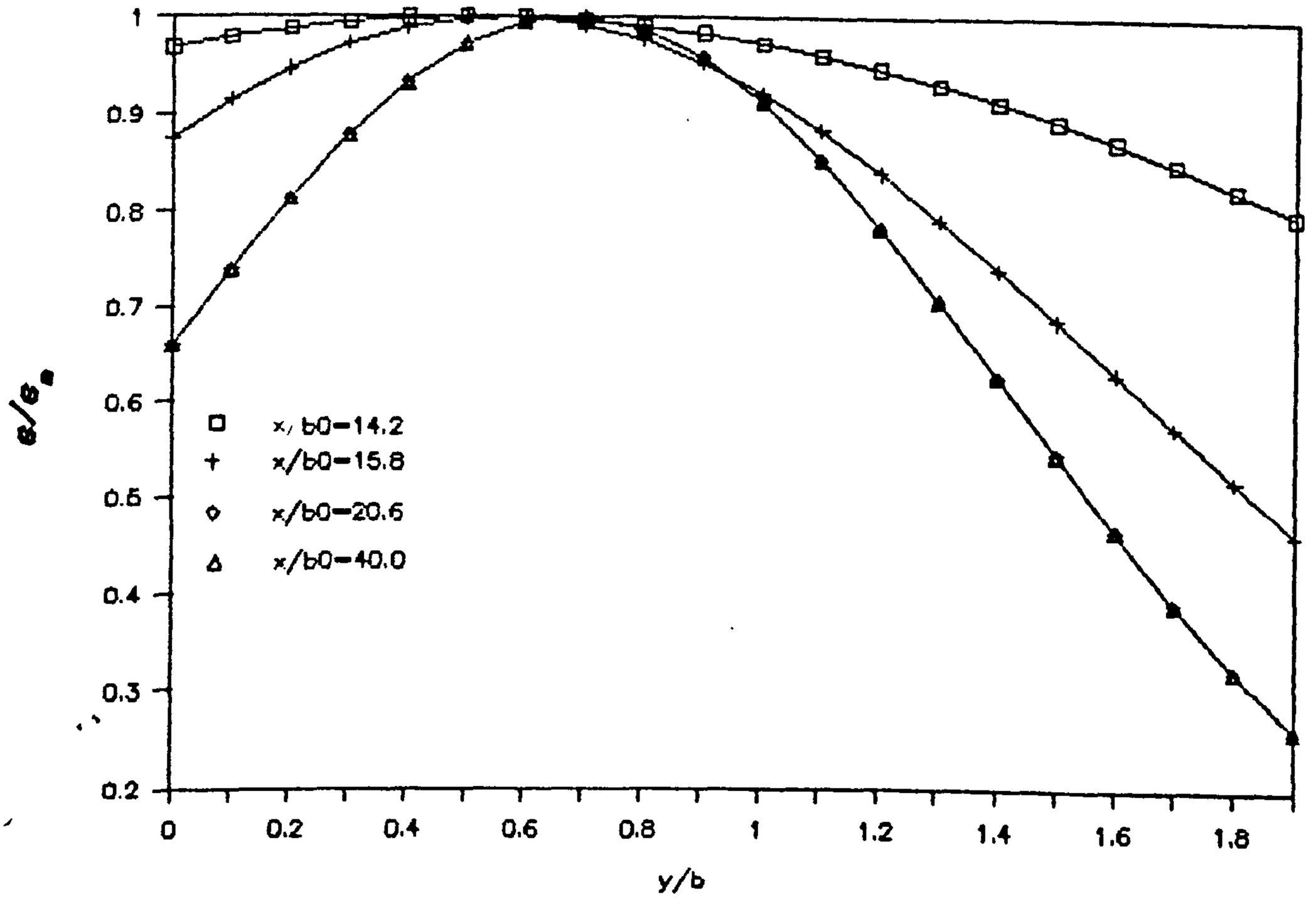

Fig. 9.5 Development of e-profile in free jet (Pred. by k-e)

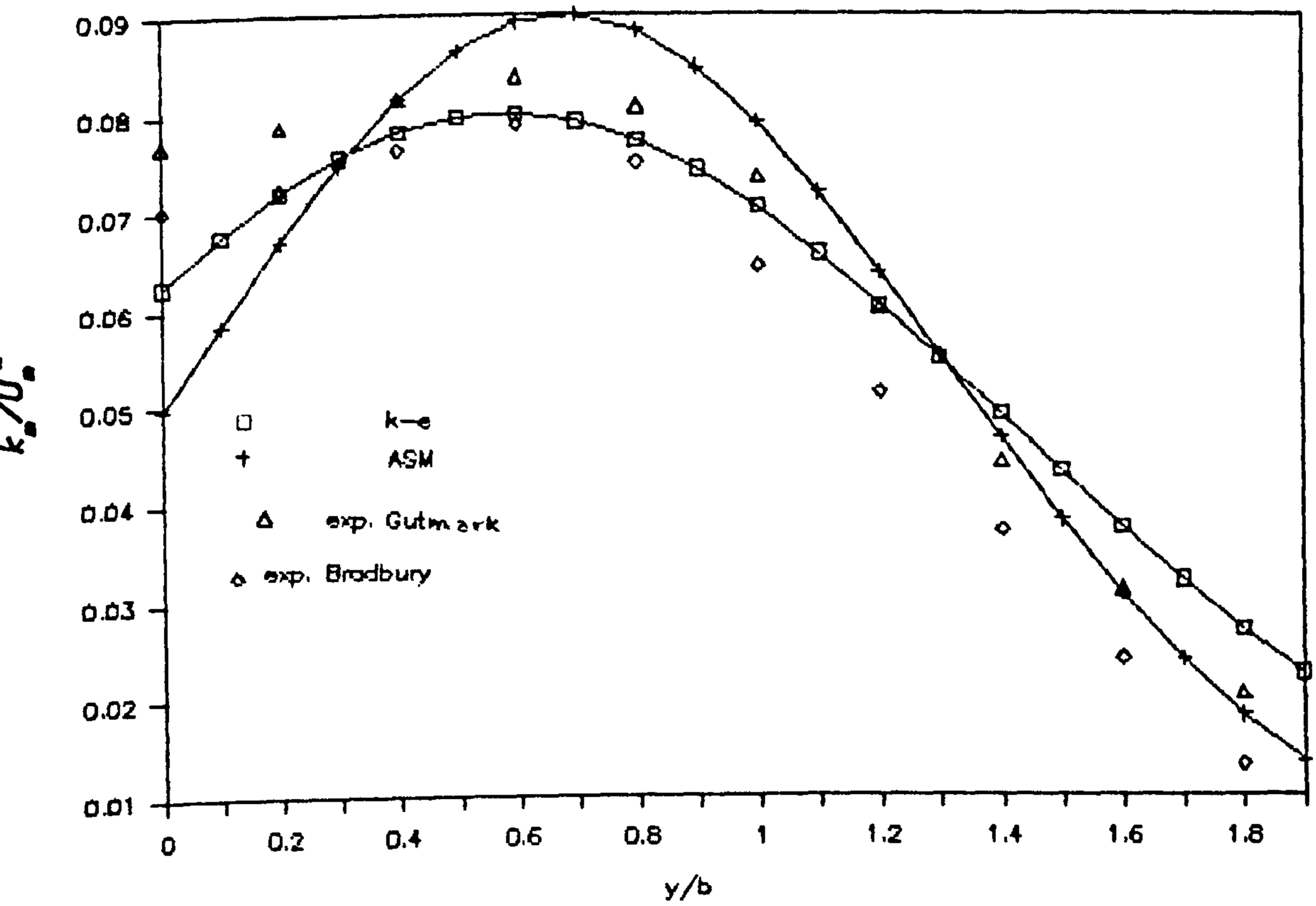

Fig. 9.6 Distribution of turb. kinetic energy in free jet

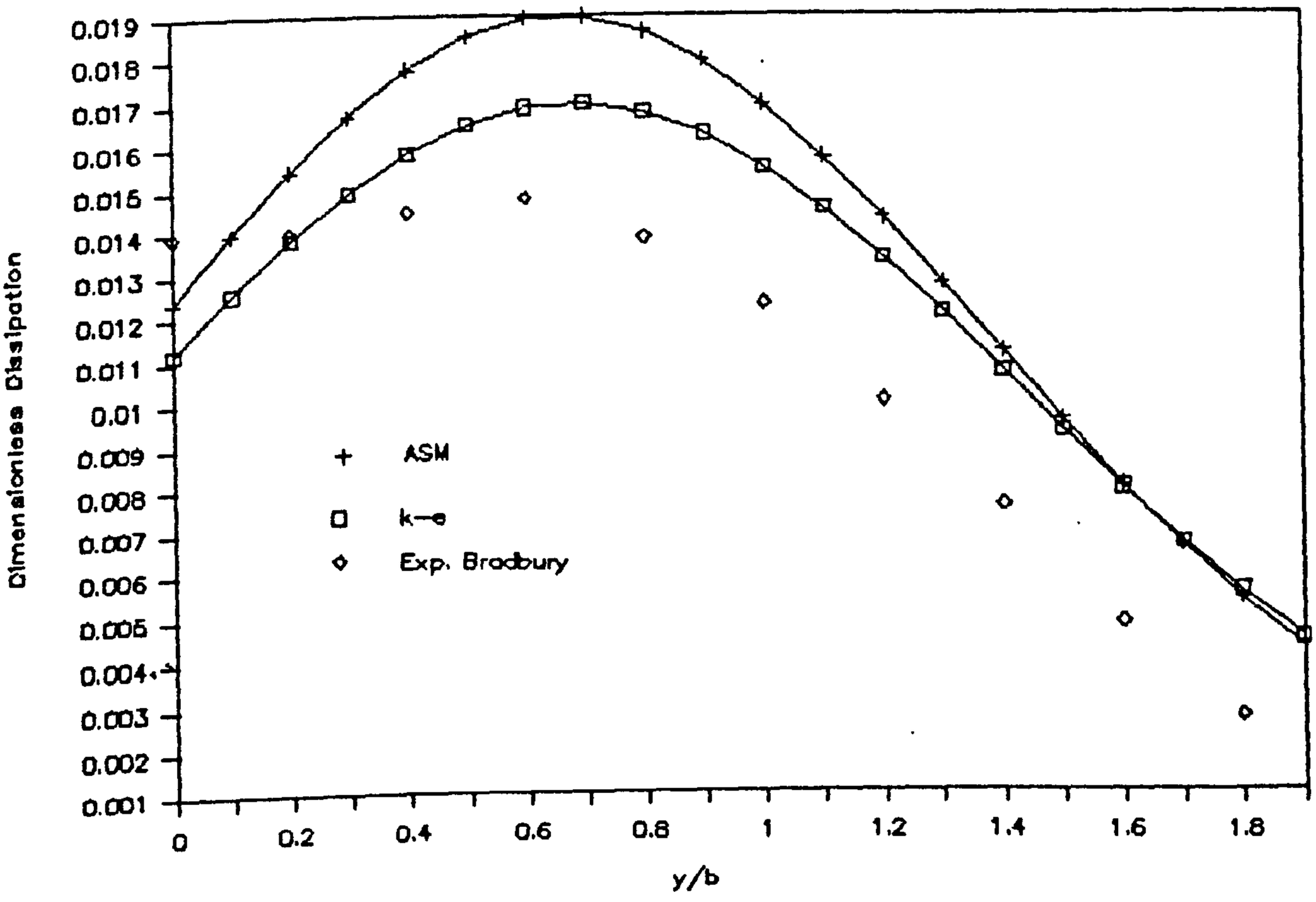

Fig. 9.7 Lateral distribution of ε in free jet

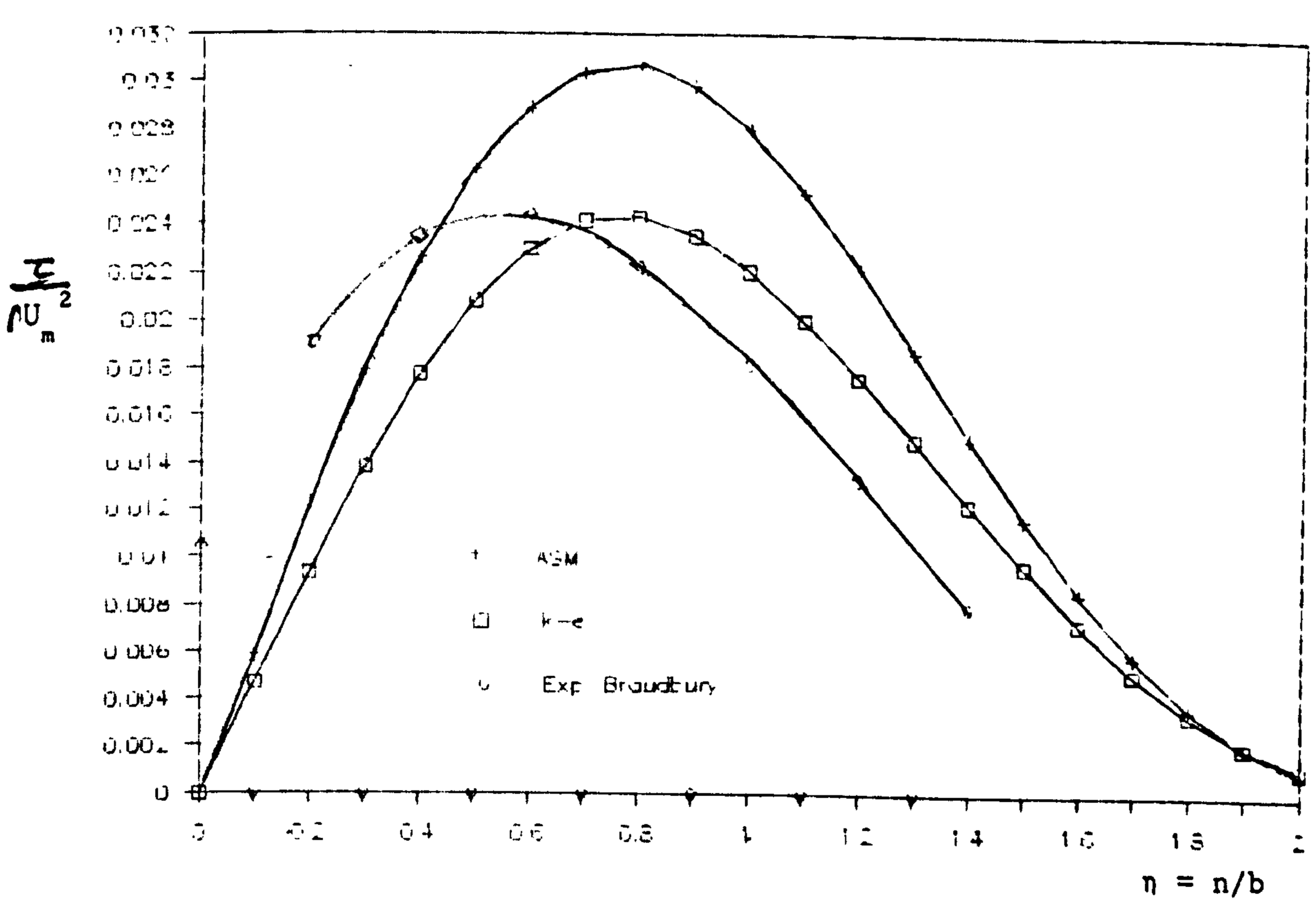

Fig. 9.8 Sheer-stress distribution in free turbulent jet

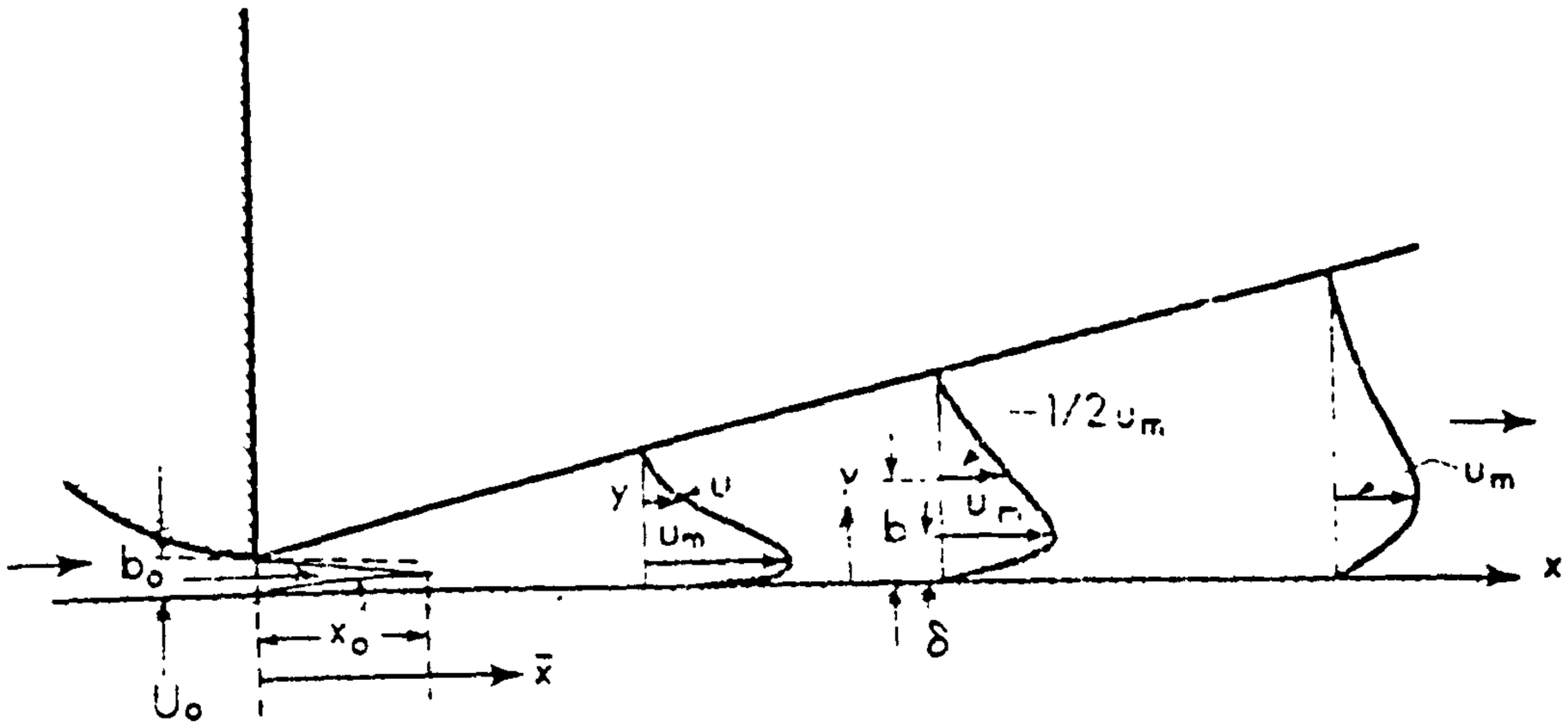

—Potential core

Fig. 9.9a Sketch of a Wall Jet

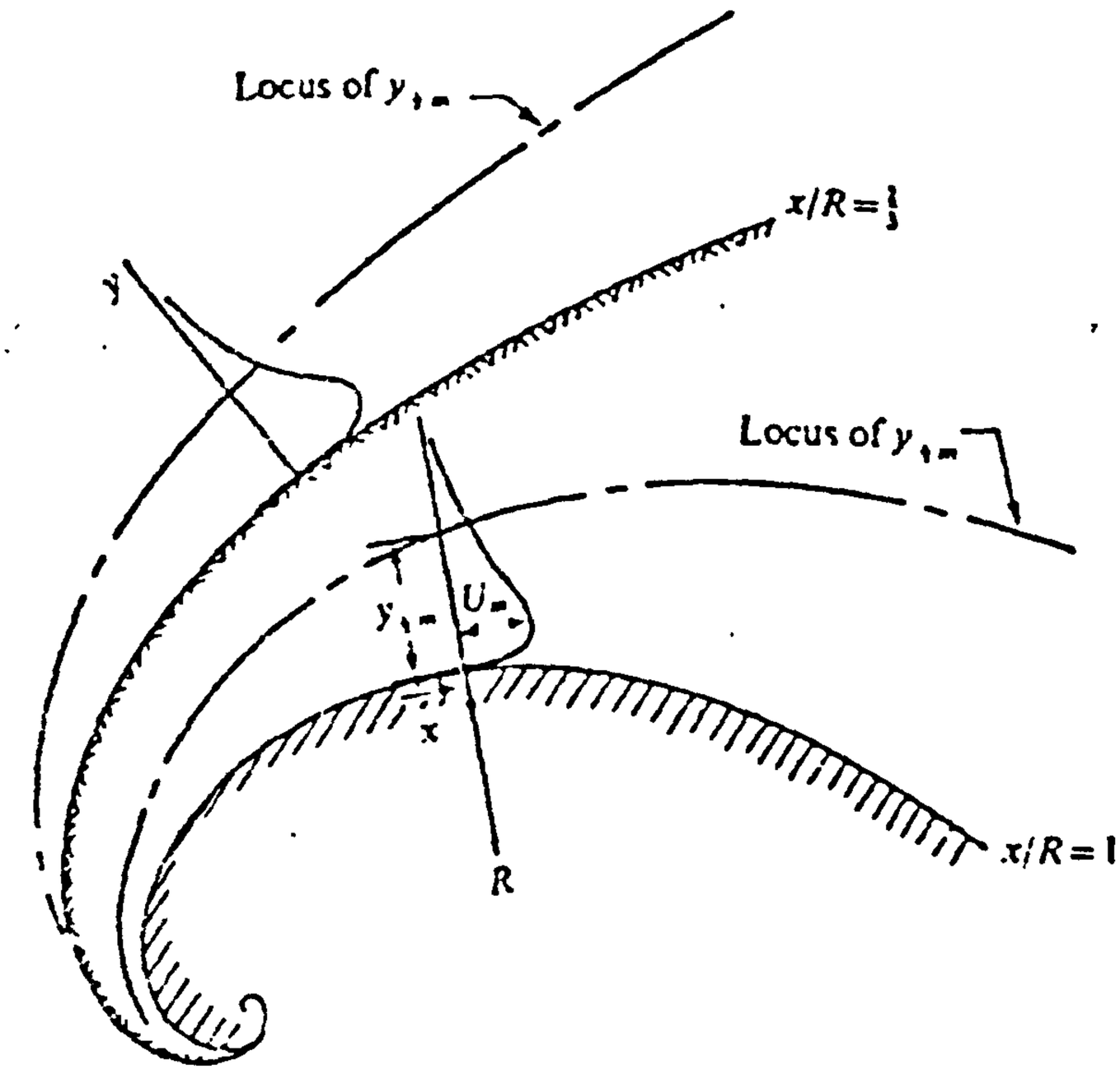

Fig. 9.9b Sketch of a Wall Jet on a Logarithmic Spiral

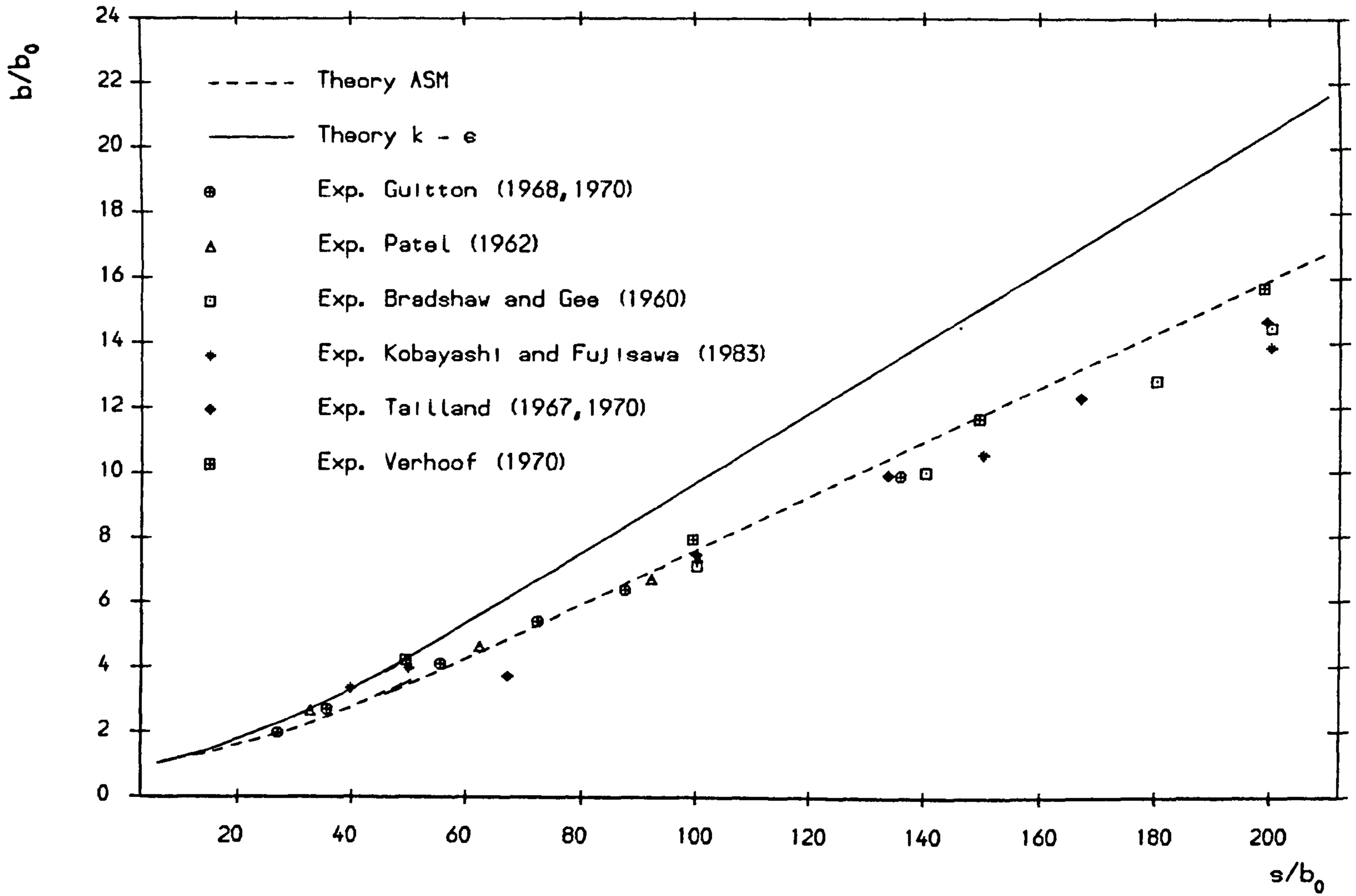

Fig. 9.10 Streamwise development of half-width for plane wall jet

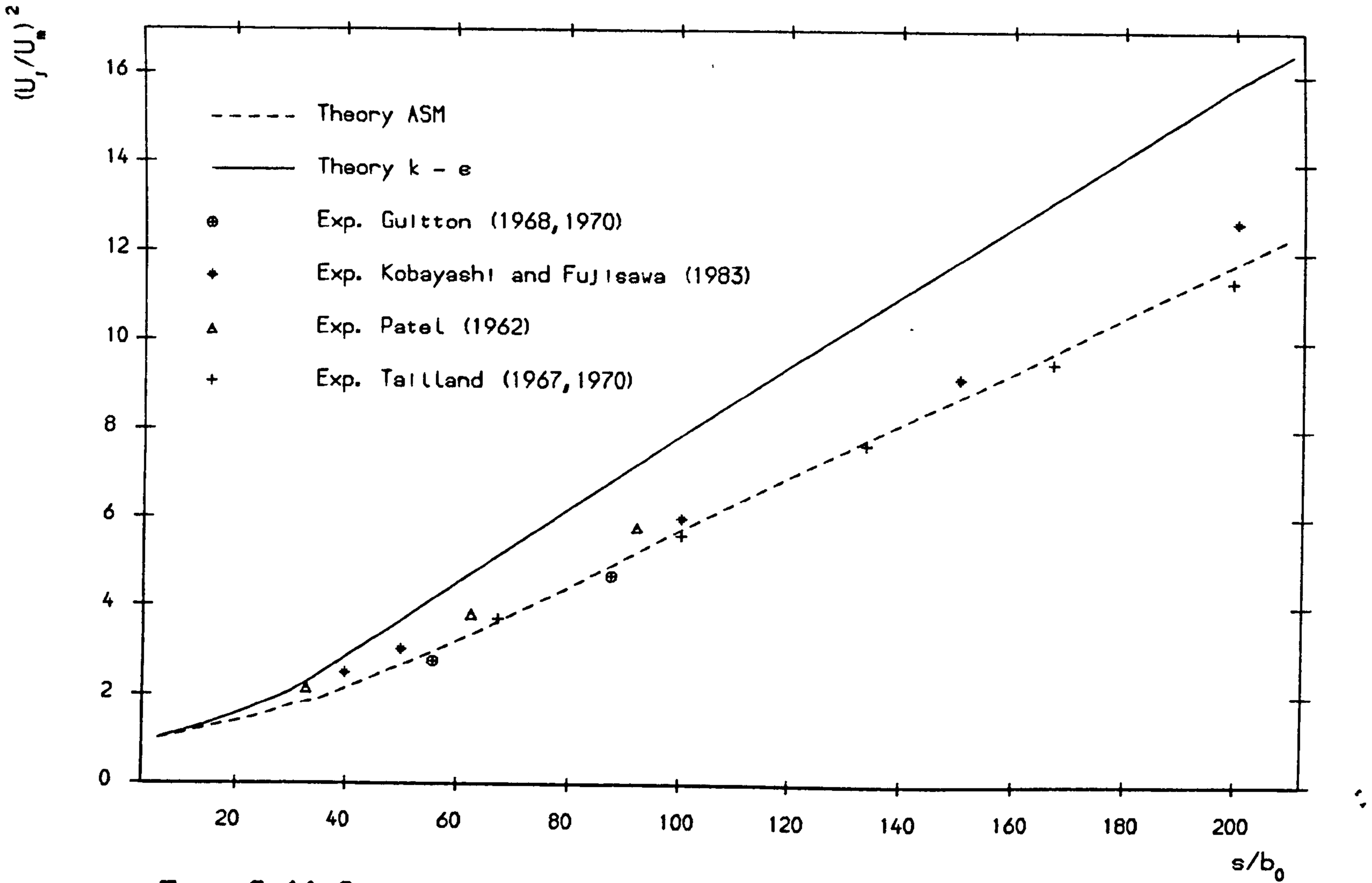

Fig. 9.11 Streamwise develop. of max. vel. for plane wall jet

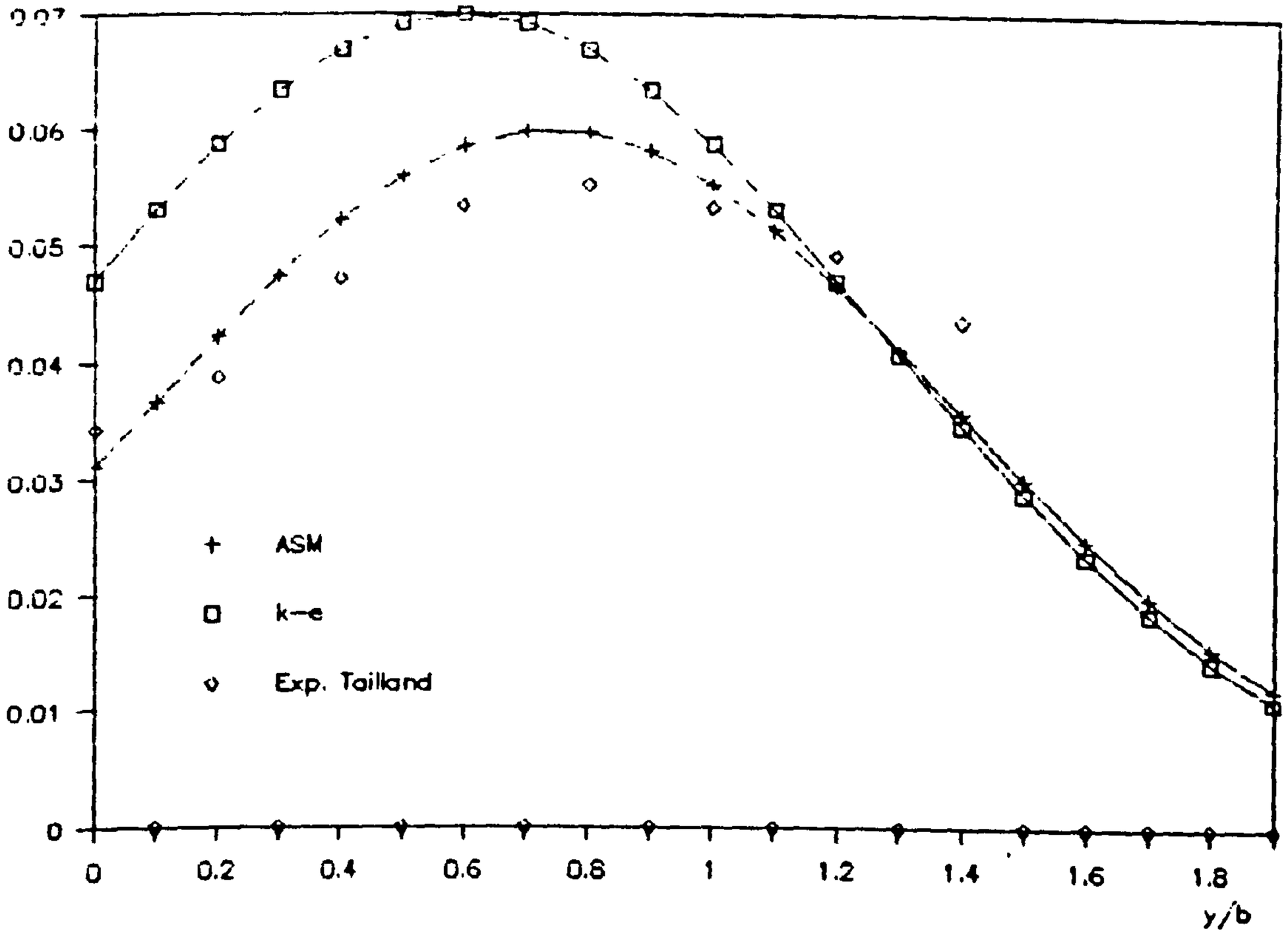

Fig. 9.12 Lateral distribution of k in plane wall jet

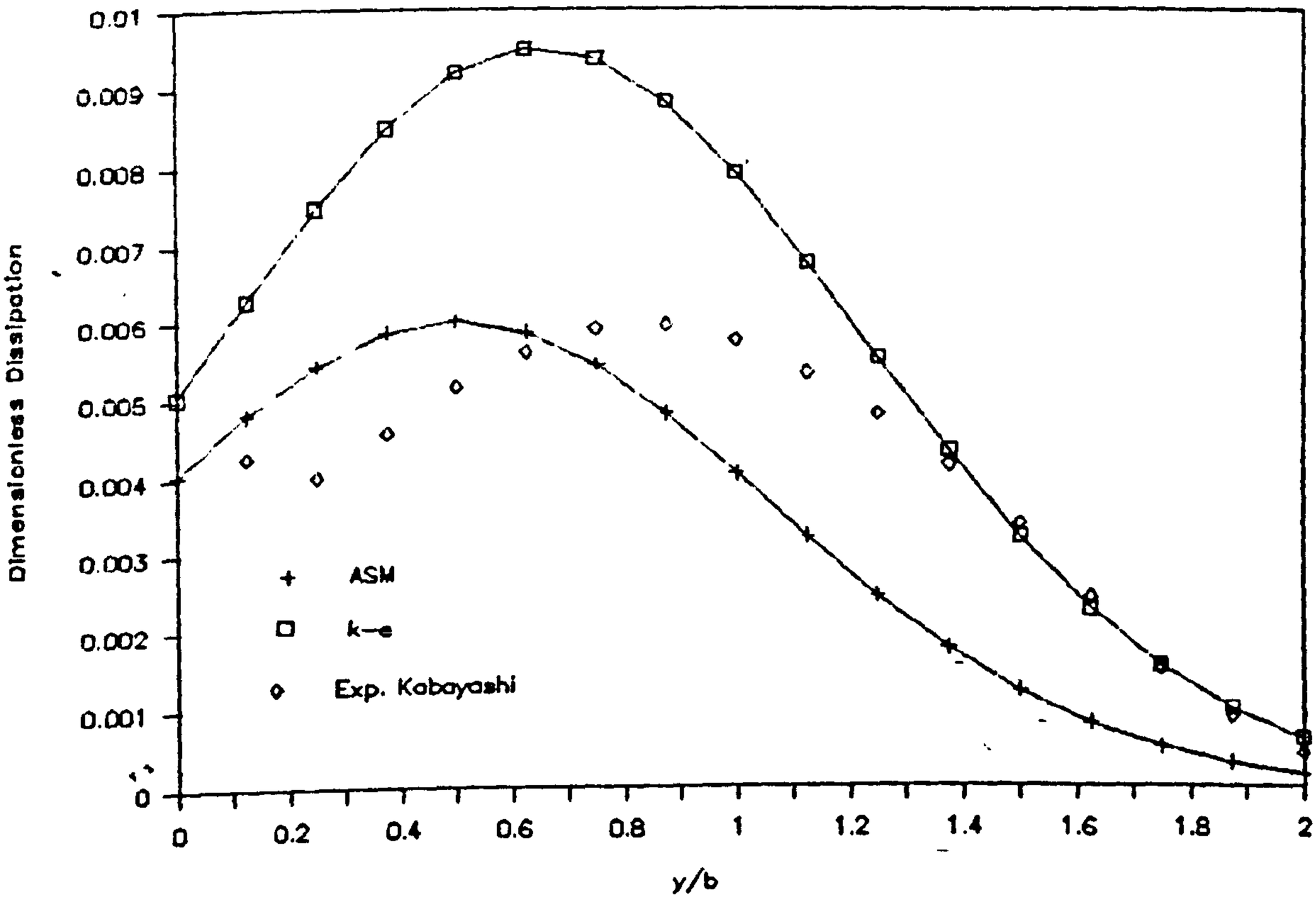

Fig. 9.13 e profile of plane wall jet

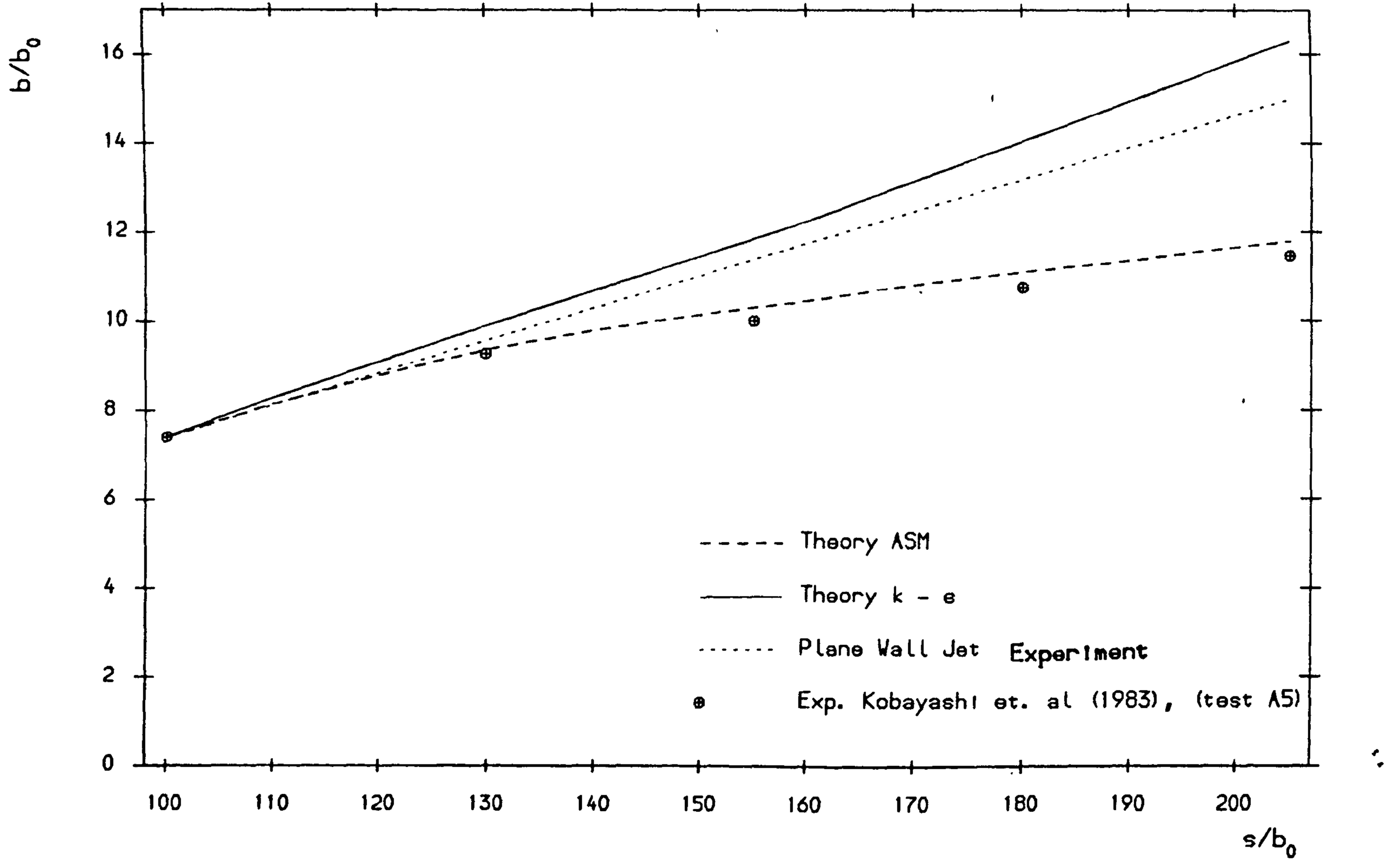

Fig. 9.14 Variation of half-width with s/b_0 for concave wll jet (R/b_0=-100)

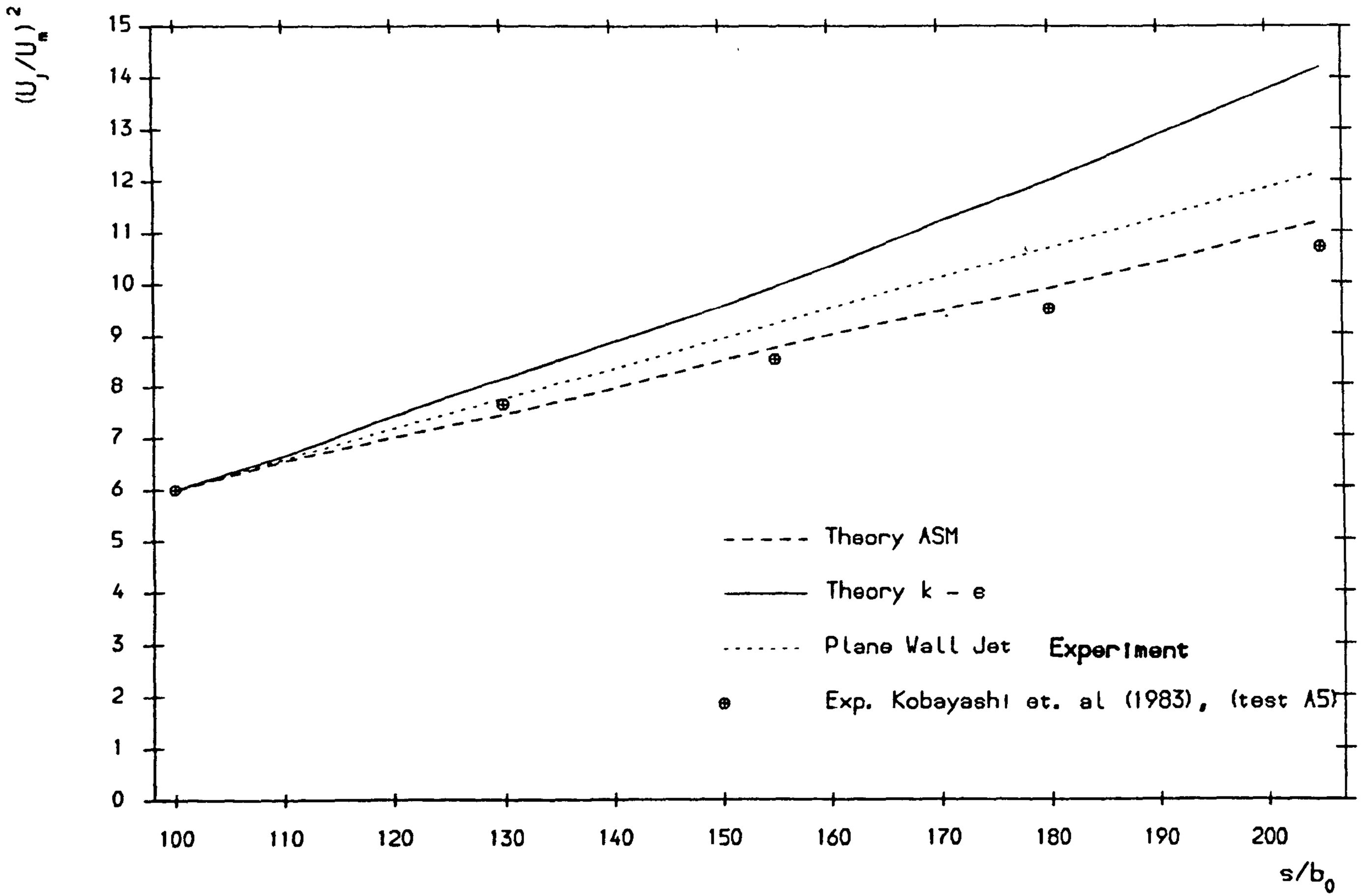

Fig. 9.15 Streamwise variation of $(U_j/U_m)^2$ for concave wall jet (R/b_0=-100)

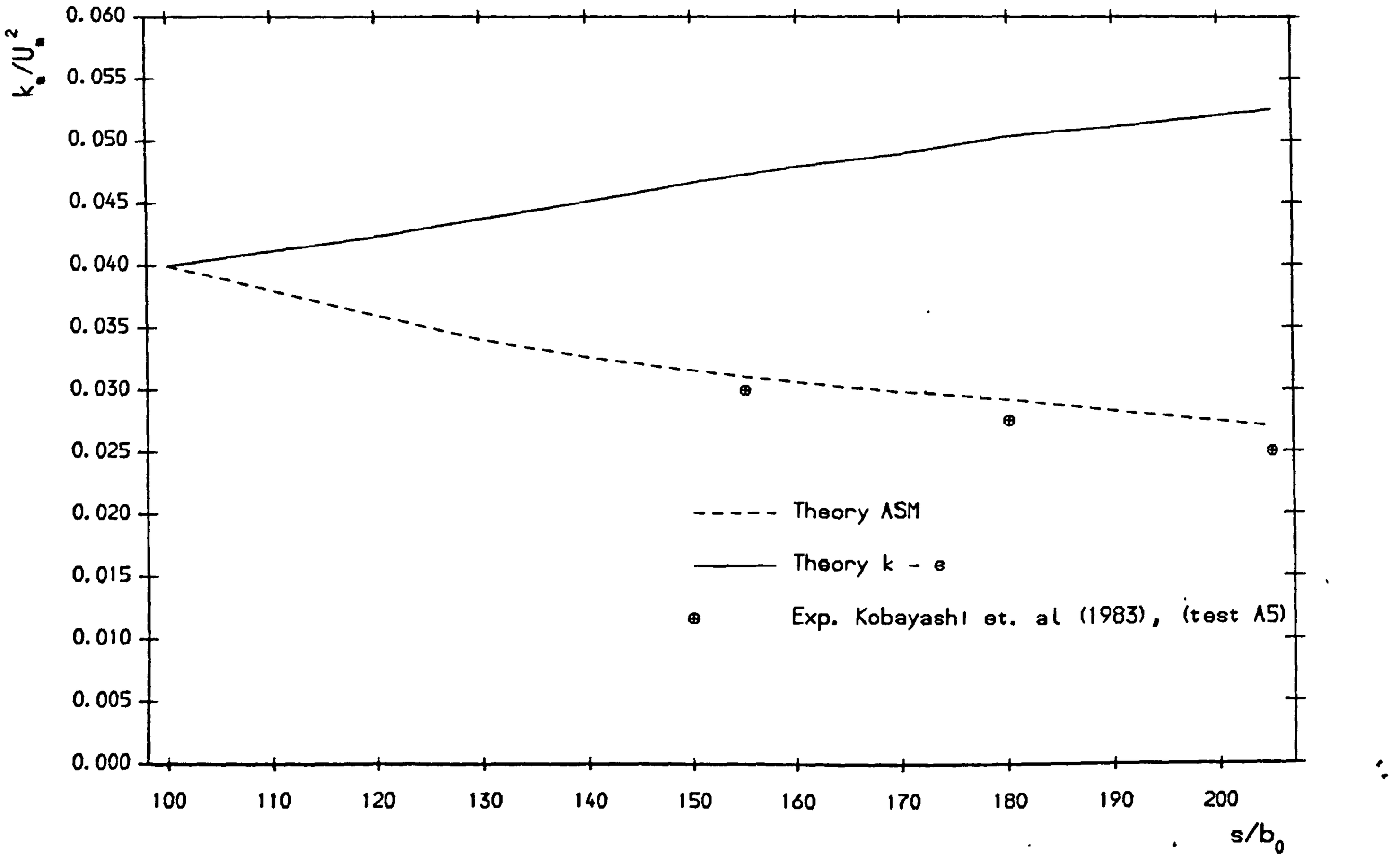

Fig. 9.16 Streamwise variation of k_e/U_e^2 for concave wall jet (R/b_0=-100)

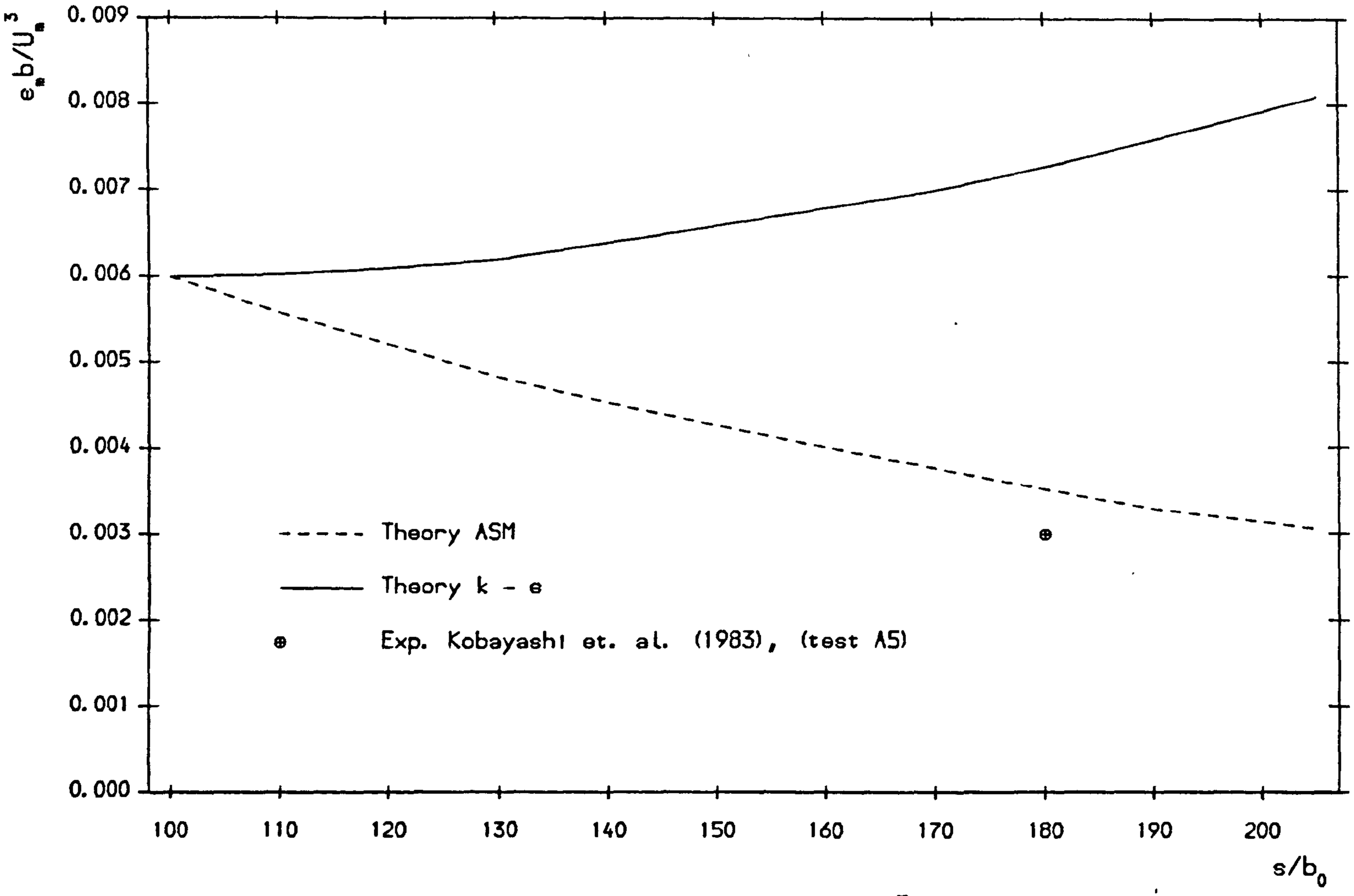

Fig. 9.17 Streamwise variation of $e_m b/U_m^3$ for concave wall jet (R/b_0=-100)

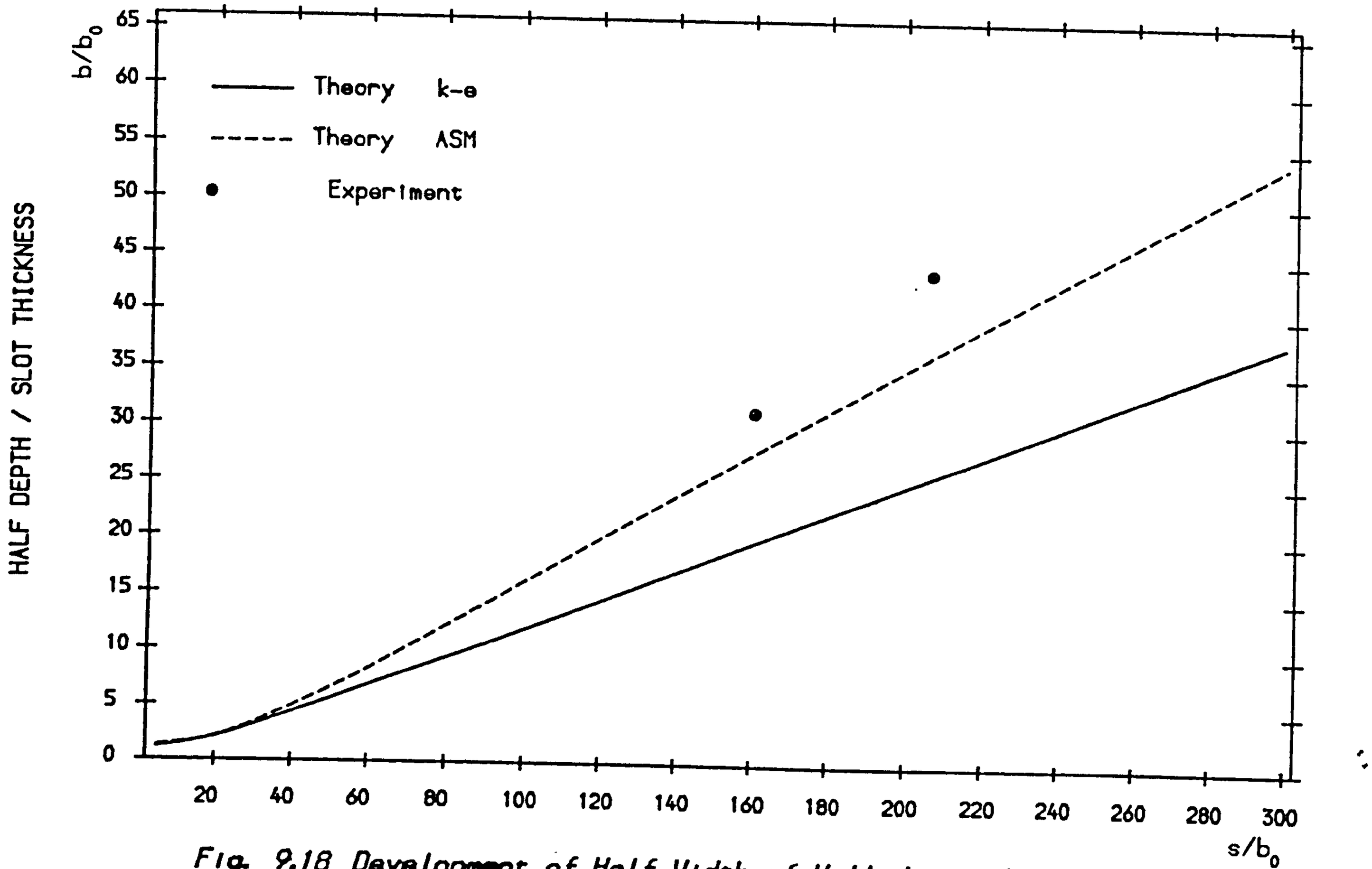

Fig. 9.18 Development of Half-Width of Wall Jet on Logar. Spiral (R/s=1, Exp. of Guitton et al. 1973)

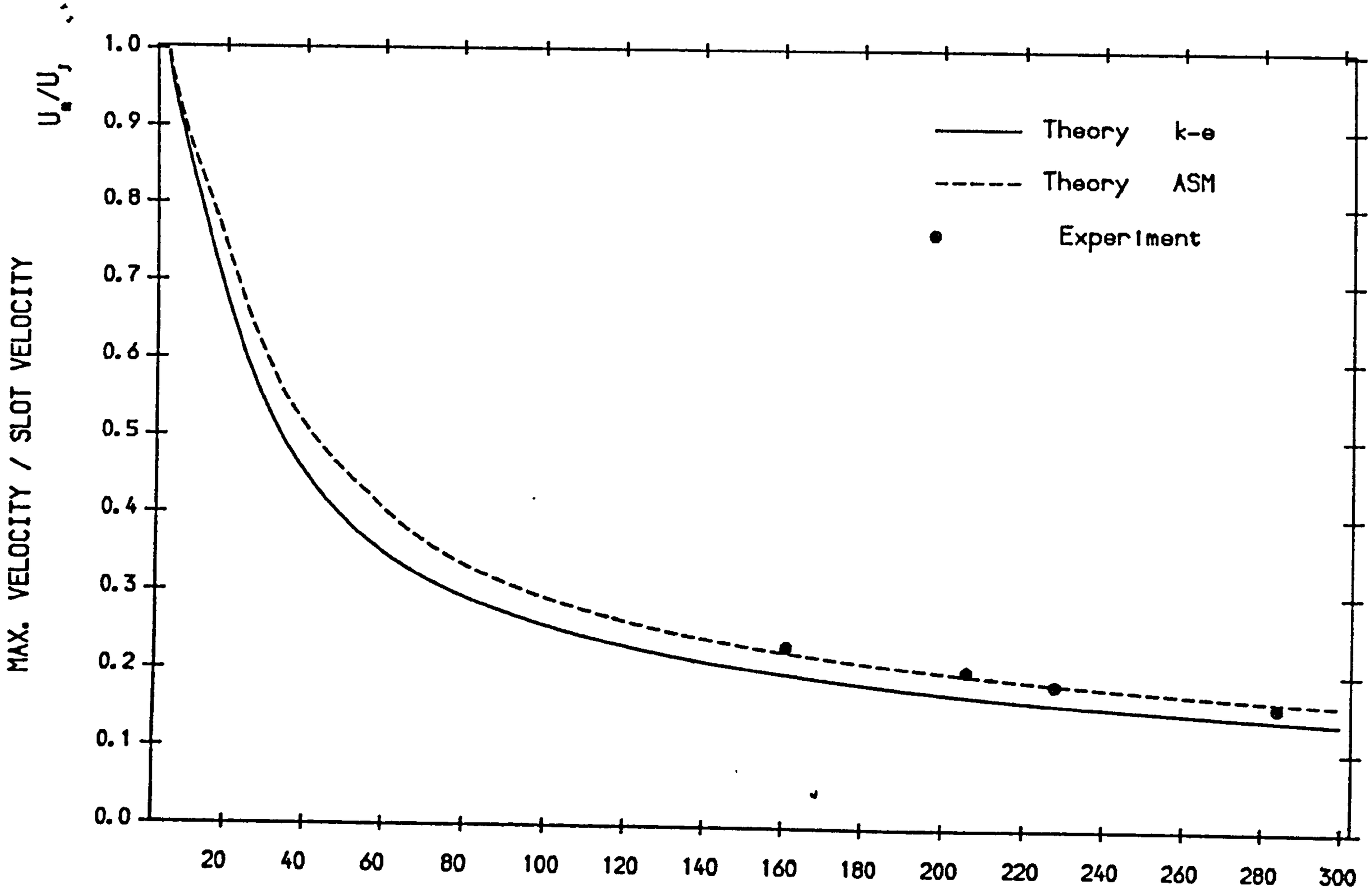

Fig. 9.19 Decay of Max. Vel. of Wall Jet on Loger. Spiral (R/s=1 , Exp. of Guitton et al. 1973)

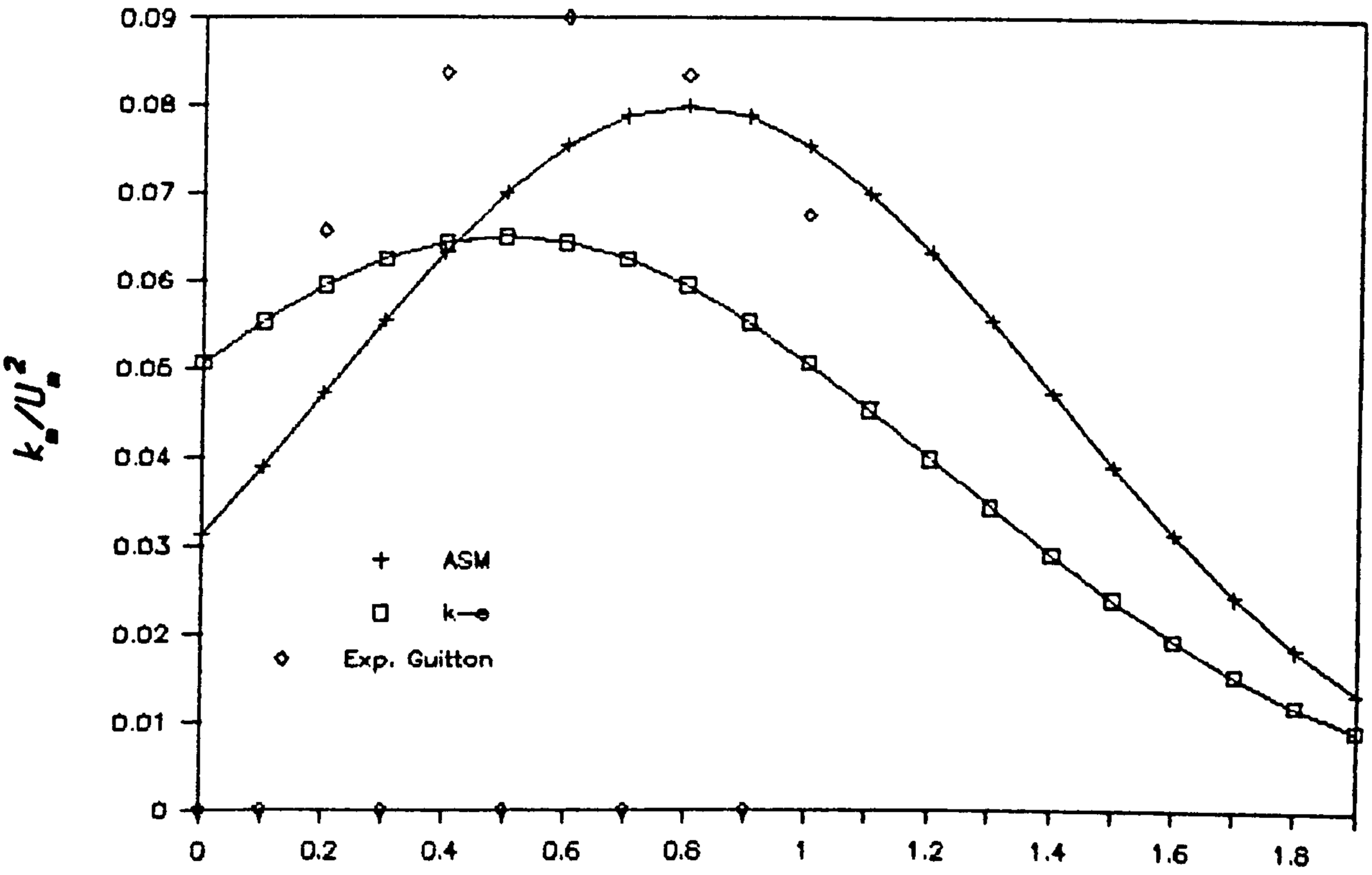

Fig. 9.20. k-profile of wall jet on logarithmic spiral (R/s=1)

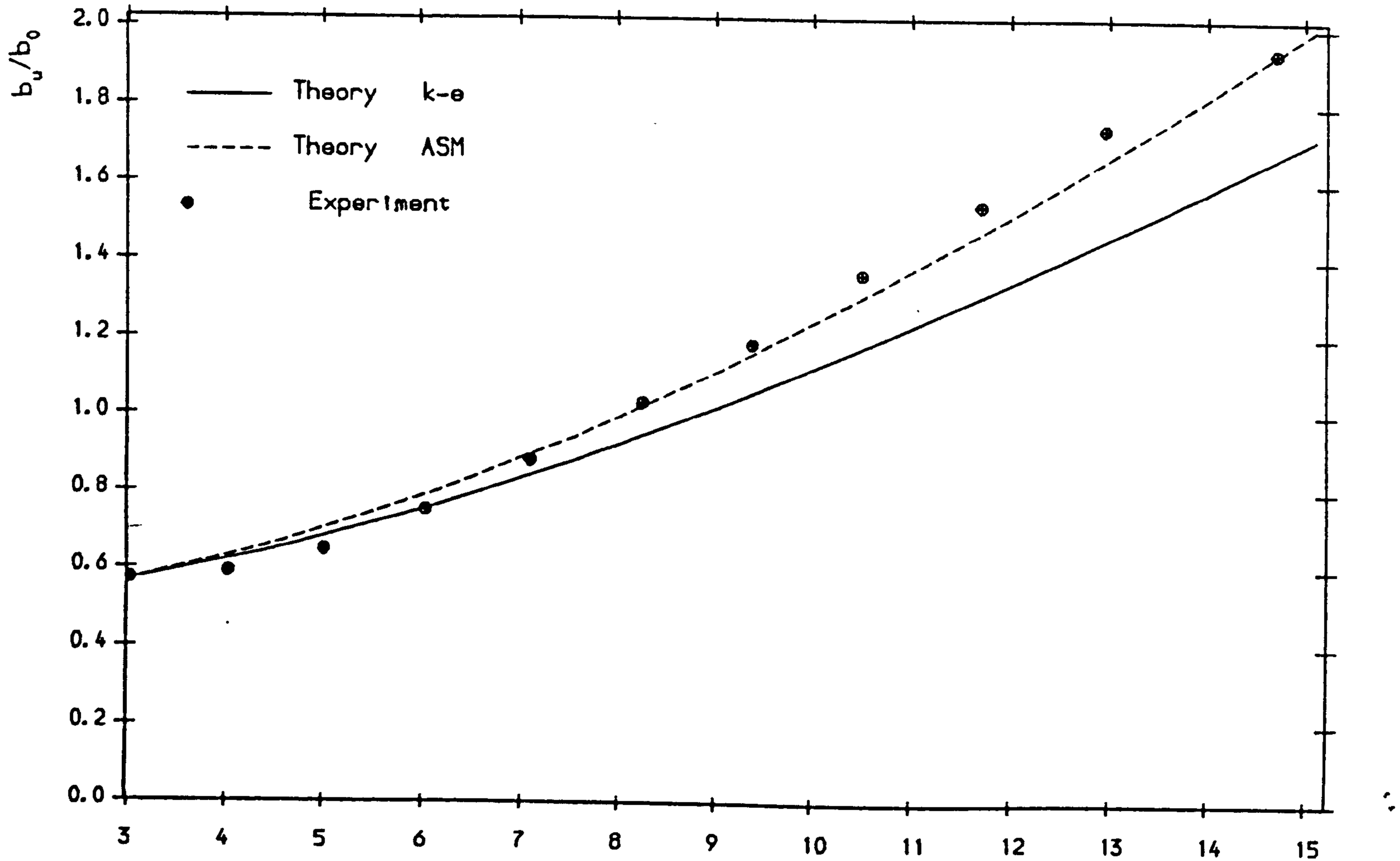

Fig. 9.21 Development of Half-Width of Offset Jet

(h/b_0=7, Exp. of Pelfrey (1984)

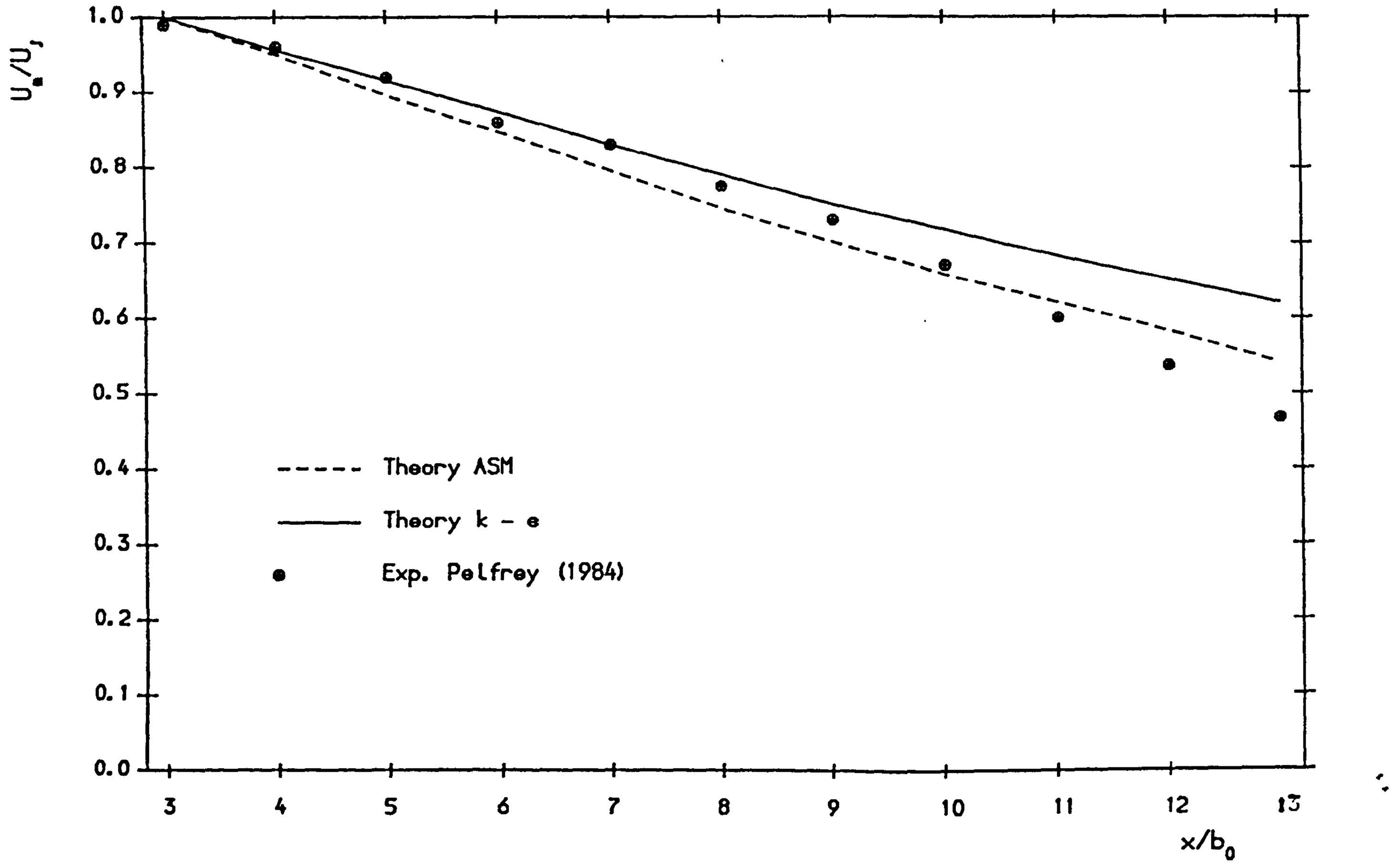

Fig. 9.22 Prediction of Decay of Max. Vel. for Offset Jet (h/b_0=7, Exp. of Pelfrey 1984)

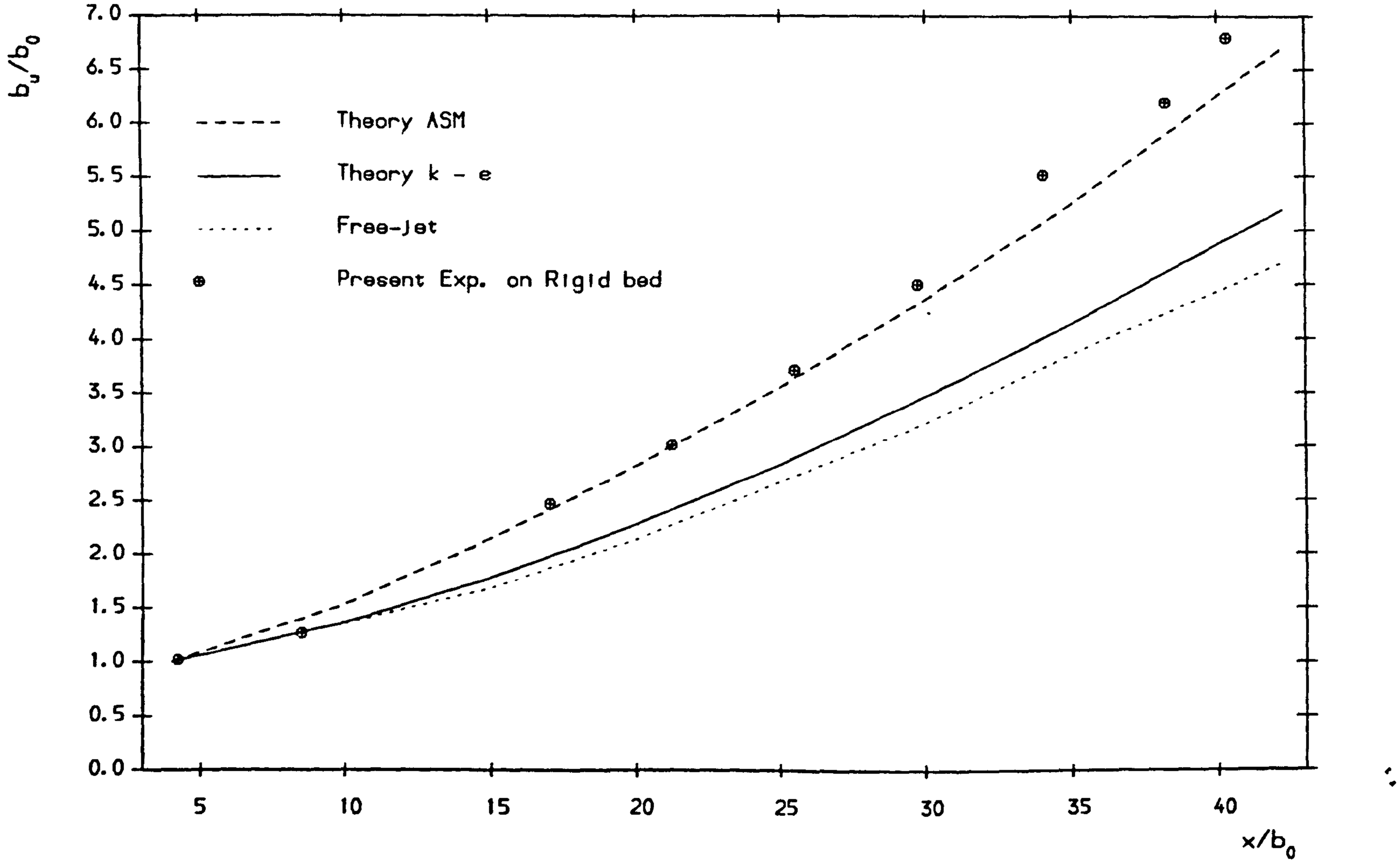

Fig. 9.23-a Development of half-width for offset-jet (h/b_o=26.2)

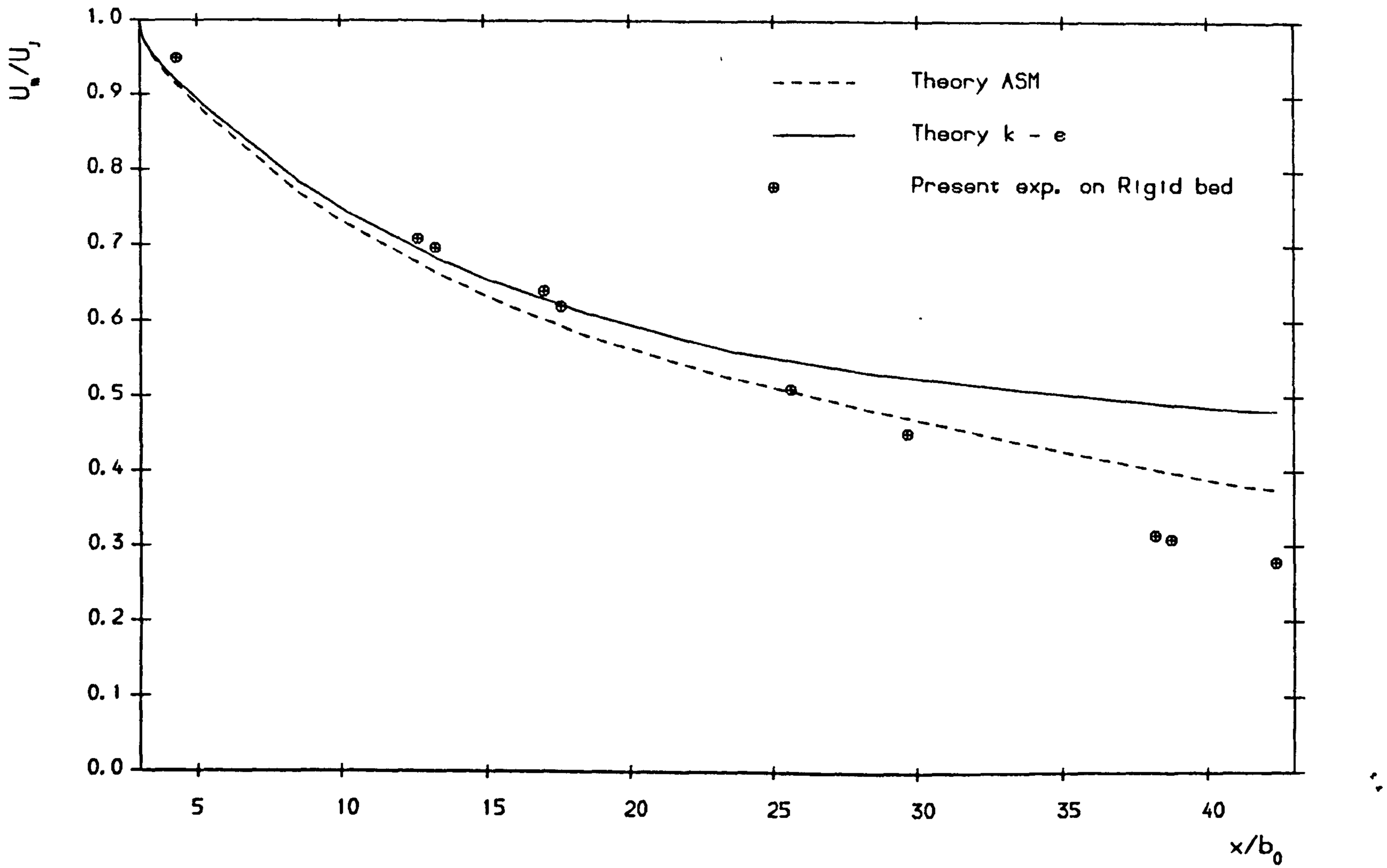

Fig. 9.23-b Decay of Max. Velocity for Offset Jet (h/b_o=26.2)

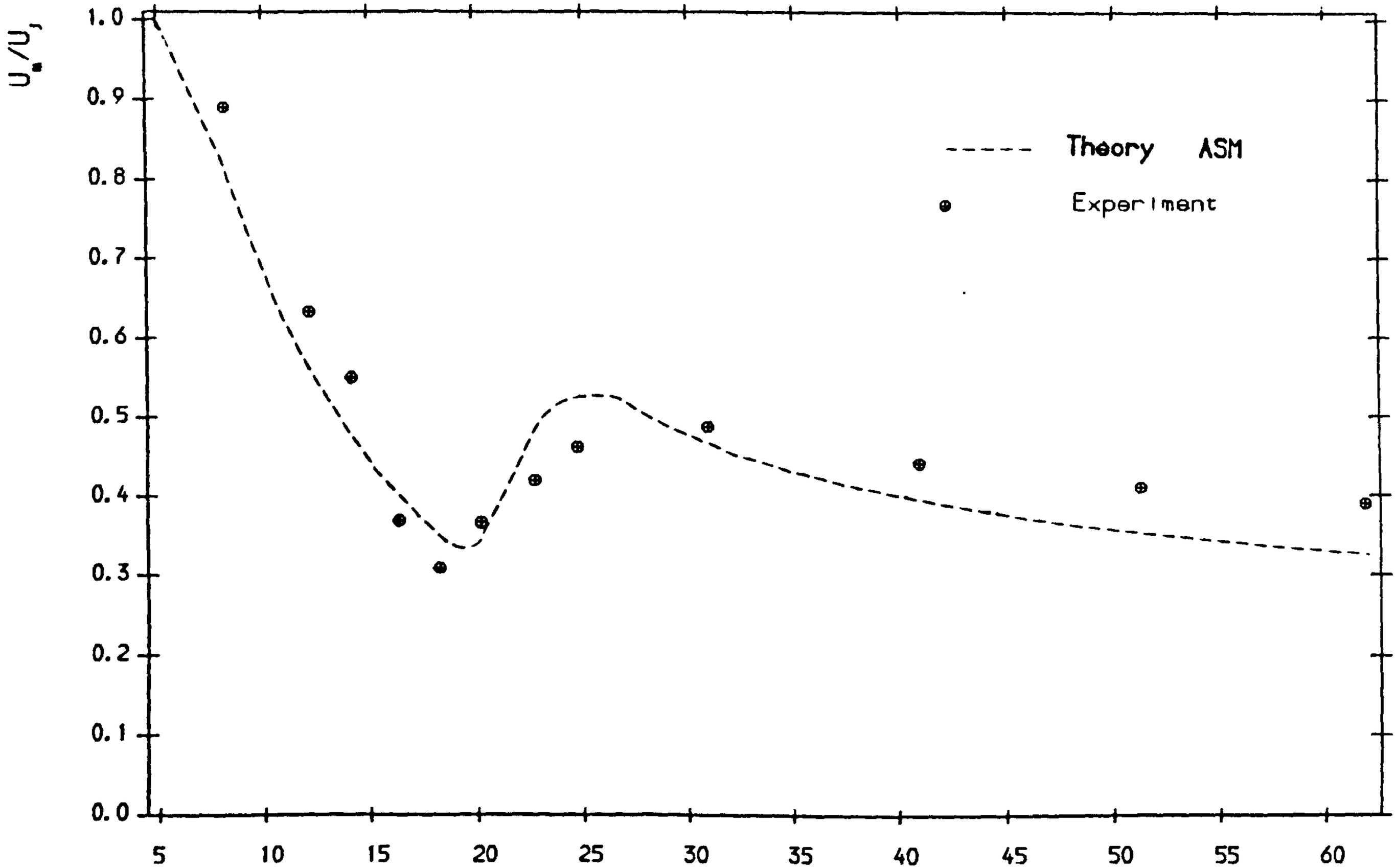

Fig. 9.24 Decay of Max. Vel. of Offset Jet (h/b_0=8.7, Ex p. of Hoch 1979)

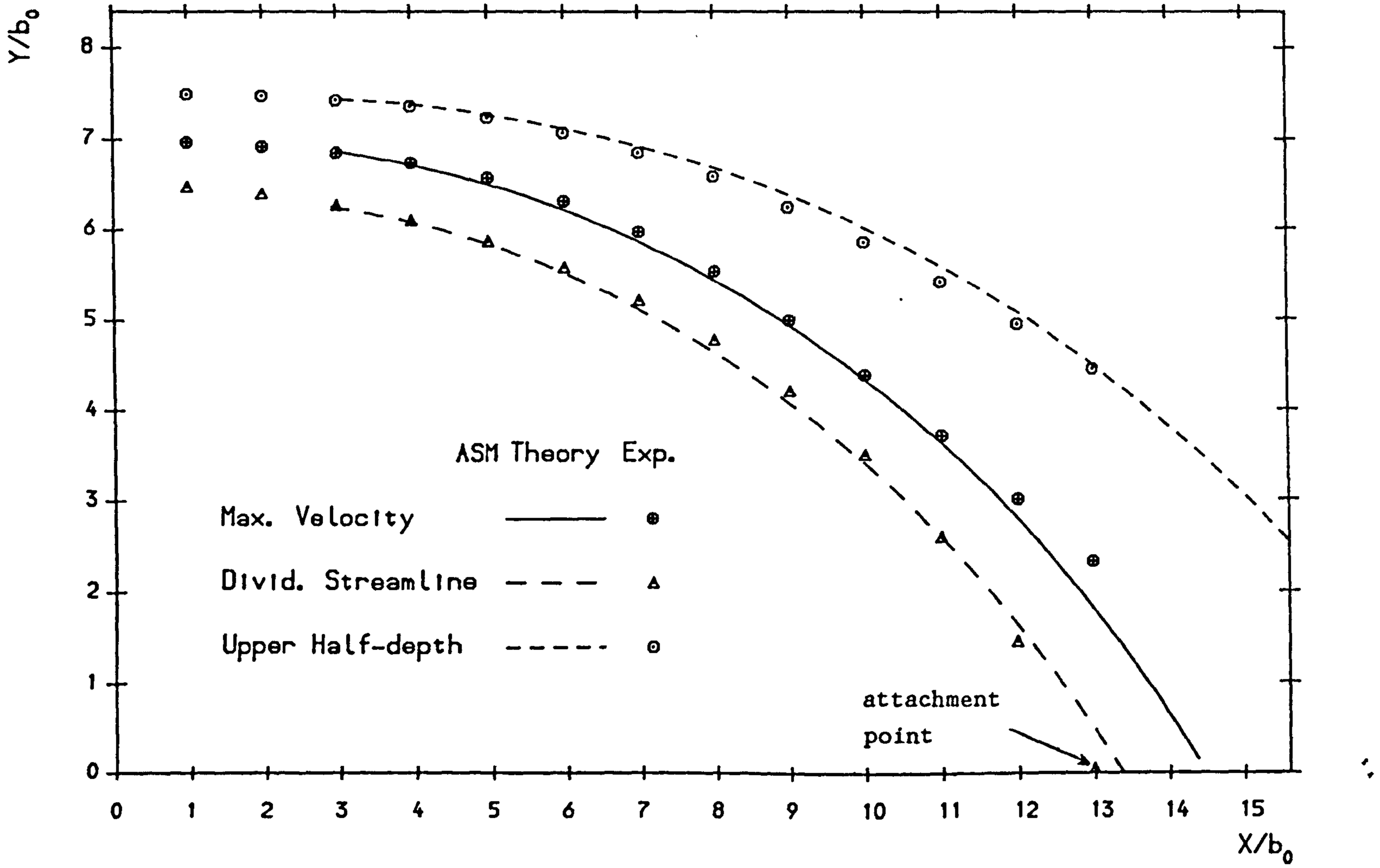

Fig. 9.25 Pred. of Different Trajectories of Offset Jet with ASM (h/b_0=7, Exp. of Pelfrey 1984)

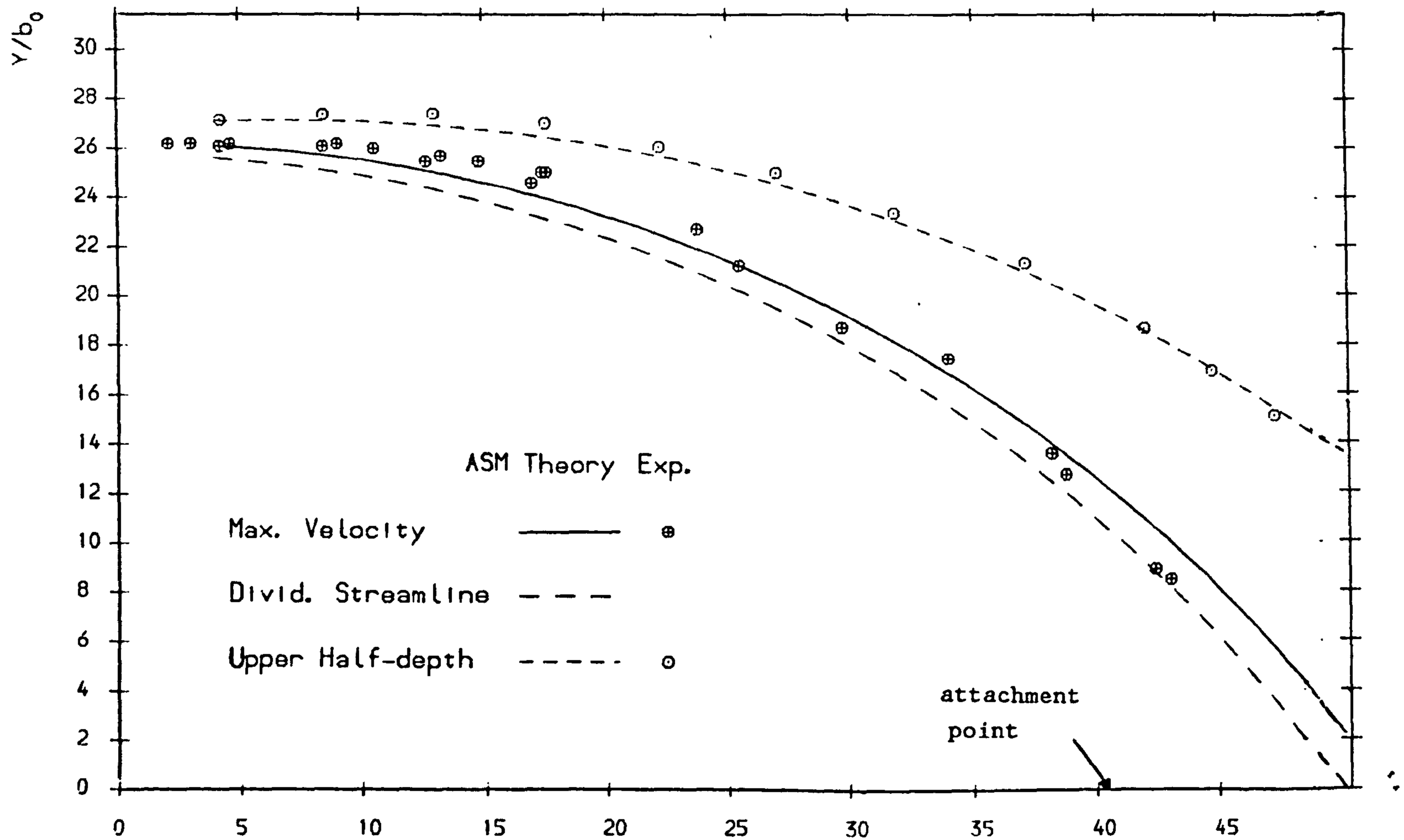

Fig. 9.26 Pred. of Different Trajectories of Offset Jet with ASM (h/b_0=26.2, Pres. Exp.)

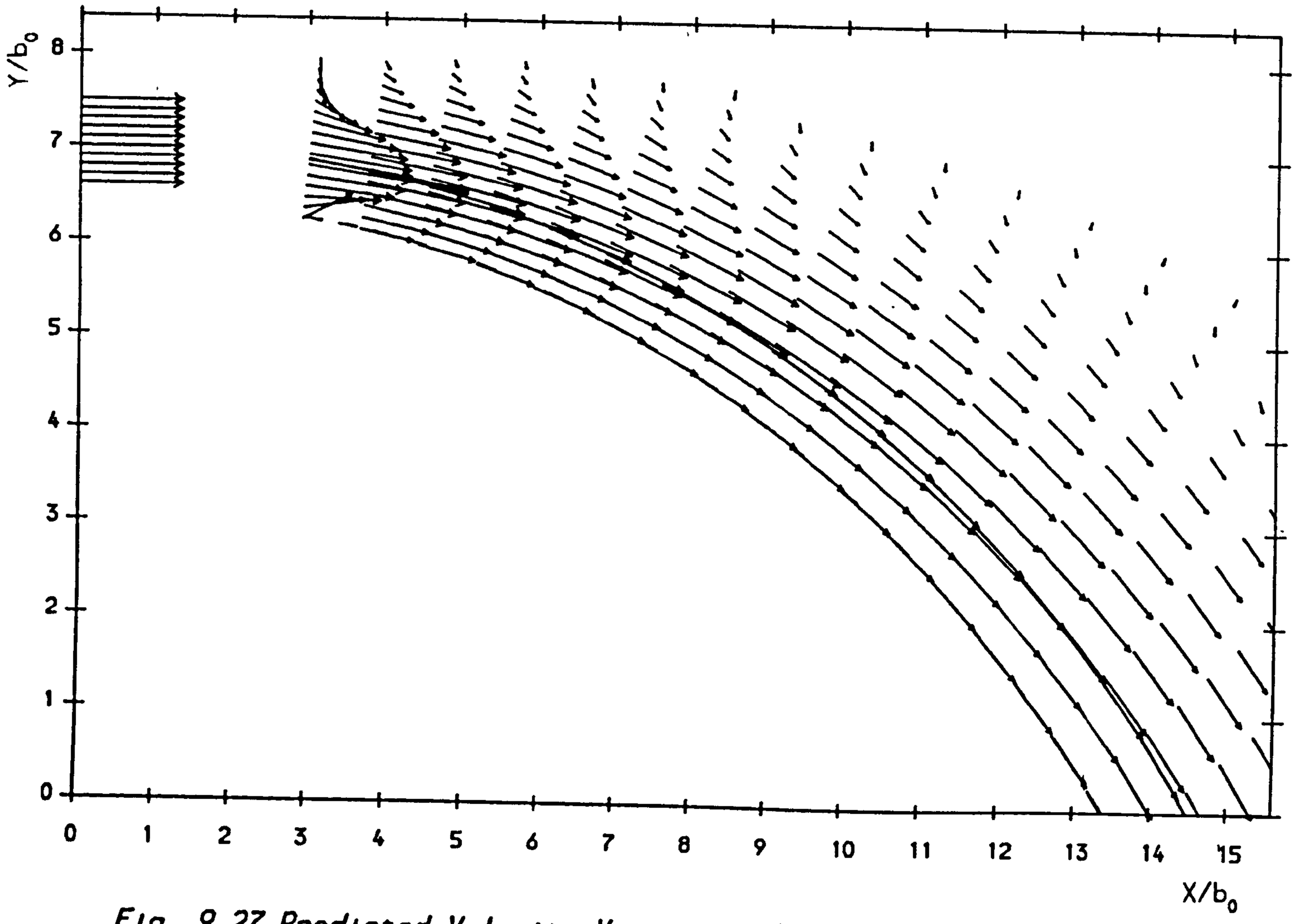

Fig. 9.27 Predicted Velocity Vectors with ASM Model for Offset Jet, (h/b_0=7, Exp. of Pelfrey 1984)

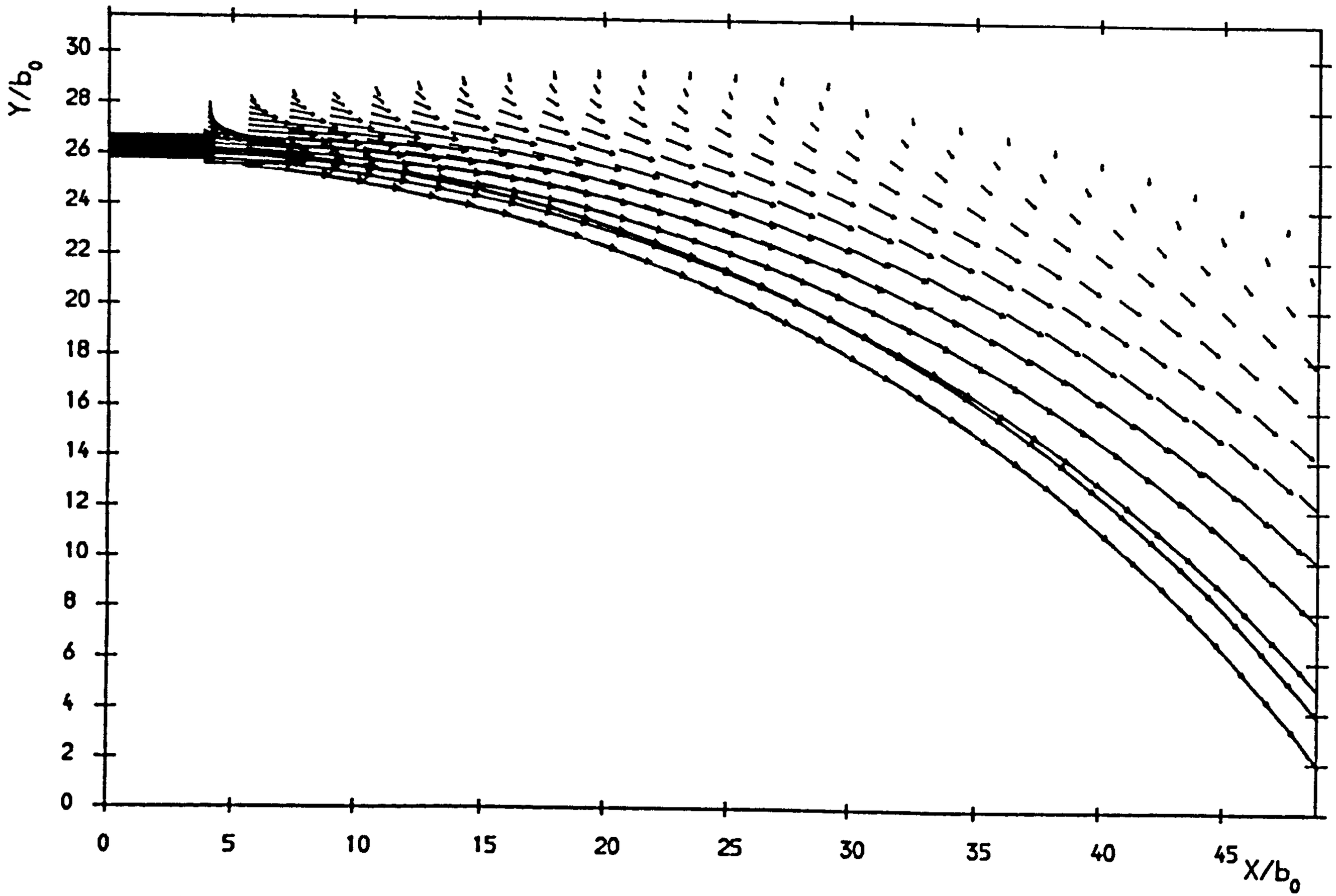

Fig. 9.28 Predicted Velocity Vectors with ASM Model for Offset Jet (h/b_0=26.2)

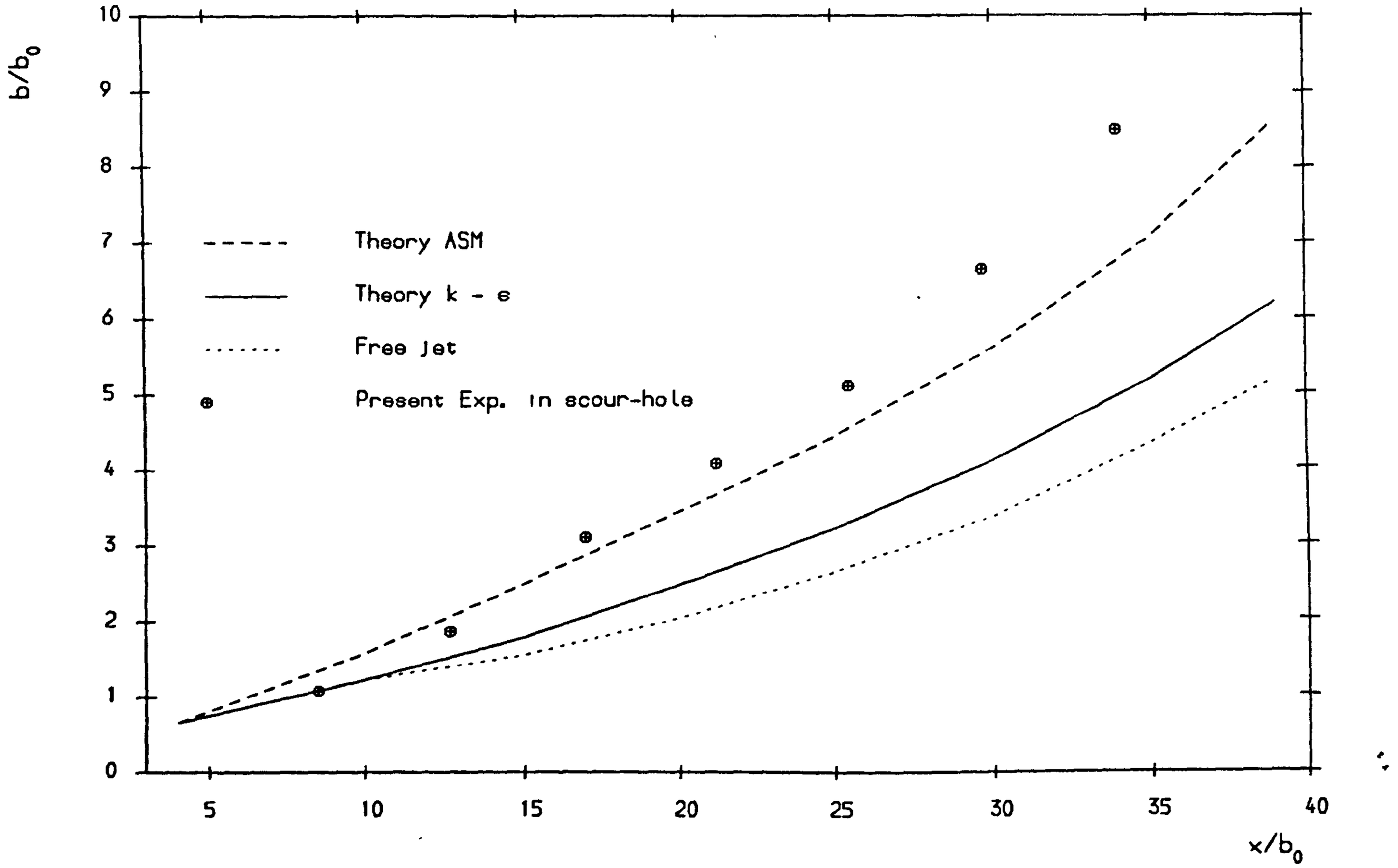

Fig. 9.29 Streamwise develop. of bu/b0 for offset-jet in scour-Hole

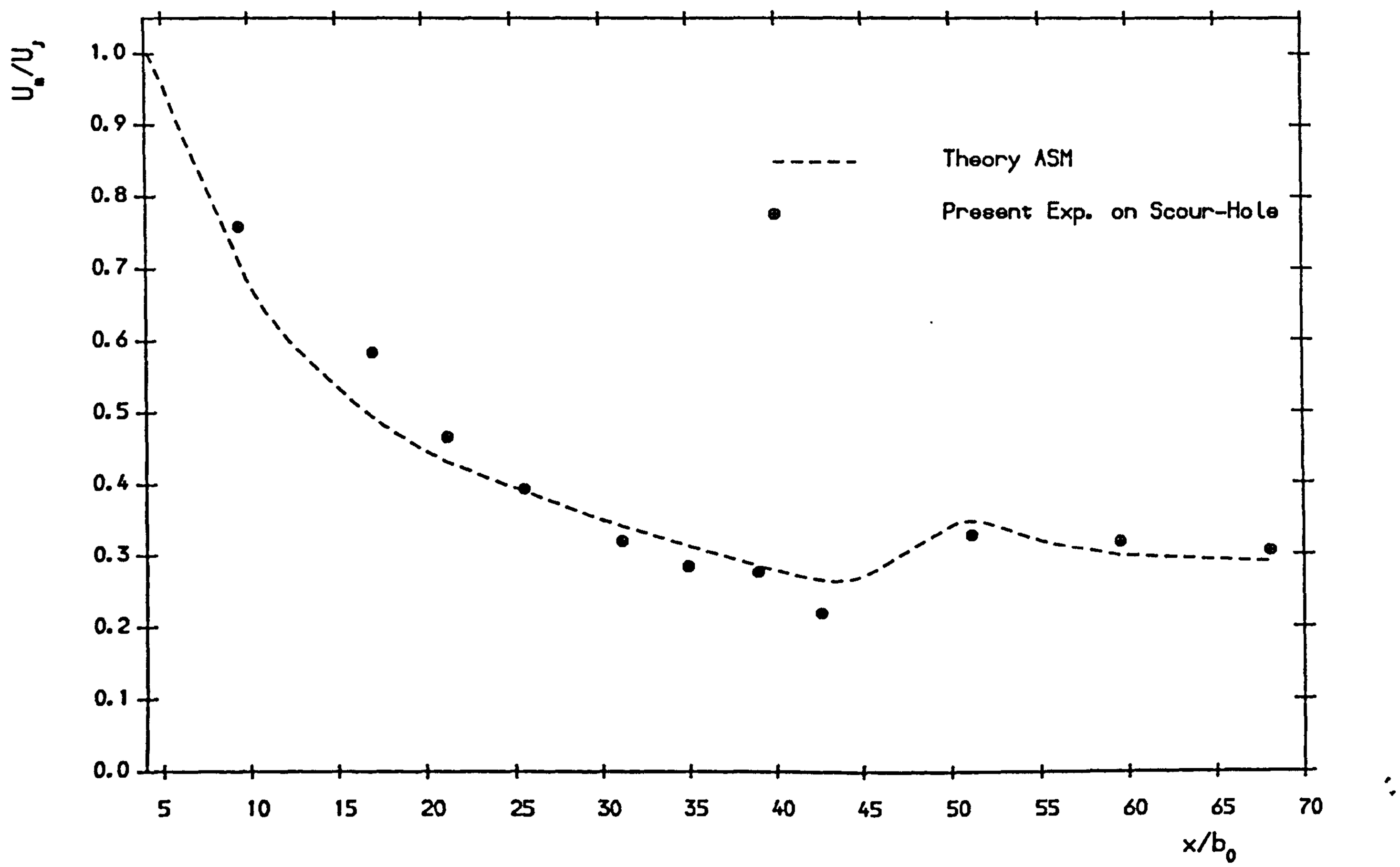

Fig. 9.30 Decay of Max. Vel. of Offset-Jet in Scour Hole

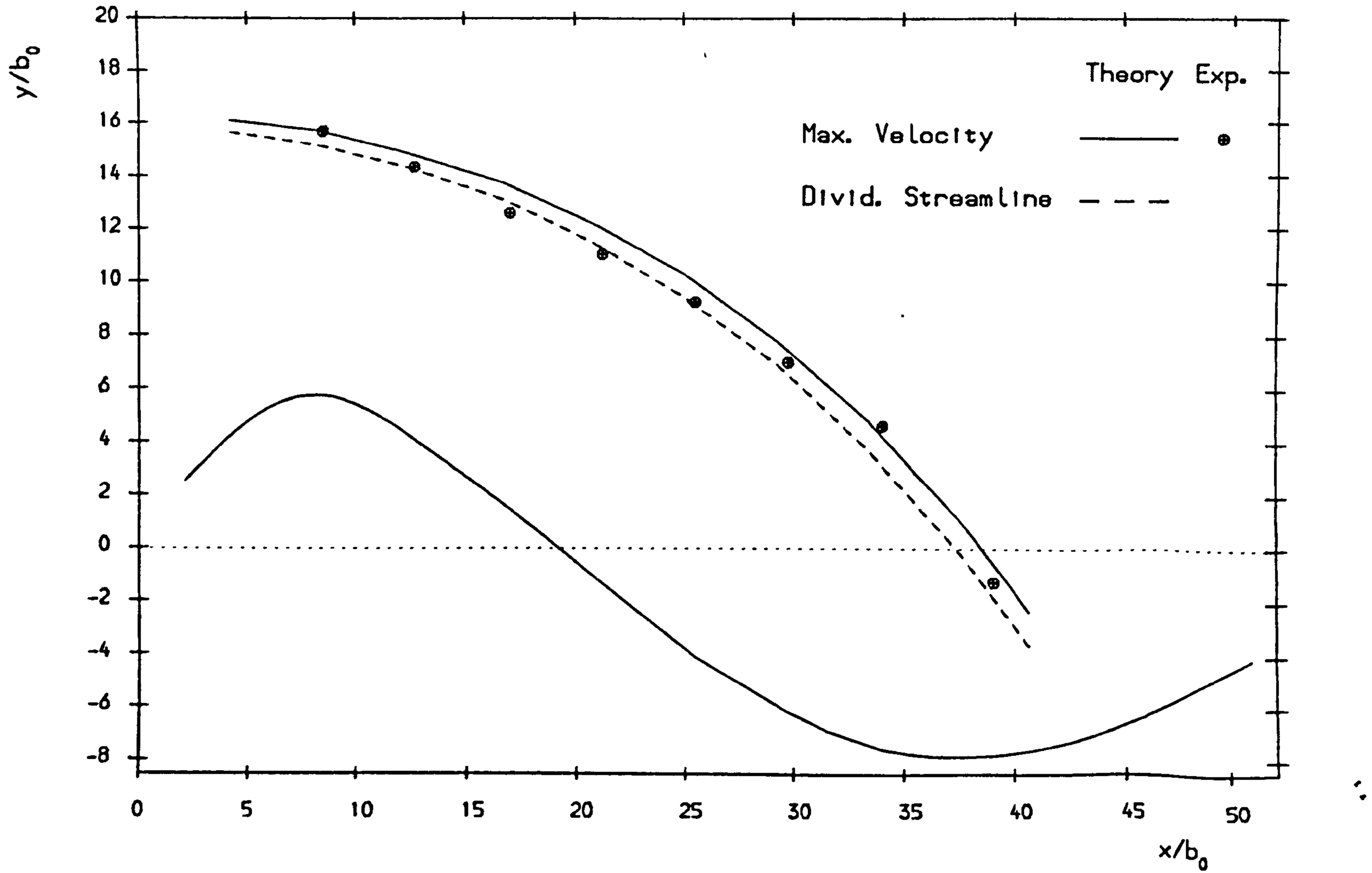

Fig. 9.31 Different Traject. for Offset Jet in the Scour Hole (Test No. S205)

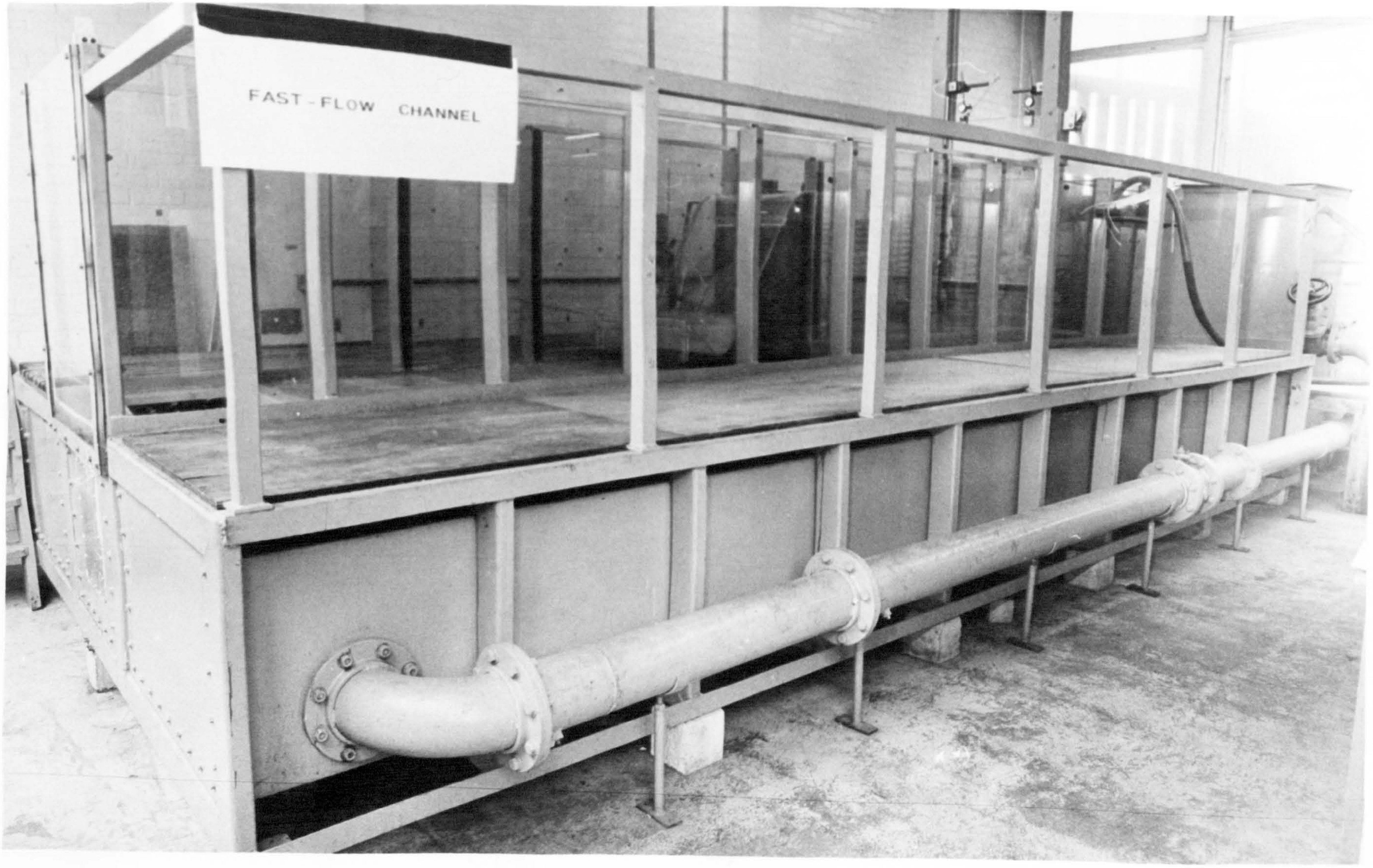

Plate 4.1 Laboratory Layout

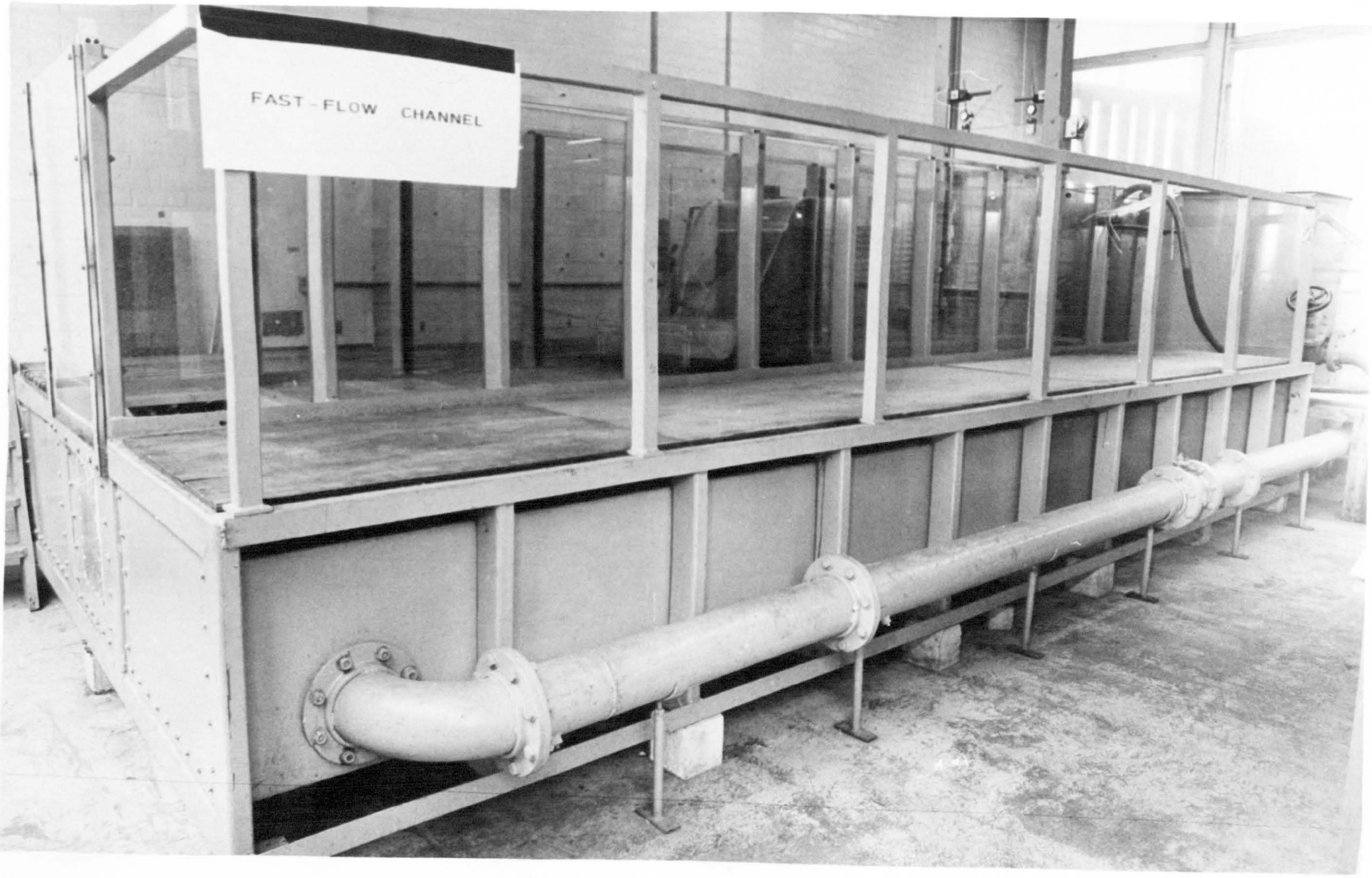

Plate 4.1 Laboratory Layout

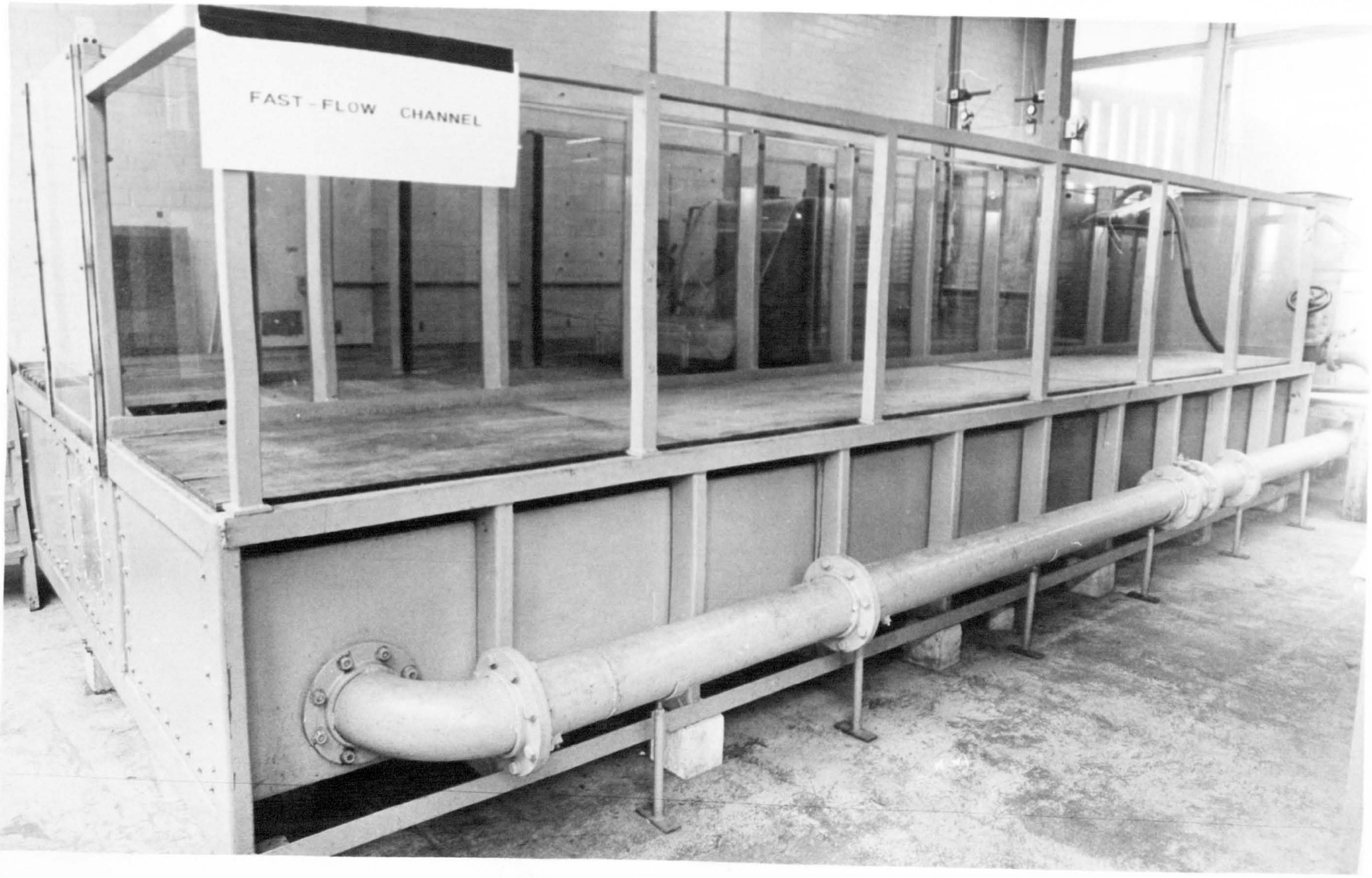

Plate 4.1 Laboratory Layout

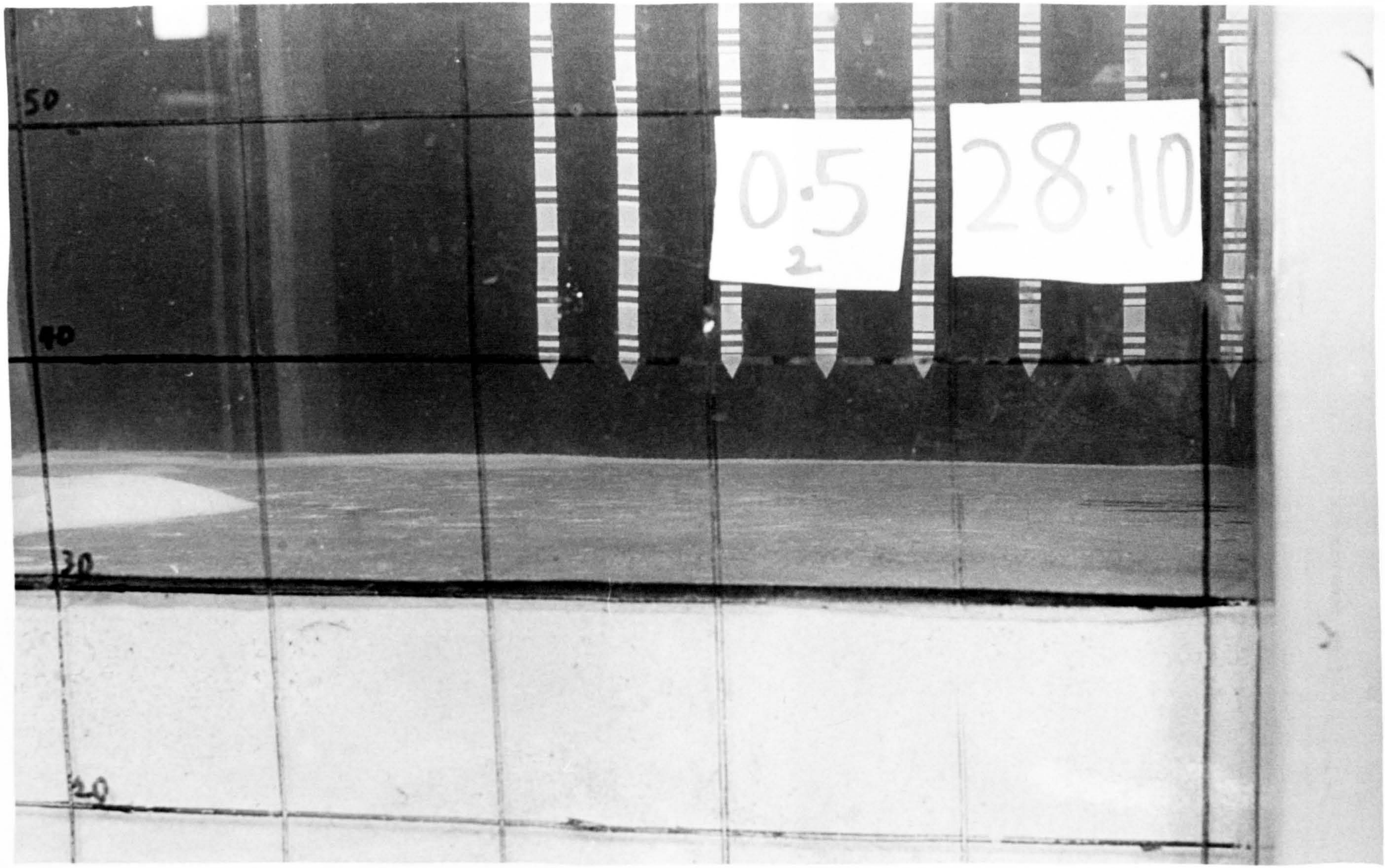

Plate 4.2 Aluminium Cover

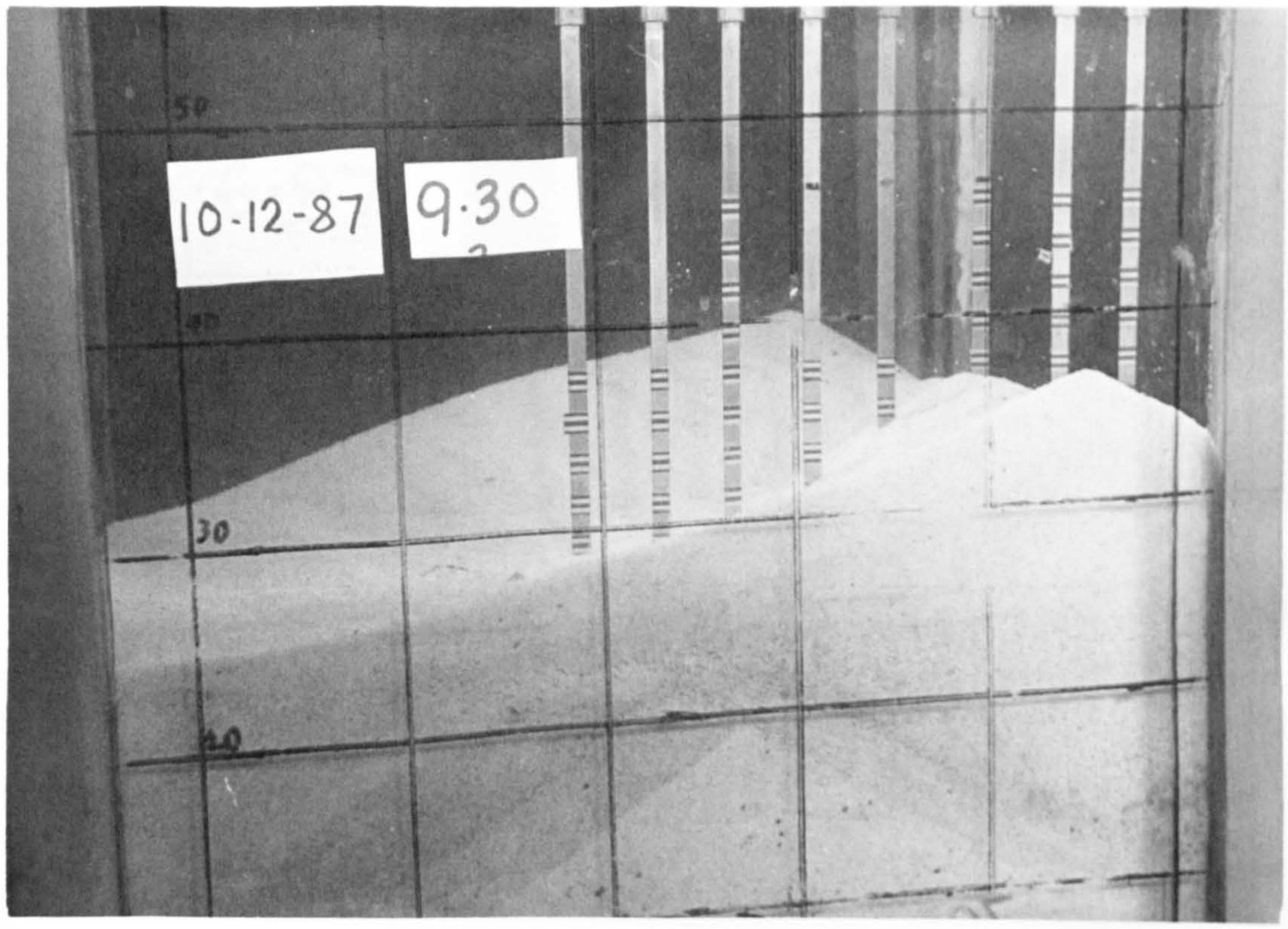

a) humping

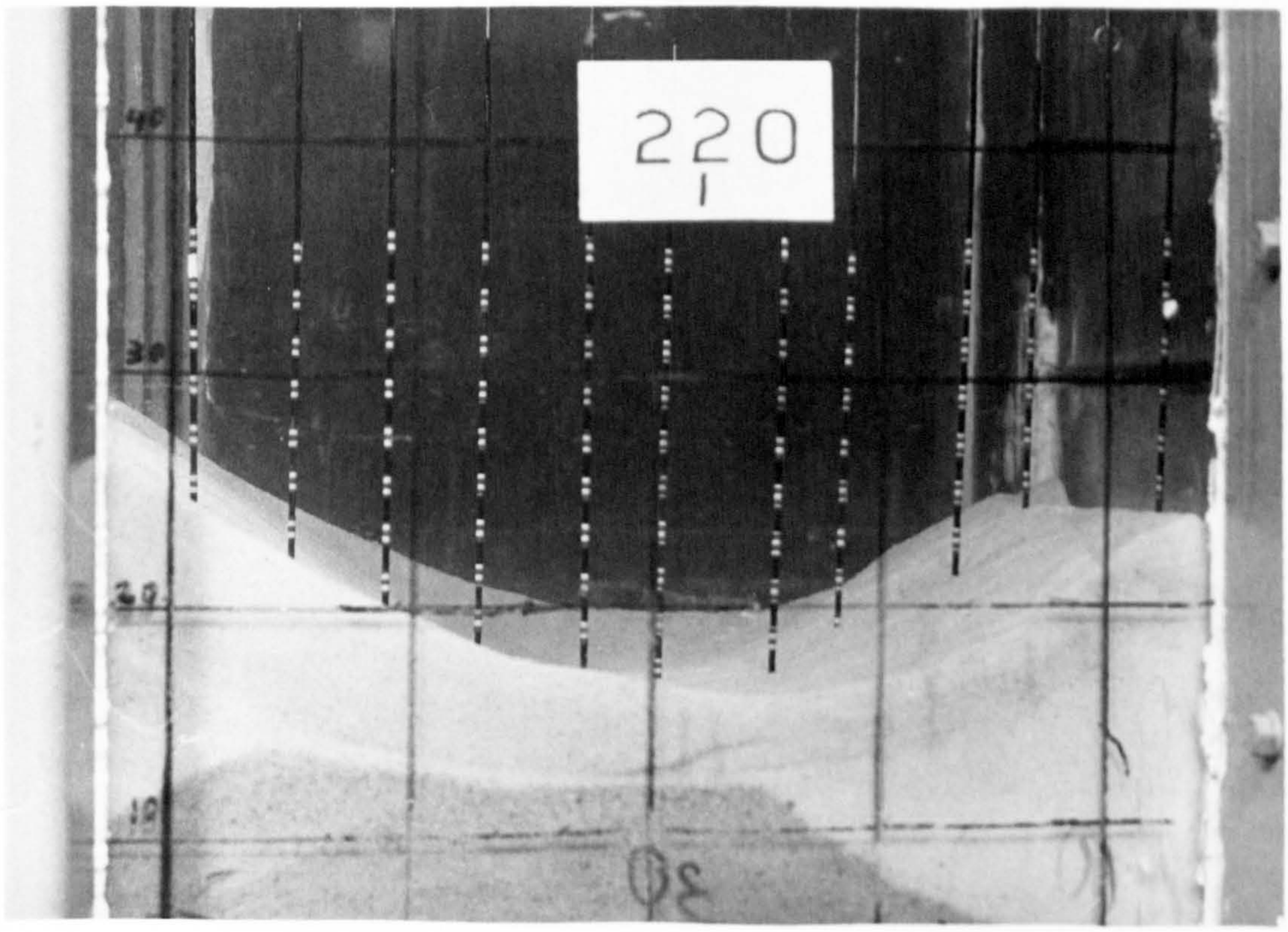

b) hollowing

Plate 4.3 Three-dimensional nature of scour holes near channel walls

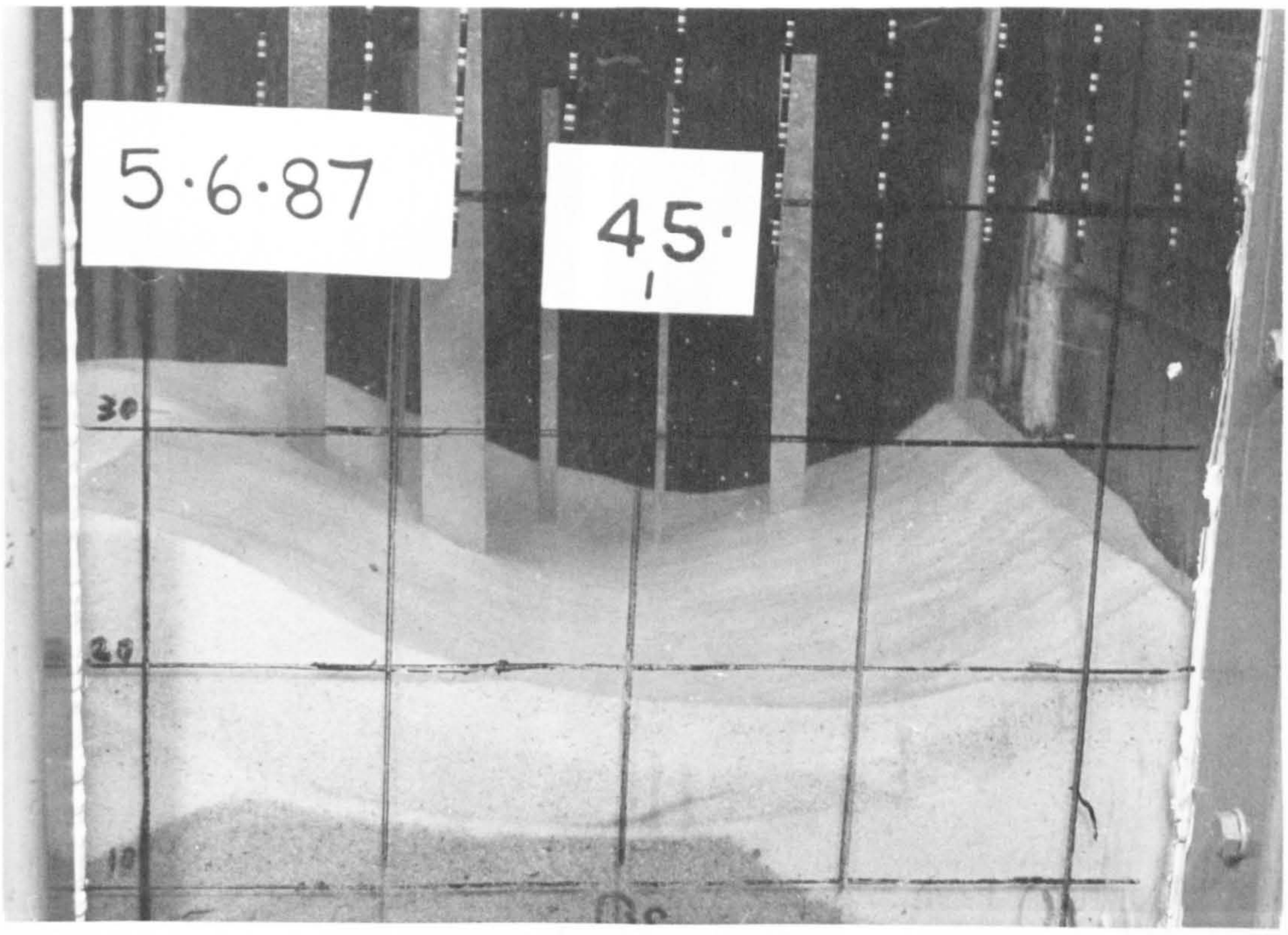

a) Strips

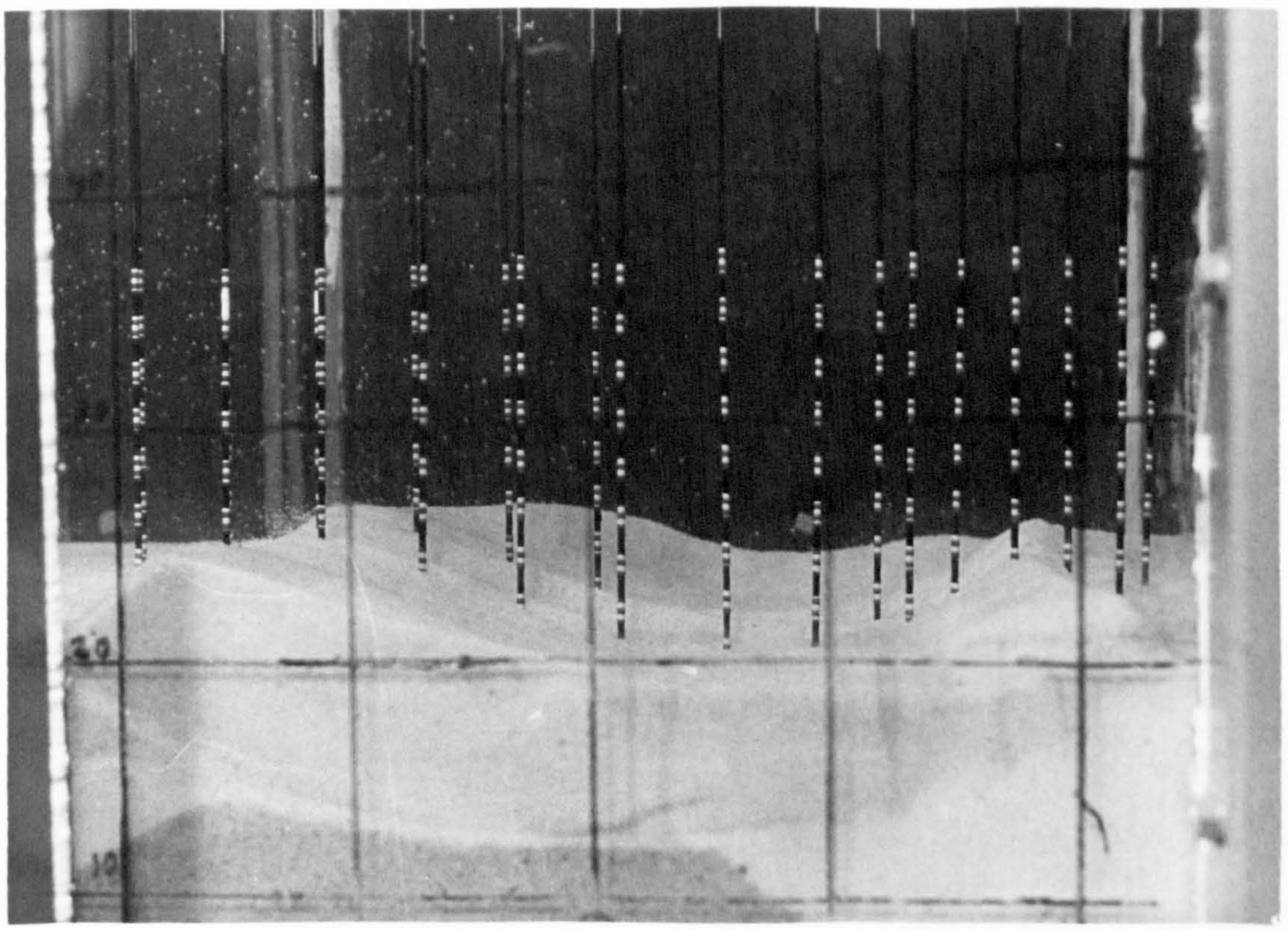

b) Rods

Plate 4.4 Different gauges for measuring scour-hole profile

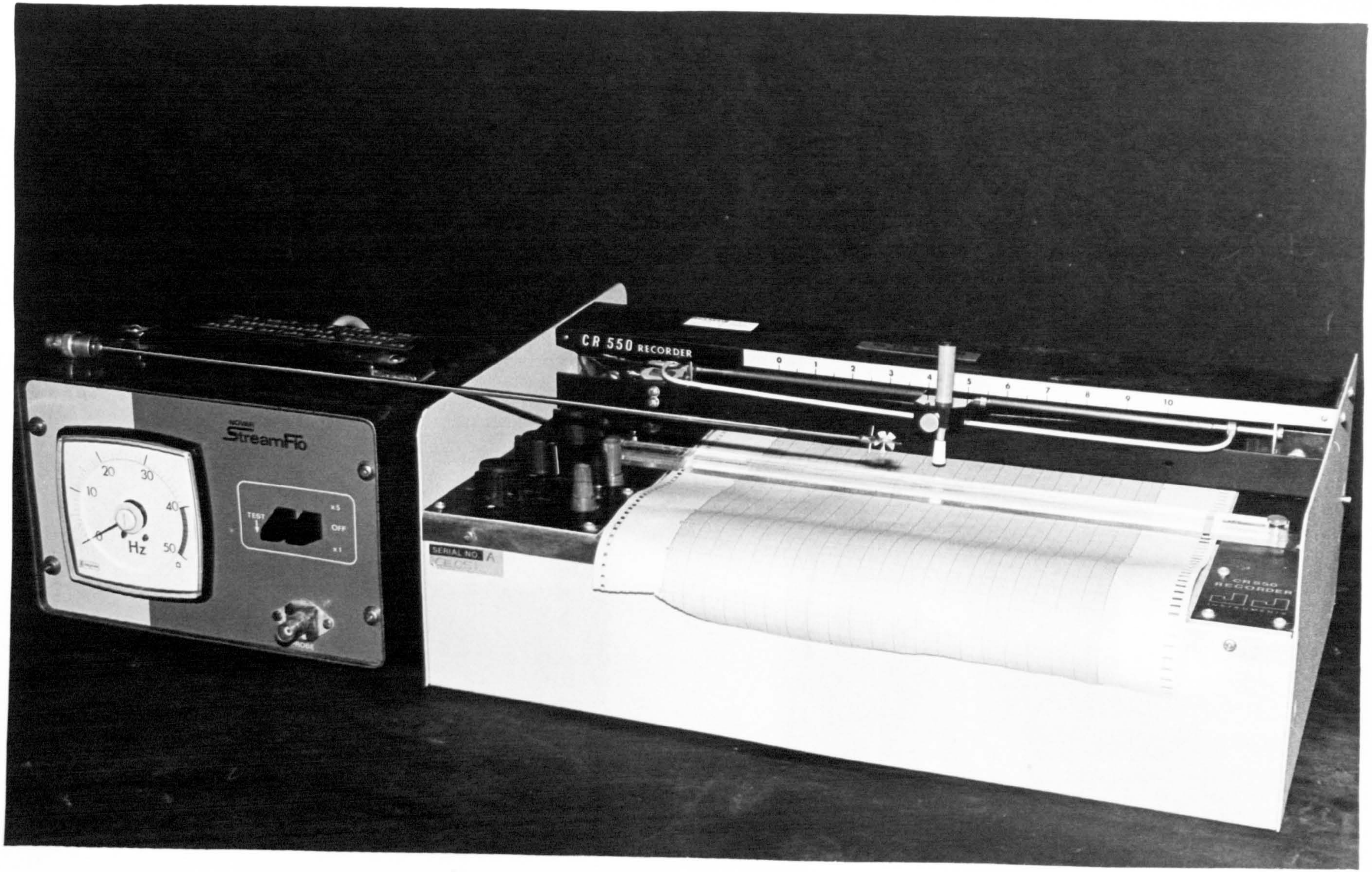

Plate 4.5 Stream-flo Current Meter, Indicator and the Speedomax Pen Recorder

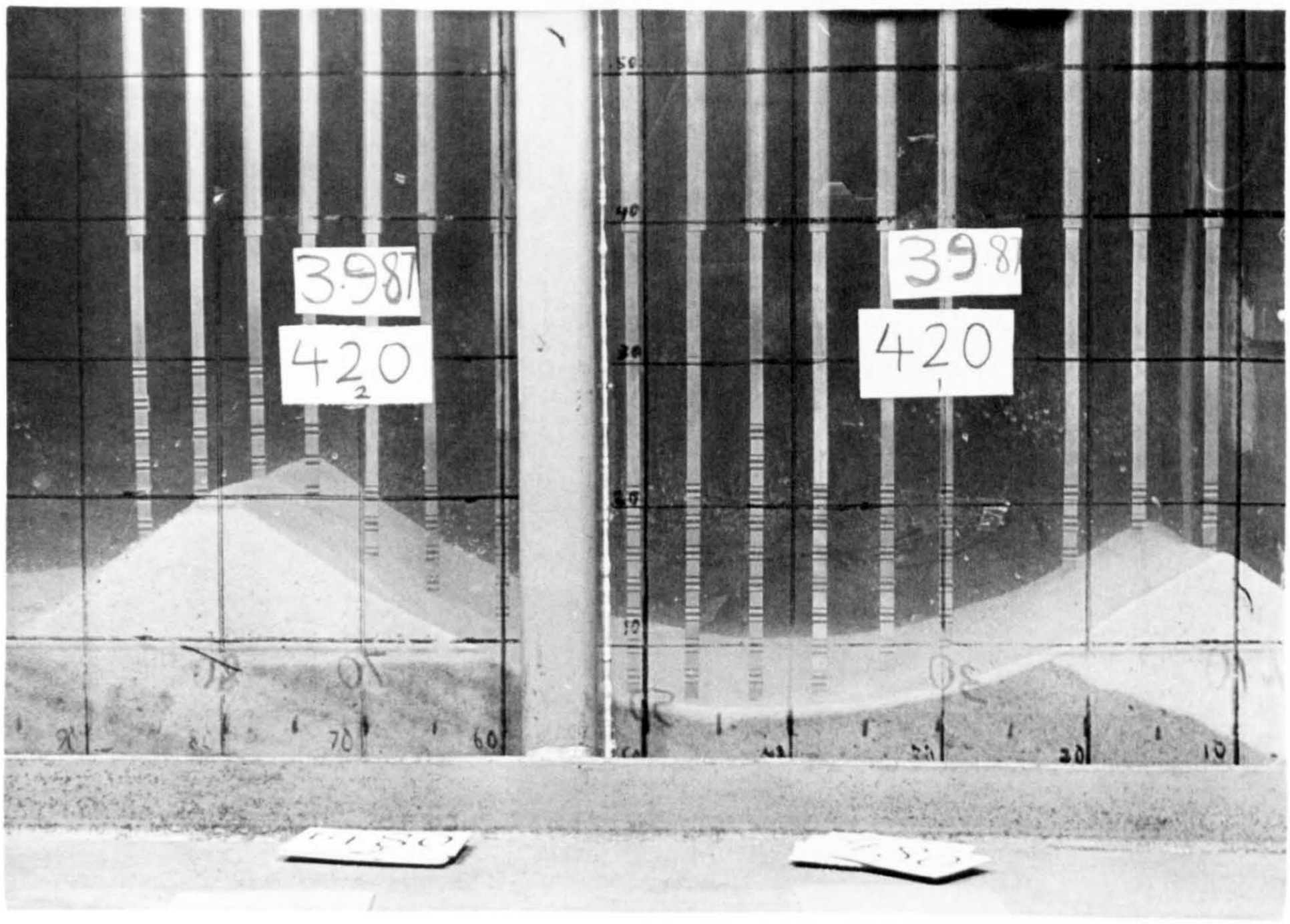

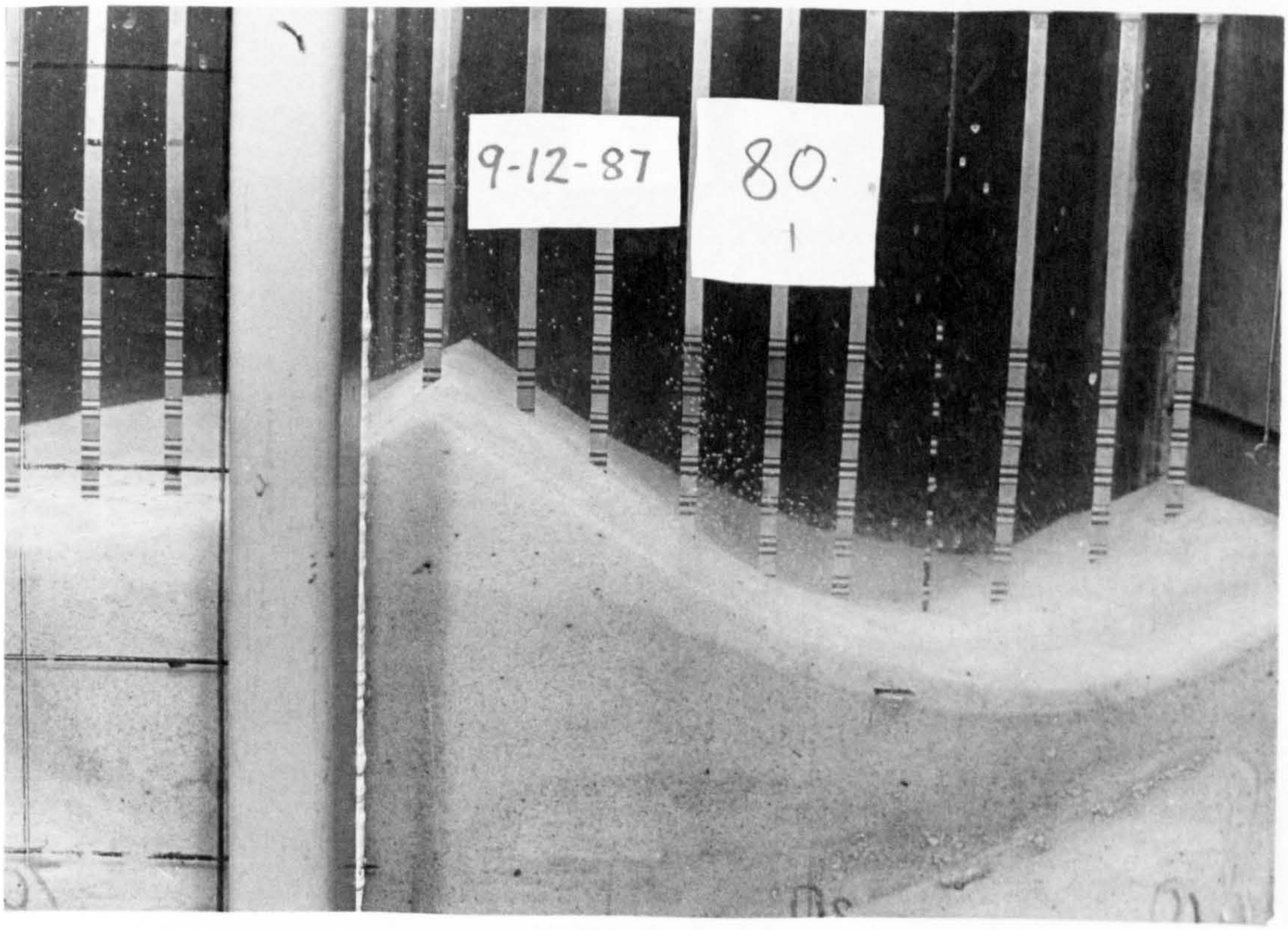

Plate 6.1 Examples of scour holes caused by offset jets

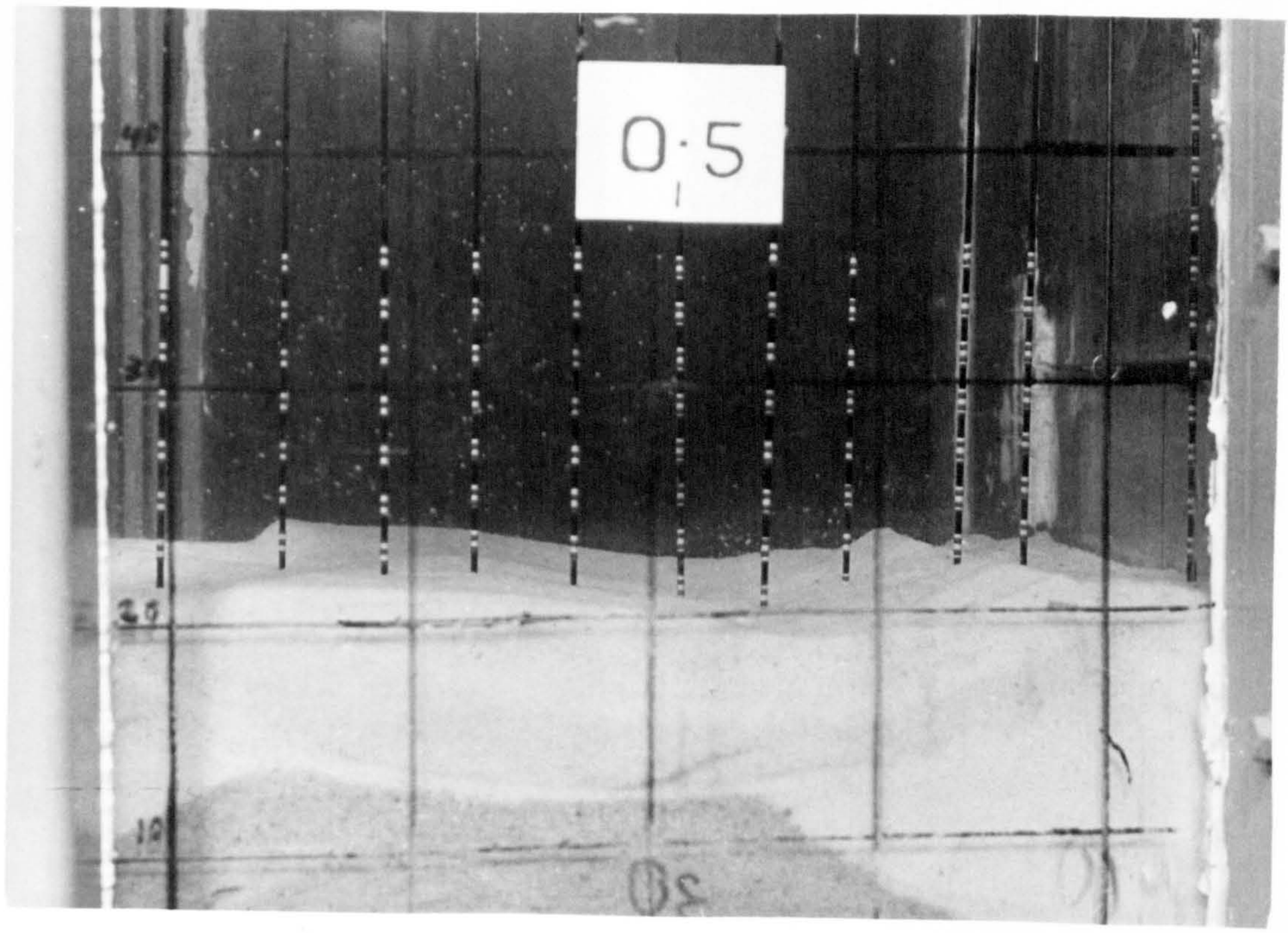

Time = 30 sec.

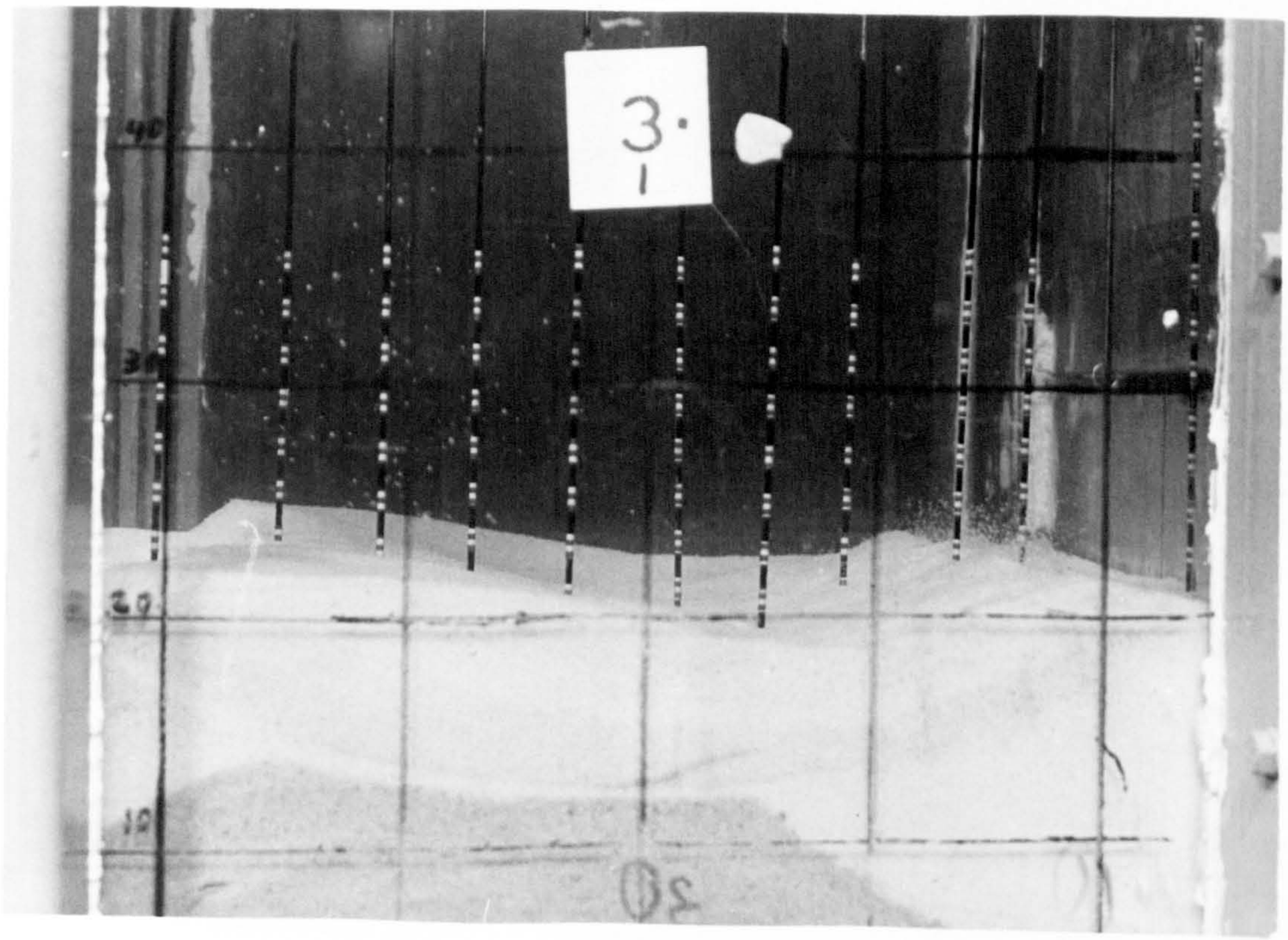

Time = 3 min.

Plate 6.2 Beginning of scour process by offset jet

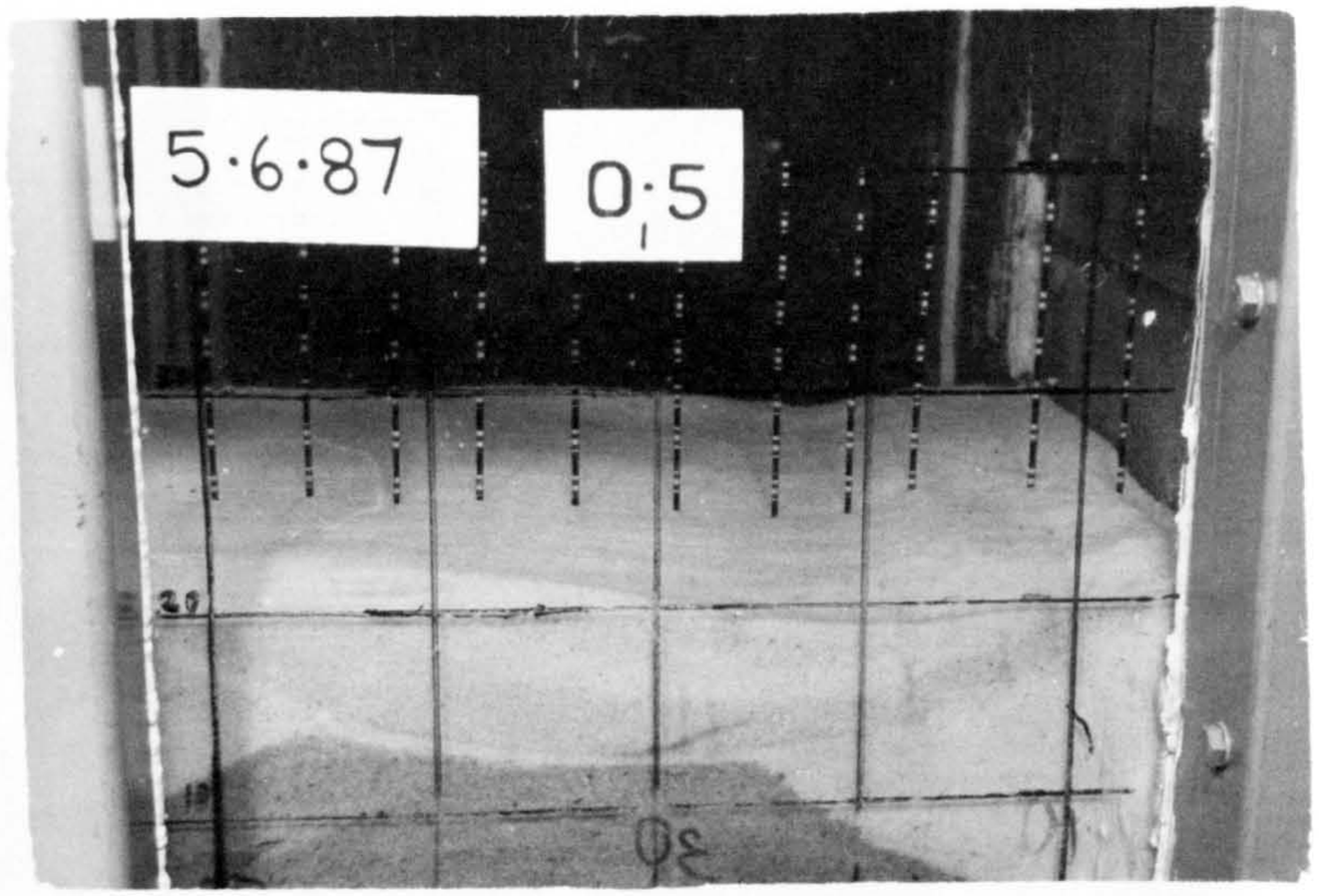

Time = 30 sec.

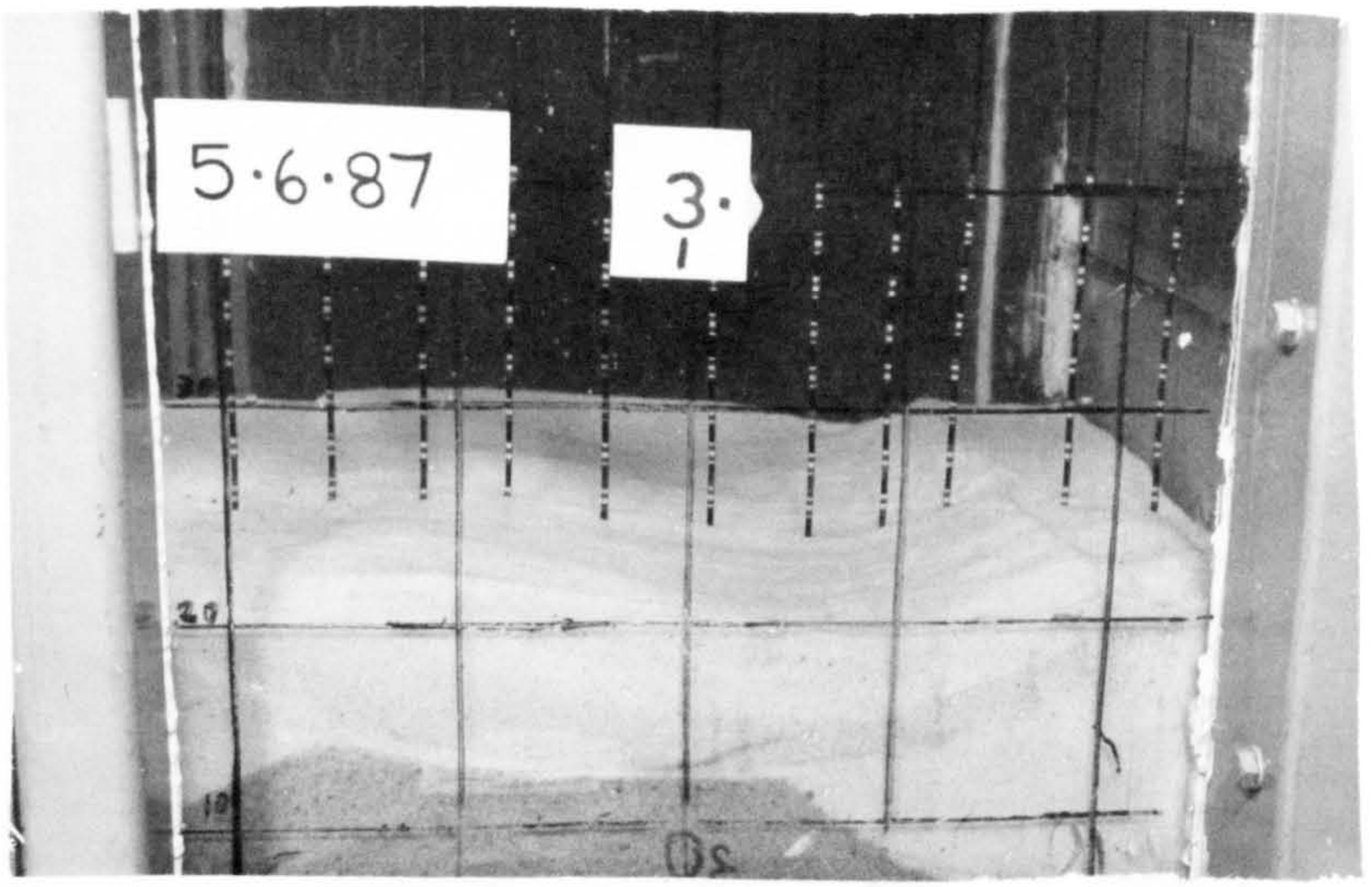

Time = 3 min.

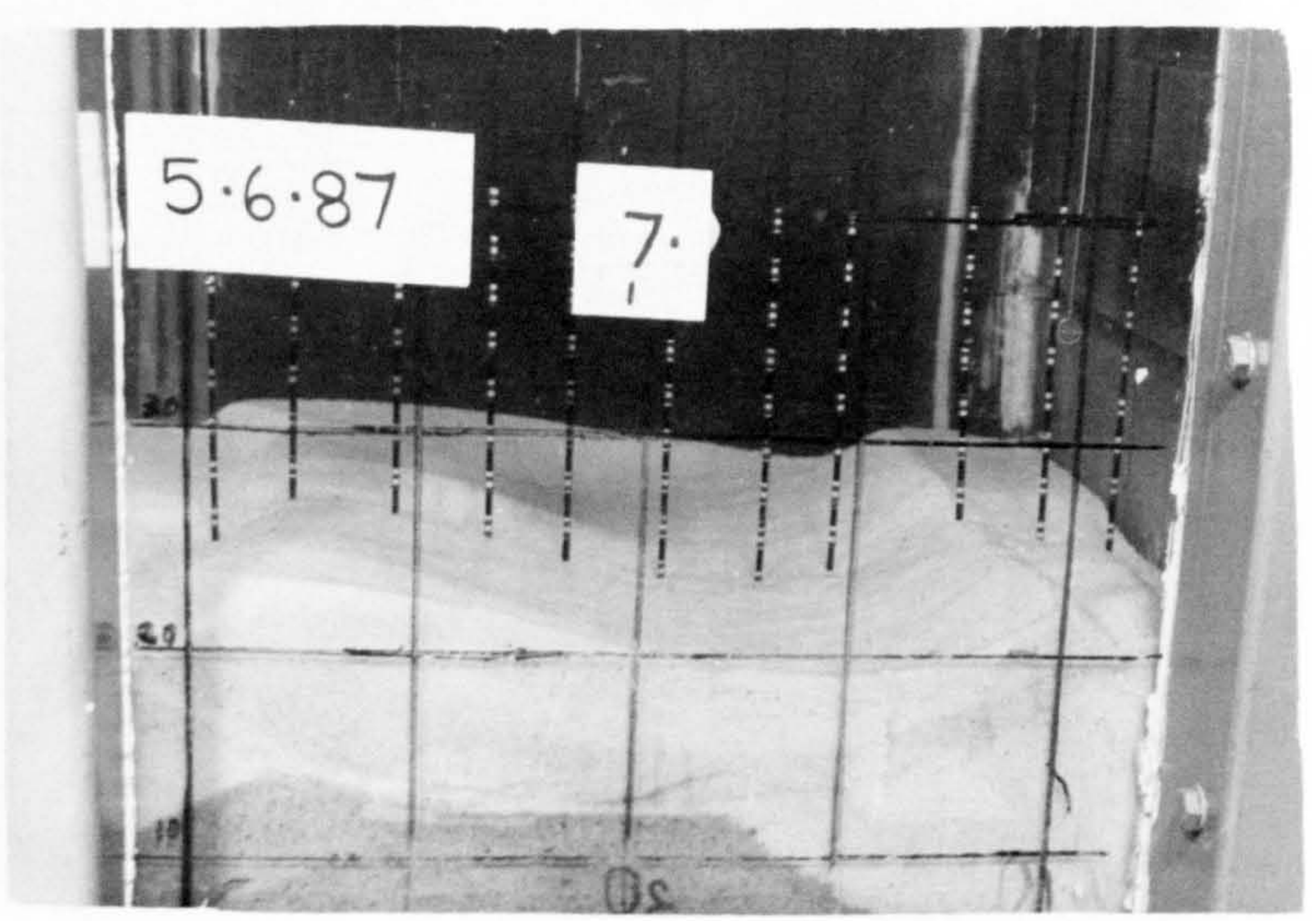

Time = 7 min.

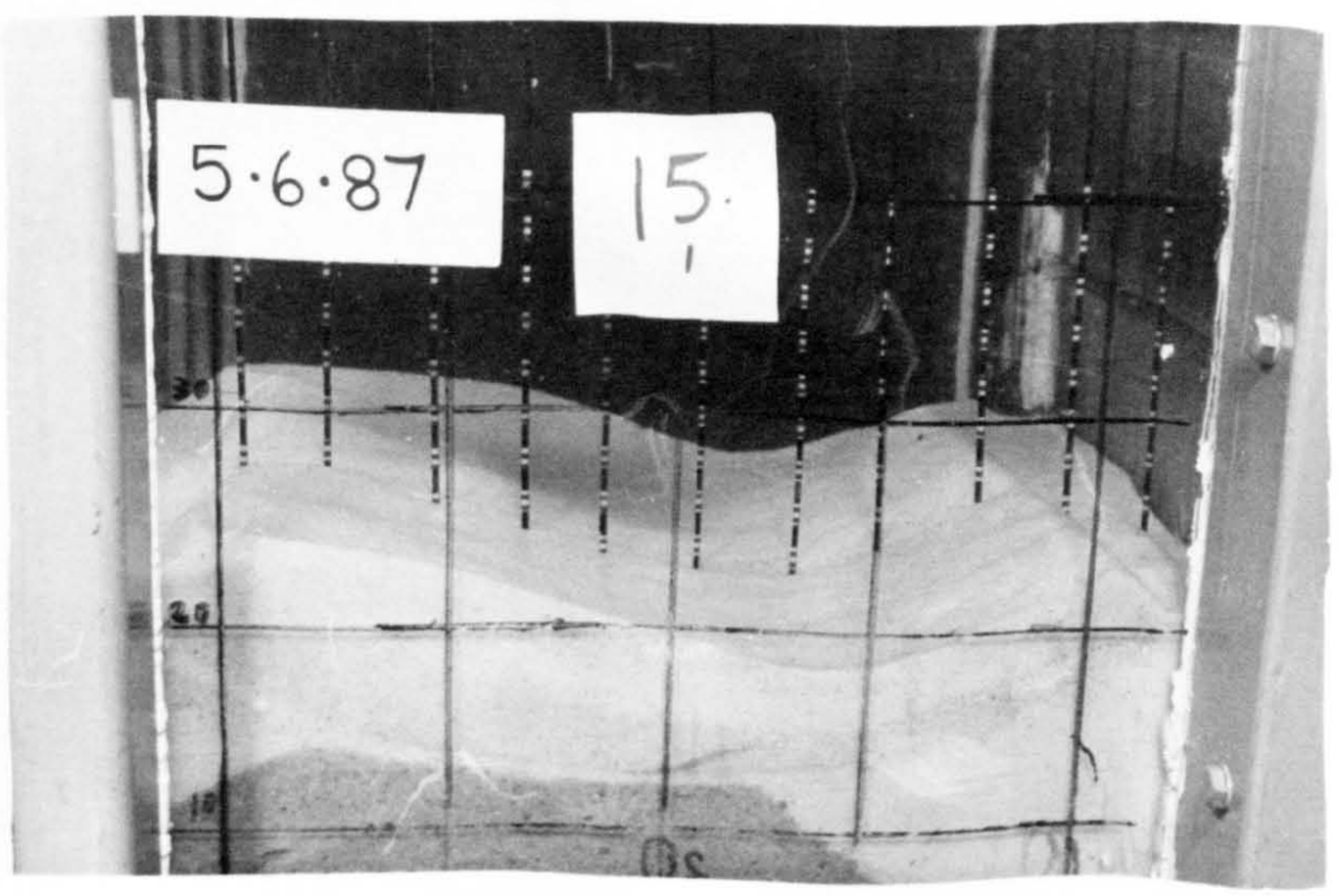

Time = 15 min.

Plate 6.3 Initial Stages of the Development of a Scour Hole by Offset Jet

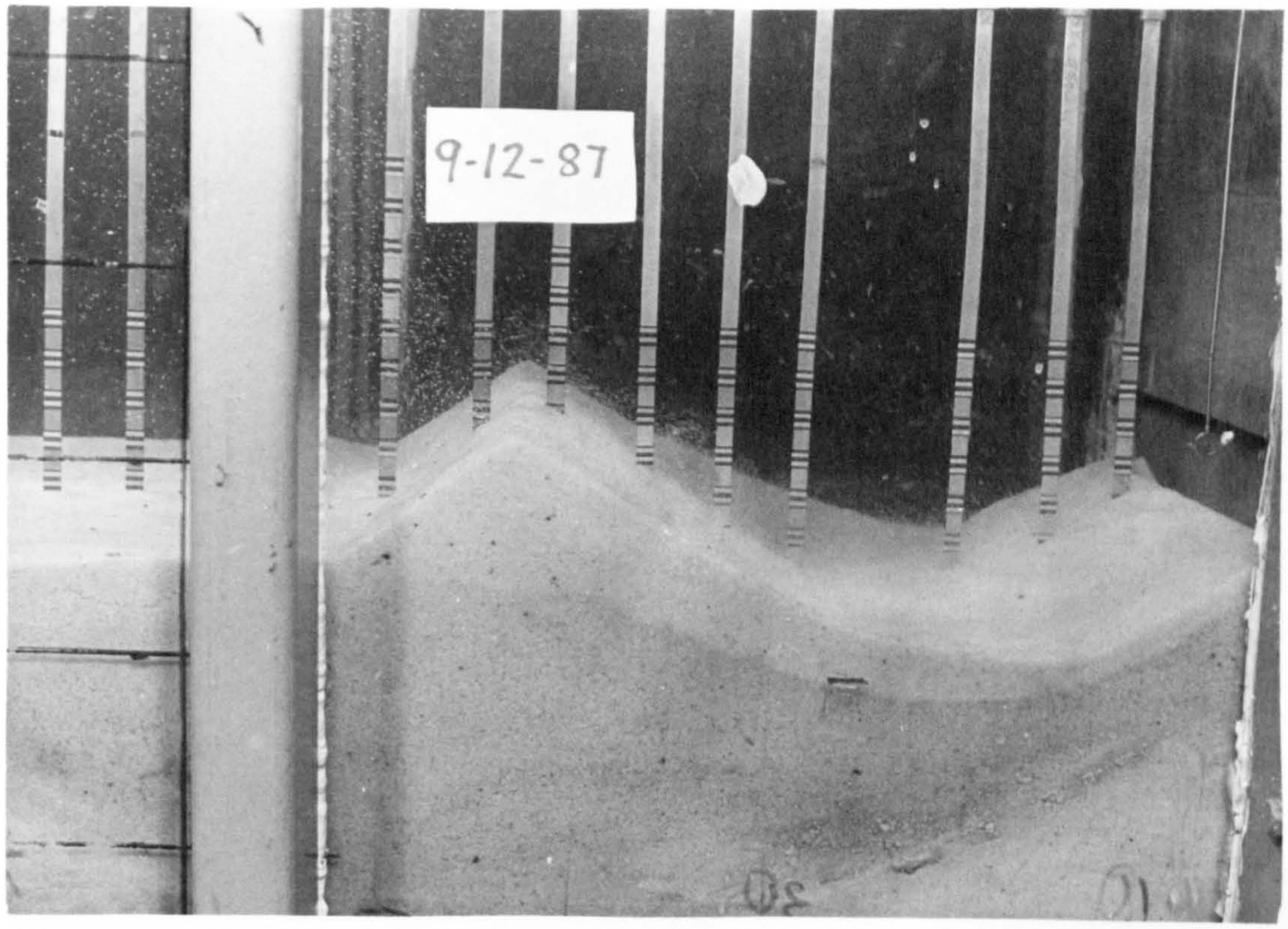

Time = 7 min.

Plate 6.4 Sands lifted from the bottom and thrown over the dune

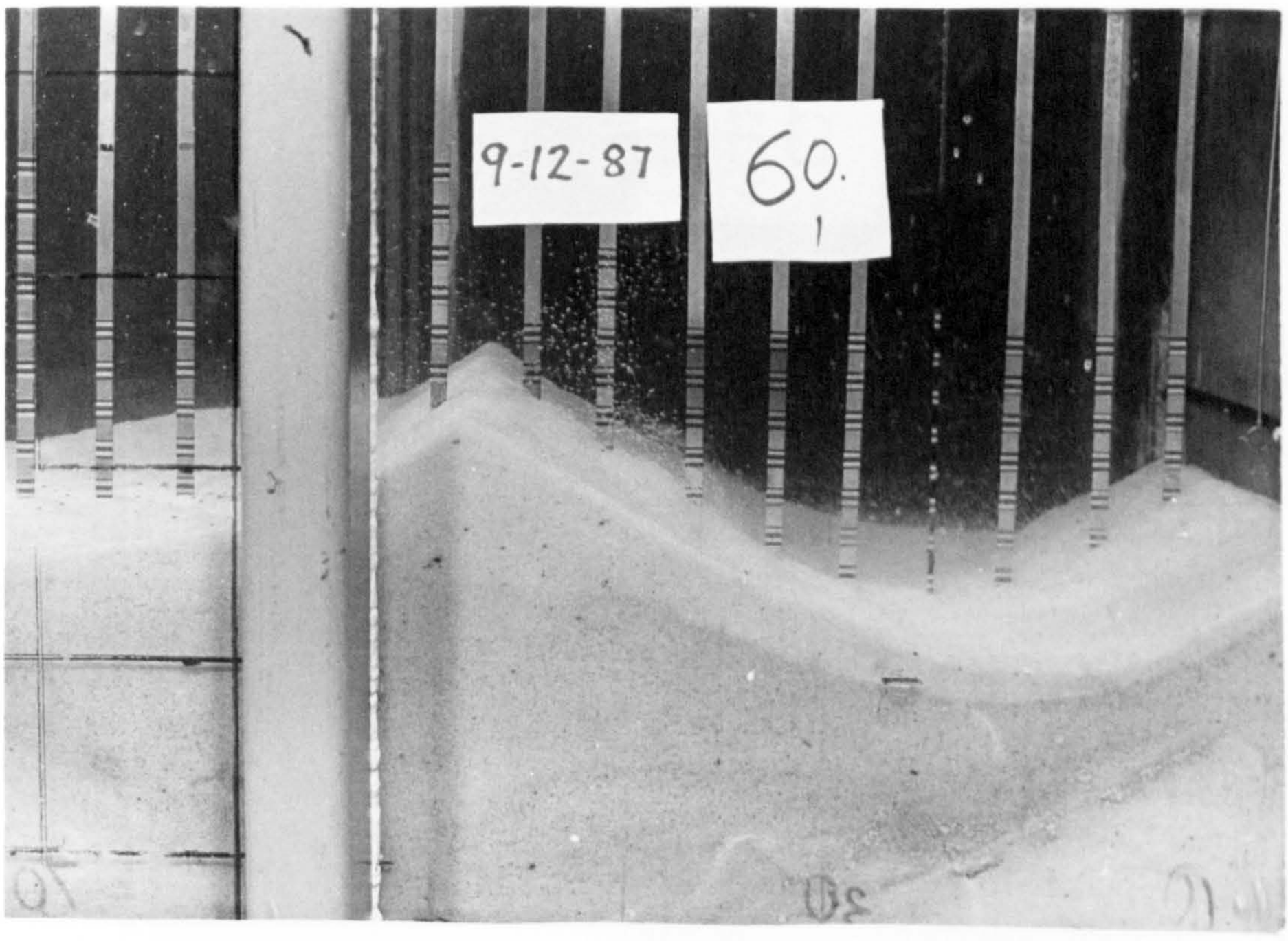

Time = 60 min.

Plate 6.5 Sands thrown mainly on top of rather over the dune

Plate 6.6 Lee of the dune (equal to the angle of repose of sand)

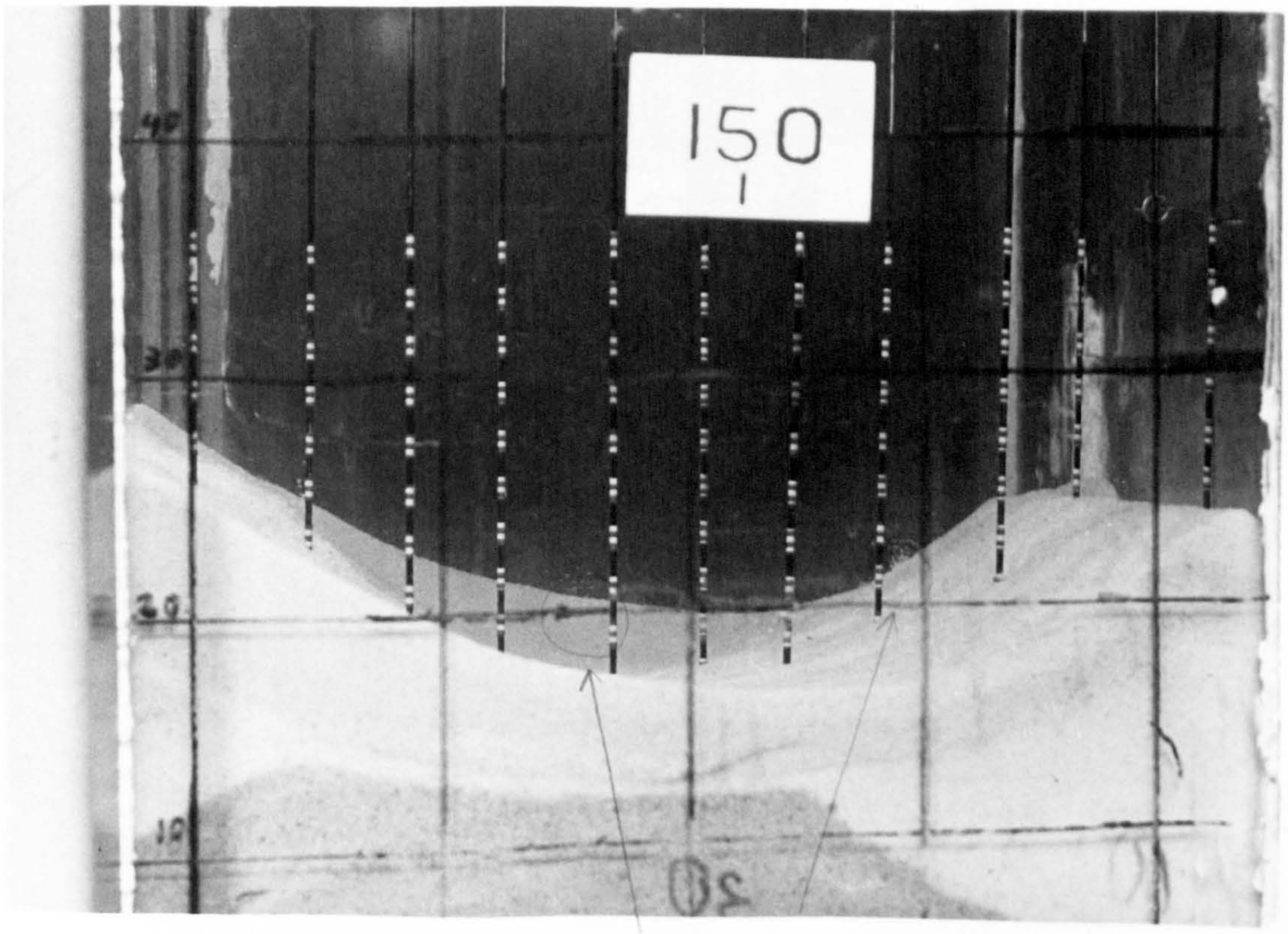

Plate 6.7 Turbulent bursts

a) Time = 15 sec.

Time = 45 sec.

Plate 6.8-a Time development of scour (test no. S051)

Time = 3 min.

Time = 22 min.

Plate 6.8-b Time development of scour (test no. S051)

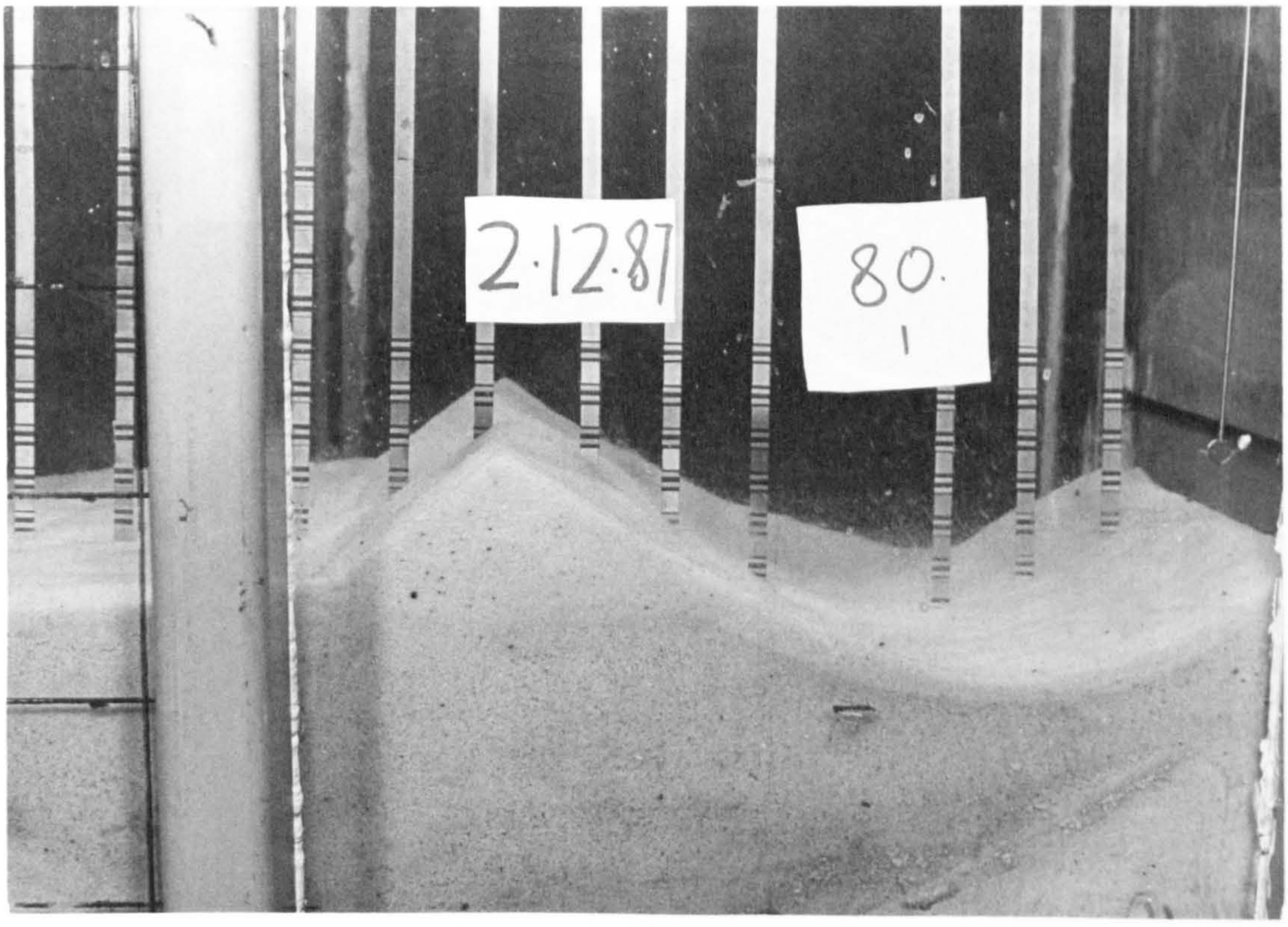

Time = 60 min.

Time = 360 min.

Plate 6.8-c Time development of scour (test no. S051)

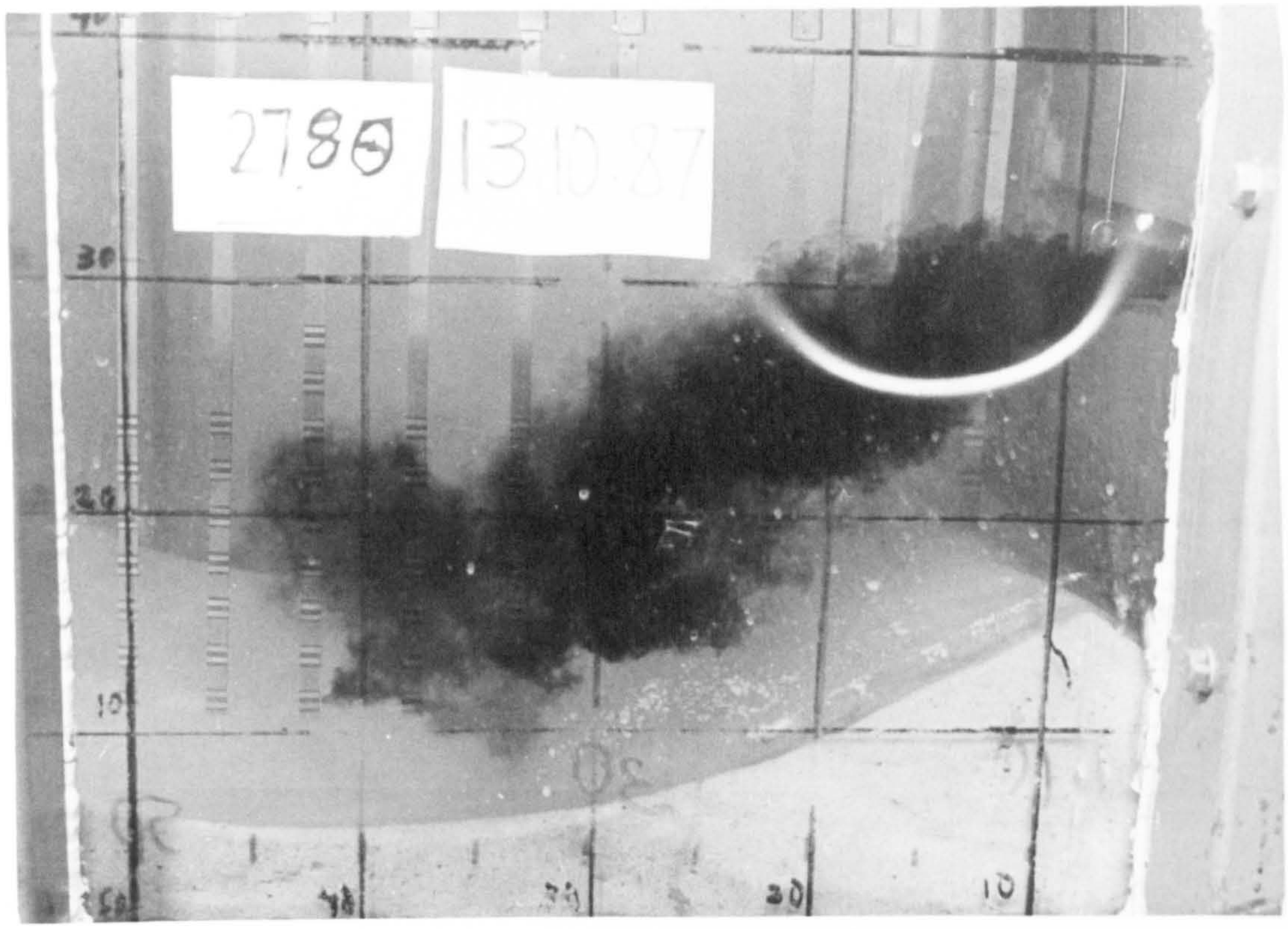

a) Pre-attachment zone

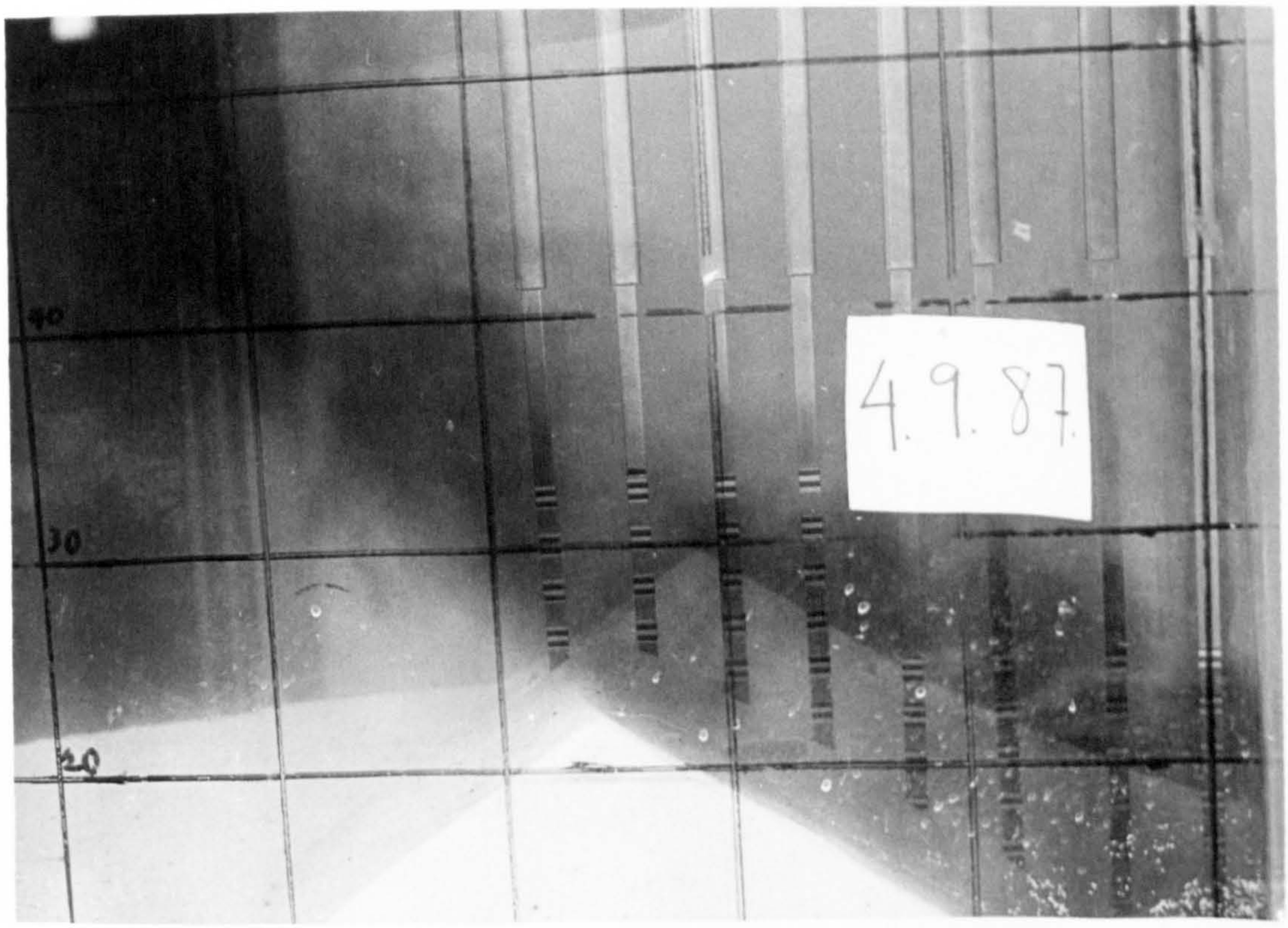

b) After attachment point

Plate 6.9 Flow behaviour in the scour hole (studied by dye injection)